Proton transfer at Carbon

Eleanor M. Higgins

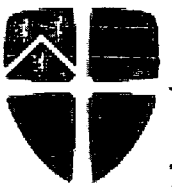

Durham University

Proton Transfer at Carbon

Eleanor M. Higgins B.Sc. (HONS.) U.C.D.

USTINOV COLLEGE

DEPARTMENT OF CHEMISTRY

DURHAM UNIVERSITY

A Thesis submitted for the degree of Doctor of Philosophy at the Durham University

September 2007

For my Grandmother

"*The great way is easy for those without preference*"

5th Zen Patriarch

Table of Contents

Abbreviations

Å	angstrom(s)
Ar	aryl
b.p.	boiling point
br.	Bra (spectral)
Bu	butyl
ca.	circa
cat.	catalyst
°C	degree centigrade
cm^{-1}	wavenumbers
^{13}C NMR	carbon 13 nuclear magnetic resonance
COD	cyclooctadiene
CO_2	carbon dioxide
Cp	cyclopentadiene
Cy	cyclohexane
δ	chemical shift
d	doublet
DMSO	dimethyl sulfoxide
DNA	deoxyribonuleic acid
D_2O	deuterium oxide
ΔE	energy change
Eqn.	equation
ESR	electron spin resonance
Et	ethyl
eV	electronvolt(s)
Fig.	Figure
fs	femtosecond
g	gram(s)
HCl	hydrochloric acid
^{1}H NMR	proton nuclear magnetic resonance

HOMO	highest occupied molecular orbital
hr	hour(s)
Hz	hertz
IR	infra red
IUPAC	International Union of Pure and Applied Chemistry
J	coupling constants
k	rate constant
K	kelvin
K	equilibrium constants
K_a	acidity constant
kcal	kilocalorie(s)
kJ	kilojoule(s)
λ	wavelength
L	litre(s)
LDA	lithium di-*iso*propylamide
lit.	literature
ln	natural logarithm
log	logarithm
LUMO	lowest unoccupied molecular orbital
M	moles/litre (Molar)
m-	*meta*
m	multiplet
Me	methyl
Mes	mesityl
min	minute(s)
mL	millilitre(s)
mm	millmeter(s)
mmol	millimole(s)
mol	mole(s)
m.p.	melting point
ms	millisecond(s)

m/z	mass per unit charge
NAD^+	nicotinamide adenine carbene
NHC	N-Heterocyclic carbene
o-	*ortho*
p-	*para*
Ph	phenyl
pm	picomitres
ppm	parts per million
ps	picosecond
Q_{net}	Löwdin net atomic charge
R	alkyl substituent
Rf	retention factor
RNA	ribonucleic acid
ρ	reaction constant
σ	substituent constant
s	second(s)
s	singlet (spectral)
t	triplet (spectral)
THF	tetrahydrofuran
t.l.c.	thin layer chromatography
μCi/l	microcurrie per litre
μL	microlitre(s)
UV	ultraviolet
VIS	visible
wk	week
wt.	weight

Abstract

This thesis describes the determination of the pK_a values of a number of carbon acids in D_2O at 25 °C and fixed ionic strength (KCl). Second-order rate constants for the deprotonation of these carbon acids by deuteroxide ion k_{DO} ($M^{-1}s^{-1}$), in D_2O at 25 °C were determined by ^1H NMR spectroscopy. These k_{DO} values could be used to calculate values for k_{HO} ($M^{-1}s^{-1}$), the second-order rate constant for deprotonation of the carbon acid by hydroxide ion to give the corresponding conjugate base in water. This thesis deals with three different groups of carbon acids: the conjugate acids of N-heterocyclic carbenes, diketopiperazines, and thalidomide and thalidomide analogues.

Diaminocarbenes are of significant interest as ligands in organometallic catalysis and in medicinal chemistry. The syntheses and determination of the pK_a values of a series of the azolium ions including 1,3-disubstituted imidazolium ions, 4,5-dihydroimidazolium ions, and 3,4,5-trihydropyrimidinium ions are described. Values for k_{HO} ($M^{-1}s^{-1}$), the second order-rate constant for deprotonation at C2 of each azolium ion, were determined as described above. Evidence is presented that the reverse rate constant for carbene protonation by solvent water is limited by solvent reorganization and occurs with a rate constant of $k_{HOH} = k_{reorg} = 10^{11}$ s^{-1}. Values for k_{HO} and k_{HOH} permitted the calculation of reliable carbon acid pK_as for ionization of the azolium ions in water. The effects of the N-substituents and ring size of the heterocycle on k_{HO} and pK_a values are discussed. The relative hydrolytic stabilities of the azolium ions is also discussed.

Diketopiperazines (DKPs) are an important class of biological compound. The synthesis and determination of the pK_a values of bis-D-proline and bis-L-proline diketopiperazine are described. Values for k_{HO} ($M^{-1}s^{-1}$), the second order-rate constant for deprotonation at the α-carbon of the DKP were determined as described above. Evidence is presented that the reverse rate of protonation of the DKP enolates by solvent water is likely to be less than diffusion controlled. Hence, the pK_a values were determined by extrapolation from a Brønsted plot of log k_{HO} values against pK_a values of other neutral simple carbon acids. The DKP k_{HO} and pK_a values are compared with analogous values for acyclic peptide analogues.

Thalidomide and analogues such as the chemokine inhibitors, N-(2-Oxo-piperidine-3yl)propionamide and N-(2-Oxo-azapan-3-yl)propionamide, have been of considerable interest to the pharmaceutical industry for some time. Determination of the rates of hydrolysis and the pK_a values for thalidomide and the analogues in D_2O at 25 °C and fixed ionic strength (KCl) are described. The pK_a values were determined from a Brønsted plot of log k_{HO} values against pK_a of other neutral simple carbon acids in a similar manner to that performed for the diketopiperazines. The rates of hydrolysis and the relative stereointegrity of the species are discussed.

Chapter 1

Introduction

1. Foreword

Factors that effect carbon acidity have long been of interest. Simple carbon acids are found in almost all areas of chemistry and biology. Yet until recently detailed studies of structural and solvent effects on their acidities had not been pursued due to the unavailability of sensitive experimental methods for the determination of high pK_a values

Scheme 1.1 shows the equation for deprotonation of a carbon acid to form the corresponding conjugate base in solvent water, where K_a (Equation 1.1) is the equilibrium constant for this dissociation process. The negative logarithm of the equilibrium constant or acid dissociation constant K_a is referred to as the pK_a (Equation 1.2), and is the common unit of comparison for acid strengths. The magnitude of the K_a value is dependent on the relative stabilities of the carbon acid and the carbanion conjugate base in solution. High pK_a values of simple carbon acids such as amino acids are mainly due to the instability the carbanion (or enolate) conjugate base.

Scheme 1.1:

$$K_a = \frac{[(R_1,R_2,R_3)C^-][H_3O^+]}{[(R_1,R_2,R_3)CH]} \qquad \textbf{(Equation 1.1)}$$

$$pK_a = -\log K_a \qquad \textbf{(Equation 1.2)}$$

Unfortunately it is not easy to directly measure the high pK_a values for very weak acids due the small concentrations of the carbanion conjugate base at equilibrium. However, recent technological advances have led to improved sensitivities of experimental methods such as high resolution NMR spectroscopy and have made such high pK_a values accessible. The main focus of this thesis is the determination of pK_a values for weak carbon acids in aqueous solution. This chapter will overview general methods for the determination of pK_a values in solution, and mechanisms and structure-reactivity studies of proton transfer at carbon.

1.1 Strong carbon acids.

Strong carbon acids are usually classed as those with a pK_a in the pH range 1 – 14. The relatively high acidities of these acids depend on the unusually high stability of their corresponding carbanion conjugate bases. This is dependent on resonance and inductive effects on carbanion stability. Strong carbon acids typically have at least one electron withdrawing substituent close to the carbanion centre. This includes carbon acids such as the nitroalkanes, (nitromethane pK_a 10.2),[1] diones (pentane-2,4-dione pK_a 9[1] or malonaldehyde pK_a 5),[1, 2] sulfones and dicyanoalkanes (dicyanomethane pK_a 11).[2]

Where the carbanionic carbon is conjugated with a carbon-oxygen, -nitrogen or -sulphur multiple bond, the stability of the ion is increased significantly since the charge is transferred in varying amounts towards the electronegative atom, and away from carbon (see Scheme 1.2). An electron-withdrawing nitro group strongly stabilises a carbanion centre as in **(1)** by resonance delocalisation of negative charge onto the nitro group **(2)**. Nitro groups effectively stabilise adjacent carbanions, even making them stable in water (dinitromethane, pK_a 3.6).[3] The strongly electron withdrawing nitro group produces a carbanion in which the negative charge has been almost completely removed from the carbon atom. Similarly, the negative charge on carbanion **(3)** may be delocalised onto the adjacent carbonyl group to give enolate **(4)**. Again the major contributor to the resonance hybrid is the enolate ion with the negative charge on oxygen rather than on carbon. However in general carbonyl groups are less efficient than nitro groups at removing the negative charge (compare dinitromethane and acetylacetone, pK_a 8.95[1] in water). Cyano and sulfonyl groups are less effective still at the stabilisation of adjacent negative charge (**(5)** – **(9)**). All of the aforementioned substituents have an electron-withdrawing inductive effect which works in concert with the resonance effect to stabilise the carbanion.

Scheme 1.2:

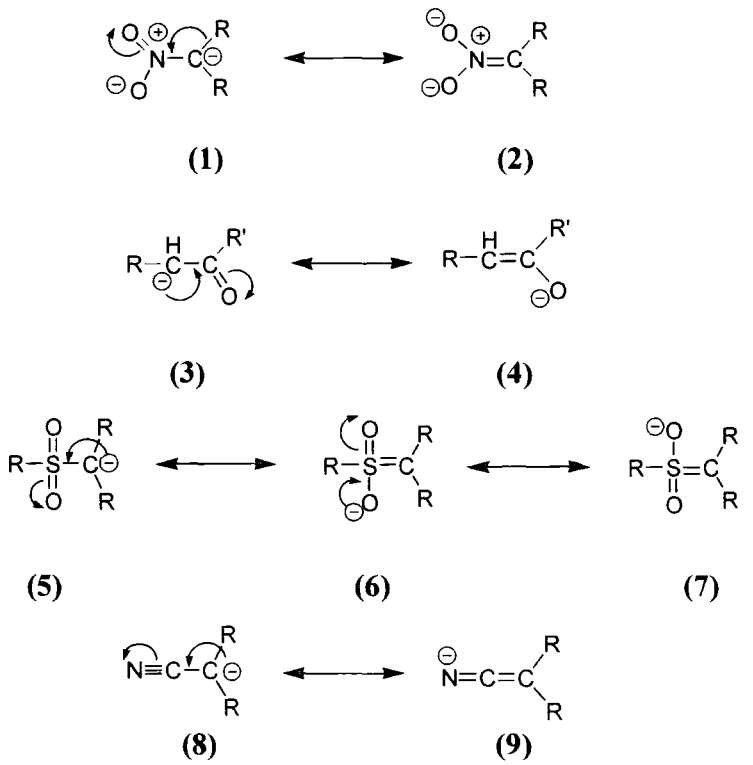

(1) **(2)**

(3) **(4)**

(5) **(6)** **(7)**

(8) **(9)**

The presence of sulphur or phosphorus adjacent to the carbanion causes an increase in stability such as in sulfides or phosphines. Possibly this is due to overlap of the occupied carbanionic *p*-orbitals with an empty *d*-orbital on sulphur or phosphorous, although in the case of sulphur this is disputed.[4] Halogen substituents close to the carbanion centre exert a strong stabilising electron-withdrawing inductive effect. The effect of a polyhalogenated carbonyl group such as in trifluoromethyl diketone (pK_a 7.3)[3] is similar to the effects of a nitro group (nitropropane-2-one pK_a 6.0).[3]

Overall, functional groups in the α-position stabilise carbanions in the order illustrated in Scheme 1.3.

Scheme 1.3:

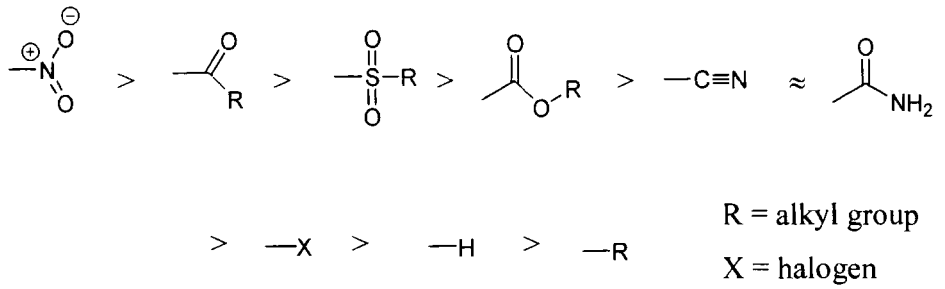

1.2 Weak carbon acids.

Carbon acids with pK_a values above pH 14 - historically called pseudo-acids – are generally classed as weak carbon acids. These range from conjugate acids of amino acids (p$K_a \approx 21$)[5] [6]to carbene precursors such as the azolium ions studied in this work. Early attempts to determine the acidity of these weak acids provided inaccurate absolute pK_a values but did indicate a general order of carbanion stability. The basic order of relative stabilities of simple carbanions from this early work[7] is shown in Scheme 1.4.

Scheme 1.4:

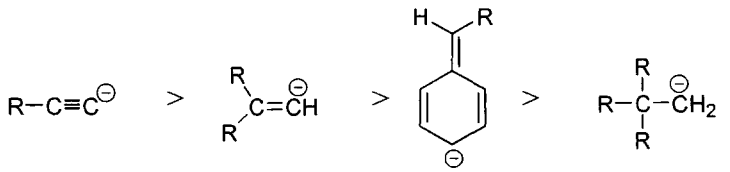

(8) **(9)** **(10)** **(11)**

Increasing the *s*-character of a carbanion increases stability. This can be seen from the order of stabilities in Scheme 1.4. The *sp*-hybridized acetylene **(8)** is significantly more acidic than sp^2-hybridized ethylene **(9)**. Ethane **(11)** with 25% *s*-character is the least acidic. The increased *s*-character implies that in general the electrons at the carbanion centre are closer to the electropositive nucleus and hence the carbanions are lower in energy. Cyclopropyl carbanions are more stable than methyl for this reason, as ring strain forces there to be more *s*-character.

Further within a series of simple alkyl carbanions such as **(11)** the following order stabilities could be predicted: methyl > primary > secondary > tertiary. This order of

stability can be interpreted to be solely the result of field effects since resonance effect are not present. More electron-donating alkyl groups result in a greater charge density at the central carbon atom relative to methyl, which decreases the stability of the carbanion. The results of studies by Applequist[8] also showed that β-branching decreases carbanion stability.

1.3 Experimental methods for pK_a determination.

Early studies on carbon acidity were limited to relatively acidic carbon acids such as nitroalkanes[9,10] and diones[11] with pK_a values within the pH range 1 - 14. Direct quantification of the amounts of carbon acid and carbanion present at equilibrium is straightforward for strong acids. A variety of methods may be used to determine the concentration of carbon acid and carbanion present at equilibrium including different spectroscopic techniques. For substrates containing chromophores, UV-Vis spectrophotometry is a particularly useful and sensitive method, and has been a popular method since the early days of studies of carbon acidity. As early as 1939 Zucker *et al*[12] reported the measurement of basic ionization constants of acetophenone derivatives by changes in their ultraviolet absorption spectra on ionization in sulphuric acid/water solutions.

Early attempts at the determination of pK_a values for weak carbon acids were made in harsh experimental conditions at high temperature and high concentrations of strong bases to promote ionization.[3, 13] Estimations of pK_a values could be made by extrapolation back to milder conditions. Given the extent of these extrapolations, the resulting pK_a values were subject to considerable error. However the determination of relative acidities of such weak acids was more straightforward. Early attempts to establish the order of carbanion stability were commonly made in non-polar media such as pentane, by quantitatively comparing the equilibrium mixtures formed by halogen–metal interchange reactions[8, 14-18] (shown in Scheme 1.5, X = halogen) using NMR spectroscopic analysis.

Scheme 1.5:

$$RX + R'M \rightleftharpoons RM + R'X$$

This reaction is formally similar to the acid-base equilibria traditionally used except that the two bases compete for a halogen rather than a hydrogen atom. Dessy *et al* used this method to predict a number of pK_a values for aryl alkanes and alkanes such as cyclohexane, which is predicted to have a pK_a of 44.[7]

Early studies of weak carbon acids also focused on the determination of the acidities, or the rates of carbanion formation, as a means of estimating relative carbanion stabilities. More weakly acidic solvents, such as dimethyl sulfoxide (DMSO), acetonitrile, or amines were popular media for the study of kinetic acidities of very weak acids. Better solvation of the carbanion may occur in water than in solvents such as DMSO, and so the pK_a values obtained in the latter poorer solvating solvent tend to be higher with varying degrees of difference. Rates obtained in non-aqueous media could be extrapolated to aqueous media for the purposes of comparison using the Grunwald Winstein equation (Equation 1.3), Traditionally this equation correlates the rate constant for solvolysis of a substrate, k_s, with the solvent ionizing power, Y, at 25° C. The rate constant k_0 is the rate constant for solvolysis in a reference solvent (80:20 Ethanol : Water). The parameter m is a characteristic of the substrate and reflects the sensitivity of the reaction to the solvent ionizing power. It is assigned the value unity for *t*-butyl chloride. Despite being initially mainly applied to S_N1 solvolysis, Equation 1.3 has been widely applied to other reaction types.

$$\log(k_s/k_0) = mY \qquad \text{(Equation 1.3)}$$

Bonhoeffer *et al*[9] applied an isotope exchange method to directly measure the rate of ionization of a number of carbon acids. In this early study the proportion of deuterated product was determined in a number of ways depending on the substrate. Electrical conductivity measurements were used in the case of nitromethane.

For acetonitrile, the deuterated content of the salt of acetic acid hydrolysis product can be determined. Finally, deuterium content of exchanged acetone was estimated by combusting the distilled exchange product followed by elemental analysis. This measured the kinetic acidity rather than the thermodynamic acidity of the carbon acids studied. Measurements of the rates of hydrogen exchange enabled the comparison of the kinetic acidities of a number of carbon acids against a base where the positions of the equilibria could not be measured because of the weakness of the acids.

More recently, significant work has been done to accurately determine the acidity constants of carbon acids under ambient rather than harsh conditions. As a result the effect of substitution on carbon acidity is more understood. Kresge and Keeffe used techniques like stopped flow spectrophotometry to access rates of ketonisation of enolates such as 2-indanone, (pK_a 12.2)[19] , as well as compiling detailed information of rates of enolization and ketonisation for other simple carbon acids[20]. Significant computational, and experimental work has been done by Bernasconi[21, 22] to establish better knowledge of a wide range of acidities and substituent effects in accordance with transition state theory and intrinsic barriers to their reaction.

1.3.1 Experimental determination of carbon acid pK_a values using a kinetic method

The acidity constant (K_a) (Equation 1.3) can be written as the ratio of rate constants for the forward and reverse directions of the acid dissociation equilibrium (Scheme 1.6): The rate constant for carbanion formation (k_f, $dm^3mol^{-1}s^{-1}$) and the rate constant for the reverse protonation of the carbanion (k_r, s^{-1}). If these two rate constants may be ascertained by kinetic methods then a pK_a value may be determined. Given this method is applied in this thesis for pK_a determination, it will be described in more detail. For weak carbon acids the forward direction of the equilibrium is relatively slow, and thus the rate constant k_f is accessible by a variety of methods including the earlier method of isotope exchange. The reverse rate of reprotonation of the carbanion is fast, and thus the determination of k_r is more challenging.

Scheme 1.6:

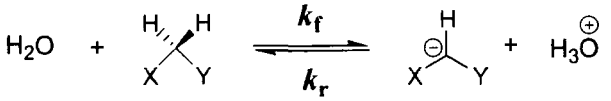

$$K_a = \frac{[H_3O^+][CHXY^-]}{[CH_2XY]} = \frac{k_f}{k_r} \qquad \textbf{(Equation 1.3)}$$

1.3.1.1 Determination of the rate constant for carbanion formation k_f.

Given the reverse protonation step of the equilibrium in Scheme 1.6 is fast, the carbanion formed is usually short lived. Rapid non-rate-limiting trapping of this carbanion by reaction with a scavenger such as a halogen molecule enables the rate-limiting formation of the carbanion to be measured directly. This method among others described by Kresge and Keeffe[20] is used widely in the study of rates of enolization of ketones (see Scheme 1.7) where **(A)** is the acid-catalyzed mechanism for enolization of the ketone followed by trapping of the enol by scavenger X and **(B)** is the base-catalyzed mechanism followed by trapping of the enol by scavenger X

Scheme 1.7:

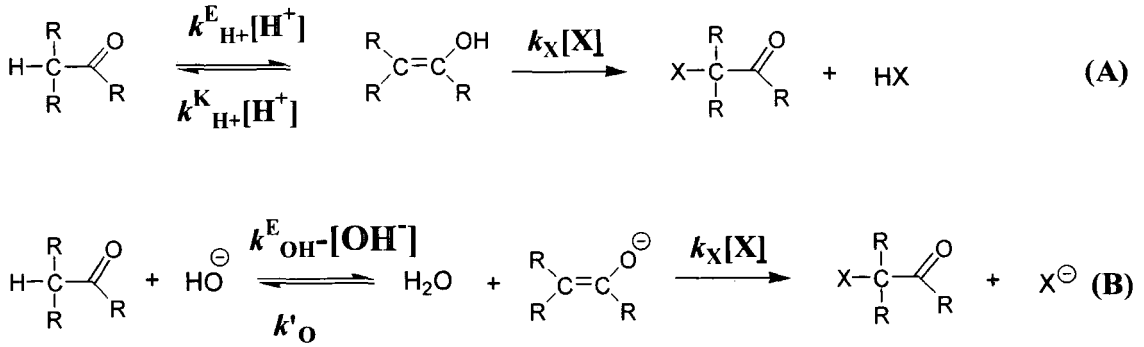

Halogenation is the most commonly used way of studying enolization kinetics. Studies in this area have shown that the rate of halogenation of simple enols by reacting with Cl_2, Br_2 and I_2 approaches the rate of diffusion[23] and is to some extent dependent on substrate structure[24] When the rate of halogenation (k_X[X]) is very fast relative to ketonization of

the enol/enolate ($k^{K}_{H+}[H^+]$, or k'_O), the values for the forward rate constants (k^{E}_{H+}, and k^{E}_{OH-}) can be read from the slopes of linear plots of the experimental rate constant (k_{obs}, s^{-1}) against catalyst concentration ($[H^+]$ or $[HO^-]$) in dilute aqueous solution. In this case the rate of halogenation will be zero-order in the concentration of halogen, and first order in catalyst concentration. The uncatalysed rate of enolization (k^{E}_{0}, s^{-1}) can be read from the intercept of these plots. However these intercepts are often only a small part of k_{obs} and imprecise. A better estimate can be obtained from studies of buffer catalysis in solutions where the concentration of hydronium or hydroxide ion is low and constant. A plot of the experimental rate constant (k_{obs}, s^{-1}) against the concentration of buffer at constant pH yields an intercept, a substantial part of which is the rate of uncatalysed reaction (k^{E}_{0}, s^{-1}).

At higher acid concentrations the halogenation step can become at least partly rate-determining as ketonization is acid catalyzed while halogenation of the enol is not[12, 25, 26]. In the case of base-catalyzed enolization reactions followed by halogenation of the enolate intermediate, enolate formation was found to be rate-limiting only in the presence of high concentrations of halogen[27] (see Scheme 1.7 B). Numerous other problems, including multiple halogenations and multiple-side reactions can complicate the kinetic analysis especially if the reaction is monitored by following the disappearance of halogen. A better option is to monitor the disappearance of the substrate.

Isotope exchange techniques have been used for some time to monitor not only the rates of enolization, but rates of ionization of weak carbon acids in general and there are many early examples of this such as those mentioned previously[9]. With the improvement in instrumental methods such as mass spectrometry and NMR spectroscopy the precision of measurement of ionization rates in this way has increased dramatically, allowing accurate estimation of pK_a values in the range 15 – 35 [5, 6, 28-30].These methods now allow the more accurate quantification of small amounts of label incorporated into the carbon acid after exchange. The limits for detection of deuterium enrichment are moderately low at around 1%, while for radioactive tritium detection limits currently estimated to be ~ 20 μCi/l[31]

which is significantly lower. The site of isotope exchange is also readily identifiable by ^{1}H NMR spectroscopy.

Scheme 1.8:

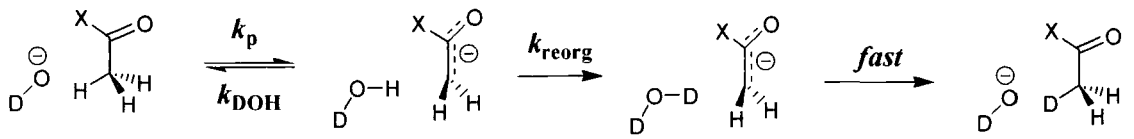

A typical deuterium-exchange reaction is shown in Scheme 1.8. Typically the deuterium label is present in large excess by conducting the experiments in 100% D_2O. A dilute solution of the unlabelled carbon acid is deprotonated by a base such as deuteroxide ion in a proton transfer step (k_p). The resulting carbanion forms an intimate ion pair with the solvent molecule DOH. The HOD solvent molecule undergoes a rapid solvent reorganization step (k_{reorg}) and is replaced by a fully isotopically labelled solvent molecule. Redeuteration by D_2O is rapid and effectively irreversible due to the large excess of deuterium relative to the acidic protons of substrate (110 M D in D_2O compared with ~10 mM H from substrate). In this situation the observed experimental rate constant (k_{obs}, s^{-1}) can be expressed as in Equation 1.4.

$$k_{obs} = k_{D2O} + k_{DO}[DO^-]. \qquad \textbf{(Equation 1.4)}$$

Specific or general base catalysis may be observed depending on the nature of the carbon acid. For specific catalysis to be observed the solvent reorganisation step must be rate-limiting. In this situation the observed experimental rate constant for deuterium exchange at a given concentration of deuteroxide ion (k_{obs}, s^{-1}) can be expressed as in Equation 1.4 *i.e.* there is no general base-catalysis term.

For general catalysis to be observed the proton transfer must be rate-limiting. In this situation the observed experimental rate constant for deuterium exchange at a given concentration of deuteroxide ion (k_{obs}, s^{-1}) can be expressed as in Equation 1.5 and includes a general base-catalysed term.

$$k_{obs} = k_{D2O} + k_{DO}[DO^-] + k_B[B] \qquad \textbf{(Equation 1.5)}$$

In certain cases, solvent isotope effects on the observed experimental rate constants for exchange must be considered. This is discussed in greater detail in the results of Chapter 2.

Isotope exchange using tritium as label is more experimentally difficult. Tritium is used at tracer levels. To enable accurate quantification of tritium label in exchange product usually requires the difficult and time-consuming separation of reactant, product and solvent species that may contain label. It was studied in detail by Kresge and Powell.[32] The radioactive nature of tritium makes this method extremely sensitive, with the obvious downside of radioactive waste being produced.

Other methods of determining rate constants for carbanion formation include using oxidants as enol scavengers. Oxidants such as Cr(IV),[33] Mn(III) pyrophosphate,[34] Hg(II),[35] and Ru(III)[36] react with the enolic form of aldehydes and ketones in acid solution. Usually the process to be monitored is a zero-order disappearance of a limiting amount of oxidant in the presence of an excess of substrate and as such it is necessary to know the stoichiometry with respect to the scavenger.

Base-promoted eliminations of acyl compounds which occur via an E1cB mechanism can be useful in studying enolization. It is possible to alter the rate determining step by altering the leaving group. Depending on the leaving group ability the mechanism may be $(E1cB)_R$ (poor leaving groups, step 2 rate–controlling) or $(E1cB)_I$ (better leaving groups, enolization rate–controlling). With leaving groups between these two extremes the reversibility of the enolization step can be controlled using buffer acids.

1.3.1.2 Determination of the rate constant for carbanion protonation, k_r.

The rate constant for reprotonation of the carbanion conjugate base of weak carbon acids (k_r, s^{-1}) (Scheme 1.6) is usually extremely fast. Carbanions formed from stronger carbon acids benefit from resonance and inductive stabilization from one or more strong electron-withdrawing substituents, while weak carbon acids do not. Many studies of reactive intermediates have been done, with a focus on determining absolute rate constants by directly monitoring the disappearance of the intermediate generated by flash photolysis[37, 38]. However there is a simpler, indirect method detailed by Richard *et al*[39] which references the unknown rate constant for reaction of the intermediate carbanions with solvent water or an acid catalyst to that for a second reaction which serves as a "clock". These reference rate constants for reactions used as clocks are known with good precision, and are typically limited by the rate constant for a physical transport step which is largely independent of the structure of the carbanion.

Scheme 1.9:

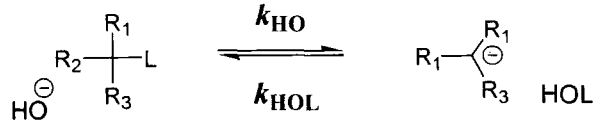

$$pK_a = pK_W + \log\left(\frac{k_{HOH}}{k_{HO}}\right) \qquad \textbf{(Equation 1.6)}$$

The route of reverse reprotonation of the carbanion intermediate depends on the forward route of carbanion formation. The law of microscopic reversibility determines that the protonation route must be the same as the deprotonation route, as protonation must occur via the lowest energy pathway. There are three possible routes for protonation of weak carbon acid, the upper limits of which are limited by a physical transport step or "clock" (Scheme 1.10). The first is deprotonation by hydroxide ion, which would mean protonation by solvent water (A). The second involves deprotonation by a Brønsted base B, where protonation occurs via the conjugate acid BH^+ (B). Thirdly, deprotonation may occur by solvent water and subsequent reverse protonation by hydronium ion (C).

Scheme 1.10:

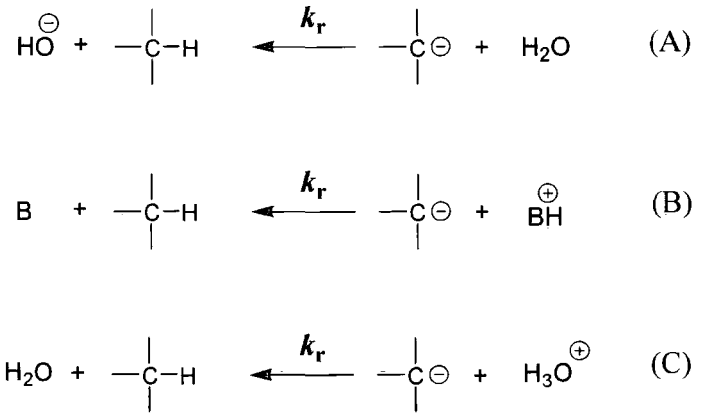

The upper limit on k_r is achieved in each case when reprotonation is limited, not by a chemical step, but rather by the physical transport process of arranging the reacting acid into a reactive position for protonation.

The limiting rate constant $(k_{HOH})_{lim}$ (s^{-1}) for protonation of carbanions by solvent water is the rate constant for rotation of a water molecule into a position where proton transfer can take place. It is measured as the rate constant for the dielectric relaxation (reorganization) of solvent water, ($k_{reorg} \approx 10^{11}$, s^{-1}).[40] Solvent reorganization serves as a clock for reactions where the carbanions - formed in water - only exist for the time it takes for solvent reorganization to occur. The primary deuterium isotope effect for this process was determined from the hydroxide-ion-catalyzed exchange of hydrons from water into acetonitrile and succinonitrile which proceed through the α-cyano carbanions **(12)** and **(13)** respectively (see Figure 1.1) and was found to be close to three.[40] The value of $(k_{DO})_H/(k_{HO})_D$ for hydron exchange at CL_3CN is expected to lie between an upper limit of $(k_{DO})_H/(k_{HO})_D \approx (1.8)(4) = 7.2$ when proton transfer is rate-determining, where 1.8 is the secondary solvent isotope effect observed for the lyoxide-ion-catalyzed deprotonation of $NCCH_2CH_2SR$ and $NCCH_2CH(CN)SR$,[40, 41] and 4 is the primary isotope effect observed for the deprotonation of these carbon acids[40, 42] and a lower limit of $(k_{DO})_H/(k_{HO})_D = 2.4$ when reorganization of solvent is rate-determining so that the full equilibrium difference in the basicities of deuterioxide and hydroxide ions is expressed in the transition state Hence the observed ratios of $(k_{DO})_H/(k_{HO})_D = 3.3$ and 2.9 for the hydron-exchange

reactions of acetonitrile and succinonitrile respectively, are considerably smaller than those expected for rate-determining deprotonation of the substrate, and they are consistent with a pathway in which solvent reorganization is largely rate-determining for hydron exchange. This is good evidence that the isotope-dependant chemical barrier to protonation of these carbanions by solvent water (k_{HOL}) is smaller than the isotope independent barrier to solvent reorganization. A linear correlation of k_{HOH} (s^{-1}) for protonation and log k_{HO} ($M^{-1}s^{-1}$) for deprotonation can be drawn with slopes of +0.60 and −0.40 respectively with the pK_a values of neutral α-carbonyl carbon acids in water.[6, 43, 44] Results show that the value of k_{HOH} (s^{-1}) increases with decreasing carbanion stability but levels off when proton transfer is limited by solvent reorganization ($(k_{HOH})_{lim} \approx 10^{11}$, s^{-1}).

Figure 1.1

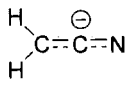

(12)

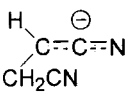

(13)

This levelling off occurs for an enolate that is formed by deprotonation of a carbon acid of p$K_a \approx 30$. For example, the estimated second-order-rate constant for hydroxide ion-catalyzed carbanion formation in H_2O by removal of the α-proton of acetate ion is (k_{HO} = 3.5×10^{-9} $M^{-1}s^{-1}$)[43] If the linear correlation of log k_{HOH} values against pK_a were to continue, this would require a pK_a = 38 for acetate ion and an estimated $k_{HOH} = 3 \times 10^{15}$ s^{-1} for protonation of the enolate dianion of acetate by solvent water. This extrapolated lifetime of the enolate dianion intermediate is shorter than the time for a bond vibration ($\approx 10^{-13}$ s).[45] If the enolate dianion forms as an intermediate of the deuterium exchange reaction of acetate ion, the rate of reprotonation must be limited by the rate of solvent reorganization $k_{HOH} = (k_{HOH})_{lim} = 10^{11}$ s^{-1}. This gives a pK_a = 33.5 for acetate ion (see Scheme 1.9 & Equation 1.6).

The limiting rate constant $(k_{BH^+})_{lim}$ ($M^{-1}s^{-1}$) for protonation of carbanions by a buffer acid is the rate constant for diffusion together of the buffer acid and carbanion in solution. In the case of ethyl acetate **(14)**, a Brønsted coefficient of β = +1.09 was determined as the slope of a plot of log k_B against pK_{BH+} values for general base catalyzed deuterium

exchange catalyzed by 3-substituted quinuclidine bases in D_2O solution.[44] In this case k_B ($M^{-1}s^{-1}$) is the second order rate constant for general base catalysed exchange of the α-protons of ethyl acetate for deuterium. This reaction proceeds through the ester enolate **(15)** (X = OEt). The Brønsted β value obtained is evidence that complete proton transfer from the carbon acid to the catalytic base has occurred before the rate-limiting step is reached. This requires that the rate-determining step for formation of the free enolate (k_B) is the diffusional separation of a reversibly formed enolate-ammonium ion complex (see Scheme 1.11). The reverse protonation of the enolate ion by ammonium conjugate acid is limited by the diffusion together of these species in solution with a second order rate constant $k_{BH^+} \approx 5 \times 10^9$ M^{-1} s^{-1}. [44] Combining these two rate constants for deprotonation of ethyl acetate by quinuclidine (pK_a = 11.5) (Equation 1.7) gave pK_a 25.6 for ethyl acetate in water, and similarly pK_a 28.4 for acetamide[43] as the corresponding enolate also undergoes diffusion-controlled protonation by buffer acids.

Scheme 1.11:

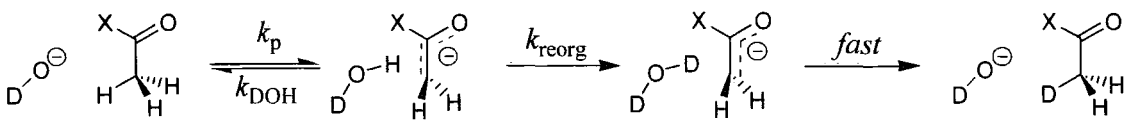

(14) **(15)**

$$pK_a = pK_{BH^+} + \log\left(\frac{k_{BH^+}}{k_B}\right) \qquad \textbf{(Equation 1.7)}$$

The third possible reaction clock for proton transfer to carbon is that of the limiting rate constant for protonation of a Brønsted base by hydronium ion ($k \approx 10^{10}$ M^{-1} s^{-1}). Values in the range $(1 - 4) \times 10^{10}$ $M^{-1}s^{-1}$ have been reported for protonation of amines by H_3O^+[46] and a rate constant of $k = 4 \times 10^{10}$ $M^{-1}s^{-1}$ has been measured for the diffusion-controlled protonation of CN^- by H_3O^+.[47] The similarity of the localized CN^- carbanion to the thiazolium ylide led to the use of this clock for proton transfer in the determination of the pK_a values of a range of thiazolium ions including thiamin (pK_a = 18.0).[48] The assumption of diffusion-controlled reprotonation of thiazolium ylides by H_3O^+ is

supported by the Brønsted β values ≥ 0.95 for catalysis of thiazolium C2-proton exchange by buffer bases. This indicates that the reverse protonation reaction has a Brønsted α value ≤ 0.05 and that protonation is diffusion-controlled with strong acids.[48]

1.4 Original mechanistic studies of proton transfer at carbon.

It is now well-established that proton transfer to and from carbon can occur with acid and base catalysis as alluded to in previous sections of this chapter. Most of the detailed mechanistic studies of catalysis of proton transfer have been carried out on simple carbonyl acids. For these compounds such as acetaldehyde - and analogously in other simple carbon acids - conversion to the enol isomer involves the removal of a hydrogen from carbon and placement of a hydrogen on oxygen. This process is both general-acid- and general-base-catalyzed, indicating both that the hydrogens move as protons, and that proton transfer is rate determining.

The earliest demonstration of general-acid-catalysis in aqueous solution was by Dawson and Powis[49] using acetone, with later work by Bell[50] and Lidwell[51] providing additional examples of both general-acid and general-base-catalysis in the enolization of simple carbonyl compounds. Enolization was also one of the first reactions for which kinetic isotope effects were determined. It was found by Reitz that the enolization of acetone catalyzed by hydronium ions is twice as fast in D_2O than in H_2O solution.[52] These reported kinetic solvent isotope effects were quickly followed by more diagnostic substrate kinetic isotope effects of k_H/k_D = 8, determined by comparing the rates of hydronium-ion-catalyzed enolization of protio and deuterated acetone.[53] Large isotope effects like these are a clear indication that the isotopically substituted bonds are being broken in the rate determining step and as such require mechanisms where proton transfer is rate limiting.

Mechanisms that could satisfy this requirement are classified according to their transition state composition and the timing of these proton transfers. Proton transfer can occur sequentially in a consecutive pathway, or by a concerted pathway. However a concerted

mechanism would require a transition state containing a proton donor, a proton acceptor and substrate, and this has been largely discounted as the preferred mechanism by experimental evidence. A detailed discussion of the possible mechanisms for enolization by Kresge and Keeffe[20] outlines the arguments for and against a concerted mechanism and as such it will not be discussed here.

The focus of this work is on base-catalysis of exchange in simple carbon acids. In the case of enolization reactions this requires proton removal from carbon to precede proton replacement on oxygen. There are two variations in the mechanism depending on which proton transfer step is rate determining. Reaction could occur through rate-limiting proton transfer from carbon followed by rapid protonation on oxygen (Scheme 1.12 **A**), or through a rapid pre-equilibrium deprotonation from carbon followed by rate-limiting reprotonation on oxygen (Scheme 1.12, **B**).

Scheme 1.12:

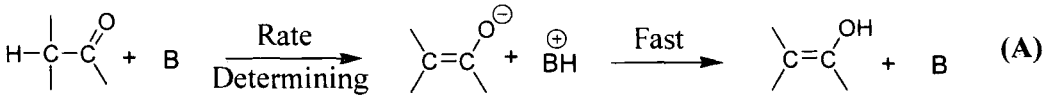

The rate-determining step in Equation **A** (Scheme 1.12) is carbon-hydrogen bond breaking. Hence a substrate kinetic isotope effect would be expected for this pathway. However this is not diagnostic as Equation **B** may also produce a substrate isotope effect depending on the method used to monitor the reaction.

One example of the latter is when monitoring the consumption of an electrophilic reagent that scavenges the enolate faster than reketonization. In this case the rate measured would

refer to the initial step in Equation **B** only. The carbon–hydrogen bond breaking in this step means that a substrate isotope effect would be produced.

Additional mechanistic information is required to distinguish between pathways **A** and **B**. For example, if Equation **A** is correct, then keto-enol equilibrium constants calculated from the base-catalyzed enolization and ketonization rate constants $K_E = k_E/k_K$ would be different from keto-enol equilibrium constants derived from acid-catalyzed rate constants. Alternatively, mechanistic information may be obtained from the nature of Brønsted correlations for base catalyzed enolization.

1.5 Linear free energy relationships.

One of the earliest examples of linear free energy relationships is the Brønsted relationship (Equation 1.8 and 1.9). This relationship is between the catalytic constants for a reaction catalyzed by a family of general acids or bases, such as carboxylic acids or tertiary amines, and the relevant values for these acid/base catalysts. The Brønsted rate law quantifies general-acid and general-base catalysis and the coefficients α and β, are constants dependant on reaction conditions but independent of the catalyst and are a function of the change between initial state and transition state of a reactant molecule. These coefficients are determined from a semilogarithmic plot of the catalytic constant k_{HA} (or k_{A^-}) against pK_a values of the catalytic acids or bases. The magnitude of the Brønsted coefficient is taken as a measure of the extent of proton transfer in the transition state of the general acid/base catalysed reaction which involves rate limiting proton transfer at the substrate.

$$\text{Log } k_{HA} = \alpha \log K_{HA} + C = -\alpha\, pK_{HA} + C \qquad \textbf{(Equation 1.8)}$$

$$\text{Log } k_{A^-} = -\beta \log K_{HA} + C = \beta\, pK_{HA} + C \qquad \textbf{(Equation 1.9)}$$

For general-acid-catalysed reactions if the proton is minimally transferred in the transition state then a poor proton donor will be as effective as a good proton donor

making α small. Alternatively, if proton transfer is almost complete at the transition state a stronger acid will be a much more effective catalyst and α will be close to unity (see Figure 1.2). In this way the experimentally measured α value provides information about the nature of the transition state.

Figure 1.2:

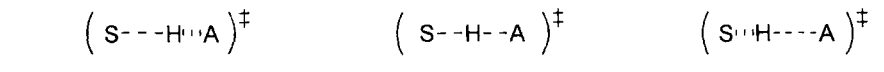

Little proton transfer at the transition state	Proton half transferred in transition state	Near complete proton transfer at transition state
$\alpha \rightarrow 0$	**$\alpha \sim 0.5$**	**$\alpha \rightarrow 1$**

Similarly with general-base-catalysed enolization of acetone by carboxylate ions, values of $\beta = 0.88$[51] and 0.89[54] imply a late transition state with the proton almost completely transferred. This agrees with the highly energy-absorbing nature of the rate-determining proton transfer step $\Delta G^{\circ} = 21$ kcal mol^{-1}. [20] Strongly endothermic reactions like these are expected to have late, product like transition states.[55, 56]

Values of $\alpha = 0.57$[51] and 0.56[57] were determined for enolization of acetone catalyzed by carboxylic acids, implying a central transition state with the proton approximately half way between substrate and acceptor. However, this rate determining step is preceded by a pre-equilibrium of protonation of the carbonyl oxygen on acetone (see Scheme 1.13), making the rate-limiting step a base-catalysed process with a Brønsted coefficient of $1 - \alpha = 0.43$[51] or 0.44.[57] This suggests a slightly less than half transferred proton in the transition state and is in agreement with the slightly exothermic nature of this reaction step $\Delta G^{\circ} = -1$ kcal mol^{-1}.[20]

Scheme 1.13

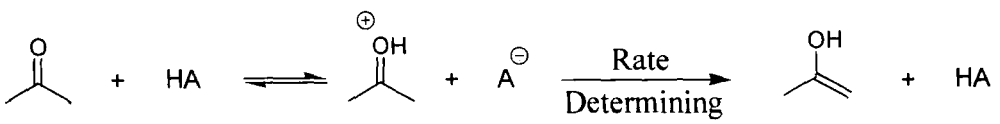

An unusually large value of $\beta = 1.09$[58] for the deprotonation of ethyl acetate catalysed by a series of 3-substituted quinuclidine bases shows that there is essentially complete proton transfer from ethyl acetate to the tertiary amine base in the rate-limiting transition state for this reaction and hence the rates of these thermodynamically uphill proton transfers are limited by diffusional separation of the intimate ion pair to give free enolate and protonated ammonium ion in solution. This means that reverse protonation is diffusion controlled and also marks the abrupt change from a rate-limiting chemical step to a rate limiting transport step. This is described by Richard *et al* as one of the "reaction clocks" for carbanions.

In situations where ambiguity exists about a mechanistic pathway, such as a hydrolysis reaction where nucleophilic catalysis and mechanistic general-base-catalysis are possible with the family of bases used, a plot of log k_B against pK_{BH+} giving a β value outside the range 0 and 1 would be evidence of the presence of nucleophilic catalysis. In this case the plot of log k_B against pK_{BH+} expresses an empirical relationship between catalytic effectiveness and base strength for the family of nucleophiles and proton transfer is not involved at all.

1.5.1 Anomalous α and β values.

Anomalous Brønsted coefficients are found in a number of cases for simple carbon acids where linear correlations have produced coefficients outside the range 0-1. Notably this is the case for some nitroalkanes[59] where there is an inverse relationship between the rates of proton abstraction and acidities in the series CH_3NO_2, $MeCH_2NO_2$ and Me_2CHNO_2. Here there is a progressive decrease in the rates of deprotonation by hydroxide (relative rates 113:18:1.0), whereas the acidities change in the opposite manner. (relative pK_a's 10.2, 8.5, and 7.7).[10] Similarly, the logarithmic rates of deprotonation of $ArCHMeNO_2$, and $ArCH_2CHMeNO_2$ by hydroxide ion in 50% v/v aqueous methanol correlate with their pK_a values with α-values of 1.31 and 1.61 respectively.[59] This means that the coefficients for protonation of the $ArCMeNO_2^-$ and $ArCH_2CMeNO_2^-$ ions by solvent

must be −0.31 and −0.61 respectively, since the sum of Brønsted coefficients for the forward and reverse reactions must equal unity.

Scheme 1.14

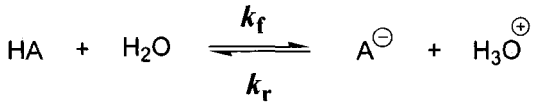

$$K_a = \frac{k_f}{k_r} \qquad \textbf{(Equation 1.9)}$$

Restriction of the Brønsted coefficients to values between 0 and 1 arose from the application of the Brønsted relationship predominantly to oxygen or nitrogen acids and bases such as carboxylic acids and carboxylate ions, amines and ammonium ions, pyridinium ions and pyridines. Here the position of the equilibrium (K_a) is more sensitive to structural changes than the microscopic rate constants (k_f and k_r) (see Scheme 1.14). However for carbon acids which must undergo extensive structural reorganization to form an ion, substituent effects on k_f and k_r can differ from those on K_a when delocalization of charge lags behind deprotonation. This can lead to Brønsted correlations where α or β lie outside the 0 – 1 range. This is described by Bernasconi[60] as the principle of non-perfect synchronization. In the series CH_3NO_2, $MeCH_2NO_2$ and Me_2CHNO_2, proton abstraction by hydroxide is retarded by methyl substitution, but proton abstraction by the nitronate ion ($CH_2{=}NO_2^-$) from the solvent is slowed to an even greater extent. This results in a negative Brønsted coefficient for a plot of log k_f vs. log K_a ($\alpha \cong -0.7$) and a coefficient larger than 1 for a plot of log k_r vs. log K_{BH+} ($\beta \cong 1.7$).

Scheme 1.15

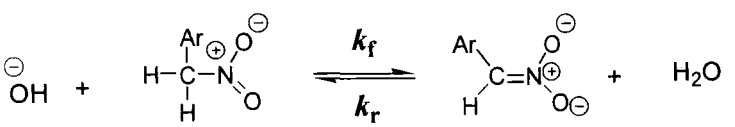

The strongly electron withdrawing nitro group produces a carbanion in which the negative charge has been almost completely removed from the carbon atom (see Scheme 1.15). However as resonance delocalization of negative charge lags behind deprotonation,

there is still substantial negative charge on α-C at the transition state which is disfavoured by methyl substitution. In the product, the methyl groups are remote from the negative charge so the inductive electron donating effect of the methyl groups does not disfavour the build up of negative charge on O. Instead the methyl groups stabilise the C=N bond hyperconjugatively, increasing thermodynamic acidity.

This removal of charge from the carbon slows down the rate at which the carbon can pick up a proton to form the conjugate acid. Thus nitroalkanes such as nitromethane have a higher acid strength than is consistent with the rate of reprotonation because the carbanion is resonance stabilized.

Scheme 1.16

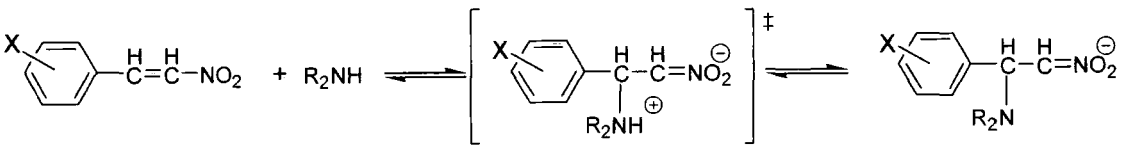

This effect is negated by the addition of π-donor substituents to the nitroalkanes such as 4-MeOPh or 4-Me_2NPh, seen in the reaction of piperidine with substituted β-nitrostyrenes[61] (see Scheme 1.16) .These substituents lead to resonance stabilization of the olefin (**B,** Scheme 1.17) which results in a reduction of the equilibrium constants (K_a) for the nitroalkanes derivatives. This would be expected to also lower the forward reaction rate (k_f), however this resonance not only stabilizes the olefin but pre-organizes the electronic structure to be more product-like, facilitating the delocalization of the negative charge starting to develop in the transition state. The result is more like the structure (**C**) where the transition state is stabilised and the intrinsic barrier to reaction is lowered. Without this pre-organization delocalization of the incipient negative charge into the nitro group lags behind bond formation and resemble structure (**D**).

Scheme 1.17

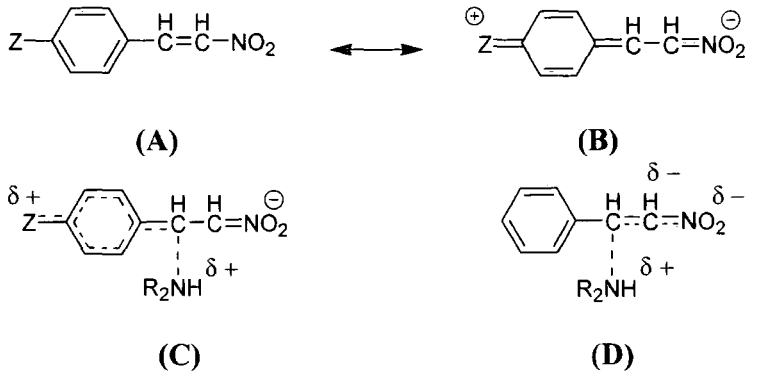

Similar if less pronounced behaviour is expected from carbonyl groups, which are less efficient than nitro groups at removing the negative charge from carbon. Cyano groups and sulfones are less effective still. However halogenated carbonyl compounds such as trifluoropentane-2.4-dione (pK_a 7.0) have an increased efficiency towards removal of the negative charge from carbon in the transition state and have effects comparable to similar nitro compounds (nitropropane-2-one pK_a 6.0).

As well as negative deviations, positive deviations from the Brønsted relationship for carbon acids are seen for reactions of compounds containing two carbonyl or carbethoxy groups. Cyano and sulfone containing carbon acids give the greatest positive deviation from the correlation for carbon acids. Changing ring size can also create anomalous Brønsted coefficients such as seen in cyclic ketoesters. 5-Membered rings ionize similarly to their straight chain analogues, showing a slight positive deviation, however 6-membered rings ionize much more slowly and are weaker acids.

1.5.2 Brønsted coefficients and Marcus theory.

The Brønsted relations are historically the earliest examples of linear Gibbs energy relations. Log k is proportional to the Gibbs energy of activation for the catalysed reaction and log K is proportional to the Gibbs energy of ionization of the catalyst. These relationships between Brønsted coefficients and free energy of reactions are quantified in simple reaction theories such as that due to Marcus.[62, 63] Marcus theory expresses the

activation barrier to a proton transfer reaction, $\Delta G^{\ddagger}$, as a quadratic function of ΔG_0 the free energy of reaction (see Equation 1.10). In this equation λ is the intrinsic barrier to reaction, which is the value of $\Delta G^{\ddagger}$ when the free energy of reaction, $\Delta G_0 = 0$. Differentiation of Equation 1.10 gives an expression for α (equivalent to the Brønsted α). The result is that when $\Delta G_0 = 0$ then $\alpha = ½$. For exothermic reactions $\alpha < ½$ for endothermic reactions $\alpha > ½$.

$$\Delta G^{\ddagger} = \lambda\left(1 + \frac{\Delta G_0}{4\lambda}\right)^2 \qquad \textbf{(Equation 1.10)}$$

$$\alpha \equiv \frac{\delta\Delta G^{\ddagger}}{\delta\Delta G_0} = \frac{1}{2} + \frac{\Delta G_0}{8\lambda} \qquad \textbf{(Equation 1.11)}$$

Curvature would be expected in Brønsted relations based on the Marcus expression, however is seldom seen for keto-enol interconversions. One reason is because it is often difficult to span a wide enough pK_a range due to the inherent slow nature of proton transfer at carbon. The second reason is that the Marcus equation assumes that the intrinsic barrier, λ, remains constant as ΔG_0 is varied. In some cases, a decrease in intrinsic barrier for enolization is observed as ΔG_0 becomes more unfavourable. This has been observed by Amyes and Richard in a Brønsted correlation of second order-rate constants for hydroxide ion catalyzed deprotonation at α-carbon versus carbon acid pK_a values for a range of neutral α-carbonyl compounds.[44]

1.5.3 Eigen plots for carbon acids.

Sharp curves may be seen in some Brønsted-type correlations known as Eigen plots.[46] Scheme 1.18 shows an Eigen plot for the reaction of two acids (HX and HY). As indicated in the last section there is a relationship between the rate constant for proton transfer (represented by $\Delta G^{\ddagger}$) and the pK_a difference of the donor and acceptor acids (related to ΔG_0). Normal acids and bases undergo a diffusion-controlled proton transfer.

When there is a large difference in pK_a between the two acids the rate of proton transfer is independent of the pK difference. The rate of proton transfer should be independent of the pK difference as long as the pK value of the acceptor is greater than that of the donor and hence proton transfer will be diffusion-controlled. In the vicinity of $\Delta pK \approx 0$, there is a relatively sharp transition to a linear dependence of log k on ΔpK, since at this point the reverse reaction becomes diffusion-controlled. For $pK_{HX} = pK_{HY}$ there is an equal probability for proton transfer to occur in both directions. If the slopes d(log k)/d(ΔpK) of the curves are denoted α for the forward reaction and β for the reverse reaction the result is as shown in Scheme 1.18.

Scheme 1.18:

$\alpha = 0, \beta = 1$ for $pK_{HY} > pK_{HX}$

$\alpha = 1, \beta = 0$ for $pK_{HY} < pK_{HY}$

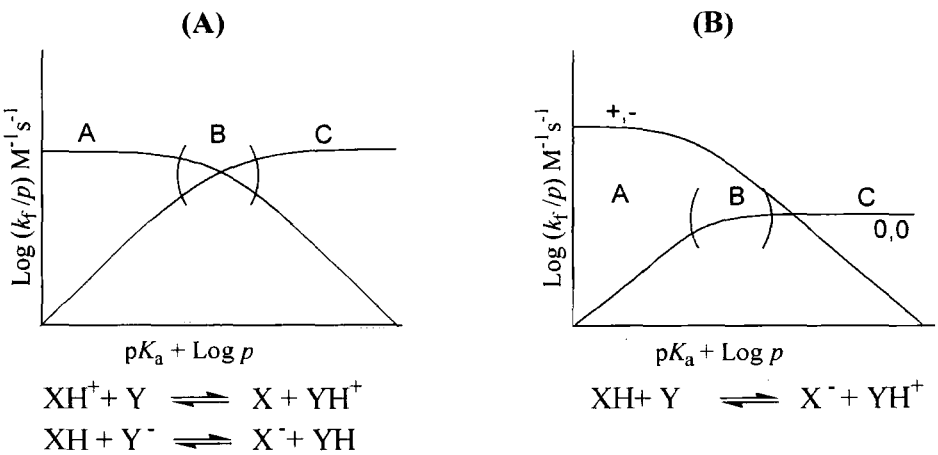

In the vicinity of $pK_{HY} = pK_{XY}$ there is a relatively sharp transition in the slopes α and β between 0 and 1. For proton transfer reactions where there is a symmetrical balance of charge such as in Scheme 1.18 **(A)** the curves for the forward and reverse reactions should be symmetrical. However many proton transfer reactions present an asymmetry of charge, (Scheme 1.18 **(B)**). In these cases the limiting values for the diffusion-controlled reactions are different for the forward and reverse directions, hence the α and β curves become asymmetric with respect to $\Delta pK = 0$. Similarly, any hindrances to the reaction which have different effects on the forward and reverse reaction rates will result in

altered symmetry of the α and β curves. For base catalyzed reactions the β curve is of importance and so will be the focus of this discussion.

For "normal acids" the Eigen plot for a base catalyzed reaction shows three distinct areas of curvature, (see Scheme 1.19) The Brønsted coefficient β = 1, **(A)** (Scheme 1.19), denotes the p*K* range in which there is rate-determining proton transfer. There is a narrow pK_a range over which both rate-determining proton transfer and non-rate-determining proton transfer are equally likely to occur, hence $0 < \beta < 1$, **(B)** It is in this region of rate-limiting proton transfer that Marcus curvature can be observed. The rate limiting step of the reaction changes from rate-determining proton transfer, β = 1, **(A)**, to non-rate-determining proton transfer, β = 0, **(C)**, where rate of proton transfer is independent of the pK_a of the reacting base.

Scheme 1.19:

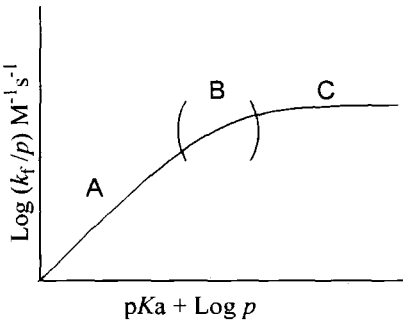

Correlations of the rate constants for proton transfer with thermodynamic driving force of electronegative proton donor and acceptor atoms such as oxygen or nitrogen show distinct curvature over a narrow range of pK_a values as described previously.[46] The rate-limiting step for reactions involving these heteroatoms is diffusion-controlled formation of an encounter complex between reactants (step 1, Scheme 1.20). For thermodynamically favourable proton transfer the Brønsted coefficient is 0. For unfavourable proton transfer the Brønsted coefficient is 1 (Step 3 rate-limiting, Scheme 1.20). Reactions between heteroatoms are almost thermoneutral and there is a narrow range of thermodynamic driving force for which the proton transfer step is partly rate determining (step 2, Scheme 1.20). In this range the slope of the correlation changes

sharply from 0.0 to 1.0. Distinct Eigen curves of this nature reflect the low intrinsic barriers to proton transfer between heteroatoms and the intrinsic rate constant for thermoneutral proton transfer is close to diffusion controlled.

Scheme 1.20:

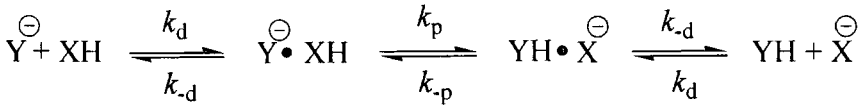

Step 1 Step 2 Step 3

In contrast, for weak carbon acids Brønsted plots rarely show normal or even detectable Eigen curvature. The intrinsically high barriers to proton transfer from carbon means that the change from rate-determining proton transfer to non-rate-determining proton transfer occurs over a large range of pK_a values. For example the intrinsic rate constant for thermoneutral proton transfer between α-carbonyl carbon and hydroxide ion is small, usually producing linear Brønsted correlations of rate constants for proton transfer from carbon with slopes of less than 1, even with a high thermodynamic barrier to proton transfer. A statistically corrected Brønsted-type correlation of log k_{HO} for deprotonation of neutral α-carbonyl carbon acids by hydroxide ion remains linear with a slope of –0.40 as the pK_a of the carbon acid is increased from a thermodynamically favourable 10 to a highly unfavourable 28.[43] A downward curve in the Brønsted plot from -0.40 to -1.0 occurs at pK_a = 31 corresponding to a favourable thermodynamic driving force of 21 kcal/mol. This very large driving force is required to overcome the large intrinsic barrier of around 10 kcal/mol and reduce the observed barrier to protonation of the enolate to that for reorganization of solvent.[64]

1.6 Biological relevance.

The heterolytic cleavage of stable C-H bonds is an important step in metabolism and the effective working of many biological systems. In biology the problem of low rates of ionization of weak carbon acids is circumvented by the use of enzymes. Proton transfer is the first step of many enzyme-catalyzed processes such as racemization, elimination,

carboxylation, aldol and Claisen condensation reactions, allylic isomeriation and phosphoryl transfer.

The relative reactivity of carbon acids in non-enzymatic proton transfer is determined predominantly from their pK_a values, where recent work by Richard *et al*[6, 58, 65] among others including this work have determined pK_a values for weak carbon acids where direct measurement of the equilibrium concentrations is not possible.

By determining the mechanism and second order rate constants for non-enzymatic proton transfer in water from such weak carbon acids to Brønsted bases (k_B, M^{-1} s^{-1}) we get an idea of the kind of thermodynamic barriers overcome by enzymes in converting their substrates to the required products. The catalytic efficiency of enzymes, given by k_{cat}/K_M (the catalytic rate divided by the Michaelis-Menton constant) for these enzyme-catalyzed reactions is in the range $10^5 - 10^8$ M^{-1} s^{-1}. This is a limited range for these rate constants when compared with the wide range of values for second-order-rate constants (k_B, M^{-1} s^{-1}) determined in solution for the strong and weak carbon acid enzyme substrates. The small differences in enzyme-catalyzed rates often do not reflect the huge variation in reactivities of the respective substrates.

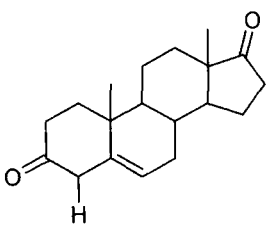

(16) pK_a ≈ 13

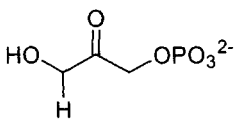

(17) pK_a ≈ 18

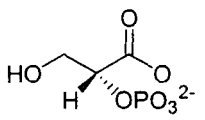

(18) pK_a >34

Carbon acids **(16)** – **(18)** are three biologically important molecules with widely differing pK_a values. The β-γ-unsaturated steroid **(16)** (pK_a 13)[66] and the α-proton of 2-phosphoglycerate **(18)** (pK_a >34) differ by upwards of 21 pK_a units which corresponds to over 29 kcal mol^{-1} difference in thermodynamic barriers to reaction in solution. By contrast the difference in the enzyme-catalyzed isomerization of steroid **(16)** (k_{cat}/K_M = 3 × 10^8 $M^{-1}s^{-1}$)[66] and the elimination reaction of 2-phosphoglycerate **(18)** (k_{cat}/K_M = 1.4 ×

10^6 $M^{-1}s^{-1}$)[67] which both start with C-H bond cleavage, corresponds to only 3 kcal mol^{-1} difference in activation barriers for the enzyme-catalyzed reactions. Deprotonation of steroid **(16)** by ketosteroid-isomerase, and of dihydroxyacetone phosphate **(17)** by triosephosphate isomerase[68] both have k_{cat}/K_M values approaching the diffusion-controlled limit while the pK_a values of the substrates differs by 5 pK_a units. There are a number of different strategies used by enzymes to facilitate the catalysis of the difficult deprotonation of weak carbon acid such as **(16)** – **(18)**.

1.6.1 Thiol esters of carboxylic acids.

The rate of deprotonation of α-carbonyl carbon acids is increased by conversion of the carboxylate anion ($pK_a \approx 34$) to a thiol ester of coenzyme A. The pK_a of α-protons of simple thiol esters[30] is around 21, which is close to a pK_a of 19 for acetone.[69] Substitution of the sulphur at the thiol ester crotonyl CoA for an oxygen to give crotonyl oxyCoA produces a 280-fold decrease in k_{cat}/K_M, and a 330 fold decrease in k_{cat} for crotonase-catalysed hydration (see Scheme 1.21), which corresponds to 3.4 kcal mol^{-1} difference in stability of the transition states for deprotonation of the two enzyme-bound carbon acid substrates in the reverse elimination reaction direction. This can be compared to the to the difference of 5.5 kcal mol^{-1} in the activation barriers for deprotonation of ethyl thioacetate,[30] and ethyl acetate[58] by 3-quinuclidinone in solution. The differences in the activation barriers for the enzyme-catalysed and general-base-catalyzed proton-transfer reactions are very similar in this case. This indicates that the stabilizations of the enolate intermediates formed by deprotonation of the crotonase substrates are similar. The greater energetic cost of activating an α-carbonyl proton with an oxygen ester compared to the cost for a thiol ester is offset by the *ca* 5.5 kcal mol^{-1} increase in stabilization of the transition state, making catalysis much more efficient for the deprotonation of α-carbonyl carbon of oxygen esters.

Scheme 1.21:

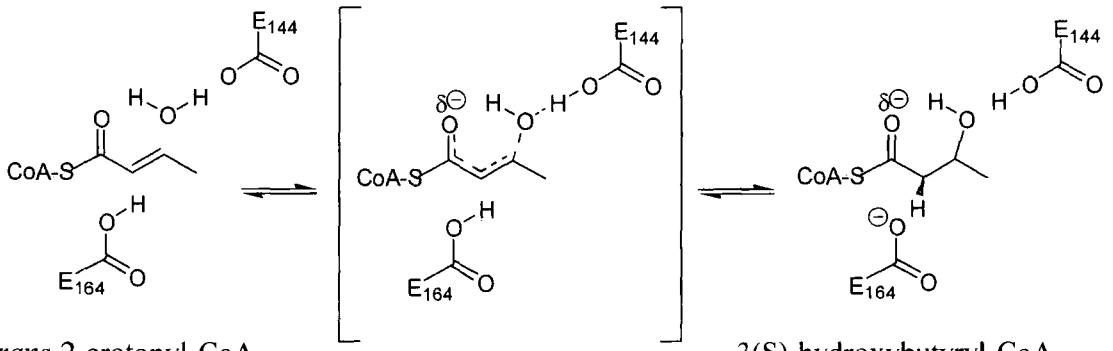

trans-2-crotonyl-CoA 3(S)-hydroxybutyryl-CoA

1.6.2 The enolase superfamily and metal ions.

An important development in enzymology has been the identification of the enolase superfamily of enzymes. These were named for the member whose function is most central to living systems. These enzymes have been shown to all pursue a common strategy to abstract the very weakly acidic α-protons of carboxylate anions.[70] Most bind a single divalent metal ion. Enolase itself uses two divalent metal ions to neutralise the formally tetranionic enolate intermediate of 2-phosphoglycerate.[71] The defining feature of enzymes in this superfamily is the metal ion-coordinating active site. Here conserved interactions between the protein, metal ion and bound substrate labilize the α-protons of bound carboxylate anion substrates.[70] These active sites need to be flexible to facilitate evolution of the enzymes by mutation in order to modify the substrate–binding specificities, or perform other roles at subsequent steps to carbanion formation such as expelling the leaving group in elimination reactions.[72] This has resulted in an occurrence of low substrate specificity, and even low reaction specificity for catalysis by individual enzymes. This may be the cost of the rapid evolution of these enzymes, which are seen to have a wide range of enzyme chemistries and activities. The catalytic assembly which is conserved throughout this family of enzymes may be thought of as the definitive assembly determined to solve the difficult problem of abstracting very weakly acidic α-protons from carboxylate anions.

1.6.3 Deprotonation of the α-amino carbon of amino acids.

The pK_a's of the α-amino carbon of amino acids such as glycine depends greatly on the ionization state of the amino acid. Glycine, in its anionic form for instance has a p$K_a \approx 34$ while the formally neutral zwitterionic N-protonated form of glycine has a much reduced value of *ca* 29. Furthermore the cationic N-protonated glycine methyl ester has a p$K_a \approx$ 21.[6] It is suggested that this cationic form is the catalytically active ionization state of amino acid substrates for enzymes like proline racemase, or glutamate racemase. These catalyse the stepwise racemization of amino acids through deprotonation of the bound substrate followed by non-stereospecific reprotonation of the planar enolate intermediate. This is discussed further in Chapter 3.

1.6.4 General strategies for enzymatic catalysis of deprotonation at carbon.

As discussed earlier in the chapter, simple substituents can have profound effects on the acidity of carbon acids. Dramatic increases in non-enzymatic proton transfer are brought about by substituents which stabilise the negative charge on the carbanion products, simple examples of which are reflected in Nature.

Formation of an iminium adduct **(20)** between acetone and glycine methyl ester **(19)** causes a reduction in the pK_a value of the α-proton by 7 units (see Figure 1.3). This is also seen in the formation of iminium ion adducts between α-amino acids and the enzyme cofactor pyridoxal phosphate.[73] Greater charge delocalization from the amino acid adduct into pyridoxal phosphate emphasizes the more important facilitation of transamination reactions by increasing charge density on the azomethine carbon of the iminium ion adduct.

Figure 1.3:

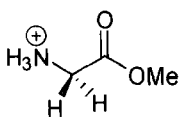

(19) pK_a 21

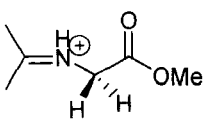

(20) pK_a 14

The α-amide substituent at the ketone **(22)** decreases the pK_a by 4 units compared to the parent ketone **(21)** (see Figure 1.4)[74] due to stabilizing electrostatic interactions between the enolate anion and the partial positive charge at the amide nitrogen. This is reflected in the mechanism for decarboxylation of orotidine 5'-monophosphate (OMP) by OMP-decarboxylase[75] (shown in Scheme 1.22) where delocalization of the negative charge on the carbanion significantly reduces the pK_a of the substrate in an analogous fashion. This is coupled with an enzyme active site with a low dielectric constant which favours the zwitterionic form of the substrate.

Figure 1.4:

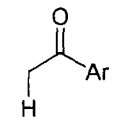

(21) pK_a 18.7

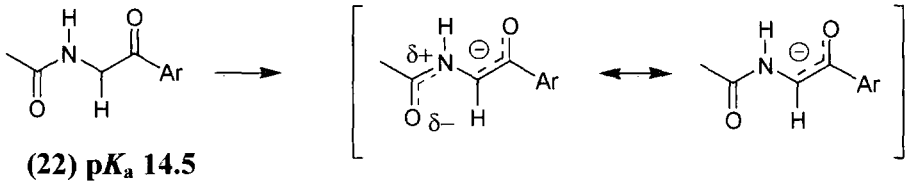

(22) pK_a 14.5

Scheme 1.22:

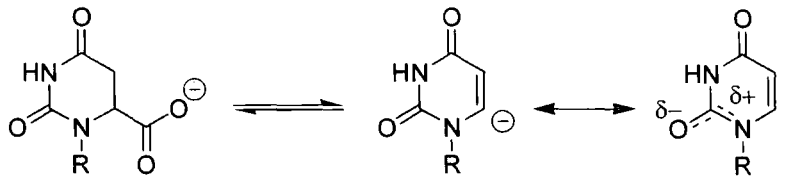

(OMP)

Despite numerous studies on the mechanism for non-enzymatic deprotonation of carbon and the stability of the anionic intermediates of enzyme-catalyzed reactions it remains unclear how the interactions between bound substrate and catalyst active site are manifested in the transition state for proton transfer to provide the observed accelerations in enzymatic rates. Model studies show stabilization of the zwitterionic enolates by intramolecular electrostatic interactions which are enhanced by the non-polar enzyme active sites. Studies also show that the use of metal ions is very important in producing the large rate accelerations seen for the catalysis of removal of the α-protons of carboxylate anions. These effects may also be enhanced by a low dielectric constant in

the enzyme active site. However the importance of these contributing forces is not fully known and further study is required in this area.

References

(1) Pearson, R. G., Dillon, R. L., *J. Am. Chem. Soc.* **1953**, *75*, 2439.
(2) K. Bowden, R. S. *Tetrahedron,* **1965**, *21*, 216-266.
(3) Pearson, R. G., Dillon, R. L., *J. Am. Chem. Soc.* **1953**, *75*, 664.
(4) Bernardi, F., Csizmadia, I. G., Mangini, A., Schlegel, H. B., Whangbo, M. H., Wolfe, S. *J. Am. Chem. Soc.* **1977**, *97*, 2209.
(5) Richard, J. P., Rios, A., Amyes,T. L., *J. Am. Chem. Soc.* **2002**, *124*, 8251.
(6) Richard, J. P., Rios, A., Amyes,T. L., *J. Am. Chem. Soc.* **2000**, *122*, 9373.
(7) Dessy, R. E., Kitching, W., Psarras, T., Salinger, R., Chen, A., Chivers, T., *J. Am. Chem. Soc.* **1966**, *88*, 460.
(8) Applequist, D. E., O'Brien, D. F. *J. Am. Chem. Soc.* **1963**, *6*, 743.
(9) Bonhoeffer, K. F., Gib, K. H., Reitz, O. *J. Chem. Phys.* **1939**, *7*, 664.
(10) Turnbull, D., Maron, S. H. *J. Am. Chem. Soc.* **1943**, *65*, 212.
(11) Edinoff, M. L. *J. Am. Chem. Soc.* **1945**, *67*.
(12) Zucker, L., Hammett, L. P. *J. Am. Chem. Soc.* **1939**, *61*, 2785.
(13) Pearson, R. G., Mills, J. M. *J. Am. Chem. Soc.* **1950**, *72*, 1692.
(14) Gilman, H., Moore, F. W., Baine, O. *ibid.* **1941**, *63*, 2479.
(15) Gilman, H., Spatz, S. M. *ibid.* **1941**, *63*, 1553.
(16) Gilman, H., Haubein, A. H., O'Donnell, G., Woods, L. A. *ibid.* **1945**, *67*, 922.
(17) Gilman, H., Haubein, A. H., *ibid.* **1945**, *67*, 1033.
(18) Jones, R. G., Gilman, H. *Organic Reactions,* **1951**, *VI*, 339.
(19) Keeffe, J. R., Kresge, A. J., Yin, Y. *J. Am. Chem. Soc.* **1987**, *110*, 1982.
(20) Kresge, A. J., Keeffe, J. R. *The Chemistry of Enols*, John Wiley and Sons Ltd., 1990.
(21) Bernasconi, C. F., Wenzel, P.J. *J. Org. Chem.* **2003**, *68*, 6879.
(22) Bernasconi, C. F. Ni, J. X. *J. Am. Chem. Soc.* **1992**, *115*, 5060.
(23) Dubois, J. E., El-Alaoui, M., Toullec, J. *J. Am. Chem. Soc.* **1981**, *103*, 5393.
(24) Hochstrasser, R., Kresge, J. A., Schepp, N. P., Wirz, J. *J. Am. Chem. Soc.* **1988**, *110*, 7875.
(25) Zucker, L., Hammett, L. P. *J. Am. Chem. Soc.* **1939**, *61*, 2791.
(26) Zucker, L., Hammett, L. P. *J. Am. Chem. Soc.* **1939**, *61*, 2779.
(27) Chiang, Y., Kresge, J. A., Tang, Y. S., Wirz, J. *J. Am. Chem. Soc.* **1984**, *106*, 460.
(28) Amyes, T., L. Diver, S. T., Richard J. P., Rivas, F. M., Toth, K. *J. Am. Chem. Soc.* **2003**, *126*, 4366.
(29) Williams, G. M., E.P.; Amyes, T. L.; Wood, T. D.; Richard, J. P. *Biochemistry,* **2003**, *42*, 8354.
(30) Amyes, T. L., Richard, J. P. *J. Am. Chem. Soc.* **1992**, *114*, 10297.
(31) Kherani, N. P. *Nuclear Instruments and Methods in Physics Research Section A: Accelerators, Spectrometers, Detectors and Associated Equipment,* **2001**, *484*, 650.
(32) Kresge, A. J., Powell, M. F. *Int. J. Chem. Kinet.* **1982**, *14*, 19.

(33) Best, P. A., Litter, J. S., Waters, W. A., *J. Chem. Soc.* **1962**, 822.
(34) Drummond, A. Y., Waters, W. A., *J. Chem. Soc.* **1955**, 497.
(35) Litter, J. S. *J. Chem. Soc.* 827.
(36) Audsley, A. J., LItter, J. S., Easton, G., *J. Chem. Soc., Perkin Trans.* **1980**, *2*, 657.
(37) McClelland, R. A. *Tetrahedron,* **1996**, *52*, 6823.
(38) Chiang, Y., Kresge, A. J. *Science,* **1991**, *253*, 395.
(39) Richard, J. P., Amyes, T. L., Toteva, M. M. *Acc.Chem. Res.* **2001**, *34*, 981.
(40) Richard, J. P., Williams, G., Gao, J. *J. Am.Chem. Soc.* **1999**, *121*, 715.
(41) Fishbein, J. C., Jencks, W. P., *J. Am Chem. Soc.* **1988**, *110*, 5075.
(42) Fishbein, J. C., Jencks, W. P., *J. Am.Chem. Soc.* **1988**, *110*, 5087.
(43) Richard, J. P. W., G.; O'Donoghue, A. C.; Amyes, T. L. *J. Am. Chem. Soc.* **2002**, *124*, 2957.
(44) Amyes, T. L., Richard, J. P. *J. Am.Chem. Soc.* **1996**, *122*, 9373.
(45) Jenks, W. P. *Chem. Soc. Rev.* **1981**, *10*, 345.
(46) Eigen, M. *Angew. Chem. Int. Ed. Engl.* **1964**, *3*, 1.
(47) Bednar, R. A., Jencks, W. P., *J. Am. Chem. Soc.* **1985**, *107*, 7117.
(48) Washabaugh, M. W., Jencks, W. P., *Biochemistry,* **1988**, *27*, 5044.
(49) Dawson, H. M., Powis, F., *J. Chem. Soc.* **1913**, 2135.
(50) Bell, R. P. *Acid-Base Catalysis*, Oxford University Press: London, 1941.
(51) Bell, R. P., Lidwell, O. M., *Proc. R. Soc.* **1940**, *176*, 88.
(52) Reitz, O. *Naturwissenschaften,* **1939**, *24*, 814.
(53) Reitz, O. *Z. Phys. Chem. A.* **1937**, *179*, 119.
(54) Venimadhavan, S., Shelly, K. P., Stewart, R., *J. Org. Chem.* **1989**, *54*, 2483.
(55) Hammond, G. S. *J. Am. Chem. Soc.* **1955**, *77*, 334.
(56) Jenks, W. P., *Chem. Rev.* **1985**, *85*, 511.
(57) Venimadhavan, S., Shelly, K. P., Stewart, R., Nagarajan, K., *Can. J. Chem.* **1989**, *67*, 1274.
(58) Amyes, T. L., Richard, J. P. *J. Am. Chem. Soc* **1996**, *118*, 3129.
(59) Bordwell, F. G., Boyle, W. J., Hautala, Jr. J. A., Yee, K. C., **1969**, *91*, 4002.
(60) Bernasconi, C. F. *Acc. Chem. Res.* **1987**, *20*, 301.
(61) Bernasconi, C. F., Schuck, D. F., *J. Org. Chem* **1992**, *57*, 2365.
(62) Capon, B., ZuccoC., *J. Am. Chem. Soc* **1982**, *104*, 7567.
(63) Kresge, A. J. *Chem. Soc. Rev.*, **1973**, *2*, 475.
(64) Guthrie, J. P. *J. Am. Chem. Soc.* **1991**, *113*, 7249.
(65) Rios, A., Richard, J. P., Amyes, T. L., *J. Am. Chem. Soc.* **2002**, *124*, 8251.
(66) Hawkinson, D., Eames, T. C. M., Pollak, R. M., *Biochemistry,* **1991**, *30*, 10849.
(67) Poner, R. K., Cleland, W W., Reed, G. H., *Biochemistry,* **2001**, *40*, 8009.
(68) Knowles, J. R., Albery, W. J., *Acc. Chem. Res.* **1977**, *10*, 105.
(69) Chiang, Y., Kresge, A. J., Tang Y. S., Wirz, J., *J. Am. Chem. Soc.* **1984**, *106*, 460.
(70) Babbit, P. C., Hasson, M. S., Wedekind, J. E., Palmer, D. R. J., Barrett, W. C., Reed G. H., Rayment, I., Ringe, D., Kenyon, G. L., Gerlt, J. A., *Biochemistry.* **1996**, *35*, 16489.
(71) Larsen. T. M., W., J. E., Rayment, I., Reed, G. H., *Biochemistry.* **1996**, *35*, 4349.
(72) Hasson M. S., S., I., Moulia, J., Taylor, K., Barrett, W., Kenyon, G. L., Babbit, P. C., Gerlt, J. A., Petsko, G. A., Ringe, D., *Proc. Natl. Acad. Sci. USA.*, **1998**, *95*, 10396.

(73) Dixon, J. E., Bruics, T. C., *Biochemistry,* **1973**, *12*, 4762.
(74) Chiang, Y., Griesbeck, A. G., Heckroth, H., Hellrung, B., Kresge, A. J. Meng, Q., O'Donoghue, A. C., Richard, J. P., Wirz, J., *J. Am. Chem. Soc.* **2001**, *123*, 8979.
(75) Beak, P., Spiegel, B., *J. Am. Chem. Soc.* **1976**, *98*, 3601.

Chapter 2

N-Heterocyclic carbene conjugate acids

2.0 Introduction

2.1 Foreword.

Pioneering work by Buchner and Curtius[1, 2] in 1885 brought carbenes into the public eye as chemical curiosities. Since then carbenes have played an important role as transient intermediates. To date, these species have been the subject of much synthetic and biological interest. The structure, reactivity and kinetic stability of carbenes are vital to preparative chemistry as well as theoretical knowledge of their nucleophilic character. The following chapter provides an introduction to carbenes, reviewing previous work relevant to this topic and the experimentally determined rates of ionization of the conjugate acids of diaminocarbenes and their estimated pK_a values.

2.1.1. Characterization of carbenes

Carbenes are neutral compounds, containing a divalent carbon atom. The valence shell of the divalent carbon atom has six electrons similar to carbocations (see Table 2.1.) however carbene behaviour is distinctly different from that of carbocations or other carbon derivatives The carbene carbon atom is linked to two adjacent groups by covalent bonds[3] giving either a linear or bent geometry.

Table 2.1:

Derivatives		Covalent bonds	Valence electrons
Carbanions	$-C^-$	3	8
Radicals	$-C\cdot$	3	7
Carbocations	$-C^+$	3	6
Carbenes	–C:	2	6

Carbenes contain two nonbonding electrons on divalent carbon. These may have either antiparallel spins (singlet state) or parallel spins (triplet state). A singlet state (S_0) requires one orbital to be filled with two spin-paired electrons (Figure 2.1 (a)), while the other is empty, and a triplet state (T_1) requires two half filled orbitals (Figure 2.1 (b)) and can be considered a diradical. Singlet carbenes are electron deficient species, but possess an ambiphilic nature. They can be likened to carbocations due to the vacant p-orbital, however they also contain a nonbonding pair of electrons making them comparable to carbanions. The electrophilic or nucleophilic character of singlet carbenes depends on the ability of the adjacent groups to supply or withdraw electrons to or from the carbene centre.

Figure 2.1:

(a) Singlet carbene

(b) Triplet carbene

2.1.2. Structure of carbenes

Spectroscopic investigations have shown that the linear or bent geometry of a carbene depends on the ground state multiplicity. Indeed, the ground-state spin multiplicity is a fundamental feature of carbenes that dictates their reactivity.[4] Linear geometry implies an sp-hybridized carbene centre, with two degenerate orbitals (p_x and p_y). The six electrons are distributed between two σ-orbitals and two higher energy p-orbitals. Electrons in the degenerate p-orbitals remain unpaired due to electron-repulsion (Figure 2.2).

Figure 2.2:

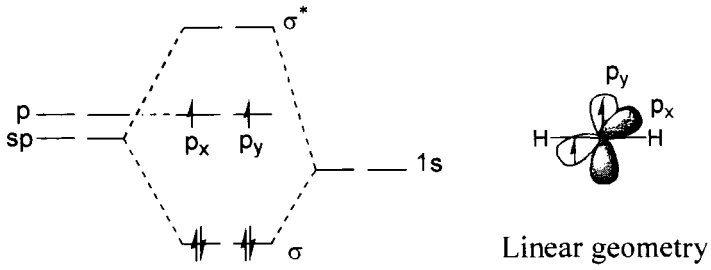

Linear geometry

This linear geometry associated with a triplet carbene is an extreme case adopted by few carbenes, such as those with very bulky substituents, restricting the carbene geometry.[1] Most carbenes have a bent geometry, where the degeneracy of the two non-bonding orbitals is broken and bond angles are between 100 – 150°. This suggests a trigonal sp^2-hybridization state. Singlet sp^2-hybridized carbenes have three sp^2-orbitals and one p-orbital to distribute six electrons. All the electrons can be paired, with each pair occupying one of the p_x and σ-orbitals (singlet state) (Figure 2.3 (a))or the two highest energy orbitals each contain one unpaired electron (triplet state)[5] (Figure 2.3 (b)).

Figure 2.3:

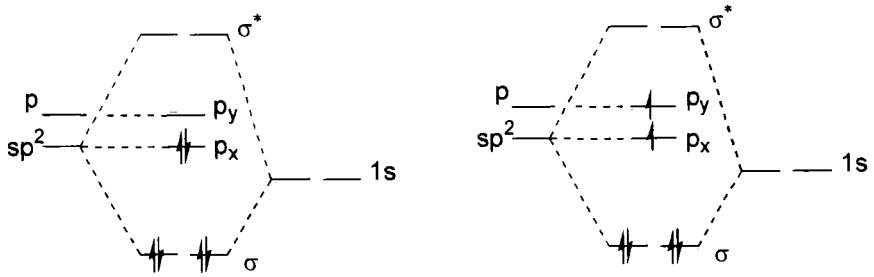

(a) **(b)**

In the singlet state the virtually unchanged p_y-orbital is renamed p_π ,while the p_x-orbital acquires s character and so becomes a σ-orbital (see Figure 2.4).[6]

Figure 2.4:

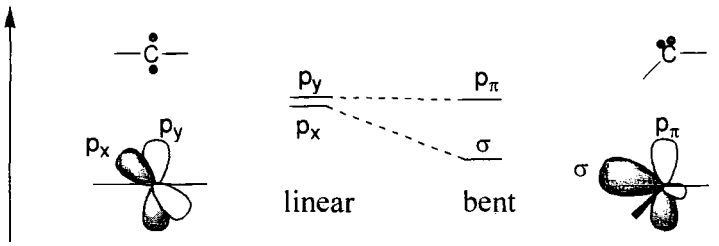

Four electronic configurations of the frontier orbitals can be envisaged (Figure 2.5.). When the two nonbonding electrons are in two different orbitals with parallel spin (triplet state) the molecule is described by $\sigma\ ^1p_\pi{}^1$configuration ($^3B_1$ state). Alternatively, the electrons may be paired in the same σ or p_π -orbital in a singlet state ($^1A_1$ state). There are two different $^1A_1$ states with σ^2 generally the more stable configuration. Finally an excited singlet state is possible (B_1 state) with $\sigma\ ^1p_\pi{}^1$ configuration. A comprehensive review of this area of carbene chemistry is given in a review by Bourissou *et al.*[1]

Figure 2.5:

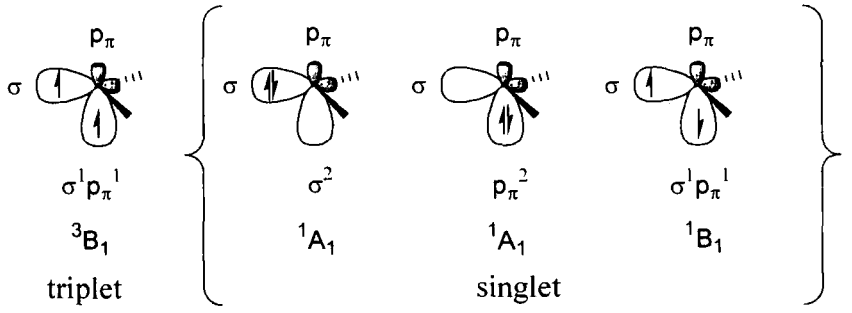

2.1.3. Reactivity and stability of carbenes

2.1.3.1 Ground state spin multiplicity

The reactivity of a carbene is dictated by its ground state spin multiplicity. This is dependent on the mode of carbene generation. Triplet carbenes, with two half filled

orbitals, act as diradicals and as such undergo two-step radical processes. The lone pair and vacant orbital incline singlet carbenes to be more ambiphilic in character and react via single–step bond insertions. The relative stabilities of singlet and triplet states is a function of the electronegativity of the carbene substituents. The singlet ground state is favoured by a large $\sigma - p_\pi$ separation, with the singlet–triplet energy gap differing depending on stabilization from the substituents. The singlet-triplet energy gap may be defined according to Equation 2.1, where for $:CF_2$, ΔE_{st} = 57 kcal mol^{-1} indicating a large orbital separation,[7] while for $:CH_2$,ΔE_{st} = -9.2 kcal mol^{-1} making a triplet state favourable.[8]

$$\Delta E_{st} = E(\text{singlet}) - E(\text{triplet}) \qquad \textbf{(Equation 2.1)}$$

Due to the paramagnetic character of triplet carbenes, they can be observed by electron spin resonance (ESR) spectroscopy, provided they have sufficient lifetimes. Molecular orbital calculations have led to the prediction of methylene H-C-H bond angles for methylene of 135° for the triplet and 105° for the singlet state. These results agree with experimental determinations of the geometry by ESR spectroscopy for $:CH_2$, which estimate an angle of 125 – 140° for the triplet state and 102° for the singlet state The orbital occupancy also explains the smaller angle in single carbenes, which have an electron- repelling lone pair. (Figure 2.1(a)).

Most carbenes are more stable in a triplet form as the energy gained by pairing the two electrons in the σ-orbital is insufficient to overcome the repulsion that exists between the two electrons in the same orbital. For most triplet carbenes the singlet spin state lies only 40 kJ mol^{-1} above the triplet ground state, and so is favoured by a large σ - p_π separation. A calculated energy value of at least 2 eV is necessary to impose a singlet ground state. A value below 1.5 eV results in a triplet ground state.[1, 9] In this way ground state spin multiplicities act similarly to strong field-low spin and weak field-high spin configuration in Crystal Field Theory.

2.1.3.2 Substituent effects

The effect of substituents can be analyzed in terms of both electronic and steric effects.

2.1.3.2.1 Electronic effects

(i) Inductive effects

The influence of the substituents electronegativity on the carbene multiplicity has been examined[4] and it is now established that σ-electron-withdrawing substituents favor the singlet versus the triplet state. These substituents inductively stabilize the σ-nonbonding orbital by increasing its s-character and leave the p_π–orbital unchanged Thus increasing the σ-p_π gap. Conversely, σ-electron-donating substituents induce a small σ-p_π separation, favoring the triplet state (Figure 2.6).[1]

Figure 2.6:

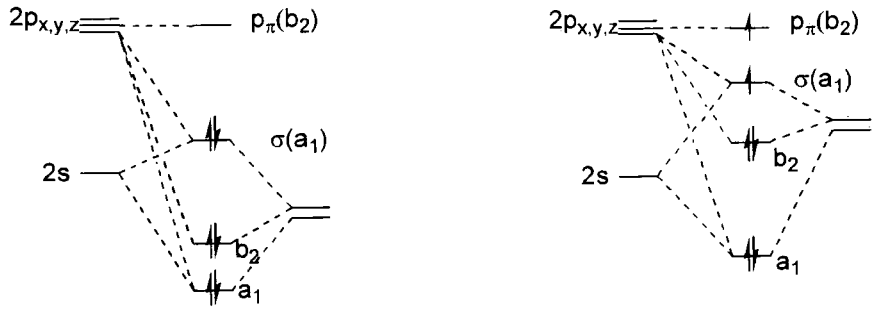

σ-electron-withdrawing substituents

σ-electron-donating substituents

Inductively electron-donating substituents disrupt the degeneracy of the p-orbitals and increase the nucleophilicity and thermodynamic stability of the carbon atom. A change from triplet to singlet state can be seen when substituents such as lithium are changed to hydrogen and fluorine (Figure 2.7).

Figure 2.7:

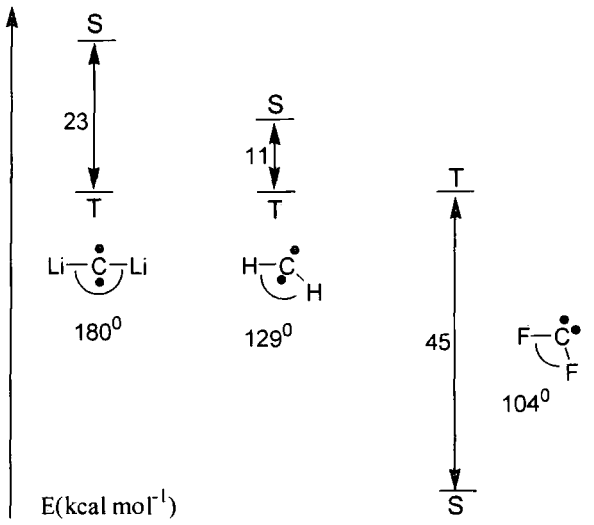

One of the best examples of this orbital separation is seen with diaminocarbenes, which are the only singlet carbenes to date isolated in crystalline form. Diaminocarbenes have a pronounced low energy HOMO and a high energy LUMO arising from the π-donating (mesomeric) and σ-withdrawing (inductive) "push–pull" effect[10] of the amino substituents (Figure 2.8).

Figure 2.8:

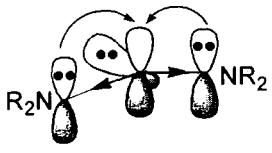

(ii) Mesomeric effects

Mesomeric effects are often more significant than inductive effects in determining the ground state multiplicity of a carbene. These effects consist of interactions between the carbene carbon orbitals (s, p_π, or p_x, p_y) and appropriate p or π-orbitals of the two carbene substituents. Carbenes with two π-electron-donating substituents, designated X (e.g. F, Cl, Br, I, NR_2, PR_3, OR, SR,) are predicted to be bent singlet carbenes.[1, 11] Interactions with the symmetric combinations of substituent lone pairs (b_1) increases the energy of the vacant p_π-orbital, which increases the σ-p_π separation as the σ-orbital remains relatively

unchanged. Hence the singlet state is favoured (Figure 1.9). The electronegativity of the π-electron-donating substituent X, compared to that of carbon is what dictates he relative position of the σ-orbital and the nonsymmetric combination of substituent lone pairs (a_2) In Figure 2.9 (a) the orbitals are close in energy. Donation from the X-substituent lone pairs results in a polarized six-electron, three-centre π system in which the carbon-substituent bonds gain some double-bond character with a negative charge on the carbene carbon. Representative examples of this stabilization include the transient dimethoxycarbenes[12] and dihalocarbanes,[7] along with more stable diaminocarbenes[1] which are the focus of this chapter.

Figure 2.9:

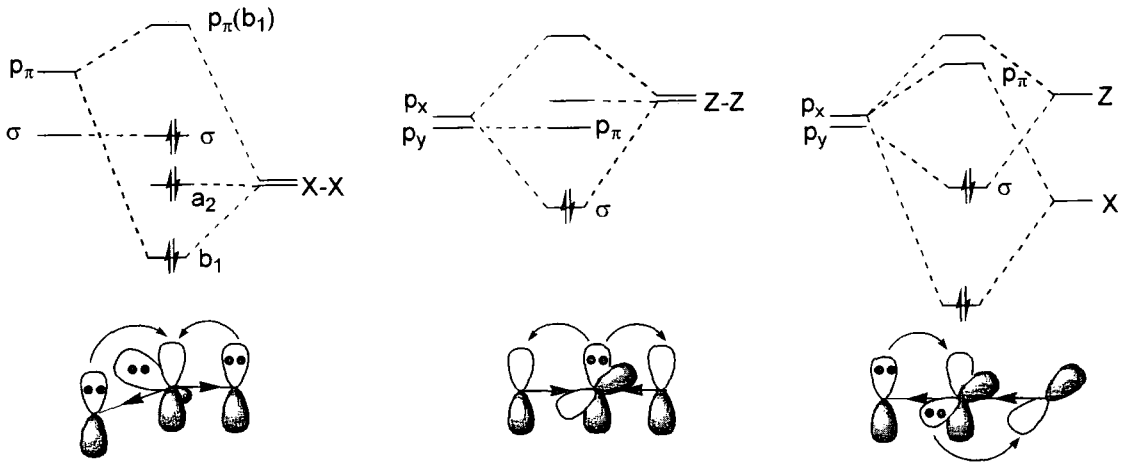

(a) **(b)** **(c)**

Carbenes with two π-electron-withdrawing substituents – Z substituents – (e.g. COR, CN, CF_3, BR_2, SiR_3, PR_3^+) are predicted to be linear singlet carbenes, with interactions between the symmetric combination of the substituent vacant orbitals and the p_y-orbital perpendicular to the valence plane (Figure 2.9 (b)). This breaks the degeneracy of the p-orbitals causing these linear carbenes to have a singlet ground state.[1, 11] This substitution pattern produces a two-electron, three-centre π-system. Multiple bond character is seen in the C–Z bonds also with a positive charge on the central carbon. Examples of such carbenes are dicarbomethoxycarbenes[13] and diborylcarbenes.[1]

A combination of one π-electron-withdrawing and one π-electron-donating substituent create both types of electronic interactions. These are quasi-linear carbenes (Figure 2.9 (c)). The vacant orbital on the Z-substituent interacts with p_x-orbital, while the lone pair on the X-substituent interacts with the p_y-orbital. Both effects are stabilizing as the vacant p_y-orbital is destabilized and the filled p_x-orbital is stabilized, thus favouring the singlet state. A polarized allene-type system with X–C and C-Z multiple bonds arises from these two electronic interactions, examples of this are transient halogencarboethoxycarbenes[14] and more stable phosphinosilylcarbenes.[1]

2.1.3.2.2 Steric effects

In situations where electronic effects are not strong, steric effects may dictate the ground state spin multiplicity. Bulky substituents are clearly seen to stabilize all types of carbene and hinder dimerization. A linear geometry will be favoured when the frontier orbitals are degenerate, since stabilization of the triplet state relative to the singlet is maximized (Figure 2.9 (b)). Increasing the steric bulk of the carbene substituents broadens the carbene bond angle thereby favouring the triplet state.[15] At an angle below 90° the energy of the singlet state for methylene drops below that of the triplet state.[11] Dimethylcarbene, with a bond angle of 111° also has a bent singlet ground state. Ditertbutylcarbene, and diadamantylcarbene have bond angles of 143° and 152° respectively and are both triplet carbenes.[1]

However evidence suggests that steric effects are not the main factors governing carbene stability. A number of bulky N-substituted imidazolyl carbenes have been isolated (N-substituent: 1-adamantyl, mesityl, *p*-tolyl and *p*-chlorophenyl).[16] The stability of these carbenes is evidently mainly due to the electronic interactions present, regardless of the presence or absence of steric bulk, as it was also possible to isolate a less bulky analogue (N-substituent: methyl).[17] Steric parameters do however affect the long term stability of N-heterocyclic carbenes.[18, 19]

2.1.3.3 π-Interactions (cyclic delocalization and/or resonance)

The original synthesis of the imidazolyl carbene was rationalized by Dixon and Arduengo.[20, 21] They attributed the extraordinary stability of these carbenes to the inductive effects of the neighbouring nitrogen atoms. Dixon and Arduengo assumed that delocalization of the nitrogen lone pairs into the empty p-orbital would stabilize the electron-deficient carbene centre. The high electron density of the nitrogen lone pairs of imidazole and the C4-C5 double bond were presumed to provide enough kinetic stabilization, enabling the species to be isolated in crystalline form. However, the importance and extent of aromatic-delocalization for carbene stability remained controversial.

While π-interactions in the imidazole ring contribute to the stability of these carbenes to some degree, they do not appear to be a dominant stabilizing factor, or even a necessary presence.[8] A further study by Cioslowski[22] concluded that the π-donation by nitrogen lone pairs plays only a minor role, compared to the inductive effect of nitrogen. Controversy was brought to an end in 1996 by Heinemann[23] and Boehme,[24] who independently investigated the importance of aromaticity in imidazole-2-ylidenes. They concluded that cyclic electron delocalization does indeed occur in the imidazole-2-ylidenes, and in fact brings additional stabilization of *ca.* 25 kcal mol^{-1} to the imidazole-2-ylidene relative to the imidazolium ion precursor.[1, 23]

Nitrogen(N)-substituted carbenes are still relatively stable in the absence of stabilization by aromaticity. A stable imidazolin–2–ylidene carbene[25] and even acyclic diaminocarbenes[26] have been isolated proving this to be the case.

The most significant mode of stabilization of the divalent site is the strong N-C-N delocalization, and the interaction of the carbene centre with the π-bonding σ-attracting amino substituents.[1, 27]

2.1.4. Historical background

The importance of carbenes in organic chemistry has been apparent since they were first known to exist. However it has taken until the last 10 - 15 years for these species to be characterized and even isolated.[21] The first attempts at carbene preparation were made in 1835 by Dumas and Péligot. The attempt was to prepare methylene by dehydrating methanol using phosphorus pentoxide or concentrated sulphuric acid.[28] At the time the existence of carbenes was considered reasonable as the tetravalency of carbon had not been established. Further studies were undertaken by Buchner and Curtius in 1885,[2] and by Nef (1895) and Gomberg (1900). In the early twentieth century Staudinger showed that carbenes generated from diazo compounds or ketenes were highly reactive species. Their unusual reactivity was attributed to their defiance of the octet rule, having only a six valence-electron shell. At the time, this revelation ended the interest in generating stable carbenes as it was considered an unattainable goal.

Interest was reawakened in the 1950s by Doering and Hoffmann[29] who introduced carbene intermediates to organic chemistry. This was followed by work by Skell,[30] Breslow[31] and Wanzlick[32] who witnessed the extraordinary stability of carbenes with amino substituents. Carbenes were introduced to inorganic and organometallic chemistry by Fischer and Maasböl [33] in 1964 with the synthesis of stable metallo-carbenes such as **(23)** To date, such metal carbene complexes have become hugely significant as catalysts in organic synthesis in organic synthesis catalysis, and macromolecular chemistry[28]

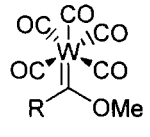

(23)

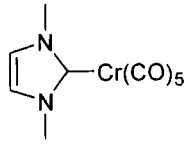

(24)

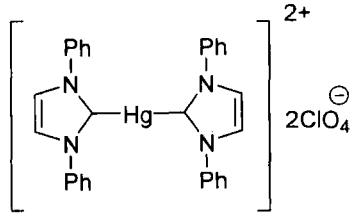

(25)

Soon after the synthesis of **(23)**, reports by Őfele [34] and Wanzlick *et al*[35] described the then unusual complexes **(24)** and **(25)** with N-heterocyclic carbenes as ligands, obtained from metal containing precursors and imidazolium salts of sufficient acidity.[28] Wanzlick

recognized that the stability of carbenes could be dramatically increased by the presence of α-amino substituents. Based on this he attempted to prepare the 1,3-diphenylimidazolidin-2-ylidene **(27)** by thermal elimination of chloroform from **(26)** (Scheme 2.1)[1] However only the dimeric electron-rich olefin **(28)** was isolated instead of the free carbene. More recently Denk *et al.*[36] suggested that an equilibrium may exist between these two species.

Scheme 2.1:

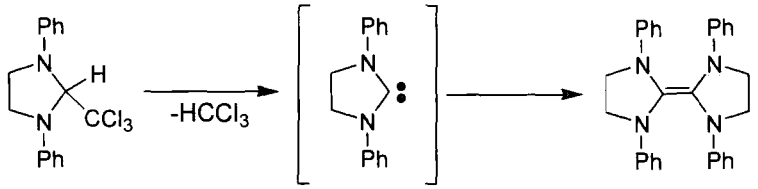

(26) **(27)** **(28)**

In 1970, Wanzlick *et al*[37] demonstrated that deprotonation of imidazolium salts by potassium *t*-butoxide could result in the corresponding imidazole-2-ylidenes. These were trapped as metal containing dimers and not isolated.[1, 10, 38] Later, the first Schrock-type carbene complex **(29)** was isolated and Hoffmann discovered that the ground state spin multiplicity depended on the separation between the σ and π-orbitals. A singlet state for carbenes such as methylene required a separation of at least 2 eV This splitting was attributed to interactions between the unoccupied carbene p-orbital with an aromatic system of (4n + 2) π-electrons.

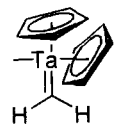

(29)

Further attempts to isolate these heteroatom-substituted carbenes were made in the 1980s by Igua *et al*,[39] with the supposed synthesis of phosphinocarbenes, λ^5–phospha–acetylene. However no differentiation was seen between carbene and double bond reactivity with this compound. Notably, a general synthesis of metal-carbene complexes was developed by Lampert *et al.* This involved the treatment of electron-rich olefins with transition metal complexes such as $[RhCl(Ph_3)_3]$.[1]

It was not until 1991 that Arduengo *et al* succeeded in isolating the first table free carbene under inert conditions[21] with close to quantitative deprotonation of 1,3-di-1-adamantylimidazolium chloride **(30)** to give the corresponding carbene (Scheme 2.2). This colourless crystalline solid had a melting point of 240 – 241 °C without decomposition, making it surprisingly thermally stable.

Scheme 2.2:

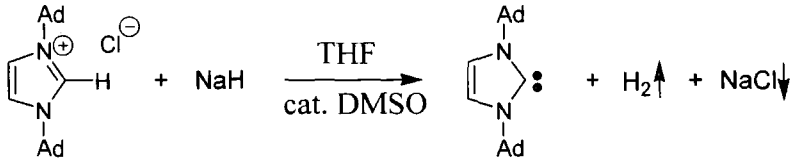

(30) Ad = Adamantyl **(31)**

This was the start of a new upsurge in interest in the preparation of free carbenes and their metal complexes. Fierce activity was prompted by the development of a new versatile two step approach to thermally stable alkyl-substituted N-heterocyclic carbenes by Kuhn *et al*[40] (Scheme 2.3). This involved the reduction of imidazole-2(3*H*)-thiones **(32)** with potassium in boiling THF to form the corresponding carbene **(33)**

Scheme 2.3:

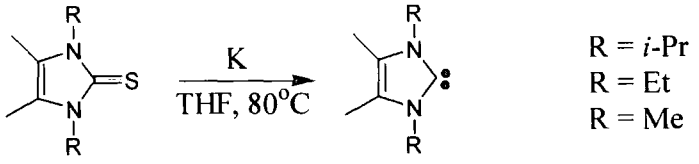

(32) **(33)**

Work by Herrmann *et al*[10] showed that deprotonation of imidazolium salts (such as in Scheme 2.2) occurred faster in solvent liquid ammonia (homogeneous phase) and a number of different N-functionalized carbenes were prepared in this way.

In 1995 the first commercially available stable carbene was produced due to the thermal elimination of methanol *in vacuo* from 5-methoxy-1,3,4-triphenyl-4,5-dihydro-5-ylidene **(34)** to produce 1,2,4-triazol-5-ylidene **(35)** (Scheme 2.4).

Scheme 2.4:

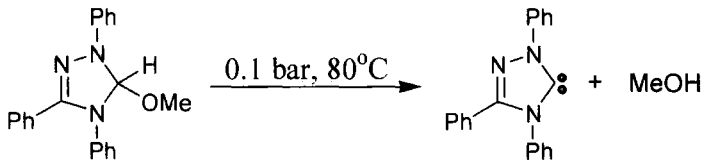

(34) **(35)**

2.1.5 Stable carbenes

2.1.5.1 Triplet carbenes

Triplet carbenes were originally regarded as being too reactive to be isolated. They cannot be stabilized through thermodynamic effects thus rely on steric protection for stabilization. The main difficulty in isolating triplet carbenes stems from the occurrence of unfavourable side reactions such as dimerization and intra/intermolecular hydrogen abstraction. Attempts to minimise these side reactions focus on increasing steric bulk around the carbene centre and avoiding the presence of alkyl groups near the carbene centre.

The first report of a relatively stable triplet carbene was by Tomioka *et al*[41] in 1995 who synthesized 2,2',4,4',6,6'-hexabromodiphenylcarbene **(36)**. This was achieved by photolysis of the parent diazo-compound. This compound was crystalline and stable without significant decomposition at room temperature and had a half life of 1 s in 2-methyltetrahydrofuran (120 K), determined by laser flash photolysis (LFP). The chlorine equivalent was less stable, due to the decrease in steric bulk of chlorine compared to bromine.

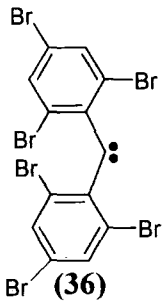

(36)

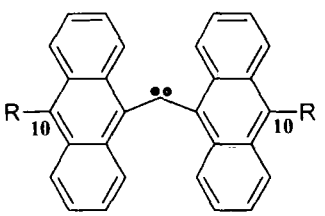

(37)

In 2001, carbene **(37, R = H)** was produced with a view to its extensive delocalization of nonbonded electrons promoting greater thermodynamic stability, and the perpendicular geometry was expected to increase the kinetic stability.[42] However carbene **(37, R = H)** had a half-life of only 0.5 μs in degassed benzene solution. Trimerization occurred, attributed to a "leaking" of the delocalized electrons from the carbene centre to position 10. Introducing substituents such as **(37, R = Ph)** to this position dramatically increased the half-life of the triplet carbene to ~ 19 minutes in degassed benzene at room temperature.

2.1.5.2 Singlet carbenes

In addition to imidazolyl carbenes, there have been a number of other stable singlet carbenes synthesized. These include imidazolin-2-ylidenes **(38)**, tetrahydropyrimid-2-ylidenes **(39)**, 1,3-thiazol-2-ylidenes **(40)**, acyclic diaminocarbenes **(41)**, aminooxycarbenes **(42)** and aminothiocarbenes **(43)** (Figure 2.10).[1] For all these compounds the carbene centre bears two π-donor group substituents, at least one of which is an amino group due to the superior π-donor ability and stabilizing effect of amino versus alkoxy groups.[1] Single crystal X-ray diffraction studies have been used to determine the solid state structures of derivatives of some of the compounds shown in Figure 2.10. The observed N-C-N bond angles at the carbene centres (100 – 110°)[20, 21] conform with the expected bond angles for singlet carbenes of this type. The angles are generally smaller than the typical angles for corresponding imidazolium salts (108.5 – 109.7°).[10] This has been attributed to the longer N-C bond of imidazolium salts as opposed to the shorter F-C bond in CF_2:. A larger value of 121.0° for the acyclic diaminocarbene is likely a result of strong steric effects.

Typically, the two nitrogen atoms are in an almost planar environment, with short N-C-N bond lengths (1.33 – 1.38 Å), indicating that donation of the nitrogen lone pairs to the carbene centre gives some double bond character.[24] This is supported by the high barriers to rotation about the N-C bond for **(41)** and **(42)**.

Figure 2.10:

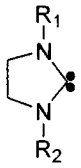

(38)

$R_1 = R_2$ = Mes, *t*-Bu, Me, Et, *i*-Pr

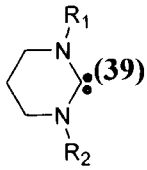

(39)

$R_1 = R_2$ = *i*-Pr, Et

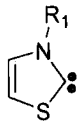

(40)

$R_1 = R_2$ = 2,6-(*i*-Pr)$_2$C$_6$H$_3$, Me

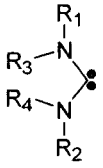

(41)

$R_1 = R_2 = R_3 = R_4$ = *i*-Pr, piperidine, Me

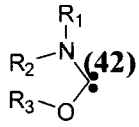

(42)

$R_1 = R_2$ = *i*-Pr, R_3 = 2,6-(*t*-Bu)$_2$C$_6$H$_3$
$R_1 = R_2$ = Me, R_3 = 2,6-(*t*-Bu)$_2$C$_6$H$_3$
$R_1 = R_2$ = *i*-Pr, R_3 = 2,6-(Me)$_2$C$_6$H$_3$
$R_1 = R_2$ = piperidine, R_3 = Me

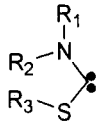

(43)

$R_1 = R_2$ = Me,
R_3 = 2,6-(*t*-Bu)$_2$C$_6$H$_3$

Therefore cyclic or acyclic diaminocarbenes are best described by resonance forms **(44a)** and **(44b)** summarized by **(44c)** (Figure 2.11). Aminooxycarbenes and aminothiocarbenes are best represented by **(45a)** and **(46a)** respectively.

The stability of singlet carbenes is mainly due to thermodynamic stabilization through electronic effects. However kinetic stabilization i.e. steric hindrance can sometimes play an important role. The question of how much aromaticity contributes to the overall stability of the 6π-electron five membered ring carbenes was pondered,[24] and it was eventually decided that cyclic delocalization does indeed occur in the imidazol-2-ylidenes, but to a lesser extent than in the imidazolium ion precursor.

Aromaticity is not the major stabilizing effect for imidazole-2-ylidenes.The interaction of the carbene centre with π-donating σ-attracting amino substituents outweighs the effects of aromatic stabilization. This makes it possible for aminocarbenes of the types **(39), (41), (42)** and **(43)** to also be isolated. Several reviews[1, 10, 28, 38, 43] have detailed the numerous routes now available for the production of stable nucleophilic carbenes, either

cyclic or acyclic. Although substantial progress has been made there remain questions about the reactive nature of these carbon derivatives.

Figure 2.11:

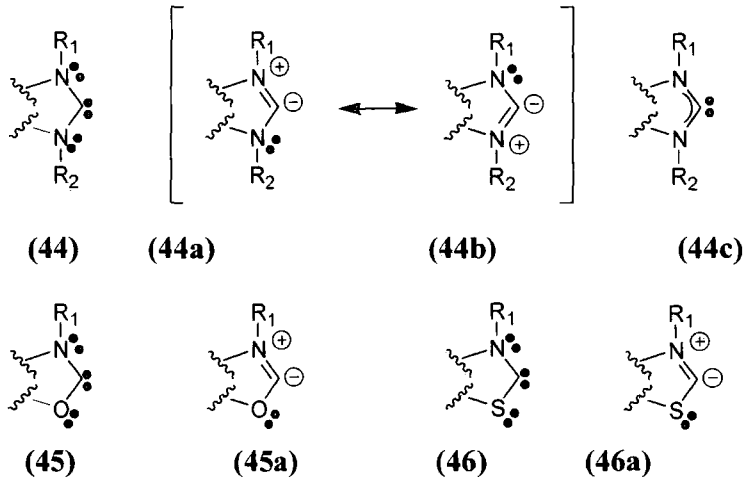

(44) **(44a)** **(44b)** **(44c)**

(45) **(45a)** **(46)** **(46a)**

2.1.6 Protonation equilibria of carbenes.

The structure and chemical reactivities of these strong carbon bases has become an advancing and progressive area of research. Physical organic studies in this area are sparse. However the synthesis and isolation of stable imidazole-2-ylidenes and studies of their binding affinities to metal ions have contributed to our basic understanding of carbenes. Knowledge of their nucleophilic character is essential for their application in organometallic chemistry, where they are noted as important ligands for transition-metal centred catalyst design.

The electron pair of a singlet carbene can accept a proton to give a carbocation. Similarly addition of a hydride ion results in the formation of a carbanion (Scheme 2.5). However the acid–base chemistry of carbenes is relatively unstudied, particularly solution pK_a values of the conjugate acids of carbenes are rare.

Scheme 2.5:

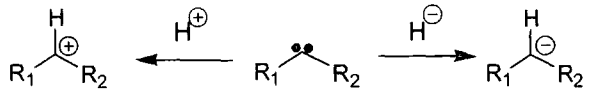

Carbocation Carbene Carbanion

The study of pK_a values of the conjugate acids of carbenes was difficult prior to the advent of modern analytical and time-resolved spectroscopic techniques. This is mainly due to the short lifetimes of carbenes in solution and correspondingly high conjugate acid pK_a values. A pK_a value of 18 was determined for thiazolium ion **(47)**, which is effectively a resonance-stabilized carbocation. Scheme 2.6 shows the relevant carbon a dissociation equilibrium between the thiazolium ion conjugate acid **(48)** and carbene **(49)**, corresponding to the K_a value.

Scheme 2.6:

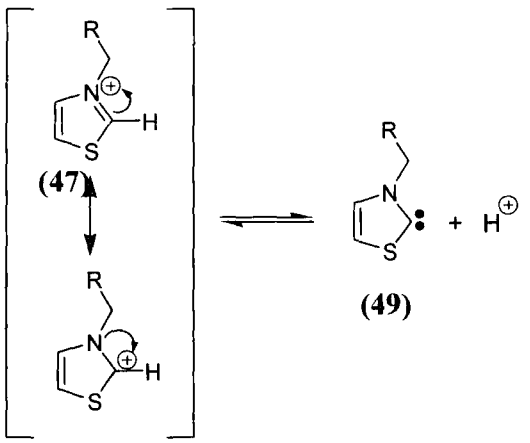

(48) **(49)**

According to the equilibrium in Scheme 2.6, the acidity constant K_a may be written as in Equation 2.2. Hence for pK_a = 18, the ratio of carbene/thiazolium ion in 1 M HCl is 10^{-18} and at the other extreme of pH range - in 1 M NaOH - this ratio is 10^{-4} illustrating that within the normal pH range, the concentration of carbene is too small to be directly detectible by conventional spectroscopic and potentiometric methods.

$$K_a = \frac{[(49)][H^+]}{[(48)]} \qquad \textbf{(Equation 2.2)}$$

Substituent polarizability, field and resonance effects have been analysed by means of gas phase protonation equilibria (proton affinities).[44] However little information is available on substituent effects on the protonation equilibria of carbenes in solution.

2.1.7 Acid-base chemistry of N-heterocyclic carbenes

In recent years, mainly theoretical studies have been done to determine factors controlling the nucleophilicity and related basicity of N-heterocyclic carbenes. Nolan studied the binding affinity of several N-heterocyclic carbenes to $[Cp^*RuCl]_4$ ($Cp^* = \eta^5$-C_5Me_5),[45] which suggested an increased nucleophilicity of N,N'-dialkyl-substituted carbenes over N,N'-aryl-substituted carbenes. A study by Lee *et al*, examined the stretching frequencies of the C-O bond in $[Cr(CO)_5L]$ (L = N-heterocyclic carbenes, diaminocarbenes, phosphines),[46] which suggested among other things that acyclic diaminocarbenes are more basic than the corresponding cyclic diaminocarbenes. There remains relatively little experimental data pertaining to the effects of structural change on the nucleophilicity or basicity of these carbenes.

Azolium ions may be deprotonated in basic conditions to form a resonance hybrid of an ylide and a carbene (Scheme 2.7). The ylide **(44a)** has been shown to be the major contributing form to the resonance hybrid from structural measurements of the N-C2 bond length of diaminocarbenes, which has significant double bond character.

Scheme 2.7:

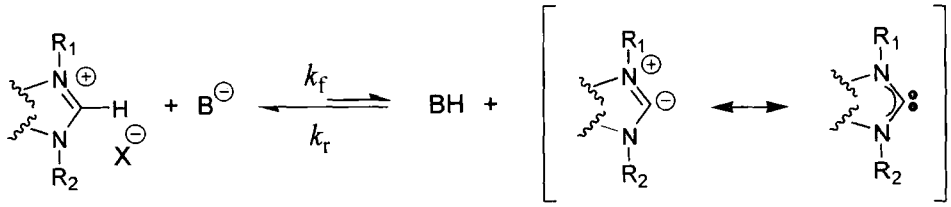

Azolium ion **(50)** | Ylide (Y) **(44a)** | Carbene **(44c)**

The few estimated pK_a values that are available for azolium ions show that these species are only very weakly acidic. The concentration of ylide at equilibrium is generally too

small to be directly measured conventionally. An alternative approach, described in Chapter 1, to determining the acidity constants, K_a of azolium ions has been employed in this work (see Equation 2.3).

$$K_a = \frac{k_f}{k_r} \qquad \textbf{(Equation 2.3)}$$

This is discussed further in Section 2.2.2 and 2.4.

2.1.8 Kinetic acidities of azolium ions by deuterium exchange

The kinetic acidities of azolium ions have been in question for some time with numerous studies undertaken of substituent effects on the rate of carbene formation. Carbene formation is thermodynamically unfavourable, so according to the Hammond postulate, the transition state for carbene formation should more resemble the carbene product than the parent imidazolium ion.

Historically, the following order of reactivity of azolium ions towards deuteroxide ion-catalyzed H/D-exchange was established[47]: oxazolium **(51)** > thiazolium **(52)** > imidazolium ions **(53)** (see Scheme 2.8).

Scheme 2.8:

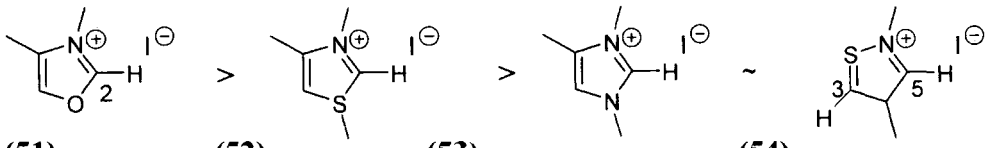

(51) **(52)** **(53)** **(54)**

k_{DO} ($M^{-1}s^{-1}$)[47]	H(2) 3.8 x 10^7	H(2) 3.7 x 10^5	H(2) 1.3 x 10^2	H(3) 1.6 x 10^1 H(5) 3.0 x 10^2

The presence of more electronegative substituents α to the C–H undergoing exchange was shown to increase the rate constants for H/D-exchange.[48] Aldrich *et al*[49] calculated that oxazolium ions and ylides contained a positive Löwdin net atomic charge, (Q_{net}) values for C2 compared to thiazolium and imidazolium ions, thus providing less nucleophilic character for oxazolium ions and producing higher rates of ring opening in the presence of nucleophilic bases. Aldrich suggested that differing degrees of solvation

and hydrogen bonding experienced by the oxazolium ions compared to other azolium ions afforded their differing rates of observed H/D-exchange. It was thought that thiazolium ions benefited from stability gained through interactions between the negative charge on the ylide and the d-orbitals of sulfur. However, theoretical studies by Scheffers-Sap,[50] showed that the polarizing influence of sulfur in thiazolium ions is the major source of stabilization of the negative charge at the C2 position rather than a d-σ-orbital overlap.

More recently, results by Amyes *el al*[51] concluded that N-substituted imidazole-2-ylidenes are in fact more stable than corresponding thiazol-2-ylidenes, based on a comparison of thermodynamic rather than kinetic acidities in water. The effect of the X-substituent (X = N or S) on the carbon basicity of these carbenes was investigated in the thermodynamic cycle shown in Scheme 2.9.

Scheme 2.9:

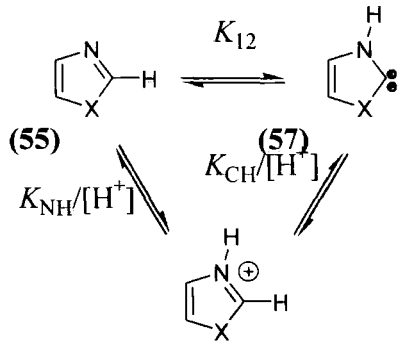

$$\text{Log } K_{12} = pK_{NH} - pK_{CH} \qquad \textbf{(Equation 2.4)}$$

The effect of the X-substituent on both the equilibrium constant for N-protonation of the neutral azole **(55)** to the azolium cation **(56)** and the subsequent ionization of cation **(56)** to carbene **(57)** is mirrored in the equilibrium constant for the 1,2-H shift of imidazole-2-ylidenes or thiazol-2-ylidenes (Equation 2.4) to give the corresponding azoles in water. It was concluded that the smaller C2 acidity of the imidazolium cation (X = NH) by 5.3 kcal mol^{-1} in water relative to the thiazolium cation (X = S), reflected the greater stability of the imidazolium cation relative to the neutral azole by 6.4 kcal mol^{-1} and not the

greater stability of thiazol-2-ylidene relative to imidazole-2-ylidene. In fact a 1.1 kcal mol^{-1} greater stability of imidazole-2-ylidene relative to the neutral azole was calculated. There have been limited studies of N-substituent effects on the acidity of the C2-H of azolium ions. However for derivatives of thiazolium ions **(58)**, Washabaugh and Jencks[52, 53] have studied catalysis of H/D exchange by deuteroxide ion, where k_{DO} is the second order rate constant for deuteroxide ion-catalyzed exchange (see Figure 2.12).

Figure 2.12:

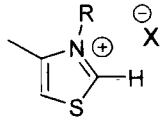

(58)

	k_{DO} ($M^{-1}s^{-1}$) 30° C
R = Et	3.24×10^5
i-Pr	3.80×10^5
Me	4.27×10^5
$CH_2CH_2CO_2^{\ominus}$	4.27×10^5
$CH_2CH{=}CH_2$	9.77×10^5
$CH_2CO_2^{\ominus}$	1.07×10^6
CH_2Ph	2.14×10^6
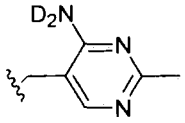	3.39×10^6
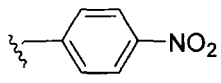	6.03×10^6
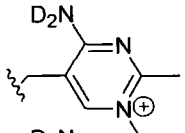	7.59×10^6
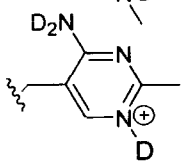	8.32×10^6
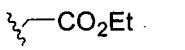	8.71×10^6
CH_2CN	4.68×10^7

The highly localized negative charge that builds up at the C2 position during deprotonation of thiazolium ion **(58)** may only be stabilized inductively, as there is a CH_2-linker to the substituent in each case. Hence the differences in the observed rate constants for deuteroxide ion-catalyzed exchange may be assigned to the relative inductive effects of the N-substituents. Similar substituent effects are expected in

imidazolium ions, however quantitative comparison of the effects of structural changes cannot be made due to a lack of structurally homologous examples and comparable reaction conditions. The few available literature values are listed in Table 2.2.

Table 2.2:

Imidazolium ion		X^-	Temp °C	k_{DO} ($M^{-1}s^{-1}$)	Reference
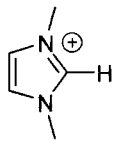	**(59)**	I^-	31	3.0×10^2	a
		I^-	31	2.0×10^2	b
		I^-	25	2.47×10^2	c
		I^-	25	2.7×10^2	d
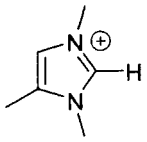	**(60)**	I^-	34.4	1.3×10^5	e
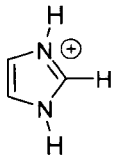	**(61)**	I^-	25	3.69×10^1	c
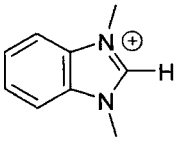	**(62)**	Cl^-	31	4.3×10^4	b,c
		I^-	25	5.74×10^3	c
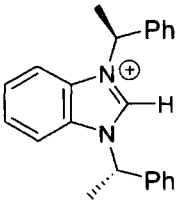	**(63)**	Cl^-	25	1.48×10^4	c

a. Olofson,[48] b. Schroeder,[54] c. Amyes,[55] d. Wong,[56] e. Haake[47]

The k_{DO} value obtained by Amyes *et al* for imidazolium ion **(59)** was found to differ from the previously reported value by Wong and Keck[56] at 25° C by 8.5 % (see Table 2.1.2). Addition of the fused benzene ring to the imidazolium ion **(62)** causes a 23-fold increase in k_{DO} values. However literature shows a 143 – 215-fold effect at 31° C. The

observed relative kinetic acidities may be explained by increased charge dispersion and decreased parent ion solvation in the order **(61)** → **(59)** → **(62)** → **(63)** and also the inductive effect of benzyl groups can be seen, **(62)** → **(63)**[55]

2.1.9 Thermodynamic acidities of azolium ions.

Few pK_a values for azolium derivatives from H/D exchange are available in the literature, and only one systematic study of substituent effects on these values for thiazolium ions exists. pK_a values for derivatives of thiazolium ion **(64)** were determined to be in the range 17 – 19 by Washabaugh and Jencks[52] (see Table 2.13), while the pK_a values for imidazolium ions such as 1,3-di-isopropyl-4,5-dimethylimidazol-ylidene were estimated to be higher than this.

Table 2.13:

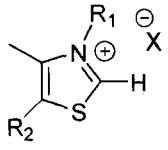

(64)

R_1	R_2	pK_a (D_2O)[a]	pK_a (DO^-)[a]
Me	H	18.7	18.9
CH_2Ph	H		18.2
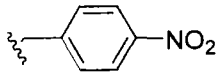	H	17.8	17.8
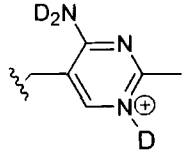	H	17.7	17.6
CH_2CN	H	16.9	16.9
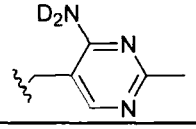	CH_2CH_2OH		18.0

(a) pK_a for the thiazolium C2 proton in H_2O, calculated from rate constants for catalysis by D_2O and DO^-.[52]

Alder *et al*[57] studied the basicity of 1,3-di-*iso*propyl-4,5-dimethylimidazol-ylidene **(65a)** (see Scheme 2.10) in deuterated DMSO and THF. The imidazolium ylide **(65)** was generated quantitatively in DMSO solution by deprotonation of the conjugate acid **(66)** using potassium hydride (see Scheme 2.10). A hydrocarbon indicator RH was then added

to the ylide solution and equilibrium occurred. The position of the equilibrium was determined by ^{1}H NMR spectroscopy. This showed that ylide **(65a)** deprotonated fluorene (pK_a = 22.9) and 2,3-benzophenone (pK_a = 23.5), but not 9-phenylxanthrene (pK_a = 27.7) or triphenylmethane (pK_a = 30.6). Hence a pK_a value of 24.0 (± 3.0) was determined for the conjugate acid of 1,3-di-*iso*propyl-4,5-dimethylimidazol-2-ylidene in DMSO solution. However corrections were not made for ionic strength or ion pairing in DMSO. In THF, ylide **(65a)** was found to have decreased basicity, as it could deprotonate indene (pK_a = 20.1) and 9-phenylfluorene (pK_a = 18.5) but not fluorene. This is possibly due to favourable formation of the formally neutral ylidic species in solvents of lower polarity such as THF.

Investigations were made by Kim and Streitweiser[58] of the basicity of 1,3-di-*t*-butylimidazol-2-ylidene **(65b)** (see Scheme 2.10) in THF and DMSO using a method for deducing the dissociation constant of ion pairs to free ions from UV-vis spectroscopy. This study also demonstrated the increase in basicity of ylide **(65b)** in DMSO (pK_a = 22.7) compared to the "effective basicity" found in THF (ion pair pK = 20). This difference in basicity may be attributed to the appreciable ion-pairing which occurs for a number of salts in DMSO, and reflects the greater stabilization of the protonated form of the carbene by hydrogen bonding in DMSO rather than the carbene itself.

Scheme 2.10

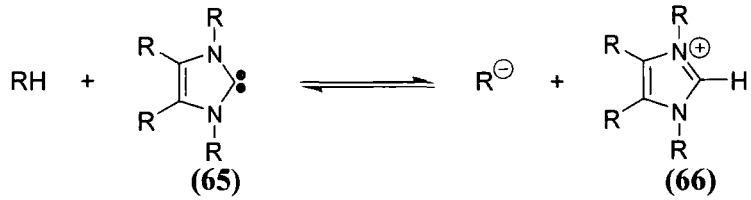

(65) **(66)**

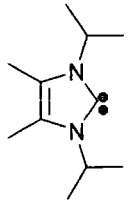

(65a)

RH = Fluorene
Benzophenone
Triphenylmethane
Indene
9-phenylfluorene

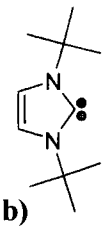

(65b)

RH = Cyclopentadiene
Dimethyl sulfoxide
Dimethyl ether

Amyes *et al*[55] determined the pK_a values for imidazolium ions **(59)**, **(61)**, **(62)** and **(63)** in water by combining the second-order rate constants for deuteroxide ion-catalyzed H/D exchange at C2-H with the rate constant for the reverse protonation of the carbenes by water as described in Section 2.2. The resulting pK_a values were: 1,3-bis((S)-α-methybenzyl)benzylimidazolium chloride, **(63)**, (21.2), 1,3-diethylbenzylimidazolium iodide, **(62)**, (21.6), 1,3-dimethylimidazolium iodide, **(59)**, (23.0), imidazolium iodide, **(61)**, (23.8). A small decrease in pK_a by 1.4 units can be seen on benzylation of the imidazolium ions, and the effect of N-methylation of imidazolium iodide **(61)** to give **(59)** on the pK_a value is also small.

An estimate of the pK_a value for the conjugate acid of dimethoxycarbene **(67)** was made by means of a thermodynamic cycle[59] which interrelates pK_a, pK_R and pK_{H2O} (see Scheme 2.11). The equilibrium for the reaction of the carbocation **(68)** with water, to form the corresponding alcohol **(69)** is represented by pK_R whereas pK_{H2O} relates to the equilibrium for hydration of carbene **(67)** to give the alcohol **(69)**. A pK_a value of 15.5 for carbocation **(68)**, can be estimated using Equation 2.4.

Scheme 2.11:

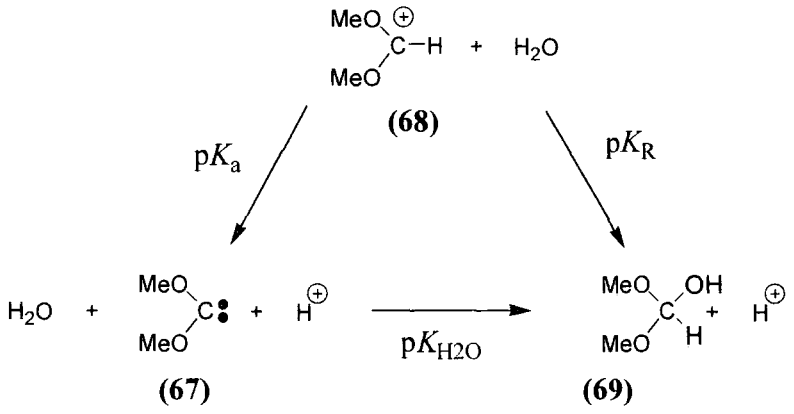

$pK_a = pK_R - pK_{H2O}$ **(Equation 2.5)**

In comparison with other azolium ions such as thiazolium ions (Figure 1.12, pK_a 17 – 19)[52] and imidazolium ions **(59)** (pK_a = 24 in DMSO)[57] and **(65)** (pK_a = 23 in water)[55] these results were suggested to be consistent with the expected trend that azolium ions are more stable than dimethoxy cations, as a nitrogen substituent is more electron donating than oxygen or sulfur.

Recently a computational study by Dixon and Arduengo[60] reported accurate predictions of the heats of formation for the unsubstituted model compound **(70)** as well as the ability of this carbene to react with other species such as a proton, a hydride ion or H_2. This was calculated using high levels of ab initio electronic structure theory. The proton affinity of the carbene was reported to be 250.5 kcal mol^{-1} at 298 K, which is very high for such a simple compound with no substituents.

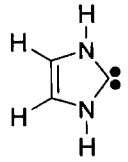

(70)

To date there has been no systematic study of the effects of the change in N-substituent or on the acidity of the C2-H of imidazolium ions. In particular there are no published literature data of the acidity of the non-aromatic analogous imidazolinium ions.

By comparison of the acid-base equilibria, steric effects such as ring strain on carbene stability will be examined. There is little or no information on how structural changes would affect nucleophilicity of N-heterocyclic carbenes, knowledge of their related basic character is limited. As carbenes are implicated as intermediates in many reactions, the ability to predict their basicities has implications for experimental design of synthetic procedures. A better understanding of the factors affecting the basicity and nucleophilicity of N-heterocyclic carbenes and their interrelations would have great potential for future synthetic applications and biological exploitations. Relative basicities may be predicted by comparing pK_a values for the conjugate acid azolium ions.

2.1.10 Applications of N-heterocyclic carbenes.

The vacant orbital in diaminocarbenes is of very high energy due to the strong π-donation of the amino substituents. Consequently they are strong nucleophiles, but very weak electrophiles. This is especially true of N-heterocyclic carbenes (NHCs) which have many catalytic applications in organic and inorganic chemistry. In the last decade the rise in the use of NHC ligands in organometallic catalysis has been so marked that this class of ligands can now be considered as broadly catalytically useful, comparable with cyclopentadienyl and phosphine ligands. Perhaps the best example of the beneficial effect of NHC ligands is the later generation Grubbs alkene metathesis catalysts, **(71)**,[61, 62] where replacement of one PCy_3 (Cy = cyclohexyl) of the classic bis-phosphine ruthenium catalyst with an NHC results in a great improvement in activity. At first, NHCs were considered as mere phosphine mimics, however now it is clear that NHCs have a chemistry that is original, novel, useful and much more complex than originally supposed. Their electronic properties are well illustrated in metallocene chemistry with the isolation of 14-electron chromium(II) complexes,[63] **(72)**, and biscarbene complexes by displacement of a Cp ligand of nickelocene,[64] **(73)**.

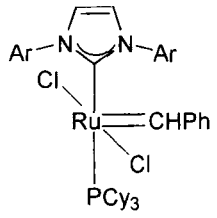

(71)

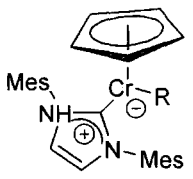

(72)

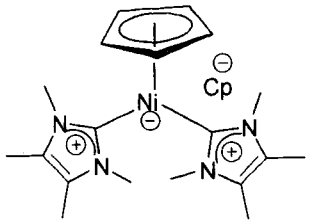

(73)

Carbene complexes are classed as either Fischer-type complexes or Schrock-type complexes depending on the nature of the formal metal-carbon double bond (See Figure 2.13). Fischer-type complexes have a metal-carbon bond with donor-acceptor character resulting from the superposition of carbene to metal σ-donation and metal to carbene π-backbonding. Schrock-type carbene complexes have an essentially covalent metal-carbene bond resulting from the interaction of a triplet carbene with a triplet metal fragment. Consequently low-valent metal fragments and carbenes with at least one π-donor group would produce Fischer-type complexes, while metals in high oxidation states and carbene ligands bearing alkyl substituents would produce Schrock-type complexes.

Figure 2.13:

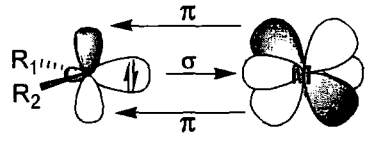

donor-acceptor bonding in
Fischer–carbene complex

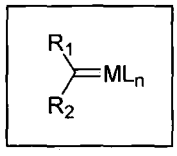

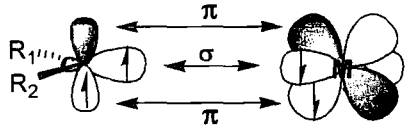

covalent bonding in
Schrock–carbene complex

N-Heterocyclic carbene complexes may be classified as Fischer-type complexes due to the presence of two π-donor substituents. Imidazol-2-ylidene was first suggested to bind to a transition metal center through σ-donation only.[10] This notion was further corroborated by calculations on transition metal complexes of the type ClM ← NHC, M = Cu, Ag, Au.[65] However, a significant amount of π-interaction between group 11 metals and NHC ligands was recently proposed on the basis of structural data.[66, 67] This proposal was further supported in theoretical calculations and the π-back-bonding

interactions for a diaminocarbene model compound were estimated to contribute approximately 15–30% of the complexes overall orbital interaction energy.[68]

Structural data obtained from single crystal X-ray diffraction studies show little to no variation in geometric detail of NHC ligands from one complex to another. The internal angle at the carbon atom increases slightly on coordination of the carbene to the metal centre and the N-C distances also increase on coordination so as to be in between the N-C distance of the free carbene and the parent imidazolium salt.

2.1.11 Catalytic applications

Early comparisons of NHCs with the commonly known ligands such as phosphines has lead to widespread investigation of the catalytic activity of organometallic complexes containing both imidazole-2-ylidene and saturated imidazolin-2-ylidenes ligands. In organometallic chemistry this has resulted in the use of metal carbene complexes in Heck-type reactions including the Mizoroki-Heck reaction itself and related reactions such as Sonogashira coupling. Also investigated are the reactions of various aryl halides with amines (Buchwald-Hartwig amination) organomagnesium (Kumada-Tamao-Corriu reaction), organoboron (Suzuki-Miyaura reaction), organosilicon, and organotin (Stille reaction) reagents.[28]

N-heterocyclic carbenes have proven extremely useful in olefin metathesis, as supporting ligands in ruthenium-catalyzed furan synthesis,[69] and in hydrosilation, hydrogenation and hydroformylation reactions of olefins.[70] Investigations have also focused on NHC-based chiral systems.[71]

2.1.11.1 Heck-type coupling reactions

Palladium carbene complexes, such as complexes **(74)** and **(75)**, have proved successful as catalysts for the Heck olefination of aryl halide and related C-C coupling reactions (see Scheme 2.12). Along with high oxygen and moisture tolerances and negligible carbene dissociation, these complexes exhibit a high thermal and hydrolytic durability associated with extremely stable M-C bonds.[18]

Scheme 2.12:

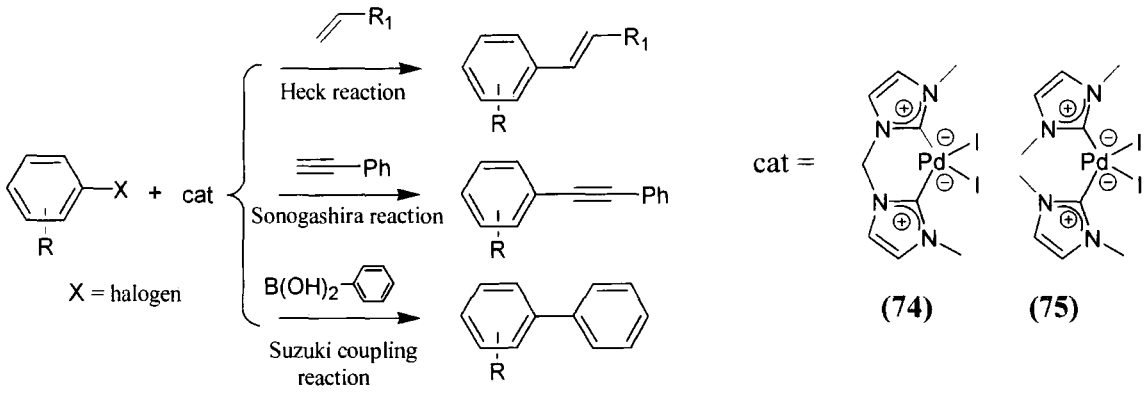

The Sonogashira reaction – the coupling of terminal alkynes with aryl or vinyl halides in a palladium-catalyzed reaction – was not generally applicable to alkyl electrophiles. Recent work by Eckhardt *et al*[72] has established that Pd/N-heterocyclic carbene based catalysts are effective for these reactions with both primary alkyl bromides and iodides under mild conditions. Particularly, the use of an N-adamantyl-substituted imidazole derived carbene ligand proved effective for coupling n-nonyl bromide and 1-octyne where the use of numerous phosphine ligands failed to produce reaction.

2.1.11.2 Hydrosilation reactions

The hydrosilation of terminal alkenes and alkynes and ketones has been known to be catalyzed by carbene-metal complexes for some time.[10] The reaction, catalyzed by rhodium(I)-carbene complexes, (where NHC = imidazol-2-ylidene) such as [RhC(η^4-1,5-COD)(NHC)], [RhCl(PPh_3)$_2$(NHC)], and [RhCl(CO)(PPH_3)(NHC)], results in selective anti-Markovnikov addition for the silane (see Scheme 2.13). These catalysts again demonstrate high stability, with long lifetimes and negligible decomposition of catalyst,

Scheme 2.13:

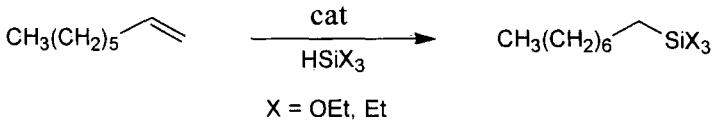

An increase in rates of hydrosilation of alkynes is also seen in the presence in ultraviolet light. In comparison, hydrosilation reactions using analogous rhodium-phosphine

catalysts [$RhCl(PPh_3)_3$] produced much lower yields, with no observed response to UV light.

2.1.11.3 Olefin metathesis

Olefin metathesis is a widely used reaction in organic and polymer chemistry and encompasses ring opening polymerization (ROMP), acyclic diene methathesis (ADMET) and ring closing metathesis (RCM) of acyclic olefins. Of the three catalyst types available for this reaction, the most effective and versatile is the second generation Grubbs catalyst **(79)**.[73] The substitution of a phosphine group on **(78)** for an NHC ligand created a catalyst which exhibited a similarly high reactivity to the Mo and W complexes **(77)** developed by Schrock, while maintaining the high functional group tolerance and air and moisture stability of the first generation Grubbs catalyst **(78)**.[73]

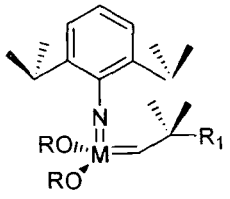

(77)

M= Mo, W
R = alkyl, ary
R_1 = Me, Ph

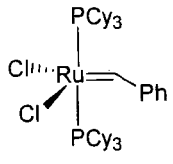

(78)

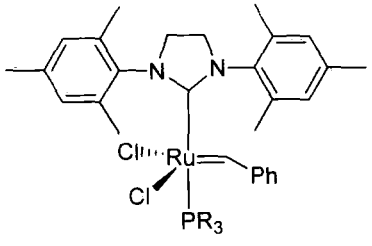

(79)

R = *p*-$CF_3C_6H_4$, *p*-ClC_6H_4, *p*-FC_6H_4, C_6H_4, *p*-$CH_3C_6H_4$, *p*-$CH_3OC_6H_4$

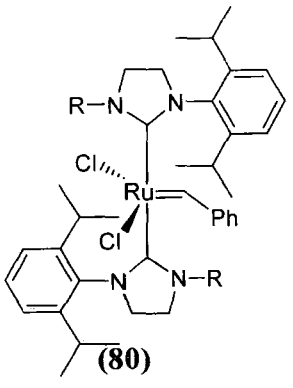

(80)

R = Me, Cy

Studies were carried out by Grubbs *et al*[73,62] on the mechanism and activity of ruthenium olefin metathesis catalysis. It as determined that, in the bis-phosphine catalysts, initiation of the catalytic cycle is preceded by dissociative substitution of one of the phosphine ligands (PR_3, see Scheme 2.14) from species **(81)** with an olefin substrate. This phosphine dissociation is a critical step along the olefin metathesis reaction coordinate. From a study on the relationship between phosphine ligand donor strength relative to the rate of dissociation of the ligand from catalyst, it was found that species with bulky and

electron-donating phosphine ligands produced the highest catalytic activity. The increased trans-effects of the larger and more basic phosphine ligand were believed to promote rapid dissociation of the second phosphine ligand to produce the reactive fourteen-electron species, **(82)**, which then entered the catalytic cycle (k_2). However recoordination of PR_3 was found to be competitive with substrate binding ($k_{-1}/k_2 >> 1$). The introduction of an N-heterocyclic carbene ligand such as in **(79)** showed that these larger and more electron-donating NHC ligand produced significant increases in catalytic activity. It was found that although dissociation of the phosphine (k_1) from these NHC-containing catalysts was relatively inefficient compared to the bis-phosphine complexes, coordination of the olefin occurs much more readily compared to rebinding of PR_3 ($k_{-1}/k_2 \sim 1$ and [olefin] is high). Thus the NHC complexes produce a greater olefin metathesis turnover before recombination the phosphine. Thus the presence of an NHC ligand increased the lifetime of the reactive species **(82)**, leading to an increased turnover of substrate relative to the corresponding phosphine analogue. Overall, introduction of the NHC ligand dramatically increased the activity and efficiency of the catalyst.

Later studies have focused on modification of the NHC ligand rather than the phosphine with a view to increasing the application of the catalyst.[74] Recent research by Ledoux *et al*[75] on N-alkyl-N'-mesityl-substituted NHCs as ligands showed substantial change from alteration of the amino group such as in catalyst **(80)**. Results showed an increase in reactivity due to increased rates of dissociation of the NHC ligand that are comparable to that of phosphine ligands, however this also resulted in a decrease in stability of the catalyst.

Scheme 2.14:

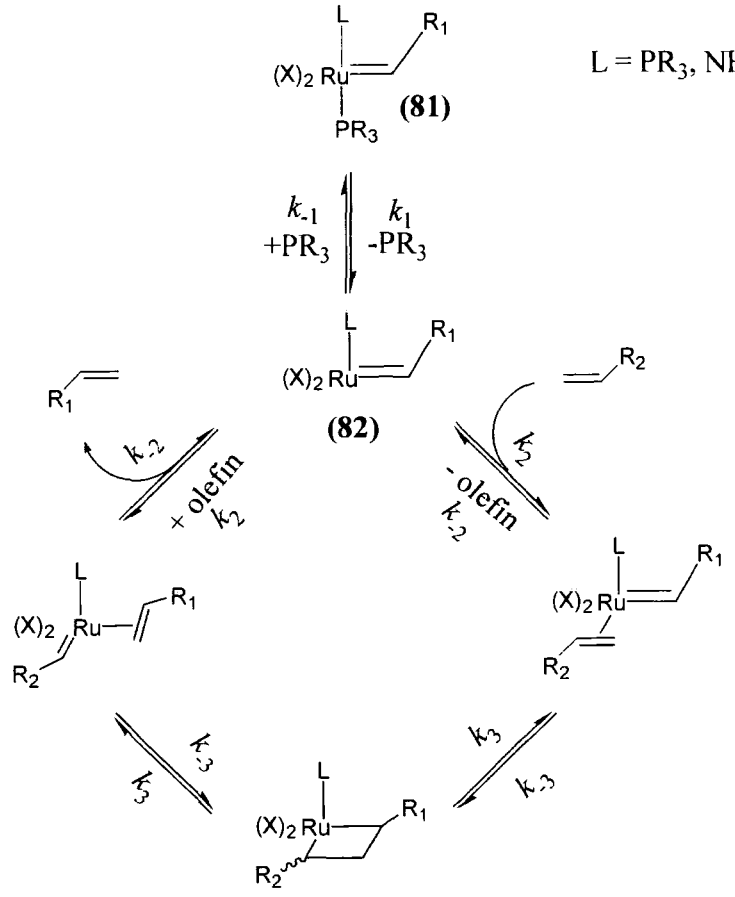

2.1.11.4 Asymmetric catalysis

Attempts to make chiral N-heterocyclic carbene ligands have focused on generation of chiral centres at C4 and C5 of the imidazolinyl backbone, or at a position on the nitrogen substituents, commonly for imidazolyl systems. These chiral carbene derivatives have been used directly as organocatalysts or more commonly have been incorporated in metal complexes such as ruthenium complex **(83)** for asymmetric organometallic catalysis.

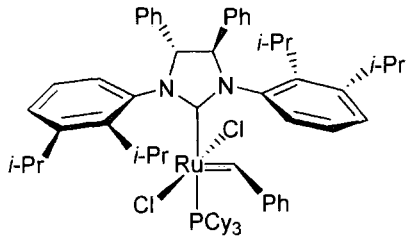

(83)

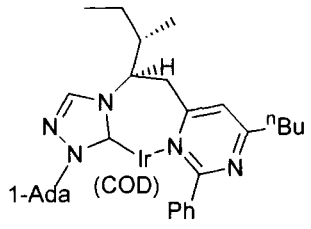

(84)

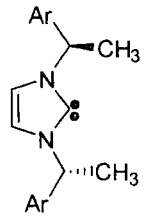

(85)

Over the past two decades several metal complexes have been made containing these types of ligands including triazole based analogues. Enantiomerically pure complexes featuring chiral metal centres, chiral N-substituents and chiral ring frameworks or backbones have been isolated and tested in asymmetric catalysis.[71] However progress has been limited due to the lack of a guiding paradigm for ligand design. Until recently applications were mostly limited to enantioselective hydrosilation[76] and Mizoroki-Heck reactions.[77] However work by Chen *et al*[78] on hydrogenation of unfunctionalized alkenes using iridium complex **(84)**[78] has also produced promising results. Suzuki *et al*[79] have investigated asymmetric acylation of 1-(1-naphthyl)ethanol achieving up to 68% ees using catalyst **(85)**.

2.1.11.5 Biological relevance

The imidazole motif is encountered frequently in living systems, sparking interest in potential complex formations of NHCs and metals from bioinorganic chemists. The purine bases in DNA and RNA as well as the amino acid histidine contain the imidazole moiety, the latter playing an important role as a nucleophilic catalyst in proteins and enzymes.[19]

NHC-metal complexes may be formed from caffeine **(86)** purine **(87)** and porphyrin **(88)** precursors. Through investigation of the properties of these complexes, possible methods for formation of complexes under physiological conditions or *in vivo* has been addressed. The carbene conjugate bases of **(86)** and **(87)** produce metal–NHC complexes with

Ruthenium, mercury and gold giving some possible explanation for the mutagenicity of such metals.[19]

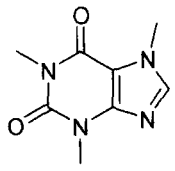

(86)

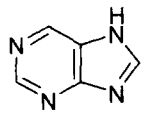

(87)

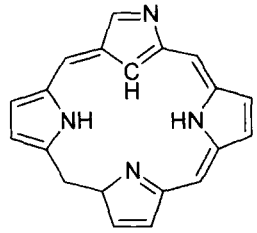

(88)

Porphyrins and their respective metal complexes occur as active sites in a number of enzymes. Isolation of porphyrins such as **(88)** complexed with palladium, silver and copper has been reported and studied with regard to their similarity to NHC complexes.

The imidazole moiety is also found in many natural products isolated in the search for anticancer agents and novel compounds for the pharmaceutical industry. One of the most abundant sources of new material is sponges such as those from the genus *Leucetta*, which have provided compounds exhibiting antitumour and cytotoxic properties including the biologically active imidazole alkaloid *Isonaamidine E*, a yellow amorphous solid **(89)**.[80]

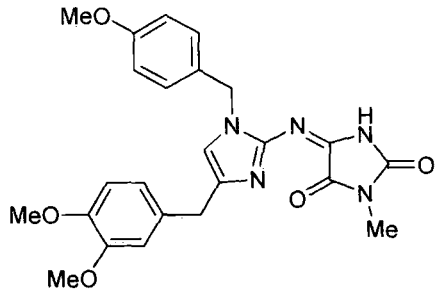

(89)

2.1.11.6 Thiamin-dependent enzyme reactions

Acceleration of reaction rates through covalent catalysis takes place through the transient formation of a catalyst-substrate covalent bond, usually formed by the reaction of a nucleophilic group on the catalyst with an electrophilic group of the substrate. Many amino acid sidechains of enzymes may function as covalent nucleophilic catalysts *e.g.* the

imidazole side chain of histidine. Several coenzymes function in association with their apoenzymes as covalent catalysts. One such coenzyme is thiamine **(90A)** and pyrophosphate derivative **(90B)** (see Figure 2.14).

Figure 2.14:

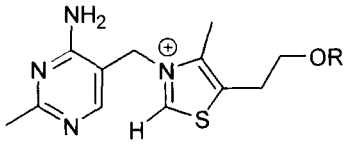

(90) acidic proton

(A) Thiamin: R = H

(B) TPP : R = 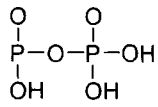

Thiamin **(90A)** and pyrophosphate derivative **(90B)** contain substituted pyrimidine and thiazolium heterocycles. Both function as coenzymes for the decarboxylation of α-keto acids such as pyruvate decarboxylation,[81] and for transketolase reactions. Thiamin (Vitamin B_1) **(90A)** is a naturally occurring thiazolium salt. Activity of thiamin **(90A)** as a catalyst in both thiamin-dependent enzyme reactions and non-enzymatic model reactions is initiated by the base-catalyzed abstraction of the C2-H (acidic proton) forming a thiazolium ylide. This very reactive thiazolium ylide or dipolar carbanion is both a potent carbon nucleophile and a reasonably stable leaving group and is the active form of the coenzyme.

The ability of the ylidic form of the thiazolium ring in thiamin **(90A)** to add to carbonyl groups and act as an electron-sink, makes it the favoured coenzyme in α-keto acid decarboxylation reactions. This essential vitamin is neither synthesized in the body or stored in significant amounts in tissues and so must be obtained from dietary sources. In humans a deficiency in vitamin B_1 leads to a fatal condition known as Beriberi.[81]

To effectively act as a catalyst in biological systems the thiazolium ylide generated through abstraction of the acidic proton of thiamin (see Figure 2.14) must be generated under physiological conditions. Mizuhara reported the catalytic action of thiamin in water at room temperature at an optimum pH of 8.4 for the decarboxylation of pyruvic acid.[82] Breslow[83] illustrated how catalysis of formation of benzoin from benzaldehyde is dependent on the formation of a stable ylide. Breslow demonstrated the generation of

this ylide in water by observing the C2–H/D exchange reaction of 3,4-dimethylthiazolium bromide at pH 7 with a half life of approximately 20 minutes. It was noted however that certain thiazolium ions, which were unstable in basic solution, were ineffective catalysts. This was due to the formation of a water adduct or a ring opened hydrolysis product. The ability of thiamin to form enough of the stable ylide, without undergoing hydrolysis under physiological conditions is related to its acidity constant indicating a delicate balance in these systems exists. It was suggested that enough inductive stabilization of the ylide of thiamin is provided by the benzylic N-substituent, shifting the equilibrium more in favour of ylide formation.

Many structural factors influence the acidity of thiazolium and related azolium ions. The governing mechanisms for catalytic activity of these ions in biological reactions is of great interest, as is their rate of C2-H exchange, for a greater understanding of biological systems. To this end, thiazolium and possibly imidazolium ions and their dependent enzymes may be studied and developed.

2.1.11.7 Medicinal properties

Along with the interest in natural products containing the imidazole moiety, NHC metal complexes have been investigated for their possible pharmaceutical properties[19] In general, no relevant dissociation equilibria are expected under physiological conditions due to the strong metal-ligand bond. This enables these complexes to be used to deliver tailor made structures to cells *in vivo*. Complexes such as rhodium(I) [(η^4-COD)Rh(NHC)Cl] and ruthenium(II) [(η^6-cumene)Ru(NHC)Cl_2] (where NHC imidazolidin-2-ylidene) have exhibited some antimicrobial activity against *Gram*-negative *Escherichia coli* and *Pseudomomonas aeruginosa* bacteria with some promising results. However more work is needed for the future therapeutic use of these complexes.

Many drugs based on the imidazole ring system have been synthesized. In the body the monosubstitued imidazole histamine, **(91)**, is derived from the essential amino acid histidine **(92)** by decarboxylation and both are intimately involved in catalysis in the body

requiring proton transfers. Over the last hundred years the numerous effects of histamine have been investigated. Histamine has effects on smooth muscle contraction and lowering of blood pressure. Upon injury histamine is released from skin cells. It is also involved in allergic reactions and regulation of gastric acid secretion.

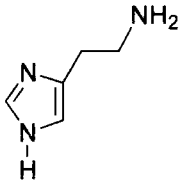

(91)

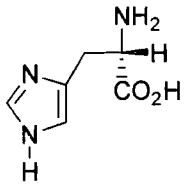

(92)

Antihistamines such as cimetidine, **(93)**, were developed in the 1970s. This blocked both H_1 and H_2 histamine receptors and was the first non-surgical treatment for peptic ulcers. Another example is the drug 2-nitroimidazole (azomycin) **(94)**, a naturally occurring antibiotic, which is active against intestinal infections. Metronidazole, **(95)**, is an antiprotozoal, used in the treatment of amoebic dysentery and as a radiosensitizer in X-ray therapy. Antihypertensive agents have been investigated such as losartan, **(96)**, and antifungal agents such as bifonazole, **(97)**.

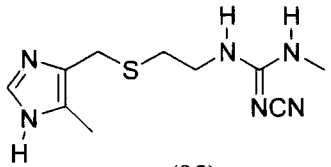

(93)

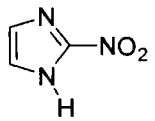

(94)

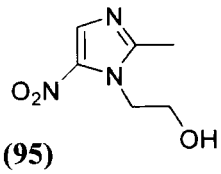

(95)

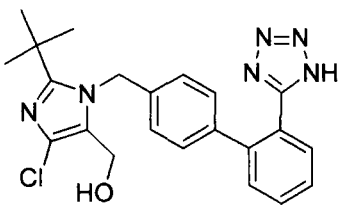

(96)

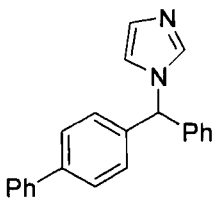

(97)

Silver has been recognized as an antimicrobial agent for centuries[84] The use of silver complexes such as silver nitrate and silver sulfonamides is well established in the treatment of burns and other wounds. Silver-carbene complexes such as **(98)** have proved useful as metal transferring agents, allowing a slow release of metal in the infected area and hence increasing effectiveness of the antimicrobial silver. The N-substituents can also be tailored to provide greater solubility in aqueous media.[84]

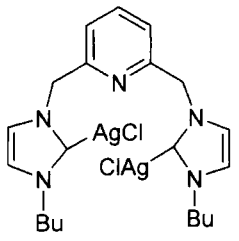

(98)

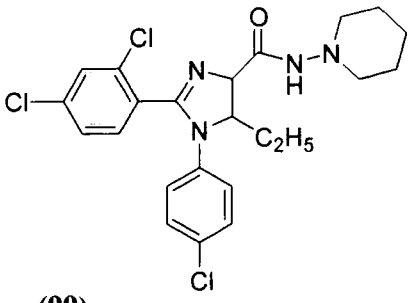

(99)

More recently, imidazole, thiazole and triazole – containing compounds have been investigated as possible CB_1 antagonists, similar to naturally occurring cannabinoids, derived from Indian hemp[85]. These compounds have been used for centuries in medicine and have potential applications in the treatment of neuroinflamatory disorders, cognitive disorders, septic shock, obesity psychosis, addiction and gastrointestinal disorders. In particular the 1,2-diarylimidazoles such as **(99)** have shown positive results in the treatment of hypothermia and hypotension in rodents.

The structure of DNA is a logical starting point in the search for drugs to combat cancer and viruses. Analogues of nucleosides in which heterocycle or sugar has been modified have been produced. Complexes such as acyclovir, **((100) R = H)**, an analogue of 2'-deoxyguanine, **(101)**, is used in the treatment of herpes virus infections, while structurally similar ganciclover **((100) R = CH_2OH)** is used to treat AIDS patients and recipients of organ transplants.

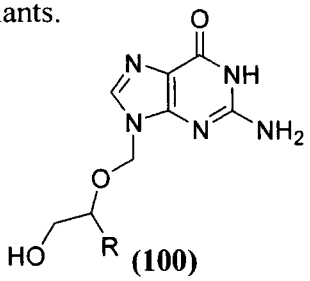

(100)

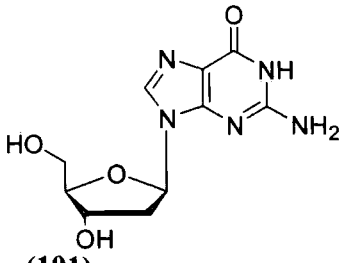

(101)

Despite the ubiquity of imidazoles in biomedical treatments, the exact mechanism of action is unknown. Metal carbene complexes may prove to be significant in enzyme catalyzed processes and in their medicinal effects.

2.2 Results

2.2.1. Synthesis

The synthesis of imidazolium ions **(104)** and 4,5-dihydroimidazolim ions **(106)** was achieved using a multicomponent reaction scheme. The method involved the formation of a substituted glyoxal diimine **(103)** by reaction of glyoxal (either neat or 40% w/w) **(102)** with the appropriate substituted aryl or alkyl amine. Reaction conditions were varied according to the product that was being formed.

Scheme 2.15:

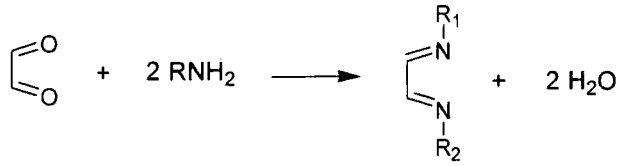

(102) **(103)**

The glyoxal diimine **(103)** could be reacted further to form the required imidazolium or dihydroimidazolium ring. The imidazolium salts **(104)** were prepared by cyclizing the diimine directly by reaction with chloromethyl ethyl ether (Scheme 2.16) The following imidazolium salts were prepared as outlined in Scheme 2.16: 1,3-bis(2,4,6-trimethylphenyl)imidazolium chloride **(109)**; 1,3bis(*p*-methoxyphenyl)imidazolium chloride **(110)**; 1,3-bis(2,6-di-*iso*propylphenyl)imidazolium chloride **(112)**; 1,3-bis(3,5-di-*t*-butylphenyl) imidazolium chloride.

Scheme 2.16:

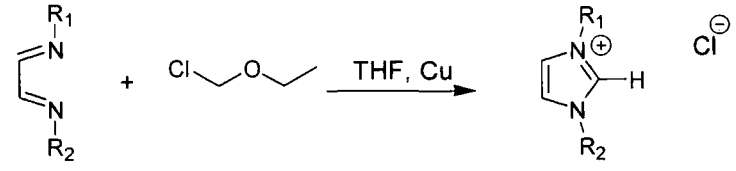

(103) **(104)**

The saturated 4,5-dihydroimidazolium rings were prepared by reducing the diimine **(103)** with sodium borohydride, or lithium aluminium hydride followed by addition of HCl. This resulted in the formation of the corresponding diamine or its hydrochloride salt

(105) (Scheme 2.17).The diamine could then be further reacted with triethyl orthoformate and ammonium tetrafluoroborate to form the 4,5-dihydroimidazolium tetrafluoroborate salt **(106)**.

Scheme 2.17:

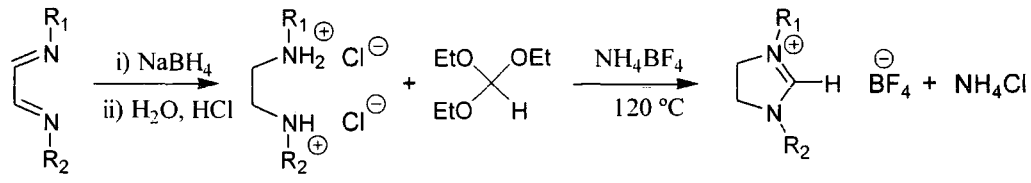

(103) **(105)** **(106)**

The tetrafluoroborate counterion could then be easily exchanged for a chloride counterion using ion exchange chromatography. This increased the solubility of the salts in aqueous solution. Also, where possible, the aim was to have a common anion for all of the imidazolium and dihydroimidazolium ions studied. The following dihydroimidazolium salts were prepared as outlined in Scheme 2.17: 1,3-bis(2,4,6-trimethylphenyl)-4,5-dihydroimidazolium chloride **(116)**; 1,3-bis(*p*-methoxyphenyl)-4,5-dihydroimidazolium chloride **(117)**; 1,3-bis(2,6-di-*iso*propylphenyl)-4,5-dihydroimidazolium chloride **(118)**.

The 1,3-dimethyl-4,5-dihyroimidazolium chloride salt was prepared in a similar manner. The diamine **(108)** was synthesized directly by treating 1,2-dichloroethane **(107)** with a solution of methylamine **(106)** in water[86] (Scheme 2.18). The dimethyl diamine was then reacted further as described above.

Scheme 2.18:

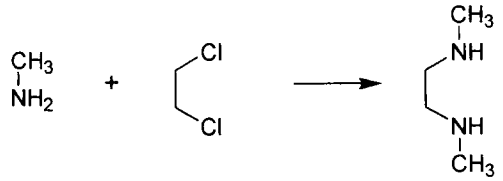

(106) **(107)** **(108)**

2.2.2. Deuterium exchange reactions followed by ^{1}H NMR spectroscopy

The H/D exchange reactions of the imidazolium ions **(109)** – **(115)**, 4,5-dihydroimidazolium ions **(116)** – **(118)** and cyclic/acyclic formadines **(120)** – **(123)** were analyzed using 300, 400 and 500 MHz ^{1}H NMR spectroscopy. The disappearance of the peak due to the C2-H in the ^{1}H NMR spectrum was monitored at 25 °C and mostly at ionic strength I = 1.0 (KCl). In the cases of 1,3-bis(*p*-methoxyphenyl)imidazolium chloride **(110)** and 1,3-bis(*p*-chlorophenyl)imidazolium chloride **(111)**, reactions were run at ionic strength I = 0.5 (KCl) while reactions were run at ionic strength I = 0.25 (KCl) for 1,3-bis(*p*-methoxyphenyl)4,5-dihydroimidazolium chloride **(117)**. This was due to the insolubility of the substrates at higher ionic strength values. From these ^{1}H NMR data the first and second order-rate constants for the deprotonation of substrate by deuteroxide ion in D_2O to give the corresponding diaminocarbene (or ylide) could be estimated.

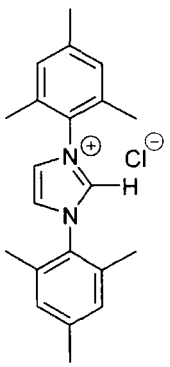

(109)

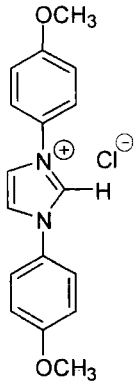

(110)

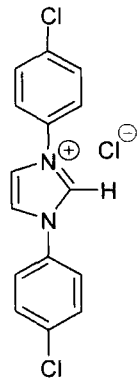

(111)

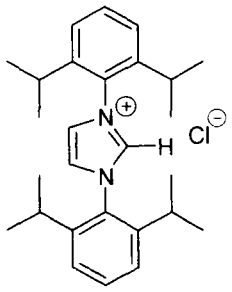

(112)

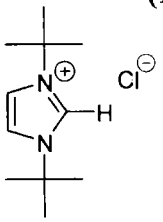

(113)

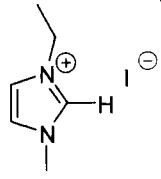

(114)

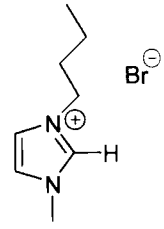

(115)

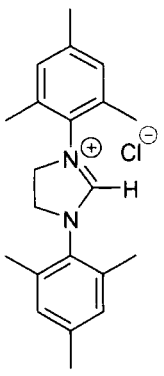

(116)

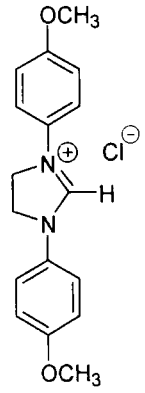

(117)

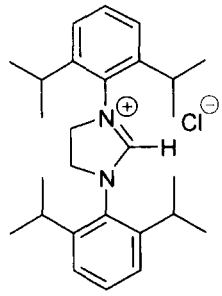

(118)

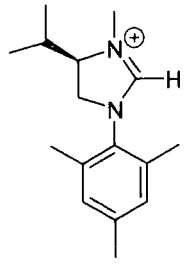

(119)

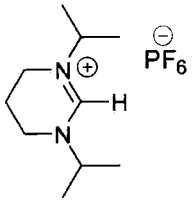

(120)

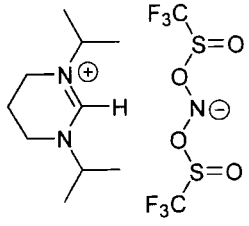

(121)

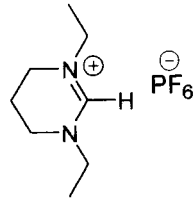

(122)

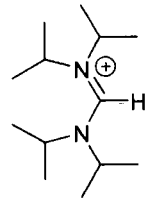

(123)

Scheme 2.19 shows a detailed mechanism for the deuterium exchange reaction of the azolium ions. The azolium ion **(124)** can be deprotonated by a base at the C2 position in D_2O solution to form the corresponding carbene **(126)** or ylide **(125)**. For low azolium ion concentrations, the concentration of DOH formed during this process is negligible in solvent D_2O which means that reprotonation by DOH will also be negligible. Thus carbene formation can be followed by effectively irreversible formation of the deuterium exchange product **(127)**.

It was found that for the following azolium ions a competing hydrolysis reaction occurred in parallel with the deuterium exchange reaction: 1,3-bis(di-*iso*propyl)-4,5,6 trihydropyrimidin-1-ium hexafluorophosphate **(120)**, 1,3-bis(diethyl)-4,5,6 trihydropyrimidin-1-ium hexafluorophosphate **(122)** and tetraisopropyl formadinium hexafluorophosphate **(123)**. A likely mechanism for this hydrolysis reaction is shown in Scheme 2.20.

Scheme 2.19:

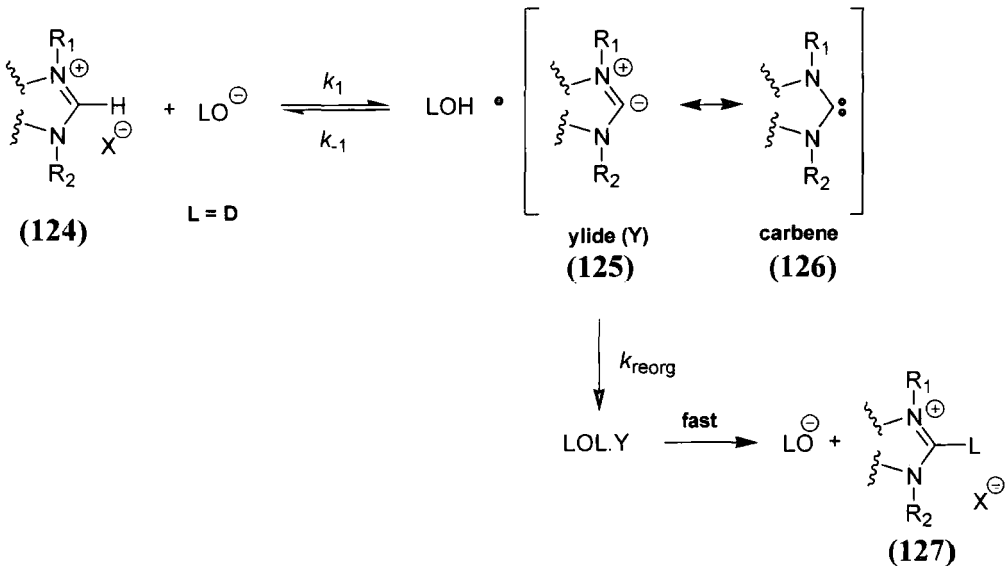

Nucleophilic attack of deuteroxide ion at the iminium carbon of azolium ion **(124)** would give the adduct **(128)**. Ring opening of this adduct by D_2O would result in formation of protonated formamide **(129)**, which could be deprotonated by deuteroxide ion to give formamide product **(130)**. In the case of an imidazolium ion the potential hydrolysis product formamide **(131)** would be a tautomer of the imine **(132)** (Scheme 2.21). However peaks due to predicted hydrolysis products were not observed in ^1H NMR spectra for any of the imidazolium ions **(109)** – **(115)** or the aryl-substituted 4,5-dihydrolimidazolium ions **(116)** –**(119)** during the timescale for the deuterium exchange reactions.

Scheme 2.20:

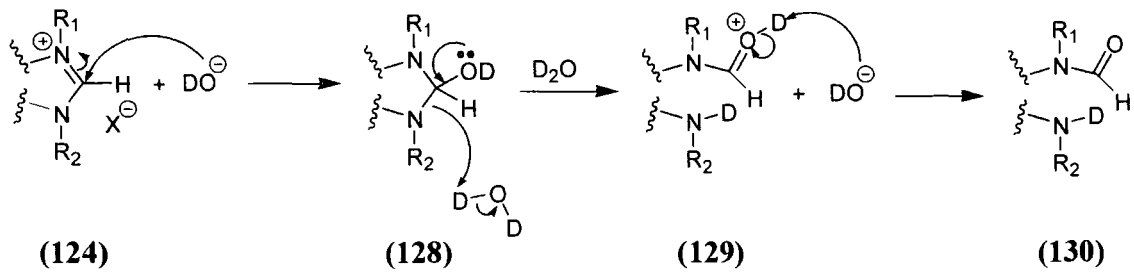

Scheme 2.21:

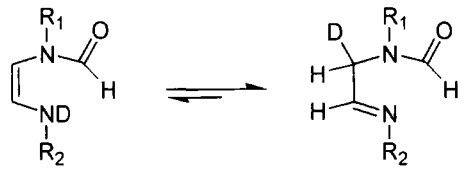

(131) **(132)**

A typical exchange experiment was run in D_2O at 25 °C and ionic strength I = 1(KCl) and was quenched at different time points during the reaction. The signal due to the C2-H of all azolium ions generally appears as a singlet at 7.0 - 9.7 ppm. The signals due to the aromatic imidazolium C4 and C5 protons are in the 7.3 -8.0 ppm range and appear usually as broad singlets for the symmetric substrates, however long range coupling to the C2-H can be observed in some cases. The signal due to the C4 and C5 on the asymmetric aromatic azolium ions appear as doublets in the 7.3 – 8.0 ppm region. The signals due to the 4,5-dihydroimidazolium C4 and C5 protons appear as singlets at 4.0 - 4.6 ppm. The signals due to the ring protons of six membered pyrimidinium ions appear as multiplets at 1 – 4 ppm. In this work no decay of peaks due to exchange of hydrogen for deuterium is seen at any carbon other than at C2. This is seen by comparison over time of all peak areas to a constant peak area due to an internal standard. In the cases of azolium ions **(120)**, **(122)** and **(123)** a competing hydrolysis reaction was observed as already mentioned. For the reaction of these ions, peaks due to hydrolysis products were clearly identifiable and could be quantified.

Two internal standards were required in this work. Generally the internal standard used was tetramethylammonium deuteriosulphate (TMADS). In situations where this could not be used due to overlap of substrate or buffer ^1H NMR peaks with the signal due to TMADS, the alternative internal standard used was *tert*-butanol. The signal due to the twelve methyl hydrogens of the internal standard, tetramethylammonium deuteriosulfate, appears as a broad singlet at 3.0 – 3.2 ppm. Coupling to ^{15}N by the methyl hydrogens is evident by triplet splitting at the top of this singlet in high resolution spectra. The signal due to the nine hydrogens of the internal standard *tert*-butanol appears as a singlet at 1.2 –

1.3 ppm. The hydrogens of the internal standards used do not undergo exchange in the reaction conditions investigated.

The progress of the deuterium exchange reactions was monitored by determining the integrated area of the singlet due to the C2-H over time relative to the integrated area of peaks due to internal standard which is at a constant concentration throughout the experiment. The fraction of substrate remaining, f(s), was determined from Equation 2.6. Competing hydrolysis of some substrates required the f(s) value determined using Equation 2.6 to be corrected for disappearance of the C2-H due to hydrolysis. The hydrolysis product could be quantified by analysis of resolved ^{1}H NMR peaks due to this product

$$f(s) = \frac{(A_{C(2)-H} / A_{Std})_t}{(A_{C(2)-H} / A_{Std})_{t=0}} \qquad \textbf{(Equation 2.6)}$$

The observed pseudo-first-order rate constants for deuterium exchange of the C2-H, k_{obs} was determined as the slope of semi-logarithmic plots of H/D exchange progress against time (Equation 2.7) These plots were linear for the half-lives examined with 4 – 7 data points.

$$\ln f(s) = -k_{obs}t \qquad \textbf{(Equation 2.7)}$$

The pseudo-first-order rate constant for deuterium exchange is formally the sum of the first order rate constants for exchange catalyzed by solvent, deuteroxide ion and buffer base (Equation 2.8).

$$k_{obs} = k_{D2O} + k_{DO}[DO^-] + k_B[B] \qquad \textbf{(Equation 2.8)}$$

The contribution of the buffer term ($k_B[B^-]$, s^{-1}) has been investigated during the course of this work, (Section 2.2.3). General base catalysis of exchange is not detected for several representative substrates, so the buffer term in Equation 2.8 may be neglected.

The value for deprotonation by solvent water (k_{D2O}, s^{-1}) is expected to be considerably lower than the other contributing terms. For thiazolium ions k_{D2O} was estimated to be 1.5 $\times$ 10^{-8} s^{-1}.[52] Imidazolium ions have a significantly slower rate of exchange, with k_{DO} values 20 – 400,000-fold smaller that that for thiazolium ions. Thus the contribution of k_{D2O} to the overall observed rate of exchange (k_{obs}, s^{-1}) is expected to be significantly less for imidazolium ions and so this contributing term will also be neglected.

Hence, the experimentally observed rate constant (k_{obs}, s^{-1}) obtained in this work may be expressed as simply the product of the second-order-rate constant for deuteroxide ion-catalyzed exchange (k_{DO}, $M^{-1}s^{-1}$) and the concentration of deuteroxide [DO^-] shown in Equation 2.9.

$$k_{obs} = k_{DO}[DO^-] \qquad \textbf{(Equation 2.9)}$$

The second-order rate constants for the deuterium exchange of the C2-H for deuterium, catalyzed by deuteroxide ion, (k_{DO}, $M^{-1}s^{-1}$), may be obtained from the slope of the plot of k_{obs} (s^{-1}) against deuteroxide concentration.

2.2.2.1. 1,3-Bis(2,4,6-trimethylphenyl)imidazolium chloride (109)

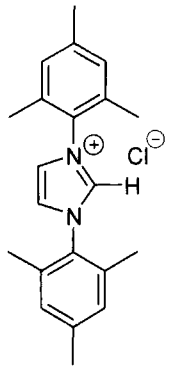

(109)

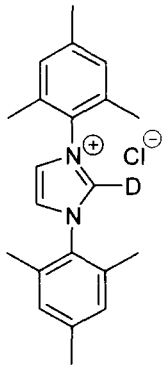

(109')

Rates of deuteroxide ion-catalysed exchange of the C2-H of imidazolium ion **(109)** to form the corresponding deuterated product **(109')** were determined by 300 MHz ^{1}H NMR spectroscopy.

Figure 2.15 shows representative ^{1}H NMR spectra of imidazolium ion **(109)** (5mM, pD 4.69), obtained during the exchange for deuterium of the C2-H in D_2O at 25 °C and I = 1.0 (KCl). Deuterium exchange at C2 results in the disappearance of the singlet peak due to the C2-H at 9.10 ppm (A).This is measured relative to the internal standard peak. The signal due to the equivalent C4-H and C5-H of the imidazole ring usually appears as a broad singlet at 7.78 ppm (B) The peak due to the *m*-CHs on the phenyl ring appears as a singlet at 7.13 ppm (C). The signals due to the *o*-CH_3 and *p*-CH_3 groups appear as singlets at 2.30 ppm and 2.08 ppm respectively. H/D exchange is not observed at any position other than at C2 under these experimental conditions, indicated by comparison of all the signals due to imidazolium ion **(109)** in the spectrum to the internal standard peak at 3.13 ppm (D). In the reaction timeframe there is no change in the total integrated area for the signals due to all other protons relative to the constant peak area of the broad triplet at 3.13 ppm due to the internal standard.

Figure 2.15: Representative ^{1}H NMR spectra at 400 MHz of imidazolium ion (109) (5 mM, pD 4.69), obtained during exchange of the C2-H for deuterium in D_2O at 25 °C and I = 1.0 (KCl). The percentage of deuterium exchange is indicated above each spectrum.

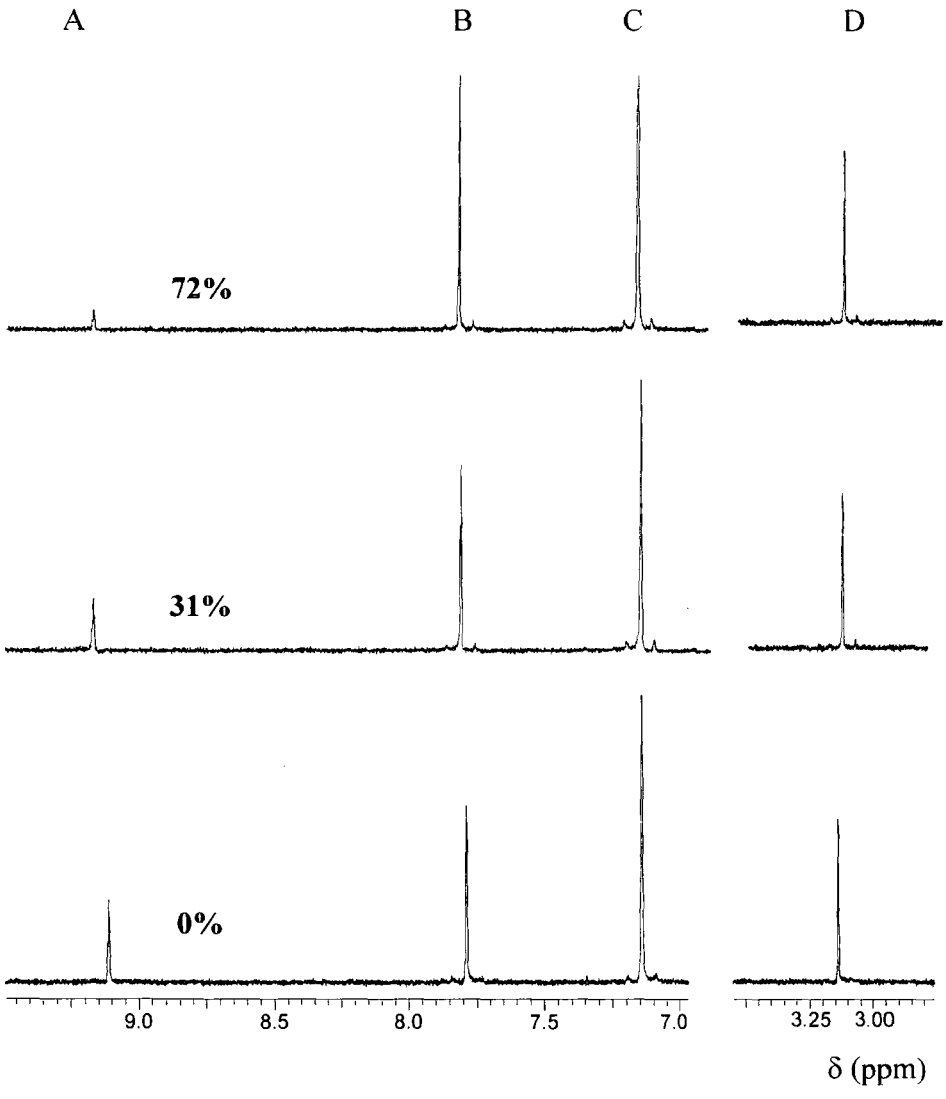

Reaction data and the experimental first-order rate constants for deuterium exchange (k_{obs}, s^{-1}) at different pD values in 50 and 100 mM acetate buffers are shown in Table 2.1, and 2.2 respectively. The values for k_{obs} (s^{-1}) shown in Tables 2.1 – 2.2 were obtained from the slopes of semilogarithmic plots (Figure 2.16 – 2.17) of the fraction of unexchanged substrate against time.

Table 2.1: First-order rate constants for exchange of the C2-H of imidazolium ion (109) for deuterium in acetate buffers (50 mM) in D_2O at 25 °C and I = 1.0 (KCl).

$[DO^-]^a$ (M)	Time (s)	$f(s)^b$	Ln $f(s)$	$k_{obs}{}^c$ (s^{-1})
1.55×10^{-9} (pD 5.93)	0	1.000	0.000	6.55×10^{-5}
	2.16×10^3	0.880	-0.128	
	7.28×10^3	0.679	-0.388	
	9.24×10^3	0.532	-0.630	
	9.89×10^3	0.536	-0.624	
	1.04×10^4	0.504	-0.686	
6.93×10^{-10} (pD 5.58)	0	1.000	0.000	2.71×10^{-5}
	1.20×10^3	0.990	-0.010	
	2.43×10^3	0.986	-0.014	
	4.87×10^3	0.896	-0.110	
	6.15×10^3	0.853	-0.159	
6.01×10^{-10} (pD 5.52)	0	1.000	0.000	2.82×10^{-5}
	1.88×10^3	0.979	-0.021	
	3.68×10^3	0.930	-0.073	
	5.43×10^3	0.873	-0.136	
	7.22×10^3	0.829	-0.187	
	9.08×10^3	0.783	-0.244	
2.32×10^{-10} (pD 5.12)	0	1.000	0.000	1.51×10^{-5}
	3.13×10^3	1.015	0.015	
	4.80×10^3	0.980	-0.020	
	7.20×10^3	0.940	-0.061	
	9.60×10^3	0.908	-0.096	
	1.20×10^4	0.839	-0.175	
8.27×10^{-11} (pD 4.66)	0	1.000	0.000	3.15×10^{-6}
	8.35×10^4	0.746	-0.293	
	1.23×10^5	0.619	-0.480	
	1.74×10^5	0.550	-0.597	
	2.57×10^5	0.447	-0.805	
4.54×10^{-11} (pD 4.40)	0	1.000	0.000	1.81×10^{-6}
	6.00×10^4	0.931	-0.072	
	1.47×10^5	0.735	-0.307	
	2.60×10^5	0.595	-0.520	
	4.92×10^5	0.419	-0.869	

(a) Measurements were made in 50mM acetate buffers in the pD 4.40 – 5.93 range. $[DO^-]$ was calculated using $[DO^-] = (10^{pD-pK_w})/\gamma_{OL}$ with $pK_w = 14.87$, where $\gamma_{OL} = 0.75$ is the activity correction of lyoxide ion under our experimental conditions. (b) The fraction of unexchanged substrate remaining $f(s)$, was calculated according to Equation 2.6 Measurements were made at an initial substrate concentration of 5 mM. (c) The value of the first-order rate constant (k_{obs}) was obtained from the slope of the plot of ln $f(s)$ against time shown in Figure. 2.16a - 2.16b.

Table 2.2: First-order rate constants for exchange of the C2-H of imidazolium ion (109) for deuterium in acetate buffers (100 mM) in D_2O at 25 °C and I = 1.0 (KCl).

$[DO^-]^a$ (M)	Time (s)	$f(s)^b$	Ln $f(s)$	$k_{obs}{}^c$ (s^{-1})
1.79×10^{-9} (pD 6.00)	0	1.000	0.000	7.29×10^{-5}
	4.35×10^{3}	0.745	-0.294	
	1.07×10^{4}	0.464	-0.768	
	1.35×10^{4}	0.372	-0.989	
	1.86×10^{4}	0.259	-1.351	
	2.09×10^{4}	0.222	-1.505	
7.17×10^{-10} (pD 5.60)	0	1.000	0.000	3.16×10^{-5}
	1.21×10^{3}	0.949	-0.052	
	2.51×10^{3}	0.929	-0.073	
	3.62×10^{3}	0.914	-0.090	
	4.95×10^{3}	0.844	-0.170	
	6.01×10^{3}	0.824	-0.194	
6.51×10^{-10} (pD 5.56)	0	1.000	0.000	2.02×10^{-5}
	9.68×10^{2}	0.966	-0.034	
	1.78×10^{3}	0.945	-0.057	
	2.68×10^{3}	0.944	-0.058	
	3.65×10^{3}	0.931	-0.071	
	4.47×10^{3}	0.901	-0.104	
9.01×10^{-11} (pD 4.70)	0	1.000	0.000	2.93×10^{-6}
	6.66×10^{4}	0.759	-0.276	
	9.74×10^{4}	0.682	-0.383	
	2.67×10^{5}	0.496	-0.702	
	4.12×10^{5}	0.272	-1.301	
4.33×10^{-11} (pD 4.38)	0	1.000	0.000	2.21×10^{-6}
	6.94×10^{4}	0.834	-0.182	
	2.40×10^{5}	0.651	-0.429	
	2.59×10^{5}	0.566	-0.569	
	5.01×10^{5}	0.323	-1.131	

(a) Measurements were made in 100mM acetate buffers in the pD 4.38 – 6.00 range. $[DO^-]$ was calculated using $[DO^-] = (10^{pD-pKw})/\gamma_{OL}$ with $pK_w = 14.87$, where $\gamma_{OL} = 0.75$ is the activity correction of lyoxide ion under our experimental conditions. (b) The fraction of unexchanged substrate remaining $f(s)$, was calculated according to Equation 2.6 Measurements were made at an initial substrate concentration of 5 mM. (c) The value of the first-order rate constant (k_{obs}) was obtained from the slope of the plot of ln $f(s)$ against time shown in Fig. 2.17a - 2.17b.

Figure 2.16a: Semi-logarithmic plot of the fraction of remaining C2-H against time for the deuterium exchange reaction of imidazolium ion (109) in 50 mM acetate buffer at pD 5.11, 5.58, 5.52 and 5.93.

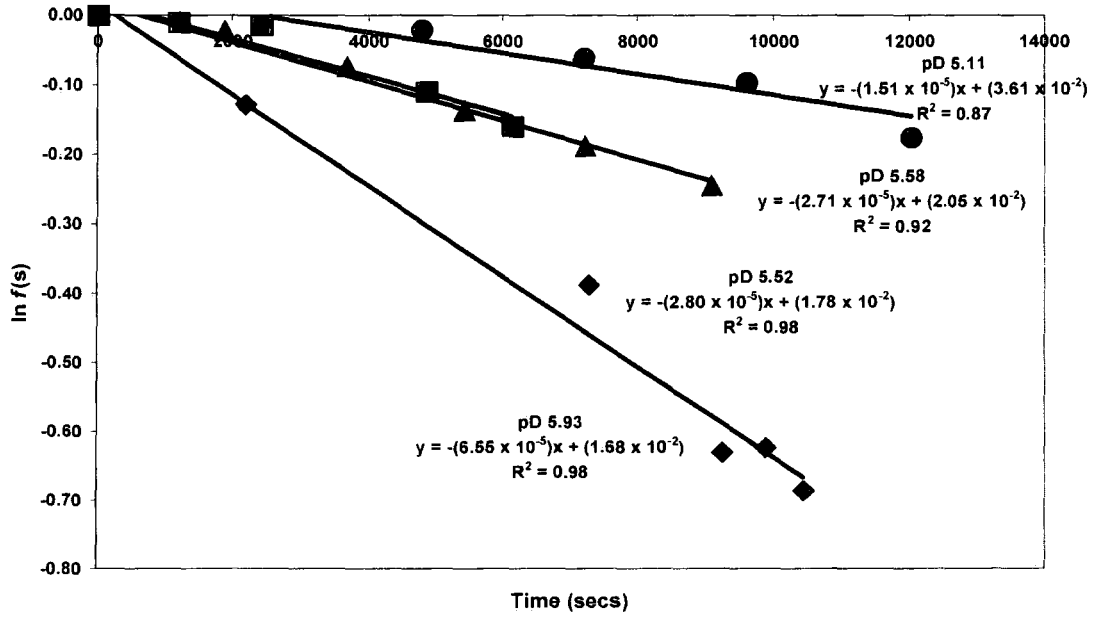

Figure 2.16b: Semi-logarithmic plot of the fraction of remaining C2-H against time for the deuterium exchange reaction of imidazolium ion (109) in 50 mM acetate buffer at pD 4.40 and 4.66

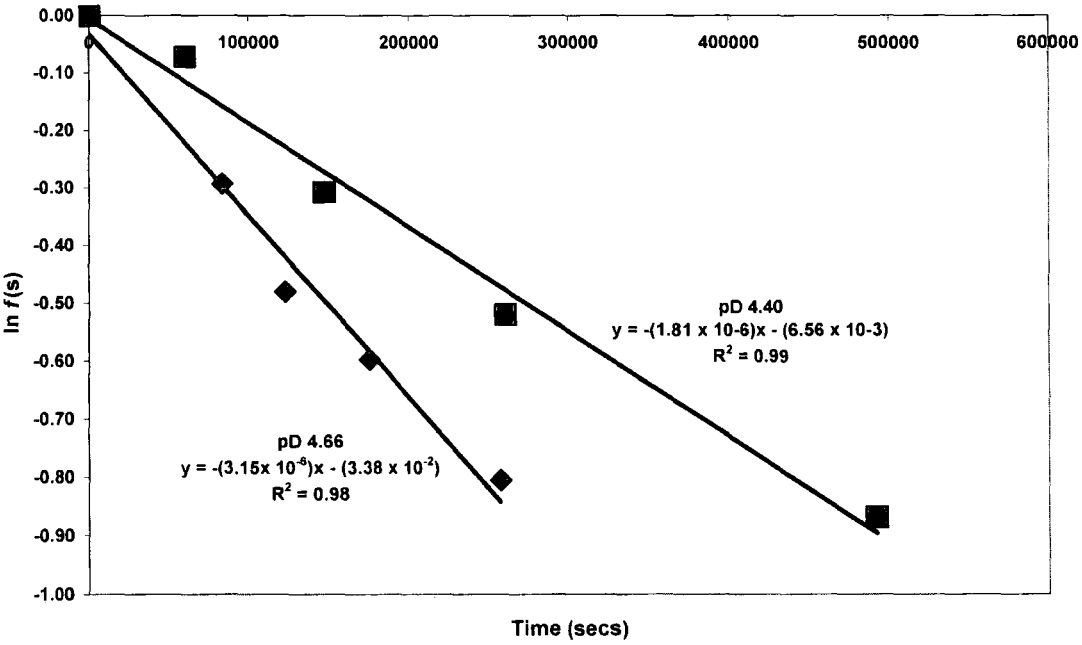

Figure 2.17a: Semi-logarithmic plot of the fraction of remaining C2-H against time for the deuterium exchange reaction of imidazolium ion (109) in 100 mM acetate buffer at pD 5.60 and 6.0.

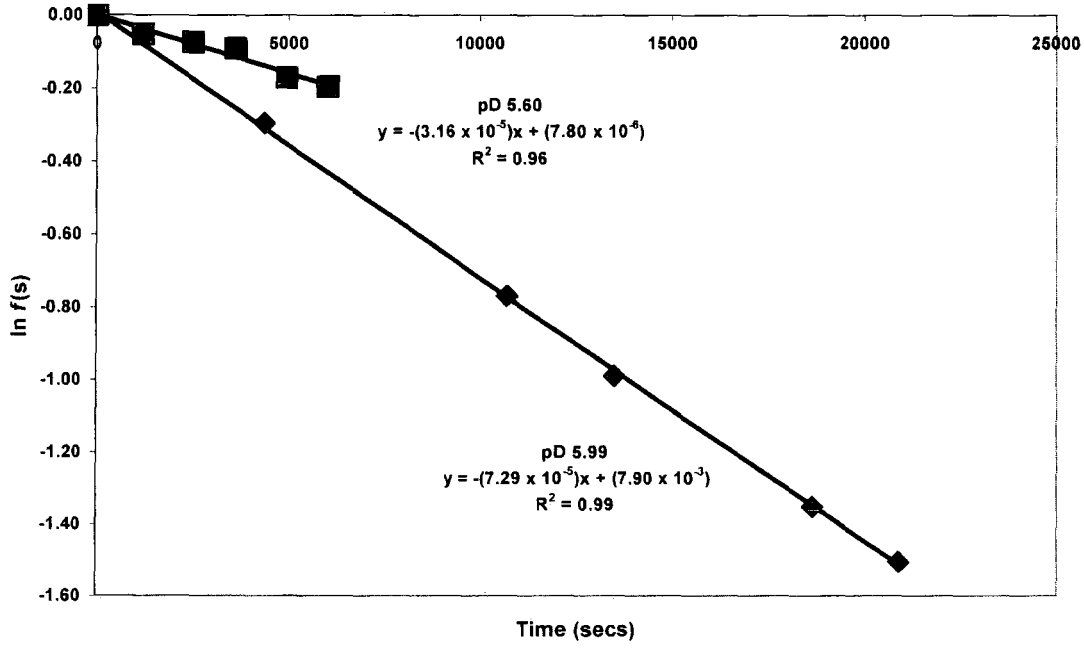

Figure 2.17b: Semi-logarithmic plot of the fraction of remaining C2-H against time for the deuterium exchange reaction of imidazolium ion (109) in 100 mM acetate buffer at pD 4.38 and 4.70.

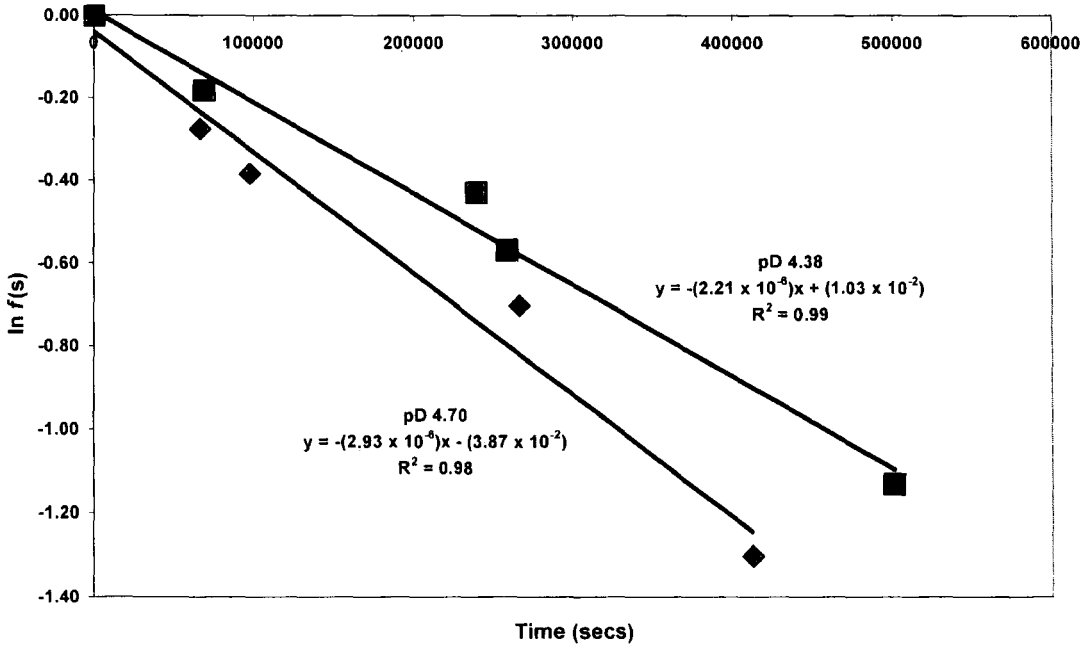

The combined reaction data of imidazolium ion **(109)** in acetate buffer solution is shown in Table 2.3. The second-order rate constant for deuteroxide ion-catalysed exchange was calculated from the slope of the plot of k_{obs} against the concentration of deuteroxide ion as shown in Figure 2.18.

Table 2.3: First and second-order rate constants for exchange of the C2-H of imidazolium ion (109) for deuterium in D_2O at 25 °C and I = 1.0 (KCl).

Buffer Conc. (M)	$[DO^-]$ (M)	k_{obs} (s^{-1})	k_{DO}[a] ($M^{-1}s^{-1}$)
0.1	1.79×10^{-9}	7.29×10^{-5}	4.08×10^{4}
	7.17×10^{-10}	3.16×10^{-5}	
	6.51×10^{-10}	2.02×10^{-5}	
	9.01×10^{-11}	2.93×10^{-6}	
	4.33×10^{-11}	2.21×10^{-6}	
0.05	1.55×10^{-9}	6.55×10^{-5}	4.12×10^{4}
	6.93×10^{-10}	2.71×10^{-5}	
	6.01×10^{-10}	2.82×10^{-5}	
	2.32×10^{-10}	1.51×10^{-5}	
	8.27×10^{-11}	3.15×10^{-6}	
	4.54×10^{-11}	1.81×10^{-6}	

(a) The second-order rate constant, (k_{DO}), was obtained from the slope of the plot of k_{obs} against $[DO^-]$ in Figure. 2.18.

Figure 2.18: Plot of k_{obs} against [DO^-] for the H/D exchange reaction of imidazolium ion (112) in D_2O at 25 °C and I = 1.0 (KCl).

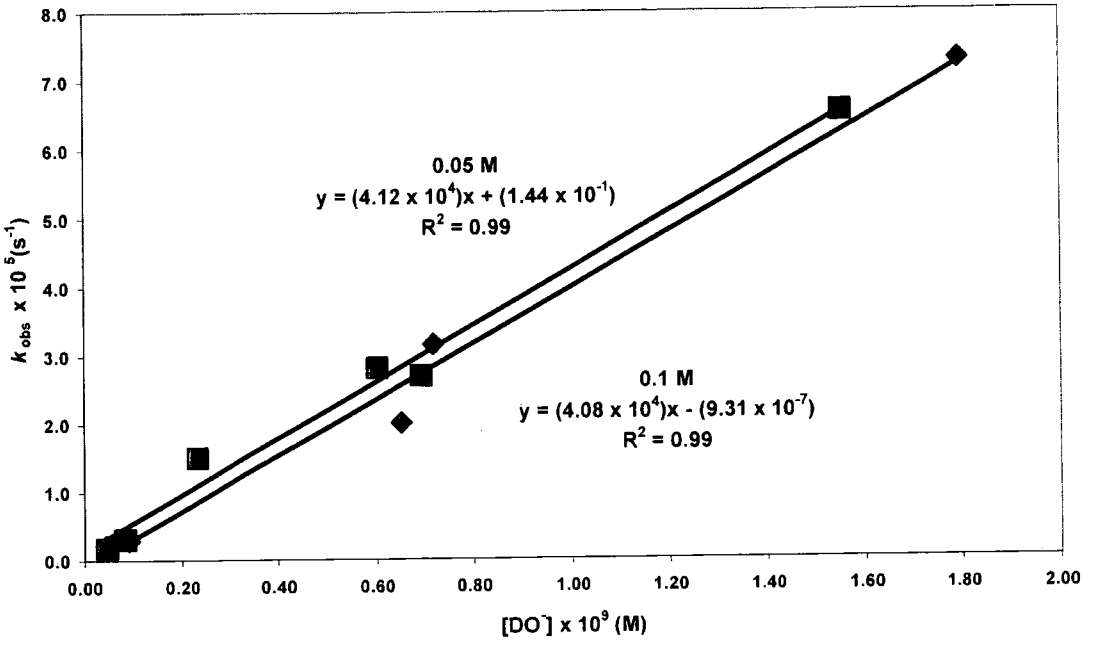

2.2.2.2 1.3-Bis(2,4,6-trimethylphenyl)4,5-dihydroimidazolium chloride (116).

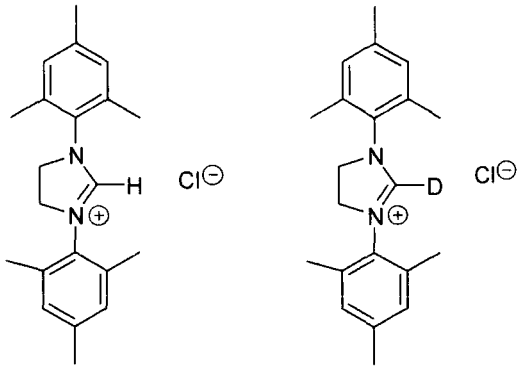

(116) **(116')**

Rates of deuteroxide ion-catalyzed exchange of the C2-H of imidazolinium ion **(116)** to form the corresponding deuterated product **(116')**, were determined by 300 MHz ^{1}H NMR spectroscopy.

Figure 2.19 shows representative ^{1}H NMR spectra of imidazolinium ion **(116)** (5 mM, pH 6.76), obtained during the exchange for deuterium of the C2-H in D_2O at 25 °C and I = 1.0 (KCl). Deuterium exchange at the C2 position results in the disappearance of the singlet peak due to the C2-H at 8.49 ppm (A). This is measured relative to the internal standard peak. The signal due to the *m*-CH on the phenyl ring appears as a singlet at 7.02 ppm (B). The signal due to equivalent C4-H_2 and C5-H_2 produce a singlet at 4.39 ppm (not shown). The signals due to *o*-CH_3 groups and *p*-CH_3 appear as singlets at 2.25 ppm and 2.19 ppm respectively (not shown). H/D exchange is not observed at any position other than at C2 under these experimental conditions, indicated by comparison of all signals due to imidazolium ion **(116)** in the spectrum to the internal standard peak at 3.08 ppm (C). In the reaction timeframe there is no change in the total integrated area for the signals due to all other protons relative to the constant peak area of the broad triplet at 3.13 ppm due to the internal standard.

Figure 2.19: Representative ^{1}H NMR spectra at 300 MHz of imidazolium ion (116) (5mM, pD 6.76), obtained during exchange of the C2-H for deuterium in D_2O at 25 °C and I = 1.0 (KCl). The percentage of deuterium exchange is indicated above each spectrum.

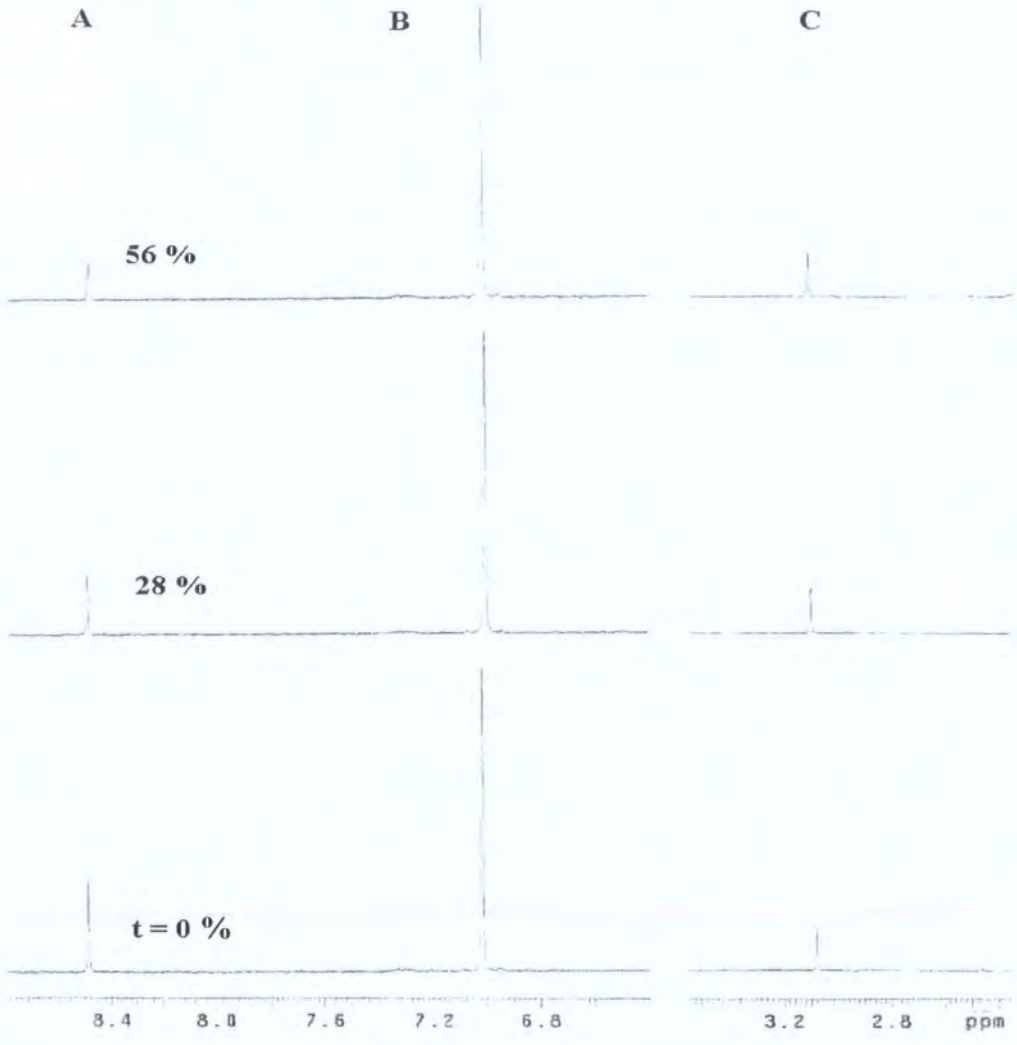

Reaction data and the experimental first-order rate constants for deuterium exchange (k_{obs}, s^{-1}) at different pD values in 50 and 100 mM phosphate buffers are shown in Tables 2.4, and 2.5 respectively. The values for k_{obs} (s^{-1}) shown in Tables 2.4 – 2.5 were obtained from the slopes of semilogarithmic plots (Figure 2.20 – 2.21) of the fraction of unexchanged substrate against time.

Table 2.4: First-order rate constants for exchange of the C2-H of imidazolium ion (116) for deuterium in phosphate buffers (50 mM) in D_2O at 25 °C and I = 1.0 (KCl).

$[DO^-]$[a] (M)	Time (s)	$f(s)$[b]	$\ln f(s)$	k_{obs}[c] (s^{-1})
7.44×10^{-8} (pD 7.62)	0	1.000	0.000	9.89×10^{-3}
	6.60×10^{2}	0.593	-0.523	
	1.22×10^{3}	0.304	-1.192	
	1.80×10^{3}	0.174	-1.748	
3.72×10^{-8} (pD 7.31)	0	1.000	0.000	5.08×10^{-4}
	6.00×10^{2}	0.727	-0.319	
	1.20×10^{3}	0.517	-0.660	
	1.80×10^{3}	0.393	-0.935	
	2.41×10^{3}	0.286	-1.250	
	3.02×10^{3}	0.216	-1.533	
8.80×10^{-9} (pD 6.69)	0	1.000	0.000	1.69×10^{-4}
	3.01×10^{3}	0.613	-0.490	
	5.41×10^{3}	0.416	-0.876	
	8.10×10^{3}	0.251	-1.383	
	1.10×10^{4}	0.173	-1.754	
	1.28×10^{4}	0.110	-2.208	
2.59×10^{-8} (pD 6.15)	0	1.000	0.000	3.01×10^{-5}
	3.65×10^{3}	0.969	-0.032	
	7.25×10^{3}	0.794	-0.230	
	1.11×10^{4}	0.707	-0.346	
	1.51×10^{4}	0.564	-0.573	
	2.26×10^{4}	0.551	-0.595	

(a) Measurements were made in 50 mM phosphate buffers in the pD 6.15 – 7.62 range. $[DO^-]$ was calculated using $[DO^-] = (10^{pD-pK_w})/\gamma_{OL}$ with $pK_w = 14.87$, where $\gamma_{OL} = 0.75$ is the activity correction of lyoxide ion under our experimental conditions. (b) The fraction of unexchanged substrate remaining $f(s)$, was calculated according to Equation 2.6. Measurements were made at an initial substrate concentration of 5 mM. (c) The value of the first-order rate constant (k_{obs}) was obtained from the slope of the plot of $\ln f(s)$ against time shown in Figure. 2.20.

Table 2.5: First-order rate constants for exchange of the C2-H of imidazolium ion (116) for deuterium in phosphate buffers (100 mM) in D_2O at 25 °C and I = 1.0 (KCl).

[DO⁻][a] (M)	Time (s)	f(s)[b]	ln f(s)	k_{obs}[c] (s^{-1})
1.45×10^{-7} (pD 7.91)	0	1.000	0.000	1.76×10^{-3}
	1.84×10^{2}	0.765	-0.268	
	2.44×10^{2}	0.686	-0.377	
	3.45×10^{2}	0.558	-0.584	
	3.90×10^{2}	0.511	-0.671	
	4.40×10^{2}	0.466	-0.764	
4.08×10^{-8} (pD 7.35)	0	1.000	0.000	4.54×10^{-4}
	6.00×10^{2}	0.767	-0.265	
	1.20×10^{3}	0.580	-0.544	
	1.80×10^{3}	0.432	-0.840	
	2.40×10^{3}	0.324	-1.128	
	3.00×10^{3}	0.265	-1.328	
1.65×10^{-8} (pD 6.96)	0	1.000	0.000	2.30×10^{-4}
	1.06×10^{3}	0.767	-0.266	
	1.80×10^{3}	0.641	-0.445	
	2.73×10^{3}	0.524	-0.647	
	3.60×10^{3}	0.406	-0.900	
	4.50×10^{3}	0.367	-1.002	
1.03×10^{-7} (pD 6.76)	0	1.000	0.000	1.43×10^{-4}
	2.82×10^{3}	0.717	-0.333	
	5.57×10^{3}	0.447	-0.804	
	8.22×10^{3}	0.310	-1.173	
	1.08×10^{4}	0.222	-1.503	
3.51×10^{-7} (pD 6.29)	0	1.000	0.000	3.36×10^{-5}
	6.00×10^{3}	0.684	-0.380	
	1.86×10^{3}	0.821	-0.198	
	1.09×10^{4}	0.624	-0.472	
	1.45×10^{4}	0.590	-0.528	

(a) Measurements were made in 100 mM phosphate buffers in pD 6.29 – 7.91 range [DO^-] was calculated using $[DO^-] = (10^{pD-pK_w})/\gamma_{OL}$ with $pK_w = 14.87$, where $\gamma_{OL} = 0.75$ is the activity correction of lyoxide ion under our experimental conditions. (b) The fraction of unexchanged substrate remaining $f(s)$, was calculated according to Equation 2.6. Measurements were made at an initial substrate concentration of 5 mM. (c) The value of the first-order rate constant (k_{obs}) was obtained from the slope of the plot of ln $f(s)$ against time shown in Figure 2.21.

Figure 2.20: Semi-logarithmic plot of the fraction of remaining C2-H against time for the deuterium exchange reaction of imidazolinium ion (116) in 50 mM phosphate buffer at pD 6.16, 6.69, 7.31, and 7.62.

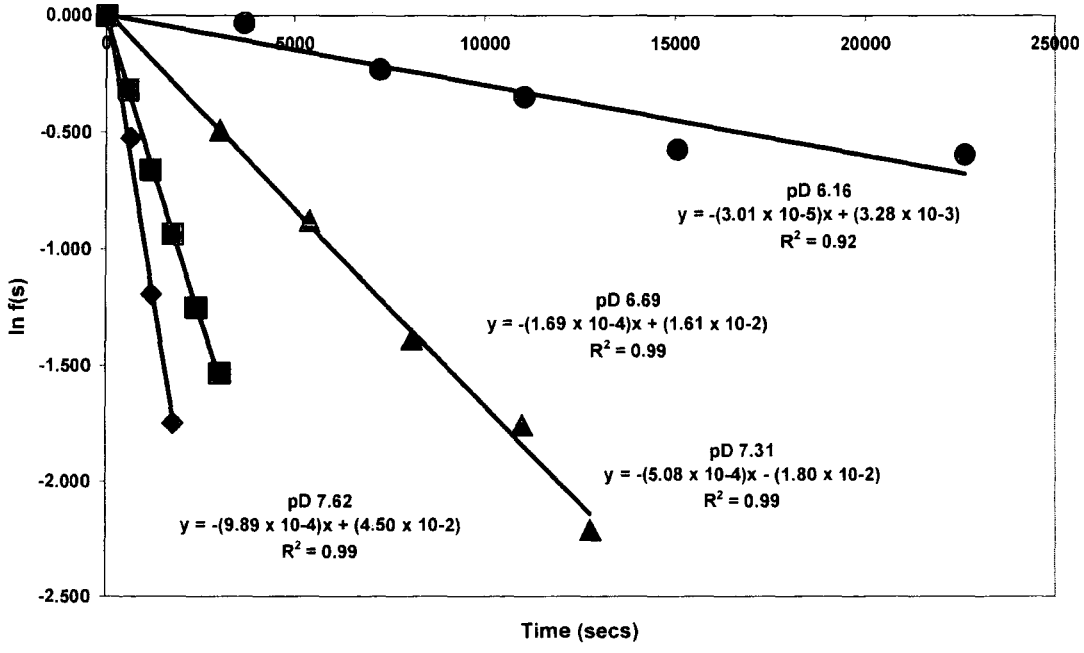

Figure 2.21: Semi-logarithmic plot of the fraction of remaining C2-H against time for the deuterium exchange reaction of imidazolinium ion (116) in 100 mM phosphate buffer at pD 6.29, 6.76, 6.96, 7.35 and 7.91.

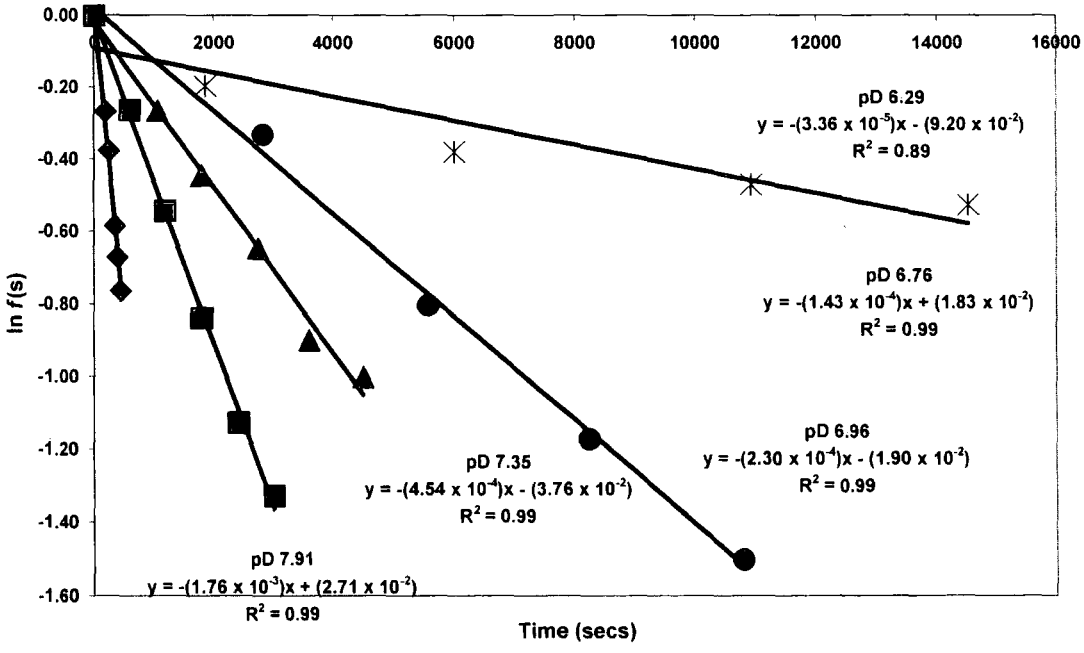

The combined reaction data of imidazolinium ion **(116)** in phosphate buffer solution is shown in Table 2.6. The second-order rate constant for deuteroxide ion-catalysed exchange was calculated from the slope of the plot of k_{obs} against the concentration of deuteroxide ion as shown in Figure 2.22.

Table 2.6: First and second-order rate constants for exchange of the C2-H of imidazolinium ion (116) for deuterium in D_2O at 25 °C and I = 1.0 (KCl).

Buffer Conc. (M)	[DO⁻] (M)	k_{obs} (s^{-1})	k_{DO}[a] ($M^{-1}s^{-1}$)
0.10	1.45×10^{-7}	1.76×10^{-3}	1.19×10^{4}
	4.08×10^{-8}	4.54×10^{-4}	
	1.65×10^{-8}	2.30×10^{-4}	
	1.03×10^{-7}	1.43×10^{-4}	
	3.51×10^{-7}	3.36×10^{-5}	
0.05	7.44×10^{-8}	9.89×10^{-3}	1.30×10^{4}
	3.72×10^{-8}	5.08×10^{-4}	
	8.80×10^{-9}	1.69×10^{-4}	
	2.59×10^{-8}	3.01×10^{-5}	

(a) The second-order rate constant, (k_{DO}), was obtained from the slope of the plot of k_{obs} against [DO⁻] in Figure 2.22.

Figure 2.22: Plot of k_{obs} against [DO⁻] for the H/D exchange reaction of imidazolinium ion (116) in D_2O at 25 °C and I = 1.0 (KCl).

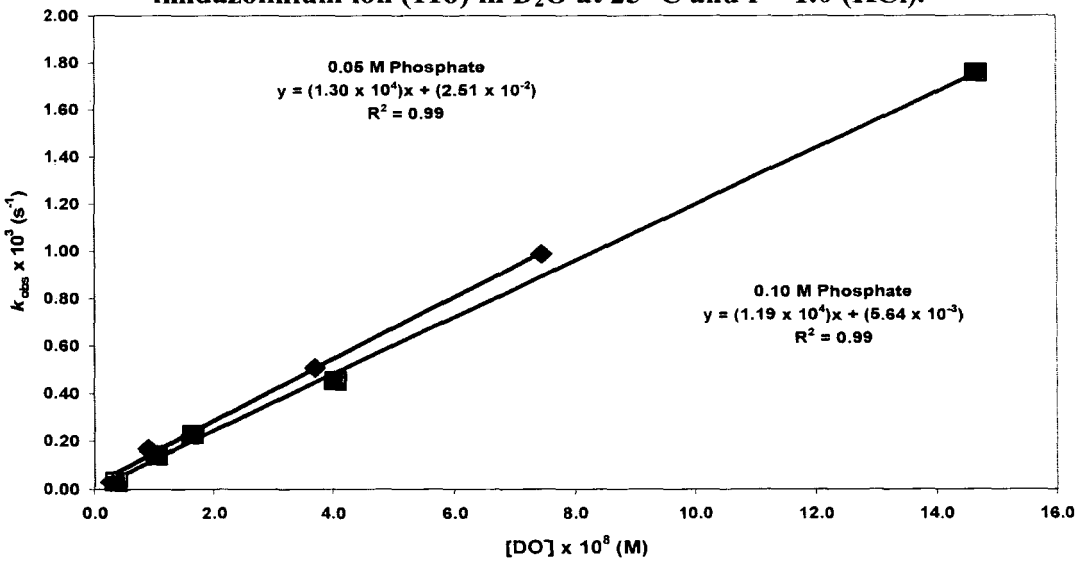

2.2.2.3. 1,3-Bis(*p*-methoxyphenyl)imidazolium chloride (110)

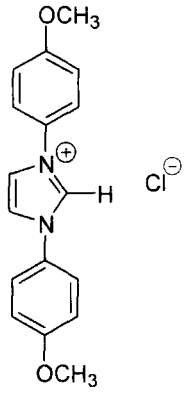

(110)

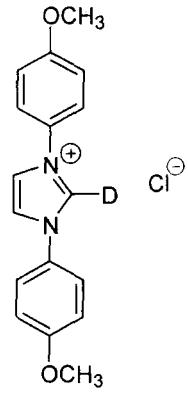

(110')

Rates of deuteroxide ion-catalyzed exchange of the C2-H of imidazolium ion **(110)** to form the corresponding deuterated product **(110')**, were determined by 500 MHz ^{1}H NMR spectroscopy.

Figure 2.23 shows representative ^{1}H NMR spectra of imidazolium ion **(110)** (1 mM, pD 6.05) obtained during the exchange for deuterium of the C2-H in D_2O at 25 °C and I = 0.5 (KCl). Deuterium exchange at the C2 position results in the disappearance of the singlet peak due to the C2-H at 9.49 pm (A). This is measured relative to the internal standard peak. The signal due to the equivalent C4-H and C5-H protons of the imidazole ring appear as a singlet at 7.90 ppm (B). The signal due to the *o*-CHs appears as a doublet at 7.59 ppm (C), due to coupling to the *m*-CH which produce a doublet at 7.16 ppm (D). The signal due to the *p*-OCH_3 appears as a singlet at 3.85 ppm. H/D exchange is not observed at any position other than at C2 under these experimental conditions, indicated by comparison of all the signals due to imidazolium ion **(110)** to the internal standard peak at 3.12 ppm (E).In the reaction timeframe there is no change in the total integrated area for the signals due to all other peaks relative to the constant peak area of the broad triplet at 3.12 ppm due to the internal standard.

Figure 2.23: Representative ^{1}H NMR spectra at 500 MHz of imidazolium ion (110) (1mM, pD 6.05), obtained during exchange of the C2-H for deuterium in D_2O at 25 °C and I = 0.5 (KCl). The percentage of deuterium exchange is indicated above each spectrum.

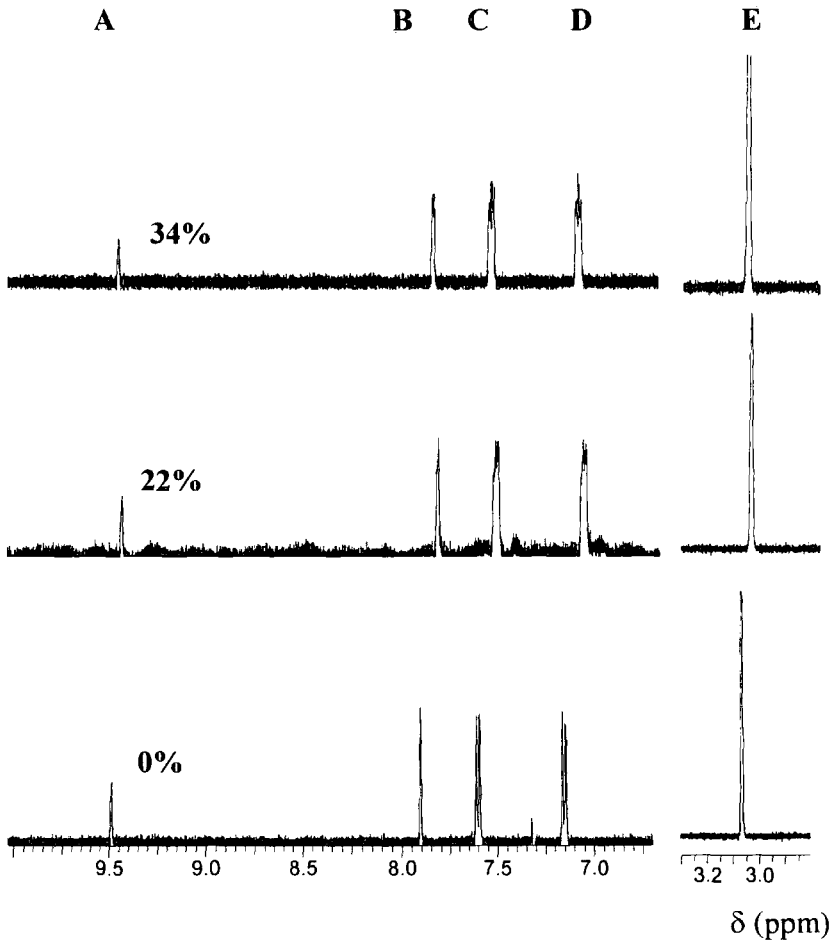

Reaction data and the experimental first-order rate constants for deuterium exchange (k_{obs}, s^{-1}) at different pD values in 100 mM acetate buffers are shown in Table 2.7. The values for k_{obs} (s^{-1}) shown in Tables 2.7 were obtained from the slopes of semilogarithmic plots (Figure 2.24) of the fraction of unexchanged substrate against time.

Table 2.7: First-order rate constants for exchange of the C2-H of imidazolium ion (110) for deuterium in acetate buffers (100 mM) in D_2O at 25 °C and I = 0.5 (KCl).

$[DO^-]^a$ (M)	Time (s)	$f(s)^b$	$\ln f(s)$	$k_{obs}{}^c$ (s^{-1})
2.05×10^{-9} (pD 6.05)	0	1.000	0.000	9.79×10^{-5}
	6.00×10^{2}	0.887	-0.120	
	1.21×10^{3}	0.809	-0.213	
	1.82×10^{3}	0.759	-0.276	
	2.41×10^{3}	0.745	-0.295	
	3.01×10^{3}	0.702	-0.356	
	3.42×10^{3}	0.653	-0.427	
5.34×10^{-10} (pD 5.47)	0	1.000	0.000	3.27×10^{-5}
	1.79×10^{3}	0.940	-0.0621	
	4.68×10^{3}	0.857	-0.154	
	5.77×10^{3}	0.817	-0.202	
	8.46×10^{3}	0.761	-0.273	
2.21×10^{-10} (pD 5.09)	0	1.000	0.000	1.0×10^{-5}
	2.06×10^{4}	0.856	-0.156	
	8.63×10^{4}	0.416	-0.877	
1.11×10^{-10} (pD 4.79)	0	1.000	0.000	4.01×10^{-6}
	4.38×10^{4}	0.869	-0.140	
	8.75×10^{4}	0.642	-0.444	
	1.20×10^{5}	0.556	-0.588	
	3.66×10^{5}	0.231	-1.467	
2.09×10^{-11} (pD 4.06)	0	1.000	0.000	1.08×10^{-6}
	1.83×10^{5}	0.779	-0.250	
	5.22×10^{5}	0.600	-0.511	
	6.94×10^{5}	0.411	-0.890	
	1.29×10^{6}	0.253	-1.376	

(a) Measurements were made in 100 mM acetate buffers in pD range 479 – 6.05 range. $[DO^-]$ was calculated using $[DO^-] = (10^{pD-pK_w})/\gamma_{OL}$ with $pK_w = 14.87$, where $\gamma_{OL} = 0.75$ is the activity correction of lyoxide ion under our experimental conditions. (b) The fraction of unexchanged substrate remaining $f(s)$, was calculated according to Equation 2.6. Measurements were made at an initial substrate concentration of 5 mM. (c) The value of the first-order rate constant (k_{obs}) was obtained from the slope of the plot of $\ln f(s)$ against time shown in Figure 2.24.

Figure 2.24: Semi-logarithmic plot of the fraction of remaining C2-H against time for the deuterium exchange reaction of imidazolium ion (110) in 100 mM acetate buffer at 4.06, 4.79, 5.09, 5.47 and 6.06.

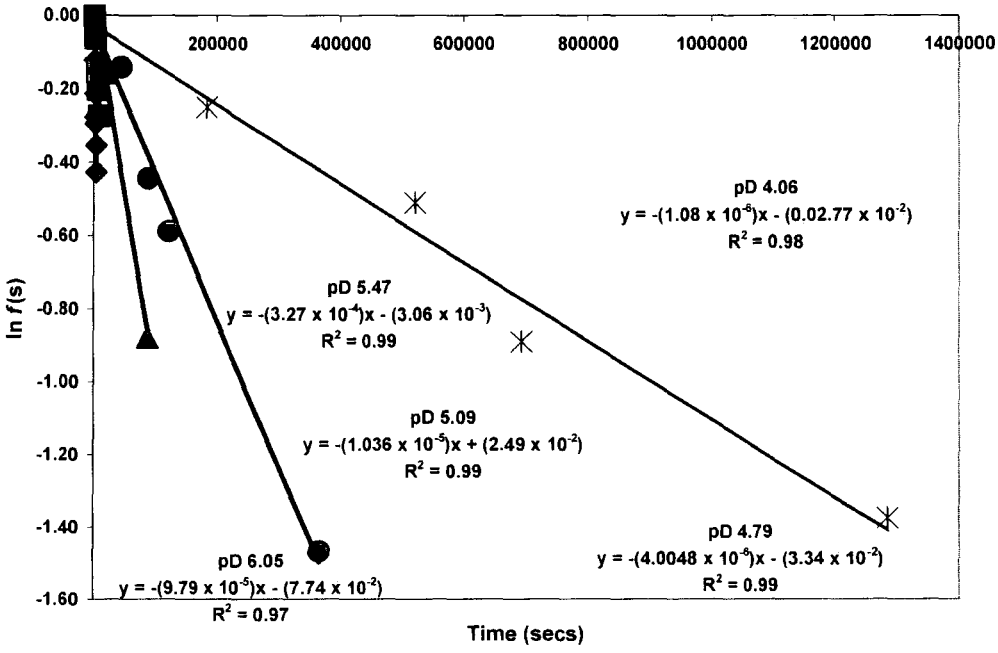

The combined reaction data of imidazolium ion **(110)** in acetate buffer solution is shown in Table 2.8. The concentration of deuteroxide ion was calculated using Equation (1.6).

Table 2.8: First and second-order rate constants for exchange of the C2-H of imidazolium ion (110) for deuterium in D_2O at 25 °C and I = 0.5 (KCl).

Buffer Conc. (M)	[DO^-] (M)	k_{obs} (s^{-1})	k_{DO}[a] ($M^{-1}s^{-1}$)
0.10	2.05×10^{-9}	9.79×10^{-5}	4.80×10^{4}
	5.34×10^{-10}	3.27×10^{-5}	
	2.21×10^{-10}	1.04×10^{-5}	
	1.11×10^{-10}	4.01×10^{-6}	
	2.09×10^{-11}	1.08×10^{-6}	

(a) The second-order rate constant, (k_{DO}), was obtained from the slope of the plot of k_{obs} against [DO^-] in Figure 2.25.

Figure 2.25: Plot of k_{obs} against [DO^-] for the H/D exchange reaction of imidazolium ion (110) in D_2O at 25 °C and I = 0.5 (KCl).

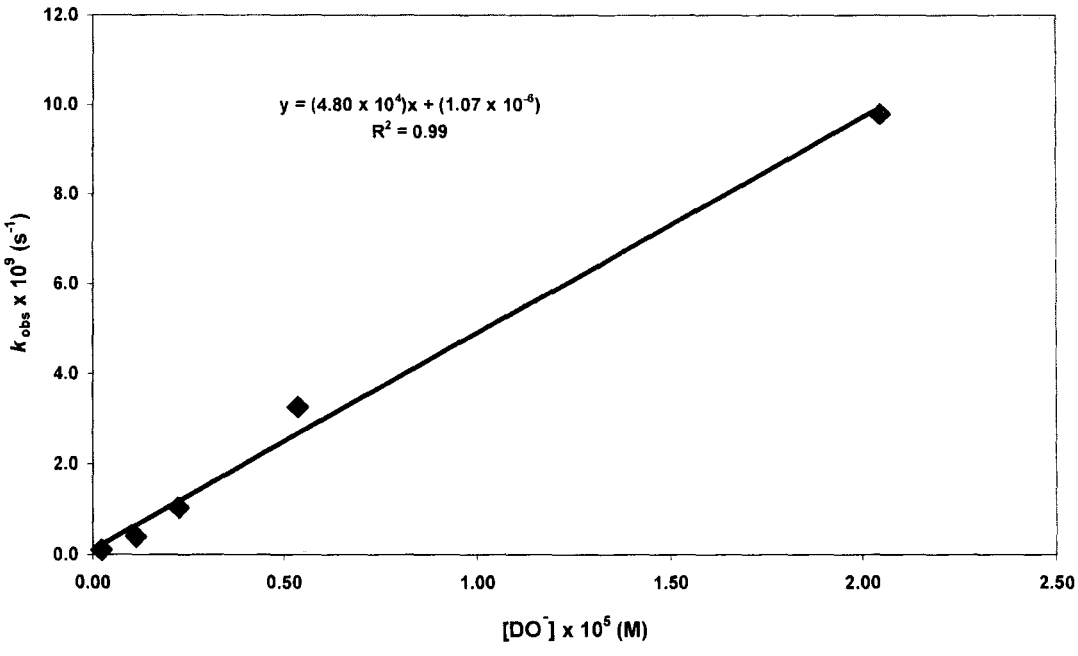

2.2.2.4. 1,3-Bis(*p*-methoxyphenyl)4,5-dihydroimidazolium Chloride (117).

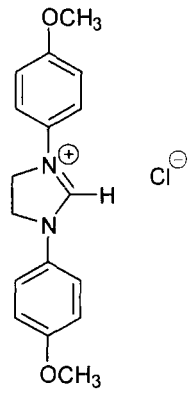

(117)

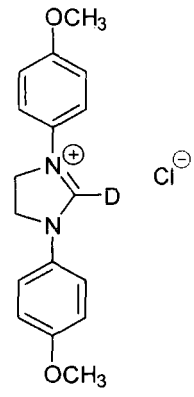

(117')

Rates of deuteroxide ion-catalyzed exchange of the C2-H of imidazolinium ion **(117)** to form the corresponding deuterated product **(117')**, were determined by 500 MHz ^{1}H NMR spectroscopy.

Figure 2.26 shows representative ^{1}H NMR spectra of imidazolinium ion **(117)** (0.1 mM pD 5.41) obtained during the exchange for deuterium of the C2-H in D_2O at 25 °C and I = 0.25 (KCl). Deuterium exchange at the C2 position results in the disappearance of the singlet peak due to the C2-H at 9.14 ppm (A). This is measured relative to the internal standard peak. The signal due to the *o*-CHs appears as a doublet at 7.28 ppm (B) and is coupled to the *m*-CHs. The signal due to the *m*-CHs appears as a doublet at 6.98 ppm (C). The signal due to the equivalent C4-H_2, and C5-H_2 appears as a singlet at 4.47 ppm (D) and the signal due to the *p*-OCH_3 appears as a singlet at 3.74 ppm (E). H/D exchange is not observed at any position other than at C2 under these experimental conditions, indicated by comparison of all the signals due to imidazolinium ion **(117)** in the spectrum to the internal standard peak at 3.12 ppm (F). In the reaction timeframe there is no change in the total integrated area for the signals due to all other protons relative to the constant peak area of the broad triplet at 3.12 ppm due to the internal standard.

Figure 2.26: Representative ^{1}H NMR spectra at 500 MHz of imidazolinium ion (117) (0.1mM, pD 5.41), obtained during exchange of the C2-H for deuterium in D_2O at 25 °C and I = 0.25 (KCl). The percentage of deuterium exchange is indicated above each spectrum.

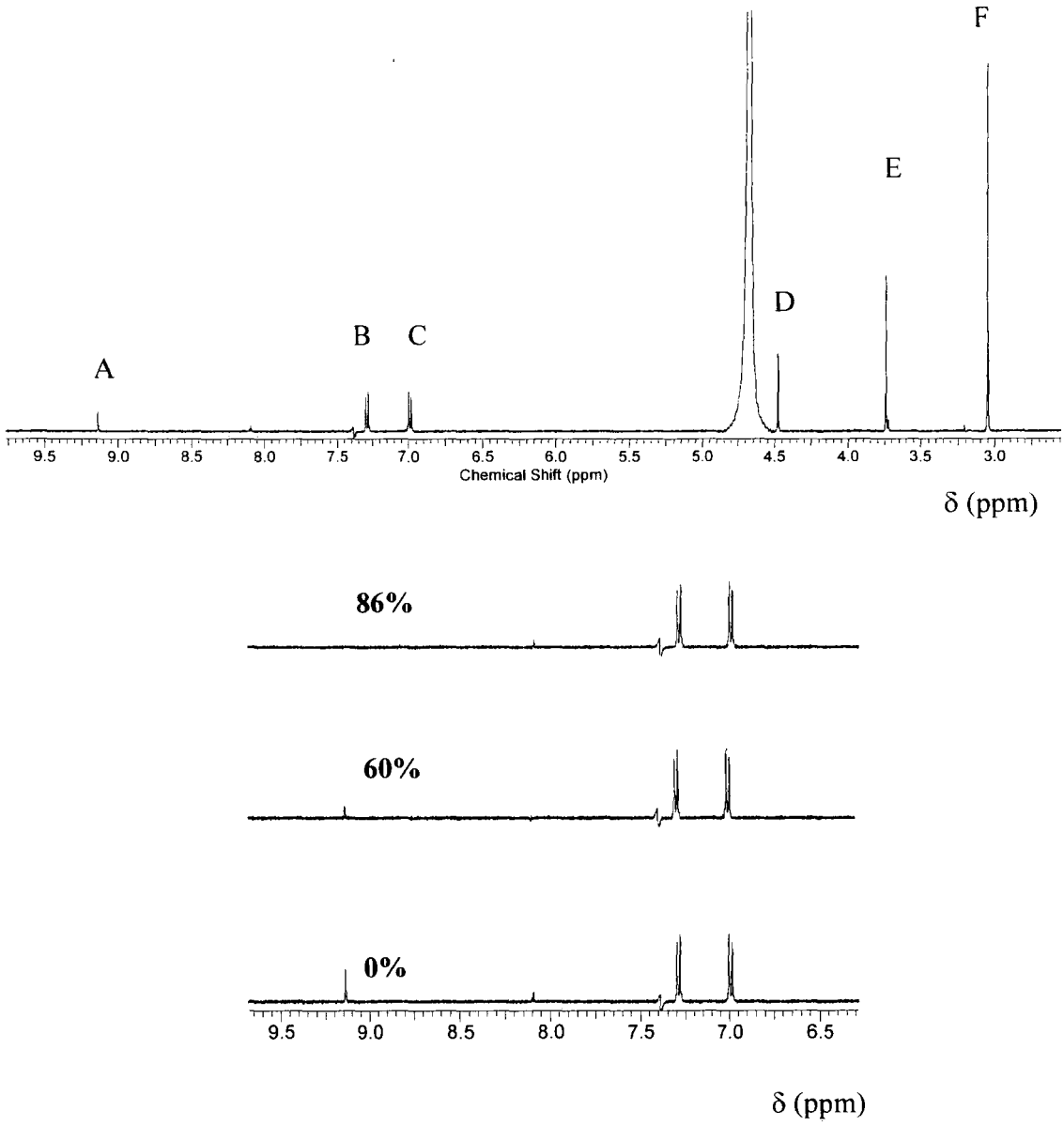

Reaction data and the experimental first-order rate constants for deuterium exchange (k_{obs}, s^{-1}) at different pD values in 100 mM acetate buffers are shown in Table 2.9. The values for k_{obs} (s^{-1}) shown in Table 2.9 are obtained from the slopes of semilogarithmic plots (Figure 2.27) of the fraction of unexchanged substrate against time.

Table 2.9: First-order rate constants for exchange of the C2-H of imidazolinium ion (117) for deuterium in acetate buffers (100 mM) in D_2O at 25 °C and I = 0.25 (KCl).

$[DO^-]^a$ (M)	Time (s)	$f(s)^b$	ln $f(s)$	$k_{obs}{}^c$ (s^{-1})
1.70×10^{-9} (pD 5.97)	0	1.000	0.000	7.66×10^{-5}
	7.17×10^{2}	0.964	-0.037	
	1.35×10^{3}	0.927	-0.075	
	2.88×10^{3}	0.798	-0.225	
	3.70×10^{3}	0.774	-0.256	
	4.49×10^{3}	0.738	-0.304	
4.67×10^{-10} (pD 5.41)	0	1.000	0.000	1.15×10^{-5}
	1.80×10^{4}	0.826	-0.192	
	5.89×10^{4}	0.396	-0.926	
	9.22×10^{4}	0.283	-1.262	
	1.50×10^{5}	0.189	-1.668	
	1.69×10^{5}	0.132	-2.024	
2.56×10^{-10} (pD 5.15)	0	1.000	0.000	5.25×10^{-6}
	5.80×10^{4}	0.543	-0.611	
	2.25×10^{5}	0.303	-1.193	
	4.41×10^{5}	0.086	-2.460	
9.95×10^{-11} (pD 4.74)	0	1.000	0.000	5.87×10^{-6}
	5.93×10^{4}	0.612	-0.490	
	1.50×10^{5}	0.306	-1.184	
	2.73×10^{5}	0.128	-2.0567	
	4.98×10^{5}	0.054	-2.914	
2.09×10^{-11} (pD 4.06)	0	1.000	0.000	1.08×10^{-6}
	1.83×10^{5}	0.779	-0.250	
	5.22×10^{5}	0.600	-0.511	
	6.94×10^{5}	0.411	-0.890	
	1.28×10^{5}	0.253	-1.376	

(a) Measurements were made in 100 mM acetate buffer in the pD 4.74 – 5.97 range. $[DO^-]$ was calculated using $[DO^-] = (10^{pD-pK_w})/\gamma_{OL}$ with $pK_w = 14.87$, where $\gamma_{OL} = 0.75$ is the activity correction of lyoxide ion under our experimental conditions. (b) Measurements were made at initial substrate concentration of 0.1 mM. (c) The value of the first-order rate constant (k_{obs}), was obtained from the slope of the plot of ln $f(s)$ against time in Figure 2.27.

Figure 2.27 Semi-logarithmic plot of the fraction of remaining C2-H against time for the deuterium exchange reaction of imidazolinium ion (117) in 100 mM acetate buffer at pD 4.06, 4.74, 5.15, 5.41, and 5.97.

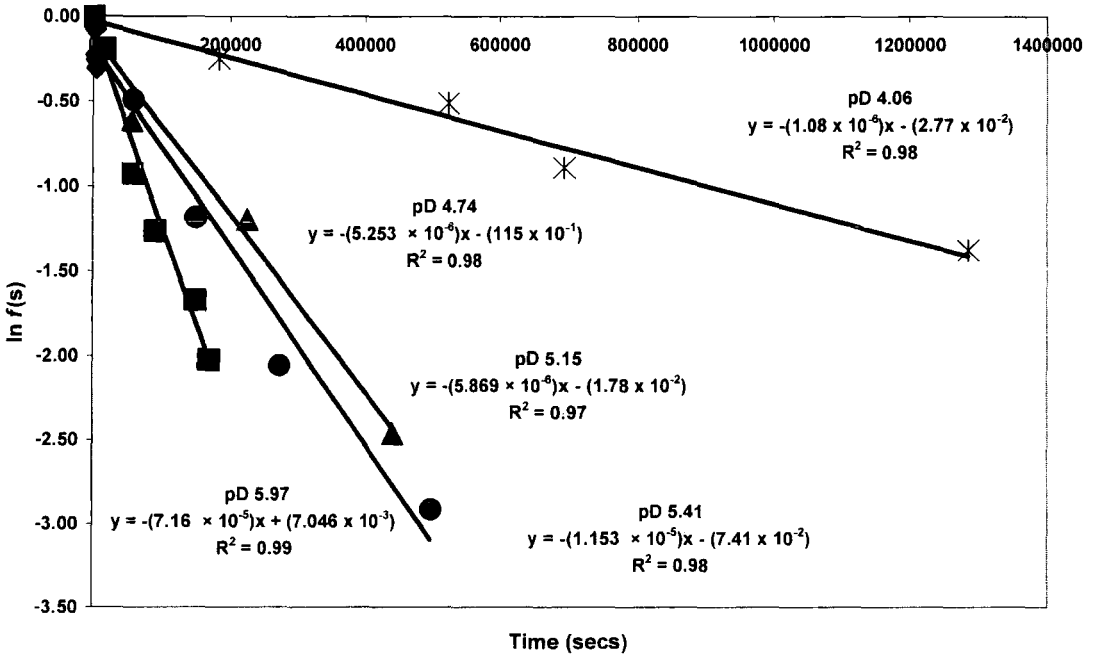

The combined reaction data of imidazolinium ion **(117)** in acetate buffer solution is shown in Table 2.10. The second-order rate constant for deuteroxide ion-catalysed exchange was calculated from the slope of the plot of k_{obs} against the concentration of deuteroxide ion as shown in Figure 2.28.

Table 2.10: First and second-order rate constants for exchange of the C2-H of imidazolinium ion (117) for deuterium in D_2O at 25 °C and I = 0.25 (KCl).

Buffer Conc. (M)	$[DO^-]$ (M)	k_{obs} (s^{-1})	k_{DO}[a] ($M^{-1}s^{-1}$)
	1.70×10^{-9}	7.17×10^{-5}	
	4.67×10^{-10}	1.15×10^{-5}	
0.10	2.56×10^{-10}	5.25×10^{-6}	4.26×10^{4}
	9.95×10^{-11}	5.87×10^{-6}	
	2.09×10^{-11}	1.08×10^{-6}	

(a) The second-order rate constant, (k_{DO}), was obtained from the slope of the plot of k_{obs} against $[DO^-]$ in Figure 2.28.

Figure 2.28: Plot of k_{obs} against $[DO^-]$ for the H/D exchange reaction of imidazolinium ion (117) in D_2O at 25 °C and I = 0.25 (KCl).

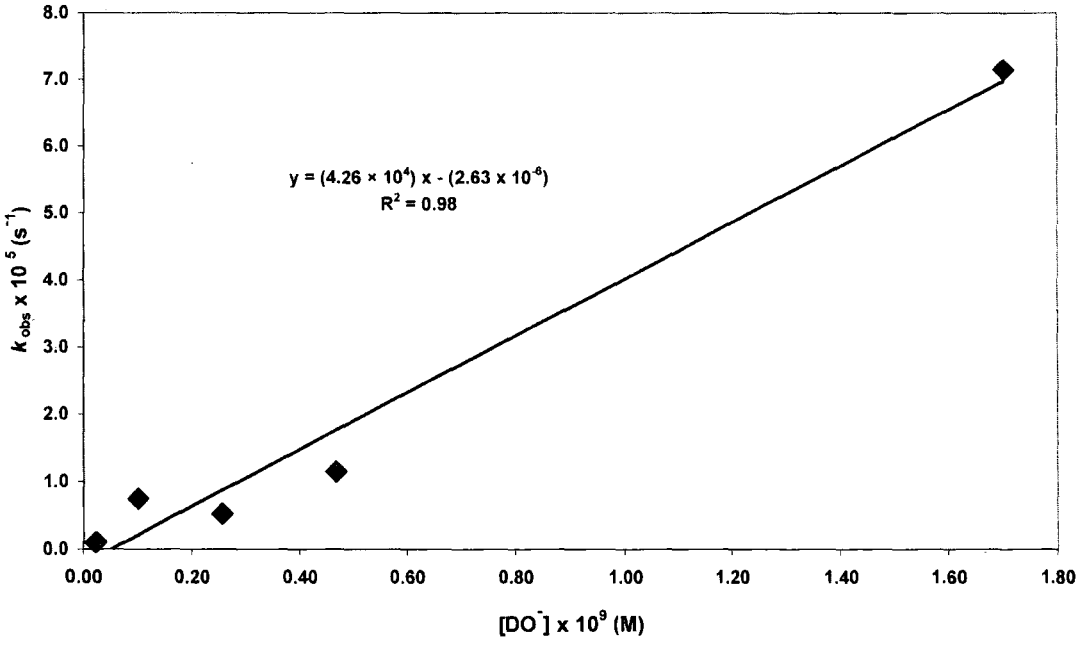

2.2.2.5. 1,3-Bis(*p*-chlorophenyl)imidazolium chloride (111)

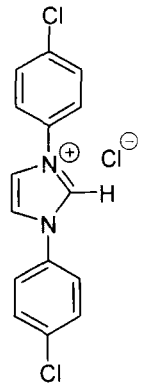

(111)

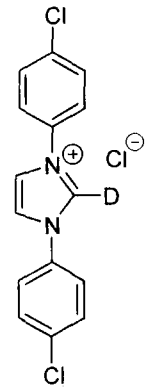

(111')

Rates of deuteroxide ion-catalyzed exchange of the C2-H of imidazolium ion **(111)** to form the corresponding deuterated product **(111')** were determined by 500 MHz ^{1}H NMR spectroscopy.

Figure 2.29 shows representative ^{1}H NMR spectra of imidazolium ion **(111)** (1.0 mM, pD 4.08) obtained during the exchange for deuterium of the C2-H in D_2O at 25 °C and I = 0.5 (KCl). Deuterium exchange at the C2 position results in the disappearance of the singlet peak due to the C2-H at 9.69 ppm (A). This is measured relative to the internal standard peak. The signal due to the *m*-CHs appears as a doublet at 7.99 ppm (B) due to coupling to the *o*-CHs. The signal due to the *o*-CH appears as a doublet at 7.62 ppm (C). The signal due to the C4-H and C5-H overlaps with the signal due to the *o*-CH at 7.60 ppm. H/D exchange is not observed at any position other than at C2 under these experimental conditions, indicated by comparison of all the signals due to imidazolium ion **(111)** in the spectrum to the internal standard peak at 3.09 ppm (D). In the reaction timeframe there is no change in the total integrated area for the signals due to all other protons relative to the constant peak area of the broad triplet at 3.09 ppm due to the internal standard.

Figure 2.29: Representative ^{1}H NMR spectra at 500 MHz of imidazolium ion (111) (0.1mM, pD 4.08), obtained during exchange of the C2-H for deuterium in D_2O at 25 °C and I = 0.5 (KCl). The percentage of deuterium exchange is indicated above each spectrum.

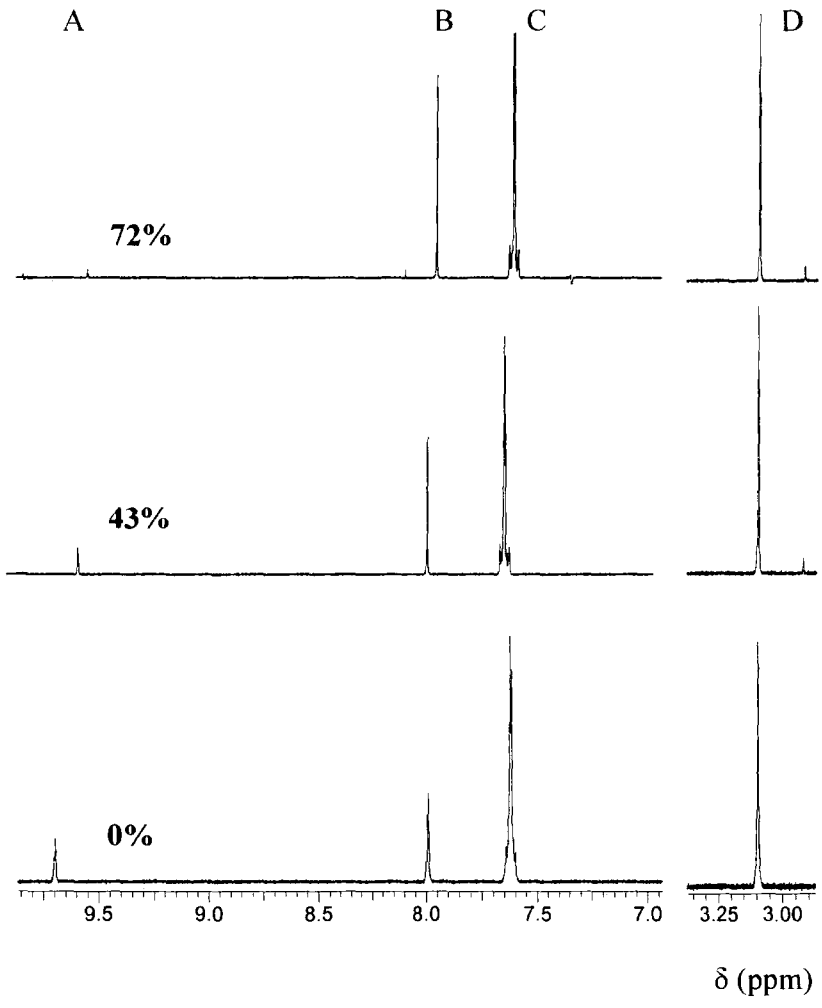

Reaction data and the experimental first-order rate constants for deuterium exchange (k_{obs}, s^{-1}) at different pD values in 100 mM acetate buffer is shown in Table 2.11. The values for k_{obs} (s^{-1}) shown in Table 2.11 were obtained from the slopes of semilogarithmic plots (Figure 2.30) of the fraction of unexchanged substrate against time.

Table 2.11: First-order rate constants for exchange of the C2-H of imidazolium ion (111) for deuterium in acetate buffers (100 mM) in D_2O at 25 °C and I = 0.5 (KCl).

$[DO^-]^a$ (M)	Time (s)	$f(s)^b$	ln $f(s)$	$k_{obs}{}^c$ (s^{-1})
1.70×10^{-9} (pD 5.97)	0	1.000	0.000	7.01×10^{-4}
	8.17×10^{2}	0.581	-0.543	
	1.20×10^{3}	0.441	-0.819	
	1.97×10^{3}	0.258	-1.356	
	2.43×10^{3}	0.183	-1.697	
	3.18×10^{3}	0.109	-2.219	
2.32×10^{-10} (pD 5.11)	0	1.000	0.000	1.62×10^{-4}
	7.20×10^{3}	0.284	-1.257	
	1.25×10^{4}	0.108	-2.228	
	2.05×10^{4}	0.0367	-3.305	
1.09×10^{-10} (pD 4.78)	0	1.000	0.000	8.18×10^{-5}
	8.71×10^{3}	0.459	-0.778	
	2.88×10^{4}	0.089	-2.420	
	3.86×10^{4}	0.0436	-3.156	
2.18×10^{-11} (pD 4.08)	0	1.000	0.000	1.71×10^{-5}
	3.88×10^{4}	0.574	-0.556	
	8.04×10^{4}	0.284	-1.258	
	1.16×10^{5}	0.132	-2.025	
	1.70×10^{5}	0.058	-2.841	

(a) Measurements were made in 100 mM acetate buffers in the pD 4.08 – 5.97 range [DO^-] was calculated using $[DO^-] = (10^{pD-pK_w})/\gamma_{OL}$ with $pK_w = 14.87$, where $\gamma_{OL} = 0.75$ is the activity correction of lyoxide ion under our experimental conditions. (b) The fraction of unexchanged substrate remaining $f(s)$, was calculated according to Equation 2.6. Measurements were made at an initial substrate concentration of 5 mM. (c) The value of the first-order rate constant (k_{obs}), was obtained from the slope of the plot of ln $f(s)$ against time in Figure 2.30.

Figure 2.30: Semi-logarithmic plot of the fraction of remaining C2-H against time for the deuterium exchange reaction of imidazolium ion (111) in 100 mM acetate buffer t pD 4.08, 4.78, 5.11 and 5.97.

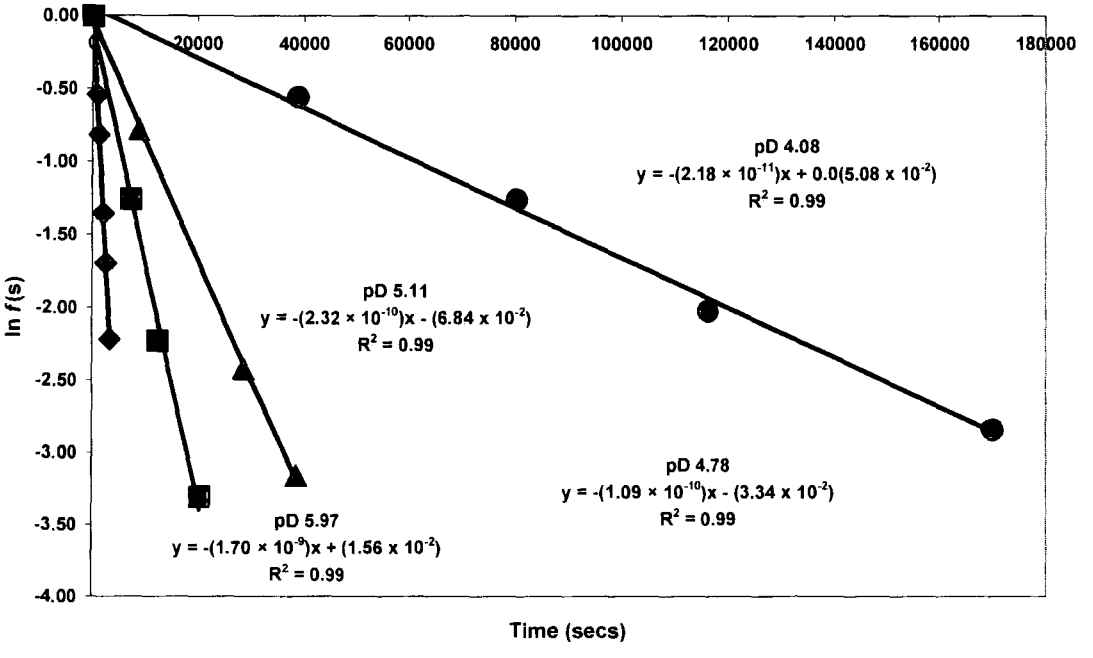

The combined reaction data of imidazolium ion **(111)** in acetate buffer solution is shown in Table 2.12. The second-order rate constant for deuteroxide ion-catalysed exchange was calculated from the slope of the plot of k_{obs} against the concentration of deuteroxide ion as shown in Figure 2.31.

Table 2.13: First and second-order rate constants for exchange of the C2-H of imidazolium ion (111) for deuterium in D_2O at 25 °C and I = 0.5 (KCl).

Buffer Conc. (M)	[DO^-] (M)	k_{obs} (s^{-1})	k_{DO}[a] ($M^{-1}s^{-1}$)
0.1	1.70×10^{-9}	7.01×10^{-4}	3.92×10^{5}
	2.32×10^{-10}	1.62×10^{-4}	
	1.09×10^{-10}	8.18×10^{-5}	
	2.18×10^{-11}	1.71×10^{-5}	

(a) The second-order rate constant, (k_{DO}), was obtained from the slope of the plot of k_{obs} against [DO^-] in Figure 2.31.

Figure 2.31: Plot of k_{obs} against [DO^-] for the H/D exchange reaction of imidazolium ion (111) in D_2O at 25 °C and I = 0.5 (KCl).

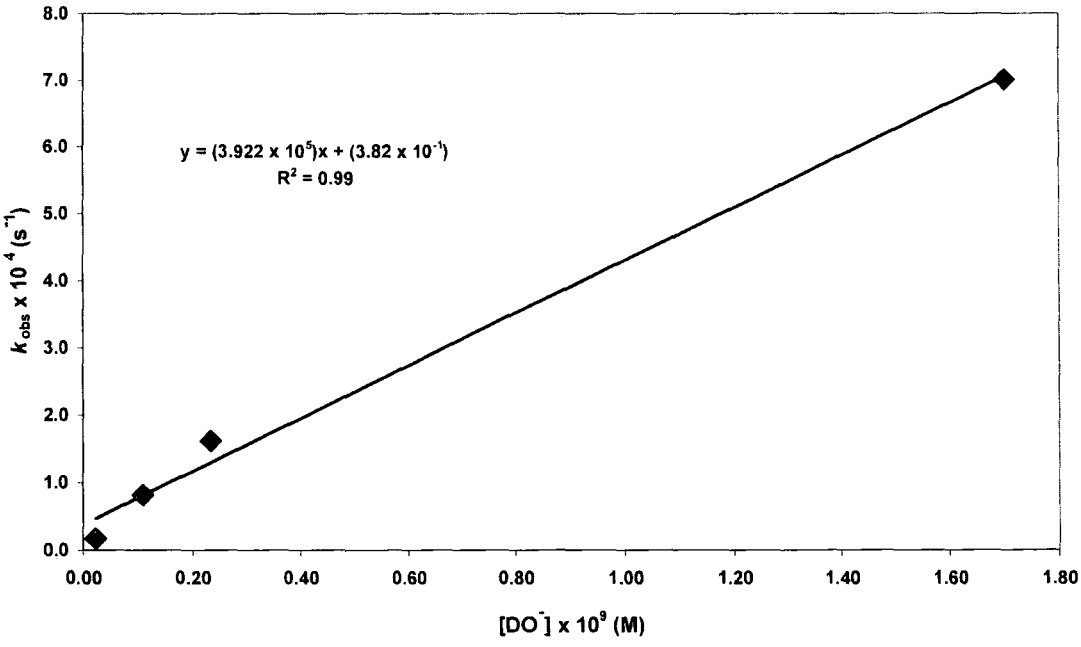

2.2.2.6. 1,3-Bis(2,6-di-*iso*propylphenyl)imidazolium chloride (112).

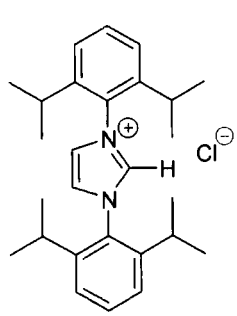

(112)

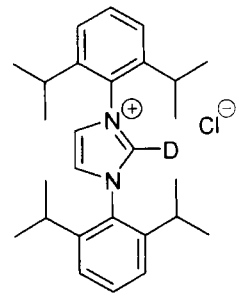

(112')

Rates of deuteroxide ion-catalyzed exchange of the C2-H of imidazolium ion **(112)** to form the corresponding deuterated product **(112')**, were determined by 500 MHz ^{1}H NMR spectroscopy.

Figure 2.32 shows representative ^{1}H NMR spectra of imidazolium ion **(112)** (2.5 mM, pD 5.97) obtained during the exchange for deuterium of the C2-H in D_2O at 25 °C and I = 1.0 (KCl). Deuterium exchange at the C2 position results in the disappearance of the singlet peak due to the C2-H at 9.57 ppm (A). The signal due to the equivalent C4-H, and C5-H appears as a singlet at 7.94 ppm (B). The signal due to the *p*-CHs appears as a triplet at 7.61 ppm (C) due to coupling to the signal due to the *m*-CHs which appears as a doublet at 7.44 ppm (D). H/D exchange is not observed at any position other than at C2 under these experimental conditions, indicated by comparison of all the signals due to imidazolium ion **(112)** in the spectrum to the internal standard peak at 3.12 ppm (E). In the reaction timeframe there is no change in the total integrated area for the signals due to all other protons relative to the constant peak area of the broad triplet at 3.12 ppm due to the internal standard.

Figure 2.32: Representative ^{1}H NMR spectra at 500 MHz of imidazolium ion (112) (2.5 mM, pD 5.97), obtained during exchange of the C2-H for deuterium in D_2O at 25 °C and I = 1.0 (KCl). The percentage of deuterium exchange is indicated above each spectrum.

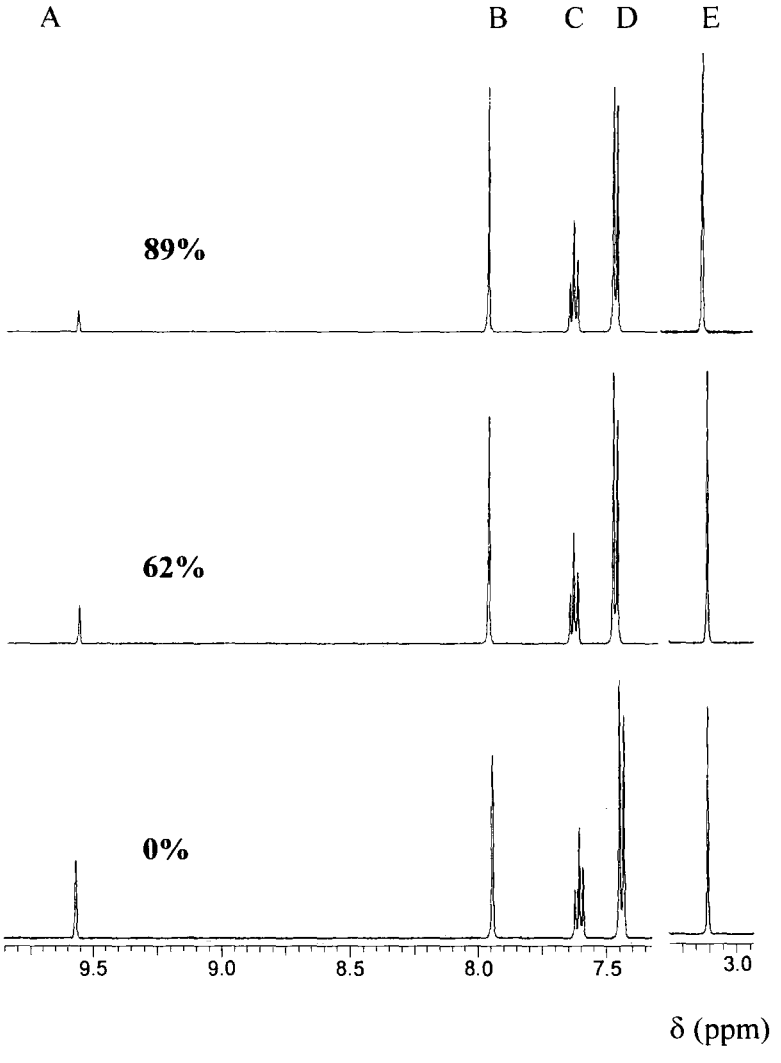

Reaction data and the experimental first-order rate constants for deuterium exchange (k_{obs}, s^{-1}) at different pD values in 100 mM phosphate buffers are shown in Table 2.14. The values for k_{obs} (s^{-1}) shown in Tables 2.14 were obtained from the slopes of semilogarithmic plots (Figure 2.33) of the fraction of unexchanged substrate against time.

Table 2.14: First-order rate constants for exchange of the C2-H of imidazolium ion (112) for deuterium in phosphate buffers (100 mM) in D_2O at 25 °C and I = 1.0 (KCl).

$[DO^-]^a$ (M)	Time (s)	$f(s)^b$	ln $f(s)$	$k_{obs}{}^c$ (s^{-1})
1.53×10^{-7} (pD 7.93)	0	1.000	0.000	3.09×10^{-3}
	2.67×10^{2}	0.446	-0.809	
	3.20×10^{2}	0.393	-0.934	
	3.86×10^{2}	0.323	-1.129	
	5.65×10^{2}	0.171	-1.766	
3.73×10^{-8} (pD 7.32)	0	1.000	0.000	8.68×10^{-4}
	3.00×10^{2}	0.599	-0.513	
	7.30×10^{2}	0.394	-0.933	
	1.09×10^{3}	0.293	-1.228	
	1446	0.245	-1.406	
	1800	0.196	-1.631	
1.54×10^{-8} (pD 6.93)	0	1.000	0.000	2.51×10^{-4}
	9.42×10^{2}	0.513	-0.668	
	1.58×10^{3}	0.419	-0.870	
	1.74×10^{3}	0.359	-1.026	
	3.12×10^{3}	0.296	-1.218	
	3.91×10^{3}	0.228	-1.479	
6.53×10^{-9} (pD 6.56)	0	1.000	0.000	1.57×10^{-4}
	1.61×10^{3}	0.599	-0.513	
	2.55×10^{3}	0.500	-0.693	
	3.75×10^{3}	0.458	-0.782	
	5.97×10^{3}	0.361	-1.020	
	6.16×10^{3}	0.31	-1.140	
	7.57×10^{3}	0.267	-1.323	
1.69×10^{-9} (pD 5.97)	0	1.000	0.000	4.05×10^{-5}
	6.08×10^{3}	0.818	-0.201	
	8.34×10^{3}	0.730	-0.313	
	1.48×10^{4}	0.505	-0.683	
	1.97×10^{4}	0.412	-0.888	
	2.71×10^{4}	0.325	-1.124	
	3.41×10^{4}	0.268	-1.316	

(a) Measurements were made in 100 mM phosphate buffers in the pD 5.97 – 7.93 range. $[DO^-]$ was calculated using $[DO^-] = (10^{pD-pK_w})/\gamma_{OL}$ with $pK_w = 14.87$, where $\gamma_{OL} = 0.75$ is the activity correction of lyoxide ion under our experimental conditions. (b) The fraction of remaining unexchanged substrate, $f(s)$, was calculated using Equation 2.6. Measurements were made at initial substrate concentration of 2.5 mM. (c) The value of the first-order rate constant (k_{obs}), was obtained from the slope of the plot of ln $f(s)$ against time in Figure 2.33.

Figure 2.33: Semi-logarithmic plot of the fraction of remaining C2-H against time for the deuterium exchange reaction of imidazolium ion (112) in 100 mM phosphate buffer at pD 5.97, 6.56, 6.9, 7.32 and 7.93.

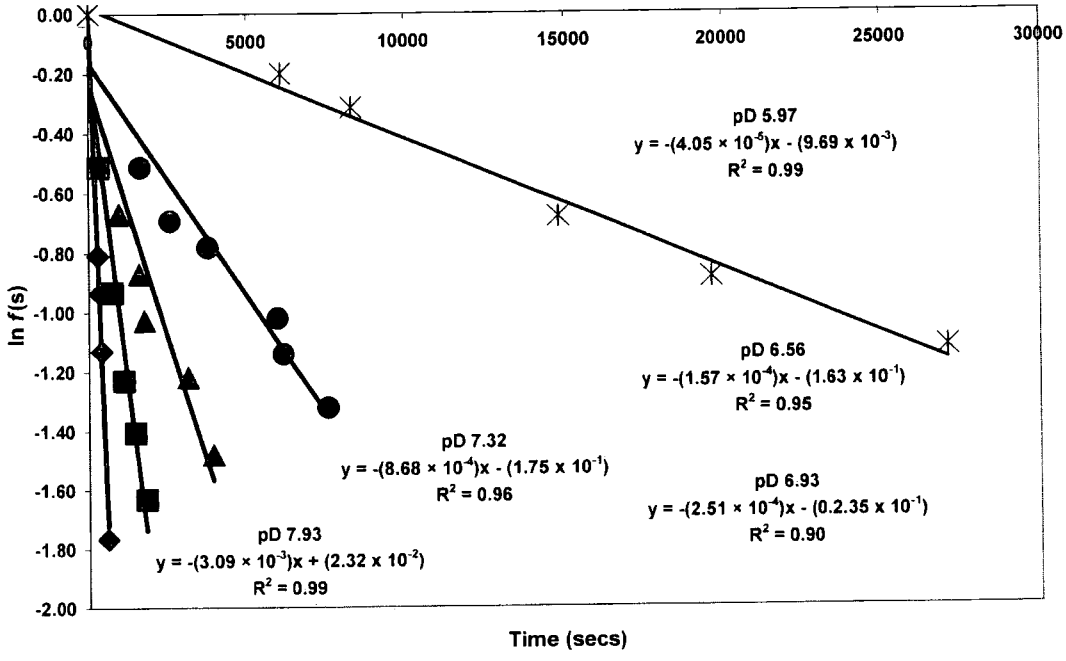

The combined reaction data of imidazolium ion **(112)** in phosphate buffer solution is shown in Table 2.15. The second-order rate constant for deuteroxide ion-catalysed exchange was calculated from the slope of the plot of k_{obs} against the concentration of deuteroxide ion as shown in Figure 2.34.

Table 2.15: First and second-order rate constants for exchange of the C2-H of imidazolium ion (112) for deuterium in D_2O at 25 °C and I = 1.0 (KCl).

Buffer Conc. (M)	$[DO^-]$ (M)	k_{obs} (s^{-1})	k_{DO}[a] ($M^{-1}s^{-1}$)
	1.53×10^{-7}	3.09×10^{-3}	
	3.73×10^{-8}	8.68×10^{-4}	
0.1	1.54×10^{-8}	2.51×10^{-4}	2.00×10^{4}
	6.53×10^{-9}	1.58×10^{-4}	
	1.69×10^{-9}	4.05×10^{-5}	

(a) The second-order rate constant, (k_{DO}), was obtained from the slope of the plot of k_{obs} against $[DO^-]$ in Figure 2.34.

Figure 2.34: Plot of k_{obs} against $[DO^-]$ for the H/D exchange reaction of imidazolium ion (112) in D_2O at 25 °C and I = 1.0 (KCl).

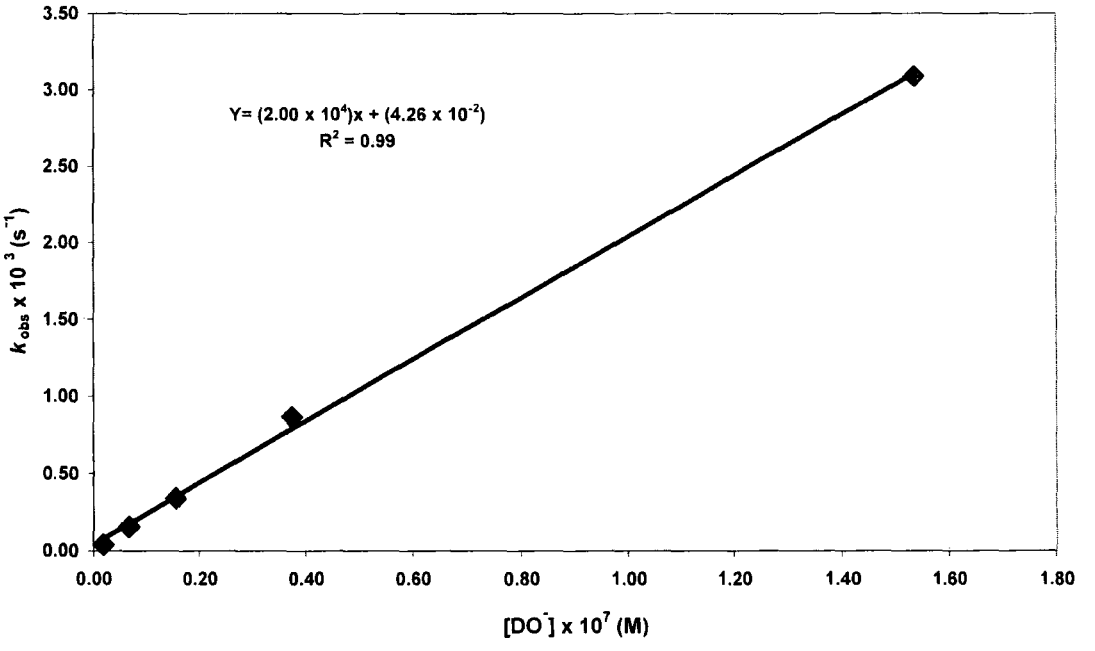

2.2.2.7 1,3-Bis(2,6-di-*iso*propylphenyl)4,5-dihydroimidazolium chloride (118)

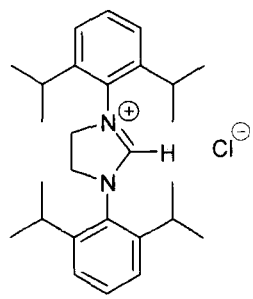

(118)

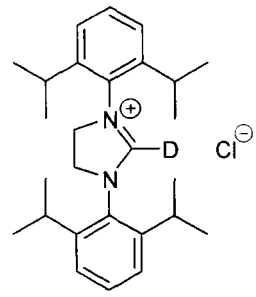

(118')

Rates of deuteroxide ion-catalyzed exchange of the C2-H of imidazolinium ion **(118)** to form the corresponding deuterated product **(118')**, were determined by 500 MHz ^{1}H NMR spectroscopy.

Figure 2.35 shows representative ^{1}H NMR spectra of imidazolinium ion **(118)**, (2.5 mM, pD 7.93) obtained during the exchange for deuterium of the C2-H in D_2O at 25 °C and I = 1.0 (KCl). Deuterium exchange at the C2 position results in the disappearance of the singlet peak due to the C2-H at 9.00 ppm (A). This is measured relative to the internal standard peak. The signal due to the *p*-CHs appears as a triplet at 7.52 ppm (B) due to coupling to the *m*-CHs which yields a doublet at 7.39 ppm (C). The signal due to the C4-H_2 and the C5-H_2 appears as a singlet at 4.51 ppm. H/D exchange is not observed at any position other than at C2 under these experimental conditions, indicated by comparison of all the signals due to imidazolium ion **(118)** in the spectrum to the internal standard peak at 3.12 ppm (D). In the reaction timeframe there is no change in the total integrated area for the signals due to all other protons relative to the constant peak area of the broad triplet at 3.12 ppm due to the internal standard.

Figure 2.35: Representative ^{1}H NMR spectra at 500 MHz of imidazolinium ion (118) (2.5 mM, pD 7.93), obtained during exchange of the C2-H for deuterium in D_2O at 25 °C and I = 1.0 (KCl). The percentage of deuterium exchange is indicated above each spectrum.

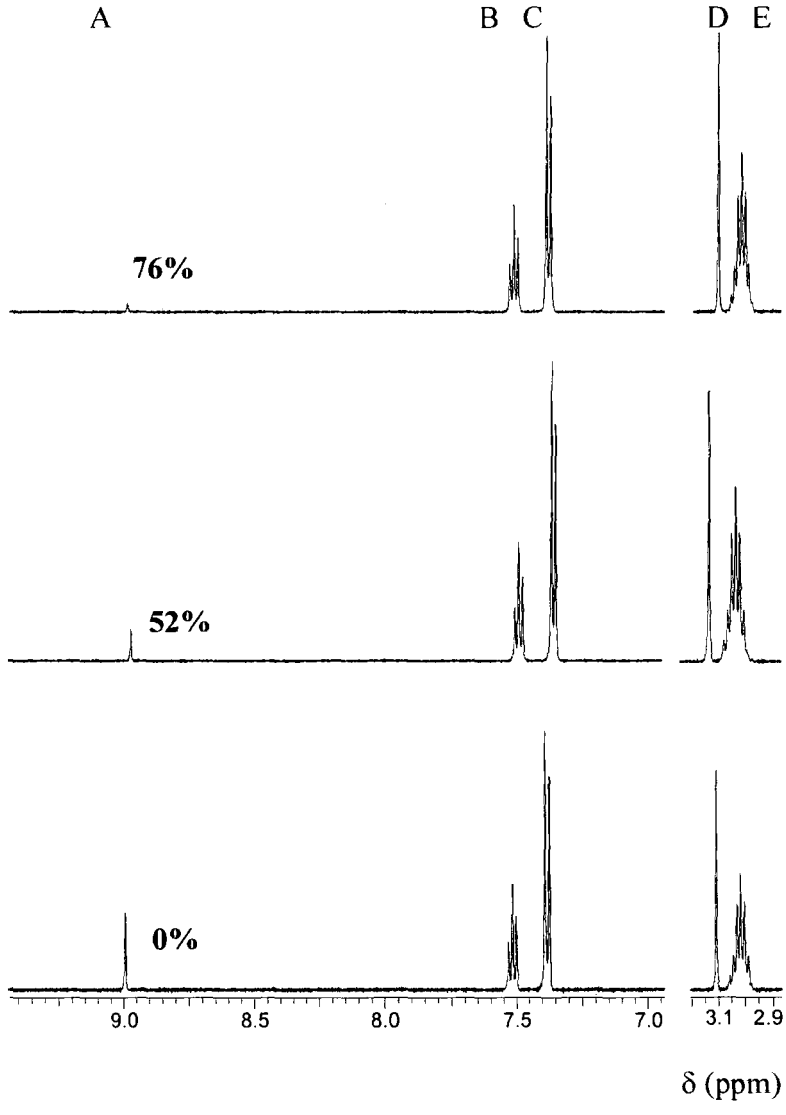

Reaction data and the experimental first-order rate constants for deuterium exchange (k_{obs}, s^{-1}) at different pD values in 100 mM phosphate buffer is shown in Table 2.16. The values for k_{obs} (s^{-1}) shown in Tables 2.16 were obtained from the slopes of semilogarithmic plots (Figure 2.36) of the fraction of unexchanged substrate against time.

Table 2.16: First-order rate constants for exchange of the C2-H of imidazolinium ion (118) for deuterium in phosphate buffers (100 mM) in D_2O at 25 °C and I = 1.0 (KCl).

$[DO^-]^a$ (M)	Time (s)	$f(s)^b$	ln $f(s)$	$k_{obs}{}^c$ (s^{-1})
1.53×10^{-7} (pD 7.93)	0	1.000	0.000	1.29×10^{-3}
	4.45×10^{2}	0.733	-0.310	
	8.40×10^{3}	0.380	-0.967	
	1.29×10^{3}	0.197	-1.626	
	1.82×10^{3}	0.102	-2.279	
	2.20×10^{3}	0.067	-2.697	
4.13×10^{-8} (pD 7.36)	0	1.000	0.000	4.18×10^{-4}
	4.53×10^{3}	0.408	-0.897	
	6.52×10^{3}	0.149	-1.904	
	8.29×10^{3}	0.078	-2.546	
	9.55×10^{3}	0.049	-3.016	
1.68×10^{-8} (pD 6.97)	0	1.000	0.000	1.56×10^{-4}
	7.68×10^{3}	0.308	-1.176	
	1.29×10^{4}	0.110	-2.205	
	1.64×10^{4}	0.099	-2.312	
	2.15×10^{4}	0.036	-3.338	
6.69×10^{-9} (pD 6.57)	0	1.000	0.000	6.24×10^{-5}
	8.00×10^{3}	0.706	-0.348	
	1.43×10^{4}	0.435	-0.832	
	1.92×10^{4}	0.305	-1.186	
	3.49×10^{4}	0.120	-2.118	
1.75×10^{-9} (pD 5.99)	0	1.000	0.000	1.73×10^{-5}
	2.80×10^{4}	0.620	-0.467	
	8.28×10^{4}	0.225	-1.490	
	1.59×10^{5}	0.065	-2.731	
	1.86×10^{5}	0.040	-3.207	

(a) Measurements were made in 100 mM phosphate buffers in the pD 5.99 – 7.93 range. $[DO^-]$ was calculated using $[DO^-] = (10^{pD-pK_w})/\gamma_{OL}$ with $pK_w = 14.87$, where $\gamma_{OL} = 0.75$ is the activity correction of lyoxide ion under our experimental conditions. (b) The fraction of remaining unexchanged substrate, $f(s)$, was calculated using Equation 2.6. Measurements were made at initial substrate concentration of 2.5 mM. (c) The value of the first-order rate constant (k_{obs}), was obtained from the slope of the plot of ln $f(s)$ against time in Figure 2.36.

Figure 2.36 Semi-logarithmic plot of the fraction of remaining C2-H against time for the deuterium exchange reaction of imidazolinium ion (118) in 100 mM phosphate buffer at pD 5.99, 6.57, 6.97, 7.36 and 7.93.

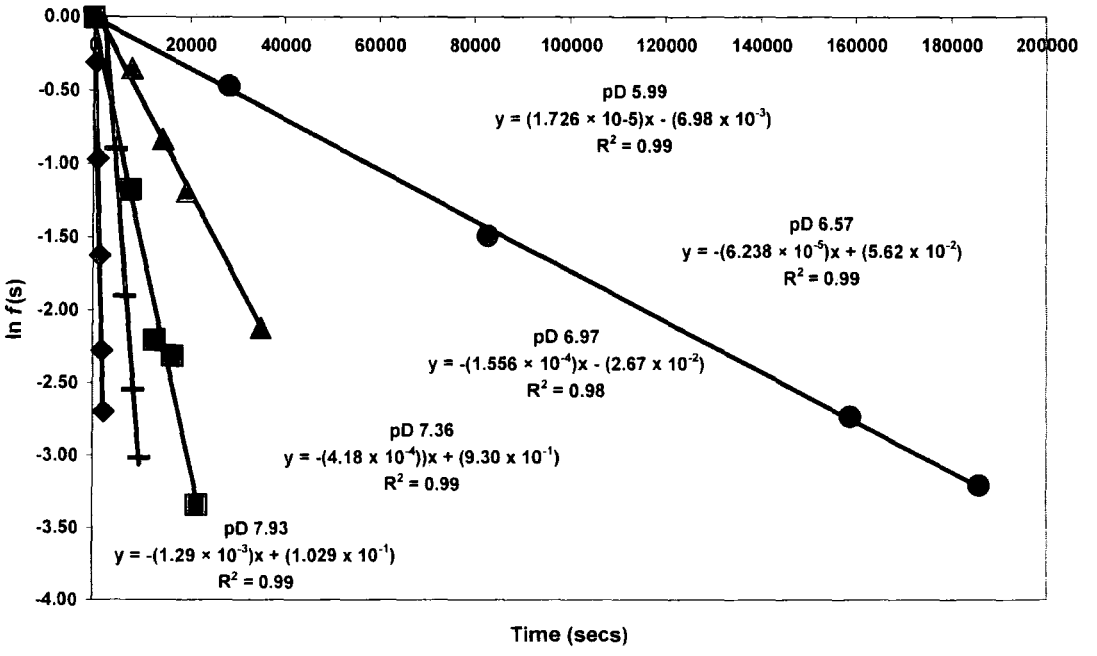

The combined reaction data of imidazolinium ion **(118)** in phosphate buffer solution is shown in Table 2.17. The concentration of deuteroxide ion was calculated using Equation (1.6).

Table 2.17: First and second-order rate constants for exchange of the C2-H of imidazolinium ion (118) for deuterium in D_2O at 25 °C and I = 1.0 (KCl).

Buffer Conc. (M)	[DO^-] (M)	k_{obs} (s^{-1})	k_{DO}[a] ($M^{-1}s^{-1}$)
	1.53×10^{-7}	1.29×10^{-3}	
	4.13×10^{-8}	4.18×10^{-4}	
0.1	1.68×10^{-8}	1.56×10^{-4}	8.37×10^{3}
	6.69×10^{-9}	6.24×10^{-5}	
	1.75×10^{-9}	1.73×10^{-5}	

(a) The second-order rate constant, (k_{DO}), was obtained from the slope of the plot of k_{obs} against [DO^-] in Figure 2.37.

Figure 2.37: Plot of k_{obs} against [DO^-] for the H/D exchange reaction of imidazolinium ion (118) in D_2O at 25 °C and I = 1.0 (KCl).

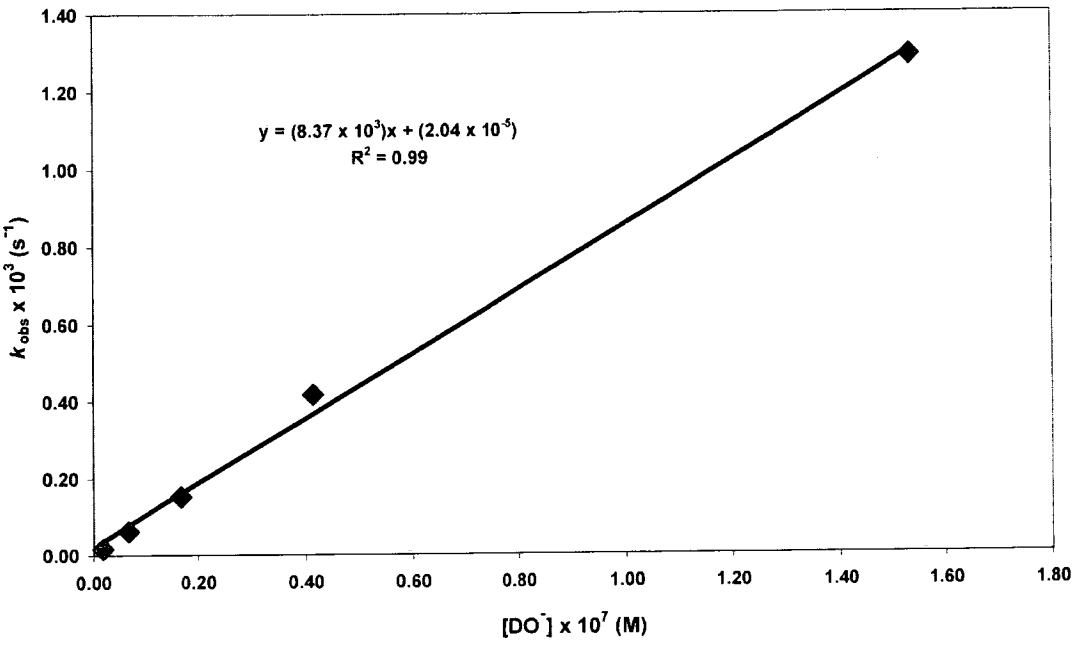

2.2.2.8 1,3-Di-*t*-butylimidazolium chloride (113).

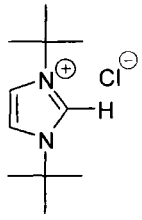

(113)

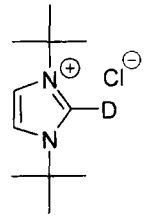

(113')

Rates of deuteroxide ion-catalyzed exchange of the C2-H of imidazolium ion **(113)** to form the corresponding deuterated product **(113')**, were determined by 500 MHz ^{1}H NMR spectroscopy.

Figure 2.38 shows representative ^{1}H NMR spectra of imidazolium ion **(113)**, (5 mM, pD 11.22) obtained during the exchange for deuterium of the C2-H in D_2O at 25 °C and I = 1.0 (KCl). Deuterium exchange at the C2 position results in the disappearance of the singlet peak due to the C2-H at 8.68 ppm (A). The signal due to the equivalent C4-H and C5-H appears as a singlet at 7.65 ppm (B). The signal due to the eighteen substituent methyl protons appears as a singlet at 1.62 ppm. No H/D exchange is observed at any position other than at C2 under these experimental conditions, indicated by comparison of all the signals due to imidazolium ion **(113)** in the spectrum to the internal standard peak at 3.17 ppm (C). In the reaction timeframe there is no change in the total integrated area for the signals due to all other protons relative to the constant peak area of the broad triplet at 3.17 ppm due to the internal standard.

Figure 2.38: Representative ^{1}H NMR spectra at 500 MHz of imidazolium ion (113) (5 mM, pD 11.22), obtained during exchange of the C2-H for deuterium in D_2O at 25 °C and I = 1.0 (KCl). The percentage of deuterium exchange is indicated above each spectrum.

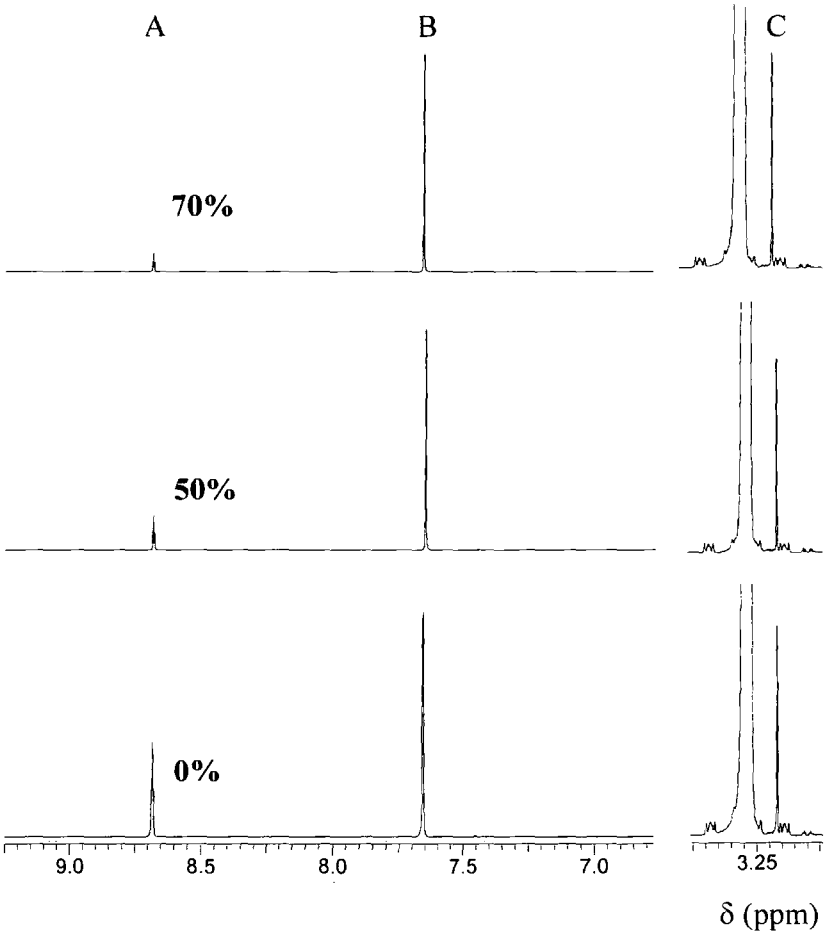

Reaction data and the experimental first-order rate constants for deuterium exchange (k_{obs}, s^{-1}) at different pD values in 100 mM quinuclidinone buffers are shown in Table 2.18. The values for k_{obs} (s^{-1}) shown in Tables 2.18 were obtained from the slopes of semilogarithmic plots (Figure 2.39) of the fraction of unexchanged substrate against time.

Table 2.18: First-order rate constants for exchange of the C2-H of imidazolium ion (113) for deuterium in quinuclidinone buffers (100 mM) in D_2O at 25 °C and I = 1.0 (KCl).

$[DO^-]$[a] (M)	Time (s)	$f(s)$[b]	ln $f(s)$	k_{obs}[c] (s^{-1})
4.01×10^{-6} (pD 9.35)	0	1.000	0.000	7.12×10^{-6}
	6.30×10^{4}	0.473	-0.749	
	9.01×10^{4}	0.459	-0.779	
	1.57×10^{5}	0.317	-1.150	
8.74×10^{-7} (pD 8.69)	0	1.000	0.000	2.70×10^{-6}
	6.34×10^{4}	0.865	-0.145	
	9.05×10^{4}	0.768	-0.264	
	1.95×10^{5}	0.624	-0.472	
	3.20×10^{5}	0.398	-0.922	
	4.06×10^{5}	0.348	-1.056	
3.42×10^{-7} (pD 8.28)	0	1.000	0.000	9.61×10^{-7}
	5.92×10^{4}	0.924	-0.080	
	2.62×10^{5}	0.704	-0.351	
	3.43×10^{5}	0.654	-0.425	
	6.78×10^{5}	0.523	-0.648	
1.48×10^{-7} (pD 7.91)	0	1.000	0.000	5.43×10^{-7}
	1.58×10^{5}	0.958	-0.042	
	9.29×10^{5}	0.619	-0.483	
	1.10×10^{6}	0.592	-0.525	
	1.62×10^{6}	0.414	-0.882	

(a) Measurements were made in 100 mM quinuclidinone buffer in the pD 7.91 – 9.35 range [DO^-] was calculated using $[DO^-] = (10^{pD-pK_w})/\gamma_{OL}$ with $pK_w = 14.87$, where $\gamma_{OL} = 0.75$ is the activity correction of lyoxide ion under our experimental conditions. (b) The fraction of unexchanged substrate remaining $f(s)$, was calculated according to Equation 2.6. Measurements were made at initial substrate concentration of 10 mM. (c) The value of the first-order rate constant (k_{obs}), was obtained from the slope of the plot of ln $f(s)$ against time in Figure 2.39.

Fig. 2.39 Semi-logarithmic plot of the fraction of remaining C2-H against time for the deuterium exchange reaction of imidazolium ion (113) in 100 mM quinuclidinone buffer at pD 7.91, 8.28, 8.69 and 9.35.

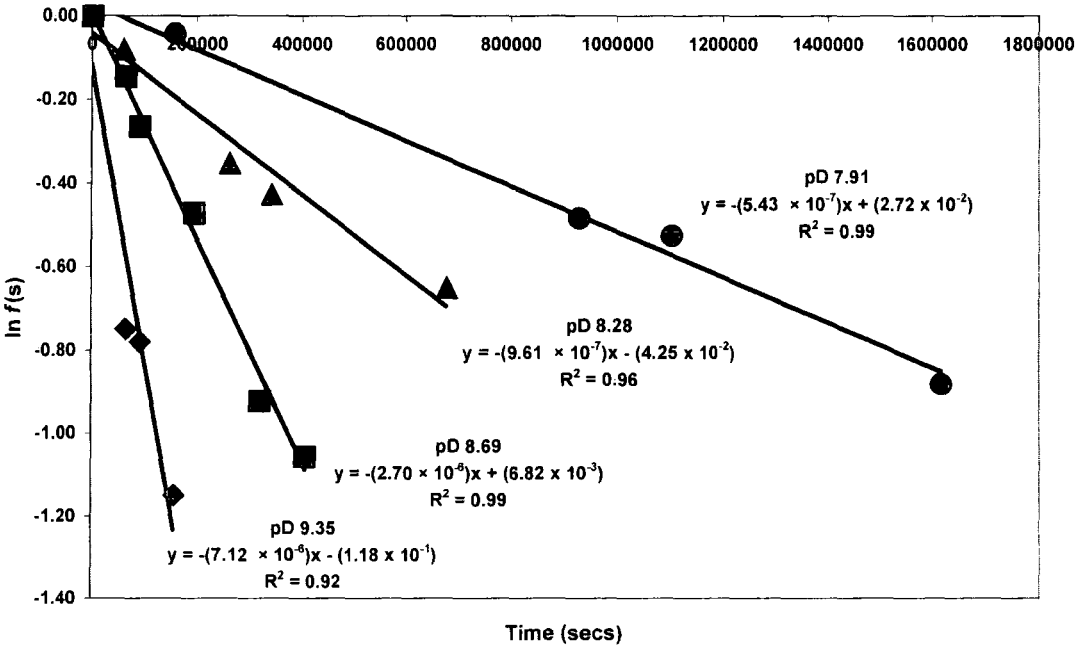

The combined reaction data of imidazolium ion **(113)** in quinuclidinone buffer solution The second-order rate constant for deuteroxide ion-catalysed exchange was calculated from the slope of the plot of k_{obs} against the concentration of deuteroxide ion as shown in Figure 2.40.

Table 2.19: First and second-order rate constants for exchange of the C2-H of imidazolium ion (113) for deuterium in D_2O at 25 °C and I = 1.0 (KCl).

Buffer Conc. (M)	$[DO^-]$ (M)	k_{obs} (s^{-1})	k_{DO}[a] ($M^{-1}s^{-1}$)
0.10	4.01×10^{-6}	7.12×10^{-6}	1.65
	8.74×10^{-7}	2.70×10^{-6}	
	3.42×10^{-7}	9.61×10^{-7}	
	1.48×10^{-7}	5.43×10^{-7}	

(a)The second-order rate constant, (k_{DO}), was obtained from the slope of the plot of k_{obs} against $[DO^-]$ in Fig. 2.40.

Figure 2.40: Plot of k_{obs} against $[DO^-]$ for the H/D exchange reaction of imidazolium ion (113) in quinuclidinone buffer in D_2O at 25 °C and I = 1.0 (KCl).

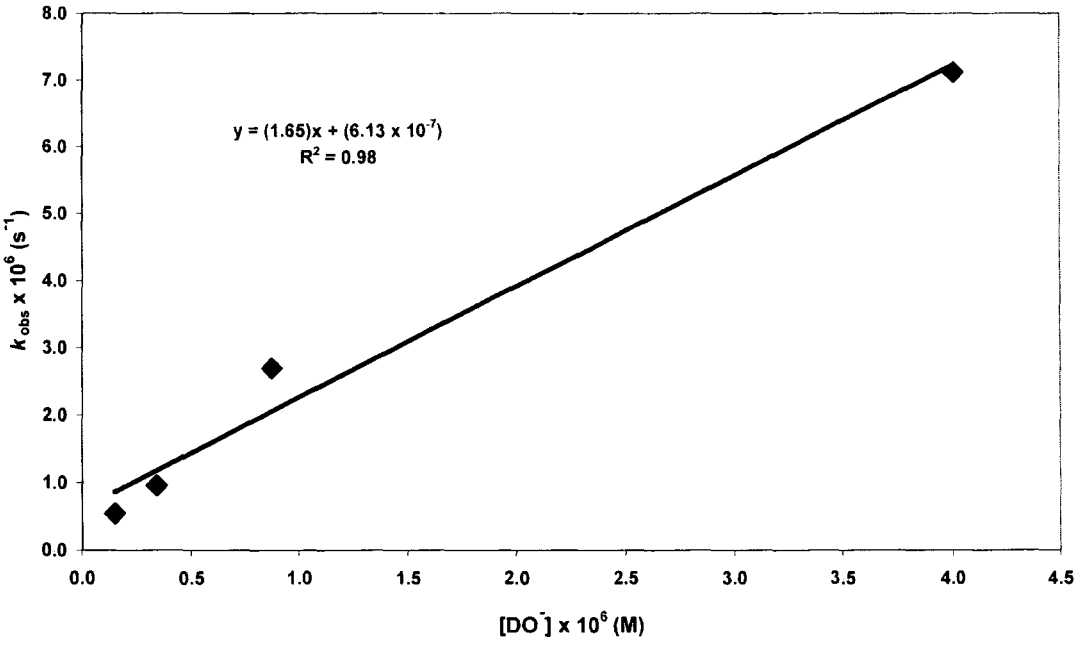

2.2.2.9. 1-Ethyl-3-methylimidazolium iodide (114)

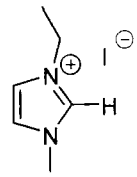

(114)

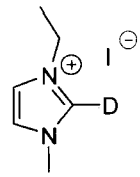

(114')

Rates of deuteroxide ion-catalyzed exchange of the C2-H of imidazolium ion **(114)** to form the corresponding deuterated product **(114')** were determined by 400 MHz ^{1}H NMR spectroscopy.

Figure 2.41 shows representative ^{1}H NMR spectra of imidazolium ion **(114)**, (10 mM, pD 7.26), obtained during the exchange for deuterium of the C2-H in D_2O at 25 °C and I = 1.0 (KCl). Deuterium exchange at the C2 position results in the disappearance of the singlet peak due to the C2-H at 8.70 ppm (A) This is measured relative to the internal standard peak. The signals due to the C4-H and C5-H appear as two triplets at 7.48 ppm (B) and 7.41 ppm (C). The signals due to the N-substituent ethyl protons appear as a quartet at 4.22 ppm and a triplet at 1.48 ppm. The signal due to the N-methyl protons appears as a singlet at 3.88 ppm. No H/D is observed at any position other than at C2 under these experimental conditions, indicated by comparison of all the signals due to imidazolium ion **(114)** in the spectrum to the internal standard peak, in this case *t*-butanol which appears as a singlet at 1.24 ppm (D). In the reaction timeframe there is no change in the total integrated area for the signals due to all other protons relative to the constant peak area of the broad triplet at 1.24 ppm due to the internal standard.

Figure 2.41: Representative ^{1}H NMR spectra at 400 MHz of imidazolium ion (114) (10 mM, pD 7.32), obtained during exchange of the C2-H for deuterium in D_2O at 25 °C and I = 1.0 (KCl). The percentage of deuterium exchange is indicated above each spectrum.

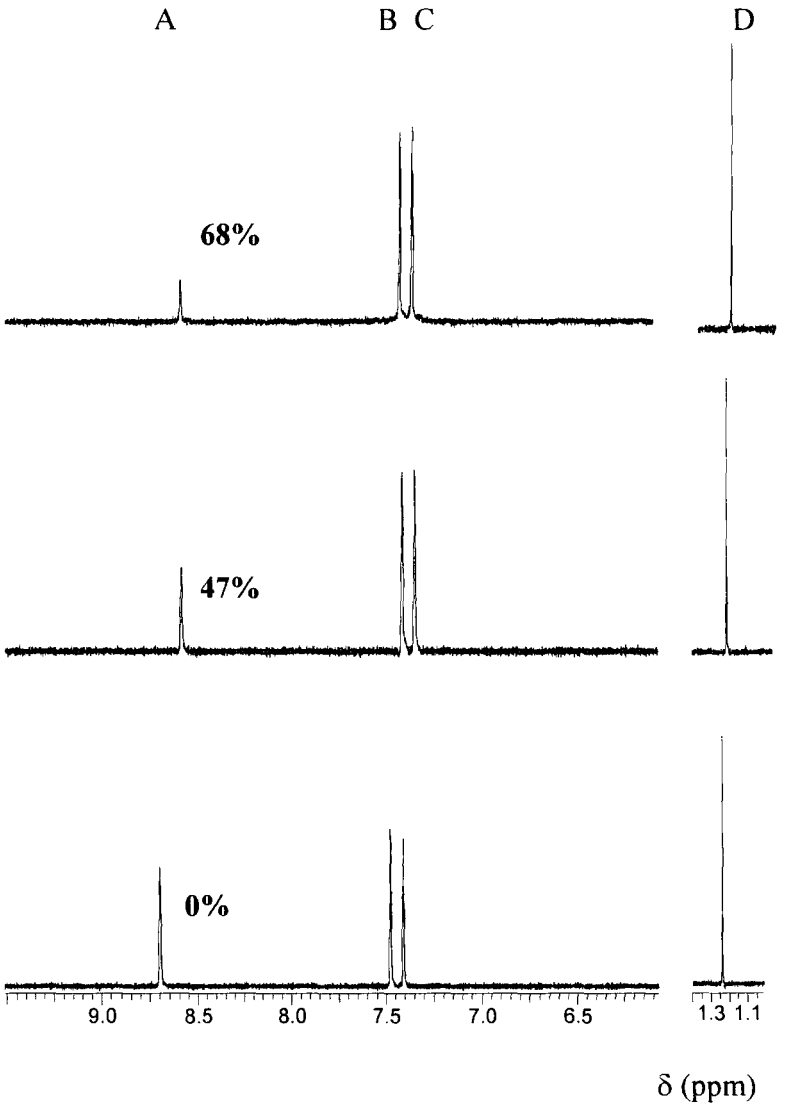

Reaction data and the experimental first-order rate constants for deuterium exchange (k_{obs}, s^{-1}) at different pD values in 100 quinuclidinone buffers shown in Table 2.20. The values for k_{obs} (s^{-1}) shown in Tables 2.20 were obtained from the slopes of

semilogarithmic plots (Figure 2.42a –b) of the fraction of unexchanged substrate against time.

Table 2.20: First-order rate constants for exchange of the C2-H of imidazolium ion (114) for deuterium in quinuclidinone buffers (100 mM) in D_2O at 25 °C and I = 1.0 (KCl).

$[DO^-]^a$ (M)	Time (s)	$f(s)^b$	ln $f(s)$	$k_{obs}{}^c$ (s^{-1})
3.70×10^{-6} (pD 9.31)	0	1.000	0.000	6.83×10^{-4}
	3.60×10^{2}	0.854	-0.158	
	7.22×10^{2}	0.684	-0.380	
	1.14×10^{3}	0.484	-0.727	
	1.56×10^{3}	0.353	-1.042	
8.41×10^{-7} (pD 8.67)	0	1.00	0.000	1.65×10^{-4}
	9.00×10^{2}	0.855	-0.157	
	1.80×10^{3}	0.782	-0.246	
	2.70×10^{3}	0.661	-0.414	
	3.60×10^{3}	0.551	-0.597	
	4.50×10^{3}	0.477	-0.740	
3.52×10^{-7} (pD 8.29)	0	1.000	0.000	6.89×10^{-5}
	4.25×10^{3}	0.733	-0.311	
	7.26×10^{3}	0.618	-0.481	
	1.05×10^{3}	0.476	-0.743	
	1.43×10^{4}	0.375	-0.980	
3.73×10^{-8} (pD 7.32)	0	1.000	0.000	6.79×10^{-6}
	9.34×10^{4}	0.529	-0.637	
	1.63×10^{5}	0.319	-1.142	
	2.54×10^{5}	0.170	-1.770	
	3.40×10^{5}	0.102	-2.287	

(a) Measurements were made in 100 mM quinuclidinone buffer the pD 7.32 – 9.31. $[DO^-]$ was calculated using $[DO^-] = (10^{pD-pKw})/\gamma_{OL}$ with $pK_w = 14.87$, where $\gamma_{OL} = 0.75$ is the activity correction of lyoxide ion under our experimental conditions. (b) The fraction of unexchanged substrate remaining $f(s)$, was calculated according to Equation 2.6. Measurements were made at initial substrate concentration of 10 mM. (c) The value of the first-order rate constant (k_{obs}), was obtained from the slope of the plot of ln $f(s)$ against time in Figure 2.42a and b.

Figure 2.42a: Semi-logarithmic plot of the fraction of remaining C2-H against time for the deuterium exchange reaction of imidazolium ion (114) in 100 mM quinuclidinone buffer at pD 8.29, 8.67 and 9.31.

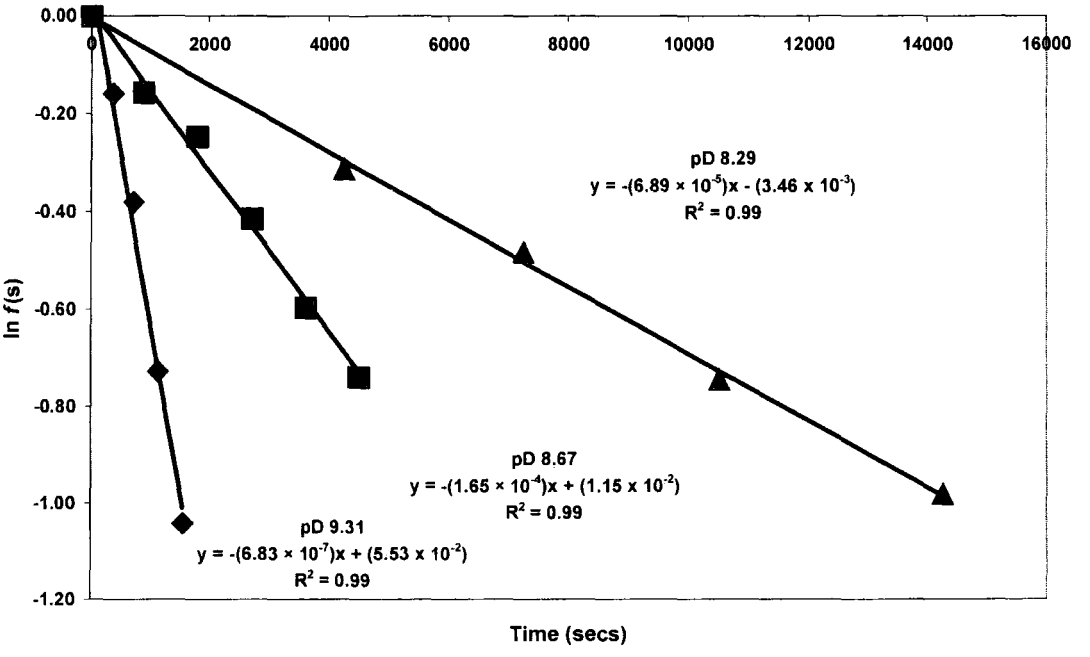

Figure 2.42b: Semi-logarithmic plot of the fraction of remaining C2-H against time for the deuterium exchange reaction of imidazolium ion (114) in 100 mM quinuclidinone buffer at pD 7.32.

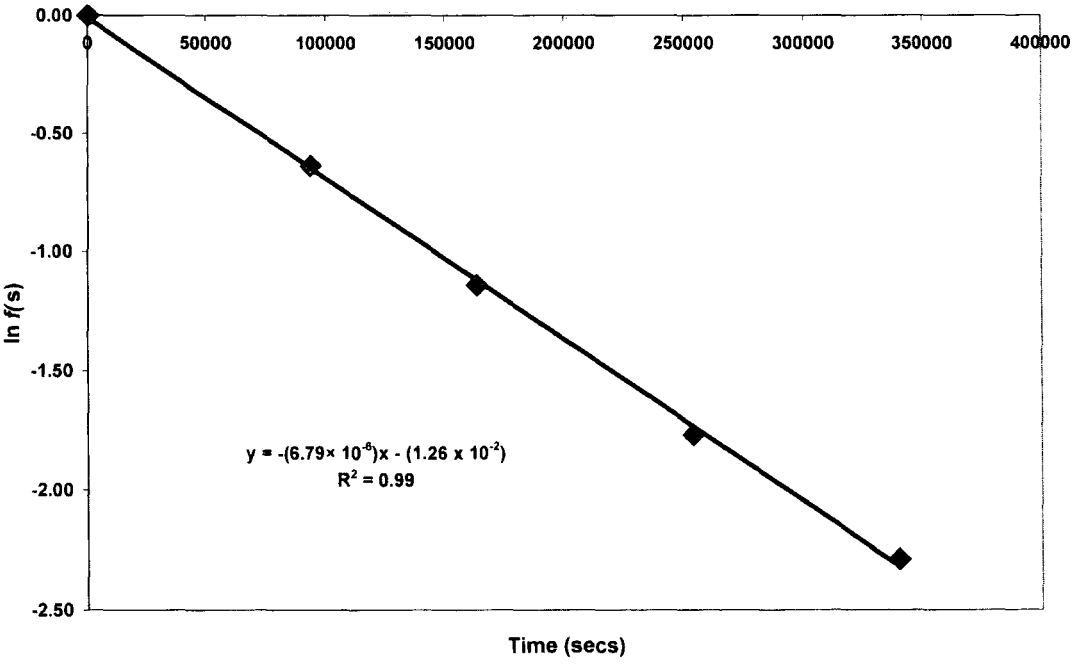

The combined reaction data of imidazolium ion **(114)** in quinuclidinone buffer solution and is shown in Table 2.21. The second-order rate constant for deuteroxide ion-catalysed exchange was calculated from the slope of the plot of k_{obs} against the concentration of deuteroxide ion as shown in Figure 2.43.

Table 2.21: First and second-order rate constants for exchange of the C2-H of imidazolium ion (114) for deuterium in D_2O at 25 °C and I = 1 (KCl).

Buffer Conc. (M)	[DO^-] (M)	k_{obs} (s^{-1})	k_{DO}[a] ($M^{-1}s^{-1}$)
0.1	3.70×10^{-6}	6.83×10^{-7}	1.84×10^{2}
	8.41×10^{-7}	1.65×10^{-4}	
	3.52×10^{-7}	6.89×10^{-5}	
	3.73×10^{-8}	6.79×10^{-6}	

(a) The second-order rate constant, (k_{DO}), was obtained from the slope of the plot of k_{obs} against [DO^-] in Figure 2.43.

Figure 2.43: Plot of k_{obs} against [DO^-] for the H/D exchange reaction of imidazolium ion (114) in D_2O at 25 °C and I = 1.0 (KCl).

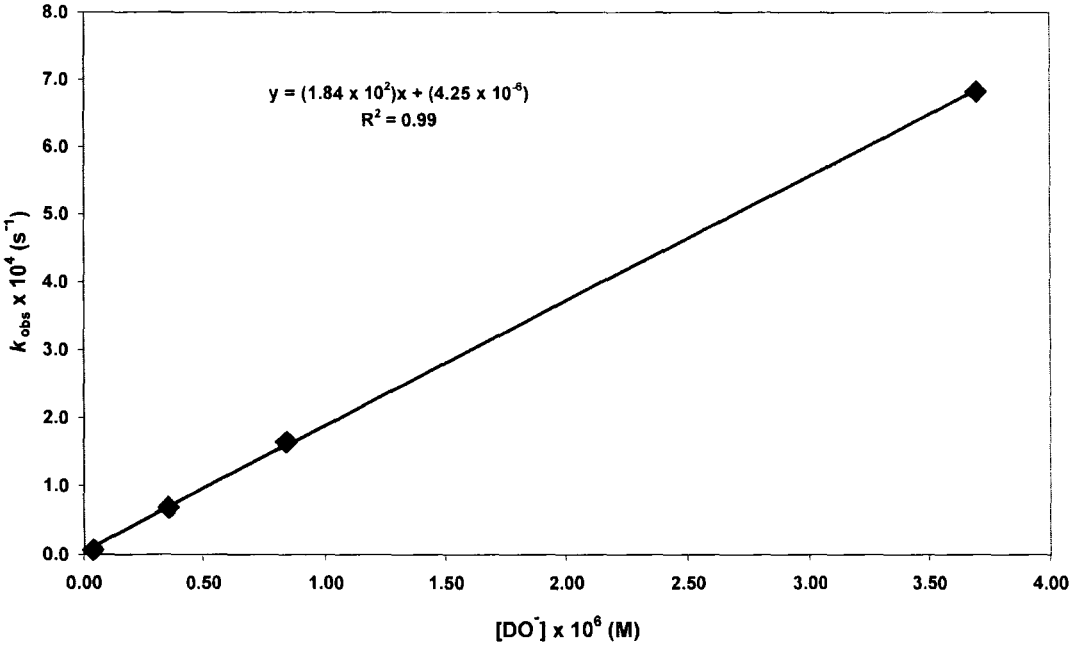

2.2.2.10. 1-Butyl-3-methylimidazolium bromide (115).

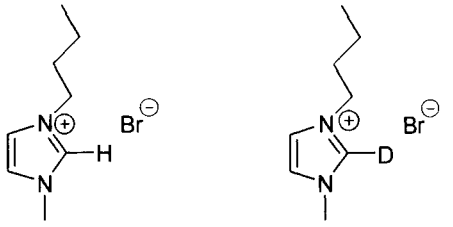

(115) **(115')**

Rates of deuteroxide ion-catalyzed exchange of the C2-H of imidazolium ion **(115)** to form the corresponding deuterated product **(115')**, were determined by 400 MHz ^{1}H NMR spectroscopy.

Figure 2.44 shows representative ^{1}H NMR spectra of imidazolium ion **(115)**, (10 mM, pD 7.31), obtained during the exchange for deuterium of the C2-H in D_2O at 25 °C and I = 1.0 (KCl). Deuterium exchange at the C2 position results in the disappearance of the singlet peak due to the C2-H at 8.66 pm (A). This is measured relative to the internal standard peak. The signals due to the C4-H and C5-H appear as two triplets at 7.43 ppm (B), and 7.38 ppm (C) respectively. The signals due to the three CH_2 groups of the N-butyl substituent appear as a triplet at 4.7 ppm, and two quintets at 1.79 ppm and 1.27 ppm (D). The signals due to the terminal CH_3 of the –butyl substituent appears as a triplet at 0.86 ppm. The signal due to the N-methyl substituent appears as a singlet at 3.84 ppm. H/D exchange is not observed at any position other than at C2 under these experimental conditions, indicated by comparison of all the signals due to imidazolium ion **(115)** in the spectrum to the internal standard peak at 1.21 ppm (E). In the timeframe for the complete exchange of the C2-H for deuterium, there is no change in the peak areas for all other protons relative to the singlet at 1.21 ppm (E) due to the internal standard.

Figure 2.44: Representative ^{1}H NMR spectra at 400 MHz of imidazolium ion (115) (10 mM, pD 7.31), obtained during exchange of the C2-H for deuterium in D_2O at 25 °C and I = 1.0 (KCl). The percentage of deuterium exchange is indicated above each spectrum.

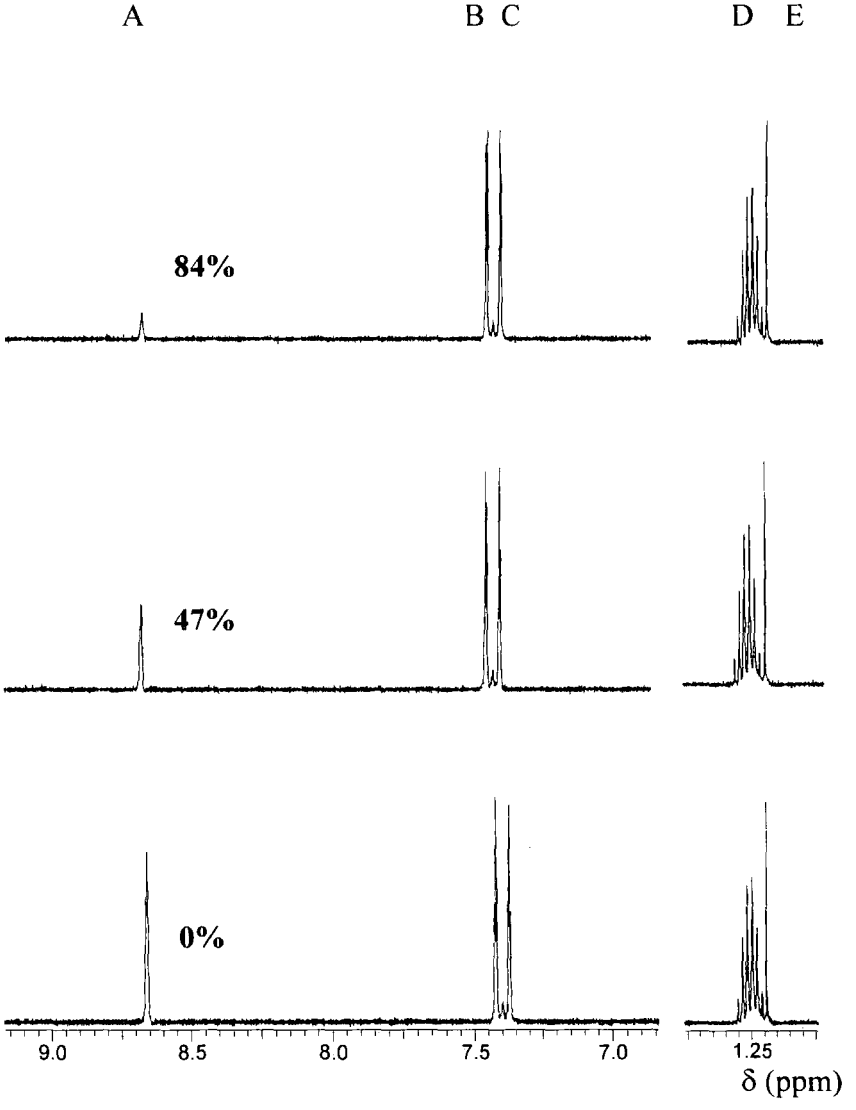

Reaction data and the experimental first-order rate constants for deuterium exchange (k_{obs} s^{-1}) at different pD values in 100 mM quinuclidinone buffers are shown in Table 2.22.

Table 2.22: First-order rate constants for exchange of the C2-H of imidazolium ion (115) for deuterium in quinuclidinone buffers (100 mM) in D_2O at 25 °C and I = 1.0 (KCl).

$[DO^-]^a$ (M)	Time (s)	$f(s)^b$	Ln $f(s)$	$k_{obs}{}^c$ (s^{-1})
3.73×10^{-6} (pD 9.32)	0	1.000	0.000	6.10×10^{-4}
	4.22×10^{2}	0.785	-0.242	
	7.20×10^{2}	0.647	-0.436	
	1.08×10^{3}	0.517	-0.660	
	1.44×10^{3}	0.423	-0.861	
	1.80×10^{3}	0.333	-1.100	
8.41×10^{-7} (pD 8.67)	0	1.000	0.000	1.25×10^{-4}
	1.80×10^{3}	0.824	-0.194	
	2.70×10^{3}	0.717	-0.334	
	3.60×10^{3}	0.677	-0.390	
	4.50×10^{3}	0.558	-0.584	
3.51×10^{-7} (pD 8.29)	0	1.000	0.000	5.81×10^{-4}
	4.33×10^{3}	0.782	-0.247	
	7.38×10^{3}	0.638	-0.451	
	1.06×10^{4}	0.545	-0.608	
	1.44×10^{4}	0.433	-0.837	
3.71×10^{-8} (pD 7.31)	0	1.000	0.000	6.63×10^{-5}
	9.35×10^{4}	0.530	-0.634	
	2.54×10^{5}	0.179	-1.721	
	3.61×10^{5}	0.092	-2.385	

(a) Measurements were made in 100 mM quinuclidinone buffer in the pD 7.31– 9.32 range. $[DO^-]$ was calculated using $[DO^-] = (10^{pD-pKw})/\gamma_{OL}$ with $pK_w = 14.87$, where $\gamma_{OL} = 0.75$ is the activity correction of lyoxide ion under our experimental conditions. (b) The fraction of unexchanged substrate remaining $f(s)$, was calculated according to Equation 2.6. Measurements were made at initial substrate concentration of 10 mM. (c) The value of the first-order rate constant (k_{obs}), was obtained from the slope of the plot of ln $f(s)$ against time shown in Figure 2.45a and b.

Figure 2.45a: Semi-logarithmic plot of the fraction of remaining C2-H against time for the deuterium exchange reaction of imidazolium ion (115) in 100 mM quinuclidinone buffers at pD 8.29, 8.67, and 9.32.

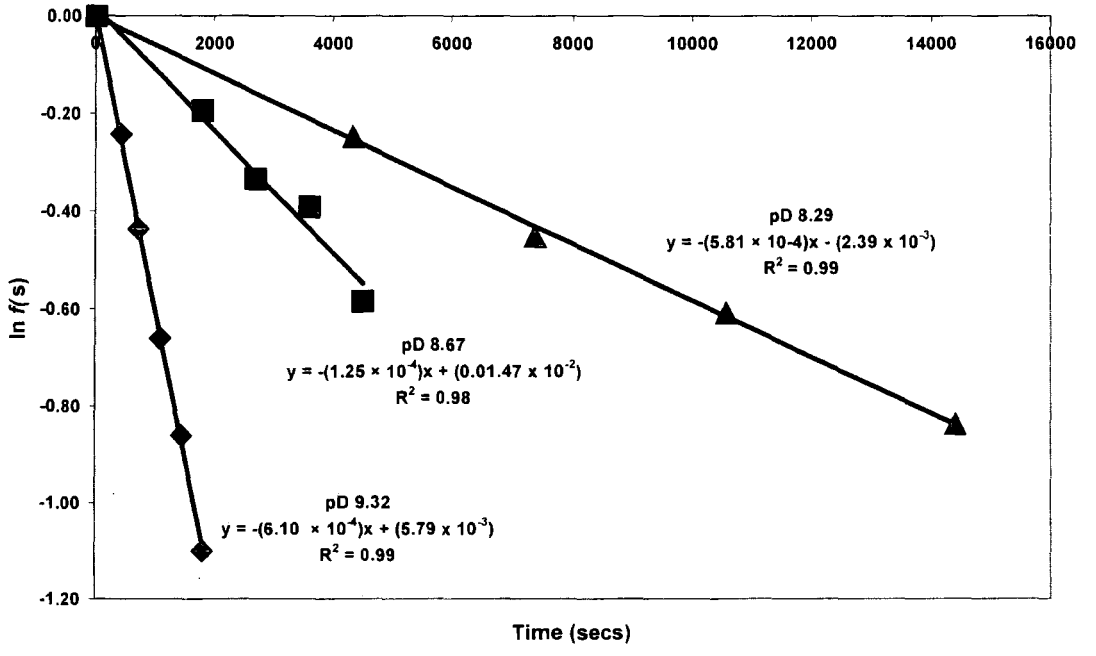

Figure 2.45b: Semi-logarithmic plot of the fraction of remaining C2-H against time for the deuterium exchange reaction of imidazolium ion (115) in 100 mM quinuclidinone buffers at pD 7.31.

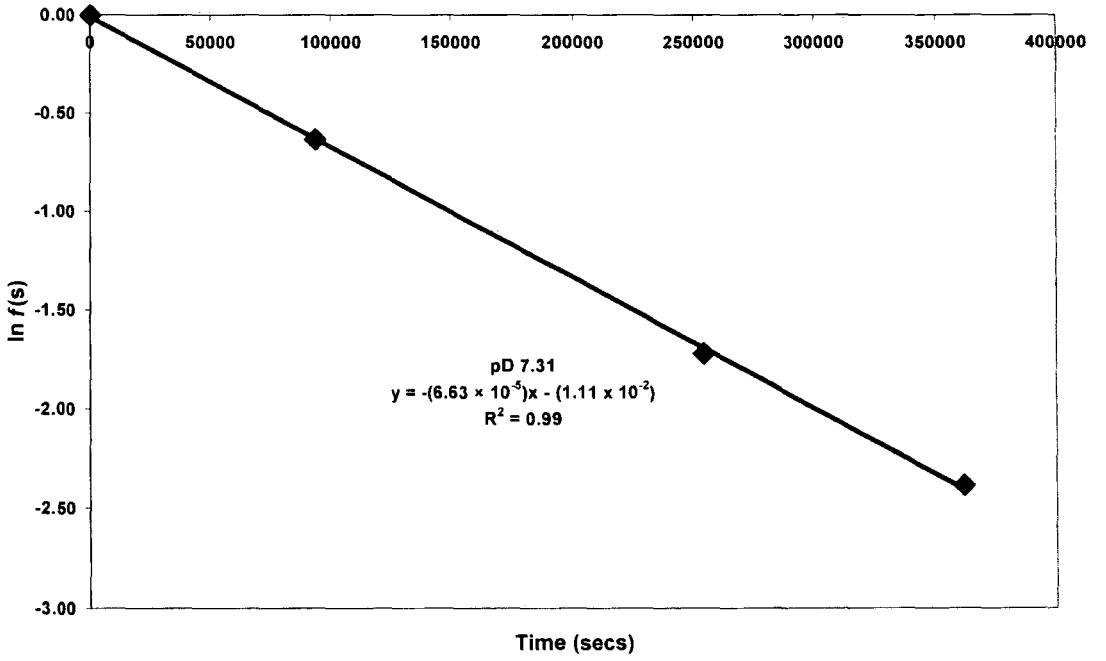

The combined reaction data for imidazolium ion **(115)** in quinuclidinone buffer solution is shown in Table 2.23. The second order rate constant for deuterium exchange (k_{DO}, $M^{-1}s^{-1}$) could be obtained from the slope of a plot of k_{obs} values against deuteroxide concentration (Figure 2.46).

Table 2.23: First and second-order rate constants or exchange of the C2-H of imidazolium ion (115) for deuterium in D_2O at 25 °C and I = 1 (KCl).

Buffer Conc. (M)	$[DO^-]$ (M)	k_{obs} (s^{-1})	k_{DO}[a] ($M^{-1}s^{-1}$)
0.1	3.73×10^{-6}	6.10×10^{-4}	1.64×10^{2}
	8.41×10^{-7}	1.25×10^{-4}	
	3.51×10^{-7}	5.81×50^{-4}	
	3.71×10^{-8}	6.63×10^{-5}	

(a)The second-order rate constant, (k_{DO}), was obtained from the slope of the plot of k_{obs} against $[DO^-]$ in Figure 2.46.

Figure 2.46: Plot of k_{obs} against $[DO^-]$ for the H/D exchange reaction of imidazolium ion (115) in D_2O at 25 °C and I = 1.0 (KCl).

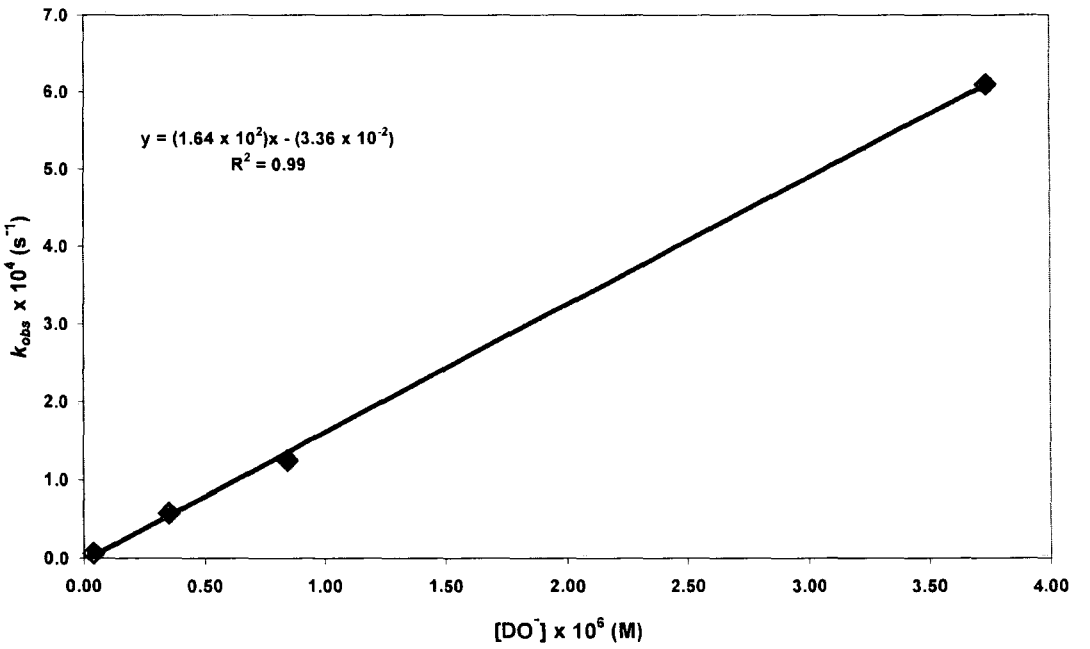

2.2.2.11. 4-Isopropyl-3-mesityl-1-methyl-4,5-dihydroimidazolium iodide (119)

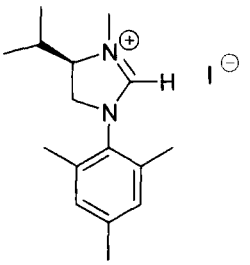

(119)

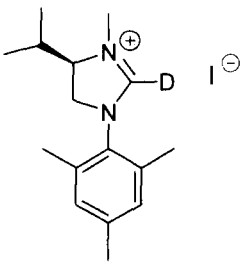

(119')

Rates of deuteroxide ion-catalyzed exchange of the C2-H of imidazolinium ion **(119)** to form the corresponding deuterated product **(119')** were determined by 400 MHz ^{1}H NMR spectroscopy.

Figure 2.47 shows a representative ^{1}H NMR spectrum of imidazolinium ion **(119)**, (5 mM, pD 6.61) before deuterium exchange has occurred. The signal due to the C2-H appears as a singlet at 8.24 ppm (A). The signal due to the two *m*-CHs of the phenyl ring appears as a singlet at 7.04 ppm (B). The signal due to the C4-H appears as a broad triplet at 4.14 ppm (C), due to coupling to the two C5-Hs. However the expected coupling to the isopropyl CH is not evident. The presence of the isopropyl substituent on C4 makes the two hydrogens on C5 diastereotopic, thus the signal due to C5-Hs appears as a poorly resolved doublet of doublets at 3.96 ppm (D) due to coupling to the C4-H. A multiplet at 2.37 ppm (G) is due to the tertiary CH of the isopropyl substituent. The signals due to the methyl groups of the isopropyl substituent at C4 appear as two doublets at 0.99 ppm (J), and 0.97 ppm (K) respectively. The signal due to the methyl group on the quaternary nitrogen appears as a singlet at 3.21 ppm (E). The two singlets at 2.24 ppm (H) and 2.20 ppm (I) are due to the *p*-CH_3 and *o*-CH_3 group respectively.

Figure 2.48 shows representative ^{1}H NMR spectra of imidazolinium ion **(119)** during the exchange reaction. Deuterium exchange at the C2 position results in the disappearance of the singlet peak due to the C2-H at 8.24 ppm (A). There is no change in the total

integrated area for the signals due to all other protons relative to the constant peak area of the broad triplet at 3.15 ppm due to internal standard (F) This is shown by comparison with the internal standard, which appears as a singlet at 3.15 ppm (F).

Figure 2.47: Representative ^{1}H NMR spectrum at 400 MHz of imidazolinium ion (119) in D_2O at 25 °C and I = 1.0 (KCl). The solvent peak at 4.67 ppm due to residual HOD has been removed for clarity.

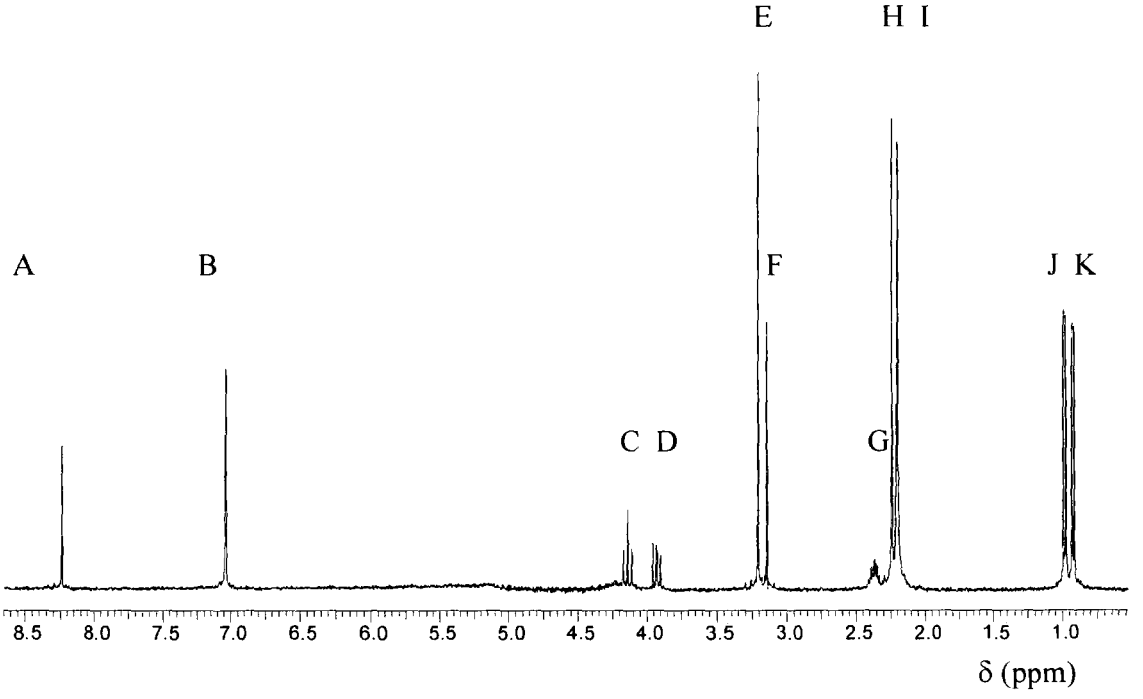

Figure 2.48: Representative ^{1}H NMR spectra at 400 MHz of imidazolinium ion (119) (5 mM, pD 6.61), obtained during exchange of the C2-H for deuterium in D_2O at 25 °C and I = 1.0 (KCl). The percentage of deuterium exchange is indicated above each spectrum.

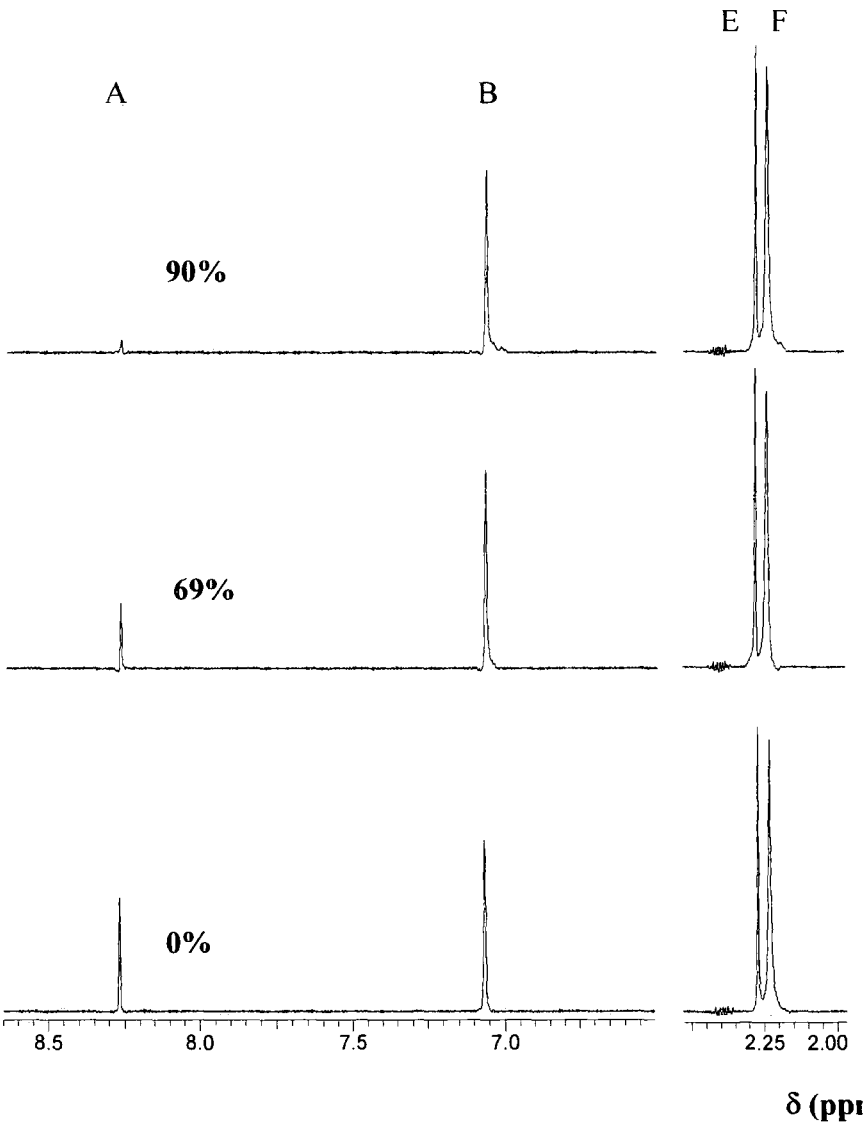

Reaction data and the experimental first-order rate constants (k_{obs}, s^{-1}) at different pD values in 50 mM phosphate buffers are shown in Table 2.24.

Table 2.24: First-order rate constants for exchange of the C2-H of imidazolinium ion (119) for deuterium in phosphate buffers (50 mM) in D_2O at 25 °C and I = 1 (KCl).

$[DO^-]^a$ (M)	Time (s)	$f(s)^b$	Ln $f(s)$	$k_{obs}{}^c$ (s^{-1})
	0	1.000	0.000	
1.87×10^{-8}	7.20×10^4	0.735	-0.308	
(pD 7.02)	3.31×10^5	0.137	-1.992	5.54×10^{-6}
	3.54×10^5	0.130	-2.038	
	4.15×10^5	0.0652	-2.731	
	0	1.000	0.000	
7.27×10^{-9}	1.75×10^5	0.682	-0.383	
(pD 6.61)	3.29×10^5	0.477	-0.740	2.66×10^{-6}
	4.17×10^5	0.439	-0.822	
	5.14×10^5	0.364	-1.012	
	0	1.000	0.000	
4.13×10^{-9}	1.75×10^5	0.909	-0.095	
(pD 6.36)	3.25×10^5	0.723	-0.325	1.51×10^{-6}
	4.16×10^5	0.599	-0.513	
	5.13×10^5	0.588	-0.531	
	0	1.000	0.000	
1.64×10^{-9}	1.75×10^5	0.971	-0.029	
(pD 5.96)	3.24×10^5	0.909	-0.095	7.02×10^{-7}
	4.15×10^5	0.780	-0.248	
	5.13×10^5	0.767	-0.266	
	6.71×10^5	0.627	-0.467	

(a) Measurements were made in 50 mM phosphate buffer in the pD 5.96 – 7.02 range. $[DO^-]$ was calculated using $[DO^-] = (10^{pD-pKw})/\gamma_{OL}$ with $pK_w = 14.87$, where $\gamma_{OL} = 0.75$ is the activity correction of lyoxide ion under our experimental conditions. (b) The fraction of unexchanged substrate remaining $f(s)$, was calculated according to Equation 2.6. Measurements were made at initial substrate concentration of 10 mM. (c) The value of the first-order rate constant (k_{obs}), was obtained from the slope of the plot of ln $f(s)$ against time in Figure 2.49.

Figure 2.49: Semi-logarithmic plot of the fraction of remaining C2-H against time for the deuterium exchange reaction of imidazolinium ion (119) in 50 mM phosphate buffer at pD 5.96, 6.36, 6.61 and 7.02.

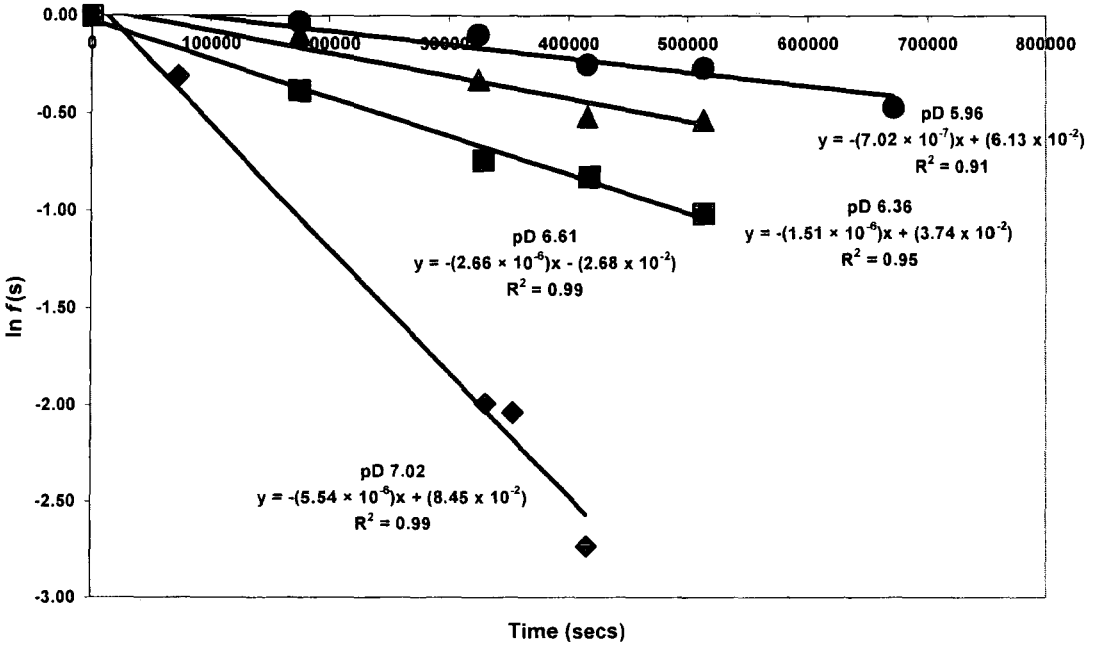

The combined reaction data for the deuterium exchange reaction of imidazolinium ion **(119)** in phosphate buffer solutions is shown in Table 2.25. The second order rate constant for deuterium exchange (k_{DO}, $M^{-1}s^{-1}$) could be obtained from the slope of a plot of k_{obs} values against deuteroxide concentration (Figure 2.50).

Table 2.25: First and second-order rate constants for exchange of the C2-H of imidazolinium ion (119) for deuterium in D_2O at 25 °C and I = 1 (KCl).

Buffer Conc. (M)	$[DO^-]$ (M)	k_{obs} (s^{-1})	k_{DO}[a] ($M^{-1}s^{-1}$)
0.05	1.87×10^{-8}	5.54×10^{-6}	3.45×10^{2}
	7.27×10^{-9}	2.66×10^{-6}	
	4.13×10^{-9}	1.51×10^{-6}	
	1.64×10^{-9}	7.02×10^{-7}	

(a)The second-order rate constant, (k_{DO}), was obtained from the slope of the plot of k_{obs} against $[DO^-]$ in Figure 2.50.

Figure 2.50: Plot of k_{obs} against [DO^-] for the H/D exchange reaction of imidazolinium ion (119) in D_2O at 25 °C and I = 1 (KCl).

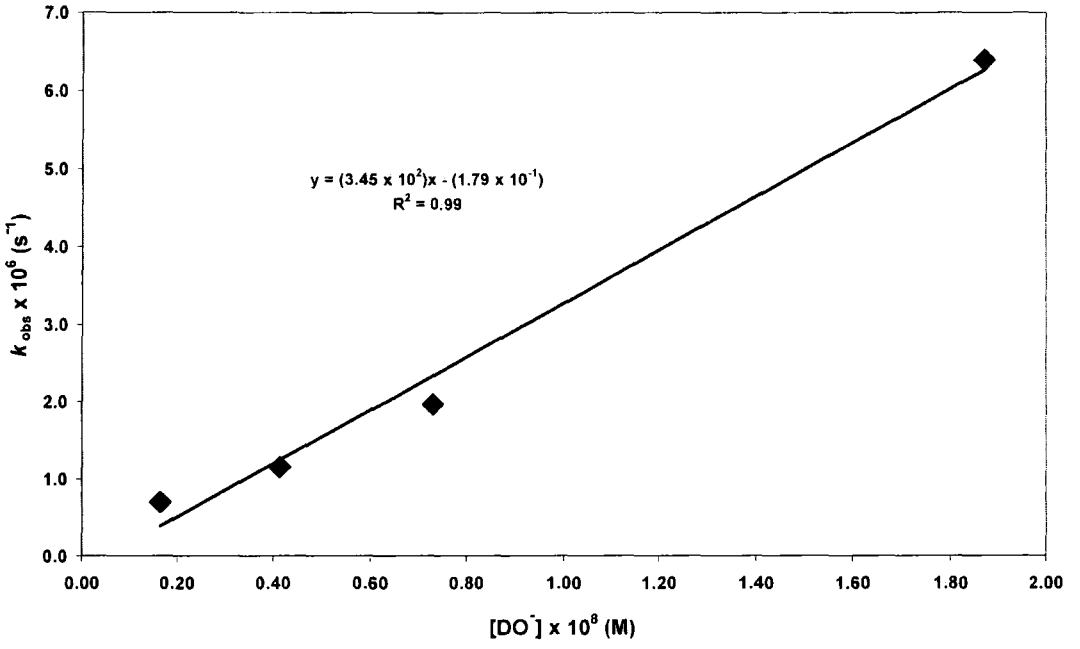

2.2.2.12 1,3-Di-*iso*propyl-4,5,6-trihydropyrimidinium hexafluoro phosphate (120).

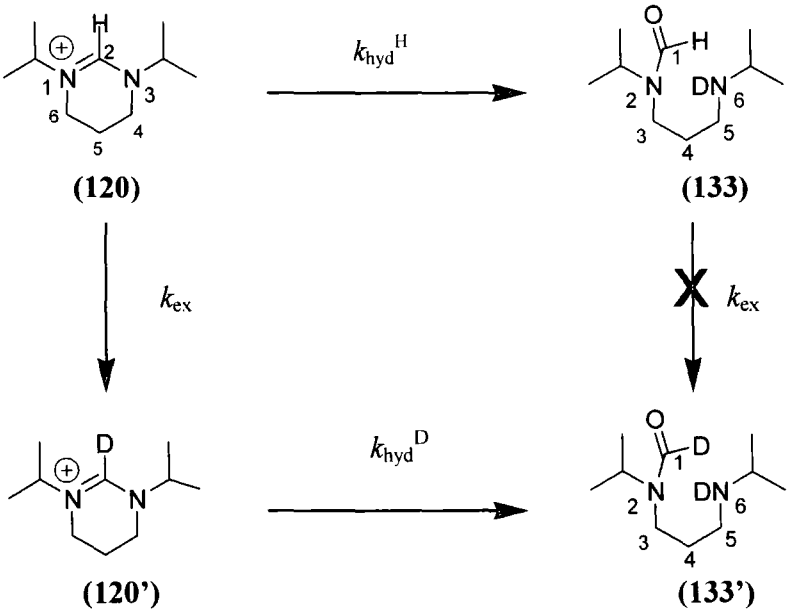

Rates of deuteroxide ion-catalysed exchange of the C2-H of 1,3-di-*iso*propyl-4,5,6-trihydropyrimidinium hexafluoro phosphate **(120)** to form the corresponding deuterated product **(120')** were determined in 0.06 – 0.14 M deuteroxide solution.

Figure 2.51(a) shows a ^{1}H NMR spectrum of trihydropyrimidinium ion **(120)** (10 mM) obtained in D_2O at 25 °C and ionic strength I = 1.0 (KCl). The peak due to the C2-H appears as a singlet a 7.88 ppm (A). The signal due to the two methinyl hydrogens of the N-isopropyl substituents appears as a septet at 3.70 ppm (B) due to coupling to the adjacent methyl protons. The signal due to C4-H_2 and C6-H_2 appears as a triplet at 3.27 ppm (C), due to coupling to C5-H_2. The signal due to the C5-H_2 appears a quintet at 1.90 ppm (D) due to coupling to the adjacent four hydrogens on C4 and C6. Finally, the peak due to the twelve methyl hydrogens of the isopropyl substituents appears as a doublet at 1.20 ppm (E) due to coupling to the two adjacent methinyl hydrogens.

Figure 2.51(b) shows representative ^{1}H NMR spectra of trihydropyrimidinium ion **(120)** (5mM, 0.12 M KOD), obtained during the exchange for deuterium of the C2-H in D_2O at 25 °C and ionic strength I = 1.0 (KCl). Reaction aliquots were quenched to pD 4 prior to ^{1}H NMR analysis. It is clear from the spectra that a competing hydrolysis reaction also occurs under these experimental conditions. As discussed in Section 2.2.2, hydrolysis of trihydropyrimidinium ion **(120)** and **(120')** would yield formadines **(133)** and **(133')** respectively. H/D-exchange is not expected to occur at C1 of formadine **(133)** as exchange of C1-H for deuterium is predicted to be significantly slower than that of the C2-H of ion **(120).**

Deuterium exchange and competing hydrolysis results in the disappearance of the singlet peak due to C2-H at 7.88 ppm (A). Hydrolysis of trihydropyrimidinium ion **(120)** prior to H/D-exchange at C2 results in the appearance of a smaller singlet at 8.10 ppm (A') due to the C1-H of formadine **(133)** only.

Over the timescale of complete disappearance of the peak due to C2-H at 7.88 ppm there are also changes elsewhere in the ^{1}H NMR spectrum due only to the formation of

formadines **(133)** and **(133')**. The signal at 1.90 ppm due to C5-H_2, a quintet, decays and a new signal appears at 1.70 ppm due to the C4-H_2 of formadines **(133)** and **(133')**. The triplets at 3.27 ppm due to C4-H_2 and C6-H_2 of ions **(120)** and **(120')** decay and two new triplets appear at 3.20 ppm and 2.90 ppm due to C3-H_2 and C5-H_2 respectively of formadines **(133)** and **(133')**. The septet at 3.70 ppm due to the methinyl hydrogens of the isopropyl substituents of trihydropyrimidinium ions **(120)** and **(120')** reduces in size by 1/2 over time and a new, smaller, septet at 2.8 ppm due to one of the two now different methinyl protons in formadines **(133)** and **(133')** appears. The signal due to the twelve methyl hydrogens at 1.20 ppm decays. Two new doublets appear at 1.26 ppm and 0.99 ppm due to the methyl groups on the N2-substituent and the methyl groups on the N6-substituent of formadines **(133)** and **(133').** It can be clearly seen that the decrease in area of the peak at 7.88 ppm is not matched by the increase in area of the peak at 8.10 ppm due to hydrolysis product as exchange is significantly faster than hydrolysis under these conditions. H/D exchange is not observed at any position other than at C2 under these experimental conditions, indicated by comparison all the signals due to trihydropyrimidinium ion **(120)** and **(120')** and formadines **(133)** and **(133')** in the spectrum to the internal standard peak at 3.10 ppm. In the reaction timeframe there is no change in the *total* integrated area for the signals due to all other protons of reactant and the corresponding relevant signals of hydrolysis product relative to the constant peak area of the broad triplet at 3.10 ppm due to the internal standard.

Figure 2.51(c) shows a ^{1}H NMR spectrum of the reaction mixture after an extended reaction time of 48 hours to ensure complete disappearance of the C2-H singlet at 7.88 ppm due to either H/D-exchange or hydrolysis of the substrate. Thus formadines **(133)** and **(133')** are present to a large extent. There is also evidence in this spectrum of further hydrolysis to formate and N,N'-di-*iso*propylethylene diamine **(134)** due to the appearance of a small septet at 4.45 ppm possibly due to the N-C*H*$(CH_3)_2$ of diamine **(134)** and a similarly small triplet at 2.00 ppm possibly due to the N-CH_2CH_2 of diamine **(134)**. Formate would produce a singlet at 7.9 ppm under these conditions. The presence of a small singlet peak at 7.90 ppm in figure 2.51(c) suggests a small quantity of formate

present in the reaction mixture. This agrees with the results of mass spectroscopic analysis of the quenched reaction mixture discussed below.

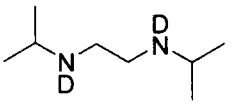

(134)

Figure 2.51(a): ^{1}H NMR spectrum of trihydropyrimidinium ion (120) in D_2O solution at ionic strength I = 1.0 (KCl) and 25 °C.

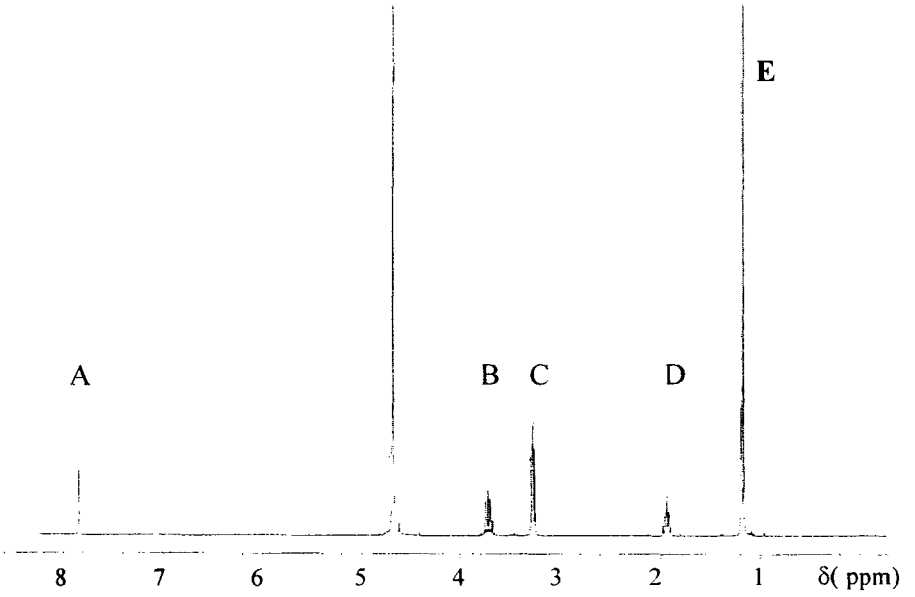

Figure 2.51(b): Representative ^{1}H NMR spectra at 300 MHz of (120) (5mM, 0.12 M KOD) obtained during the exchange reaction of C2-H for deuterium in D_2O and minimal amounts of competing hydrolysis at 25°C and ionic strength I = 1.0 (KCl).

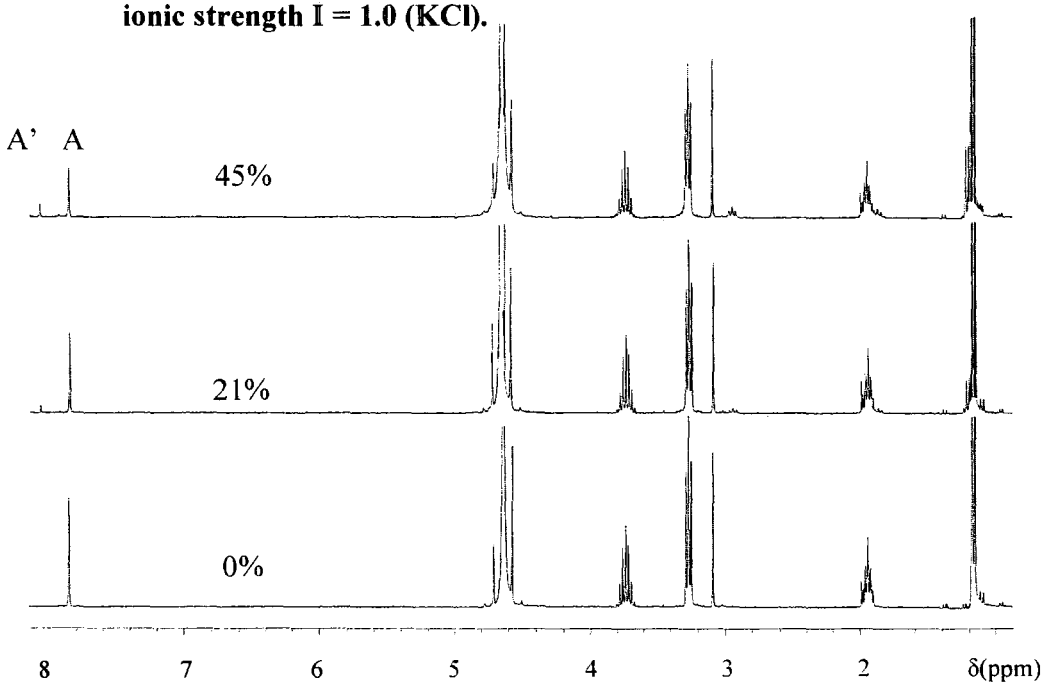

Figure 2.51(c): Representative ^{1}H NMR spectrum of the trihydropyrimidinium ion (120), displaying the peaks for the hydrolysis product (133), (133') and (134) after almost complete hydrolysis had occurred.

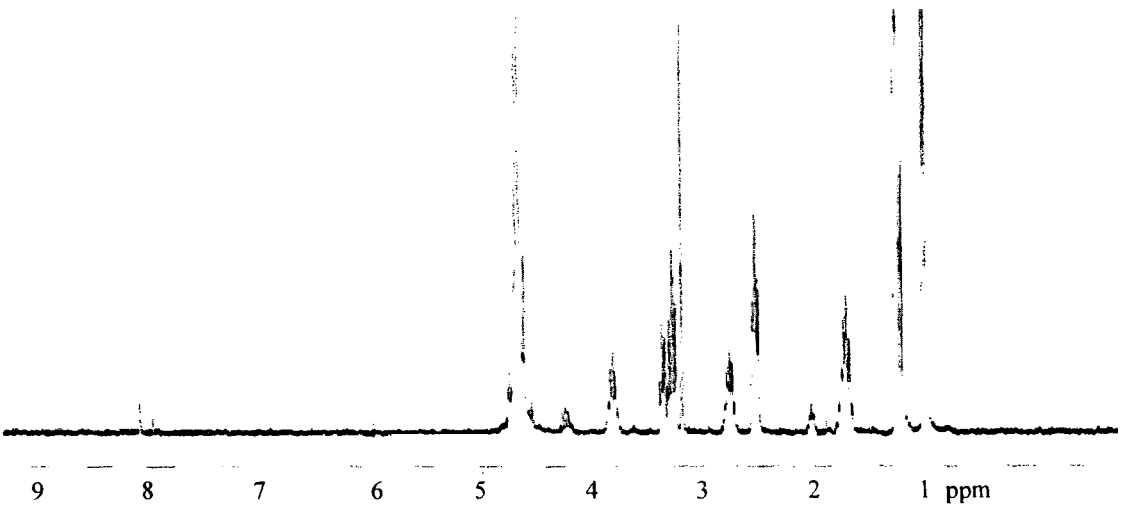

Reaction data and the experimental first-order rate constants for deuterium exchange (k_{obs}(ex), s^{-1}) and hydrolysis (k_{obs}(hyd), s^{-1}) at different pD values in deuteroxide solution are shown in Table 2.26 – 2.27. First order rate constants for the overall disappearance of substrate due to both hydrolysis and exchange (k_{obs}(hyd + ex), s^{-1}) could be determined from the slopes of semilogarithmic plots of the fraction of remaining substrate (f(s)) against time (plots not shown). The values for k_{obs}(ex) (s^{-1}) were obtained from the slopes of semilogarithmic plots (not shown) of the fraction of remaining substrate against time with correction for the formation of hydrolysis product in this period (f(s')). The values for k_{obs}(hyd) (s^{-1}) shown in Table 2.27 were calculated by subtraction of the rate constants for exchange only (k_{obs}(ex), s^{-1}) from those for overall disappearance of substrate (k_{obs}(hyd + ex), s^{-1}).

Table 2.26: Analysis of data for the reaction trihydropyrimidinium ion (120) in deuteroxide solution in D_2O at 25 °C and I = 1.0 (KCl).

[a][DO-] (M)	Time (secs)	[b]*f*(s)	[c]*f*(s')	Ln *f*(s)	Ln *f*(s')
0.140	0	1.000	1.000	0.000	0.000
	6.00×10^2	0.851	0.871	-0.161	-0.138
	1.20×10^3	0.792	0.839	-0.230	-0.176
	1.80×10^3	0.698	0.747	-0.360	-0.292
	2.28×10^3	0.642	0.710	-0.443	-0.343
	3.00×10^3	0.511	0.588	0.588	-0.531
0.120	0	1.000	1.000	0.000	0.000
	9.35×10^2	0.819	0.841	-0.200	-0.173
	1.80×10^3	0.740	0.787	-0.302	-0.239
	2.70×10^3	0.596	0.665	-0.518	-0.408
	3.60×10^3	0.526	0.614	-0.643	-0.488
	4.50×10^3	0.430	0.545	-0.843	-0.608
0.100	0	1.000	1.000	0.000	0.000
	1.20×10^3	0.849	0.883	-0.164	-0.124
	2.40×10^3	0.726	0.772	-0.321	-0.258
	3.60×10^3	0.621	0.692	-0.477	-0.368
	4.80×10^3	0.515	0.610	-0.664	-0.495
	6.00×10^3	0.418	0.533	-0.873	-0.630
0.095	0	1.000	1.000	0.000	0.000
	1.20×10^3	0.823	0.853	-0.195	-0.185
	2.41×10^3	0.695	0.737	-0.364	-0.306
	3.60×10^3	0.598	0.668	-0.514	-0.404
	4.80×10^3	0.543	0.624	-0.610	-0.471
	6.00×10^3	0.483	0.576	-0.729	-0.551
0.090	0	1.000	0.000	0.000	0.000
	1.21×10^3	0.922	0.922	-0.081	-0.081
	2.73×10^3	0.735	0.789	-0.308	-0.237
	3.60×10^3	0.677	0.733	-0.390	-0.311
	4.80×10^3	0.580	0.657	-0.545	-0.419
0.080	0	1.000	1.000	0.000	0.000
	1.80×10^3	0.913	0.913	-0.091	-0.091
	3.83×10^3	0.721	0.785	-0.327	-0.242
	5.40×10^3	0.635	0.719	-0.453	-0.330
	7.20×10^3	0.497	0.598	-0.699	-0.515
	1.26×10^4	0.314	0.454	-1.157	-0.790
0.070	0	1.000	1.000	0.000	0.000
	1.92×10^3	0.939	0.939	-0.063	-0.063
	3.42×10^3	0.832	0.880	-0.184	-0.128
	6.24×10^3	0.640	0.710	-0.446	-0.342
	7.23×10^3	0.558	0.644	-0.584	-0.440
	9.06×10^3	0.521	0.622	-0.651	-0.474

0.060	0	1.000	1.000	0.000	0.000
	2.73×10^{3}	0.866	0.866	-0.144	-0.144
	5.48×10^{3}	0.703	0.768	-0.352	-0.264
	8.10×10^{3}	0.563	0.631	-0.574	-0.460
	1.09×10^{4}	0.439	0.520	-0.822	-0.654
	1.35×10^{4}	0.436	0.538	-0.831	-0.620

(a) Measurements were made in D_2O solution, with the addition of KOD to result in the required concentration of deuteroxide. (b) f(s) is the fraction of substrate remaining at time t. This could be calculated using the following equation: $f(s) = (A_s/A_{IS})_t/(A_s/A_{IS})_{t=0}$. In this equation, A_s is the area of the singlet due to the C2-H of substrate **(120)** at 7.88 ppm, and A_{IS} is the area of the broad triplet due to internal standard at 3.10 ppm. (c) f(s') is the fraction of substrate and protonated hydrolysis product present at time t, This could be calculated by using the following equation: $f(s') = ((A_s+A_P)/A_{IS})_t/((A_s+A_P)/A_{IS})_{t=0}$ In this equation, A_s and A_{IS} are as described in footnote (b), and A_P is the area of the singlet at 8.10 ppm due to the C1-H of hydrolysis product **(133)**.

Table 2.27: First order rate constants for the C2 deprotonation and hydrolysis reactions of trihydropyrimidinium ion (120) in deuteroxide solution in D_2O at 25° C and ionic strength I = 1.0 (KCl).

$[DO^-]$ (M)	[a] k_{obs}(hyd + ex) (s^{-1})	[b] k_{obs}(ex) (s^{-1})	[c] k_{obs}(hyd) (s^{-1})
0.140	2.10×10^{-4}	1.65×10^{-4}	4.56×10^{-5}
0.120	1.84×10^{-4}	1.32×10^{-4}	5.13×10^{-5}
0.100	1.44×10^{-4}	1.04×10^{-4}	3.94×10^{-5}
0.095	1.20×10^{-4}	9.04×10^{-5}	2.97×10^{-5}
0.090	1.03×10^{-4}	8.92×10^{-5}	1.34×10^{-5}
0.080	9.53×10^{-5}	6.47×10^{-5}	3.06×10^{-5}
0.070	7.94×10^{-5}	5.86×10^{-5}	2.07×10^{-5}
0.060	6.79×10^{-5}	5.11×10^{-5}	1.68×10^{-5}

(a) The value of the first-order rate constant k_{obs}(hyd + ex), for the total disappearance of the substrate over time due to both deprotonation and hydrolysis, was obtained from the slope of the plot of ln f(s) against time. (b) The value of the first-order rate constant k_{obs}(ex) for the loss of substrate due to exchange only, was obtained from the slope of the plot of ln f(s') against time (c) The value of the first-order rate constant k_{obs}(hyd), for the loss of substrate due to hydrolysis only, was obtained by subtraction of the rate constants for the rate of deprotonation only from those for the total rate of disappearance of substrate.

Figure 2.52 shows the second order plots for the reaction of trihydropyrimidinium ion **(120)** in D_2O solution. The slope of the plot of the first order rate constants for total disappearance (♦k_{obs}(hyd+ ex), s^{-1}) against deuteroxide concentration is the second order rate constant for exchange and hydrolysis reactions of **(120)**. The slope of the plot of the

first order rate constants for exchange (■ k_{obs}(ex), s^{-1}) against deuteroxide concentration is the second order rate constant for the deuteroxide catalysed exchange of the C2-H for deuterium.

From Figure 2.52 the second-order rate constant for total disappearance of trihydropyrimidinium ion **(120)** was determined as $k_{total} = 1.70 \times 10^{-3}$ $M^{-1}s^{-1}$ and that for deuteroxide ion-catalyzed exchange at C2 as $k_{DO} = 1.48 \times 10^{-3}$ $M^{-1}s^{-1}$. From the calculated values for k_{obs}(hyd), s^{-1} (Table 2.27) the second order rate for hydrolysis of trihydropyrimidinium ion **(120)** was determined as $k_{Hyd} = 2.21 \times 10^{-4}$ $M^{-1}s^{-1}$.

Figure 2.52: Plot of k_{obs}(hyd + ex) (♦)and k_{obs}(ex) (■) against [DO^-] for the reaction of trihydropyrimidinium ion (120) in D_2O at 25 °C and ionic strength I = 1.0 (KCl)

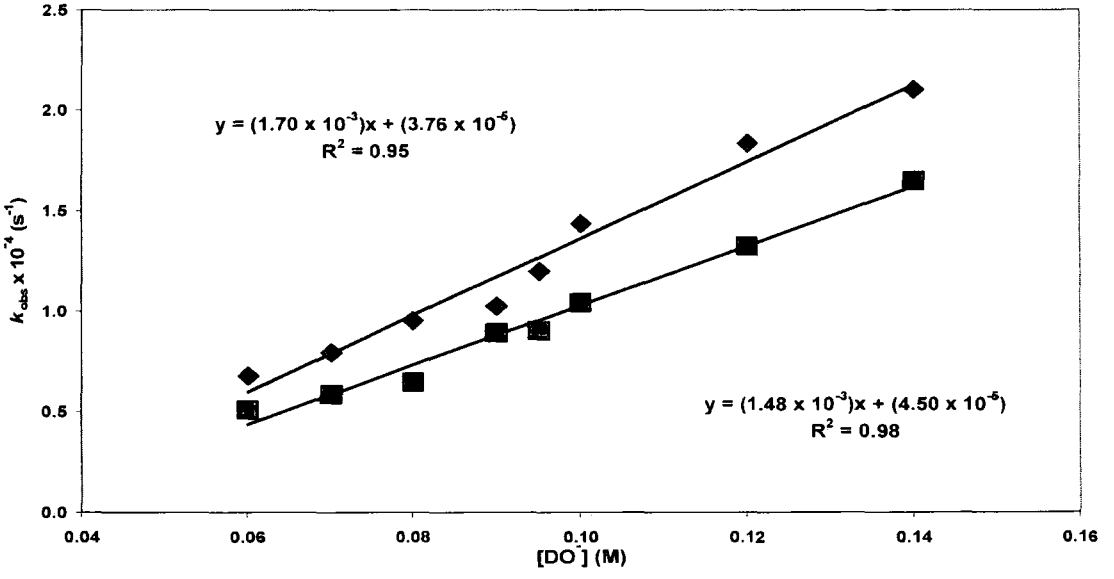

2.2.2.12.1 Mass spectrometry analysis

Mass spectrometric analysis was used to clarify further the extent of exchange which had occurred prior to hydrolysis of trihydropyrimidinium ion **(120)**. Hydrolysis reactions were run to completion under experimental conditions corresponding to those for monitoring exchange.

Upon completion of hydrolysis the reactions were quenched to pD 4 and the products were extracted into chloroform solution. This was to avoid suppression of the MS signal by high concentrations of KCl. The chloroform solution was subsequently diluted with CH_3OH before analysis. Results were analyzed using ES+ mass spectra showing peaks corresponding MW+1 of species.

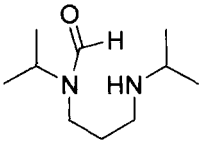

(135)

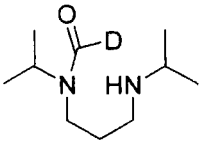

(135')

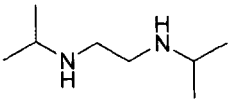

(134')

Dilutions of the product samples in methanol would replace any exchangeable N-Ds for hydrogen. Thus hydrolysis product **(133)** would yield a molecular ion peak due to **(135)** in the mass spectrum, which has a formula weight of 186.28. Hydrolysis product **(133')** would yield a molecular ion peak due to **(135')** in the mass spectrum, which has a formula weight of 187.28.

Figure 2.53 shows the mass spectra of the products after the extended reaction of trihydropyrimidinium ion **(120)** in different concentrations of deuteroxide solution. A large peak at 188.3 is likely due to the hydrolysis product **(135')**. A smaller peak at 187.2 is consistent with the hydrolysis product **(135)** that does not contain deuterium. It is clear from the mass spectral data that significant exchange has occurred prior to hydrolysis, which is consistent with the results obtained by NMR analysis. Finally the peak at 160.2 is consistent with diamine **(135')** which would be obtained from the further hydrolysis of either **(133)** or **(133')**.

Figure 2.53: Mass spectral analysis of the reaction solutions after full hydrolysis of trihydropyrimidinium ion (120).

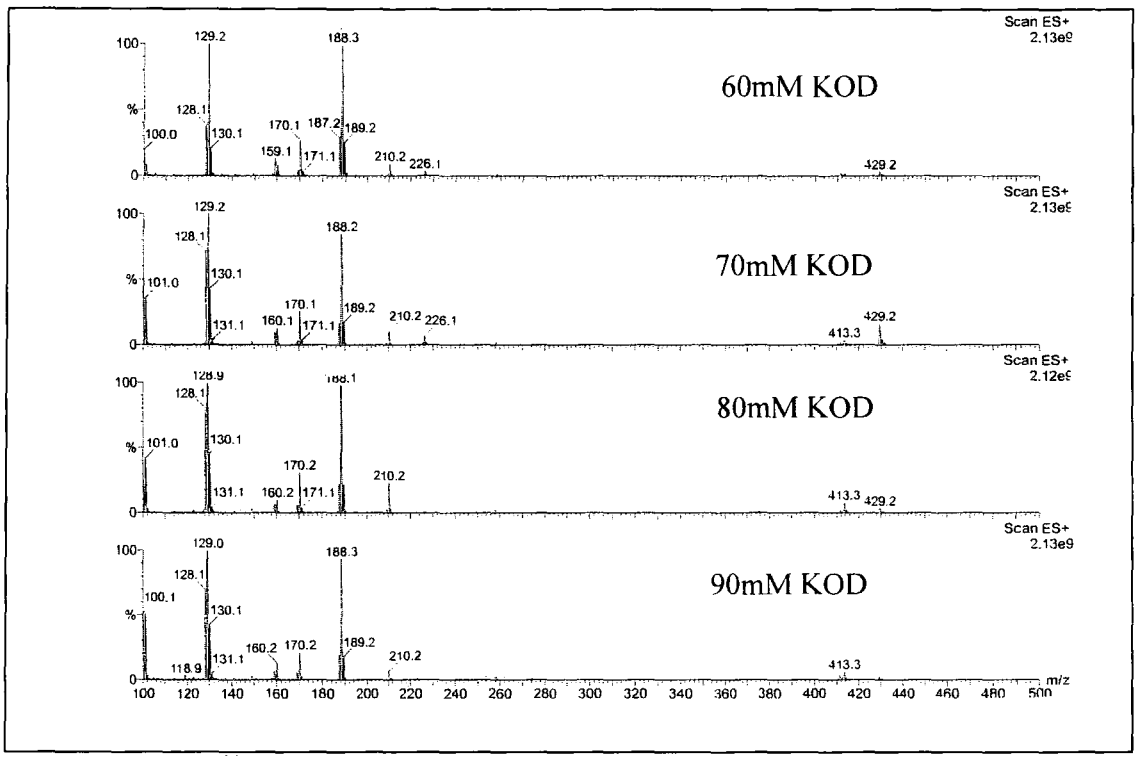

2.2.2.13. 1,3-Diethyl-4,5,6-trihydropyrimidinium hexafluoro phosphate (122)

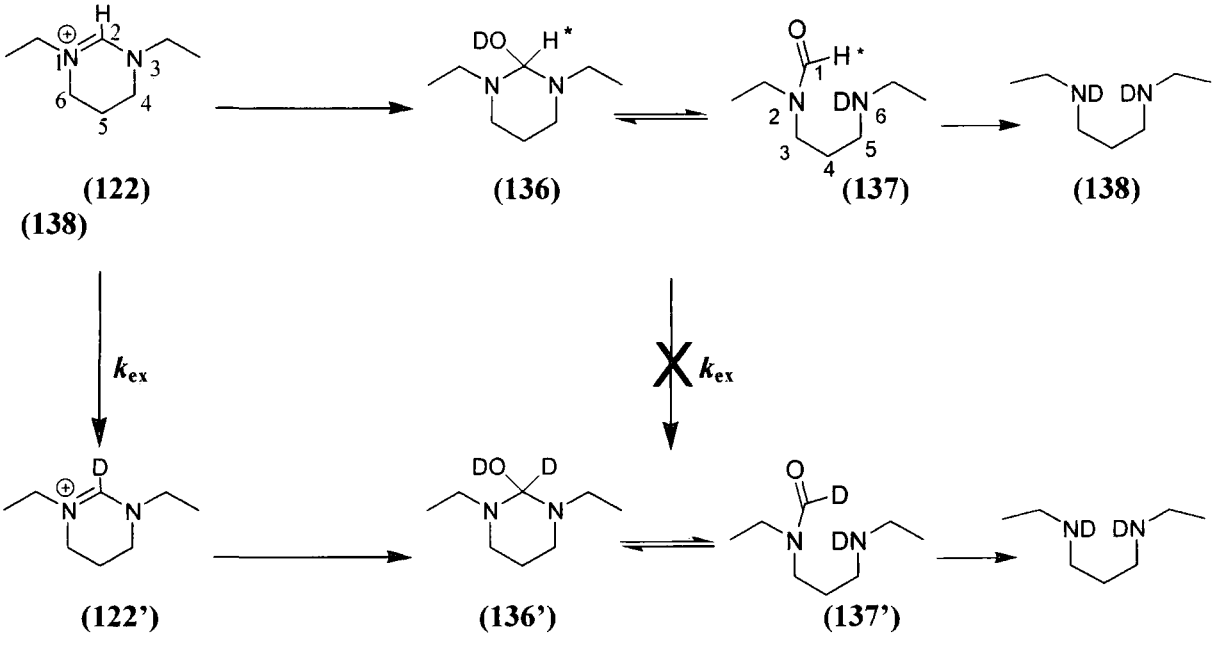

Rates of deuteroxide ion-catalysed exchange of the C2-H of 1,3-diethyl-4,5,6-trihydropyrimidinium hexafluoro phosphate **(122)** to form the corresponding deuterated product **(122')** were determined in 0.05 – 0.095 M deuteroxide solution.

Figure 2.54(a) shows a 300 MHz ^{1}H NMR spectrum of trihydropyrimidinium ion **(122)** (10 mM) in D_2O at ionic strength = 1.0 (KCl). The peak due to the C2-H appears as a singlet at 7.89 ppm (A). The signal due to the CH_2 protons of the N-ethyl substituents appear as a quartet at 3.41 ppm (B) and is coupled to the three adjacent methyl hydrogens. The peak due to the C4-H_2 and C6-H_2 appears as a triplet at 3.31 ppm (C) due to coupling to the two hydrogens of C5. The peak due to the C5-H_2 appear as a quintet at 2.05 ppm (D) due to coupling to the hydrogens on C4 and C6. Finally, the peak due to the methyl protons of the N-ethyl substituents appears as a triplet at 1.20 ppm (E) due to coupling to the two adjacent methylene hydrogens.

Figure 2.54(b) shows representative ^{1}H NMR spectra of trihydropyrimidinium ion **(122)** (5mM, 0.05 M KOD) obtained in D_2O at 25 °C and ionic strength I = 1.0 (KCl). Reaction aliquots were quenched to pD 4 prior to ^{1}H NMR analysis. As in the case of

trihydropyrimidinium ion **(120)**, Figure 2.54(b) clearly shows that hydrolysis is competitive with H/D-exchange at C2 under these experimental conditions. Hydrolysis of trihydropyrimidinium ion **(122)** and **(122')** would result in formation of formadine **(137)** and **(137')** respectively. H/D-exchange is not expected to occur at C1 of formadine **(137)** as exchange of C1-H for deuterium is predicted to be significantly slower than that of C2-H of ion **(122).**

The decay of the singlet at 7.89 ppm is accompanied by the increase in the two new singlets at 7.97 and 8.07 ppm. Integration shows that the relative areas remain constant over the timescale of the reaction.

This could be due to the formation of two different products at fixed relative rates. Alternatively it could be due to the formation of one product which is in rapid equilibrium with a second product over the timescale of the reaction (however slow interconversion on the NMR timescale so that the two species give separate distinct peaks). The most likely candidate is a hydrolysis reaction to yield an initial hemiaminal adduct **(136)**, which could be in rapid equilibrium with formamide derivative **(137)**. In this case the two new singlets at 7.97 and 8.07 ppm would be due to the C2-H of aminal **(136)** and the C1-H of formamide derivative **(137)**. Another option is a rapid equilibrium between formamide **(137)** and a hydrate adduct, however this is unlikely as N,N-dimethylformamide is unhydrated in D_2O solution. A final option is that these two new singlets are due to aldehydic protons of a mixture of initial hydrolysis products **(137)** and further hydrolysis product formate. Further hydrolysis of formamide derivative **(137)** would yield formate and diamine **(138)**. However this option is not consistent with the constant relative areas over time of the two singlets at 7.97 and 8.07 ppm. Any of the options mentioned above would be correctly accounted for by assuming that the sum of the areas of the two singlets are due to only one hydrogen of one or two products. Addition of the total area of these two new singlets at a given timepoint to the remaining area of the singlet due to the C2-H of reactant **(122)** will permit the rate of disappearance of substrate due to exchange only to be estimated.

Changes are also evident elsewhere in the ^{1}H NMR spectrum as reaction proceeds, however it is not possible fully to resolve product peaks from those for reactant. Decreases in peak areas due to all substrate hydrogens are observed over time relative to internal standard. The quintet at 2.05 ppm due to the two C5 hydrogens of substrate **(122)** decays completely over time and a new multiplet appears slightly upfield at 1.95 ppm likely due to the C5 hydrogens of hydrolysis products. Changes are also observed in the 3.31-3.41 ppm region of the spectrum where peaks due to the N-ethyl CH_2, C4-H_2 and C6-H_2 of reactant occur. A new multiplet appears at 3-3.1 ppm that integrates 1.7:1 with the new multiplet at 1.95 ppm. Two new triplets appear in the 1.02 – 1.30 ppm region. The smaller of the two new triplets is upfield of the triplet due to the parent ion **(122)** at 1.20 ppm. The larger of the two new triplets is downfield of the triplet due to the parent ion **(122)**.

Reaction data and the experimental first-order rate constants for deuterium exchange (k_{obs}(ex), s^{-1}) and hydrolysis (k_{obs}(hyd), s^{-1}) at different pD values in deuteroxide solution are shown in Table 2.28 – 2.29. First order rate constants for the overall disappearance of substrate due to both hydrolysis and exchange (k_{obs}(hyd + ex), s^{-1}) could be determined from the slopes of semilogarithmic plots of the fraction of remaining substrate (f(s)) against time (plot not shown). The values for k_{obs}(ex) (s^{-1}) were obtained from the slopes of semilogarithmic plots of the fraction of remaining substrate against time with correction for the formation of hydrolysis product in this period (f(s')). The values for k_{obs}(hyd) (s^{-1}) shown in Table 2.29 were calculated by subtraction of the rate constants for exchange only ((k_{obs}(ex), (s^{-1})) from those for overall disappearance of substrate (k_{obs}(hyd + ex), s^{-1}).

Figure 2.54(a): ^{1}H NMR Spectrum of trihydropyrimidinium ion (122) in D_2O solution at ionic strength I = 1.0 (KCl) and 25 °C.

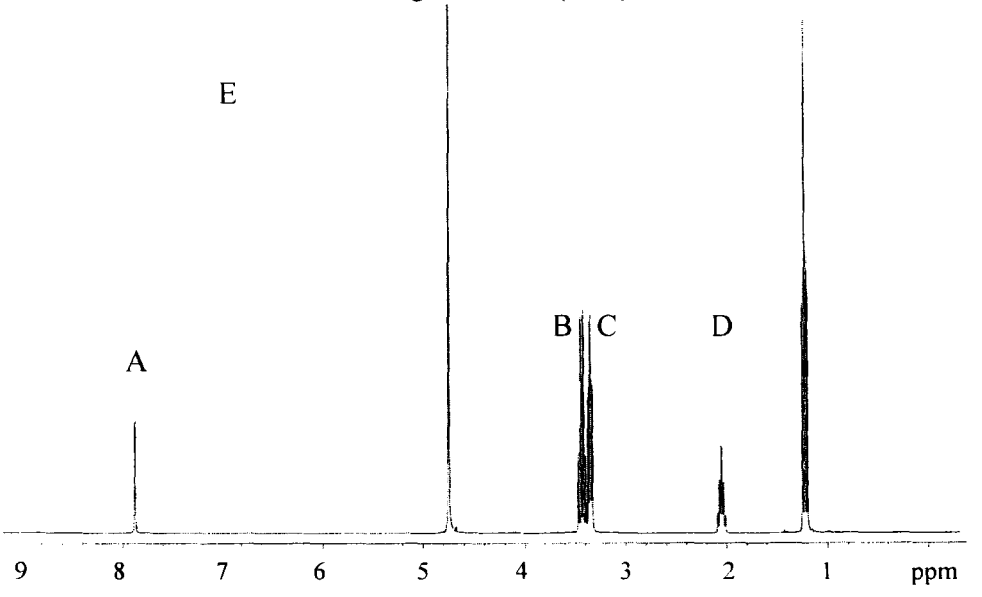

Figure2.54(b):Representative ^{1}H NMR spectra at 300 MHz of trihydropyrimidinium ion (122) (5mM, 0.05 M KOD) obtained during the exchange reaction of C2-H for deuterium, with competing hydrolysis at 25°C, and ionic strength I = 1.0 (KCl).

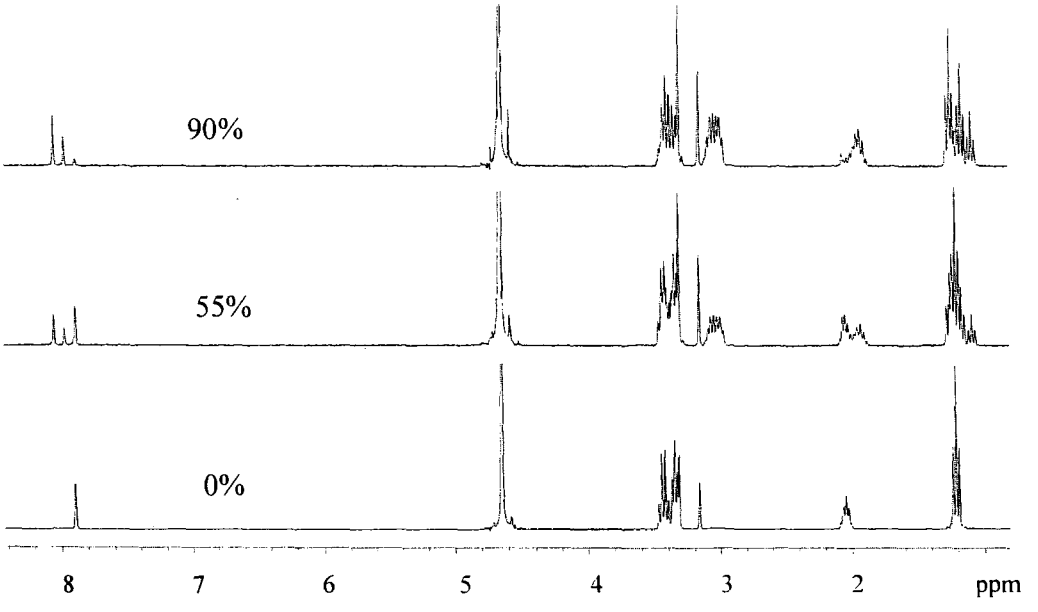

Table 2.28: Analysis of data for the reaction of trihydropyrimidinium ion (122) in deuteroxide solution in D_2O at 25 °C, ionic strength I = 1.0 (KCl).

[a][DO-] (M)	Time (secs)	[b]*f*(s)	ln *f*(s)	[c]*f*(s')	ln *f*(s')
	0	1.000	0.000	1.000	0.000
	9.15×10^{-2}	0.445	-0.890	0.933	-0.070
0.050	1.74×10^{-3}	0.190	-1.616	0.886	-0.121
	2.53×10^{-3}	0.130	-2.041	0.874	-0.135
	3.42×10^{-3}	0.092	-2.383	0.881	-0.127
	0	1.000	0.000	1.000	0.000
	6.00×10^{-2}	0.445	-0.736	0.897	-0.108
0.060	1.20×10^{-3}	0.190	-1.353	0.903	-0.102
	1.80×10^{-3}	0.130	-1.199	0.891	-0.115
	2.40×10^{-3}	0.092	-2.645	0.848	-0.165
	0	1.000	0.000	1.000	0.000
	4.20×10^{-2}	0.541	-0.614	0.896	-0.110
0.070	8.40×10^{-2}	0.278	-1.281	0.847	-0.166
	1.26×10^{-3}	0.154	-1.871	0.854	-0.158
	1.68×10^{-3}	0.098	-2.325	0.836	-0.179
	0	1.000	0.000	1.000	0.000
	3.13×10^{-2}	0.639	-0.448	0.960	-0.041
0.080	6.00×10^{-2}	0.361	-1.018	0.946	-0.055
	9.00×10^{-2}	0.190	-1.662	0.882	-0.126
	1.20×10^{3}	0.102	-2.281	0.785	-0.242
				0.877	
	0	1.000	0.000	1.000	0.000
	4.31×10^{-2}	0.559	-0.582	0.931	-0.071
0.090	5.33×10^{-2}	0.403	-0.909	0.874	-0.135
	7.20×10^{-2}	0.258	-1.356	0.847	-0.166
	9.60×10^{-2}	0.148	-1.911	0.798	-0.225
	0	1.000	0.000	1.000	0.000
	2.40×10^{-2}	0.607	-0.498	0.935	-0.067
0.095	4.80×10^{-2}	0.364	-1.012	0.898	-0.108
	7.20×10^{-2}	0.204	-1.588	0.873	-0.136
	9.60×10^{-2}	0.122	-2.104	0.901	-0.105

(a) Measurements were made in D_2O solution, with the addition of KOD to result in the required concentration of deuteroxide. (b) *f*(s) is the fraction of substrate remaining at time t. This could be calculated using the following equation: $f(s) = (A_s/A_{IS})_t/(A_s/A_{IS})_{t=0}$ In this equation, A_s is the area of singlet due to the C2-H of substrate **(122)** at 7.89 ppm, and A_{IS} is the area of the broad triplet due to the internal standard at 3.10 ppm. (c) *f*(s') is the fraction of substrate and hydrolysis product present at time t. This could be calculated by using the following equation: $f(s') = ((A_s+A_P)/A_{IS})_t/((A_s+A_p)/A_{IS})_{t=0}$ In this equation, A_s and A_{IS} are as described in footnote (b), and A_p is the sum of the areas of the singlets at 7.97 and 8.07 ppm due to hydrolysis products (see main text).

Table 2.29: First-order rate constants for the C2-deprotonation and hydrolysis reactions of trihydropyrimidinium ion (122) in deuteroxide solution in D_2O at 25° C, and ionic strength I = 1.0 (KCl).

[DO-] (M)	[a]k_{obs}(ex + hyd) (s^{-1})	[b]k_{obs}(ex) (s^{-1})	[c]k_{obs}(hyd) (s^{-1})
0.050	6.73×10^{-4}	3.78×10^{-5}	6.36×10^{-4}
0.060	9.98×10^{-4}	$5{,}62 \times 10^{-5}$	9.42×10^{-4}
0.070	1.41×10^{-3}	9.69×10^{-5}	1.31×10^{-3}
0.080	1.72×10^{-3}	1.53×10^{-4}	1.57×10^{-3}
0.090	1.93×10^{-3}	2.40×10^{-4}	1.69×10^{-3}
0.095	2.11×10^{-3}	1.31×10^{-4}	1.98×10^{-3}

(a) The value of the first-order rate constant k_{obs}(hyd + ex) for the total disappearance of the substrate over time due to both deprotonation and hydrolysis, , was obtained from the slope of the plot of ln *f*(s) against time. (b) The value of the first-order rate constant k_{obs}(ex) for the loss of substrate due to exchange only, was obtained from the slope of the plot of ln *f*(s') against time. (c) The value of the first-order rate constant k_{obs}(hyd) for the loss of substrate due to hydrolysis only, was obtained by subtraction of the rate constants for deprotonation only from those for total disappearance of substrate.

Figure 2.55 shows the second order plots for the reaction of trihydropyrimidinium ion **(122)** in D_2O solution. The slope of the plot of the first order rate constants for total disappearance ((♦)k_{obs}(hyd+ ex), s^{-1}) against deuteroxide concentration is the second order rate constant for exchange and hydrolysis reactions of ion **(122)**. The slope of the plot of the first order rate constants for exchange ((▲) k_{obs}(ex), s^{-1}) against deuteroxide concentration is the second order rate constant for the deuteroxide ion-catalysed exchange of the C2-H for deuterium.

From Figure 2.55 the second-order rate constant for total disappearance of trihydropyrimidinium ion **(122)** was determined $k_{total} = 3.18 \times 10^{-2}$ $M^{-1}s^{-1}$. The second-order rate constant for exchange of trihydropyrimidinium ion **(122)** was determined as $k_{DO} = 3.12 \times 10^{-3}$ $M^{-1}s^{-1}$. The second order rate for deuteroxide ion-catalyzed hydrolysis of trihydropyrimidinium ion **(122)** could then be estimated as $k_{Hyd} = 2.86 \times 10^{-2}$ $M^{-1}s^{-1}$.

Figure 2.55:. Plot of log k_{obs}(Hyd + ex) (♦), of k_{obs}(ex) (▲) and k_{obs}(Hyd) (■) against [DO^-] for the reaction of trihydropyrimidinium ion (122) in D_2O at 25°C and ionic strength I = 1.0 (KCl).

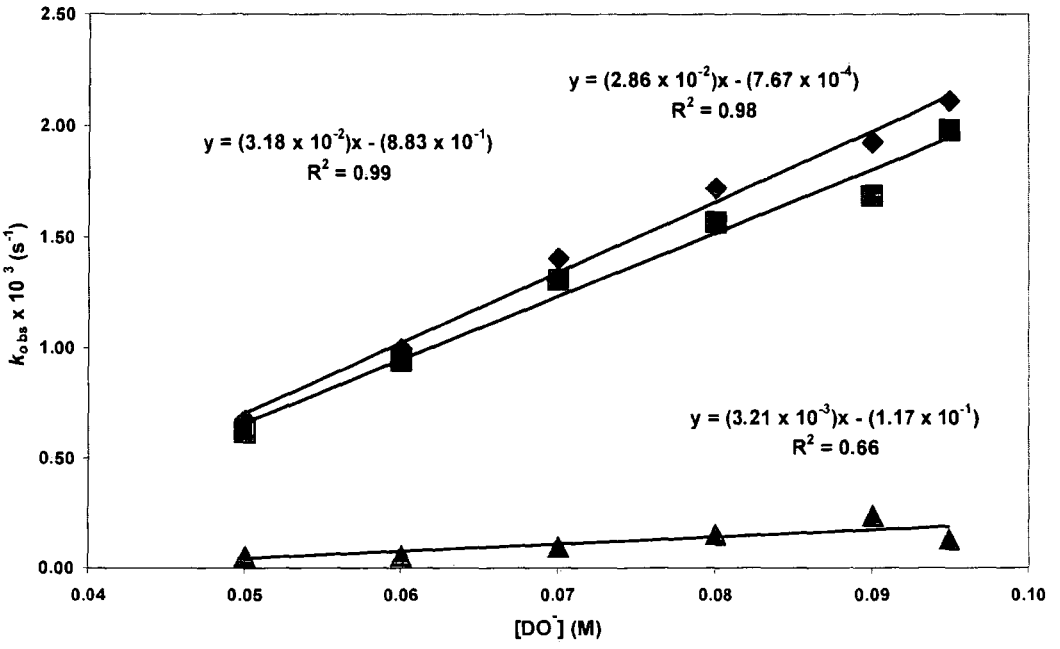

2.2.2.13.1 Mass spectrometry analysis

Mass spectrometric analysis was used as before to further clarify the fraction of exchange which had occurred prior to hydrolysis of trihydropyrimidinium ion **(122)**. Hydrolysis reactions were run to completion under experimental conditions corresponding to those run for monitoring exchange.

Upon the completion of hydrolysis, the reaction mixture was quenched to pD 4 and the products were extracted into chloroform solution to avoid suppression of the MS signal by high concentrations of KCl. The chloroform solution was subsequently diluted with methanol before analysis by GC-MS. Results were analyzed using ES+ mass spectra showing peaks corresponding MW+1 of species

Dilutions of the product samples in methanol would replace any exchangeable N-D for hydrogen. Thus hydrolysis product **(137)** would yield a molecular ion peak due to **(139)** in the mass spectrum, which has a formula weight of 158.2, and is indistinguishable from aminal **(136)**. Hydrolysis product **(138')** would yield a molecular ion peak due to **(139')** in the mass spectrum, which has a formula weight of 159.2, and is indistinguishable from aminal **(137')**.

Figure 2.56 shows the mass spectra of products of the extended reaction of trihydropyrimidinium ion **(122)** in different concentrations of deuteroxide solution. A large peak at 160.1 is likely due to the presence of **(140')**.

A small peak at 142.1 is consistent with starting material trihydropyrimidinium ion **(122)**, and a slightly larger peak at 131.1 is consistent with diamine **(139')** formed on further hydrolysis of formamide derivative **(137)**.

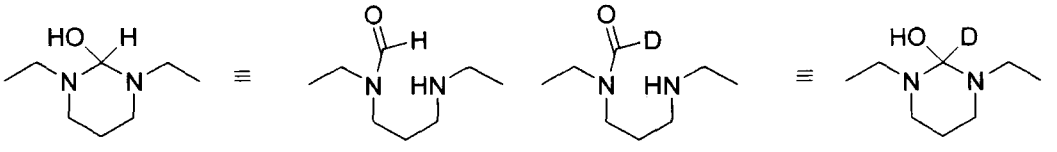

(136) **(139)** **(139')** **(136')**

(138')

The NMR exchange experiments indicated that hydrolysis was significantly faster than exchange in this case, thus the major expected product after complete hydrolysis should be **(137)** and not **(137')**. It could be that due to the longer timescale of these reactions for mass spectrometry compared to those conducted for NMR analysis that instead the hydrolysis product **(138')** is present to a greater extent in this case. It could also just be a feature of the mass spectrometry experiments. For absolute clarification by mass spectrometry, proper calibration experiments should be performed with authentic

independent samples of known relative concentrations of all reactant and product species to calibrate relative responses.

Figure 2.56: Mass spectral analysis of the reaction solutions after full hydrolysis of trihydropyrimidinium ion (122)

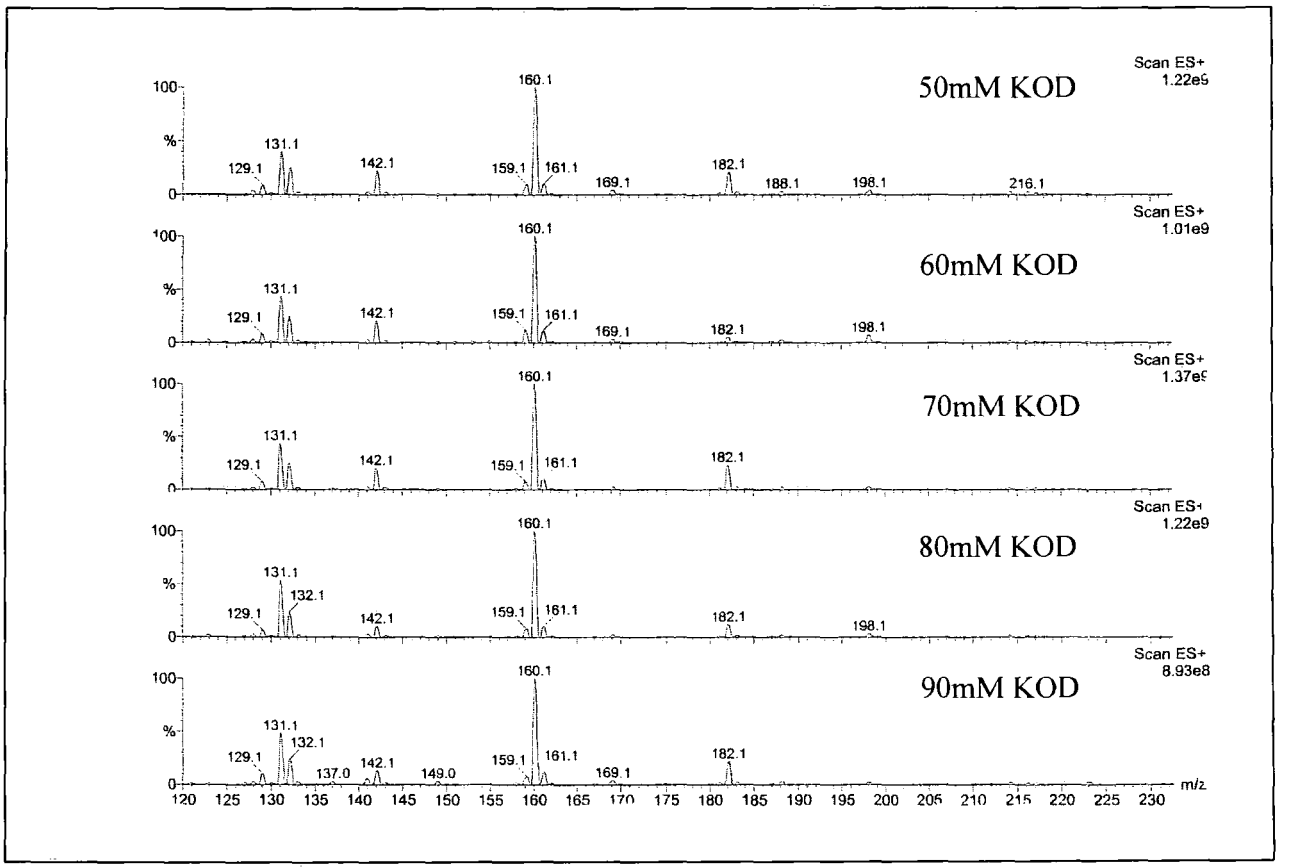

2.2.2.14 1,3-Di-*iso*propyl-4,5,6-trihydropyrimidinium, bis(trifluoromethylsulfonyl)amide (121)

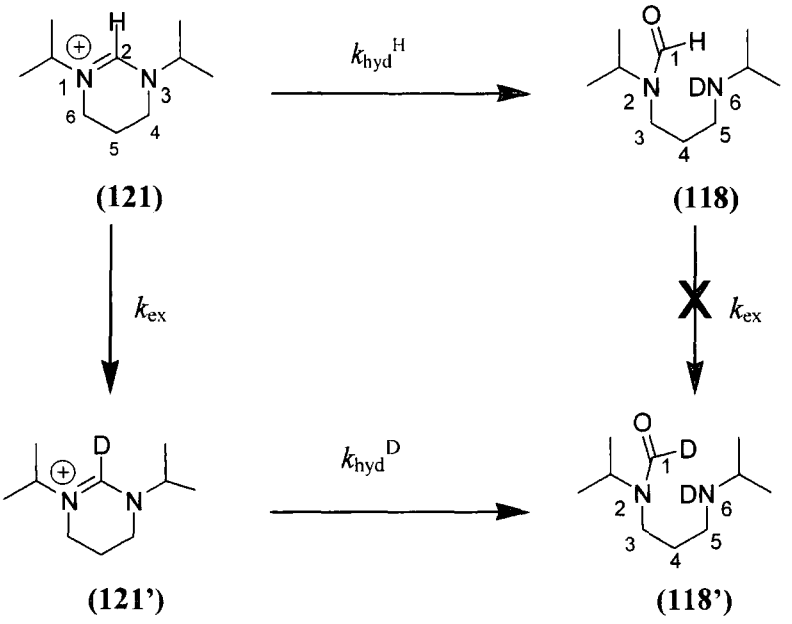

Rates of deuteroxide catalyzed exchange of the C2-H of the 1,3-di-*iso*propyl-3,4,5,6-tetrahydro-pyrimidin-1-ium bis(trifluoromethylsulfonyl)amide **(121)** to form the corresponding deuterated product **(121')** were determined in 0.08 - 0.14 M deuteroxide solution.

Figure 2.57 shows representative ^{1}H NMR spectra of trihydropyrimidinium ion **(121)** in 0.14 M KOD, obtained during the exchange of the C2-H for deuterium in D_2O at 25 °C and ionic strength I = 1.0 (KCl). The peak due to the C2-H appears as a singlet at 7.91 ppm (A). The signal due to the two equivalent methinyl hydrogens of the N-isopropyl substituents appears as a septet at 3.79 ppm (B), due to coupling to the six adjacent methyl protons. The signal due to the C4-H_2 and C6-H_2 appears as a multiplet at 3.27 ppm (C) due to coupling to C5-H_2. This peak appears to resemble a doublet of doublets, which could be due to the slight non-equivalence of the two C5 hydrogens. The signal due to C5-H_2 appears as a multiplet at 1.99 ppm (E) due to coupling to the C4, and C6 hydrogens, and also potential coupling between the two C5 hydrogens. Due to the broad

nature of the peaks, this could not be confirmed by a comparison of the coupling constants. Finally, the peak due to the twelve methyl hydrogens of the isopropyl substituents appears as a doublet at 1.20 ppm (E) due to coupling to the two adjacent methinyl hydrogens.

The result of reaction of pyrimidinium salt **(121)** in deuteroxide solution was the disappearance of a singlet peak due to the C2-H at 7.91 ppm (A). In contrast with the trihydropyrimidinium salt **(120)**, no competing hydrolysis reaction was detectible to any measurable extent under these experimental conditions. However, trihydropyrimidinium salt **(121)** was found to be significantly less soluble than **(120)** and as hydrolysis is expected to be significantly slower than exchange for this ion, as with **(120)**, it is likely that the low concentration of species **(121)** rendered it undetectable in the ^{1}H NMR spectra. In the following analysis it is assumed that no hydrolysis occurs. H/D exchange is not observed at any position other than at C2 under these experimental conditions.

Figure 2.57: Representative ^{1}H NMR spectra at 400 MHz of trihydropyrimidinium ion (121) (1mM, 0.14 M KOD) obtained during the exchange reaction of C2-H for deuterium in D_2O at 25°C and ionic strength I = 1 (KCl).

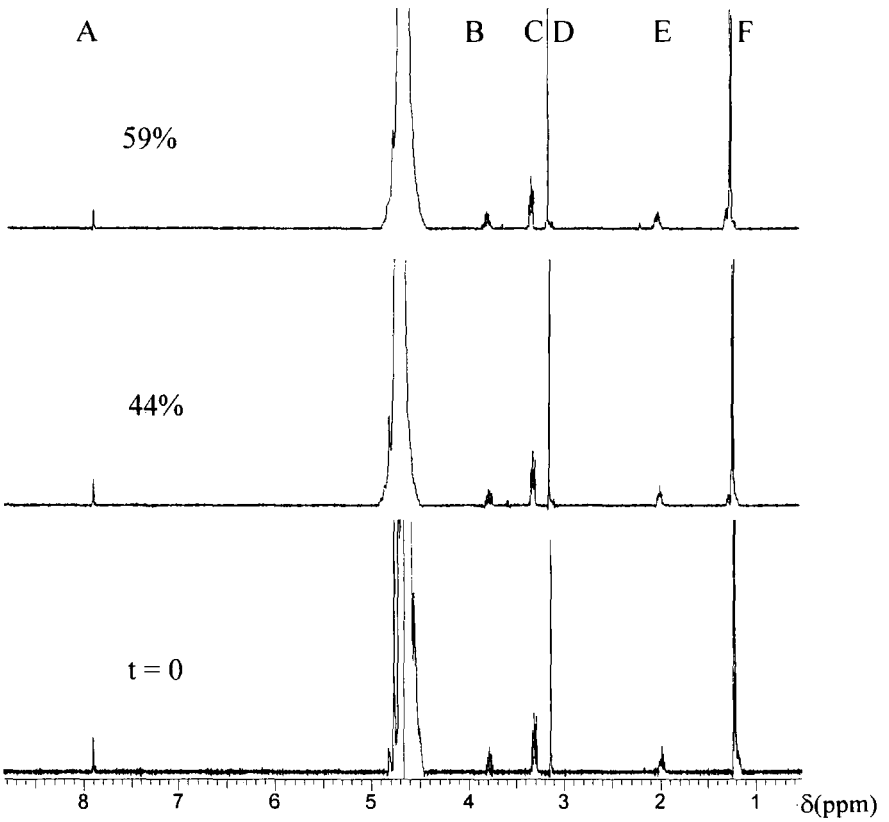

Reaction data and the experimental first-order rate constants for deuterium exchange (k_{obs}(ex), s^{-1}) at different concentrations of deuteroxide ion are shown in Table 2.30. The values for k_{obs}(ex) (s^{-1}) shown in Table 2.30 are obtained as the slopes of semilogarithmic plots of the fraction of unexchanged substrate against time.

Table 2.30: First-order rate constants for exchange of the C2-H of trihydropyrimidinium ion (121) for deuterium in deuteroxide solution in D_2O at 25 °C and ionic strength I = 1.0 (KCl).

$[DO^-]^a$ (M)	Time (s)	$f(s)^b$	$\ln f(s)^c$	$k_{obs}{}^d$ (s^{-1})
0.140	0	1.000	0.000	3.07×10^{-4}
	6.00×10^2	0.865	-0.146	
	1.20×10^3	0.681	-0.384	
	1.81×10^3	0.550	-0.597	
	3.03×10^3	0.406	-0.901	
0.100	0	1.000	0.000	1.60×10^{-4}
	1.39×10^3	0.864	-0.146	
	4.86×10^3	0.441	-0.819	
	6.06×10^3	0.407	-0.900	
0.090	0	1.000	0.000	1.29×10^{-4}
	1.20×10^3	0.829	-0.180	
	2.40×10^3	0.706	-0.349	
	3.60×10^3	0.610	-0.494	
	4.74×10^3	0.541	-0.614	
0.080	0	1.000	0.000	9.11×10^{-5}
	1.80×10^3	0.784	-0.243	
	3.66×10^3	0.739	-0.303	
	7.22×10^3	0.503	-0.688	

(a) Measurements were made in D_2O solution, with the addition of KOD to result in the required concentration of deuteroxide. (b) The fraction of remaining unexchanged substrate, $f(s)$, was calculated using Equation 2.6. The initial substrate concentration was 1 (c) Ln $f(s)$ is the natural log of the fraction of substrate remaining at time t (d) The value of the first-order rate constant $k_{obs}(ex)$, for disappearance of substrate was obtained from the slope of the plot of ln $f(s)$ against time. It is assumed that no hydrolysis is occurring.

A value for the second-order rate constant for the disappearance of trihydro-pyrimidinium ion **(121)** in deuteroxide solution was obtained from the slope of the plot of k_{obs} (s^{-1}) against deuteroxide concentration $[DO^-]$ (M). The second order rate for total loss of substrate due to deuteroxide ion-catalyzed exchange at C2 was obtained as $k_{DO} = 3.58 \times 10^{-3}\ M^{-1}s^{-1}$.

Figure 2.58: **Plot of k_{obs} against [DO^-] for the H/D exchange reaction of trihydropyrimidinium ion (121) in D_2O at 25 °C and ionic strength I = 1.0 (KCl).**

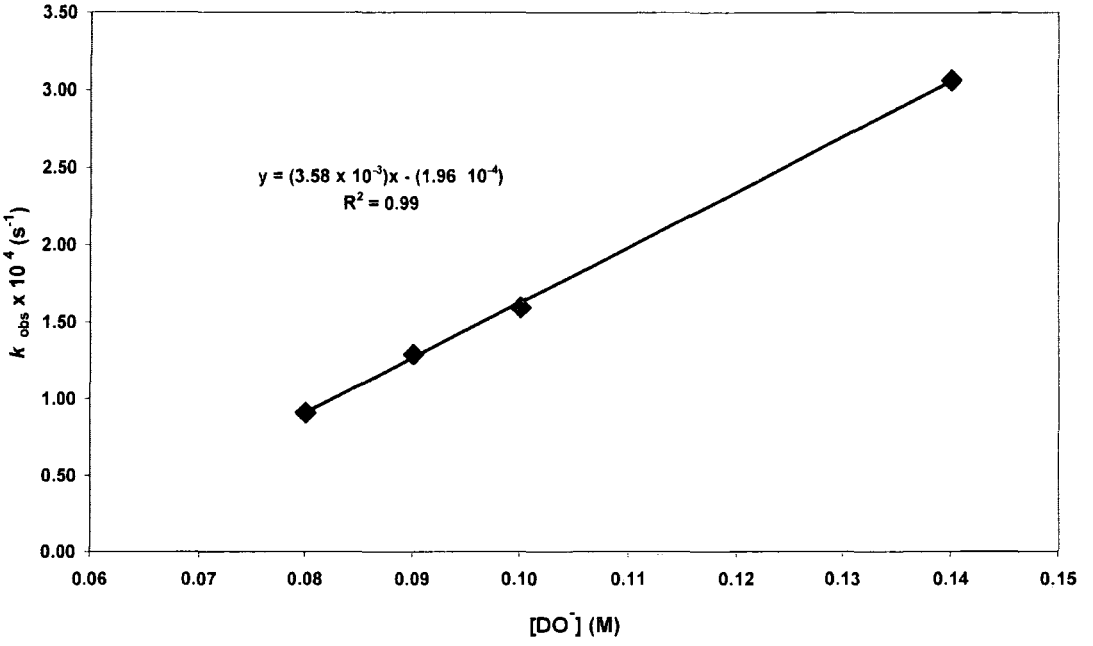

2.2.2.15 N,N'-Bis(di-*iso*propylamino) formadinium hexafluoro phosphate (123)

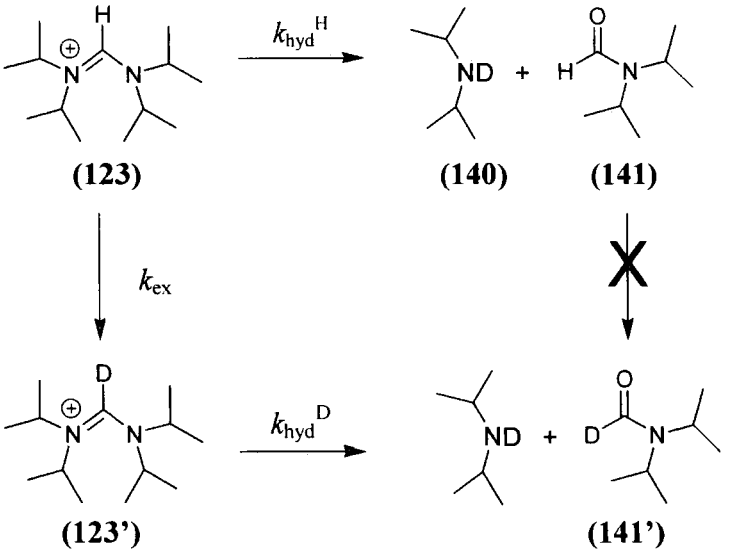

Rates of deuteroxide ion-catalysed exchange of the C2-H of acyclic formadine **(123)** to form the corresponding deuterated product **(123')** were investigated and rates of hydrolysis to form N,N'-di-*iso*propylamine **(140)** and N,N'-di-*iso*propyl formamide **(141)** were determined in the range pD 12.12 – 13.06 in quinuclidine buffers and in deuteroxide solution.

Figure 2.59 shows a ^{1}H NMR spectrum of formadine **(123)** (5 mM) obtained in D_2O solution at 25 °C and ionic strength I = 1.0 (KCl). The peak due to the C2-H appears singlet at 7.36 ppm (A). The signal due to the four methinyl C-*H*s of the four equivalent isopropyl substituents appears as a very broad septet at 4.06 ppm (B), due to coupling to the six adjacent methyl hydrogens. The signal due to the twenty four N-methyl hydrogens appears as a doublet at 1.37 ppm (C), due to coupling to the adjacent methinyl hydrogen. All other peaks in the region 0 – 3.8 ppm in the spectrum are due to quinuclidine buffers and internal standard, tetramethylammonium deuteriosulfate at 3.16 ppm.

Figure 2.60 shows representative ^{1}H NMR spectra of formadine **(123)** (5 mM, pD 12.12), obtained during the attempted exchange for deuterium of C2-H in D_2O at 25 °C and ionic strength I = 1.0 (KCl). Reaction aliquots were quenched to pD 4 prior to ^{1}H NMR analysis. It is clear from the spectra that hydrolysis of formadine **(123)** out competes H/D-exchange under these experimental conditions. The signal due to C2-H of formadine **(123)** at 7.36 ppm decayed over the course of the reaction, and this was matched by the growth of a singlet at 8.09 ppm due to the C1-H of ,N'-di-*iso*propylformamide **(141)**. The decay of the broad septet due to the four N-C*H*s of ion **(123)** was matched by the appearance of two new multiplets in the region 4.27 – 4.35 ppm due to the two N-C*H* protons of both **(140)** and **(141)**. The decay of the doublet due to the twelve methyl hydrogens of ion **(123)** was matched by the growth of two doublets at 1.25 ppm and 1.20 ppm due to the six methyl hydrogens on formamide **(142)** and a doublet at 1.08 ppm due to the six methyl hydrogens of amine **(140)** (not shown).

Figure 2.59:. ^{1}H NMR spectrum of formadine (123) in D_2O solution at ionic strength I = 1.0 (KCl) and 25 °C.

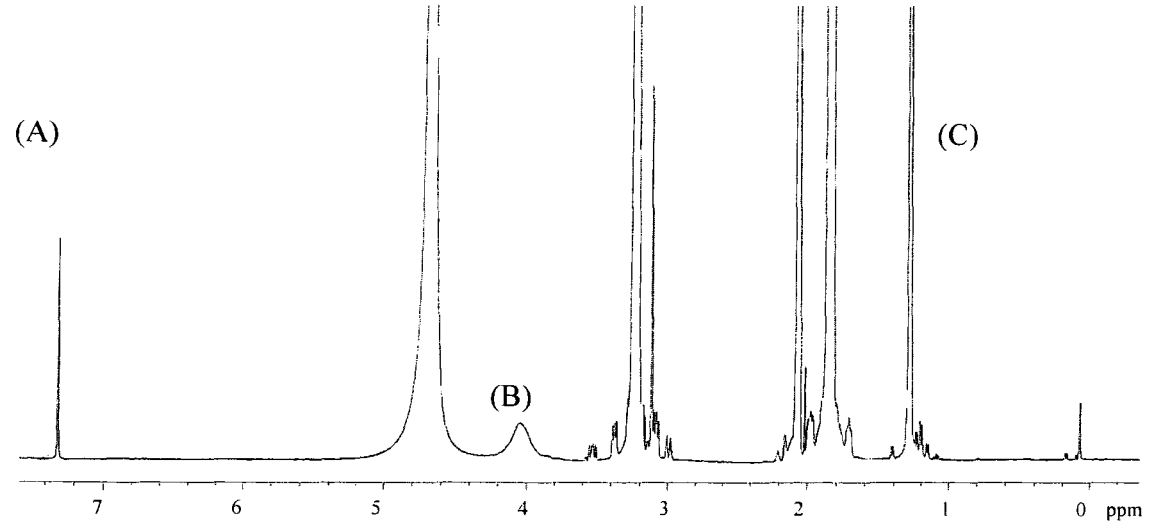

Figure 2.60: Representative ^{1}H NMR spectra at 300 MHz of acyclic formadine (123) (5 mM, pD 12.12) obtained during reaction in 100 mM quinuclidine buffers in D_2O at 25°C and ionic strength I = 1.0 (KCl).

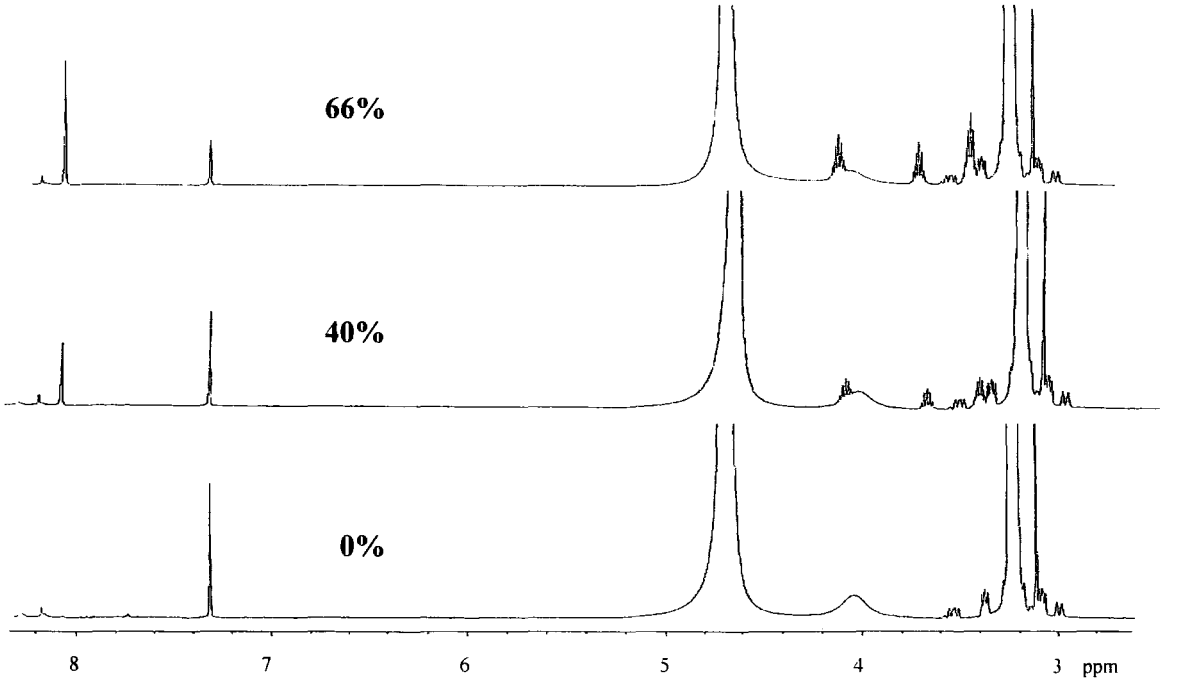

Reaction data and the experimental first-order rate constants for the hydrolysis of formadine **(123)** (k_{obs}, s^{-1}) in quinuclidine buffers at different pD values and in deuteroxide solution are shown in Table 2.31-2.32. The values for k_{obs} (s^{-1}) shown in Table 2.32 were obtained from the slopes of semilogarithmic plots (Figure 2.61) of the fraction of substrate against time. Values of f(s'), the sum of the fractions of remaining substrate and of hydrolysis product, remain close to unity over the timecourse of the reaction within experimental error. Thus deuterium exchange is not detectible under these experimental conditions and the disappearance of the signal due to the C2-H of formadine **(123)** is due entirely to hydrolysis of the substrate.

Table 2.31: First-order rate constants for disappearance of the C2-H of formadine (123) for deuterium in deuteroxide solution in D_2O at 25 °C and I = 1.0 (KCl).

[a][DO-] (M)	Time (secs)	f(s)[d]	f(s')[e]	[d]Ln f(s)[f]
2.38×10^{-3} (pD 12.12)[b]	0	1.000	1.000	0.000
	7.05×10^{5}	0.816	1.158	-0.203
	1.12×10^{6}	0.766	1.202	-0.267
	1.64×10^{6}	0.647	1.279	-0.435
1.20×10^{-2} (pD 12.82)[b]	0	1.000	1.000	0.000
	2.60×10^{5}	0.353	1.100	-1.041
	3.63×10^{5}	0.245	1.145	-1.406
	4.26×10^{5}	0.166	0.984	-1.796
	7.05×10^{5}	0.049	0.993	-3.016
2.08×10^{-2} (pD 13.06)[b]	0	1.000	1.000	0.000
	2.87×10^{4}	0.901	0.920	-0.045
	7.80×10^{4}	0.852	0.939	-0.070
	2.61×10^{5}	0.657	1.000	-0.182
	3.62×10^{5}	0.544	0.968	-0.264
	9.06×10^{5}	0.300	0.936	-0.523

	0	1.000	1.000	0.000
5.88×10^{-2}	8.47×10^{-4}	0.897	0.970	-0.109
(KOD)[c]	1.69×10^{-4}	0.753	1.083	-0.284
	2.54×10^{-4}	0.595	1.088	-0.519
	4.23×10^{-4}	0.506	1.074	-0.681

(a) $[DO^-]$ was calculated using $[DO^-] = (10^{pD-pK_w})/\gamma_{OL}$ with $pK_w = 14.87$, where $\gamma_{OL} = 0.75$ is the activity correction of lyoxide ion under our experimental conditions. (b) 100 mM quinuclidine buffer 50%, 80% and 90% FB. (c) 0.0588 M KOD (d) The fraction of unreacted substrate remaining $f(s)$, was calculated according to Equation 2.1 Measurements were made at an initial substrate concentration of 5 mM. (e) $f(s')$ is the sum of the fractions of remaining substrate and of hydrolysis product calculated as follows: $f(s') = ((A_s + A_p)/A_{IS})_t/(A_s/A_{IS})_{t=0}$ In this equation, A_s is the area of singlet due to the C2-H of substrate **(123)** at 7.36 ppm, A_{IS} is the area of the broad triplet due to internal standard at 3.16 ppm and A_p is the area of the singlet at 8.09 ppm due to the C1-H of N,N'-diisopropylformamide **(141)**.

Figure 2.61: Semi-logarithmic plot of the fraction of remaining C2-H against time for the hydrolysis of formadine (123) in 100 mM quinuclidine buffer at pD 12.12, 12.82, 13.06, and 0.059 M deuteroxide solution.

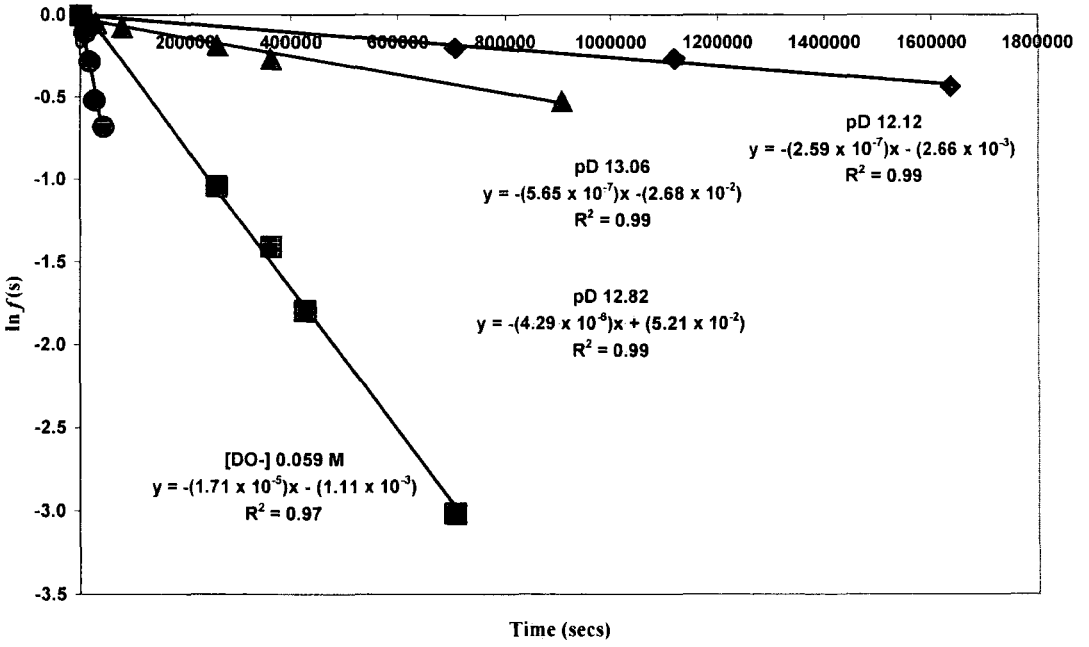

The combined reaction data for formadine **(123)** in quinuclidine buffer solution and deuteroxide solution is shown in Table 2.32.

Table 2.32: First and second-order rate constants for hydrolysis of formadine (123) in D_2O at 25 °C and I = 1.0 (KCl).

$[DO^-]$ (M)	k_{obs}[a] (s^{-1})	k_{Hyd}[b] ($M^{-1}s^{-1}$)
2.38×10^{-3}	2.59×10^{-7}	
1.20×10^{-2}	4.29×10^{-6}	
2.08×10^{-2}	5.65×10^{-7}	2.26×10^{-5}
5.88×10^{-2}	1.71×10^{-5}	

The second-order rate constant for deuteroxide ion-catalysed hydrolysis was obtained from the slope of the plot of k_{obs} against the concentration of deuteroxide ion as shown in Figure 2.62.

Figure 2.62: Plot of k_{obs} against $[DO^-]$ for the hydrolysis reaction of formadine (123) in D_2O at 25 °C and I = 1.0 (KCl).

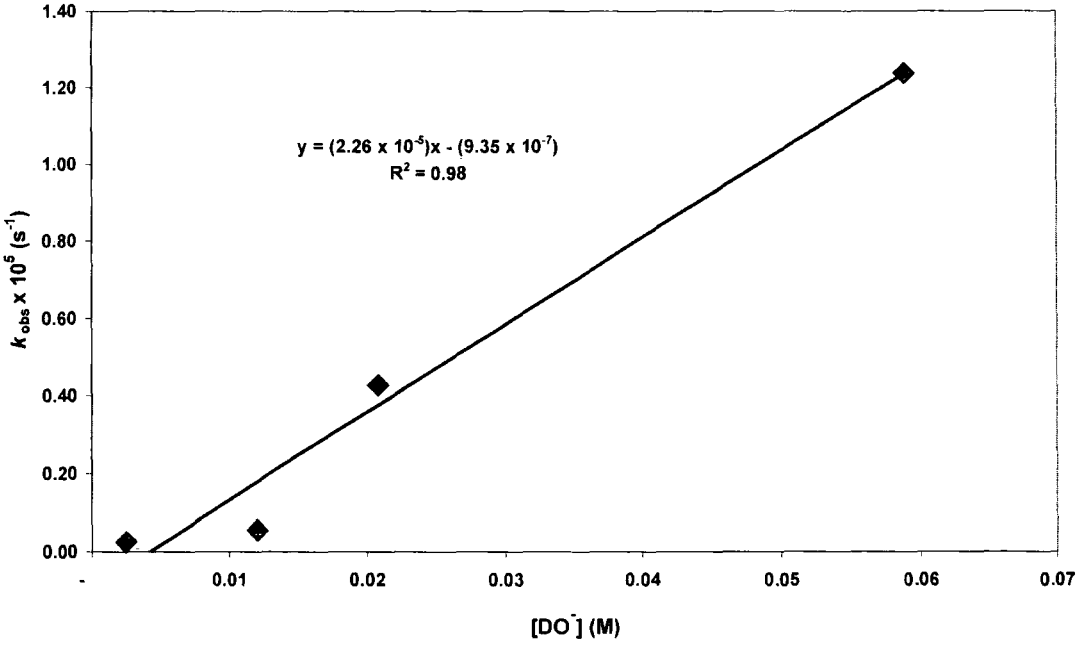

2.3. Buffer catalysis of exchange.

Scheme 2.19 shows the detailed mechanism for deuteroxide ion-catalyzed exchange of the C2-H of an azolium ion for deuterium. The proposition for this mechanism is that the reverse rate for carbene protonation is limited by solvent reorganization, (k_{reorg})[87] and that the proton transfer step is non rate-determining.

Scheme 2.19:

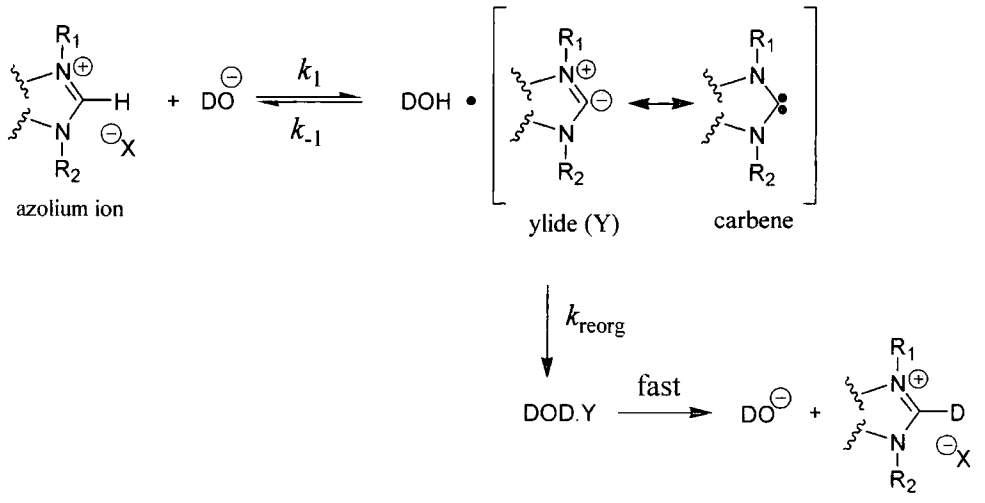

The law of microscopic reversibility states that the reverse reaction must occur via the lowest energy pathway which means that the route for reprotonation must follow the same pathway as deprotonation.

As mentioned in Section 2.2.2, the observed experimental pseudo-first-order rate constant (k_{obs}) is the sum of the contributions of all potential catalytic species to the rate of exchange, including contributions by solvent, deuteroxide, and buffer base (Equation 2.8). The value for deprotonation by solvent water (k_{D2O}) as a base is expected to be much lower than other contributing terms so can be neglected as mentioned in Section 2.2. Where there is general base catalysis of exchange, buffer catalysis (k_B[B]) may be a contributing term. Where there is no general base catalysis of exchange the observed rate constant (k_{obs}) is equal to the term for deuteroxide catalyzed exchange (k_{DO}[DO^-]). To determine the contribution of the term for general base catalysis, experiments are run at a fixed pD and at constant buffer ratio, while varying the total concentration of buffer.

Thus the concentration of deuteroxide ion is fixed while the concentration of buffer base varies. If there is general base catalysis of exchange then the observed pseudo-first-order rate constant for exchange (k_{obs}) will increase with the increasing concentration of buffer base present.

$$k_{obs} = k_{D2O} + k_{DO}[DO^-] + k_B[B] \qquad \textbf{(Equation 2.8)}$$

General base catalysis of exchange is observed when deprotonation of the substrate by DO^- is rate determining for the overall deuteroxide catalyzed exchange reaction. Brønsted bases result in an increase in the rate constant for this proton-transfer step ($k_B[B]$) because of the lyoxide ion anomaly, that is the low reactivity of lyoxide ion in proton transfer to/from carbon for its basicity. However, when reprotonation of the enolate intermediate by solvent (k_{-1}) is so fast that solvent reorganization is rate-determining for the overall deuteroxide–catalyzed reaction, general base catalysis of the overall deuterium exchange reaction is not possible as there is no way for a Brønsted base to lower the barrier to solvent reorganization.

A representative graph showing the dependence of the increase in k_{ex} on the ratio of the concentrations of the basic form of quinuclidine buffer [Buffer] and deuteroxide ion in D_2O at 25 °C is shown in Figure 2.63 for three molecules representing three distinct mechanistic differences,[88] ethyl acetate **(A)**, acetamide **(B)** and acetonitrile **(C)**.

Figure 2.63:

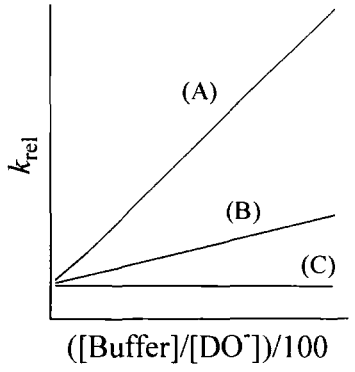

k_{rel} is the normalized rate constant for the exchange for deuterium of the first α-proton of carbon acid. k_{rel} values are calculated according to Equation 2.9. In Equation 2.9, k_{DO} is the experimental second order rate constant for deuteroxide ion catalyzed exchange which was determined in Section 2.2.2. The ratio of first order rate constants (k_{rel}) is a measure of the relative difference between the observed experimental rate constant (k_{obs}) and the deuteroxide ion catalyzed rate of exchange ($k_{DO}[DO^-]$). This equation also corrects for the small changes in pD that occur upon dilution of a buffer solution at constant ionic strength. In a situation where there is no general base catalysis of exchange this ratio should be close to unity.

$$k_{rel} = \frac{k_{obs}}{k_{DO}[DO^-]} = 1 + \frac{k_B[B]}{k_{DO}[DO^-]} \qquad \textbf{(Equation 2.9)}$$

The relatively strong buffer catalysis seen for the deuterium exchange reaction of ethyl acetate denotes a rate-limiting proton transfer step for the deuteroxide-ion catalyzed exchange reaction. The absence of detectable buffer catalysis of deuterium exchange into acetonitrile marks a change to rate-limiting solvent reorganization for the overall deuteroxide catalyzed exchange reaction. For acetamide however, weak but significant buffer catalysis of deuterium exchange is evident indicating that deuterium exchange takes place via a stepwise mechanism through an amide enolate intermediate for which the rate of reverse protonation of the enolate is less than solvent reorganization.

Results of the investigations into the existence and extent of buffer catalysis of deuterium exchange at the C2 position of the imidazolium, 4,5-dihydroimidazolium and 3,4,5,6-trihydropyrimidinium ions are reported in this section.

2.3.1 1,3-Di-*t*-butylimidazolium chloride (113)

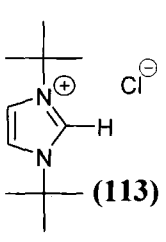

(113)

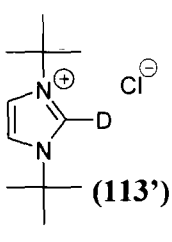

(113')

Rates of deuteroxide ion-catalyzed exchange of the C2-H of imidazolium ion **(113)** to form the corresponding deuterated product **(113')**, were determined by 500 MHz ^{1}H NMR spectroscopy. ^{1}H NMR spectral details in quinuclidine buffers at fixed pD values were exactly as described in section 2.2.2.8 for analogous exchange reactions in quinuclidine buffers at different pD values.

Deuteroxide ion-catalyzed exchange experiments were run at 10% free base and at varied total concentration of quinuclidine buffer at 25 °C and ionic strength I = 1.0 (KCl). The experimental first-order rate constants (k_{obs}, s^{-1}) obtained as the slope of the plot of the experimental data (Figure 2.64) at different quinuclidine buffer concentrations and at fixed pD are shown in Table 2.33.

Figure 2.64: Semi-logarithmic plot of the fraction of remaining C2-H against time for the deuterium exchange reaction of imidazolium ion (113) in 10% free base quinuclidine buffer (0.15 M (■), 0.25 M (▲) and 0.35 M (●)).

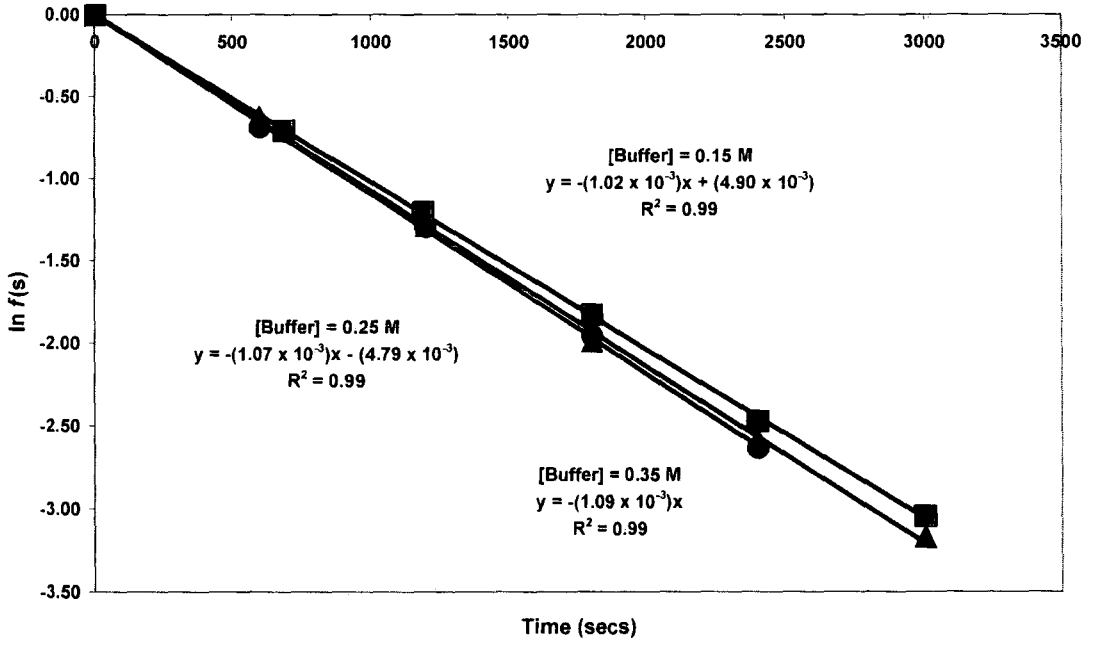

Table 2.33: First-order rate constants for exchange of the C2-H of imidazolium ion (113) for deuterium in quinuclidine buffers (10% free base) in D_2O at 25 °C and I = 1.0 (KCl).

$[Buffer]_T$[a] (M)	$[DO^-]$[b] (M)	Time (secs)	$f(s)$[c]	ln $f(s)$	k_{obs}[d] (s^{-1})
0.15	2.97×10^{-4} (pD 11.22)	0	1.000	0.000	1.02×10^{-3}
		6.90×10^{2}	0.493	-0.708	
		1.19×10^{3}	0.300	-1.203	
		1.80×10^{3}	0.161	-1.825	
		2.40×10^{3}	0.084	-2.474	
		3.00×10^{3}	0.048	-3.045	
0.25	3.00×10^{-4} (pD 11.22)	0	1.000	0.000	1.07×10^{-3}
		6.00×10^{2}	0.538	-0.621	
		1.20×10^{3}	0.277	-1.285	
		1.80×10^{3}	0.137	-1.987	
		2.40×10^{3}	0.075	-2.587	
		3.00×10^{3}	0.042	-3.169	
0.35	2.98×10^{-4} (pD 11.22)	0	1.000	0.000	1.09×10^{-3}
		6.00×10^{2}	0.503	-0.688	
		1.20×10^{3}	0.274	-1.295	
		1.80×10^{3}	0.141	-1.959	
		2.40×10^{3}	0.072	-2.634	

(a) Total concentration of quinuclidine buffers ([B] + [BH^+]) (b) Measurements were made in 10% free base quinuclidine buffer. The concentration of deuteroxide [DO^-] was calculated using $[DO^-] = (10^{pD-pK_w})/\gamma_{OL}$ with pK_w = 14.87, where γ_{OL} = 0.75 is the activity correction of lyoxide ion under our experimental conditions. (c) Measurements were made at initial substrate concentration of 10 mM. (d) The value of the first-order rate constant (k_{obs}), was obtained from the slope of the plot of ln $f(s)$ against time in Figure 2.64.

The first order-rate constants for the deuteroxide catalyzed exchange of the C2-H of imidazolium ion **(113)** are summarized in Table 2.34. Also shown in Table 2.34 are k_{rel} values which are calculated according to Equation 2.6 as described previously. In this case, the value obtained for k_{rel} is approximately 2 at each buffer concentration. As the value for k_{rel} changes little over a large range in buffer concentration it can be concluded that there is no buffer catalysis of exchange occurring in the deuteroxide catalyzed

exchange reaction of imidazolium ion **(113)**. The departure from the ideal k_{rel} value reflects the error in the k_{DO} value.

Table 2.34: Ratio of first order rate constants (k_{rel}) for the deprotonation of imidazolium ion (113) in buffered quinuclidine solution relative to unbuffered deuteroxide solution at 25 °C and ionic strength I = 1.0 (KCl).

[B][a] (M)	([B]/[DO⁻])/100[b]	k_{obs}[c] (s^{-1})	k_{rel}[d]
0.015	0.505	1.020×10^{-3}	2.078
0.025	0.833	1.068×10^{-3}	2.157
0.035	1.174	1.020×10^{-3}	2.214

(a) The concentration of quinuclidine free base form. (b) Ratio of concentrations of quinuclidine free base to deuteroxide ion (c) Observed pseudo first-order rate constant for exchange at a given quinuclidine concentration at pD 11.22. (d) k_{rel} is the ratio of observed first order-rate constant for exchange in buffered quinuclidine solution at pD 11.22 (k_{obs}) and the first order-rate of deuteroxide ion-catalyzed exchange only ($k_{DO}[DO^-]$), calculated using Equation 2.6 . In this case $k_{DO} = 1.65 \times 10^{-1}\ M^{-1}s^{-1}$.

Figure 2.65: Plot of the ratio of rate constants k_{rel} against ([B]/[DO⁻])

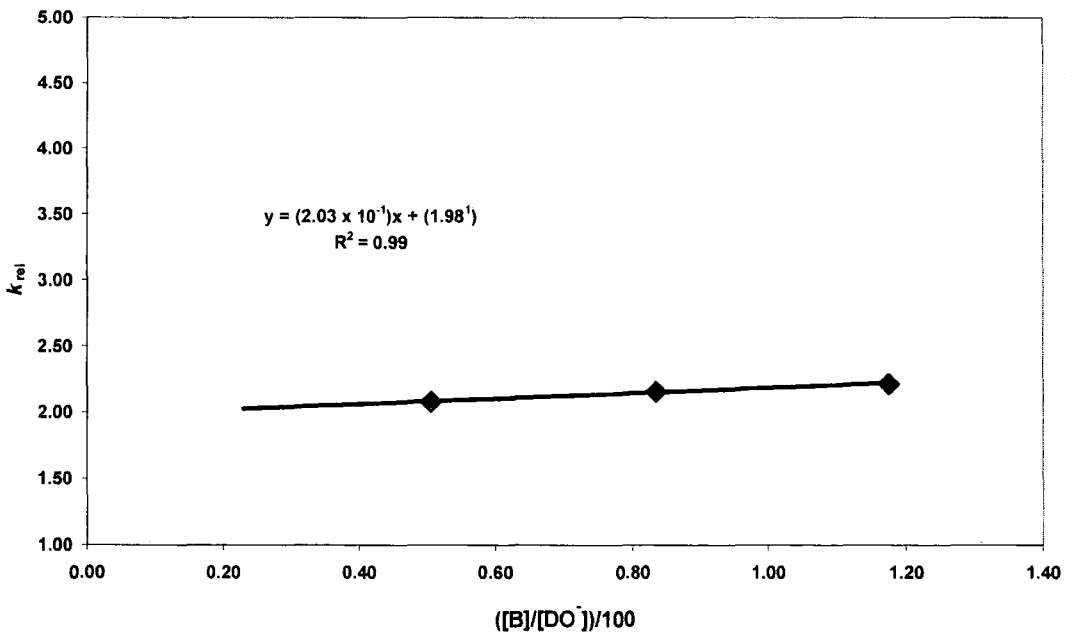

Shown in Figure 2.65 is a plot of k_{rel} values against the ratio of buffer to deuteroxide ion concentration. The slope of this plot should be the ratio of the second order rate constants for the general base and deuteroxide ion-catalyzed exchange, k_B/k_{DO} according to Equation 2.6 and the y-intercept should be unity. The deviation of the intercept from unity again reflects error in the value for k_{DO}. The slope of this plot is small in comparison to the increase in buffer concentration which indicates that general base catalysis of exchange is not significant.

2.3.2 1-Ethyl- 3-methylimidazolium chloride (142).

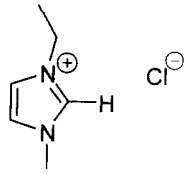

(142)

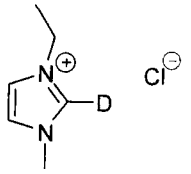

(142')

Rates of deuteroxide ion-catalyzed exchange of the C2-H of imidazolium ion **(142)** to form the corresponding deuterated product **(142')**, were determined by 500 MHz ^{1}H NMR spectroscopy.

Deuteroxide ion-catalyzed exchange experiments were run at 10% free base and in varying concentrations of quinuclidinone buffers at 25 °C and ionic strength I = 1.0 (KCl). Deuterium exchange at the C2 position results in the disappearance of the singlet peak due to the C2-H at 8.65 ppm (^{1}H NMR spectra not shown). The measured first-order rate constants (k_{obs}) at different quinuclidinone buffer concentrations at fixed pD values are shown in Table 2.35.

Table 2.35: First-order rate constants for exchange of the C2-H of imidazolium ion (142) for deuterium in quinuclidinone buffers (10% free base) in D_2O at 25 °C and I = 1.0 (KCl).

$[Buffer]_T$[a] (M)	$[DO^-]$[b] (M)	Time (secs)	$f(s)$[c]	$\ln f(s)$	k_{obs}[d] (s^{-1})
0.05	3.20×10^{-8} (pD 7.25)	0	1.000	0.000	5.92×10^{-6}
		5.72×10^{4}	0.685	-0.378	
		1.01×10^{5}	0.487	-0.720	
		1.67×10^{5}	0.336	-1.092	
		2.45×10^{5}	0.237	-1.438	
0.15	3.28×10^{-8} (pD 7.26)	0	1.000	0.000	5.79×10^{-6}
		5.65×10^{4}	0.593	-0.523	
		1.01×10^{5}	0.575	-0.553	
		1.67×10^{5}	0.303	-1.195	
		2.45×10^{5}	0.245	-1.408	
0.25	3.20×10^{-8} (pD 7.25)	0	1.000	0.000	6.46×10^{-6}
		5.70×10^{4}	0.648	-0.434	
		1.01×10^{5}	0.538	-0.619	
		1.67×10^{5}	0.315	-1.156	
		2.45×10^{5}	0.207	-1.576	
0.45	3.15×10^{-8} (pD 7.24)	0	1.000	0.000	6.84×10^{-6}
		5.69×10^{5}	0.573	-0.557	
		8.65×10^{5}	0.474	-0.747	
		1.66×10^{5}	0.266	-1.324	
		2.45×10^{5}	0.154	-1.868	
		4.03×10^{5}	0.061	-2.797	

(a) Total concentration of quinuclidinone buffers ([B] + [BH^+]) (b) Measurements were made in 10% free base quinuclidinone buffers. The concentration of deuteroxide [DO^-] was calculated using [DO^-] = $(10^{pD-pK_w})/\gamma_{OL}$ with pK_w = 14.87, where γ_{OL} = 0.75 is the activity correction of lyoxide ion under our experimental conditions. (c) Measurements were made at initial substrate concentration of 10 mM. (d) The value of the first-order rate constant (k_{obs}), was obtained from the slope of the plot of $\ln f(s)$ against time in Figure 2.66.

Figure 2.66: Semi-logarithmic plot of the fraction of remaining C2-H against time for the deuterium exchange reaction of imidazolium ion (142) in 10% free base quinuclidinone buffer (0.05 M (♦), 0.15 (■), 0.25 M (▲) and 0.45 M (—))

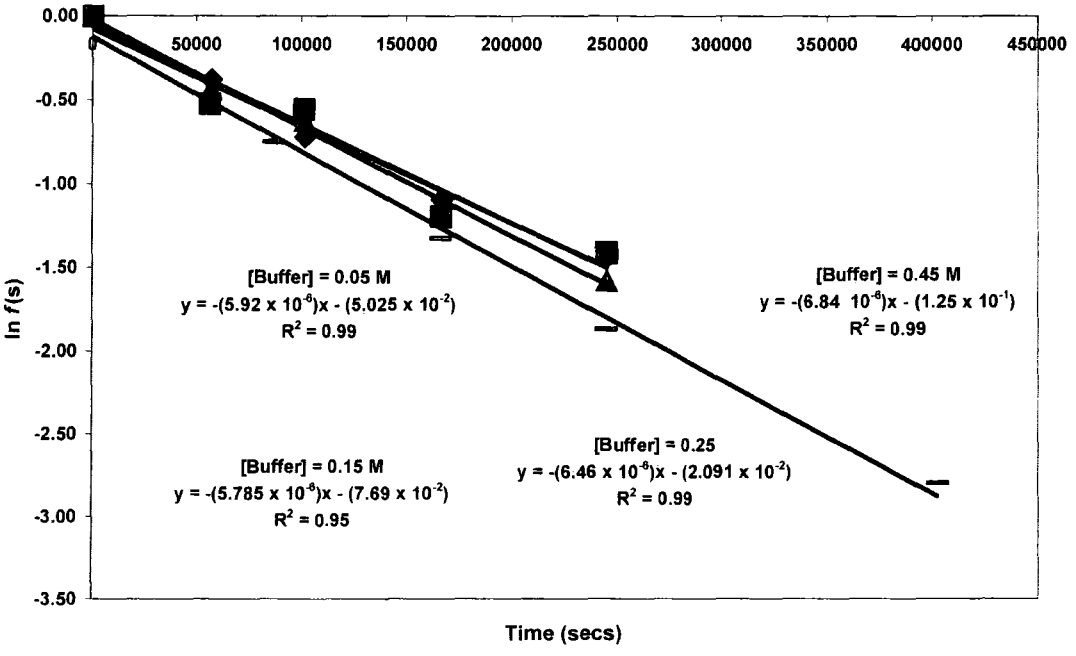

The first order-rate constants for the deuteroxide ion-catalyzed exchange of the C2-H of imidazolium ion **(142)** are summarized in Table 2.36. Also shown in Table 2.36 are k_{rel} values which are calculated according to Equation 2.6, as described in Section 2.3.1 In Equation 2.6, k_{DO} is the second order rate constant for deuteroxide ion catalyzed exchange which was determined in Section 2.2.2.9. The ratio of first order rate constants (k_{rel}) is a measure of the relative difference between the observed experimental rate constant (k_{obs}) in buffered D_2O solution at a fixed pD and the deuteroxide ion catalyzed rate of exchange ($k_{DO}[DO^-]$).

In this case, the value obtained for k_{rel} is approximately unity at each buffer concentration. As the value for k_{rel} changes little over a large range in buffer concentration it can be concluded that there is no buffer catalysis of exchange occurring in the deuteroxide catalyzed exchange reaction of imidazolium ion **(142)**.

Table 2.36: Ratio of first order rate constants (k_{rel}) for the deprotonation of imidazolium ion (142) in buffered quinuclidinone solution relative to unbuffered deuteroxide solution at 25 °C and ionic strength I = 1.0 (KCl).

[B] × 10% Free Base[a] (M)	([B]/[DO⁻]) × 10^5[b]	k_{obs} (s^{-1})	k_{rel}[c]
0.005	1.563	5.92×10^{-6}	1.004
0.015	4.573	5.79×10^{-6}	0.959
0.025	7.813	6.46×10^{-6}	1.096
0.045	14.28	6.84×10^{-6}	1.178

(a) The concentration of quinuclidinone free base form. (b) Ratio of concentrations of quinuclidinone free base to deuteroxide ion (c) Observed pseudo first-order rate constant for exchange at a given quinuclidinone concentration at pD 7.25. (d) k_{rel} is the ratio of the observed first order-rate constant for exchange in buffered quinuclidinone solution at pD 7.25 (k_{obs}) and the first order-rate of deuteroxide ion-catalyzed exchange only (k_{DO}[DO⁻]), calculated using Equation 2.6 . In this case $k_{DO} = 1.84 \times 10^2$ $M^{-1}s^{-1}$.

Figure 2.67 shows the plot of the ratio k_{rel} values against the ratio of buffer base and deuteroxide ion concentrations. The slope of this plot, k_B/k_{DO}, is very small, which indicates that general base catalysis of exchange is not significant.

Figure 2.67: Plot of the ratio of rate constant k_{rel} against ([B]/[DO⁻]).

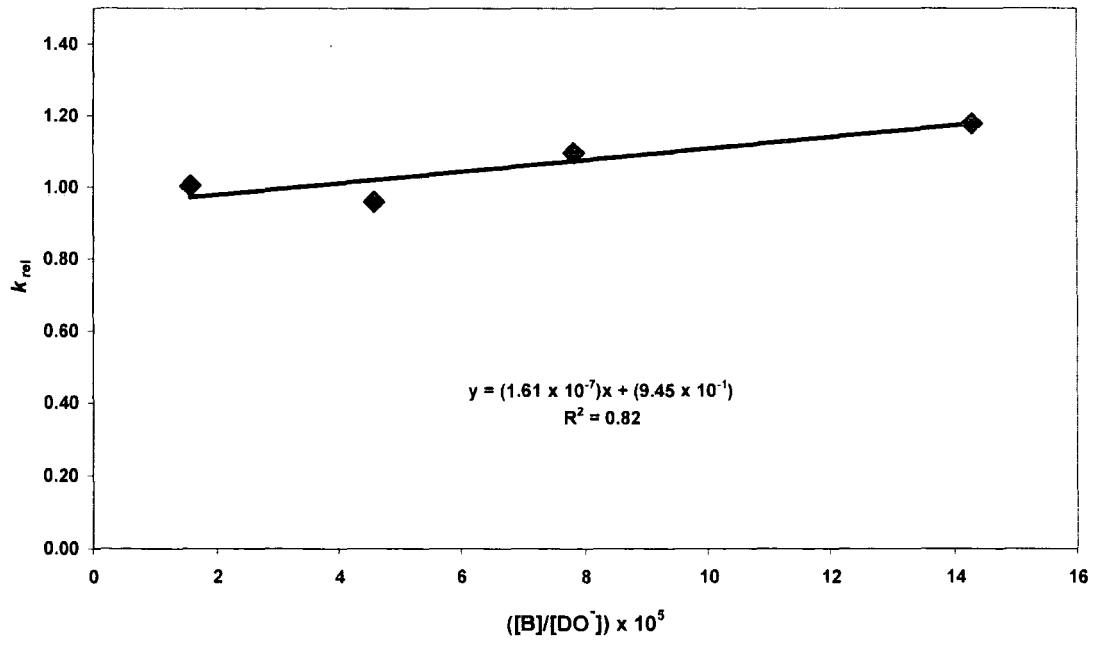

2.3.3 1,3-Bis(2,4,6-trimethylphenyl)4,5-dihydroimidazolium chloride (116).

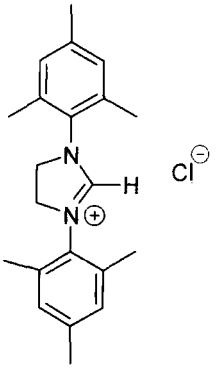

(116)

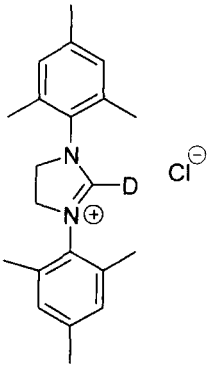

(116')

Rates of deuteroxide ion-catalyzed exchange of the C2-H of 4,5-dihydroimidazolium ion **(116)** to form the corresponding deuterated product **(116')**, were determined by 500 MHz ^{1}H NMR spectroscopy. ^{1}H NMR spectral details in phosphate buffers at fixed pD values were exactly as described in section 2.2.2.2 for analogous exchange reactions in phosphate buffers at different pD values.

Deuteroxide ion-catalyzed exchange experiments were run at 30% free base in and in varied total concentrations of phosphate buffer at 25 °C and ionic strength I= 1.0 (KCl). The experimental first-order rate constants (k_{obs}) at different phosphate buffer concentrations and at fixed pD are shown in Table 2.37.

Table 2.37: First-order rate constants for exchange of the C2-H of 4,5-dihydroimidazolium ion (116) for deuterium in phosphate buffers (30% free base) in D_2O at 25 °C and I = 1.0 (KCl).

$[Buffer]_T$[a] (M)	$[DO^-]$[b] (M)	Time (secs)	$f(s)$[c]	$\ln f(s)$	k_{obs}[d] (s^{-1})
0.10	1.03×10^{-8} (pD 6.76)	0	1.000	0.000	1.43×10^{-4}
		2.82×10^3	0.717	-0.333	
		5.57×10^3	0.447	-0.804	
		8.22×10^3	0.310	-1.173	
		1.08×10^4	0.222	-1.503	
0.20	7.04×10^{-9} (pD 6.59)	0	1.000	0.000	9.10×10^{-5}
		2.16×10^3	0.783	-0.245	
		4.73×10^3	0.660	-0.415	
		9.55×10^3	0.412	-0.887	
		1.18×10^4	0.339	-1.083	
0.40	7.39×10^{-9} (pD 6.61)	0	1.000	0.000	1.03×10^{-4}
		1.80×10^3	0.891	-0.116	
		4.39×10^3	0.703	-0.352	
		6.83×10^3	0.548	-0.601	
		9.17×10^3	0.386	-0.953	
0.50	7.56×10^{-9} (pD 6.62)	0	1.000	0.000	9.24×10^{-5}
		1.56×10^3	0.916	-0.088	
		4.17×10^3	0.750	-0.288	
		6.16×10^3	0.570	-0.563	
		8.92×10^3	0.427	-0.851	
		1.12×10^4	0.382	-0.961	

(a) Total concentration of phosphate buffer ($[K_2DPO_4] + [KD_2PO_4]$). (b) Measurements were made in 30% free base phosphate buffer. The concentration of deuteroxide $[DO^-]$ was calculated using $[DO^-] = (10^{pD-pK_w})/\gamma_{OL}$ with $pK_w = 14.87$, where $\gamma_{OL} = 0.75$ is the activity correction of lyoxide ion under our experimental conditions. (c) Measurements were made at initial substrate concentration of 10 mM. (d) The value of the first-order rate constant (k_{obs}), was obtained from the slope of the plot of $\ln f(s)$ against time in Figure 2.67.

Figure 2.67: Semi-logarithmic plot of the fraction of remaining C2-H against time for the deuterium exchange reaction of 4,5-dihydroimidazolium ion (116) in 30% free base phosphate buffer (0.1 M (■), 0.2 M (▲), 0.4 M (●) and 0.5 M (♦)).

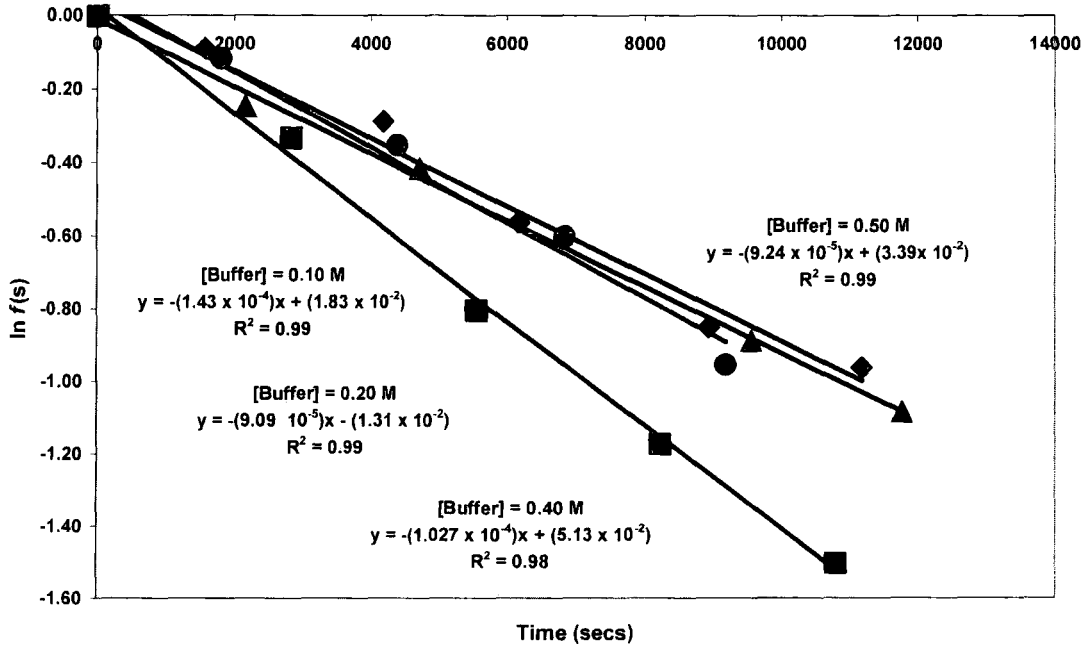

The first order-rate constants for the deuteroxide ion catalyzed exchange of the C2-H if imidazolinium ion **(116)** are summarized in Table 2.38. Also shown in Table 2.38 are k_{rel} values which are calculated according to Equation 2.6 as described in Section 2.3.1. In Equation 2.6, k_{DO} is the second order rate constant for deuteroxide ion catalyzed exchange which was determined in Section 2.2.2.2.

The value obtained for k_{rel} is approximately unity at each buffer concentration. As the value for k_{rel} changes little over a large range in buffer concentration it can be concluded that there is no buffer catalysis of exchange occurring in the deuteroxide catalyzed exchange reaction of 4,5-dihydroimidazolium ion **(116)**.

Table 2.38: Ratio of first order rate constants (k_{rel}) for the deprotonation of 4,5-dihydroimidazolium ion (95) in buffered phosphate solution relative to unbuffered deuteroxide solution at 25 °C and ionic strength I = 1.0 (KCl).

[B][a] (M)	([B]/[DO⁻]) × 10⁻⁶[b]	k_{obs}[c] (s^{-1})	k_{rel}[d]
0.030	0.291	1.43×10^{-4}	1.067
0.060	8.520	9.10×10^{-5}	0.992
0.120	16.21	1.03×10^{-4}	1.068
0.150	19.83	9.24×10^{-5}	0.939

(a) The concentration of phosphate dianion. (b) Ratio of concentrations of phosphate dianion to deuteroxide ion. (c) Observed pseudo first-order rate constant for exchange at a given phosphate dianion concentration at pD 6.6. (d) k_{rel} is the ratio of the observed first order-rate constant for exchange in buffered phosphate solution at pD 7.25 (k_{obs}) and the first order-rate of deuteroxide ion-catalyzed exchange only ($k_{DO}[DO^-]$), calculated using Equation 2.6 . In this case $k_{DO} = 1.25 \times 10^4\ M^{-1}s^{-1}$.

Figure 2.68 shows the plot of the ratio k_{rel} values against the ratio of buffer base and deuteroxide ion concentrations. The slope of this plot, k_B/k_{DO}, is very small, which indicates that general base catalysis of exchange is not significant.

Figure 2.68: Plot of the ratio of rate constant k_{rel} against ([B]/[DO⁻]) for 4,5-dihydroimidazolium ion (116).

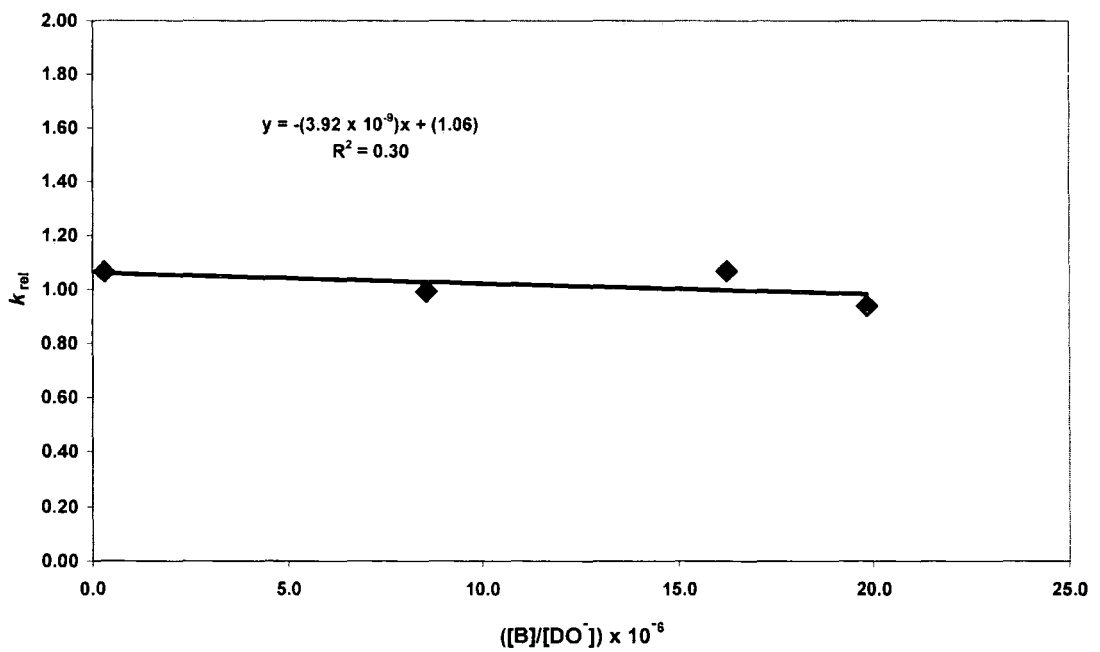

2.3.4. 1,3-Di-*iso*propyl-4,5,6-trihydropyrimidinium hexafluoro phosphate (120)

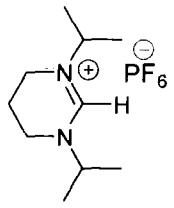

(120)

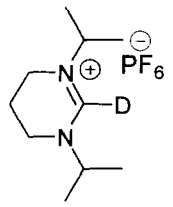

(120')

Rates of deuteroxide ion-catalyzed exchange of the C2-H of trihydropyrimidinium ion **(120)** to form the corresponding deuterated product **(120')**, were determined by 500 MHz ^{1}H NMR spectroscopy. ^{1}H NMR spectral details in deuteroxide solution at fixed pD values were exactly as described in section 2.2.2.8 for analogous exchange reactions in quinuclidine buffers at different pD values.

Deuteroxide ion-catalyzed experiments were run in quinuclidine buffers at 10% free base at varied total concentrations of quinuclidine buffer at 25 °C and ionic strength I = 1.0 (KCl). Quinuclidine buffers were used to minimize the competing hydrolysis which occurs with this substrate in KOD solution. Hence only the rate of decay of the C2-H peak due to deuterium exchange is measured this data. The measured first-order rate constants (k_{obs}) at different quinuclidine buffer concentrations and at fixed pD are shown in Table 2.39.

Table 2.39: First-order rate constants for exchange of the C2-H of tetrahydroimidazolium ion (120) for deuterium in quinuclidine buffers (10% free base) in D_2O at 25 °C and I = 1.0 (KCl).

[Buffer] (M)	$[DO^-]^b$ (M)	Time (secs)	$f(s)^c$	ln $f(s)$	$k_{obs}{}^d$ (s^{-1})
0.05	2.43×10^{-4} (pD 11.13)	0	1.000	0.000	2.48×10^{-7}
		2.43×10^5	0.936	-0.067	
		6.33×10^5	0.872	-0.137	
		8.34×10^5	0.824	-0.194	
		9.10×10^5	0.782	-0.246	
0.15	2.86×10^{-4} (pD 11.20)	0	1.000	0.000	3.24×10^{-7}
		6.32×10^5	0.808	-0.214	
		8.34×10^5	0.746	-0.294	
		9.10×10^5	0.728	-0.318	
		1.21×10^6	0.685	-0.378	
0.25	2.65×10^{-4} (pD 11.17)	0	1.000	0.000	3.19×10^{-7}
		1.57×10^5	0.917	-0.087	
		3.51×10^5	0.857	-0.154	
		5.04×10^5	0.833	-0.182	
		6.84×10^5	0.798	-0.226	

(a) Total concentration of quinuclidine buffers ([B] + $[BH^+]$) (b) Measurements were made in 10% free base quinuclidine buffer. The concentration of deuteroxide $[DO^-]$ was calculated using $[DO^-] = (10^{pD-pK_w})/\gamma_{OL}$ with $pK_w = 14.87$, where $\gamma_{OL} = 0.75$ is the activity correction of lyoxide ion under our experimental conditions. (c) Measurements were made at initial substrate concentration of 10 mM. (d) The value of the first-order rate constant (k_{obs}), was obtained from the slope of the plot of ln $f(s)$ against time in Figure 2.69.

Figure 2.69: Semi-logarithmic plot of the fraction of remaining C2-H against time for the deuterium exchange reaction of trihydropyrimidinium ion (120) in 10% free base quinuclidine buffer (0.5 M (♦), 0.15 M (■) and 0.25 M (▲)).

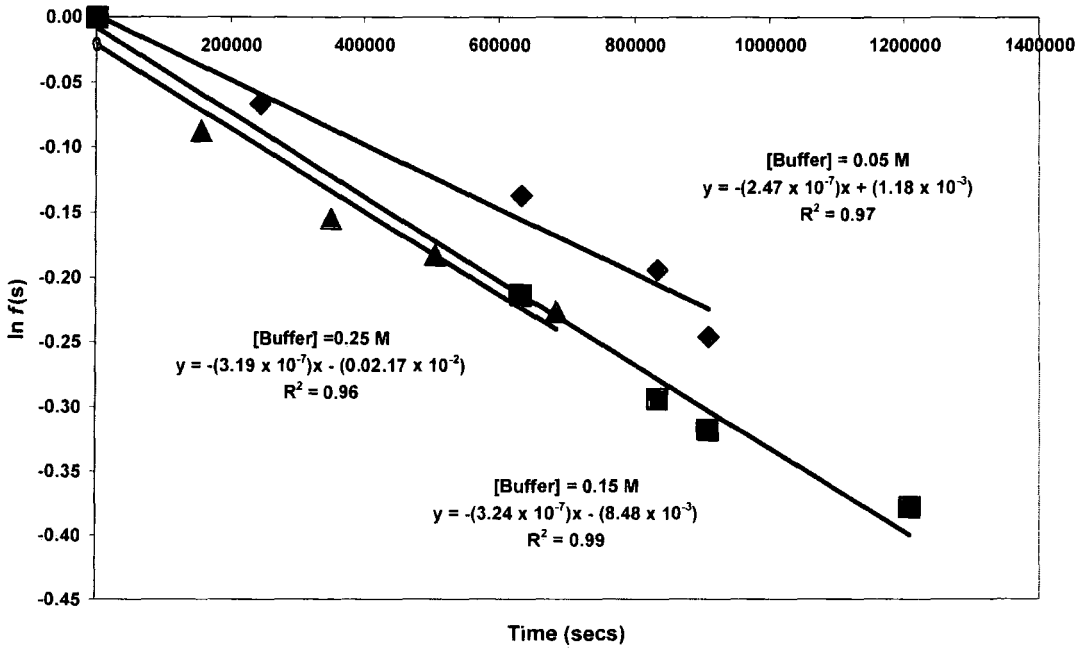

The first order-rate constants for the deuteroxide ion-catalyzed exchange of the C2-H of trihydropyrimidinium ion **(120)** are summarized in Table 2.8. Also shown in Table 2.40 are k_{rel} values which are calculated according to Equation 2.6 as described in Section 2.3.1. In Equation 2.6, k_{DO} is the second order rate constant for deuteroxide ion catalyzed exchange which was determined in Section 2.2.2.12 at different pD values. The ratio of rate constants (k_{rel}) is a measure of the relative difference between the observed experimental rate constant (k_{obs}) and the deuteroxide catalyzed rate of exchange ($k_{DO}[DO^-]$), as in Equation 2.6

The value obtained for k_{rel} is approximately 0.6 at each buffer concentration. As the value for k_{rel} changes little over a large range of buffer concentrations it can be concluded that there is little or no buffer catalysis of exchange occurring in the deuteroxide catalyzed exchange reaction of trihydropyrimidinium ion **(120)**. The departure from the ideal k_{rel} value reflects the error in the k_{DO} value.

Table 2.40: Ratio of first order rate constants (k_{rel}) for the deprotonation of tetrahydropyrimidinium ion (99) in buffered quinuclidine solution relative to unbuffered deuteroxide solution at 25 °C and ionic strength I = 1.0 (KCl).

[B] × 10% Free Base[a] (M)	([B]/[DO⁻]) × 10^{-5}[b]	k_{obs} (s^{-1})	k_{rel}[c]
0.005	0.943	2.48×10^{-7}	0.559
0.015	0.525	3.24×10^{-7}	0.647
0.025	0.206	3.19×10^{-7}	0.661

(a) The concentration of quinuclidine free base form. (b) Ratio of concentrations of quinuclidine free base to deuteroxide ion (c) Observed pseudo first-order rate constant for exchange at a given quinuclidine concentration at pD 11.2. (d) k_{rel} is the ratio of observed first order-rate constant for exchange in buffered quinuclidine solution at pD 11.2 (k_{obs}) and the first order-rate of deuteroxide ion-catalyzed exchange only (k_{DO}[DO⁻]), calculated using Equation 2.6. In this case $k_{DO} = 1.48 \times 10^{-3}$ $M^{-1}s^{-1}$.

Figure 2.70 shows the plot of k_{rel} values against the ratio of buffer to deuteroxide ion concentration. The slope of this plot should be the ratio of the second order rate constants for the general base and deuteroxide ion-catalyzed exchange, k_B/k_{DO} according to Equation 2.6 and the intercept should be unity. The deviation of the intercept from unity reflects error in the value for k_{DO}. The slope of this plot is small in comparison to the increase in buffer concentration which indicates that general base catalysis of exchange is not significant.

Figure 2.70: Plot of the ratio of rate constant k_{rel} against ([B]/[DO⁻]).

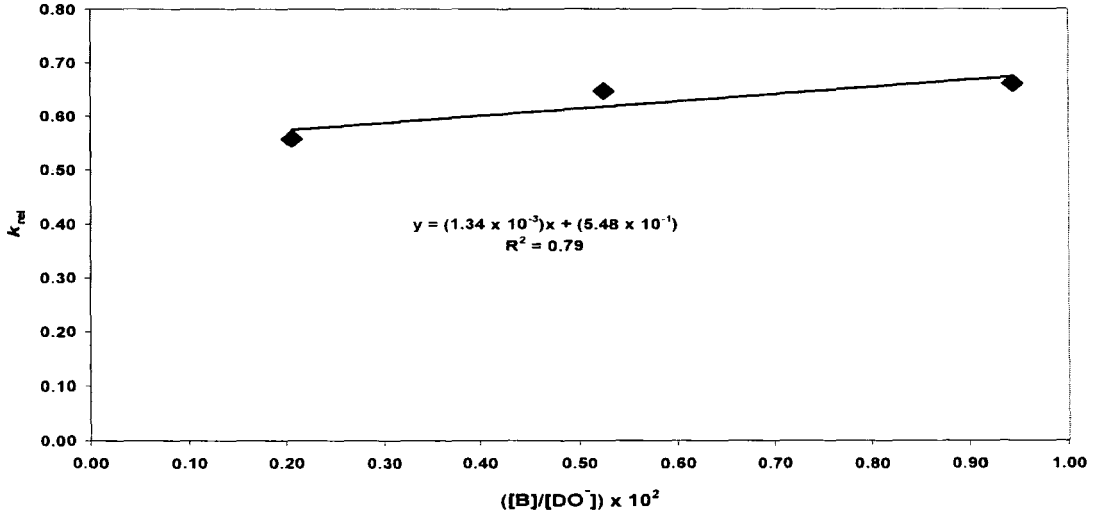

2.4. Estimation of k_{H2O} and pK_a determination.

The second-order rate constant for deuteroxide-ion catalyzed exchange (k_{DO}, $M^{-1}s^{-1}$) and for hydrolysis where relevant (k_{Hyd}, $M^{-1}s^{-1}$) for imidazolium ions **(109) – (115)**, 4,5-dihydroimidazolium ions **(116) – (119)**, trihydropyrimidinium ions **(120) – (121)** and acyclic formadine **(123)** are summarized in Table 2.41.

The second order-rate constant for hydroxide ion-catalyzed deprotonation (k_{HO}, $M^{-1}s^{-1}$) can be obtained from the experimental value k_{DO} ($M^{-1}s^{-1}$) values by using the isotope effect relationship $k_{DO}/k_{HO} = 2.4$. This secondary solvent isotope effect on the basicity of the deuteroxide ion is applicable where proton transfer is not rate-determining and exists instead as a pre-equilibrium. This secondary solvent isotope effect results from the higher basicity of the deuteroxide ion in D_2O compared to the hydroxide ion in H_2O.[89]

Combining the reaction of azolium ions and hydroxide ion with the self ionization of water, permits the estimation of a pK_a value in water for the azolium ion (Scheme 2.20). This can be calculated as in Equation 2.10. In this equation k_{HO} is the second order rate constant for hydroxide ion catalyzed deprotonation at C2 and k_{H2O} is the first order rate constant for the reverse protonation of the ylide by water.

Scheme 2.20:

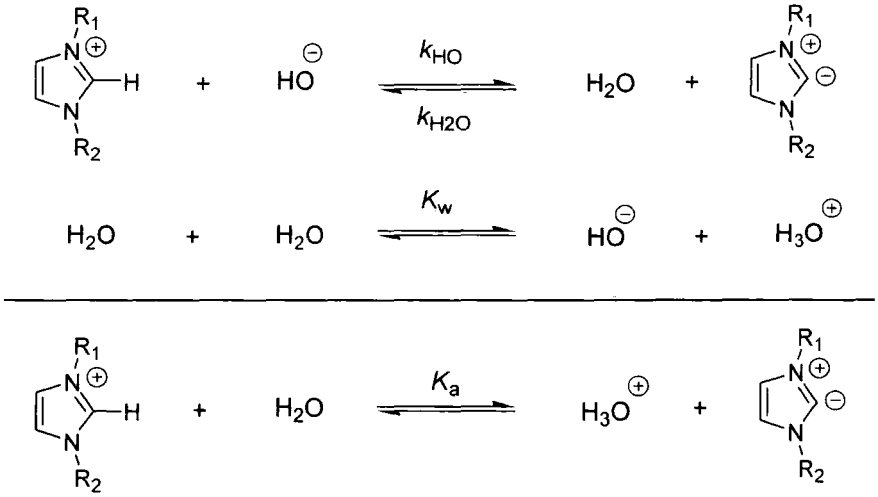

$$pK_a = pK_w + \log\left(\frac{k_{H2O}}{k_{HO}}\right) \qquad \textbf{(Equation2.10)}$$

The absence of general base catalysis of exchange for the representative azolium ions studied means that solvent reorganization is rate-determining for the overall deuteroxide ion-catalyzed reaction, as described in Section 2.3. Hence the rate constant for the reprotonation of the carbene or ylide by water (k_{H2O}, s^{-1}) can be equated with the rate constant for solvent reorganization according to Equation 2.11.

$$k_{H2O} = k_{reorg} \approx 10^{11}\ s^{-1} \qquad \textbf{(Equation 2.11)}$$

The term pK_w is derived from the ion product of water, $K_w = 10^{-14}\ M^2$ and hence pK_w = 14. The resulting pK_a values for imidazolium ions **(109)** – **(115)** and for 4,5-dihydroimidazolium ions **(116)** – **(119)** and for trihydropyrimidinium ions **(120)** – **(122)** are shown in Table 2.41.

Table 2.41: Kinetic and thermodynamic acidities of imidazolium ions (109), (110), (111) and (112) and of dihydroimidazolium ions (113), (114), (115) and trihydropyrimidinium ions (120), (121) and (122) and formadine (123).

Substrate	k_{DO} ($M^{-1}s^{-1}$)[a]	k_{HO} ($M^{-1}s^{-1}$)[b]	pK_a[c]	k_{Hyd} ($M^{-1}s^{-1}$)
Imidazolium ion				
$R_1 = R_2$ = *p*-chlorophenyl **(111)**	3.92×10^5	1.63×10^5	19.78	–
$R_1 = R_2$ = *p*-methoxyphenyl **(110)**	4.80×10^4	2.00×10^4	20.70	–
$R_1 = R_2$ = Mesityl **(109)**	4.10×10^4	1.71×10^4	20.77	–
$R_1 = R_2$ =2,6-di-*iso*propylphenyl **(112)**	2.00×10^4	8.33×10^3	21.08	–
R_1 = ethyl, R_2 = methyl **(114)**	1.84×10^2	7.67×10^1	23.12	–
R_1 = butyl, R_2 = methyl **(115)**	1.64×10^2	6.84×10^1	23.17	–
$R_1 = R_2$ = *t*-butyl **(113)**	1.66	0.69	25.16	–
4,5-dihydroimidazolium ions				
$R_1 = R_2$ = *p*-methoxyphenyl **(117)**	4.26×10^4	1.77×10^4	20.75	–
$R_1 = R_2$ = Mesityl **(116)**	1.25×10^4	5.19×10^3	21.29	–
$R_1 = R_2$ =2,6-di-*iso*propylphenyl **(118)**	8.37×10^3	3.49×10^3	21.46	–
R_1 = mesityl, R_2 = methyl, C4-*iso*propyl **(119)**	3.45×10^2	1.17×10^2	22.93	–
Trihydropyrimidinium ions				
$R_1 = R_2$ = ethyl **(122)** PF_6^-	3.48×10^{-3}	1.45×10^{-3}	27.83	2.83×10^{-2}
$R_1 = R_2$ = *iso*propyl **(121)** $N(SO_2CF_3)_2^-$	3.58×10^{-3}	1.49×10^{-3}	27.82	–
$R_1 = R_2$ = *iso*propyl **(120)** PF_6^-	1.48×10^{-3}	6.15×10^{-4}	28.21	2.21×10^{-4}
Formadine				
$R_1 = R_2 = R_3 = R_4$ = *iso*propyl **(123)**	$<2.26 \times 10^{-4}$	$<9.41 \times 10^{-5}$	>28	2.26×10^{-4}

(a) Second order rate constant for deprotonation of the substrate ion at C2 by deuteroxide ion in D_2O, (b) Second-order rate constants for deprotonation of substrate at C2 by hydroxide ion in H_2O, calculated from the experimental value for k_{DO}, using an estimated secondary solvent isotope effect of k_{DO}/k_{HO} = 2.4 (see text). (c) Carbon acid pK_a for ionization of the substrate ion at C2 in H_2O, calculated using Equation 2.10 (see text). The estimated error is ± 0.5.

2.5 Discussion

2.5.1 Synthesis of azolium ions

The successful synthesis, isolation and purification of imidazolium ions **(142)** and 4,5-dihydroimidazolium ions **(143)** depended largely on the nature of the substituents on the nitrogen atoms of the ring.

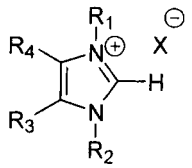

(142)

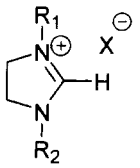

(143)

2.5.1.1 Synthesis of imidazolium ions (142)

There are several possible routes to the formation of imidazolium ions detailed in the literature. Traditionally, procedures have focused on the dissolution of imidazole in a variety of solvents such as THF,[90] methanol, [91] and DMSO.[92] This was followed by deprotonation of the imidazole by a base such as NaOH,[91] NaH,[92] KBF_4 and KPF_6[93] at varying temperatures. Alkylation was achieved by addition of two equivalents of an alkyl halide, (see Scheme 2.21) Common by-products of the alkylation reaction include elimination products of the alkyl halides.

Isolation and purification of imidazolium and 4,5-dihydroimidazolium ions is achievable in numerous ways. Organic layer components have been extracted with water, chloroform or benzene and further purified by sublimation from -30 to -80 °C, distillation or column chromatography.[94]

Scheme 2.21:

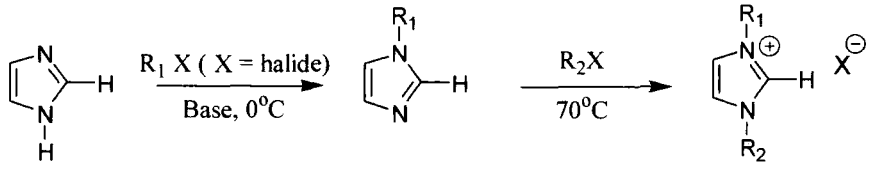

Other multicomponent procedures have been reported, such as the reaction of glyoxal, an appropriate primary alkyl or aryl amine and formaldehyde in the presence of an acid to

construct a heterocycle with the required substituents. Different counter anions for the imidazolium salt may result from the use of different acids and the incorporation of chiral amines would result in C_2-symmetric imidazolium salts.

By far the simplest and most straightforward method for this work was that of Arduengo *et al.*[95] This method involved a multicomponent reaction to build up the heterocycle with the appropriate substituents (see Scheme 2.22). Glyoxal was reacted with the appropriately substituted amine to form a diimine which precipitated out of solution upon the addition of water. This was then readily cyclized by reaction with chloromethylethyl ether in THF in the presence of copper metal to yield an imidazolium chloride salt. Typically this imidazolium salt was then precipitated out of the organic layer by the addition of water or dilute acid. However the success of this synthetic route was limited to air and water stable products. Attempts to synthesize imidazolium ions with N-alkyl substituents such as a methyl group proved difficult with this method as the imines produced were in low yield and did not precipitate. The preparation of imidazolium ions from less reactive aryl substituted amines such as *p*-nitrophenylamine also proved difficult and ultimately was not achieved in this work.

All the imidazolium ions successfully synthesized in this work were prepared by a similar synthetic route to Arduengo *et al*[95] with only minor adjustments needed depending on the nitrogen substituent. Imidazolium ions **(109)**, **(110)** and **(112)** were synthesized using the procedure outlined in Scheme 2.22. In the first step, glyoxal **(144)** was treated with two equivalents of the required primary amine to form corresponding diimine **(145)** which precipitated easily in all cases due to the large steric bulk and hydrophobicity of the two aryl groups. Diimine **(145)** was then treated with chloromethyl ethyl ether in THF to yield the corresponding imidazolium chloride. Imidazolium ion **(109)** was obtained in 48% yield after 30 minutes, imidazolium ion **(110)** in 91% yield after 2 hours, imidazolium ion **(112)** in 94% yield after 24 hours.

Scheme 2.22:

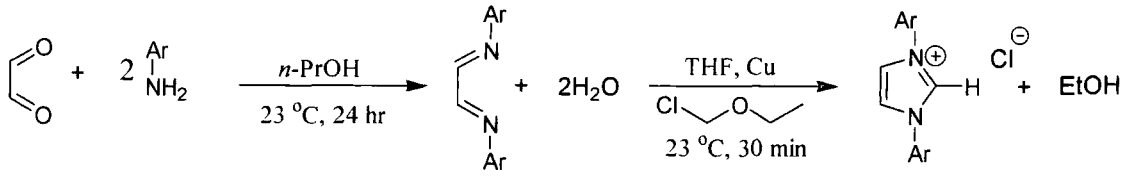

(144) **(145)**

(109) Ar = 2,4,6-trimethylphenyl
(110) Ar = *p*-methoxyphenyl
(112) Ar = 2,6-diisopropylphenyl

Imidazolium ion **(109)** was further purified by recrystallization from *n*-hexane, while imidazolium ions **(110)** and **(112)** were purified by column chromatography (1:9 methanol:dichloromethane). Imidazolium chloride **(109)** had been prepared previously[95] and the literature ^{1}H NMR data matched our results. Further confirmation of product purity was obtained by elemental analysis.

Syntheses of imidazolium ions **(110)** and **(112)** have not been published to date. The identity and purity of these imidazolium ions were confirmed by elemental analysis and by ^{1}H and ^{13}C NMR spectroscopy. The structure of 1,3-bis(*p*-methoxyphenyl)imidazolium chloride **(110)** was further confirmed by X-ray crystallography as suitable crystals formed upon purification of the crude product.

2.5.1.2 Synthesis of 4,5-dihydroimidazolium ions (143)

A similar synthetic route to that outlined in Scheme 2.22 was followed for synthesis of 4,5-dihydroimidazolium ions, however generally lower yields of products were obtained.

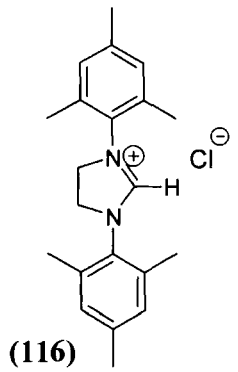

(116)

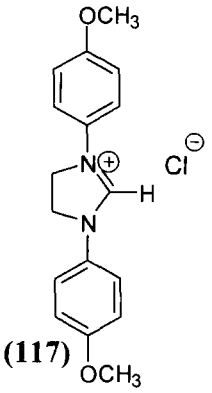

(117)

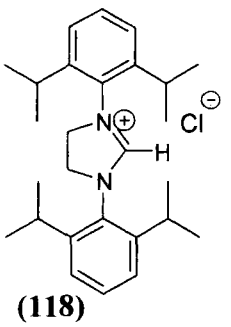

(118)

As with the synthesis of imidazolium ions **(109)** – **(112)**, the first step in the synthesis of the saturated counterparts 4,5-dihydroimidazolium ions **(116)** – **(118)** involved formation of a diimine **(145)** from the condensation of glyoxal with two equivalents of the appropriate aryl amine (Scheme 2.23). The second step in the synthesis involved reduction of the diimine. Sodium borohydride in THF was used to reduce glyoxal-bis(2,4,6-trimethylphenyl)imine followed by 24 hours stirring at room temperature and a subsequent 4 hours reflux. The reduction of glyoxal-bis(*p*-methoxyphenyl)imine and glyoxal-bis(2,6-diisopropylphenyl)imine required dissolution of the diimines in a methanol/THF mixture, followed by the addition of sodium borohydride in a sodium hydroxide and water solution at 0 °C. The reaction solutions were then refluxed for 1 and 16 hours respectively for complete reaction to form the corresponding diamine **(153)** (Scheme 2.23). Addition of HCl and water to the cooled reaction mixture produced a solid precipitate in the case of 1,3-bis(2,4,6-trimethylphenylamino)ethane. However, concentration of the reaction mixture after addition of HCl and water was required to induce precipitation of 1,3-bis(*p*-methoxyphenyl)ethane and 1,3-bis(2,6-diisopropylphenylamino)ethane as crystalline solids. Elemental analysis of the products confirmed them to be diamines and not the hydrochloride salts which were reported to form in the literature.[95]

Scheme 2.23:

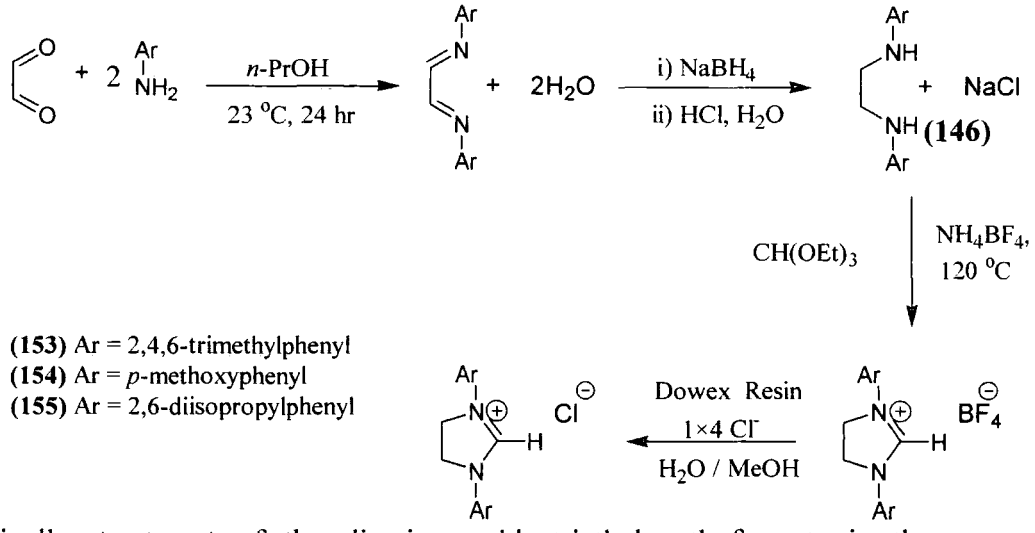

(153) Ar = 2,4,6-trimethylphenyl
(154) Ar = *p*-methoxyphenyl
(155) Ar = 2,6-diisopropylphenyl

Finally, treatment of the diamines with triethyl orthoformate in the presence of ammonium tetrafluoroborate formed 4,5-dihydroimidazolium tetrafluoroborate salts. The

yield for this final cyclization step varied dramatically. 1,3-Bis(2,4,6-trimethylphenyl)-4,5-dihydroimidazolium tetrafluoroborate **(116)** formed readily with a 96% yield, while 1,3-bis(*p*-methoxyphenyl)-4,5-dihydroimidazolium tetrafluoroborate **(117)** was obtained with a significantly lower 30% yield. Finally, 1,3-bis(2,6-diisopropylphenyl)-4,5-dihydroimidazolium tetrafluoroborate **(118)** was obtained in a 54% yield. The 4,5-dihydroimidazolium ions with tetrafluoroborate counterions were found to be insoluble in water. Hence the tetrafluoroborate counterion was exchanged for chloride ion by passing the substrates through an ion exchange column. The chloride salts of **(116)** and **(118)** showed good agreement between theoretical and experimental elemental analytical percentages, however elemental analysis of 4,5-dihydroimidazolium ion **(117)** indicated the presence of water of crystallization in the final product.

The change in counterion resulted in a large increase in solubility of 4,5-dihydroimidazolium ions **(116)**, **(117)** and **(118)** and also gave a consistent counterion throughout the series of aryl substituted imidazolium and 4,5-dihydroimidazolium ions studied.

2.5.1.3 Attempted synthesis of further imidazolium and 4,5-dihydroimidazolium ions.

Attempts were made to synthesise 1,3-bis(3,5-di-*t*-butylphenyl)-4,5-dihydroimidazolium chloride **(149)** (Scheme 2.24) however synthesis of the 1,2-bis(3,5-di-*t*-butylphenylamino)ethane **(148)** precursor was unsuccessful. It was found that reduction of 1,3-bis(3,5-di-*t*-butylphenyl)imine **(147)** required the use of lithium aluminium hydride. However the reduction was only marginally successful as the majority of the product was decomposed before it could be isolated. The synthesis of 1,3-bis(3,5-di-*t*-butylphenyl)-4,5-dihydroimidazolium tetrafluoroborate was not attempted due to the low yields of the previous step.

Scheme 2.24:

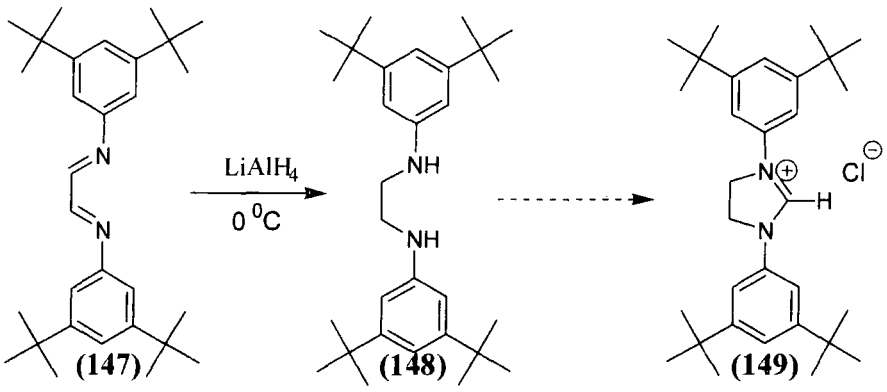

The synthesis of the glyoxal-bis(*p*-nitrophenyl)imine **(150)** precursor to the 1,3-bis(*p*-nitrophenyl)imidazolium and 4,5-dihydroimidazolium ions was subject to a number of problems (Scheme 2.25). The reaction mixture was stirred under argon at 0 °C for 2 hours and at 23 °C for 24 hours after which time the solution was visibly lighter in colour and T.L.C analysis showed a distinctive spot (R_f 0.70 ethyl acetate /dichloromethane 1:5) indicating possible product formation, and mass spectral analysis of the crude mixture showed the presence of the imine product. However attempted isolation of the product clearly resulted in hydrolysis back to starting materials and no imine product was evident in the resulting ^{1}H NMR spectra. Brief exposure to air for 2 minutes resulted in conversion of the yellow solid to orange oil. It is clear that more sensitive conditions are required for the successful isolation of diimine **(150)** to avoid possible hydrolysis back to starting materials. However, due to time limitations, further synthetic routes were not pursued.

Scheme 2.25:

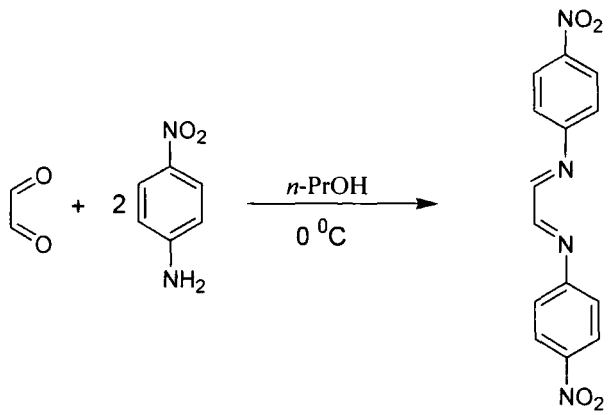

(150)

Attempts were made to synthesise 1,3-dimethyl-4,5-dihydroimidazolium ion **(155)** using the method described previously for 4,5-dihydroimidazolium ions **(116)** – **(118)** however this was found to be an ineffective method for the smaller alkyl substituted ion. An alternative approach was to couple 1,2-dichloroethane with methylamine in a substitution reaction to form 1,2-dimethylaminoethane **(152)**. This was achieved by stirring 1,2-dichloroethane with methylamine (40% wt% in H_2O) for three weeks at 23 °C followed by the addition of sodium hydroxide. This resulted in precipitate formation (NaCl) which was then removed by filtration. More sodium hydroxide was added until a distinct organic layer was formed. This was decanted off and purified by fractional distillation to give a mixture of two compounds, the diamine **(152)** and dimer **(153)**. Attempts to precipitate the hydrochloride salt of diamine **(152)** resulted only in the production of the hydrochloride salt of the dimer **(154)** and not the diamine salt.

Scheme 2.26:

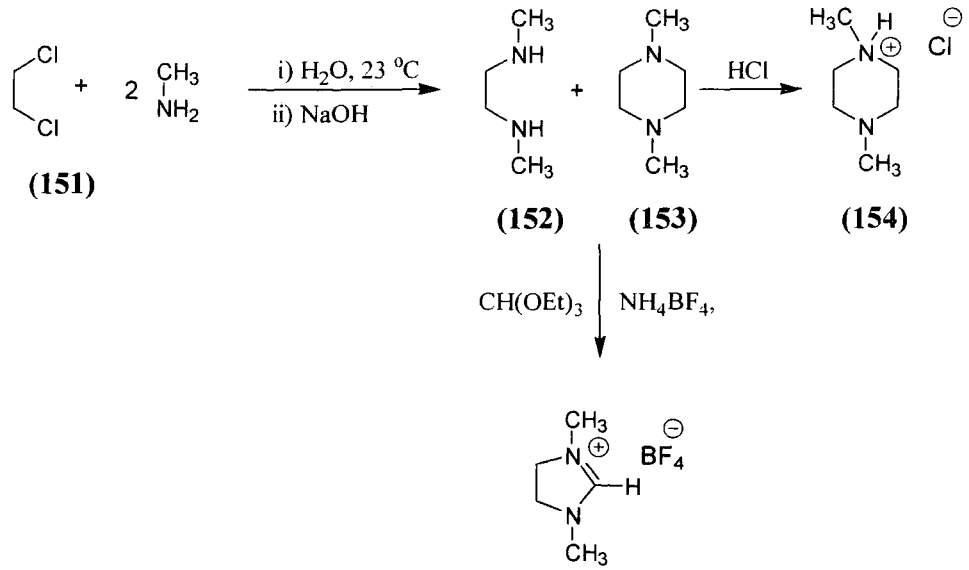

(151) **(152)** **(153)** **(154)** **(155)**

Synthesis of 1,3-dimethyl-4,5-dihydroimidazolium ion **(155)** was attempted by reacting the crude oil mixture of both diamine **(152)** and dimer **(153)** with triethyl orthoformate and ammonium tetrafluoroborate (Scheme 2.26) Mass spectral analysis showed a molecular ion peak at 100.1 corresponding to azolium ion **(155)**, however isolation of the

product proved difficult due to the low yield and rapid hydrolysis of the saturated imidazolium ring.

2.5.2 Deuterium exchange and competing reactions

Deuterium exchange reactions for all azolium ions was followed by ^{1}H NMR spectroscopy. The disappearance of the peak due to the C2-H in the ^{1}H NMR spectrum was monitored at 25 °C and mostly at ionic strength I = 1.0 (KCl) as detailed in Section 2.2.2. Under the experimental conditions for deuterium exchange, the likelihood of a number of competing parallel reactions had to be considered. These reactions include hydrolysis, dimerization and adduct formation

2.5.2.1 Hydrolytic stability of azolium ions and corresponding diaminocarbenes

In the case of imidazolium ions, the expected hydrolysis product is the acyclic, unsymmetrical formamide **(131)**, (see Scheme 2.27) which is a tautomer of imine **(133)**, and similarly for 4,5-dihydroimidazolium ions the expected hydrolysis product is formamide **(156)**. For 4,5,6-trihydropyrimidinium ions **(120)** – **(122)**, the expected hydrolysis product is the acyclic formadine **(157)**. For the acyclic N,N'-di-*iso*propyl formadine **(123)** the expected hydrolysis products are di-*iso*propyl amine **(140)** and N,N'-bis(di-*iso*propyl) formamide **(141)**.

Scheme 2.27:

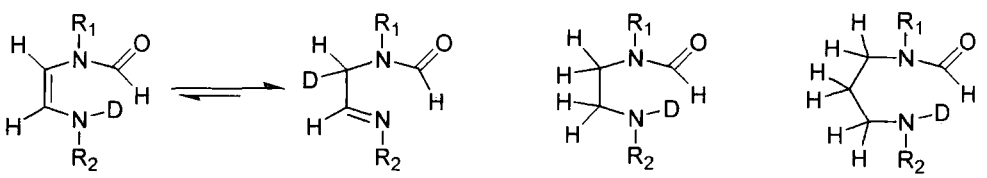

(131) **(133)** **(156)** **(157)**

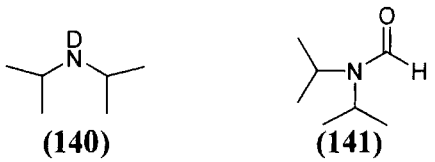

(140) **(141)**

However, during the time course for exchange of the C2-H for deuterium for imidazolium ions **(109)** – **(115)**, and for 4,5-dihydroimidazolium ions **(116)** – **(119)**, no hydrolysis products were detected by ^{1}H NMR spectroscopy, indicating that deuterium exchange is much faster than hydrolysis under reaction conditions. However an increase in ring size from five-membered 4,5-dihydroimidazolium ions to six-membered 4,5,6-trihydropyrimidinium ions significantly reduced the rate of deuterium exchange and the hydrolytic stability of the azolium ions. The significant differences in reactivity between five and six membered rings is discussed further in Section 2.5.5.2. Hydrolysis was observed in the cases of 4, 5, 6-trihydropyrimidinium ions **(120)** – **(122)** and for the acyclic formadine **(123)** (see Table 2.41). In these cases hydrolysis was seen to be competitive with deuterium exchange under the experimental conditions investigated, with the relative rates dependent on the N–substituent. The second-order rate constant for the deuteroxide-ion catalyzed hydrolysis of 1,3-di-*iso*propyl-4,5,6-trihydropyrimidinium hexafluoro phosphate **(120)** (k_{Hyd} 2.21 × 10^{-4} $M^{-1}s^{-1}$) is approximately seven fold lower than the corresponding rate constant for deuterium exchange, (k_{DO} = 1.48 × 10^{-3} $M^{-1}s^{-1}$) and 130 fold lower than obtained for hydrolysis of 1,3-diethyl-4,5,6-trihydropyrimidinium hexafluoro phosphate **(123)** (k_{Hyd} 2.86 × 10^{-2} $M^{-1}s^{-1}$). In the latter case hydrolysis is 20-fold slower than deuterium exchange (k_{DO} = 1.45 × 10^{-3} $M^{-1}s^{-1}$). The difference in rates of hydrolysis between these two compounds may be attributed to steric effects from the N-substituents. In the case of acyclic tetra-*iso*propyl formadine **(121)**, hydrolysis was seen to occur at a similarly slow rate to 1,3-di-*iso*propyl-4,5,6-trihydropyrimidinium hexafluoro phosphate **(120)**, (k_{Hyd} 4.65 × 10^{-4} $M^{-1}s^{-1}$), however deuterium exchange was not found to be competitive under any conditions, indicating a much smaller rate constant for exchange (and higher pK_a value) compared with all other azolium ions in this study.

Generally in the literature hydrolytic stability of carbenes is judged by the relative ease of formation of acyclic ring-opened hydrolysis products such as those shown above (Scheme 2.27) after initial rapid carbene protonation. The synthesis, isolation and relative stabilities of carbenes 1,3-bis(1-adamantyl)imidazol-2-ylidene **(158)**,[21] 1,3-di-*t*-butylimidazol-2-ylidene **(159)**, 1,3-di-*t*-butylimidazolin-2-ylidene, **(160)**,[96] 1,3-bis(2,4,6-

trimethylphenyl)imidazol-2-ylidene **(161)**[95] and 1,3-bis(2,4,6-trimethylphenyl)imidazolin-2-ylidene **(162)**[25] along with a few others has been reported.

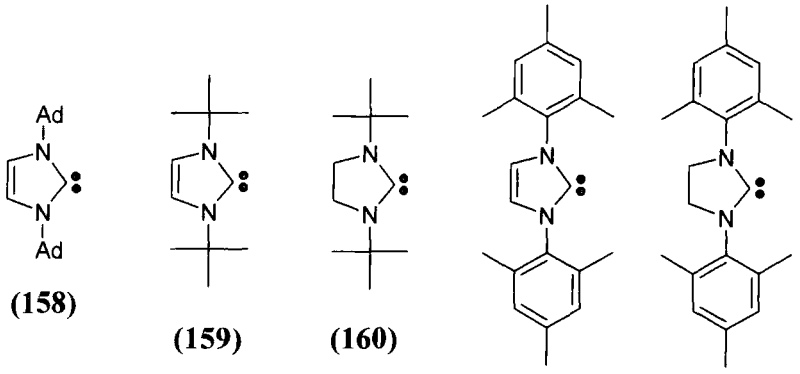

(158) **(159)** **(160)** **(161)** **(162)**

It was reported by Denk *et al*[96] that 1,3-di-*t*-butylimidazol-2-ylidene **(159)** was more stable to hydrolysis than the corresponding saturated analogue **(160)** (see Scheme 2.28). This was attributed to the aromatic stabilization of the former. In THF in the presence of one equivalent of water, carbene **(159)** is protonated to form the azolium ion **(163)**, however hydrolysis of **(163)** to acyclic formamide **(164)** does not become apparent for days, and takes months to complete. Conversely di-*t*-butylimidazolin-2-ylidene, **(160)** undergoes instantaneous hydrolysis in these conditions or on exposure to air to give, first, the protonated azolium **(165)**, and then the acyclic product **(166)**. This susceptibility of 4,5-dihydroimidazolium ions with small alkyl substituents to hydrolysis explains our failure to isolate 1,3-dimethyl-4,5-dihydroimidazolium chloride.

Arduengo *et al*[95] reported that the unsaturated 1,3-bis(2,4,6-trimethylphenyl)imidazolin-2-ylidene **(162)** showed indefinite stability in the solid state and no hydrolysis was observed during deuteroxide-catalyzed deuterium exchange reactions carried out during the course of this work. The stability of this N-aryl substituted carbene and conjugate acid appears to correlate with its ease of isolation relative to N-alkyl substituted azolium ions. The same is true for the corresponding 4,5-dihydroimidazolium counterpart.

Scheme 2.28:

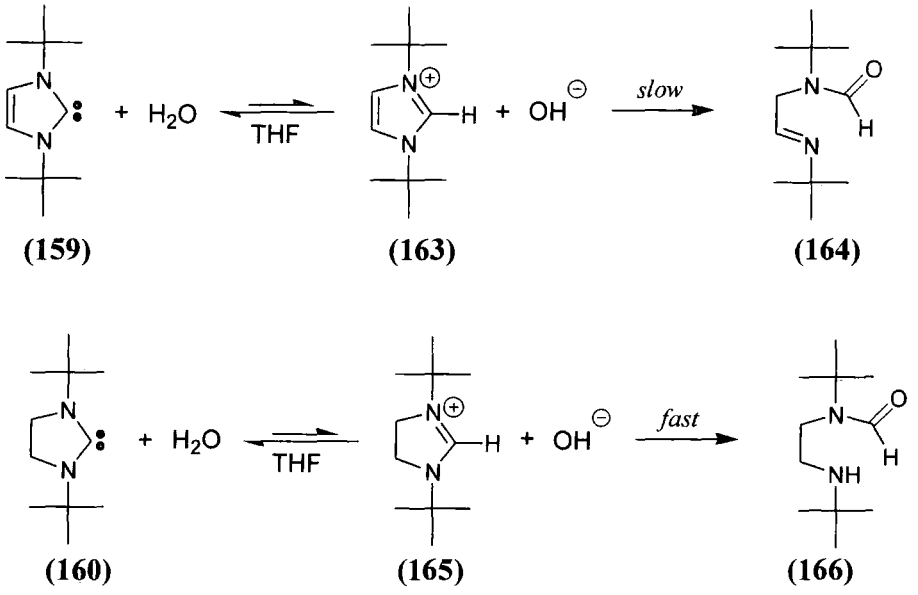

(159) **(163)** **(164)**

(160) **(165)** **(166)**

2.5.2.2 Dimerization of diaminocarbenes

Dimerization is a side reaction commonly associated with the generation of carbenes. The product of such a reaction of imidazole-2-ylidenes would be formation of a tetraazafulvalene **(167)**, a relatively stable molecule. A recent review of dimerization of diaminocarbenes by Alder *et al*[97] stated that dimerization is thermodynamically unfavourable for imidazole-2-ylidenes, the calculated activation energies being preventatively high. However it is typically 100 kJ mol^{-1} more favourable for less stable acyclic and seven-membered–ring carbenes than for five- and six-membered cyclic carbenes.[97]

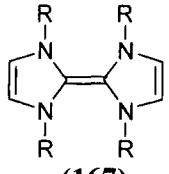

(167)

This is partly due to an increase in N-C-N bond angles and some loss of conjugation brought about by twisting about the N-C bonds. Non-aromatic imidazolin-2-ylidenes require substantial steric hindrance such as N-*t*-butyl substituents for the carbene to be stable towards dimerization.[98] Simple unhindered aromatic imidazole-2-ylidenes such as

1,3-dimethylimidazol-2-ylidene are thermodynamically stable towards dimerization due to very high calculated energy barriers to the uncatalyzed reaction.

It was first pointed out by Hoffmann *et al*[99] that singlet carbenes cannot dimerize by a least motion, head-to-head approach. The filled sp^2 lone pair orbital must approach the empty p-orbital of the other carbene (see Scheme 2.29) with a transition state resembling structure **(A).**

Scheme 2.29:

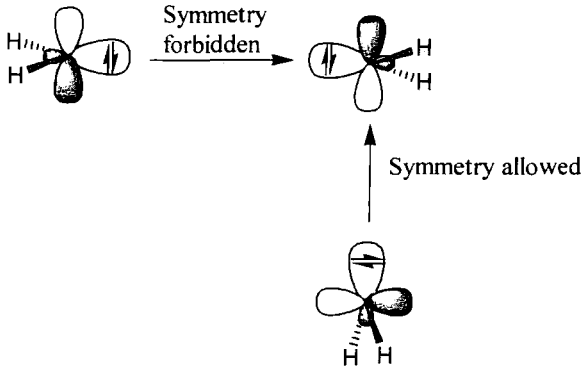

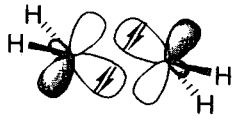

(A)
Transition state for dimerization

Diaminocarbenes can however dimerize by a proton-catalyzed mechanism. Proton-catalyzed dimerization has been seen to occur readily between a carbene and its conjugate acid formadine. The formadine/carbene reaction is likely to have a lower energy barrier than is expected for direct carbene dimerization as there are electrostatic attractions between the negative end of the carbene and the positive charge on the formadine. Also the approach of the carbene can be more perpendicular, reducing the steric effects of large N-substituents. The nucleophilic carbene attacks its protonated formadine precursor to generate the C-protonated dimer (Scheme 2.30 **(A)**). Arduengo *et al* have shown that certain imidazole-2-ylidenes form hydrogen bonds to the corresponding imidazolium ions creating an alternate route **(B)** to the C-protonated dimer. However over the course of this work there was no evidence for the formation of dimers of any of the carbenes studied, even though some of the studies were conducted in acetate buffers with pH values from 4 - 7. This is not unexpected however, as the concentration of carbene was extremely low at all times due to the high pK_a values of the

Scheme 2.30:

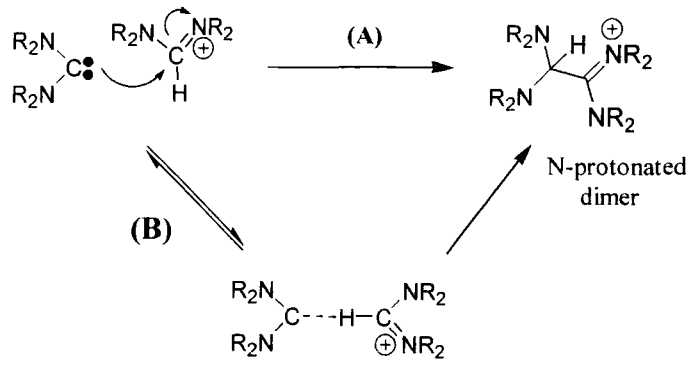

respective imidazolium and 4,5-dihydroimidazolium ions and the short lifetime of the carbene in aqueous solution, with reprotonation limited by solvent reorganization. This reprotonation by bulk solvent water would significantly out-compete any dimerization which would require one carbene molecule and one azolium ion to meet in solution.

2.5.2.3 Adduct formation

Another potential side reaction, an example of which was reported recently by Aggarwal *et al*,[100] is adduct formation between the carbene and an electrophile such as benzaldehyde. This stems from the strongly nucleophilic nature of diaminocarbenes. The use of imidazolium salts as ionic liquid solvents in Baylis-Hillmann reactions was prompted in an attempt to increase yields, however led to unexpected results (Scheme 2.31). Far from being inert, under mild basic conditions the imidazolium salts were deprotonated to give reactive nucleophiles. These were found to react with the aldehyde leading to the formation of an adduct **(168),** resulting in lower yields of the over all desired Baylis-Hillmann reaction.

As one of the supposed advantages of ionic liquids is their recyclability, this reaction poses serious consequences for their general use as solvents, as further analysis showed that reuse of the ionic liquid from one Baylis-Hillmann reaction gave a mixture of products in subsequent reactions.[100] However, from the point of view of this work, there is no evidence of adduct formation between imidazolium ions and any other species

Scheme 2.31:

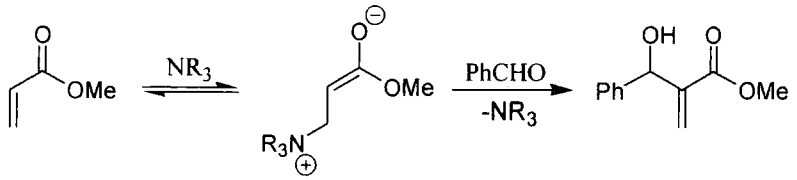

Baylis-Hillmann reaction

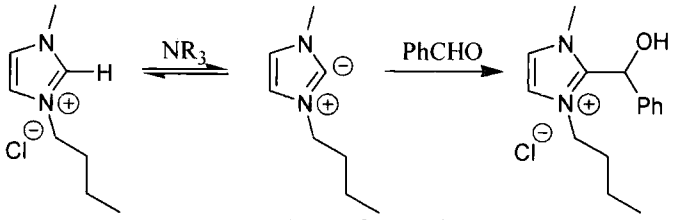

Adduct formation **(168)**

employed under these experimental conditions. Also the concentrations of imidazolium ion used is significantly lower than employed in reactions where the ionic liquids are used as solvent.

2.5.3 Mechanism for deuterium exchange catalyzed by deuteroxide ion

Scheme 2.19 shows a detailed mechanism for exchange of the C2-H of all azolium ions studied for deuterium catalyzed by deuteroxide ion. In D_2O solution with deuteroxide ion as base, the encounter of imidazolium ion (C2-L^+, (L = H)) and deuteroxide ion, results in proton abstraction to give an intimate ion pair – a carbene /LOD complex – which reacts by either of two pathways.

Firstly, reprotonation of the carbene/LOD complex by DOH (k_p), regenerates the protonated substrate. Secondly, irreversible deuteration by D_2O gives exchange product. This initially involves placement of a molecule of DOD in a position to deliver a deuteron to C2 of the carbene/LOD complex. The solvent reorganization step is irreversible and results in an exchange reaction as the concentration of DOH is negligible. The rate constant for solvent reorganization may be equated to the rate constant for dielectric relaxation of the solvent, $k_{reorg} = 10^{11}$ s^{-1}.[101-104] As mentioned in Section 2.3, reprotonation of the carbene/LOD complex is fast, hence determination of the rate constant for deuterium exchange enables estimation of the rate constant for carbene formation.

Scheme 2.32:

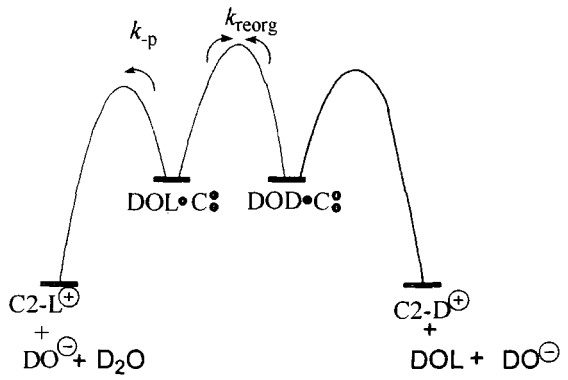

As discussed by Amyes *et al*[51] the solvent reorganization step is rate-limiting for the above mechanism in the case of deuterium exchange of the C2-H of imidazolium ions. This was concluded from the absence of buffer catalysis of the deuterium exchange reaction at C2 of 1,3-dimethylimidazolium iodide **(59)**, 1,3-dimethylbenzylimidazolium iodide **(62)** and 1,3-bis((S)-α-methylbenzyl)benzylimidazolium chloride **(63)** within an estimated 10% experimental error limit, indicating that proton transfer is non-rate-determining.

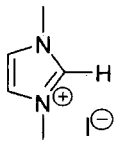

(59)

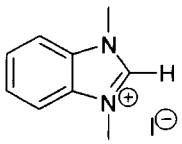

(62)

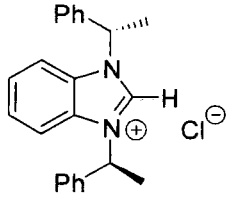

(63)

Results from similar buffer catalysis experiments carried out under our experimental conditions are in agreement with these findings (Table 2.42).

Table 2.42:

Carbene conjugate acid	Buffer	% FB[a]	[Buffer]/M[b]	pD	$[DO^-]^c$ (M^{-1})	$k_{obs}{}^d$ (s^{-1})	$k_{rel}{}^e$
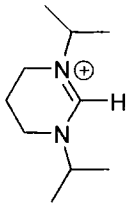 **(120)**	Quinuclidine	10	0.05	11.13	2.44×10^{-4}	2.47×10^{-7}	0.559
			0.15	11.20	2.86×10^{-4}	3.24×10^{-7}	0.647
			0.25	11.17	2.65×10^{-4}	3.19×10^{-7}	0.661
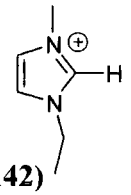 **(142)**	Quinuclidinone	10	0.05	7.25	3.20×10^{-8}	5.92×10^{-6}	0.807
			0.15	7.26	3.28×10^{-8}	5.79×10^{-6}	0.771
			0.25	7.25	3.20×10^{-8}	6.46×10^{-6}	0.880
			0.45	7.24	3.15×10^{-8}	6.84×10^{-6}	0.947
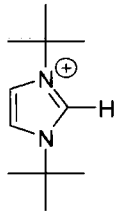 **(113)**	Quinuclidine	10	0.15	11.22	2.97×10^{-4}	1.02×10^{-3}	2.078
			0.25	11.22	3.00×10^{-4}	1.07×10^{-3}	2.157
			0.35	11.22	2.98×10^{-4}	1.02×10^{-3}	2.214
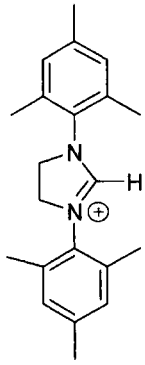 **(116)**	DPO_4^{-2}/ $D_2PO_4^-$	30	0.10	6.79	1.03×10^{-8}	1.43×10^{-4}	1.067
			0.20	6.59	7.04×10^{-9}	9.10×10^{-5}	0.992
			0.40	6.61	7.39×10^{-9}	1.03×10^{-4}	1.068
			0.50	6.62	7.56×10^{-9}	9.24×10^{-5}	0.939

(a) Fraction of buffer present in basic form. (b) Total concentration of buffer. (c) Concentration of deuteroxide ion at the pD of the experiment, calculated using $[DO^-] = 10^{(pD-pK_w)}/\gamma_{OL}$ with $pK_w = 14.87$, where $\gamma_{OL} = 0.75$ is the activity correction of lyoxide ion under our experimental conditions. (d) k_{obs} is the experimental rate constant for deuterium exchange catalyzed by deuteroxide ion at the pD of the experiment in buffered D_2O solution. (e) k_{rel} is the ratio of observed rate constant for exchange (k_{obs}) and

the rate of deuteroxide ion-catalyzed exchange only ($k_{DO}[DO^-]$) , see Equation 2.6 (Section 2.3.1). Using this equation allows for correction for small changes in pD that occur upon dilution at constant ionic strength.

Amyes *et al* reported that a two fold increase in the concentration of phosphate buffer from 50 mM to 100 mM showed no significant change in k_{ex} (s^{-1}) for 1,3-dimethylimidazolium ion **(59)**. Similarly for 1,3-dimethylbenzylimidazolium iodide **(62)** and 1,3-bis((S)-α-methylbenzyl)benzylimidazolium chloride **(63)**, rate constants for deuterium exchange at C2 in 1 M acetate buffer at pD 4.4 or 5.78 were no more than 10% larger than calculated values of $k_{obs} = k_{DO}[DO^-]$ for deuteroxide ion-catalyzed reactions of these substrates.

Similar conclusions may be drawn from the calculated k_{rel} values for the azolium ions shown in Table 2.42. For 1-ethyl-3-methylimidazolium ion **(114)** and more sterically hindered 1,3-bis(*t*-butyl)imidazolium ion **(113)** there is little variation in the values for k_{rel} for each molecule over a large concentration range of quinuclidine buffer seen from the second order rate constant of the plot of the ratio of rate constants k_{rel} against ([B]/[DO^-]) (Figures 2.66 and 2.64 respectively) . This is good evidence against the presence of buffer catalysis for these imidazolium ions. Similarly for 1,3-bis(2,4,6-trimethylphenyl)4,5-dihydroimidazolium ion **(116)** a five fold increase in the concentration of phosphate buffer resulted in negligible change in the rate constants for deuterium exchange shown by the calculated k_{rel} values, indicating no buffer catalysis. In the case of 1,3-di-*iso*propyl-4,5,6-trihydropyrimidinium ion **(120)** the increase in k_{rel} values with increasing buffer concentration is slightly greater than for the other ions. It is still unlikely that buffer catalysis contributes to the observed increase of deuterium exchange. It is more likely that the slight increase in observed rate with increased buffer concentration reflects a greater margin for error brought about by the very low acidity of these ions, coupled with a competing hydrolysis reaction.

As described in Section 2.3, the ratio of first order rate constants (k_{rel}) is a measure of the relative difference between the observed experimental rate constant (k_{obs}) and the

deuteroxide ion-catalyzed rate of exchange ($k_{DO}[DO^-]$). In a situation where there is no general base catalysis of exchange this ratio should be close to unity. The values obtained for k_{rel} in the cases of the azolium ions shown in Table 2.42 deviate from unity significantly however the associated slopes are close to zero. This confirms the absence of general base catalysis of exchange. Deviation of k_{rel} from unity in these cases reflects error from two possible sources: Either the activity coefficient for deuteroxide ion γ_{DO}, which is a value characteristic of the pH electrode used in the experiment, or the second-order rate constant k_{DO} which was determined experimentally (Section 2.2).

Earlier work by Washabaugh and Jencks[53] on analogous deuterium exchange reactions of 3,4-dimethylthiazolium ion **(169)** to give the deuterated product concluded that reverse protonation of these ions by water is limited by the physical encounter of a molecule of HOL (L = H) with the carbene/thiazolium ylide complex. Small primary isotope effects of k_H/k_T = 2.94 and k_D/k_T = 1.58 for hydron transfer from C2 of thiazolium ion **(169)** to lyoxide ion at 30° C show significant deviation from the Swain-Schaad relationship. This implies that there is significant internal return of this transferred hydron to the thiazolium carbene/ylide complex ($k_{-1}/k_{reorg} \approx 3$ for L = H, where $k_{-1} = k_p$) so that reverse protonation of thiazolium ion **(169)** by water is at least partly limited by the physical encounter of a molecule of water with the carbene.

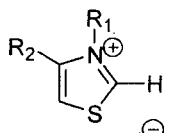

(169)

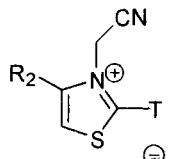

(170)

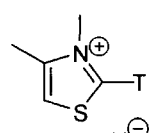

(171)

R_1,R_2 = Me

The value of k_{DO} ($M^{-1}s^{-1}$) for deprotonation at C2 of the imidazolium analogues of **(169)** in this work and in the work of Amyes *et al*[51] are 20 - 400,000-fold smaller than those for deprotonation of thiazolium ions. This implies that imidazol-2-ylidenes are less stable than thiazol-2-ylidenes relative to their azolium ion ground states. Thus deprotonation should be even more limited by the solvent reorganization step ($k_p > k_{reorg}$ in Scheme 2.32). Washabaugh and Jencks[53] also found a systematic increase in the secondary solvent isotope effect for hydron transfer in the case of thiazolium ions **(170)** and **(171)** to

lyoxide ion from k_{DO}/k_{HO} = 1.30 for **(170)**, to k_{DO}/k_{HO} = 2.35 for **(171)**. This limiting maximum value of k_{DO}/k_{HO} = 2.4, for the secondary solvent isotope effect for proton transfer at C2 should apply in the case of imidazolium ions due to their structural similarity and is consistent with proton transfer that is limited by solvent reorganization.

Finally, Amyes *et al*[51] quoted work of Peon *et al*[105] on the generation of diphenylcarbenes by femtosecond laser flash photolysis (LFP) of diphenyldiazomethane **(172)**. Using methanol as a solvent Peon *et al* determined the rate constant for proton transfer to diphenylcarbenes, k_{MeOH} = 1.1 × 10^{11} s^{-1} (τ = 9 ps). This revealed good correlation with the dielectric relaxation time of solvent (τ_{MeOH} = 6.8 ps) showing proton transfer from hydroxylic solvents to highly unstable carbenes to be limited by solvent reorganization with a limiting rate constant $k_{ROH} = k_{reorg} = 1/\tau_{ROH}$.

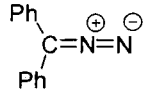

(172)

The conclusion that solvent reorganization is rate-limiting for deuteroxide ion-catalyzed exchange at the C2-H of imidazolium ions allows the definition of two vital parameters in the calculation of the corresponding pK_a values. Firstly, the value of k_{HO} may be obtained from the experimental k_{DO} values via the secondary solvent isotope relationship k_{DO}/k_{HO} = 2.4 where proton transfer is non-rate-determining and exists as a pre-equilibrium. This results from the higher basicity of deuteroxide ion in D_2O compared to hydroxide ion in H_2O. Secondly, the inference that the reverse protonation of these ylides by solvent water is limited by solvent reorganization permits the assignment of the rate constant for dielectric relaxation of solvent, k_{reorg} = 10^{11} s^{-1} as the rate constant for protonation of the carbenes by water.

2.5.4 Substituent effects on second-order rate constants for deuteroxide ion-catalyzed exchange (k_{DO}, $M^{-1}s^{-1}$).

The H/D exchange reactions of azolium ions **(109)** – **(119)** and trihydropyrimidinium ions **(120)** – **(122)** were monitored by ^1H NMR spectroscopy in D_2O solution as described in Section 2.2. The results are summarised in Table 2.41. There are no available literature values for these azolium ions in aqueous solution, however the above values are qualitatively consistent with other available literature estimates of k_{DO} values of similar imidazolium ions as described below.

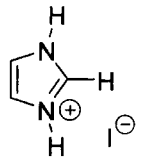

$k_{DO} = 3.69 \times 10^1\ M^{-1}s^{-1}$

(173)

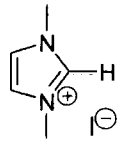

$k_{DO} = 2.47 \times 10^2\ M^{-1}s^{-1}$

(59)

2.5.4.1 Alkyl substituents effects

The effects of alkyl substitution on the kinetic acidities of the imidazolium ions studied in this work could be evaluated by comparison with the recent determination of a k_{DO} value for the parent protonated imidazolium iodide **(173)** at 25 °C, $3.69 \times 10^1\ M^{-1}s^{-1}$ by Amyes *et al.*[51] However as noted by these authors, this value is unexpectedly lower by 7-fold than that for 1,3-dimethylimidazolium iodide. The electron donating methyl substituents would be expected to stabilise the parent azolium ion more than the ylidic product, and to a greater extent than a hydrogen substituent, thus leading to a decrease in kinetic acidity. The greater kinetic acidity of 1,3-dimethylimidazolium iodide relative to imidazolium iodide can only be explained by the potential of hydrogen bonding between the parent ion and water in the latter case. Thus a better reference for comparison with the present results is the k_{DO} value for 1,3-dimethylimidazolium iodide **(59)**, $2.47 \times 10^2\ M^{-1}s^{-1}$, as in this case there is no propensity for H-bonding in aqueous solution from the parent ion to water.

The k_{DO} values determined for 1-ethyl-3-methylimidazolium iodide **(114)** and 1-butyl-3-methylimidazolium chloride **(115)** are very similar at 1.84×10^2 and 1.64×10^2 $M^{-1}s^{-1}$ respectively and are very similar to the value for 1,3-dimethylimidazolium iodide **(59)**, 2.47×10^2 $M^{-1}s^{-1}$. An almost 150-fold decrease is observed in the k_{DO} value for 1,3-bis(*t*-butyl)imidazolium chloride **(113)** 1.66 $M^{-1}s^{-1}$ from 1,3-dimethylimidazolium iodide **(59)**, which is more akin to the 230-fold decrease that was observed in the k_{DO} value for 1,3-bis(adamantyl)imidazolium chloride (1.07 $M^{-1}s^{-1}$) in previous work.[106]

The transition state for carbene formation should resemble the carbene product for these thermodynamically uphill reactions according to the Hammond postulate. Thus a factor which decreases the stability of the product carbene relative to the conjugate acid azolium ion should lead to a decrease in the rate constant for carbene formation. The systematic decrease in observed k_{DO} values appears to correlate with steric bulk and hydrophobicity of the N-alkyl substituent. This could be a result of poorer aqueous solvation of the formally neutral carbene or ylide with bulky, hydrophobic substituents relative to the charged conjugate acid salt. Alternatively this trend could result from steric hindrance to deprotonation at C2, disfavouring carbene formation.

Alkyl substituents are generally inductively electron-donating and so are expected to slightly decrease the effective positive charge on the nitrogen to which they are attached, thus potentially also decreasing the acidity of the C2-H. The alkyl groups cannot interact with the azolium ring through resonance.

Using the Hammett equation (Equation 2.12), which quantifies the sensitivity of a reaction to substituent changes, the effect of a substituent may be postulated.

$$\log\left(\frac{K_X}{K_H}\right) = \rho\sigma \qquad \textbf{(Equation 2.12)}$$

In this equation K_H is the ionization constant for benzoic acid in water at 25 °C and K_X is the corresponding constant for a *meta*- or *para*-substituted benzoic acid. The slope of the

correlation, ρ, indicates the sensitivity of the reaction to substituent changes and is defined as ρ = +1.0 for the ionization of substituted benzoic acids. The parameter, σ, is the substituent constant which is independent of the nature of the reaction and is defined as in Equation 2.13. A positive value for σ indicates an electron-withdrawing substituent, while a negative σ value denotes an electron-donating substituent.

$$\sigma_X = \log K_X - \log K_H \qquad \textbf{(Equation 2.13)}$$

However the electronic effects of substituents are composed of two main parts. A field/inductive component and a resonance component. This is highlighted by the difference between σ_p values where both inductive and resonance effects are present and σ_m values where the contribution of resonance is likely to be much less. Simply, the contribution of inductive (σ_I) and resonance (σ_R) electronic effects of a substituent can be expressed as in Equation 2.14.

$$\sigma_p = \sigma_I + \sigma_R \qquad \textbf{(Equation 2.14)}$$

Experimentally, the ionization of rigid systems such as bicyclooctane carboxylic acids **(174)**[107, 108] and quinuclidines **(175)**,[107, 109] provide an unambiguous system for defining an inductive parameter as the substituent X is firmly held in place. There is little possibility for resonance or polarization interaction between the substituent X and either the carboxylic acid or corresponding anion of **(174)** or the amino group of **(175)**. Hence the only influences that can exist on ionization of these acids are through space (field effects) and through the intervening σ bonds (inductive effects).

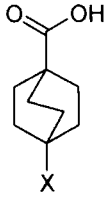

(174)

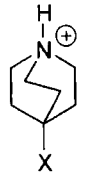

(175)

Additional σ_I values may be calculated using Equation 2.15[107] in which the coefficients α and β are evaluated via a least squares method. The intercept ϵ can be regarded as an error term and is close to zero.

$$\sigma_I = \alpha\sigma_m + \beta\sigma_p + \epsilon \qquad \textbf{(Equation 2.15)}$$

From reported σ_m values, the inductively electron-donating substituent effect is seen to lie in the order: adamantyl (σ_m = -0.12) > *t*-butyl (σ_m = -0.10) > ethyl (σ_m = -0.07) = methyl (σ_m = -0.07). Based on σ_I values only, the inductively electron-donating substituent effect lies in the order: adamantyl (σ_I = -0.07) > *t*-butyl (σ_I = -0.02)> ethyl (σ_I = 0.00) > methyl (σ_I =0.01).[107] This agrees with the increase in k_{DO} values ($M^{-1}s^{-1}$) along this series: adamantly (1.07) < *t*-butyl (1.66) < ethyl (184) < methyl (247). However there is a much larger substituent effect on the k_{DO} values in moving from ethyl to *t*-butyl and subsequently to adamantyl, than from methyl to ethyl substituents. This suggests the influence of steric effects is also important as the changes in σ values cannot account for the larger substituent effects.

2.5.4.2 Aryl substituent effects

From the work by Amyes *et al*[51] it can be seen that annelation of a benzene ring at C4 and C5 of the imidazole ring results in an increase in k_{DO} values from 1,3-dimethylimidazolium ion **(59)** by 23-fold for 1,3-dimethylbenzimidazolium iodide **(61)** and 60-fold for 1,3-bis((S)-α-methylbenzyl)benzimidazolium chloride **(62)**.

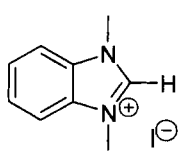

(61)

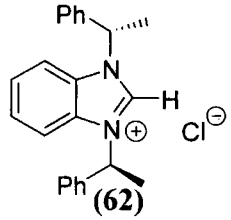

(62)

k_{DO} = 5.74×10^3 $M^{-1}s^{-1}$ 1.48×10^4 $M^{-1}s^{-1}$.

The addition of phenyl and methyl groups to the N-alkyl substituent of **(62)** resulted in a 2.6 fold increase in the value of k_{DO} relative to **(61)**. This could result from an inductive

electron-withdrawing effect of the phenyl substituent, stabilizing the negative charge at C2 of the ylide. This is significantly less than the larger 7-fold differences in k_{DO} values for N-substituted thiazolium ions **(176)** and **(177).**

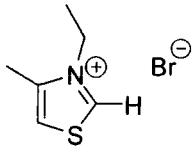

(176)

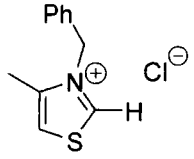

(177)

k_{DO} ($M^{-1}s^{-1}$)	3.24×10^5	2.14×10^6

The effect of aryl substituents directly attached to the nitrogen can be seen from the k_{DO} values determined for imidazolium ions **(109) – (112)** (Table 2.41). Deuteroxide-ion catalyzed exchange of all of the N,N-diarylimidazolium ions studied was 33 – 660 fold faster than for the N,N-dimethylimidazolium ion **(59).** This suggests that all of the aryl groups are acting in an electron withdrawing capacity relative to N-alkyl substituents. Electron withdrawing substituents are expected to increase to k_{DO} values due to destabilization of the cationic parent relative to the neutral ylide.

Within the series of N,N-diarylimidazolium ions the k_{DO} values increase in the order 2,6-di-*iso*propylphenyl (2.00×10^4)< 2,4,6-trimethylphenyl (4.10×10^4) < *p*-methoxyphenyl (4.80×10^4) < *p*-chlorophenyl (3.92×10^5). However over this series the rate constants only vary by up to 20 fold. The largest σ_I value is seen for *p*-chlorophenyl ($\sigma_I = 0.18$), however the value for *p*-methoxyphenyl ($\sigma_I = 0.12$) is identical to that for an unsubstituted phenyl group. It is likely that there is little to no resonance stabilization of the carbene/ylide or its conjugate acid through the phenyl ring as this would likely decrease the k_{DO} value significantly for aryl substituted imidazolium ions and greater differences between k_{DO} values for these ions would be expected. This is also evident from X-ray crystal structures of imidazolium carbenes and their azolium salt precursors, which have shown the aromatic rings are slightly out of plane with the imidazole ring,

making resonance delocalization unlikely. This is discussed in greater detail in Section 2.5.6.3.

Intercomparison of the observed k_{DO} values of imidazolium ions **(109)** – **(112)** shows that the strongly inductively electron-withdrawing *p*-chlorophenyl increases the k_{DO} value significantly compared to relatively inductively electron-donating groups such as 2,6-di-*iso*propylphenyl. However *p*-methoxyphenyl substituent produces a k_{DO} value which is less than twice that of the mesityl group and which is, significantly less than that of *p*-chlorophenyl. The methoxy substituent is electron-donating in a resonance capacity but electron-withdrawing inductively. Generally the resonance effect outweighs the inductive effect making this substituent electron-donating. In the present case, the *p*-methoxyphenyl substituent acts similarly to electron donating alkylphenyl substituents. Perhaps the cumulative effect of several alkyl groups matches that of a single methoxy group.

There is no literature data available for comparison with the series of second order rate constants for deuterium exchange of the C2-H of 4,5-dihydroimidazolium ions **(116)** – **(119)**. However the k_{DO} values for 4,5-dihydroimidazolium ions **(116), (117)** and **(118)** may be compared to their unsaturated analogues **(109), (110)** and **(112)** respectively. In the case of 1,3-bis(2,4,6-trimethylphenyl)4,5-dihydroimidazolium chloride **(116)** (1.25×10^4 $M^{-1}s^{-1}$) the k_{DO} value is 3-fold smaller than for the imidazolium ion analogue **(109)**. Similarly, for 1,3-bis(2,6-di-*iso*propylphenyl)4,5-dihydroimidazolium chloride **(118)** (8.37×10^3 $M^{-1}s^{-1}$) the k_{DO} value is 2-fold smaller than that of 1,3-bis(2,6-di-*iso*propylphenyl)imidazolium chloride **(112),** while the k_{DO} value obtained for 1,3-bis(p-methoxyphenyl)4,5-dihydroimidazolium chloride **(117)** (4.26×10^4 $M^{-1}s^{-1}$) is almost the same as analogue **(110)** (4.80×10^4 $M^{-1}s^{-1}$). This indicates that 4,5-dihydroimidazolium ylides are in general less stable relative to the parent azolium ions than their unsaturated analogues although the effect is small.

We were unable to obtain k_{DO} values for alkyl substituted 4,5-dihydroimidazolium ions due to the difficulties in synthesis. Although the 4,5-dihydroimidazolium ions discussed

above showed no evidence of hydrolysis under the experimental conditions used, it is likely that deuteroxide ion-catalyzed hydrolysis of the 4,5-dihydroimidazolium ring would be a significant competing reaction with deuterium exchange for alkyl-substituted 4,5-dihydroimidazolium ions.

2.5.4.3 Alkyl substituent effects on kinetic acidities of trihydropyrimidinium ions.

The second order rate constants for deuterium exchange of the C2-H of 4,5,6-trihydropyrimidinium ions **(120)** and **(122)** are reported in Table 2.41. In aqueous solution there is no literature data available for comparison with these values. It is apparent from comparison of these data with that of imidazolium ion **(59)**, that an increase in ring size by one carbon significantly reduces the stability of the azolium ylide formed. For deuteroxide ion-catalyzed exchange at C2 of 1,3-di-*iso*propyl-4,5,6-trihydropyrimidinium ion **(120)** (1.48×10^{-3} $M^{-1}s^{-1}$) and for 1,3-diethyl-4,5,6-trihydropyrimidinium ion **(122)** (3.48×10^{-3} $M^{-1}s^{-1}$). The k_{DO} values are 10^4-fold smaller than the value for dimethylimidazolium ion **(59)** (2.47×10^{2}). Under the experimental conditions employed these ions were also subject to competing deuteroxide ion-catalyzed hydrolysis, (Table 2.41), which was substantial for ion **(122)** (2.83×10^{-2} $M^{-1}s^{-1}$) but less significant for ion **(120)** (2.21×10^{-4} $M^{-1}s^{-1}$). This suggests that while the increase in steric bulk from ethyl to *iso*propyl substituents significantly decreases the rate of hydrolysis it has little effect on the rate of exchange.

Although N-aryl-substituted trihydropyrimidinium ions were not studied in this work it may be surmised that the rate of exchange would be much increased relative to the N,N-dialkyl analogues.

2.5.4.4 The effect of counterion on the kinetic acidities of azolium ions.

Throughout this work the counterion present for the majority of imidazolium, and 4,5-dihydroimidazolium ions was maintained as Cl^-. This increased the solubility of many of the azolium ions, most significantly the aryl substituted imidazolium ions. The chloride

salts of the more hydrophobic azolium ions such as the 1,3-bis(2,4,6-trimethylphenyl)4,5-dihydroimidazolium ion **(116),** were soluble in water while the tetrafluoroborate salts were not. However in some cases counterions such as PF_6^- or Br^- have been employed.
In non-polar solvents ion pairs are generally closely associated, however in aqueous solution they are fully solvent separated. Thus the effect of the counterion on the rate constants for C2-H/D exchange is expected to be small especially as the concentration of counterion will be hugely diluted by the concentration of chloride ion present to maintain an ionic strength of unity.

In cases where the counterion was varied, little effect on the second order rate constant for deuterium exchange at C2 was observed. For the 1-ethyl-3-methylimidazolium ion **(114)**, a change in counterion from iodide to chloride **(121)** resulted in no change in the observed second order rate constant for deuteroxide ion-catalyzed deuterium exchange, as the results are identical within the experimental error.

The second order rate constant (k_{DO}, $M^{-1}s^{-1}$) for deuteroxide ion-catalyzed exchange at C2 of 1,3-di-*iso*propyl-4,5,6-trihydropyrimidinium hexafluoro-phosphate **(120)** was found to be 1.48×10^{-3} $M^{-1}s^{-1}$. Competing hydrolysis was also evident. The change from PF_6^- to a significantly larger and more hydrophobic counterion in 1,3-di-*iso*propyl-4,5,6-trihydropyrimidinium $(CF_3SO_2)_2N^-$ **(121)**, significantly reduced the solubility of the substrate to the extent that only an overall rate of disappearance of the C2-H could be measured, $k_{total} = 3.58 \times 10^{-3}$ $M^{-1}s^{-1}$. The rate of deuteroxide ion-catalyzed exchange was estimated to be similar to than for ion **(120)**.

2.5.5 Substituent effects on carbon acid pK_a values.

In Table 2.41 pK_a values are compiled for imidazolium ions **(109) – (115)**, dihydroimidazolium ions **(116) – (119)**, and trihydropyrimidinium ions **(120) – (122)** at 25 °C in D_2O and ionic strength I = 1 (KCl).

The pK_a values in Table 2.41 are arranged in increasing order for the above mentioned azolium ions. Values obtained for imidazolium ions **(109)** – **(115)**, are broadly ranging from 19.8 for 1,3-bis(*p*-chlorophenyl)imidazolium ion **(111)** to 25.2 for 1,3-di-*t*-butylimidazolium ion **(113)**. Values obtained for dihydroimidazolium ions **(116)** – **(119)** range from 20.8 for 1,3-bis(*p*-methoxyphenyl)4,5-dihydroimidazolium ion **(117)** to 22.9 for 1-methyl-3-mesityl-4-*iso*propyl-4,5-dihydroimidazolium ion **(119)**. Values for trihydropyrimidinium ions **(120)** – **(122)** and acyclic azolium ion **(123)** were significantly higher, ranging from 27.4 for 1,3-diethyl-4,5,6-trihydropyrimidinium ion **(122)** to 28.2 for 1,3-di-*iso*propyl-4,5,6-trihydropyrimidinium ion **(120)**. The acyclic formadine **(123)** is estimated to have a pK_a > 28.

Substituent effects that are observed on k_{DO} are mirrored in the corresponding pK_a values as the only variable in Equation 2.7 in the calculation of these pK_a values is k_{HO}. The logarithmic pK_a scale does however reduce the magnitude of these observed substituent effects. These new pK_a values are consistent with previous literature estimates, and the general consensus that aryl substituents decrease the pK_a while alkyl substituents increase the pK_a.

2.5.5.1 Alkyl substituent effects on the pK_a values of azolium ions

The pK_a values of 23.1 for 1-ethyl-3-methylimidazolium iodide **(114)** and 23.2 for 1-butyl-3-methylimidazolium bromide **(115)** are almost identical to that determined by Amyes et al[51] for 1,3-dimethylimidazolium iodide **(59)** (23.0) and 0.7 units lower than the reported value for the unsubstituted imidazolium ion **(173)** in water. A further increase in pK_a value to 25.2 is seen for 1,3-di-*t*-butylimidazolium chloride **(113)**. Thus as discussed earlier, an increase in steric bulk of the N-alkyl substituents appears to disfavour carbene formation, thus leading to a decrease in the acidity of the imidazolium ion conjugate acids.

Limited further comparisons can be made with a number of available literature pK_a values for imidazolium ions in non-aqueous solvents. pK_a values of 22.7 for 1,3-di-*t*-

butylimidazolium ion **(113)** and 24.0 for 1,3-di-*iso*propyl-4,5-dimethylimidazolium ion **(163)** have been determined by Alder *et al* in DMSO.[51, 57] The differences between these two values had been attributed to the appreciable ion-pairing effect present for a number of salts in DMSO which was not accounted for in the determination of the pK_a value of 24.0 for ion **(163).**

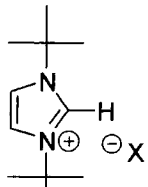

(113)

pK_a = 22.7 (DMSO)

pK_a = 20.0 (THF)

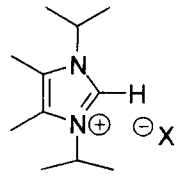

(163)

pK_a = 24.1 (DMSO)

A pK_a value of 20.0 has also been determined for ion **(113)** in THF solution. The value for imidazolium ion **(113)** in water determined in this work is consistent with these literature values for the imidazolium ions shown above in DMSO. The higher pK_a for a 1,3-di-*t*-butylimidazolium salt in water than in DMSO could be explained by the greater solvation of the charged azolium ion conjugate acid in the more polar hydroxylic medium.

Comparison can be made between these pK_a values in the range 23 – 25 determined for N,N-dialkylated imidazolium ions in aqueous solution and values determined for N-alkyl-substituted thiazolium ion **(64)** (Section 2.1.9) in the range 16.9 – 18.9. Also a value of 15.5 for dimethoxymethyl cation **(68)** (Section 2.1.9) has been determined in aqueous solution. Replacement of nitrogen by a less electronegative but more polarizable sulfur increases acidity, as does replacing both nitrogens by more electronegative oxygen.

Löwdin net atom charges (Q_{net}) have been determined by Aldrich *et al*[49] for azolium ions and corresponding ylides (Figure 2.71). As the transition state for the formation of an ylide from the corresponding azolium ion should resemble the product ylide, the

magnitude of the activation barrier to the reaction will be dependent on both the nature of the ylide and the nature of the reactant azolium ion. Substituents which destabilize the azolium ion or stabilize the ylide product will decrease the activation barrier and an increase in the rate of reaction will be observed.

Figure 2.71:

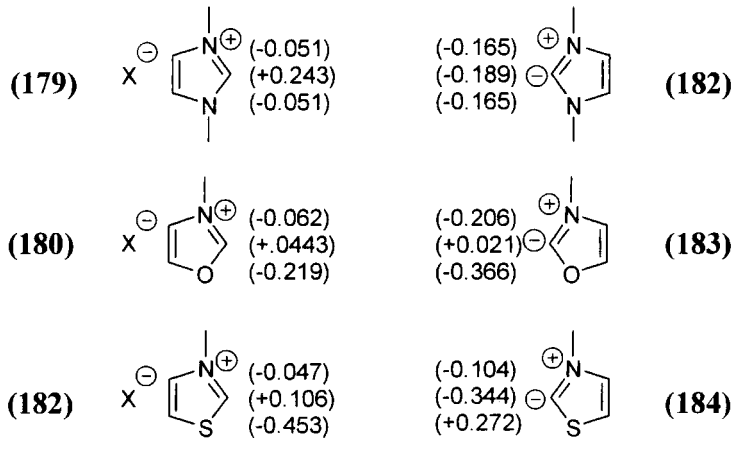

The charge at C2 of all the azolium ions in Figure 2.1 is positive. However the C2 of the thiazolium ion **(181)**, (+0.106) is less positive than that of imidazolium ion **(179)** (+0.243).

The negative charge at C2 of the thiazolium ylide **(184)** (-0.344) is more negative than that of imidazolium ylide **(182)** (-0.189) resulting from the positively charged S3 rather than a negatively charged N3. However in both cases there is an increase in negative charge of 0.43 – 0.45 units moving from the azolium ion to the ylide. This suggests that the sensitivity of both reactions to substituent charge on nitrogen should be the same, and similar Hammett ρ values should be obtained.

The slower rate of H/D-exchange obtained in this thesis for imidazolium ions over thiazolium ions is in agreement with the observations by Olofson[48] and Haake[47] that the C2-H of a thiazolium ion undergoes deuterium exchange faster than that of an imidazolium ion. The decreasing order of rate of abstraction of C2-H by deuteroxide ion under conditions of negligible buffer catalysis reported by Haake was oxazolium > thiazolium > imidazolium ions. Aldrichs' results did not agree with the difference

between oxazolium and thiazolium ions, however the increased positive charge at C2 of the oxazolium ylide (+0.021) was attributed to its favourable hydrogen bonding ability.

Studies of thermodynamic acidities in water by Amyes *et al*[51] have concluded that imidazole-2-ylidenes are in fact more stable than their thiazol-2-ylidene counterparts. However studies of other factors including differences in the degree of aromaticity, hydrogen bonding abilities of the ion and transition state, resonance contributors and solvation may further clarify the faster rate of H/D exchange and subsequently higher acidities of thiazolium ions.

2.5.5.2 Aryl substituent effects on the pK_a values of azolium ions

The increase in acidity seen on moving from imidazolium ions to benzimidazolium ions has been discussed in detail by Amyes *et al.*[51] Fusion of a benzene substituent to the C4,5 position of dimethylimidazolium ion **(59)** to give 1,3-dimethylbenzimidazolium iodide **(62)** and 1,3-bis((S)-α-methylbenzyl)benzylimidazolium chloride **(63)** and has the effect of decreasing the pK_a by 1.4 – 1.8 units. This is comparable to a difference of 1.58 pK units for the second ionization at nitrogen of imidazole (pK_a = 7.25) and benzylimidazole (pK_a 5.67).[51] This reflects the greater stabilization by hydrogen bonding between water and the quaternary nitrogen of the imidazolium cation relative to neutral imidazole.

N-Aryl substituents on the imidazole ring serve to significantly decrease the pK_a by 2.72 - 4.02 units. As discussed earlier, more electron withdrawing substituents such as *p*-chlorophenyl exert a greater stabilizing effect on the conjugate acid than less electron-withdrawing substituents such as 2,6-di-*iso*propylphenyl.

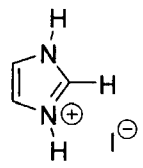

(173)

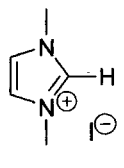

(59)

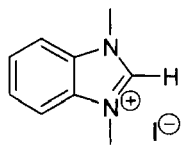

(62)

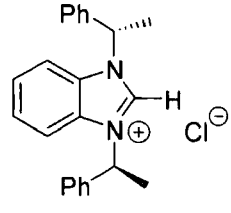

(63)

$pK_a = 23.8$ $pK_a = 23.0$ $pK_a = 21.6$ $pK_a = 21.2$

Saturation of the imidazole ring to give the N-aryl-substituted 4,5-dihydroimidazolium analogues had little effect on the pK_a. Values for N-aryl-substituted dihydroimidazolium ions **(116)** – **(119)** range from 20.8 for 1,3-bis(p-methoxyphenyl)-4,5-dihydroimidazolium chloride **(117)** to 21.5 for 1,3-bis(2,4,6-trimethylphenyl)-4,5-dihydroimidazolium chloride **(116)**. A pK_a value of 22.9 for 1-methyl-3-mesityl-4-*iso*propyl-4,5-dihydroimidazolium iodide **(119)** compared to ion **(116)** shows removal of one N-aryl-substituent has the effect of increasing the pK_a by 1.6 units. The average increase in pK_a from bis aryl- to bis alkyl-substitution of imidazolium ions is 3.4 pK units. It may be assumed that a similar increase would be seen between aryl and alkyl-substituted dihydroimidazolium ions. The difference of 1.6 pK units observed between 1,3-bis(2,4,6-trimethylphenyl)-4,5-dihydroimidazolium chloride **(116)** and 1-methyl-3-mesityl-4-*iso*propyl-5-hydroimidazolium chloride **(119)** is half of this estimated increase.

Intercomparison of the pK_a values of the imidazolium ions studied in this work shows that steric hindrance has a smaller effect on the pK_a of N-aryl-substituted imidazolium ions, than on alkyl-substituted imidazolium ions.

2.5.5.3 The effect of ring size on the pK_a of azolium ions.

As mentioned earlier in section 2.5.2.1, the effect of changing the size of the ring is evident from a comparison of the pK_a values observed for five membered dihydroimidazolium ions and six-membered for 4,5,6-trihydropyrimidinium ions. The pK_a values for dihydroimidazolium ions ranges from 20.8 – 22.9, while for trihydropyrimidinium ions this range is seen to dramatically increase by almost 5 pK units. Data for N-alkyl dihydroimidazolium ions could not be obtained due to synthetic difficulties, thus the more accurate comparison of dihydroimidazolium and trihydropyrimidinium ions with similar N-substituents cannot be made. However it may be hypothesised that since the average increase in pK_a from N-aryl-substituted imidazolium ions to N-alkyl-substituted imidazolium ions is 3.4 units, a similar difference in pK may be expected between N-aryl and N-alkyl-substituted

dihydroimidazolium ions. Thus an average pK_a value of 24.6 for alkyl-substituted dihydroimidazolium ions would be expected. A theoretical increase of over 3 pK units due solely to an increase in ring size can then be predicted.

Values for 1,3-diethyl-4,5,6-trihydropyrmidinium hexafluoro-phosphate **(122)** (pK_a = 27.8) and 1,3-di-*iso*propyl-4,5,6-trihydropyrmidinium hexafluoro-phosphate **(120)** (pK_a = 28.2) show that an increase in ring size strongly disfavours formation of the negative charge on C2 and greatly reduces the acidity of the azolium ion. This is also accompanied by competing hydrolysis reaction showing a marked decrease in ring stability. Similarly, this was the case in the alkyl substituted dihydroimidazolium ions which were initially studied in this work. Rapid decomposition via hydrolysis was observed in the attempted synthesis of 1,3-dimethyl-4,5-dihydroimidazolium tetrafluoroborate. It is likely that N-aryl substitution of the trihydropyrimidinium ions would significantly increase both the stability and acidity of trihydropyrimidinium ions, as steric hindrance would likely have a similarly significant stabilizing effect as with dihydroimidazolium ions. Further introducing aromaticity into the pyrimidinium ring would greatly increase the stability of the ring towards hydrolysis and also serve to decrease the pK_a values.

2.5.6 Comparison of kinetic and thermodynamic acidities of azolium ions with structural, thermodynamic and spectroscopic literature data.

As previously mentioned the magnitude of the second-order rate constant for hydroxide ion-catalyzed carbene formation, k_{HO} ($M^{-1}s^{-1}$), will be dependent on the stabilities of both the azolium ion precursor and the carbene or ylide. Up to this point the discussion has focused primarily on intercomparison of the new kinetic results for azolium ions studied in this work that are summarised in Table 2.41. In this section attempts will be made where possible to correlate changes in the kinetic data with X-ray crystal data and ^{13}C NMR data reported in the literature. In the case of 1,3-bis(*p*-methoxyphenyl)4,5-dihydroimidazolium chloride **(118)**, an X-ray crystal structure has been solved in this work. Values for bond lengths of the nitrogen atoms N1 and N3 to the carbene centre at

C2, bond angles of N1-C2-N3 and values for δ ^{13}C (ppm) of C2 are compared with the value of k_{HO} ($M^{-1}s^{-1}$), for the imidazolium ion counterpart of the carbene in Table 2.43.

2.5.6.1. Correlation of k_{HO} ($M^{-1}s^{-1}$) values with ^{13}C NMR chemical shifts.

^{13}C NMR spectral data for the unsaturated imidazole-2-ylidenes **(158), (159), (161)** and **(185) – (189)** shown in Table 2.43 reveal that the chemical shifts of the peaks due to C2 are in the 210 – 221 ppm range. The peak due to C2 for the saturated imidazolin-2-ylidene **(162)** was observed to be 15 – 35 ppm further downfield which is characteristic of saturated diaminocarbenes derivatives in general.[1] These values for the ^{13}C NMR chemical shifts of C2 can be compared with analogous chemical shifts of C2 of the imidazolium ion precursors. Values in similar solvents are expected to be in the range 135 – 180 ppm.

Table 2.2 shows an increasing order of the δ ^{13}C (ppm) values for C2 of the imidazole-2-ylidenes from **(158), (159), (161)** and **(185) – (189)**. By contrast the second order rate constant for hydroxide ion-catalyzed carbene formation increases across the same series. Generally, more downfield δ ^{13}C (ppm) values indicate less negative charge.

Table 2.43: Correlation of bond length, bond angle and chemical shifts at C2 for diaminocarbenes (158) – (162) and (185) – (188) with the second-order rate constant for hydroxide ion-catalyzed carbene formation k_{HO} ($M^{-1}s^{-1}$) for the corresponding imidazolium ions.

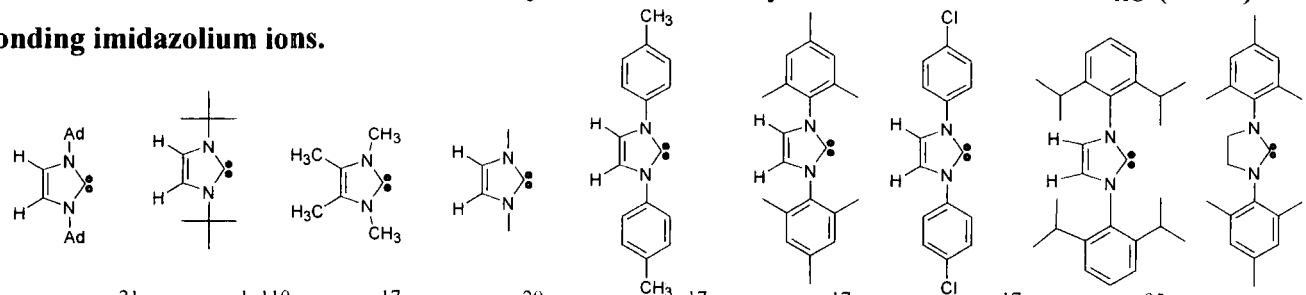

(158)[21] **(159)**[1, 110] **(185)**[17] **(186)**[20] **(187)**[17] **(161)**[17] **(188)**[17] **(189)**[95] **(162)**[17]

r(C2 - N1(3))[a] (pm)	136.7 137.3	136.8 135.7	136.3	-[h]	137.1 137.5	136.5 137.1	136.8 136.8	136.7 136.7	135.2 134.5
r(N1(3) – R)[b] (pm)	148.2 148.5	148.6 149.7	145.4	-[h]	143.0 143.0	144.1 144.2	143.0 143.0	-	142.7 143.7
θ(N1 – C2 – N3)[c] (°)	102.2	102.2	101.5	-[h]	101.2	101.4	101.7	101.4	104.7
θ(C2-N1(3)– R1(2))[d] (°)	123.4 122.1	121.7 123.8	122.9	-[h]	123.1 122.9	121.8 122.6	122.6 122.0	-	122.9 122.5
^{13}C NMR δ C2 (ppm)[e]	211.4[(i)]	213.2[(ii)]	213.7[(ii)]	215.2[(ii)]	215.8[(ii)]	219.7[(ii)]	216.3[(ii)]	220.6[(i)]	244.5[(ii)]
k_{HO} ($M^{-1}s^{-1}$)[f]	0.45	0.69	-[h]	103	-[h]	1.71×10^4	1.63×10^5	8.33×10^3	5.19×10^3
pK_a[g]	25.7[(v)]	25.2[(iii)]	-[h]	23.0[(iv)]	-[h]	20.8[(iii)]	19.8[(iii)]	21.1[(ii)]	21.3[(iii)]

(a) Bond lengths of N1 (above) and N3 (below) to the carbene centre at C2. (b) Bond length from N1 (above) and N3 (below) to the N-substituent. (c) Bond angle N1-C2-N3 at the carbene centre C2. (d) Bond angle C2-N1 (above) N3 (below) to the N-substituent. (e) ^{13}C NMR resonance values for C2 in (i) benzene $-d_6$ and (ii) THF-d_8. (f) Second-order rate constant for hydroxide-ion catalyzed carbene formation, k_{HO} ($M^{-1}s$). pK_a values determined in this work (iii), by Amyes *et al*[51] (iv), and by Sherwood[106] (v). (h) No current literature values available.

on the carbon. This may be due to inductive attenuation or stabilization of negative charge on carbon by the N-substituent, the extent of which is variable and dependant on the relative electron-withdrawing or donating inductive effects. The δ ^{13}C (ppm) values for the carbene centre for **(187), (162), (188)** and **(189)** suggests that they are more deshielded than those of **(158), (159), (185)** and **(186)**, although the values for 1,3-dimethylimidazol-2-ylidene **(186)**, and 1,3-bis(*p*-methylphenyl)imidazol-2-ylidene **(187)**, differ by only 0.6 ppm. This supports our kinetic observations that an N-aryl substituent is more electron-withdrawing than an N-alkyl substituent and leads to an increase in the rate constant for deprotonation at C2. One notable exception to this is the $\delta^{13}C$ (ppm) value for 1,3-bis(*p*-chlorophenyl)imidazol-2-ylidene **(188)**, which occurs 3.4 ppm further upfield than the value for 1,3-bis(2,4,6-trimethylphenyl)imidazol-2-ylidene **(161)**, but with a value for k_{HO} ($M^{-1}s^{-1}$) 9.5 times greater than for **(161).**

These data may also be compared to the structural data for a number of imidazolium salts. The $\delta^{13}C$ (ppm) values for the C2 of 1,3-bis(2,4,6-trimethylphenyl)imidazolium ion **(109)** (141.4), and 1,3-bis(2,4,6-trimethylphenyl)4,5-dihydroimidazolium ion **(116)** (159.9) are 78.3 – 84.2 ppm upfield compared to the corresponding ylide (Table 2.44). The $\delta^{13}C$ (ppm) values for the C2 of 1,3-bis(*p*-methoxyphenyl)imidazolium ion **(110)** 162.9, 1,3-bis(*p*-methoxyphenyl)4,5-dihydroimidazolium ion **(117)** (158.6), 1,3-bis(2,6-di-*iso*propylphenyl)imidazolium ion **(112)** (151.0), 1,3-bis(2,6-di-*iso*propylphenyl)4,5-dihydroimidazolium ion **(118)** (160.7) were determined in this work. The $\delta^{13}C$ (ppm) values for the corresponding ylides are not available in the literature. An increase in $\delta^{13}C$ (ppm) value for C2 of 18.5 ppm is seen upon saturation of the imidazole ring of 1,3-bis(2,4,6-trimethylphenyl)imidazolium ion **(109)**. A smaller increase of 9.7 ppm is seen on saturation of 1,3-bis(2,6-di-*iso*propylphenyl)imidazolium ion **(112)**. However a

decrease in the $\delta^{13}C$ (ppm) value for the C2 of 4.3 ppm is seen on saturation of 1,3-bis(*p*-methoxyphenyl)imidazolium ion **(110).** No correlation can be seen between the $\delta^{13}C$ (ppm) values of these azolium ions and the corresponding k_{HO} values.

2.5.6.2 Correlation of bond angles and lengths with k_{HO} ($M^{-1}s^{-1}$) values

As can be seen from Table 2.43, the angle at the carbene centre θ (N1-C2-N3) for imidazol-2-ylidenes ranges from 101.2° – 102.2°, while the saturated dihydroimidazolin-2-ylidene **(161)** has a bond angle of 104.7°, which is characteristic of the angles of saturated diaminocarbene derivatives in general.[1] Protonation of the carbene to give the corresponding acid increases the bond angle to between 108.7° – 109.7° for imidazolium ions **(Table 2.44)**. For dihydroimidazolium ion **(116)** the angle is similarly increased to 113.1°. This suggests that upon carbene formation the substituents crowd the carbene centre, creating more steric hindrance in the carbene/ylide compared to the corresponding acid form. Thus sterically large substituents will disfavour carbene formation mainly due to steric crowding in the carbene. This could explain the 600-fold variation in k_{HO} values for alkylimidazolium ions that cannot be accounted for solely on the basis of inductive effects.

Comparison of bond lengths in imidazol-2-ylidene **(161)** and imidazolin-2-ylidenes **(162)** shows that the absolute C2-N bond lengths are shorter in the saturated carbene than in the unsaturated. This may result in the larger N1-C2-N3 bond angle for the imidazolin-2-ylidene as a narrower angle would not be accommodated by the shorter bonds.

Average bond lengths for C2-N1(3) of the imidazol-2-ylidenes shown in Table 2.43 show little variation in the range 135.7 – 137.5 pm. The corresponding bond lengths for imidazolium ions show a decrease to 131.0 – 133.2 pm possibly due to greater π-character in the parent azolium ion. No correlation can be seen between these bond lengths and the second-order rate constant for hydroxide ion-catalyzed carbene formation.

Table 2.44: Structural data for imidazolium ions and 4,5-dihydroimidazolium ions and corresponding imidazol-2-ylidenes and imidazolin-2-ylidenes.

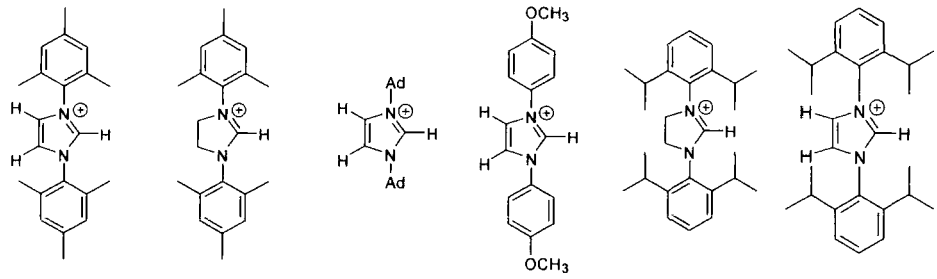

	(109)[17]	**(116)**[17]	**(190)**[21]	**(110)**	**(118)**	**(112)**[95]
r(C2 - N1(3))[a]	133.2 131.9	132.7 131.0	132.8	133.2 133.2	132.0 132.0	134.0 134.0
r(N1(3) – R1(2))[b]	144.5	-	148.2	144.5	144.5	-
θ(N1 – C2 – N3)[c]	108.7	113.1	109.7	108.6	112.4	107.6
θ(C2 – N1(3) – R1(2))[d]	125.8 127.1	127.0 126.2	-	125.7	124.5	-
^{13}C NMR δ C2 (ppm)[e]	141.4[(i)]	159.9[(i)] 160.2	-	162.9[(ii)]	160.7[(i)]	151.0
k_{HO} ($M^{-1}s^{-1}$)[f]	4.09×10^4	5.19×10^3	4.5×10^{-1}	2.00×10^4	3.49×10^3	8.33×10^3
pK_a[g]	20.8	21.3	25.7[106]	20.7	21.5	21.1

(a) Bond lengths of N1 (above) and N3 (below) to the carbene centre at C2. (b) Bond length from N1 (above) and N3 (below) to the N-substituent. (c) Bond angle N1-C2-N3 at the carbene centre C2. (d) Bond angle C2-N1 (above) N3 (below) –N-substituent. (e) ^{13}C NMR resonance values for C2 in (i) DMSO –d_6 and (ii) $CDCl_3$. (f) Second-order rate constant for hydroxide-ion catalyzed carbene formation, k_{HO} ($M^{-1}s^{-1}$), calculated from the value of k_{DO} as described in the text. (g) pK_a values determined in this work. ^{13}C NMR values determined in this work.

2.5.6.3 Planarity in the imidazol-2-ylidene and imidazolin-2-ylidene rings

As expected the aromatic imidazol-2-ylidene ring is planar, however the saturated dihydroimidazolium ring is non-planar (Figure 2.72). The crystal structure of imidazolin-2-ylidene **(162)** shows that C4 lies 90 pm above the plane, while C5 lies 148 pm below the plane. This may facilitate the larger N1-C2-N3 bond angle in the imidazolin-2-ylidene relative to the aromatic analogue. The mesityl substituents are also out of plane with the imidazoline ring, with the N1-mesityl substituent 89 pm below and the N3-mesityl substituent 82 pm above the plane.[95]

For bulky aryl-substituents such as the mesityl groups of imidazol-2-ylidene **(161)** an in-plane configuration with the imidazole ring is not possible. The substituents are twisted 80° and 71° respectively in a conrotatory direction relative to the imidazole ring creating a pseudo 2-fold axis. The *o*-methyl groups significantly hinder the imidazole ring from above and below.[17] The 2,6-di-*iso*propyl groups of imidazole-2-ylidene **(189)** exhibit very similar twisting of 78° and 65° respectively. Similar twisting also occurs with the *p*-tolyl substituents of **(177)** but to a lesser extent making the substituents nearly co-planar with the imidazolium ring, but still making conjugation unlikely. These rings are twisted 31° and 34° respectively in a similarly conrotatory fashion. A difference is seen with the *p*-chlorophenyl substituents of **(178)** which have inclinations with respect to the imidazole ring of 28° and 39°, similar to **(177)** however these are in a disrotatory direction, producing a pseudo mirror plane which is normal to the imidazole ring. This subtle difference in structure may account for the more upfield chemical shift of C2 in the ^{13}C NMR spectrum for imidazole-2-ylidene **(178)** as there seems a complex interplay between steric effects and electronic effects in the stability of these carbenes.

Figure 2.72:

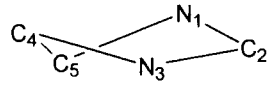

One surety however is that the consistent and significant degree of non-planarity between the central imidazole ring and the aryl-substituents in the structures that π-donation from the aryl substituents is extremely unlikely. The relatively small 20-fold variation in k_{HO} values for imidazolium and 4,5-dihydroimidazolium ions, with electronically very

different aryl substituents is consistent with the absence of any resonance substituent effects.

Similar twisting is seen in the crystal structure of 1,3-bis(2,6-di-*iso*propylphenyl)4,5-dihydroimidazolium ion **(118)** in which the N-substituents are twisted 73° and 80° respectively in a conrotatory fashion. Unusually, the crystal structure of 1,3-bis(*p*-methoxyphenyl)imidazolium ion **(110)** shows the N-substituents to be almost co-planar with minimal twisting of 4° and 0.5 ° respectively. This suggests that resonance delocalization may be possible, however this is not reflected in the low k_{HO} value observed for this ion.

2.5.6.4 Gas phase proton affinities and aqueous thermodynamic pK_a values

Proton affinities (PA) for a series of cyclic and acyclic diaminocarbenes in the gas phase have been determined experimentally (Table 2.45).[3] The PA values for the unsaturated imidazol-2-ylidene **(190)**, and the 1,3-di-*iso*propyl-4,5-dimethylimidazol-2-ylidene **(192)** are similar although the calculation methods are different. This agrees with the estimates of similar k_{HO} and pK_a values of the conjugate acids of **(161)** and **(190)**. However, the saturated imidazolin-2-ylidene **(161)** and acyclic diaminocarbene **(193)** have similar PA values despite quite different aqueous pK_a values. The values for all cases lie within the same range as that of phenylcarbene (Ph-HC:, PA = 258 kcal mol^{-1}), one of the most basic carbenes. Computational results have revealed that the amino groups of imidazole-2-ylidenes and imidazolin-2-ylidenes such as those in Table 2.45 enhance the PA more strongly than hydroxyl groups ((OH)$_2$C: = 217 kcal mol^{-1}).[3]

The PA determinations for the ylide forms of N-heterocyclic carbenes have not been determined experimentally and are only available from *ab initio* calculations.[111] The PA values for the oxazolium **(183)**, thiazolium **(184)** and imidazolium **(182)** ylides are shown in Table 2.46. These are consistent with kinetic acidities determined by Haake *et al.*[47] As described in Section 2.5.5.1, the Löwdin net atomic charge for C2 of the thiazolium ylide is 1.8-fold more negative than the corresponding charge on the imidazolium ylide. Stabilization by hydrogen bonding is thought to be most favourable when the negative

charge is largely localized at carbon. Thus as the thiazolium ion exhibits considerably more charge development it is expected that their proton affinity should be higher than that of imidazolium ions. However this is not the case as stabilization of the negative charge is thought to be accounted for by the high polarizability of the sulfur atom.

Table 2.45: Gas phase acidities of azolium ions

Entry		Method	PA (kcal mol^{-1})
(161)	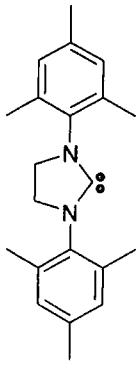	AM1	252
(191)	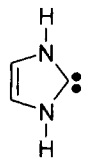	MP2/DZ	257
(192)	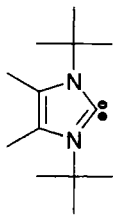	AM1	255
(193)	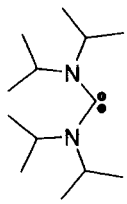	AM1	254

This was illustrated by Washabough and Jencks[53] who showed that hydrogen bonding between water and the C2 ylide of thiazolium ions is in fact quite weak.

Proton affinities for imidazolium ylides **(182)** in Table 2.46 are considerably higher than those for thiazolium **(184)** and oxazolium **(183)** ylides. Hence imidazolium ylides exhibit greater transition state stabilization by hydrogen bonding than the corresponding thiazolium and oxazolium counterparts. The increase in proton affinity in the gas phase from the oxazolyl to thiazolyl to imidazolyl ylides parallels a decrease in the rate constant for their formation in aqueous solution from azolium conjugate acids.

Table 2.46: Proton affinities for oxazolium, thiazolium and imidazolium ylides

Entry		PA (kcal mol^{-1})
(183)	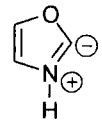	247.2
(184)	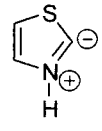	254.7
(182)	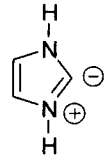	262.1

The order of decreasing basicity of the ylides according to their PA values shown in Table 2.5 is imidazolium ylide **(182)** > thiazolium ylide **(184)** > oxazolium ylide **(183)**. Since the relative order of acidity of these azolium ions in solution corresponds to the relative order of their proton affinities in the gas phase, it is suggested that intrinsic relative acidities of azolium ions are not affected by solvent.

2.5.7 N-Heterocyclic carbene "Ligands" in synthesis

As described in Section 2.1.11.3, in olefin metathesis reactions, the use of N-heterocyclic carbene ligands in ruthenium catalysts dramatically increases the activity and efficiency of the catalyst.[62]In bis-phosphine catalysts such as **(78)** the rate of dissociation (k_1) is

large and so the requisite active fourteen-electron species is formed frequently (see Section 2.1.11.3). However due to the competitiveness of recombination of the phosphine with substrate binding, this active species achieves few catalytic turnovers before it is quenched. In NHC-containing catalysts, such as **(79),** selectivity for binding of the olefin over phosphine is increased by four orders of magnitude. This was explained by the difference in electronic properties of these two ligands. The NHC-ligands are far superior donor ligand relative to the phosphine ligands, and show greater affinities for π-acidic olefinic substrates relative to σ-donating phosphine ligands. Cavell *et al* [62, 112] reported that these ligands promote and stabilise metal-to-olefin back bonding to a far greater extent than phosphine ligands in such systems.

X-ray crystallographic studies have shown that the decrease in initiation rates observed on the introduction of an NHC-ligand are not ground state effects, as the Ru-PCy_3 distance changes little when the trans ligand is changed from PCy_3 to 1,3-bis(2,4,6-trimethylphenyl)imidazol-2-ylidene (Ru-PCy_3 in **(78)**: 240.9 and 242.2 pm; Ru-PCy_3 in **(79)**: 241.9 pm). Therefore the large difference in k_1 between these catalysts may result from different reorganizational energies associated with the transition state for phosphine dissociation.

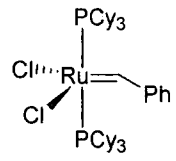

(78)

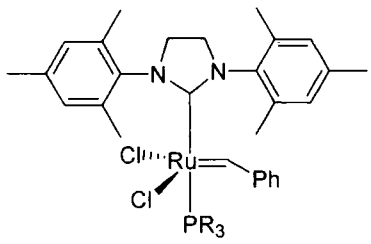

(79)

The distribution of steric bulk around the Ru-centre could also be an important factor affecting the initiation rates of the catalyst. Both PR_3 and the NHC-ligands are large, however the steric effects are very different for each case. This may lead to either destabilizing interactions in bis-phosphine complexes or stabilizing interactions in NHC-containing complexes leading to changes in the activation energy for phosphine loss.

With ligands such as phosphines the potential donor abilities of the ligand have often been predicted from the pK_a value of its conjugate acid. Thus a more basic ligand with higher conjugate acid pK_a value is usually a better donor. Whether this is the case with N-heterocyclic carbenes as ligands is not clear. However, intercomparison of the limited number of NHC ligands studied mechanistic detail by Grubbs *et al*[62] indicated that this may be possible. Comparison of 1,3-bis(2,4,6-trimethylphenyl)imidazol-2-ylidene **(161)** (pK_a = 21.3), and 1,3-bis(2,4,6-trimethylphenyl)-imidazolin-2-ylidene **(165)** (pK_a =20.8), as ligands showed that the saturated imidazolin-2-ylidene ligand **(162)** was a better donor than its unsaturated analogue **(161)** and was more active for polymerization of cyclooctadiene. Although both ligands are highly effective relative to phosphine, replacement of the saturated 1,3-bis(2,4,6-trimethylphenyl)-imidazolin-2-ylidene ligand with the unsaturated analogue suppressed the rate of dissociation of phosphine (k_1) by close to an order of magnitude. Numerous attempts were made by Grubbs *et al* to synthesise effective catalysts with alternative alkyl-substituted or aryl-substituted N-heterocyclic carbene ligands such as **(196).** However, without *ortho*-substituents the complexes either would not substitute for the phosphine, would decompose rapidly or gave double substitution. Only the mesityl substituted ligand gave a stable system with the correct substitution.

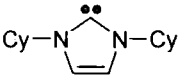

(193)

More work is needed to determine whether nucleophilicity is a reflection of basicity for these ligands, or whether steric effects are a major contributing factor in their success as ligands. The pK_a values determined in this work may be beneficial to this end.

More recently, studies by Grubbs *et al*[113] focused on modification of the amino substituent have resulted in the development of more specialized Ru-catalysts such as **(194)**, a highly active chiral ruthenium catalyst for use in asymmetric ring-closing olefin metathesis (ARCM). This catalyst produced up to 90% ees in ARCM, and AROCM

reactions of alkenyl ethers and alkyl silyl ethers, and **(195)** a water soluble catalyst, effective for aqueous environments.

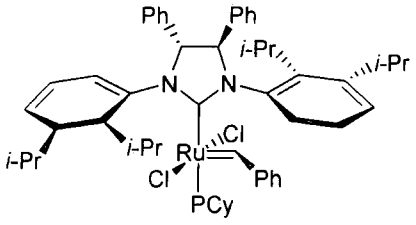

(194)

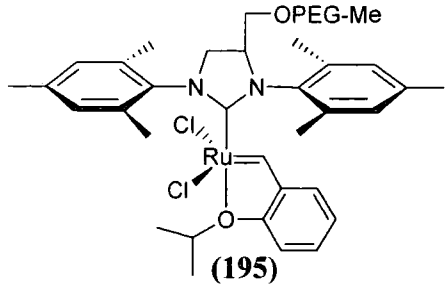

(195)

It remains to be determined what the main contributions are from these NHC-ligands to the Ru-catalysts. Whether donor ability can be predicted accurately from the pK_a of their conjugate acids of these carbenes and to what extent steric effects influence the reactivity of the catalysts is unknown.

References:

(1) Bourissou, D., Guerret, O., Gabbai, F. P., Bertrand, G., *Chem. Rev* **2000**, *100*, 39.
(2) Buchner, E., Curtius, T., *Ber. Dtsch. Chem. Ges.* **1885**, *8*, 2377.
(3) Krimse, W. *Carbene Chemistry*, 2nd ed.; Academic Press, Inc.: New York, 1971.
(4) Schuster, G. B. *Adv. Phys. Org. Chem.* **1986**, *22*, 311.
(5) Clayden, J., Greeves, N., Wrren, S., Wothers, p., *Orgnaic Chemisry.*; Oxford University Press: New York, 2001.
(6) Enders, D., Balensiefer, T., *Acc. Chem. Res* **2004**, *37*, 534.
(7) Koda, S. *Chem. Phys. Lett.* **1978**, *55*, 353.
(8) Jenson, P., Binker, P. R., *J. Chem. Phys.* **1988**, *89*, 1327.
(9) Hoffmann, R. *J. Am. Chem. Soc.* **1968**, *90*, 1475.
(10) Herrmann, W. A., Köcher, C., *Angew. Chem.,Int. Ed. Engl.* **1997**, *36*, 2162.
(11) Irikura, K. K., Goddard, W. A. III., *J. Am. Chem. Soc.* **1992**, *114*, 48.
(12) Du, X. M., Fan, H., Goodman, J. L.,Kesselmayer, M. A., Krogh-Jesprsen, K., LaVila, J. A., Moss, R., Shen, S., Sheridan, R. S., *J. Am. Chem. Soc.* **1990**, *112*, 1920.
(13) Wang, j. L., Toscano, J., Platz, M. S., Nikolaev, V., Popik, V., *J. Am. Chem. Soc.* **1995**, *117*, 5477.
(14) Moss, R. A., Mallon, C. B., Ho, C. T., *J. Am. Chem. Soc.* **1977**, *99*, 4105.
(15) Gilbert, B. C., Griller, D., Nazran, A. S., *J. Org. Chem.* **1985**, *50*, 4738.
(16) Arduengo, A. J., III, Georlich, J. R., Marshall, W. J., *J. Am. Chem. Soc.* **1997**, *119*, 12742.
(17) Arduengo, A. J., III, Dias, H. V. R., Harlow, R. L., Kline, M., *J. Am. Chem. Soc.* **1992**, *114*, 5530.
(18) Herrmann, W. A., Elison, M., Fischer, J., Köcher, C., Artus, G. R. J., *Angew. Chem.,Int. Ed. Engl.* **1995**, *34*, 2371.
(19) Herrmann, W. A., Weskamp, T., Böhm, V. P. W., *Adv. Organomet. Chem.* **2001**, *48*, 1.
(20) Dixon, D. A., Arduengo,A. J., *J. Phys Chem.* **1991**, *95*, 4180.
(21) Arduengo, A. J., III, Harlow, R. L., Kline, M., *J. Am. Chem. Soc.* **1991**, *113*, 361.
(22) Cioslowski, J. *Int. J. Quantum Chem., Quantum Chem. Symp.* **1993**, *27*, 309.
(23) Heinemann, C., Müller, T., Apeloig, Y., Schwatrz, H., *J. Am. Chem. Soc.* **1996**, *118*, 2023.
(24) Boehme, C., Frenking, G., *J. Am. Chem. Soc.* **1996**, *118*, 2039.
(25) Arduengo, A. J., III, Goerlich, J. R., Marshall, W. J., *J. Am. Chem. Soc.* **1995**, *117*, 11027.
(26) Alder, R. W., Allen, P. R., Murray, M.,Orpen, A., Boehme, C. A., *Angew. Chem., Int. Ed. Engl.* **1996**, *35*, 1121.
(27) Lehmann, J. F., Urquhart, S. G., Ennis, L. E., Hitchcock, A. P., *Organometallics* **1999**, *18*, 1862.
(28) Hermann, W. A., Weskamp, T., Böhm, V. P. W., *Adv. Organomet. Chem.* **2001**, *48*, 1.
(29) Deoring, W. V. E., Hoffmann, A. K., *J. Am. Chem. Soc.* **1954**, *75*, 6162.
(30) Skell, P. S., Sandler, S. R., *J. Am. Chem. Soc.* **1958**, *80*, 2024.
(31) Breslow, R. *J. Am. Chem. Soc.* **1958**, *80*, 3719.

(32) Wanzlick, H. W. *Angew. Chem., Int. Ed. Engl.* **1962**, *1*, 75.
(33) Fischer, E. O., Maasböl, A., *Angew. Chem.* **1964**, *6*.
(34) Őfele, K. *J. Angew. Chem.* **1968**, *80*, 1032.
(35) Wanzlick, H. W., Schonherr, H., *Angew. Chem., Int. Ed. Engl.* **1968**, *7*, 141.
(36) Denk, M. K., Hatano, J., Ma, M., *Tetrahedron Lett.* **1999**, *40*, 2057.
(37) Wanzlick, H. W., Schonherr, H., *Chem. Ber.* **1970**, *103*, 1037.
(38) Hermann, W. A., Köcher, C., *Angew. Chem.,Int. Ed. Engl.* **1997**, *36*, 2162.
(39) Igua, A., Grutmacher, H., Baceiredo, A., Bertrand, G., *J. Am. Chem. Soc.* **1988**, *110*, 6463.
(40) Kuhn, N., Kratz, T., *Synthesis* **1993**, 561.
(41) Tomioka, H., Watanabe, T., Hirai, K., Takui, T., Itoh, K., *J. Am. Chem. Soc.* **1995**, *117*, 6376.
(42) Tomioka, H., Iwamoto, E., Itakura, H. Hirai, K., *J. Am. Chem. Soc.* **2001**, *412*, 626.
(43) Hermann, W. A. *Angew. Chem. Int. Ed.* **2002**, *41*.
(44) Krimse, W. *Advances in Carbene Chemistry.* **2001**, *3*, 1.
(45) Nolan, S. P., Jaapour, L., *Adv. Organomet. Chem.* **2000**, *46*, 181.
(46) Lee, M. T., Hu, C. H., *Organometallics* **2004**, *23*, 976 - 983.
(47) Haake, P., Bauscher, L. P., Miller, W. B., *J. Am. Chem. Soc.* **1969**, *91*, 1113.
(48) Olofson, R. A., Thompson, W. R., Michelman, J. S., *J. Am. Chem. Soc.* **1964**, *86*, 1865.
(49) Aldrich, H. S., Alworth, W. L., Clement, N. R., *J. Am. Chem. Soc.* **1978**, *100*, 2362.
(50) Scheffers-Sap, M. M. E., Buck, H. M., *J. Am. Chem. Soc.* **1979**, *101*, 4807.
(51) Amyes, T., L. Diver, S. T., Richard J. P., Rivas, F. M., Toth, K. *J. Am. Chem. Soc.* **2004**, *126*, 4366.
(52) Washabaugh, M. W., Jencks, W. P., *Biochemistry* **1988**, *27*, 5044.
(53) Washabaugh, M. W., Jencks, W. P., *J. Am. Chem. Soc.* **1989**, *111*, 674.
(54) Schroeder, M. A., Makino, R. C., *Tetrahedron* **1973**, *29*, 3469.
(55) Amyes, T., L. Diver, S. T., Richard J. P., Rivas, F. M., Toth, K. *J. Am. Chem. Soc.* **2003**, *126*, 4366.
(56) Wong, J. L., Keck, J. H. Jr., *J. Org. Chem.* **1974**, *39*, 2398.
(57) Alder, R. W., Allen, P. R., Williams, S. J., *J. Chem. Soc., Chem. Commun.* **1995**, 1267.
(58) Kim, Y. J., Streitwieser, A., *J. Am. Chem. Soc.* **2002**, *124*, 5757.
(59) Guthrie, J. P., More O'Ferrall, R. A., O'Donoghue, A. C., Waghorne, E. W., Zrinski, I., *J. Phys. Org. Chem.* **2003**, *16*, 582.
(60) Dixon, D. A., Arduengo,A. J., *J. Phys Chem. A.* **2006**, *110*, 1968.
(61) Love, J. A., Sanford, M. S., Day, M. W., Grubbs, R. H., *J. Am. Chem. Soc.* **2001**, *125*, 10103.
(62) Sanford, M. S., Love, J. A., Grubbs, R. H., *J. Am. Chem. Soc.* **2001**, *123*, 6543.
(63) Voges, M. H., Romming, C., Tilset, M., *Organometallics* **1999**, *18*, 529.
(64) Abernathy, C. D., Clyburne, R., Bruneau, p. H., Dixeuf, P. H., *J. Am. Chem. Soc.* **1999**, *121*, 2329.
(65) Boehme, C., Frenking, G., *J. Am. Chem. Soc.* **1996**, *118*, 2039.

(66) Tulloch, A. D. D., Danopoulos, A. A., Kleinhenz, S., Light, M. E., Hursthouse, M. B., Eastham, G., *Organometallics* **2001**, *20*, 2027.
(67) Hu, X. L., Tank, Y. J., Gantzel, P., Meyer, K., *Organometallics* **2003**, *22*, 612.
(68) Hu, X. L., Castro-Rodriguez, I., Olsen, K., Meyer, K., *Organometallics* **2004**, *23*, 755.
(69) Çetinkaya, B., Özdemir, R., Bruneau, P. H., Dixneuf, P. H., *J. Mol. Catal. A.* **1997**, *118*, L1.
(70) Köcher, C., Herrmann, W. A., *J. Organomet. Chem.* **1998**, *532*, 261.
(71) Herrmann, W. A., Goossen, L. J., Spiegler, M., *Organometallics* **1998**, *17*, 2162.
(72) Eckhardt, M., Fu, G. C., *J. Am. Chem. Soc.* **2003**, *125*, 13642.
(73) Love, J. A., Sanford, M. S., Day, M. W., Grubbs, R. H., *J. Am. Chem. Soc.* **2003**, *125*, 10103.
(74) Hong, S. H., Grubbs, R. H., *J. Am. Chem. Soc.* **2006**, *128*, 3508.
(75) Ledoux, N., Allaert, B., Linden, A., Van er Voort, P., Verpoort, F., *Organometallics* **2007**, *26*, 1052.
(76) Enders, D., Gielen, H., Breuer, K., *Mol. Online* **1998**, *2*, 105.
(77) Enders, D., Gielen, H., Raabe, G. R. J., Teles, J. H., *Chem. Ber.* **1996**, *129*, 1483.
(78) Chen, D., Banphavichit, V., Reibenspies, J., Burgess, K., *Organometallics* **2007**, *26*, 855.
(79) Suzuki, Y.; Muramatsu, K.; Yamauchi, K.; Morie, Y.; Sato, M. *Tetrahedron* **2006**, *62*, 305-310.
(80) Blunt, J. W., Cop, B. R., Munro, M. H. G., Northcote, P. T., Prinsep, M. R., *Nat. Prod. Rep.* **2003**, *20*, 1.
(81) Voet, D., Voet, J. G., Pratt, C. W. *Fundamentals of Biochemistry.*; John Wiley & Sins Inc.: New York, 1999.
(82) Mizuhara, S., Handler, P., *J. Am. Chem. Soc.* **1954**, *76*, 571.
(83) Breslow, R. *Ann. N. Y. Acad. Sci.* **1962**, *98*, 445.
(84) Melaiye, A., Simons, R. S., Milsted, A., Pingitore, F., Wasdemiotis, C., Tessier, C. A., Youngs, W. J., *J. Med. Chem.* **2004**, *47*, 973.
(85) Lange, H. M., Stuivenberg, H. H. V., Coolen, H. K. A. C. Adolfs, T. J. P., McCreary, A. C., Kieszer, H. G., als, H. C., Veerman, W.,Borst, A. J. M., de Looff, W., Verveer, P. C., Kruse, C. G., *J. Am. Chem. Soc.* **2005**, *48*, 1823.
(86) Denk, M. K. K., M. J.; Niyogi, D. F.; Gill, N. K.; *Tetrahedron* **2003**, *59*, 7565-7570.
(87) Richard, J. P.; Amyes, T. L.; Toteva, M. M. *Accounts of Chemical Research* **2001**, *34*, 981-988.
(88) Richard, J. P. W., G.; O'Donoghue, A. C.; Amyes, T. L. *J. Am. Chem. Soc.* **2002**, *124*, 2957-2968.
(89) Kresge, A. J., More O'Ferrall, R. A., Powell, M. F. *Isot. Org. Chem.* **1987**, 7-177.
(90) Harwood, L. M., Moody, C. J., Percy, J. M., *Experimental Organic Chemistry*; Blackwell Scientific Ltd., 1999.
(91) Häring, M. *Helv. Chim. Acta.* **1959**, *42*, 1845.
(92) Kashima, C., Harada, Y., Hosomi, A., *Heterocycles* **1993**, *35*, 433.
(93) Dullius, J. E. L., Suarez, P. A. Z., Einloft, S., de Souza, R. F., Dupont, J., Fischer, J., De Cian, A., *Organometallics* **1998**, *17*, 815.

(94) Diez-Barra, E., de la Hoz, A., Sánchez-Migallón, A., Tejeda, J., *Synth. Commun.* **1993**, *23*, 1783.
(95) Arduengo, A. J., III, Krafczyk, R., Schmutzler, R., *Tetrahedron* **1999**, *55*, 14523.
(96) Denk, M. K., Rodenzo, J. M., Gupta, S., Lough, A. J., *J. Organomet. Chem.* **2001**, *617-618*, 242.
(97) Alder, R. W., Blake, M. E., Chaker, L., Hervey, J. N., Paolini, F., Schütz, J., *Angew. Chem. Int. Ed.* **2004**, *43*, 5896.
(98) Denk, M. K., Thadani, A., Hatano, J., Lough, A. J., *Angew. Chem.* **1997**, *109*, 2719.
(99) Hoffmann, R. G., F., Mallory, F. B., *J. Am. Chem. Soc.* **1970**, *92*, 1460.
(100) Aggarwal, V. K., Emme, I., Mereu, A., *Chem. Commun.* **2002**, 1612.
(101) Giese, K., Kaatze, U., Pottel, R., *J. Phys. Chem.* **1970**, *74*, 3718.
(102) Richard, J. P., Williams, G., Cao, J., *J. Am. Chem. Soc.* **1999**, *121*, 715.
(103) Kaatze, U. *J. Chem. Eng. Data* **1989**, *34*, 371.
(104) Kaatze, U., Pottel, R., Schumacher, A., *J. Phys. Chem.* **1992**, *96*, 6017.
(105) Peon, J., Polshakov, D., Kohler, B., *J. Am. Chem. Soc.* **2002**, *124*, 6428.
(106) Sherwood, J. A., University College Dublin, Dublin, 2004.
(107) Hansch, C., Leo, A., Taft, R. W., *Chem. Rev.* **1991**, *91*, 165.
(108) Roberts, J. D., Moreland, W. T. Jr., *J. Am. Chem. Soc.* **1953**, *75*, 2167.
(109) Grob, C. A., Schlageter, M. G., *Helv. Chim. Acta.* **1976**, *59*, 264.
(110) Arduengo, A. J. I., Bock, H., Chen, C., Denk, M., Dixon, D. A., Green, J. C., Herrmann, W. A., Jones, N. L., Wagner, M., West, R., *J. Am. Chem. Soc.* **1994**, *116*, 6641.
(111) Sauers, R. R. *Tetrahedron Lett.* **1996**, *37*, 149.
(112) McGuinness, D. S., Cavell, K. J., Skeleton, B. W., White, A. H., *Organometallics* **1999**, *18*, 1596.
(113) Funk, T., Berlin, J. M., Grubbs, R. H., *J. Am. Chem. Soc.* **2006**, *128*, 1840.

Chapter 3

Diketopiperazines

3.0 Introduction

3.1 Foreword

Amino acids are the basic building blocks of proteins and peptides. The simplicity and universality of these species has lead to a diverse and important area of research. To date, Richard *et al*[1-4] have accurately estimated the acidities of several amino acids in water under physiological conditions. However there remains a substantial amount of amino acids and amino acid derivatives such as diketopiperazines that have not been studied. The characterization of the chemical reactivity of this important class of biological compound depends on this data, along with the explanation for the origin of rate acceleration for enzyme-catalysed racemization of amino acids. Since deprotonation of the amino acid is commonly the first step in many racemization reactions it is the focus of our interest. Our approach involves examining how the rate constants for this reaction might depend on the protonation state of the enzyme bound amino acid, and if an alteration of this is what produces enzyme-catalysed rate acceleration.

In a more general sense, understanding the effects of α-substitution on the rate and equilibrium constants for the ionization of weak carbon acids in aqueous solution is of interest for similar reasons as stated above. These simple carbon acids play a large role in many processes, biological and otherwise, and to understand their chemical reactivities is to open the door to deciphering the processes in which they are involved.

This chapter deals with diketopiperazines, cyclic dipeptides which are common in many biological systems, and increasingly appear as molecules of interest in medicinal chemistry.

3.1.1 Amino acids

Amino acids consist of an amino group, a carboxyl group, a carbon α to the carboxyl group equipped with an acidic hydrogen and variable *R*-group, the simplest being glycine where the *R*-group is simply another hydrogen.

Of the three sites on the amino acid which contain acidic protons the carboxy site is the most acidic with an average pK_a value of five. The conjugate acid of the amino group generally has a pK_a of nine or ten and the acidic proton on the α-carbon has been shown to have an average pK_a value of twenty five.[1] This proton is attached to the chiral centre of the amino acid and so controls the stereochemistry of the molecule. The only weakly acidic proton bestows a high degree of stereochemical integrity to the amino acid and so racemization is usually very slow in aqueous solution under physiological conditions. Half lives can be in the order of thousands of years as is the case for epimerizaton of isoleucine in bones which is greater than 100,000 years.[5] Aspartyl residues in several mammalian tissues including dentine, ocular lens nuclei and myelin have been shown to undergo racemization at 0.1% per year.[6] However the acidity of the α-proton of an amino acid is dependent on the ionization state of the amino acid.[1]

3.1.1.1 Relative rates of racemization.

There has been some research on the racemization of amino acids in aqueous solution mostly in the form of non-systematic studies. As was the case with other weak carbon acids these reactions were thought too slow to be studied in any reasonable way. Studies have been carried out under harsh conditions at temperatures of 110° - 180° C and often in up to six molar acid.[7-12] These data are not applicable to biological systems. However racemization of amino acids does regularly occur during peptide synthesis under what would be considered mild conditions.[13] More recently Richard *et al*[1, 14, 15] determined a number of racemization rates of amino acids and amino acid derivatives along with other simple carbon acids, under controlled and considerably milder conditions than previously used.

Despite the relatively slow rates of racemization of amino acid residues in proteins and during peptide synthesis, studies have shown this process to be faster in peptides than the amino acid monomers, and relative rates of racemization of different amino acid residues in protein have been reported with a general ratio of 5:7 for monomer racemization compared to peptide residue racemization.[7, 8] This is mainly due to the mechanism by which amino acids are believed to racemize, which is *via* a high-energy enolate intermediate as described in Chapter 1.

Racemization is essential for a number of key functions in biological systems as a means to obtain the D-configuration amino acids which cannot be obtained from dietary sources and so must occur at sufficiently high rates under biological conditions to satisfy this need. This is accomplished in Nature by way of enzyme-catalysed racemization using enzymes such as amino acid racemases. These catalyse the conversion of enantiomerically pure L-configuration amino acids to a 50:50 mixture of the L- and D configuration. These racemases come in two groups, those that use the coenzyme pyridoxal phosphate such as alanine racemase (PLP-dependent amino acid racemases), and those that do not, such as glutmate racemase (PLP-independent amino acid racemases). General mechanisms by which these two classes of racemases function have been elucidated by site directed mutagenesis and kinetic studies. Although the finer detail varies from enzyme to enzyme, the basic mechanism is similar.[16]

3.1.1.2 Racemization of amino acids

Amino acids undergo racemization in solution by way of a high-energy enolate intermediate (see Scheme 3.1). The amino acid **(196)** is deprotonated by a base **(B)** at the α-carbon, forming a high-energy planar enolate intermediate **(197)**, which may be reprotonated to produce a racemic mixture of L and D configuration amino acid. As discussed previously in Chapter 1, the rate-determining step in this reaction is enolate formation followed by rapid reprotonation by the conjugate acid of the base (BH^+). It is possible to follow enolization reactions of amino acid by monitoring the optical rotation of the reaction mixture. As the solution containing pure L or D-amino acid becomes

racemic the specific optical rotation value $[\alpha]_D$ approaches 0°. Therefore no trapping agents are required to monitor the rate of reaction as with other enolization reactions. Often however an isotope exchange method is employed to monitor the rate of enolization in amino acids such as the H/D exchange method described in Chapter 1 and used in this work.

Scheme 3.1:

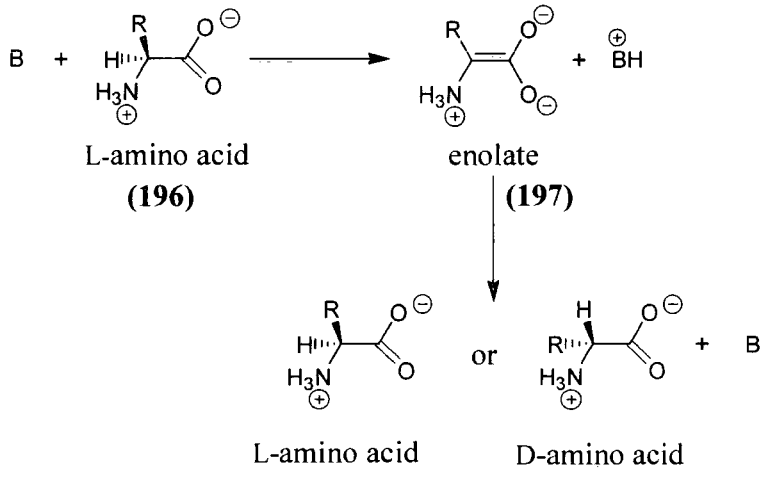

3.1.1.3 Ionization states of amino acids.

The acidity of the α-proton of the amino acids depends greatly on the ionization state of the species, and amino acids can theoretically have three ionization states (see Scheme 3.2).Taking the most simple example, deprotonation of the glycine anion **(198)**, to give the enolate dianion ($(K_a)_{anion}$) is much less favourable than deprotonation of the essentially neutral zwitterion **(199)** ($(K_a)_{neutral}$) which has been shown to have a pK_a of 28.9 ± 0.5.[1] The most favourable deprotonation should be that of the cationic form **(200)** ($(K_a)_{cation}$) with its overall positive charge. There is difficulty in measuring the latter rate directly as a decrease in pH, which is required to produce the cationic ionization state, **(200)** means a corresponding decrease in concentration of hydroxide ion which catalyses the reaction. However these relative rates have been determined using glycine derivatives where the charge at the substrate is held constant by fixing the ionization state by methylation of the carboxyl group of glycine producing glycine methyl ester, or by permethylation of the amino group to give betaine ($^+Me_3N\text{-}CH_2\text{-}CO_2^-$ pK_a = 27.3 ± 1.2) and betaine methyl ester ($^+Me_3N\text{-}CH_2\text{-}CO_2Me$ pK_a = 18.0 ± 1.0). These values are

comparable to the pK_a values of simple carbon acids such as ethyl acetate[17] pK_a = 25.6 ±0.5. and acetamide pK_a = 28.4.[14]

Scheme 3.2:

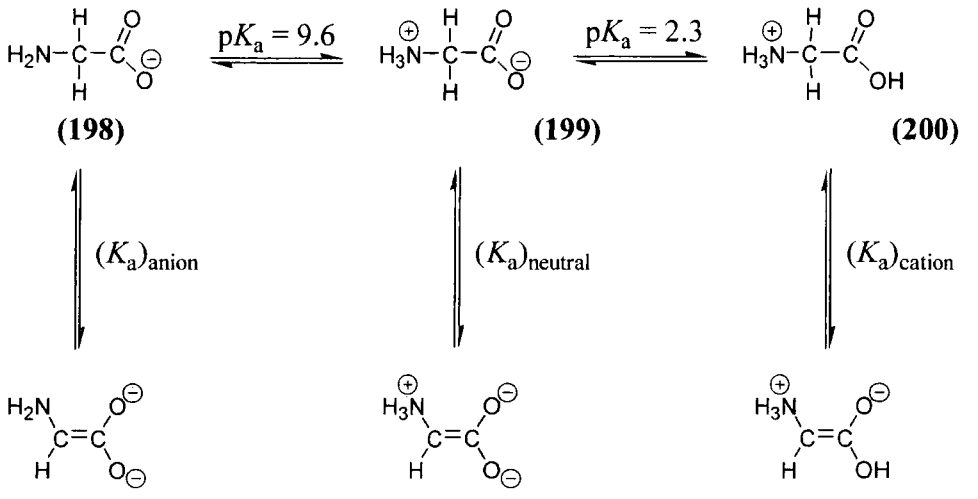

The difference in carbon acid pK_a values of the ionization states of glycine reflects the significant differences in their intrinsic reactivities. A large positive deviation by cationic carbon acids is seen from the linear rate-equilibrium correlation for deprotonation of neutral aldehydes ketones and esters. This reflects the existence of a smaller Marcus intrinsic barrier and hence faster deprotonation of cationic carbon acids by hydroxide than of neutral α-carbonyl carbon acids, as the thermodynamic driving force for the deprotonation is similar. Smaller deviations are seen for the zwitterionic amino acids and derivatives, however much of the positive deviation from the correlation is masked by the approach of the rate of the reverse protonation to the limiting rate constant k_{reorg}.[1]

The zwitterionic form of an amino acid is likely to be the form present at physiological pH for a number of reasons. Firstly the pK_a of an ammonium ion NH_4^+ is 9.3,[18] and even simple ammonium ions have pK_a's averaging 10 ($C_2H_5NH_3^+$, pK_a = 10.6),[19] so at pH 7 protonation of the amino end is most probable. Conversely, a typical carboxylic acid has a pK_a of around 5 such as methanoic acid pK_a = 4.8,[18] so at physiological pH the carboxyl group of the amino acid will be essentially deprotonated.

The acidity of the α-carbon depends not only on the ionization state of the amino acid but also on its position in a peptide chain. The α-amino carbon at the N-protonated N-terminus of a peptide or protein is estimated to undergo deprotonation 130-times faster than the α-amino carbon at the corresponding internal amino acid residue.[3] This is significant when it comes to interpreting the reactivities of amino acid residues in peptide and in proteins. Superficially in the case of archaeological artefact dating, the different rates of racemization of alanine at the N-terminus of a peptide and at an internal residue gives a short and long timescale on which the age of the tissue can be measured as an internal residue will racemize more slowly than an N-terminal residue.[20] More importantly this has implications on the reactivity of residues in enzyme active sites, and in protein folding in the enzymes themselves.

3.1.2 Amino acid racemases

There are relatively few amino acid racemases. Of those known, two distinct groups have emerged. Pyridoxal phosphate-dependent amino acid racemases, such as alanine racemase, and serine racemase, and pyridoxal phosphate-independent amino acid racemases, like glutamate racemase, aspartate racemase and proline racemase.

The mechanism for racemization in both PLP-dependent, and PLP-independent amino acid racemases makes use of two catalytic bases in the active site. In alanine racemase these are Tyr265 and Lys39 which bind the pyridoxal phosphate. Scheme 3.3 shows the proposed mechanism of the alanine racemase enzymatic reaction in which the substrate carboxy-group directly participates in the catalysis by mediating the proton transfer between the two catalytic bases, Lys39 and Tyr265. The phenolic hydroxyl group of Tyr265 removes the α-proton from L-alanine in the external aldimine with pyridoxal phosphate and concertedly donates a proton to the carboxylate group of the aldimine (**A – B**). This proton transfer is made possible by the formation of a sterically favourable six membered ring (**C**). The resulting carboxy-group then donates a proton to the ε-amino group of Lys39 (**D**) and again, in a concerted manner, Lys39 donates a proton to the α-

carbon to form D-alanine. The advantages of this mechanism is that both the ε-amino group of Lys39 and the phenolic OH group of Tyr265 are allowed to maintain their neutral states throughout the catalytic steps, also the proton on the carboxylate group stabilizes the carbanion structures **(C – D)**. The mechanism shown in Scheme 3.3 is shown without formation of a quinonoid intermediate because alanine racemase has Arg219 at the site interacting with the pyridine nitrogen of the cofactor, which destabilizes the quinonoid intermediate. Although the formation of this intermediate was thought to be a key step of PLP enzyme reactions, quantum mechanical calculations have not supported this mechanism.[21]

Scheme 3.3:

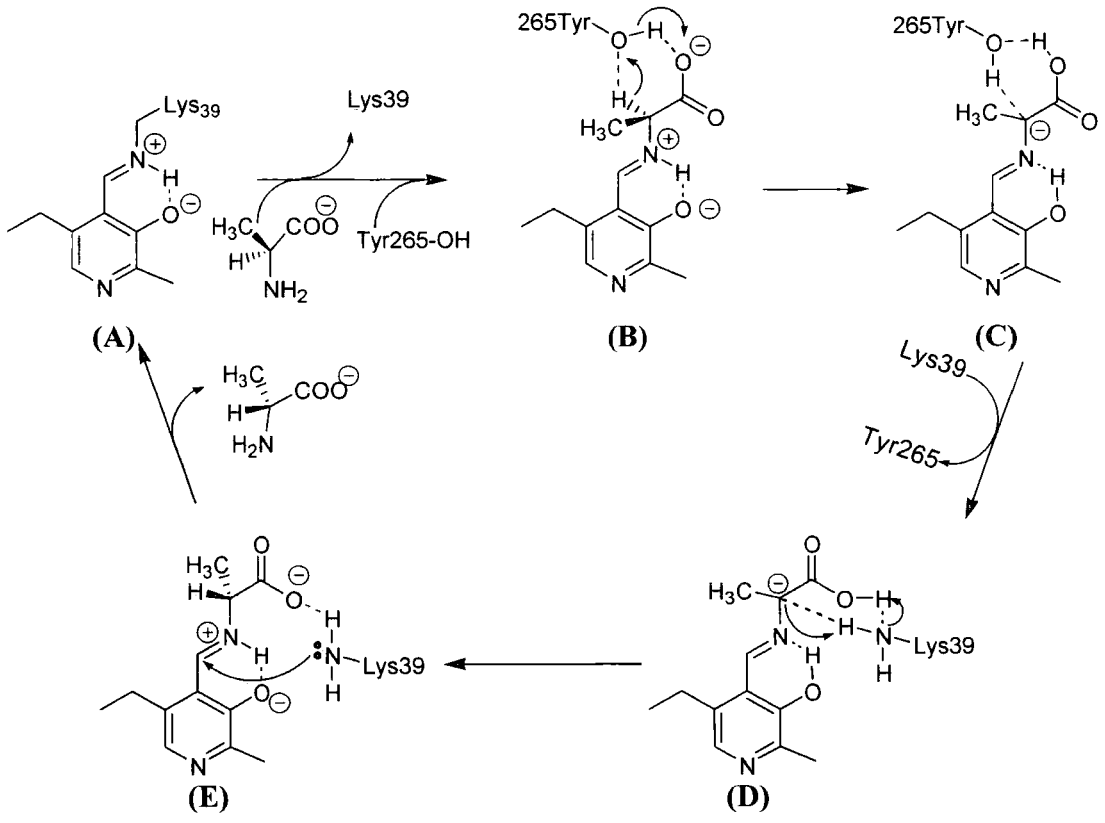

PLP-independent amino acid racemases, such as glutamate racemase contain two cysteine thiols in their active site. These act as a general acid/base catalysts (see Scheme 3.4). One cysteine serves to deprotonate the amino acid substrate at the α-position, and the other reprotonates the resulting intermediate carbanion on the opposite face, thus generating the enantiomeric product.

Scheme 3.4:

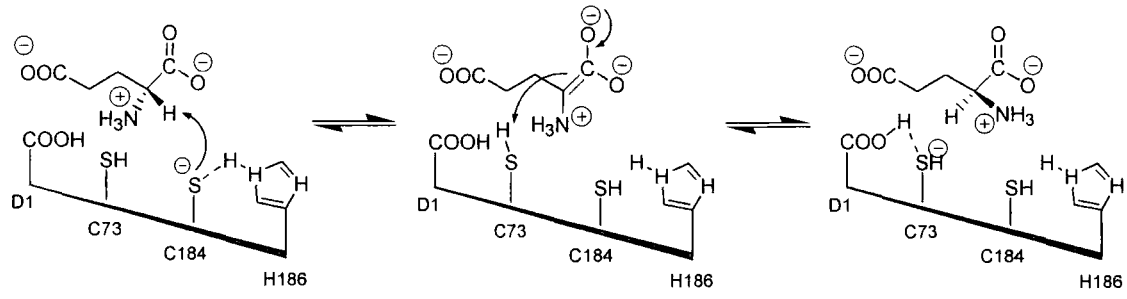

PLP-independent amino acid racemases have thiol anions in their active site in contrast to other neutral carbon acid deprotonating enzymes such as triosephosphate isomerase,[22] and ketosteroid isomerase which utilise carboxylate anions in their active site as base/acid catalysts. The result of this is that amino acid racemases have a low dielectric constant, favouring the conversion of the substrate to the zwitterionic enol intermediate. The transfer of anions to a non-polar active site from polar water solvent requires some desolvation of negative charge, for this reason thiols are better than oxygen in this situation. The side chains themselves have been shown not to have a significant effect in lowering the thermodynamic barrier to reaction, but once in the active site the energetic price for desolvating a thiol is less than that of a carboxylate.

3.1.3 Diketopiperazines

Peptides are involved in a large number of physiological and biological processes, such as metabolism, reproduction, cellular communication, and immune responses. They occur naturally as both linear compounds, which form well known helices, β-sheets and proteins, and also as a wide variety of monocyclic and polycyclic proteins and peptides.

Diketopiperazines (DKPs), or dioxopiperazines are the smallest cyclic peptides that can exist i.e. cyclic dipeptides. Their abundance in nature is becoming increasingly widely appreciated and has encouraged medicinal chemists to use DKPs as a way around the limitations of peptides. Constraining the nitrogen atoms of an α-amino amide in a ring changes its physical properties. Cyclization reduces the susceptibility of the amide bond

to metabolic cleavage reactions and reduces conformational mobility. These changes can produce more drug-like properties in a molecule, and enhance more favourable interactions with macromolecules.

3.1.3.1 Isomers of diketopiperazines.

There are three possible isomers which can be obtained from cyclization of a dipeptide. While these isomers share a piperazine core, the strategies for their synthesis and their potential applications differ.

2,3-Diketopiperazines **(201)** (see Figure 3.1) are frequently used in medicinal chemistry. They can be found in natural products such as the antibiotics piperacillin,[23] cefoperazone,[24] and bicyclomycin.[25] 2,5-Diketopiperazines **(202)** are head to tail dipeptide dimers, and a common naturally occurring structural motif. Despite their apparently considerable biological activity, which is more recently coming to light, they were mostly viewed as unwanted by-products of peptide synthesis. 2,6-Diketopiperazines **(203)**, are the third possible isomer. These are head to head cyclic dipeptides. These molecules have been the focus of investigation as antiproliferative agents through the inhibition of DNA topoisomerase II.[26]

Figure 3.1:

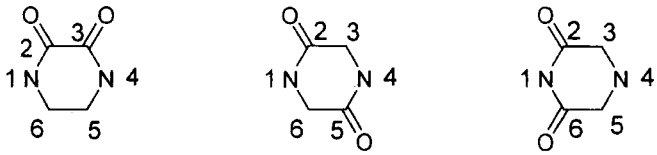

(201) **(202)** **(203)**

A detailed review comparing recently reported synthetic routes for the production of these different isomers has been published.[27] The focus of this work is on 2,5-diketopiperazines, **(202)** and so apart from this brief mention, the other isomers will not be discussed further.

Although 2,5-DKP formation was for a long time regarded as a troublesome side reaction during peptide chain assembly, recent, and more accurate identification of new 2,5-DKPs

has led to a fuller realisation of the potential properties of these small peptides as both potential drugs and drug precursors. 2,5-DKPs were found to be inhibitors of various enzymes, including topoisomerases, collagenase-1, as well as bradykinin antagonists, modulators of plasminogen activator inhibitor-1 and opioid receptor agonists and antagonists.[28] Figure 3.2 shows a range of naturally occurring, planar DKPs, D-Pro-D-Phe, **(204)**, D-Pro-D-Leu, **(205)**, D-Pro-D-Val, **(206)**, D-Pro-D-Ile, **(207)** and *trans*-4-OH D-Pro-D-Phe, **(208)**, found from one strain of marine bacteria, *Vibrio Anguillarium*, which exhibit significant antibacterial activity.[29] However the L-L forms of these molecules, also naturally occurring from entirely different sources, have no antibacterial activity.

Figure 3.2:

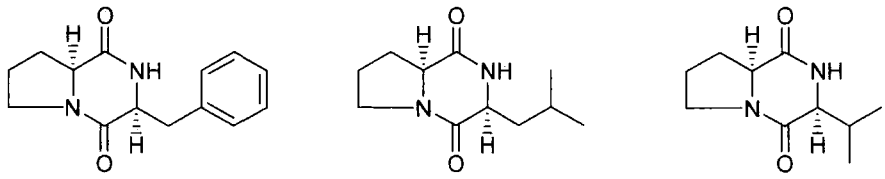

(204) **(205)** **(206)**

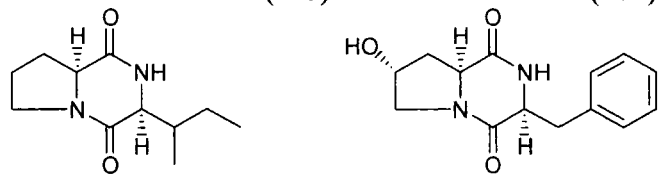

(207) **(208)**

The L-L enantiomers of DKPs **(204)-(208)** occur in a cyanobacterium from sponge *Calyx podatypa, Pseudomonas aeruginosa,*[29] from roasted coffee,[30] and other sources.[31-34] The L-L enantiomer of **(208)** is produced in *Jaspidae* sponge.[32] Although the L-L enantiomers of these compounds have no antibacterial function some are used by Gram-negative bacteria in cell-cell communications and gene expression regulation in response to population density.[35, 36] These discoveries have indicated the important relationship between the stereochemistry of the DKPs and their inherent activity.

As is observable from compounds **(204)-(208)** the amino acid D/L-proline is common in many biologically active 2,5-DKPs.

These compounds are extremely attractive as synthons in organic chemistry, as precursors to larger biomolecules. Considerable interest is stimulated in these compounds by the ability to quickly, efficiently and reliably build very large and well defined aggregates such as molecular tapes, **(209)**, through intermolecular hydrogen bonding[37] (see Figure 3.3). These aggregates can span a range of structures and sizes which makes them potentially very versatile in their application.

Figure 3.3:

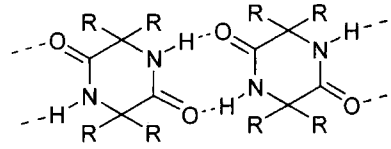

(209)

A diketopiperazine can be viewed as a small, constrained scaffold with up to six points of diversity. DKPs are expected to be significantly more stable than their linear precursors and the corresponding monomers[29] and so are potentially useful tools in the process of drug discovery, both as probes into the three-dimensional structure of active site or as leads to new biologically active agents.

There is little information on the reactivity of these compounds considering their abundance and significant biological activity. The very diverse nature of their structures has created a wide field in which to conduct a structure-reactivity study with the only question being where to start.

3.1.3.2 Synthesis of 2,5-diketopiperazines

Most homogeneous 2,5-DKPs can be prepared simply by heating the free amino acid methyl esters in a sealed tube. This is even effective for amino acids with reactive side chains.[38] Possibly the oldest method of unsymmetrical DKP synthesis consists of treatment of the dipeptide ester with methanolic ammonia, however the strongly basic medium can lead to epimerization, as do other base-catalyzed cyclization methods.[39] A more stereochemically robust method described by Nitecki *et al*[40] consists of Boc-

dipeptidyl methyl ester N-protection with formic acid, followed by reflux of the dipeptidyl ester formate salt in 2-butanol/toluene and removal of the formic acid through azeotropic distillation. However other side reactions occur which complicate this method.[41] A later and more simple approach described by Ueda *et al*[42] was the reflux of dipeptidyl methyl esters in low-boiling solvents, particularly methanol, or other alkyl esters in 2-butanol containing 0.1 – 2 M acetic acid.[43] 2,5-Diketopiperazines may be formed directly from Z-protected dipeptidyl methyl esters through simultaneous deprotection and cyclization, such as through the use of catalytic transfer hydrogenation at elevated temperatures.[44] Often the preparation of unsymmetrical 2,5-DKPs is performed by reacting appropriate N-carboxy anhydrides, **(210)**, with amino acid ethyl esters **(211)**.[45] An advantage of this method is the absence of condensation by-products which would require removal (see scheme 3.5). In some cases even one-pot procedures have been adopted.[46]

Scheme 3.5:

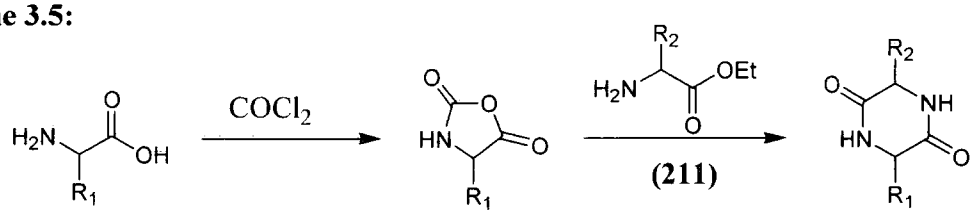

To promote cyclization, less reactive dipeptidyl alkyl esters may be converted to an active ester form, such as succinimido esters by deprotection of the N-terminally Boc-protected precursors with trifluoroacetic acid, followed by cyclization in pyridine.[47] However, preparation of active esters from protected dipeptide acids is not always straightforward. Often epimerization occurs during esterification. There are also various solid–phase synthesis methods available for DKP preparation, including those employing linkers based on *o*-nitrophenyl,[48] *p*-thiophenyl,[49] and 4-bromomethyl-3-nitrobenzoylaminobenzyl esters.[50] Resins such as Kaiser oxime resin,[51] and even standard Merrifield peptide synthesis resin may be used under optimized reaction conditions.[52]

3.1.3.3 Mechanism of 2,5-diketopiperazine formation.

The planar backbone amide bonds of polypeptides occur mainly in the *trans*-conformation. Planarity is maintained through a high rotational energy barrier due to partial double bond character of the peptide bond. The energy difference between *trans* and *cis*-peptide bond isomers is of the order of 2.5 kcal mol^{-1}. Intramolecular attack of the amino group of a dipeptide derivative on the terminal carboxy group is only possible from a folded conformation containing a *cis*-peptide bond (see Scheme 3.6).

Scheme 3.6:

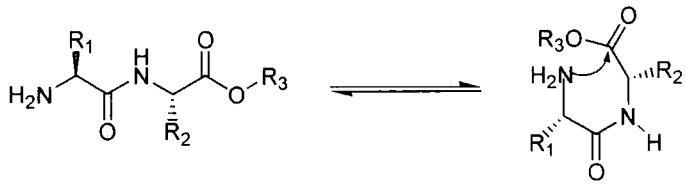

The low abundance of *cis*-peptide bonds in naturally occurring polypeptides was attributed mainly to steric conflict between adjacent C_α-substituents in *cis*-conformation, a theory which was supported by mechanistic studies. However the actual occurrence of *cis*-peptide bonds in known protein structures does not correlate with residue side chain bulk. Similarly the relative ease of 2,5-DKP formation from a number of dipeptide derivatives cannot be explained adequately by steric interactions between side chains in *trans* and *cis*-isomers. Most notably for dipeptides with α-alkyl amino acid residues, despite the steric crowding in the *cis*-isomer such peptides have been observed to cyclize readily. Factors such as overall proximity between terminal amino and carbonyl group, as well as stabilizing intramolecular interactions may be involved.[53]

3.1.3.4 Structure of 2,5-diketopiperazines

The presence of two *cis*-peptide bonds dictates that *cis*-2,5-DKP rings must be nearly planar, although very flat twist forms of boats and chairs are also possible.[54] Minimization of steric conflict between side chains of the ring is a major influence on 2,5-DKP ring conformation.[55] Generally, if the dihedral bond angles between α-carbons

and the carbonyl and amino groups are termed Ψ, and Φ, respectively and the amide N-C bond ω, then the general constraints shown in Figure 3.4 apply.[56]

Figure 3.4:

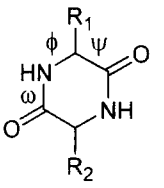

$$0° < |\phi| - |\Psi| < 50° \; ; \; 0° < |\omega| < 8° \; ; \; |\phi| \approx |\omega + \Psi|$$

The rigid nature of DKP molecules was suggested as early as the 1930's[57] and was later confirmed by optical rotatory dispersion experiments[58] and X-ray crystallographic analysis of the structures.[59] Aromatic side chains on DKP molecules were found to influence the ring conformation by tending to overlap with the DKP ring. Such interactions are likely due to dipole-dipole interactions, the amide group providing the dipole and the aromatic ring supplying a polarizable π-electron cloud. There are three basic conformations, **(212)**, **(213)** and **(214)**, that can be rationalized from the various combinations of aromatic and non-aromatic side chains of *cis*-DKPs (see Figure 3.5). Only a planar ring conformation is likely to be important for *trans*-DKPs.[60]

Figure 3.5:

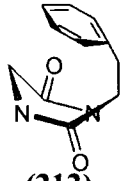

(212)

Flagpole boat

cyclo-[Gly-Xaa]

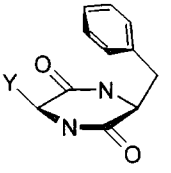

(213)

Planar

cyclo-[Xaa-Yaa]

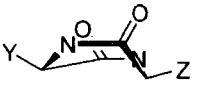

(214)

Bowsprit boat

cyclo-[Yaa-Zaa]

Xaa = Aromatic residue

Yaa, Zaa = Non aromatic residues

3.1.3.5 Proline 2,5-diketopiperazines

As mentioned earlier, L/D-proline is a very common amino acid constituent in DKP structures, found in a myriad of sources throughout the natural world. It is surprisingly common in biologically active structures that have been found (See Figure 3.2). The prevalence of proline in some classes of cyclopeptides such as phakellistatines (see Figure 3.6) found in marine environments and in higher plants has defined these peptides as "proline rich". [61] Phakellistatin 7, **(215)**, a "proline rich" biomolecule is comprised of two Pro-Pro tracts in a constrained decapeptidic macrocyclic framework.

Figure 3.6:

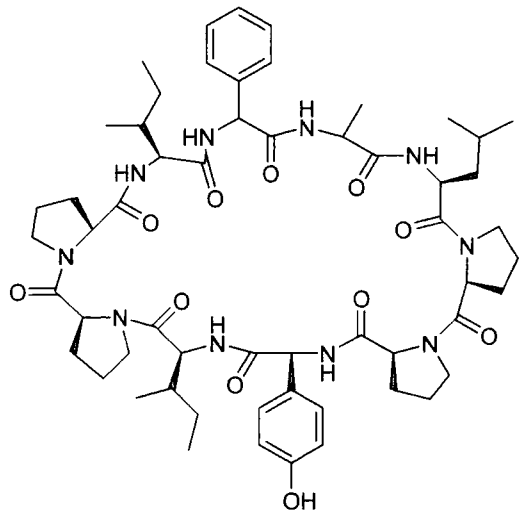

(215)

The biologically active cyclo-(His-Pro) DKP (CHP), **(216)** (see Figure 3.7), is the proposed major metabolite of thyrotropin releasing hormone (TRH) **(217)**, a simple tripeptide discovered first in the hypothalamus, and subsequently in the gastrointestinal tract.[62, 63] The metabolite CHP exhibits similar and dissimilar properties to the parent hormone and shows a wider tissue distribution[64] and resistance to plasma degradation[62]. Specific binding sites exist for CHP along with evidence that it also originated from non-TRH sources[62]. This DKP is reported to possess antagonistic activity to ethanol narcosis in mammals[65], and to induce satiety in rats[66]. It also is reported to influence gut mobility and gastric acid secretion.[62]

Figure 3.7:

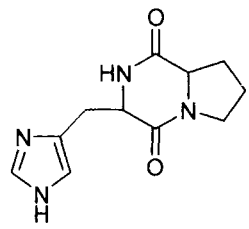

(216)

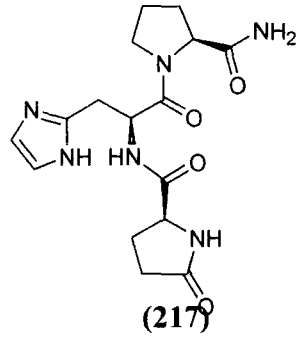

(217)

As a dietary supplement, often in the form of powdered animal prostates, CHP, **(216)**, has been shown to improve the symptoms of type 2 diabetes by aiding the absorbance of zinc into the body through the digestive tract.[67] CHP has also been found in significant and consistent amounts in cows' milk, although the role of CHP obtained in dietary milk is not established.

The apparent importance of proline in natural systems, coupled with the ease of synthesis of bis-proline makes it a good candidate for preliminary structure-reactivity studies. The very generous donation of bis–D-Proline from Dr David Fox (University of Warwick) prompted these investigations. In this work, the rates of racemization of bis-D-proline, and bis-L-proline are measured and compared.

3.2 Results

3.2.1 Synthesis of diketopiperazines.

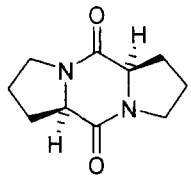

(218)

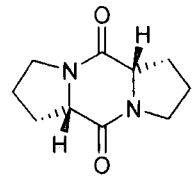

(219)

Synthesis of the diketopiperazines, bis-D-proline **(218)** and bis-L-proline **(219)**, involved a single step dehydration/cyclization method (Scheme 3.7). Heating of enantiomerically pure proline monomer **(220)** to high temperatures resulted in cyclization of the amino acids to give the corresponding diketopiperazines **(221)** in high yield.

Scheme 3.7:

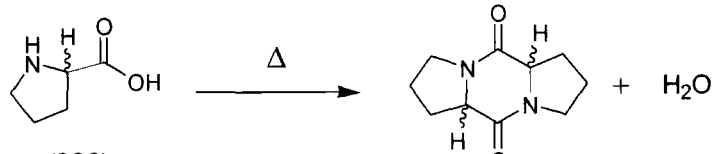

(220) **(221)**

Synthesis of bis-D/L-proline diketopiperazine was attempted using a multicomponent reaction scheme. This first step involved N-protection of the enantiomerically pure D-proline with benzyl chloride **(222)**, and potassium hydroxide, to produce the N-benzyl-D-proline **(223)** (Scheme 3.8). The N-protected D-proline **(223)** could then be coupled to L-proline methyl ester using the standard coupling reagent dicyclohexylcarbodiimide (DCC) in the presence of *o*-benzotriazole-N,N,N',N'-tetramethyl-uronium-hexafluoro phosphate (HBTU) and triethylamine (TEA) (Scheme 3.9). The D/L-dipeptide could then be deprotected over a palladium catalyst and cyclized to produce the bis-D/L-proline diketopiperazine **(227)**[68] (Scheme 3.10). However this synthesis proved ultimately unsuccessful as the final cyclization of the dipeptide **(226)** did not occur.

Scheme 3.8:

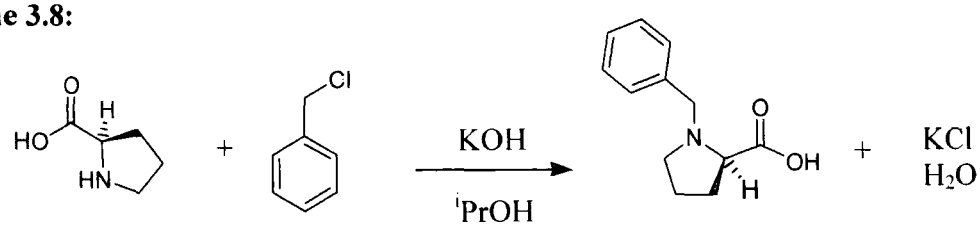

(222) **(223)**

Scheme 3.9:

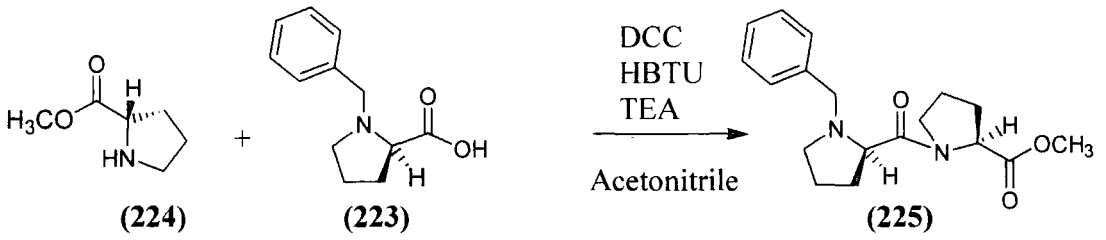

(224) **(223)** **(225)**

Scheme 3.10:

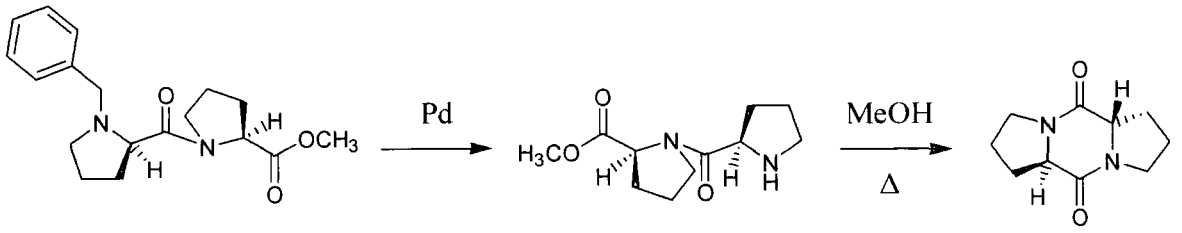

(225) **(226)** **(227)**

3.2.2. Deuterium exchange followed by ^{1}H NMR spectroscopy.

The H/D exchange reactions of the diketopiperazines (DKPs) **(218)** and **(219)** were analyzed using 300 and 500 MHz ^{1}H NMR spectroscopy. The disappearance of the peak due to the C3-H and C6-H in the ^{1}H NMR spectrum was monitored at 25 °C and at ionic strength I = 1.0 (KCl). From these ^{1}H NMR data the first and second order-rate constants for the deprotonation of substrate by deuteroxide ion in D_2O to give the corresponding enolate intermediate could be estimated.

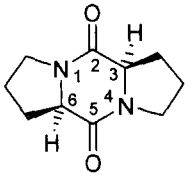

(218)

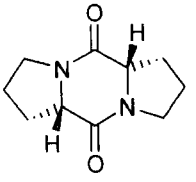

(219)

A detailed mechanism for exchange of the C3-H and C6-H of DKP **(218)** and **(219)** for deuterium is shown in Scheme 3.11. Amino acids can be deprotonated by a base in solvent to form the corresponding enolate **(228)**. This can then be redeuterated by fully isotopically labeled solvent or buffer conjugate acid to form the exchange product **(229)**. For low amino acid concentrations, the concentration of the proton containing DOH formed during this process is negligible in solvent D_2O, meaning reprotonation by DOH to generate the protonated substrate will also be negligible. Thus enolate formation is followed by effectively irreversible formation of the deuterium exchange product. Reprotonation is rapid, hence an estimate of the rate constant for enolate formation may be obtained by determining the rate constant for deuterium exchange.

A typical exchange experiment was run at 25 °C and ionic strength I = 1.0 (KCl). Aliquots were taken and quenched at different time points during the reaction. The signal due to the C3-H and C6-H appears as a broad triplet 4.2 – 4.5 ppm range.

Scheme 3.11:

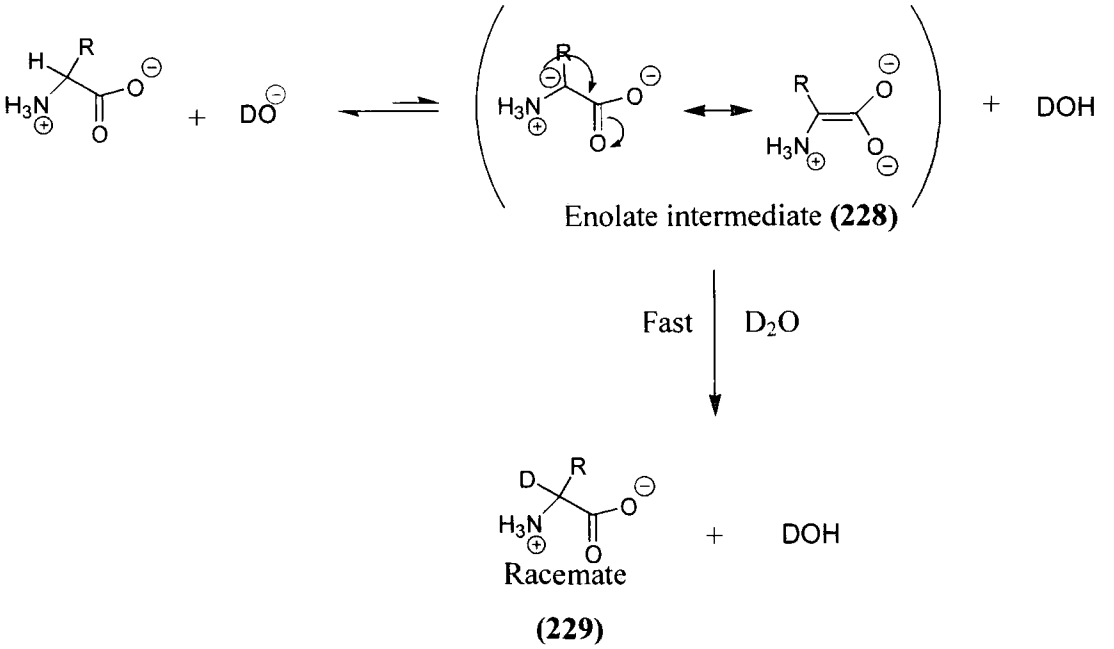

In this work decay of peaks due to exchange of hydrogen for deuterium is not observed at any carbon other than that at C3 and C6. As with the azolium ions, this is seen by comparison over time of all peak areas to a constant peak area due to the internal standard tetramethylammonium deuteriosulfate, which appears as a broad singlet at 3.0 – 3.3 ppm.

A possible competing reaction with deuterium exchange of the C3-H and C6-H of diketopiperazines **(218)** and **(219)** is base-catalyzed hydrolysis at one of the carbonyl carbons of the diketopiperazines, (Scheme 3.12), which would lead to hydrolysis product **(230)**.

Scheme 3.12:

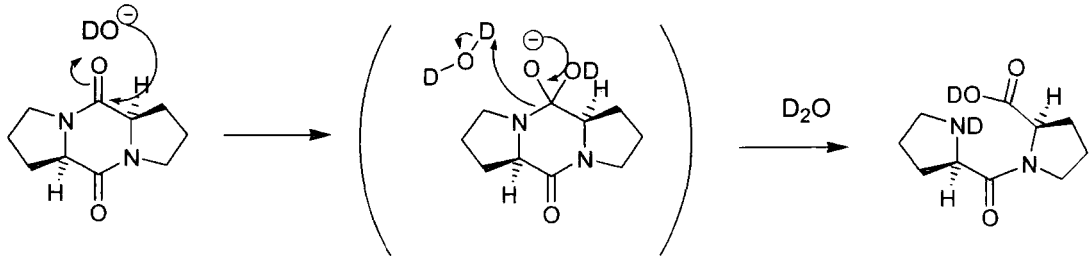

(230)

However no such hydrolysis products were detected by ^{1}H NMR spectroscopy during H/D exchange. Under these experimental conditions deuterium exchange is much faster than hydrolysis for these compounds. Significant hydrolysis is not expected to be seen for these diketopiperazines due to the inherent stability displayed by diketopiperazines in general compared to the analogous acyclic dipeptides.[69]

The progress of the deuterium exchange reactions for diketopiperazines **(218)** and **(219)** was monitored as described in Section 2.2.2. The pseudo-first-order rate constant for deuterium exchange (k_{obs}, s^{-1}) could formally be the sum of the first-order rate constants for exchange catalyzed by solvent, deuteroxide ion and buffer base (Equation 2.3). The value for deprotonation by solvent water (k_{D2O}, s^{-1}) is expected to be considerably lower than the other two contributing terms.[4, 69] The contribution of the buffer term (k_B [B^-], $M^{-1}s^{-1}$) is expected to be significant in this case due to the increased stability of the enolate

intermediate by resonance delocalization of the negative charge. In this case the proton transfer step is expected to be rate limiting for deuteroxide ion-catalyzed exchange, and not the solvent reorganization step Hence the experimentally observed pseudo-first-order rate constant (k_{obs}, s^{-1}) obtained for DKPs **(218)** and **(219)** in this work may be expressed as the sum of the pseudo-first-order rate constant for deuteroxide ion-catalyzed exchange (k_{DO} [DO^-] , s^{-1}) and base catalyzed exchange (k_B [B], s^{-1}) shown in Equation 3.1.

$$k_{obs} = k_{DO}[DO^-] + k_B[B] \qquad \textbf{(Equation 3.1)}$$

Fortunately, deuterium exchange for the DKPs under investigation in this project could be directly monitored in unbuffered deuteroxide solution. Thus the general base catalysis term (k_B [B], s^{-1}) could be ignored.

The second-order-rate constant for the exchange of the C3-H and C6-H for deuterium, catalyzed by deuteroxide ion (k_{DO}, $M^{-1}s^{-1}$), could be obtained as the slope of the plot of k_{obs} (s^{-1}) against deuteroxide concentration.

3.2.2.1. Bis-D-proline diketopiperazine (218)

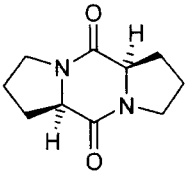

(218)

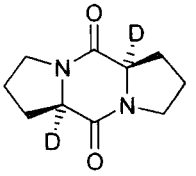

(218')

Rates of deuteroxide ion-cataysed H/D exchange of the C3 and C6 hydrogens of DKP **(218)** to form the corresponding deuterated product **(218')** were determined by 300 MHz ^{1}H NMR spectroscopy.

Figure 3.8 shows representative ^{1}H NMR spectra of DKP **(218)** (10mM substrate, 20mM KOD) obtained during the exchange for deuterium of the C3 and C6 hydrogens in D_2O solution at 25 °C and ionic strength I = 1.0 (KCl). Deuterium exchange at C3 and C6 results in the disappearance of a triplet peak due to the C3 and C6 hydrognes at 4.68 ppm (A). The signal due to the four COCHCH_2 hydrogens appears as two broad multiplets at 2.29 – 2.32 ppm, and 1.9 – 2.13 ppm respectively (not shown) due to coupling to the two adjacent C3 and C6 hydrogens and NCH_2CH_2 protons. The signal due to the four NCH_2CH_2 protons appears as a broad multiplet at 1.95 – 2.13 ppm, overlapping the signal due to COCHCH_2 and coupled to adjacent protons. The signal due to the four NCH_2 protons appears as a broad multiplet at 3.42 – 3.64 ppm (B), due to coupling to the adjacent NCH_2C$\underline{H_2}$.

H/D exchange is not observed at any position other than at C3 and C6 under these experimental conditions, indicated by comparison of all the signals due to DKP **(218)** in the spectrum to the peak due to the internal standard tetramethylammonium deuteriosulfate at 3.22 ppm (C) In the reaction timeframe there is no change in the total integrated area for the signals due to all other protons relative to the constant peak area of the broad triplet at 3.22 ppm due to the internal standard.

Figure 3.8: Representative ^{1}H NMR spectra at 300 MHz of DKP (218) (10mM, 20mM KOD), obtained during exchange of the C3 and C6 hydrogens for deuterium in D_2O at 25 °C and ionic strength I = 1.0 (KCl). The percentage of deuterium exchange is indicated above each spectrum.

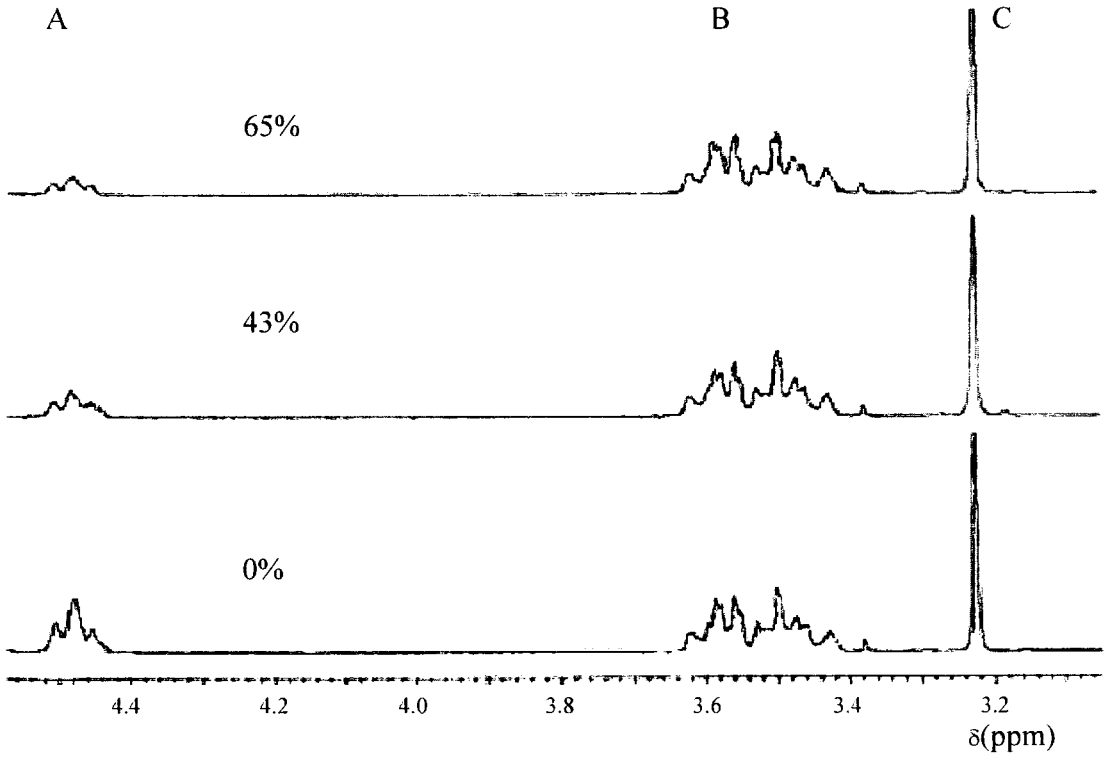

Reaction data and the experimental first-order rate constants for deuterium exchange (k_{obs}, s^{-1}) at different concentrations of deuteroxide are shown in Table 3.1. The values for k_{obs} (s^{-1}) are obtained from the slopes of semi-logarithmic plots (Figure 3.8) of the fraction of unexchanged substrate $f(s)$ against time. The value for $f(s)$ is calculated using Equation 3.2, where $A_{C(3+6)-H}$ is the area of the peak at 4.68 ppm due to the C3 and C6 hydrogens and $A_{I.S}$ is the area of the peak due to the internal standard.

$$f(s) = \left(\frac{(A_{C(3+6)-H})_t}{(A_{I.S.})_t} \right) \Big/ \left(\frac{(A_{C(3+6)-H})_{t=0}}{(A_{I.S.})_{t=0}} \right) \qquad \textbf{(Equation 3.2)}$$

Table 3.1: First-order rate constants for the exchange of the C3 and C6 hydrogens of DKP (218) for deuterium in KOD solution in D_2O at 25 °C and ionic strength I = 1.0 (KCl).

$[DO^-]^a$ (M)	Time (s)	$f(s)^b$	Lnf(s)	$k_{obs}{}^c$ (s^{-1})
0.03	0	1.000	0.000	2.54×10^{-4}
	9.00×10^2	0.783	-0.245	
	180×10^3	0.630	-0.462	
	2.70×10^3	0.487	-0.719	
	3.60×10^3	0.383	-0.960	
	4.51×10^3	0.325	-1.124	
0.02	0	1.000	0.000	1.66×10^{-4}
	1.50×10^3	0.761	-0.273	
	3.06×10^3	0.578	-0.548	
	$4,57 \times 10^3$	0.454	-0.790	
	6.00×10^3	0.352	-1.044	
	7.50×10^3	0.292	-1.231	
0.015	0	1.000	0.000	1.19×10^{-4}
	1.96×10^3	0.803	-0.115	
	3.60×10^3	0.664	-0.259	
	5.40×10^3	0.518	-0.438	
	7.32×10^3	0.407	-0.587	
	9.02×10^3	0.352	-0.757	
0.01	0	1.000	0.000	6.14×10^{-5}
	2.55×10^3	0.892	-0.115	
	4.81×10^3	0.772	-0.259	
	7.68×10^3	0.645	-0.438	
	9.90×10^3	0.556	-0.587	
	1.25×10^4	0.469	-0.757	
0.005	0	1.000	0.000	2.79×10^{-5}
	3.00×10^3	0.898	-0.108	
	6.00×10^3	0.826	-0.191	
	9.00×10^3	0.759	-0.276	
	1.20×10^4	0.708	-0.345	
	1.50×10^4	0.652	-0.428	

(a) Measurements were made in KOD solution. (b) The fraction of unexchanged substrate remaining f(s) was calculated according to Equation 3.2. Measurements were made at an initial substrate concentration of 10 mM. (c) The value of the first-order rate constant (k_{obs}) was obtained as the slope of the plot of ln f(s) against time shown in Figure 3.9.

Figure 3.9: Semi-logarithmic plot of the fraction of remaining C3 and C6 hydrogens against time for the deuterium exchange reaction of DKP (218) in 5 mM (♦), 10 mM (■), 15 mM (▲), 20 mM (—) 30 mM (●) KOD solution at 25 °C and ionic strength I = 1.0 (KCl).

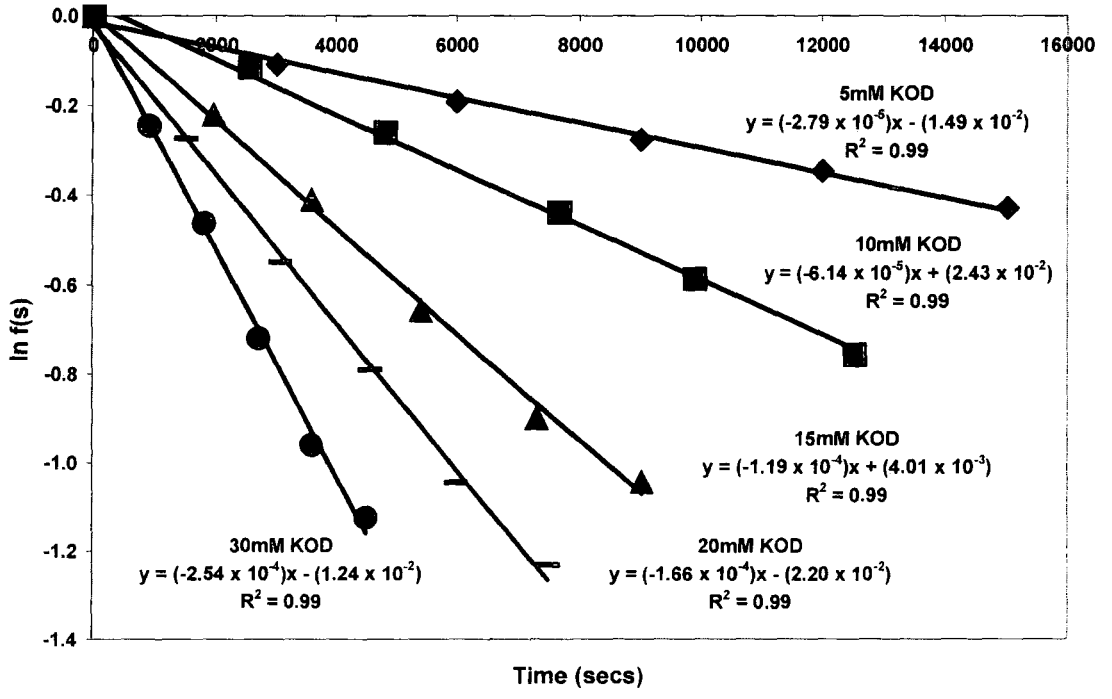

The first-order-rates of exchange (k_{obs}, s^{-1}) are shown in Table 3.2. The second-order rate constant for deuteroxide ion-catalysed exchange, $k_{DO} = 9.27 \times 10^{-3}$ $M^{-1}s^{-1}$ was calculated from the slope of the plot of the first-order-rate constants k_{obs} against the concentration of deuteroxide ion as shown in Figure 3.10.

Table 3.2: First and second-order rate constants for exchange of the C3 and C6 hydrogens of DKP (218) for deuterium in D_2O at 25 °C and ionic strength I = 1 (KCl).

$[DO^-]$ (M)	k_{obs} (s^{-1})	k_{DO}[b] ($M^{-1}s^{-1}$)
0.030	2.54×10^{-4}	
0.020	1.66×10^{-4}	
0.015	1.19×10^{-4}	9.27×10^{-3}
0.010	6.14×10^{-5}	
0.005	2.79×10^{-5}	

(a) The second-order rate constant, (k_{DO}), was obtained as the slope of the plot of k_{obs} against [DO^-] in Figure. 3.10.

Figure 3.10: Plot of k_{obs} against $[DO^-]$ for the H/D exchange reaction of DKP (218) in D_2O at 25 °C and ionic strength I = 1.0 (KCl).

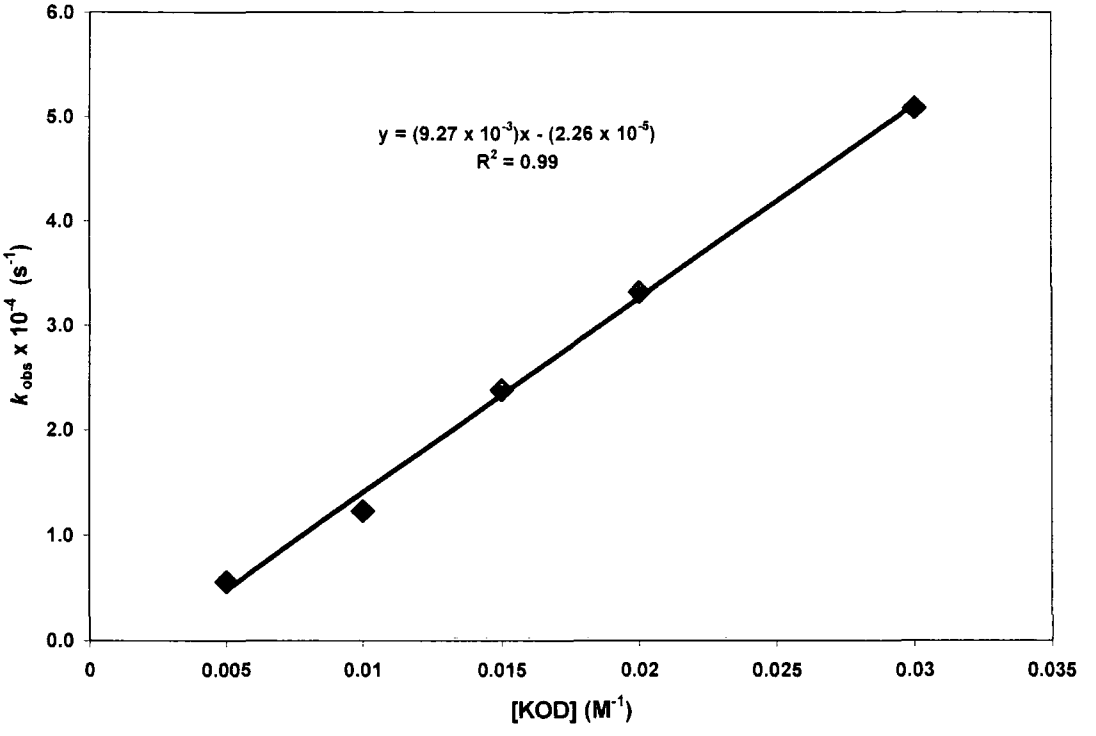

3.2.2.2 Bis-L-proline diketopiperazine (219)

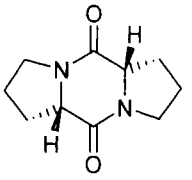

(219)

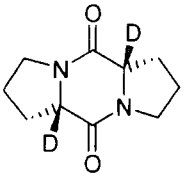

(219')

Rates of deuteroxide ion- cataysed H/D exchange of the C3 and C6 hydrogens of DKP **(219)** to form the corresponding deuterated product **(219')** were determined by 300 MHz ^{1}H NMR spectroscopy.

Figure 3.11 shows representative ^{1}H NMR spectra of DKP **(219)** (10mM substrate, 20mM KOD) obtained during the exchange for deuterium of the C3 and C6 hydrognes in D_2O solution at 25 °C and ionic strength I = 1.0 (KCl). Deuterium exchange at C3 and C6 results in the disappearance of a triplet peak due to the C3-H and C6-H at 4.68 ppm (A). The signal due to the four COCHCH_2 hydrogens appears as two broad multiplets at 2.29 – 2.32 ppm, and 1.9 – 2.13 ppm respectively (not shown) due to coupling to the two adjacent C3 and C6 hydrogens and NCH_2CH_2 protons. The signal due to the four NCH_2CH_2 protons appears as a broad multiplet at 1.95 – 2.13 ppm (not shown), overlapping the signal due to COCHCH_2 and coupled to adjacent protons. The signal due to the four NCH_2 protons appears as a broad multiplet at 3.42 – 3.64 ppm (B), due to coupling to the adjacent NCH_2C$\underline{H_2}$.

H/D exchange is not observed at any position other than at C3 and C6 under these experimental conditions, indicated by comparison of all the signals due to DKP **(219)** in the spectrum to the peak due to the internal standard, tetramethylammonium deuteriosulfate, at 3.22 ppm (C). In the reaction timeframe there is no change in the total integrated area for the signals due to all other protons relative to the constant peak area of the broad triplet at 3.22 ppm due to the internal standard.

Figure 3.11: Representative ^{1}H NMR spectra at 300 MHz of DKP (219) (10mM, 20mM KOD), obtained during exchange of the C3 and C6 hydrogens for deuterium in D_2O at 25 °C and ionic strength I = 1.0 (KCl). The percentage of deuterium exchange is indicated above each spectrum.

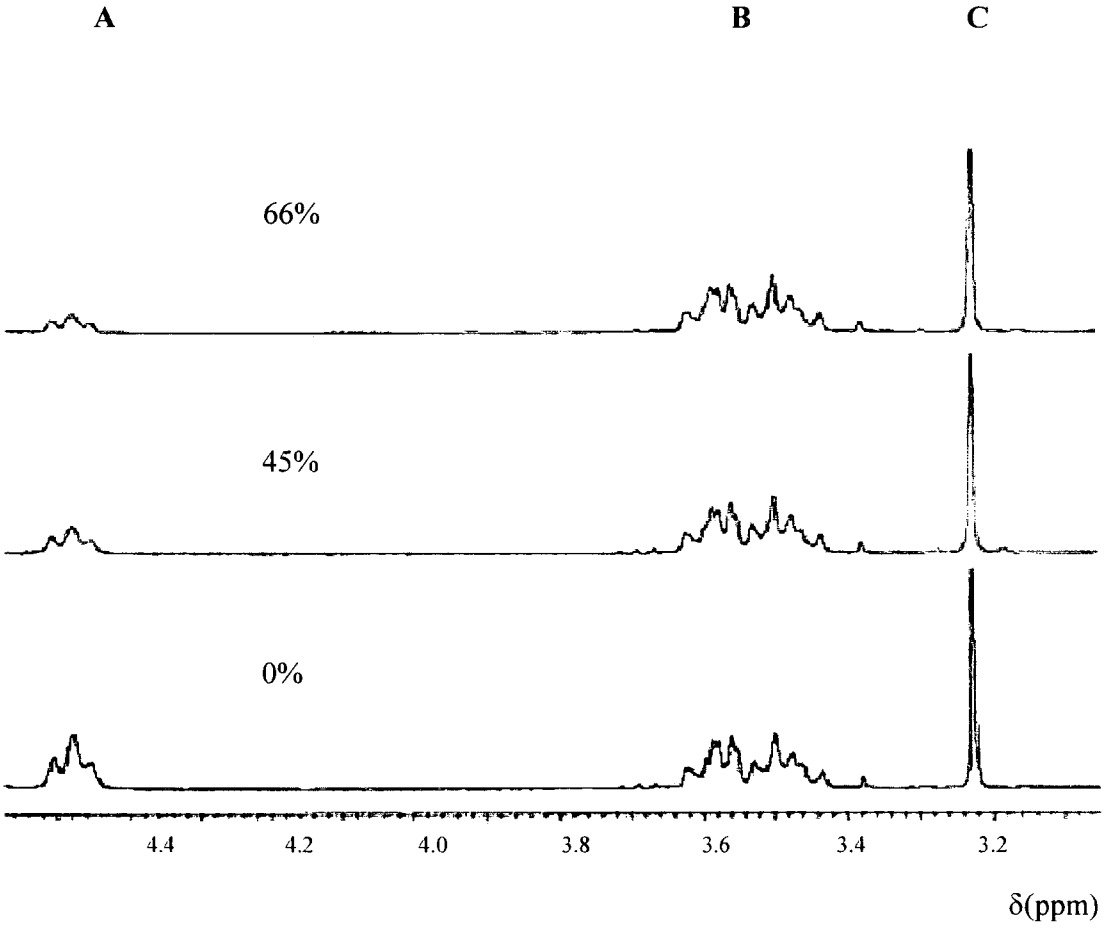

Reaction data and the experimental first-order rate constants for deuterium exchange (k_{obs}, s^{-1}) at different concentrations of deuteroxide are shown in Table 3.3. The values for k_{obs} (s^{-1}) are obtained from the slopes of semi-logarithmic plots (Figure 3.12) of the fraction of unexchanged substrate $f(s)$ against time. As described previously, the value for $f(s)$ is calculated using Equation 3.2, where $A_{C(3+6)-H}$ is the area of the peak at 4.68 ppm due to the C3 and C6 hydrogens and $A_{I.S}$ is the area of the peak due to the internal standard.

Table 3.3: First-order rate constants for the exchange of C3 and C6 hydrogens of DKP (219) for deuterium in KOD solution in D_2O at 25 °C and ionic strength I = 1.0 (KCl).

$[DO^-]^a$ (M)	Time (s)	$f(s)^b$	Lnf(s)	$k_{obs}{}^c$ (s^{-1})
0.030	0	1	0.000	2.46×10^{-4}
	9.00×10^2	0.936	-0.168	
	1.80×10^3	0.866	-0.426	
	2.70×10^3	0.795	-0.596	
	3.61×10^3	0.734	-0.894	
	4.51×10^3	0.697	-1.082	
0.020	0	1.000	0.000	1.66×10^{-4}
	2.04×10^3	0.755	-0.281	
	4.70×10^3	0.460	-0.777	
	7.50×10^3	0.295	-1.220	
0.015	0	1	0.000	1.23×10^{-4}
	1.81×10^3	0.804	-0.218	
	3.60×10^3	0.646	-0.437	
	5.40×10^3	0.515	-0.664	
	7.20×10^3	0.415	-0.879	
	9.00×10^3	0.331	-1.106	
0.010	0	1	0.000	7.00×10^{-5}
	2.40×10^3	0.855	-0.157	
	4.79×10^3	0.725	-0.322	
	7.20×10^3	0.602	-0.507	
	9.65×10^3	0.512	-0.669	
	1.20×10^4	0.436	-0.830	
0.005	0	1	0.000	2.49×10^{-5}
	3.00×10^3	0.936	-0.066	
	6.00×10^3	0.866	-0.144	
	9.00×10^3	0.795	-0.229	
	1.20×10^4	0.734	-0.309	
	1.50×10^4	0.697	-0.361	

(b) Measurements were made in KOD solution. (b) The fraction of unexchanged substrate remaining f(s) was calculated according to Equation 3.2. Measurements were made at an initial substrate concentration of 10 mM. (c) The value of the first-order rate constant (k_{obs}) was obtained as the slope of the plot of ln$f$(s) against time shown in Figure 3.12.

Figure 3.12: **Semi-logarithmic plot of the fraction of remaining C3 and C6 hydrogens against time for the deuterium exchange reaction of DKP (219) in 5 mM (♦), 10 mM (■), 15 mM (▲), 20 mM (—) 30 mM (●) KOD solution at 25 °C and ionic strength I = 1.0 (KCl).**

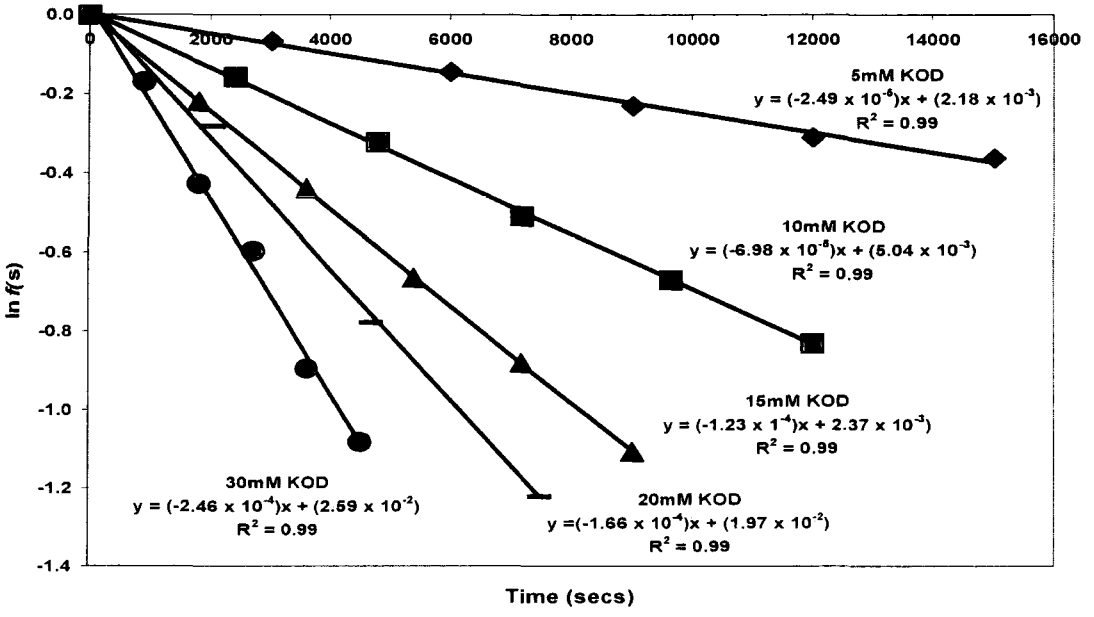

First-order-rate constants for exchange (k_{obs}, s^{-1}) are summarized in Table 3.4. The second-order rate constant for deuteroxide ion-catalysed exchange, $k_{DO} = 8.89 \times 10^{-3}$ $M^{-1}s^{-1}$ was calculated from the slope of the plot of the first-order-rate constant k_{obs} against the concentration of deuteroxide ion as shown in Figure 3.13.

Table 3.4: First and second-order rate constants for exchange of the C3 and C6 hydrogens of DKP (219) for deuterium in D_2O at 25 °C and ionic strength I = 1.0 (KCl).

$[DO^-]$ (M)	k_{obs} (s^{-1})	k_{DO}[a] ($M^{-1}s^{-1}$)
0.030	2.46×10^{-4}	
0.020	1.66×10^{-4}	
0.015	1.23×10^{-4}	8.89×10^{-3}
0.010	7.00×10^{-5}	
0.005	2.49×10^{-5}	

(a) The second-order rate constant, (k_{DO}), was obtained from the slope of the plot of k_{obs} against $[DO^-]$ in Figure. 3.10.

Figure 3.13: Plot of k_{obs} against $[DO^-]$ for the H/D exchange reaction of DKP (219) in D_2O at 25 °C and ionic strength I = 1.0 (KCl).

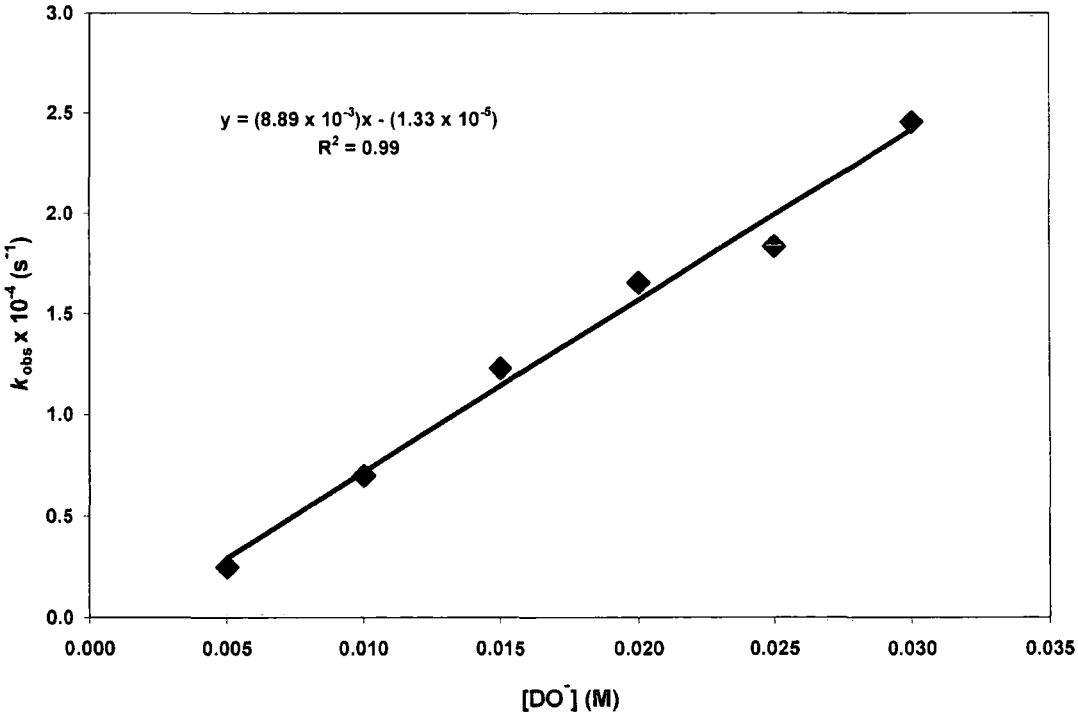

3.2.3 Estimation of k_{H2O} and pK_a determination.

The slopes of the plots of the experimental pseudo-first-order rate constants (k_{obs}, s^{-1}) against the concentration of deuteroxide ion for DKPs **(218)** and **(219)** gives the second order rate constants (k_{DO}, $M^{-1}s^{-1}$) for deuteroxide ion-catalyzed exchange of the two acidic protons of these cyclic substrates. The k_{DO} values were obtained as = 9.27×10^{-3} $M^{-1}s^{-1}$ and $k_{DO} = 8.89 \times 10^{-3}$ $M^{-1}s^{-1}$ respectively.

The second-order rate constant for hydroxide-ion catalyzed deprotonation (k_{HO}, $M^{-1}s^{-1}$) can be obtained from the experimental k_{DO} value ($M^{-1}s^{-1}$) by using an equilibrium secondary isotope effect relationship: $k_{DO}/k_{HO} = 2.0$ The secondary solvent deuterium isotope effect for deprotonation of these carbon acids by lyoxide ion is expected to be larger than $k_{DO}/k_{HO} = 1.46$ for deprotonation of acetone.[70] However there is no evidence that it is close to the maximum value of $k_{DO}/k_{HO} = 2.4$ for deprotonation to form very unstable carbanions for which isotope exchange is limited by solvent reorganization. Therefore, an intermediate value of $k_{DO}/k_{HO} = 2.0$ is used as the secondary solvent isotope effect for deprotonation of the carbon acids discussed in this chapter.

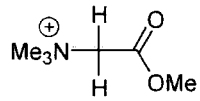

(231)

The reverse rate of protonation of betaine methyl ester **(231)** by solvent water is estimated to be 4×10^6 s^{-1}.[71] This is far below the limiting rate constants determined for the 'clocks' described by Richard *et al*[72] detailed in Chapter 1. Thus a value for k_{HOH} in this case can only be accessed by direct measurement. However there are extensive linear rate-equilibrium correlations of log k_{HO} (M^{-1}, s^{-1}) for the hydroxide ion-catalyzed formation of the enolates of simple aldehydes, ketones and esters with the pK_a of the parent acid.[73-75] Hence the pK_a values of DKPs **(218)** and **(219)** may be estimated from a Brønsted plot of log k_{HO} values against pK_a of other neutral simple carbon acids where both literature parameters have been statistically corrected to represent a single acidic proton in the molecule (see Table 3.5 and Figure 3.14). An estimate of the pK_a values for DKPs **(218)** and **(219)** can be calculated from the equation of the line in Figure 3.14

together with the experimental k_{HO} values for these cyclic substrates. The negative of the slope of the Brønsted correlation in Figure 3.14 is the Brønsted coefficient, $\beta = 0.40$. pK_a values of 22.5 and 22.6 could be interpolated for DKPs **(218)** and **(219)** respectively.

Table 3.5: Kinetic acidity of C3-H and C6-H of DKPs (218) and (219) and other simple carbon acids of similar acidity.

Carbon Acid	p[a]	k_{HO} $(M^{-1}s^{-1})$[b]	k_{HO}/p $(M^{-1}s^{-1})$[d]	pK_a[e]	pK_a + Log p[g]
Ph_2CHCHO	1	254	254	10.4	10.4
t-$PhCH_2CHO$	2			12.3	12.6
c-$PhCH_2CHO$	2	20	10	13.1	13.4
CH_3CHO	3	1.17	0.39	16.7	17.2
CH_3COPh	3	0.25	0.083	18.3	18.8
CH_3COCH_3	6	0.22	0.037	19.3	20.1
CH_3COSEt	3	2.0×10^{-2}	6.7×10^{-3}	21.0	21.5
Bis-L-Proline DKP	**2**	**4.4×10^{-3} [c]**	**2.2×10^{-3}**	**22.6[f]**	22.9
Bis-D-Proline DKP	**2**	**4.6×10^{-3} [c]**	**2.3×10^{-3}**	**22.5[f]**	22.8
CH_3COOEt	3	1.2×10^{-3}	4.0×10^{-4}	25.6	26.1
CH_3CONH_2	3	9.5×10^{-6}	3.2×10^{-6}	28.4	28.9

(a) p is the number of identical acidic protons in the carbon acid. (b) k_{HO} is the second order rate constant for the hydroxide-catalyzed deprotonation of the carbon acid. (c) Experimentally determined in this work. (d) The second order-rate constant for the hydroxide-catalyzed deprotonation of a *single acidic proton* of the carbon acid. (e) Literature pK_a values.[75] (f) Interpolated using the equation that fits the linear plot in Figure 3.14 together with experimental k_{HO} values. (g) Carbon acid pK_a values corrected to represent the ionisation of one acidic proton. (h) Interpolated using the equation to the linear plot in Figure 3.14 together with experimental k_{HO} values.

Figure 3.14: Brønsted plot of statistically corrected second order rate constants k_{HO} for hydroxide ion catalysed deprotonation of carbon acids (♦) against corresponding pK_a values using the literature data in Table 3.5. The interpolated data points for DKPs (218) and (219) are also indicated (●).

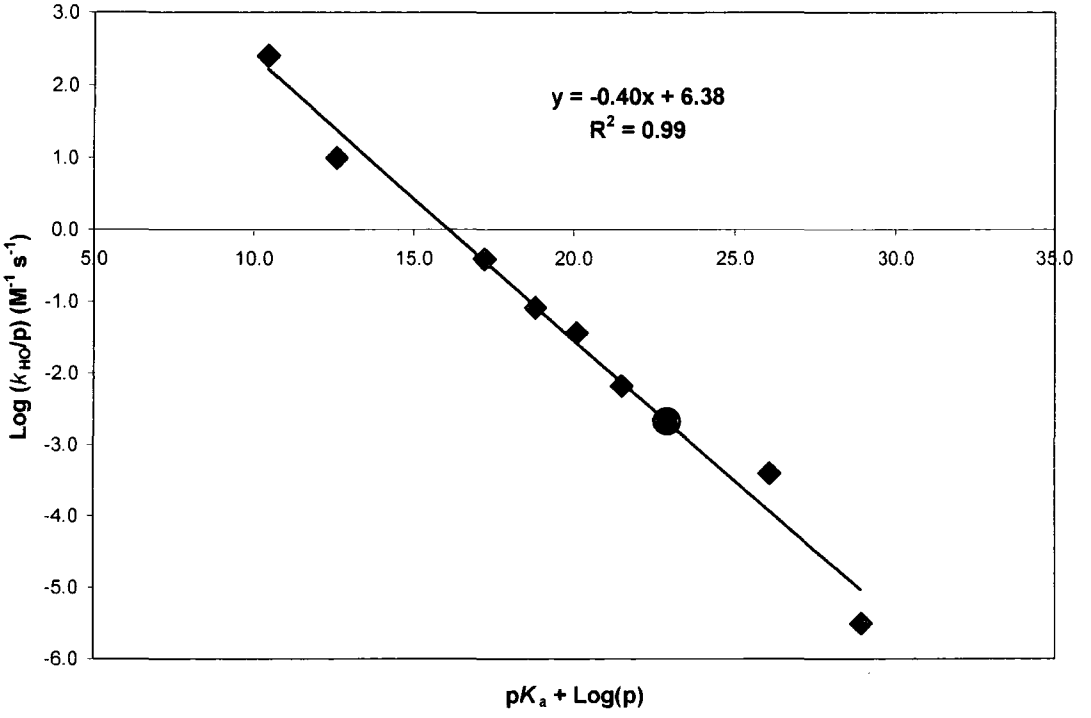

3.3 Discussion

3.3.1 Structure of diketopiperazines

The cyclic structure of diketopiperazines gives rise to their unique properties, which have lead to diverse application of the DKP motif in biological systems. Besides the obvious difference in shape, a major difference between dipeptides and the corresponding DKPs is in charge. Removal of the negative charge at the C-terminal through DKP formation would potentially increase the α-carbon acidity significantly, whereas removal of the positive charge on the N-terminal would have the opposite effect. DKPs possess an atypical *cis* amide bond. X-ray crystallographic analysis of crystalline DKPs along with Dreiding models[12, 76] have shown that rather than being completely rigid molecules, they possess a slight flexibility. DKPs exist in either a flat or slightly puckered boat form in which puckering increases with substitution. *Cyclic*-Gly-Gly[12, 77] is planar, while *cyclic*-L-Ala-L-Ala has a slightly skewed boat conformation with the methyl substituents in a quasi-equatorial position.[12, 78] In contrast DKPs containing proline must adopt a non planar boat conformation reflecting the constraints imposed on the DKP ring by fusion to the pyrrolidine ring.[79] Quantum mechanical studies using a CNDO/2 method confirmed considerable the flexibility of the DKP ring. However as folding of the ring increased the more rigid and less stable boat conformations tended to be favoured.

Figure 3.15:

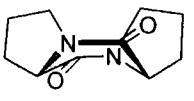

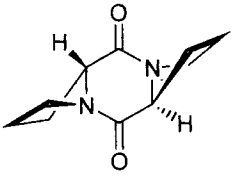

For proline-containing DKPs it is energetically unfavorable to adopt a planar DKP ring conformation[56, 80] (Figure 3.15). Planarity would require the five-membered proline ring to be severely twisted. The pyrrolidine rings strongly favor a near-planar conformation, which is only possible if the DKP ring assumes a boat-like conformation. In the case of bis-L-proline DKP **(218)** or bis-D-proline DKP **(219)** an even stronger stabilization of the DKP boat form would be expected as in these cases the $C\alpha - C\beta$ bonds of the two Pro residues are in pseudo-equatorial positions. In the case of bis-D/L-proline DKP only the

planar DKP ring conformation is possible, with the two pyrrolidine rings taking up half-chair conformations.

The preference of these rings for planarity may inhibit the cyclization of bis-D/L-proline dipeptide **(226),** as the product DKP **(227)** would likely be a highly strained structure.

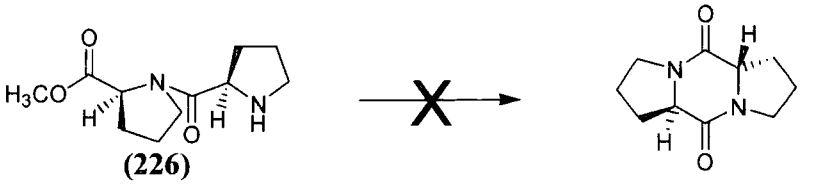

(226) **(227)**

3.3.2 Effects of cyclization on acidity

A number of reports of relative rates of epimerization of DKPs, dipeptides and free amino acids may be found the literature.[81] However, until recently no absolute values for these rates were reported. The relative acidities of amino acids and amino acid derivatives were usually determined under harsh conditions and high temperatures and often the conclusions drawn were contradictory. In many studies, using epimerization-forcing conditions of high temperatures (100 -120 °C), the rate of DKP epimerization was seen to be initially rapid but decreased over time. This was presumed to be due to hydrolysis of the DKP to the dipeptide. It was shown under these conditions for Gly-Ala dipeptide that equilibria exist between the DKP and dipeptides, H-Ala-Gly-OH, and H-Gly-Ala-OH.[82] This was also observed for aspartame (H-Asp-Phe-OMe) and the corresponding DKP. A detailed study of the decomposition and epimerization of aspartame as a function of pH and temperature showed rapid, pH-dependent interconversion of the dipeptide and DKP which was reflected in the changing rates of epimerization and hydrolysis of the individual species.[81]

Smith and Sol[49, 83] reported that in some dipeptides, the rate of racemization of amino acids in a carboxyl, C-terminal position was faster than in the amino N-terminal position at pH 7.6. This was attributed to neighboring group stabilization of the carbanion intermediate. However, Mittere and Kriausakul[84] reported that N-terminal isoleucine

epimerized faster than C-terminal Ile at pH 6. Furthermore, the rate of epimerization of Ile in DKP was found to be less than that for N-terminal Ile and similar to that of C-terminal Ile at pH 8. A detailed study by Gaines *et al*[81] of the rates of hydrolysis and epimerization of aspartame and the corresponding DKP lead to the proposed general order for the relative rates of racemization in free and peptide-bound amino acids in various ionic forms (Scheme 3.13).

Scheme 3.13:

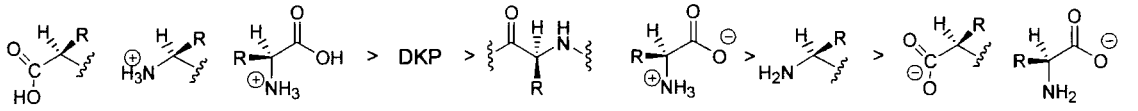

It was noted that the rates of racemization of amino acids (Asp and Phe) in the DKP was slower than that of the protonated N-terminal Phe in Phe-Asp dipeptide but more rapid than the un-protonated N-terminal amino acids in the dipeptide.[81] A study of the first order rate constants for racemization of the amino terminal of dipeptides, Gly-Ala, Ala-Gly and *cyclic*-Gly-Ala showed that the rate of racemization of the DKP (k_{rac} = 0.15 h^{-1}) was twice as fast as Gly-Ala, (k_{rac} = 0.066 h^{-1}), but nearly seven-fold faster than Ala-Gly dipeptide (k_{rac} = 0.020 h^{-1}).

A dipolar resonance of the amide linkage may significantly enhance the racemization rates in DKPs and at internal positions in peptides (Scheme 3.14), with longer peptide chains conveying greater stability to the resonance form thus increasing the rate of racemization at internal amino acid residues in central positions in peptide chains.

Scheme 3.14:

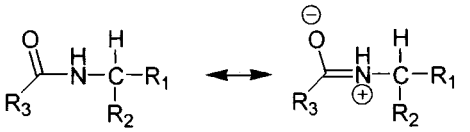

If this is the case, the rates of racemization of α-protons at internal amino acid residues are predicted to be comparable to or greater than those in DKPs. In support of this theory, it was found that in deuterium exchange reactions of the α-methylene protons of Gly-Gly-

Gly, Gly-Gly and glycine in D_2O at pD 13.3, monitored by ^1H NMR at 100 MHz, no deuterium exchange into glycine or the dipeptide was observed after 21 hours, however significant deuterium exchange into the internal amino acid residue of the tripeptide was detected after only five hours.[3, 85]

3.3.3 Epimerization involving diketopiperazines

It has been observed that in aqueous solution, the initial formation of a dipeptide is slower than the subsequent condensation of residues to form a peptide chain. Along with initial condensation, dipeptides and diketopiperazines.

Scheme 3.15:

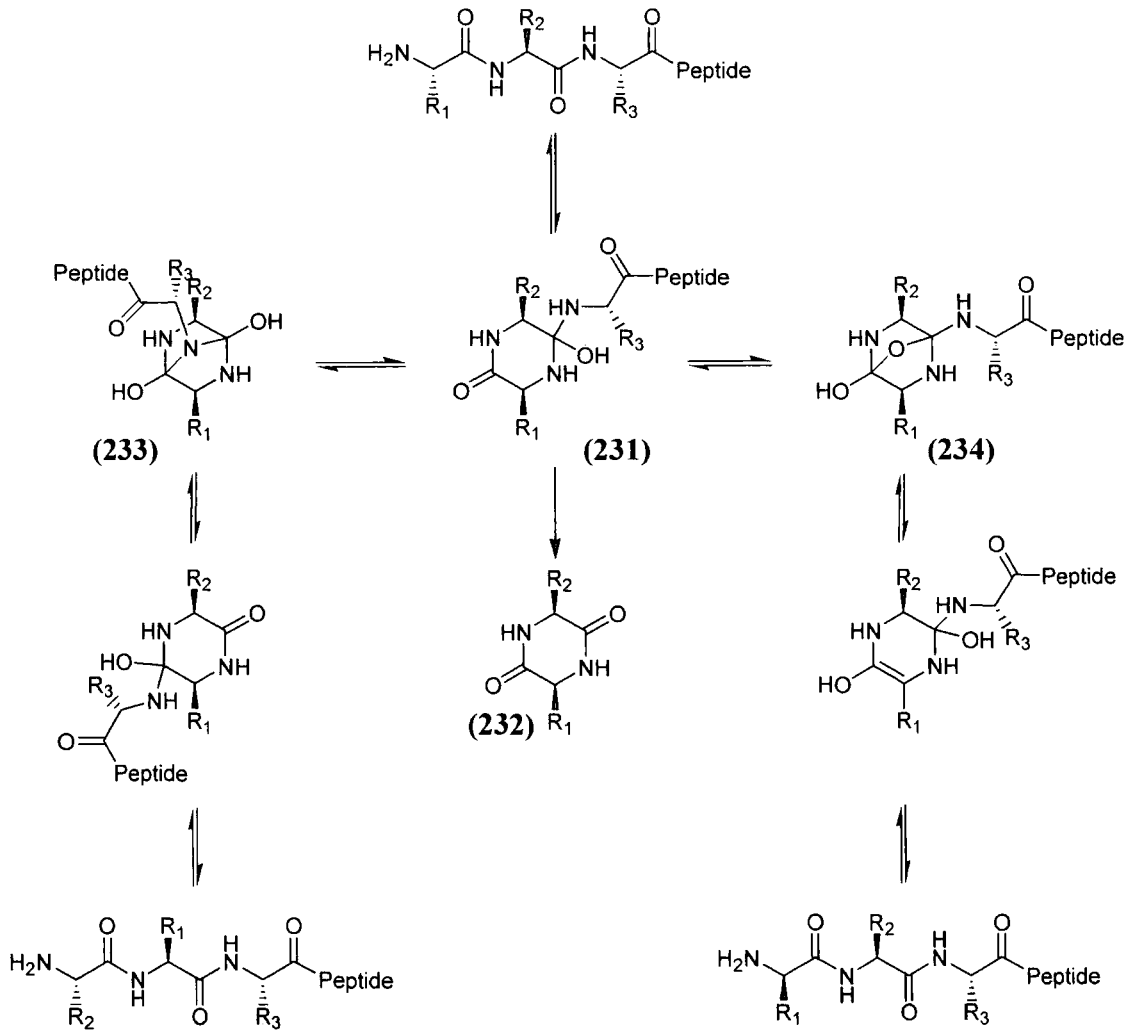

are formed via hydrolysis of the longer polypeptide chain.[86] Peptides containing a glycine residue in position 3 may undergo rearrangement *via* formation of DKP intermediates. This can involve sequence inversion of the first two amino acid residues and epimerization at position 1 (Scheme 3.15).[56, 87] Alternatively, peptides containing amino acids other than glycine at position 3 tend to favour epimerization over rearrangement. The proposed mechanism for these experimental observations involves attack of the *N*-terminal amino group on the carbonyl group of the second residue of the polypeptide sequence. The resulting tetrahedral DKP-like intermediate **(231)** may either decompose to the DKP **(232)** via chain scission. Alternatively, it can form a bicyclic structure by transannular attack on the first carbonyl group by the newly formed amino group **(233),** resulting in rearranged products, or it may form a bicyclic structure **(234)** by attack of the newly formed hydroxyl group on the carbonyl group leading to epimerized products. For many dipeptides cyclization to give the diketopiperazine competes with hydrolysis to form the free amino acids. However, in the simplest case of glycylglycine, cyclization to form the DKP was found to be less rapid than hydrolysis.[86] During the deuterium exchange reactions of Gly-Gly in D_2O at pD 8.2 – 9.2 at 25 °C, monitored by ^1H NMR there was no detectable (<5%) formation of 2,5-DKP. This was evident as formation of the diketopiperazine would result in scrambling of the initially incorporated deuterium at the more acidic N-terminal position such as the scrambling seen in Scheme 3.13. This shows that deuterium exchange into Gly-Gly does not occur through the formation of a low concentration of DKP that is in equilibrium with Gly-Gly dipeptide[3] Instead racemization of the dipeptide Gly-Gly occurs via deprotonation to form a planar enolate intermediate as described in Section 3.1.

3.3.4 Kinetic acidities of amino acids

There are few reliable estimates of the pK_a values for the α-protons of amino acids available in the literature. Rios *et al*[2, 3] estimated the k_{DO} values and subsequently the pK_a values for glycine and a number of glycine derivatives shown in Table 3.6. From this data a clear picture may be obtained as to the effect of the ionization state on the acidity of the

α-proton of the amino acid and its derivatives. It is also clear that the position of the α-proton in a peptide chain has a profound effect on the acidity of the proton. In agreement with the general order of reactivity proposed by Smith and Sol,[82] the rate constant for the hydroxide ion-catalyzed exchange reaction of the N-terminal α-amino proton of N-protonated Gly-Gly-Gly **(235)** (k_{HO} = 0.12, $M^{-1}s^{-1}$), is reported to be 590-fold larger than that for the internal α-amino proton of Gly-Gly-Gly **(236)** ($k_{HO} = 1.9 \times 10^{-4}$ $M^{-1}s^{-1}$).

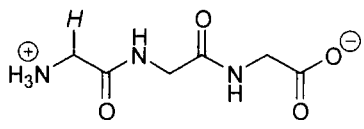

(235)

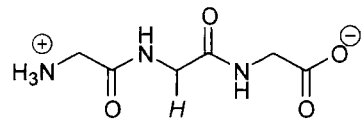

(236)

The effect of the presence of the terminal carboxylate anion of tripeptide **(236)** on the kinetic acidity of the internal proton is likely to be only a 4–5-fold decrease in the k_{HO} value and an even smaller effect is expected on the N-terminal α-carbon which is more shielded from interaction with the C-terminal carboxylate anion. Neutralization of the negative charge at acetylglycine to give acetylglycinamide results in a 4.7-fold increase in k_{HO} value for deuterium exchange into the acetyl methyl group. The separation of the acetyl methyl group and the anionic C-terminal of acetylglycine is similar to that of the internal α-CH_2 group and the anionic C-terminal of tripeptide **(236).** Therefore a similar increase in k_{HO} is expected to result from the shielding of the internal α-CH_2 groups from the anionic C-terminal of a polyglycine chain. Hence, the data suggests that, neglecting the local effects of conformation and microenvironment, the racemization reaction of N-protonated N-terminal amino acids residue at a protein or peptide is around 130-fold faster than that of an identical internal amino acid residue. This is in turn 20-fold faster than the racemization reaction of the free zwitterionic amino acid, (glycine zwitterion, $k_{HO} = 4.5 \times 10^{-5}$ $M^{-1}s^{-1}$).[71]

Table 3.6:

Amino Acid Derivative	k_{DO} ($M^{-1}s^{-1}$)[a]	k_{HO} ($M^{-1}s^{-1}$)[b]	pK_a[c]	reference
$^{+}H_3NCH_2CO_2Me$	6.0	4.1 *i*	21.0 ± 1.0	71
$^{+}Me_3NCH_2CO_2Me$	5.7×10^{2}	3.9×10^{2} *i*	18.0 ± 1.0	71
$^{+}H_3NCH_2CO_2^{-}$	8.9×10^{-5}	4.5×10^{-5} *i*	28.9 ± 0.5	71
$^{+}Me_3NCH_2CO_2^{-}$	6.6×10^{-4}	3.3×10^{-4} *ii*	27.3 ± 1.2	71
$CH_3CONHCHCO_2^{-}$	4.5×10^{-6}	2.3×10^{-6} *ii*	30.8	3
$CH_3CONHCHCO_2^{-}$	1.9×10^{-6}	9.5×10^{-7} *ii*	30.3	3
$CH_3CONHCHCONH_2$	2.1×10^{-5}	1.1×10^{-5} *ii*	23.9	3
$CH_3CONHCHCONH_2$	2.6×10^{-3}	1.3×10^{-3} *ii*	29.1	3
$^{+}H_3NCH_2CONHCH_2COO^{-}$	3.5×10^{-2}	1.8×10^{-2} *ii*	26.7	3
$^{+}H_3NCH_2CONHCH_2CONHCH_2CO_2^{-}$	0.23	0.12 *ii*	25.1	3
$^{+}H_3NCH_2CONHCH_2CONHCH_2CO_2^{-}$	3.9×10^{-4}	1.9×10^{-4} *ii*	25.9	3
N-protonated-L- proline-OMe	5.3	3.6 *i*	21 ± 1.0	4
L-proline zwitterion	-	-	29 ± 1.0[d]	4
Bis-L-proline DKP	8.89×10^{-3}	4.45×10^{-3} *ii*	22.6	e
Bis-D-proline DKP	9.27×10^{-3}	4.64×10^{-3} *ii*	22.5	e

(a) Second order-rate constant for deprotonation of the carbon acid by deuteroxide ion in D_2O. (b) Second order-rate constant for deprotonation of the carbon acid by hydroxide ion in H_2O, calculated from the value of k_{DO} using an estimated secondary solvent deuterium isotope effect of (*i*) k_{DO}/k_{HO} = 1.46 (*ii*) k_{DO}/k_{HO} = 2.0. (c) pK_a for ionization of the carbon acid in water at ionic strength I = 1.0 (KCl). (d) Estimated value. (e) Value obtained in this work.

Also shown in Table 3.6 are the estimated k_{DO} and k_{HO} values and pK_a of N-protonated proline methyl ester, determined in D_2O at 25 °C.[4] The carbon acid pK_a for N-protonated proline methyl ester is estimated to be the same as that for N-protonated glycine methyl

ester (pK_a = 21 ± 1.0). This is because the statistically corrected second order-rate constant for hydroxide ion-catalyzed deprotonation of one of the α-amino hydrogens of N-protonated glycine methyl ester (k_{HO} = 2.1 $M^{-1}s^{-1}$)[3] and N-protonated proline methyl ester (k_{HO} = 3.6 $M^{-1}s^{-1}$)[4] are expected to be at the same position on a good linear correlation between log k_{HO} for deprotonation of the α-carbonyl carbon of cationic ketones and esters and the pK_a of the corresponding carbon acid. The deuterium exchange reaction of the parent L-proline zwitterion has not been examined in the literature, however the very similar reactivity of N-protonated glycine methyl ester and N-protonated proline methyl ester as regards deprotonation by lyoxide ion shows that the effect of the bridging trimethylene group at proline zwitterion on carbon acidity is small. The conclusion that may be drawn is that the values of k_{HO} and pK_a for α-carbon deprotonation of proline zwitterion should be similar to $k_{HO} = 4.5 \times 10^{-5}$ $M^{-1}s^{-1}$ and pK_a = 28.9 ± 0.5 for glycine zwitterion.[3, 71] Therefore proline zwitterion is estimated to have a $pK_a = 29 \pm 1.0$[4] (Scheme 3.14)

Scheme 3.14:

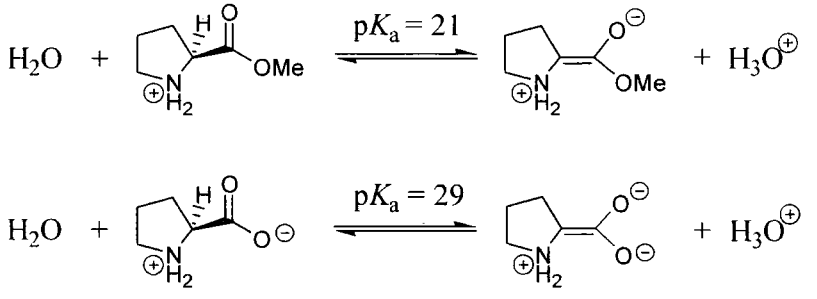

According to the k_{HO} values determined in this work for bis-L and bis-D-proline, (k_{HO} = 4.45×10^{-3} $M^{-1}s^{-1}$ and 4.64×10^{-3} $M^{-1}s^{-1}$ respectively) these species form relatively stable enolates in aqueous solution. There are no comparable values of k_{HO} for an analogous acyclic bis-proline dipeptide. However, as described previously for the pK_a of proline zwitterion, estimations for this can be made from the available literature information. The second order-rate constant for the hydroxide ion-catalyzed deprotonation of the N-terminal α-carbon of glycylglycine dipeptide is $k_{HO} = 1.8 \times 10^{-2}$ M^{-1} s^{-1}. It can be assumed that the 230-fold difference in reactivity between glycine methyl ester and

glycine dipeptide is similar to the difference in reactivity of proline methyl ester and proline dipeptide. This would give an estimated value for deprotonation at the N-terminal position of polyproline dipeptide of $k_{HO} = 1.58 \times 10^{-2}$ M^{-1} s^{-1}. However this value refers to deprotonation of the single α–hydrogen at the N-terminal of prolylproline whereas the data for proline DKPs is for deprotonation of two equivalent hydrogens. Thus the k_{HO} values determined for bis-L- and bis-D-proline in this work reported in Table 3.6 must be reduced by 2-fold to give k_{HO} values of 2.23×10^{-3} and 2.32×10^{-3} M^{-1} s^{-1} respectively, before comparison with the estimated value for prolylproline. Hence the N-terminal α–hydrogen of prolylproline is 5–fold more reactive towards deprotonation by hydroxide ion than either DKP **(218)** or **(219).** Values for deprotonation of the α–hydrogens at the C-terminal of prolylproline may not be estimated as analogous data for glycylglycine is not available. However the effect of DKP formation in **(218)** and **(219)** is to increase reactivity towards deprotonation by hydroxide ion by 51– fold relative to the predicted k_{HO} value of 4.5×10^{-5} M^{-1} s^{-1} for proline zwitterion. Finally the similar k_{HO} values for **(218)** and **(219)** is expected as the two DKPs are known to adopt similar conformations with the diketopiperazine ring in a boat conformation and the two pyrrolidine rings in near-planar conformations as discussed earlier. A different k_{HO} value could have been expected for the bis-D/L-proline DKP as in this case the diketopiperazine ring is planar and the two pyrrolidine rings have half-chair conformations.

3.3.5 pK_a values for bis-proline diketopiperazine

The second order-rate constants for deprotonation of the C3-H by hydroxide ion, ($k_{HO} = 4.45 \times 10^{-3}$ M^{-1} s^{-1} for DKP **(218)**, and 4.64×10^{-3} M^{-1} s^{-1} for DKP **(219)** were calculated from the respective experimental second order rate constants for deuteroxide ion-catalyzed deprotonation, k_{DO}, assuming a primary isotope effect of $k_{DO}/ k_{HO} = 2.0$ (see Section 3.2.3). A reverse rate constant for protonation of the DKP enolate cannot not be assigned using a clock as the k_{HO} values for **(218)** and **(219)** are greater than that for ethyl acetate $k_{HO} = 1.2 \times 10^{-3}$ M^{-1} s^{-1}. Thus the reverse rate of protonation of the DKP enolates is likely to be less than for protonation of the enolate of ethyl acetate. Protonation of the latter enolate by the conjugate acid of a series of quinuclidinium ions has been shown to

be diffusion controlled giving a Brønsted β-value of unity. Thus the reverse rate constant for protonation of the enolate of the DKP is likely less than diffusion controlled and would be subject to general base catalysis of exchange as in the case of glycine methyl ester where a Brønsted β = 0.91 for the formation of the corresponding enolate shows that reverse protonation is limited by proton transfer from the parent acid to a general base catalyst. Therefore, pK_a values must be extrapolated from the Brønsted plot of comparable carbon acids[75] (see Table 3.5 and Figure 3.14). A pK_a value of 22.6 for bis-L-proline DKP **(218)** and 22.5 for bis-D-proline DKP **(219)** were estimated from this plot. These values show an increase of 1.5 - 1.6 pK units from the pK_a value of 21.0 for N-protonated proline methyl ester. A much larger decrease of 6.4 – 6.5 pK units is expected from the estimated pK_a value of 29 for proline zwitterion. The estimated large increase in stability of the DKP enolate relative to the enolate of proline zwitterion is likely due the absence of charge in the parent cyclic dipeptide. Although formally neutral, proline zwitterion still has two distinct centres of charge. However there is a much smaller difference in pK_a between bis-proline DKP and the positively charged N-protonated proline methyl ester. The indication is that cyclization of the dipeptide to form a diketopiperazine significantly increases the stability of the enolate and hence increases the acidity of the C3-H.

References:

(1) Richard, J. P., Rios, A., Amyes,T. L., *J. Am. Chem. Soc.* **2000**, *122*, 9373.
(2) Rios, A., Richard, J. P., *J. Am. Chem. Soc.* **1997**, *119*, 8375.
(3) Rios, A., Richard, J. P., Amyes, T. L., *J. Am. Chem. Soc.* **2002**, *124*, 8251.
(4) Williams, G. M., E.P.; Amyes, T. L.; Wood, T. D.; Richard, J. P. *Biochemistry.* **2003**, *42*, 8354.
(5) Baba, J. L., Kvenvolden, K. A., Peterson, E., *Nature* **1973**, *245*, 308.
(6) Helfman, P. M., Baba, J. L., *Proc. Nat. Acad. Sci. U.S.A.* **1975**, *72*, 297.
(7) Caspó, J., Caspó-Kiss, Z., Wágner, L., Tálos, T., Martin, T.G., Folstad, S., Tivestan, A., Némethy, S., *Analytica Chemica Acta.* **1997**, *339*, 99.
(8) Sienberg, S. M., Masters, P. M., Baba, J. L., *Bioorg. Chem.* **1984**, *12*, 349.
(9) Stroud, E. D., Fife, D. J., Smith, G. G., *J. Org. Chem.* **1983**, *48*, 5268.
(10) Baum, R., Smith, G. G., *J. Am. Chem. Soc.* **1986**, *52*, 2248.
(11) Smith, G. G., Reddy G. V., *J. Org. Chem.* **1989**, *54*, 4529.
(12) Smith, G. G., Evans, R. C., Baum, R., *J. Am. Chem. Soc.* **1986**, *108*, 7327.
(13) Zhao, M., Baba, J. L., Ahern, T., *J. Bioorg. Chem.* **1989**, *17*, 36.
(14) Richard, J. P., Rios, A., Amyes,T. L., *J. Am. Chem. Soc* **2002**, *124*, 8251.
(15) Richard, J. P., Williams, G., O'Donoghue, A. C., Amyes, T. L. *J. Am. Chem. Soc.* **2002**, *124*, 2957.
(16) Yoshimura, T., Nobuyoshi, E., *J. Biosc. Bioeng.* **2003**, *96*, 103.
(17) Amyes, T. L., Richard, J. P. *J. Am. Chem. Soc.* **1996**, *122*, 9373.
(18) Brown, M. D., Häfliger *Determinations of Organic Structures by Physical Methods*, Braude and Nachod, Academic Press: New York, 1955.
(19) Hall *J. Am. Chem. Soc.* **1957**, *79*, 5441.
(20) Robins, J., Jones, M., Matisoo-Smith, E.; Auckland University, Private Bag 92019: Auckland, 2001.
(21) Wantabe, A., Yoshimura, T., Milami, B., Hayashi, H., Kagamiyama, H., Esaki, N., *J. Boil. Chem.* **1999**, *277*, 19166.
(22) O'Donoghue, A. C., Amyes, T. L., Richard, J. P., *Biochemistry.* **2005**, *44*, 2610.
(23) Fu, K. P., Neu, H. C., *Antimicrob. Agents Chemother.* **1978**, *13*, 358.
(24) Neu, H., Fu, K. P., Aswapokee, N., Asqapokee, P., Kung, K., *Antimicrob. Agents Chemother.* **1979**, *16*, 150.
(25) Miyoshi, T., Miyairi, N., Aoki, H., Kohnsaka, M., Sakai, H., Imanaka, H., *J. Antibiot.* **1972**, *25*, 569.
(26) Andoh, T. *Biochemie.* **1998**, *80*, 235.
(27) Dinsmore, C. J., Behore, D. C., *Tetrahedron* **2002**, *58*, 3297.
(28) Acharya, A. N., Ostresh, J. M., Houghten, R. A., *J. Comb. Chem.* **2001**, *3*, 612.
(29) Fdhila, F., Vázquez,V.,Sánchez, J. L., Riguera, R., *J. Nat. Prod.* **2003**, *66*, 1299.
(30) Stierle, A. C., Cardellina, J. H. II., Singleton, F. L., *Expermentia* **1988**, *44*, 1021.
(31) Young, P. E., Madison, V., Blout, E. R., *J. Am. Chem. Soc.* **1976**, *18*.
(32) Keil, B., Polonsky, J., nouaille, F., Lederer, E., *Helv. Chim. Acta.* **1975**, *58*, 4.
(33) Ginz, M., Engehardt, U. H., *J. Agric. Food Chem.* **2000**, *48*, 3528.
(34) Schmitz, F. J., Vandera, H. D. J., Hollenbeak, K. H., Enwall, C. E. L., Gopichand, Y., *J. Org. Chem.* **1983**, *48*, 3941.
(35) De Kievit, T. R., Barbara, H, Iglewski, B.H., *Infect. Immun.* **2000**, *8*, 4839.

(36) Degrassi, G., Aguilar, C., Bosco, M., Zaharev, S., Pongor, S., Venturi, V., *V. Curr. Microbiol.* **2002**, *45*, 250.
(37) Chin, D. N., Tayhas, G., Palmore, R., Whiesides, G. M., *J. Am. Chem. Soc.* **1999**, *121*, 2115.
(38) Adamson, D. W. *J. Chem. Soc.* **1943**, 39.
(39) Rosenmund, P., Kaiser, K., *Angew. Chem. Int. Ed. Engl.* **1970**, *9*, 162.
(40) Nitecki, D. E., Halpern, B., Westley, J. W., *J. Org. Chem.* **1968**, *33*, 864.
(41) Lee, S., Kanmera, T., Aoyagi, H., Izumiya., *Int. J. Peptide Protein Res.* **1979**, *1*, 207.
(42) Ueda, T., Saito M., Kato, T., Izumiya, N., *Bull. Chem. Soc. Jpn.* **1983**, *56*, 568.
(43) Suzuki, K., Sasaki, Y., Endo, N., Mihara, Y., *Chem. Pharm. Bull.* **1981**, *29*, 233.
(44) Lyrs, M. S., Lipton, M. A., *Bioorg. Med. Chem. Lett.* **1993**, *3*, 2061.
(45) Schoellkopf, U. *Tetrahedron* **1983**, *39*, 2085.
(46) González, A., Vorob'eva, S. L., Linares, A., *Tetrahedron: Asymmerty* **1995**, *6*, 1357.
(47) Bergeron, R. J., Phanstiel, O., Yao, G. W., Milstein, S., Weiar, W. R., *J. Am. Chem. Soc.* **1994**, *116*, 8479.
(48) Fridkin, M., Patchornik, A., Katchalsi, E., *J. Am. Chem. Soc.* **1965**, *87*, 4646.
(49) Flanigan, E., Marscha, G. R., *Tetrahedron Lett.* **1970**, 2403.
(50) Giralt, E., Eritja, R., Josa, J., Kuklinski, C., Pedroso, E., *Synthesis* **1985**, 181.
(51) Oesapay, G., Bouvier, M.,Taylor, J. W., *Tehniques in Protein Chemistry II* **1991**, 221.
(52) Kowalski, J., Lipton, M. A., *Tetrahedron Lett.* **1996**, *37*, 5839.
(53) Fischer, S., Dunbrack, R. L., Karplus, M., *J. Am. Chem. Soc.* **1994**, *116*, 11931.
(54) Song, S., Asher, S. A., Krimm, S., Shaw, K. D., *J. Am. Chem. Soc.* **1991**, *113*, 1155.
(55) Web, L. E., Lin, C. F., *J. Am. Chem. Soc* **1971**, *93*, 3818.
(56) Fischer, P. M. *J. Peptide Sci.* **2003**, *9*, 9.
(57) Corey, R. B. *J. Am. Chem. Soc.* **1938**, *60*, 1598.
(58) Balasubramanian, D., Wetlaufer, D. B., *J. Am. Chem. Soc* **1966**, *88*, 3449.
(59) Benedetti, E., Corradini, P., Goodman M., Pedone, C., *Proc. Natl. Acad. Sci. USA.*, **1969**, *62*, 650.
(60) Basu, G., Kubasik, M., Anglos, D., Kuki, A., *J. Phys. Chem.* **1993**, *97*, 3956.
(61) Napolitano, A., Bruno, I., Riccio, R., Gomez-Paloma, L., *Tetrahedron* **2005**, *61*, 6808.
(62) Duntas, L., Nelson, D. K., Gra, B. M., Rosenthals, J., Maier, V., *Neuropeptides* **1993**, *25*, 357.
(63) Martino, E., Lermark, A., Seo, H., Steiner, D. F., Refetoff, S., *Proc. Natl. Acad. Aci. USA.*, **1978**, *75*, 4265.
(64) Prasad, C., Mori,M., Wilber, J. F., *Peptides* **1982**, *3*, 591.
(65) Prasad, C., Matsui T., Peterkofski, A., *Nature* **1977**, *268*, 142.
(66) Wilber, J. F., Mori., Pegues, J., Prasad, C., *Trans. Assoc. Am. Physicians* **1983**, *96*, 131.
(67) Song, M. K., Rosenthal, M. J., Kang, K. W., *Diabetes Research* **1996**, *31*, 157.
(68) Toshihisa, U. M., S.;Tetsuo, K.; Nobuo, I. *Bull. Chem. Soc. Jpn.* **1983**, *56*, 568 - 572.

(69) Prasad, C. *Peptides* **1994**, *16*, 151.
(70) Pocker, Y. *Chem. Ind.* **1959**, 1383.
(71) Rios, A., Amyes, T. L., Richard, J. P., *J. Am. Chem. Soc* **2000**, *122*, 9373.
(72) Richard, J. P., Amyes, T. L., Toteva, M. M. *Acc. Chem. Res* **2001**, *34*, 981.
(73) Keefe, J. R., Kresge, A. J., *The Chemistry of Enols*; John Wiley and Sons: Chichester, 1990.
(74) Amyes, T. L., Richard, J. P. *J. Am. Chem. Soc.* **1992**, *114*, 10297.
(75) Amyes, T. L., Richard, J. P. *J. Am. Chem. Soc* .**1996**, *118*, 3129.
(76) Ciarkwolski, J. *Biopolymers* **1984**, *23*, 397.
(77) Degeilh, R., Marsh, R. E., *Acta. Crystallogr.* **1959**, *12*, 1007.
(78) Sletten, E. *J. Am. Chem. Soc.* **1970**, *92*, 172.
(79) Karle, I. L. *J. Am. Chem. Soc.* **1972**, *94*, 81.
(80) Siemion, I. Z. *Liebigs Ann. Chem.* **1971**, *748*, 88.
(81) Gaines, S. M., Bada, J. L., *J. Org. Chem.* **1988**, *53*, 2757.
(82) Smith, G. G., Evans, R. C., Baum, R., *J. Am. Chem. Soc.* **1987**, *108*, 7327.
(83) Smith, G. G., de Sol, B. S., *Science (Washington D.C.)* **1980**, *207*, 765.
(84) Mitterer, R. M., Kriausakul, N., *Org. Geochem.* **1984**, *7*, 91.
(85) Fridkin, M., Wilchek, M., Shinblatt, M., *Biochem. Biophys. Res. Commun.* **1970**, *38*, 458.
(86) Li, J., Brill, T. B., *J. Phys. Chem.* **2003**, *107*, 8575.
(87) Sepetov, N. F., Krymsky, M.A., Ovchinnikov, M.V., Bespalova; Z.D., Isakova, O.L., Soucek, M., Leb, l. M., *Peptide Res.* **1991**, *4*, 308.

Chapter 4

Thalidomide and analogues

4.0 Foreword.

A precedent was set in the pharmaceutical industry when in 1961 thalidomide was banned after it was identified as the cause of horrific birth defects in thousands of babies across the world. However, the effects of this drug are numerous and complex. It is now back in widespread use as a treatment for a myriad of diseases ranging from leprosy to cancer.

The numerous side effects associated with the use of this drug have encouraged the development of analogues of thalidomide, to maximise the therapeutic value of the molecule while reducing the negative side effects.

In this chapter the rates of racemization and rates of hydrolysis are reported for thalidomide and two analogues under consistent experimental conditions. This allows good comparison of rates of hydrolysis and gives information of the relative stereointegrity of the species investigated.

4.1 Introduction

Thalidomide **(237)** is a notorious compound in today's pharmaceutical industry as the most publicised example of the need for enantiomerically pure pharmaceutical products. The use of thalidomide **(237)** as a barbiturate replacement, and as an anti-nausea agent during early pregnancy in the 1950's caused the most horrific side effects. In the babies that survived to birth - around 10,000 children - thalidomide caused teratogenicity and neuropathy, blindness and deafness. This foetal fatality and/or extreme deformity lead to the complete ban of this drug in 1961. The teratogenic side effects were attributed to presence of the *S*-enantiomer[1] **(238)** in the racemic mixture dispensed, while the *R*-enantiomer **(239)** worked as the sedative drug required. However enantiomeric purification of thalidomide was found to be ineffective at alleviating this problem. The low stereointegrity displayed by thalidomide in the body implied that racemization occurred *in vivo*, making it impossible to separate the enantiomers.

Figure 4.1:

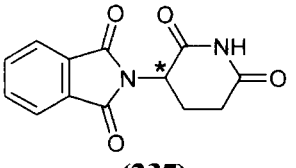

(237)

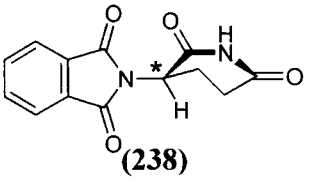

(238)

(-)-(*S*)-thalidomide

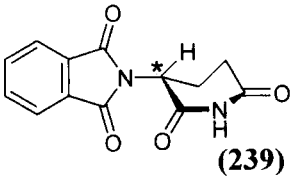

(239)

(+)-(*R*)-thalidomide

Despite the risks of use of this drug, thalidomide is still a prescribed drug today under very strict controls of usage. It is the treatment choice in countries such as Brazil for diseases like erythema nodosum leprosum, a complication of leprosy, and is effective in treating certain strains of Hansons Disease.[2, 3] This lead to approval of the drug by the FDA in 1998.

Since then the uses of thalidomide have increased dramatically. Areas of development include immunosupression in the treatment of graft V. host diseases[4, 5] and inflammatory dermatosis[6] Thalidomide also shows significant antiangiogenic activity[7, 8] and inhibition of (TNF)-α-release. This may be linked with a teratogenic capability and is associated predominantly with the *S*-enantiomer. The *R*-enantiomer is linked to the sedative and hypnotic effect associated with the drug. Little mechanistic information regarding the effects of thalidomide is available. The mechanism of action remains unknown, as do the effects of the separate enantiomers and metabolites, dose and concentration effects, despite the extensive biological studies that have been conducted. The latter studies have been reviewed in detail by Eriksson *et al.*[9]

The aqueous solubility of *Rac*-thalidomide is reported to be 50 μg mL^{-1} with a solubility up to five times higher for the pure enantiomers. Absorption of the drug is slow and the enantiomers undergo spontaneous hydrolysis and rapid chiral inversion at physiological pH. Breakdown of thalidomide in the body occurs predominantly via pH-dependant spontaneous hydrolysis in all body fluids. However the *S*-enantiomer is broken down significantly faster than the *R*-enantiomer. The overall half-life is around 8 hours in the body for both enantiomers.[9]

4.1.1 pH-Dependence of reactions of thalidomide

Breakdown of thalidomide is carried out mainly by pH-dependent, spontaneous hydrolysis in all body fluids, giving an apparent mean clearance of between 4 and 14 hours with the *S*-enantiomer exhibiting a slightly faster rate of decomposition than the *R*-enantiomer.[10] Enzymatic metabolism, and renal excretion do not appear to be major pathways for clearance of the drug.[11] All the substituted amide bonds on thalidomide are sensitive to hydrolysis at pH 7.4, however it was found that from pH 6-7 the phthalimide ring cleaves, while above pH 7 the glutarimide moiety hydrolyses. Both rates of inversion and hydrolysis are thought to increase with pH between pH 7-7.5.[12] The current literature suggests that inversion is twice is fast as hydrolysis in blood and plasma.[10] The enantiomers of thalidomide are not extensively bound to blood or plasma components in

the human body, however there is evidence that inversion of thalidomide is catalysed by Serum Albumin, and to a lesser extent human plasma. The hydrolysis is dependent on pH alone and it has not been found to be subject to catalysis from another source in the body.

4.1.2 Metabolism of thalidomide

In 1965 Schumacher *et al* reported that twelve hydrolysis products were formed from the splitting of amide bonds in thalidomide.[13] This was later followed by Reist *et al*[14] who reported that thalidomide underwent base-catalyzed inversion and hydrolysis, as did a number of it's hydrolytic metabolites (shown in Scheme 4.1). The main urinary metabolites found in humans in this study were 2-phthalimidoglutaramic acid, **(240)**, (about 50%) and α-(*o*-carboxybenzamido)glutarimide, **(241)** (about 30%). Teratogenic activity was found to be produced only by three metabolites, all of which contained the phthalimide moiety.

Scheme 4.1:

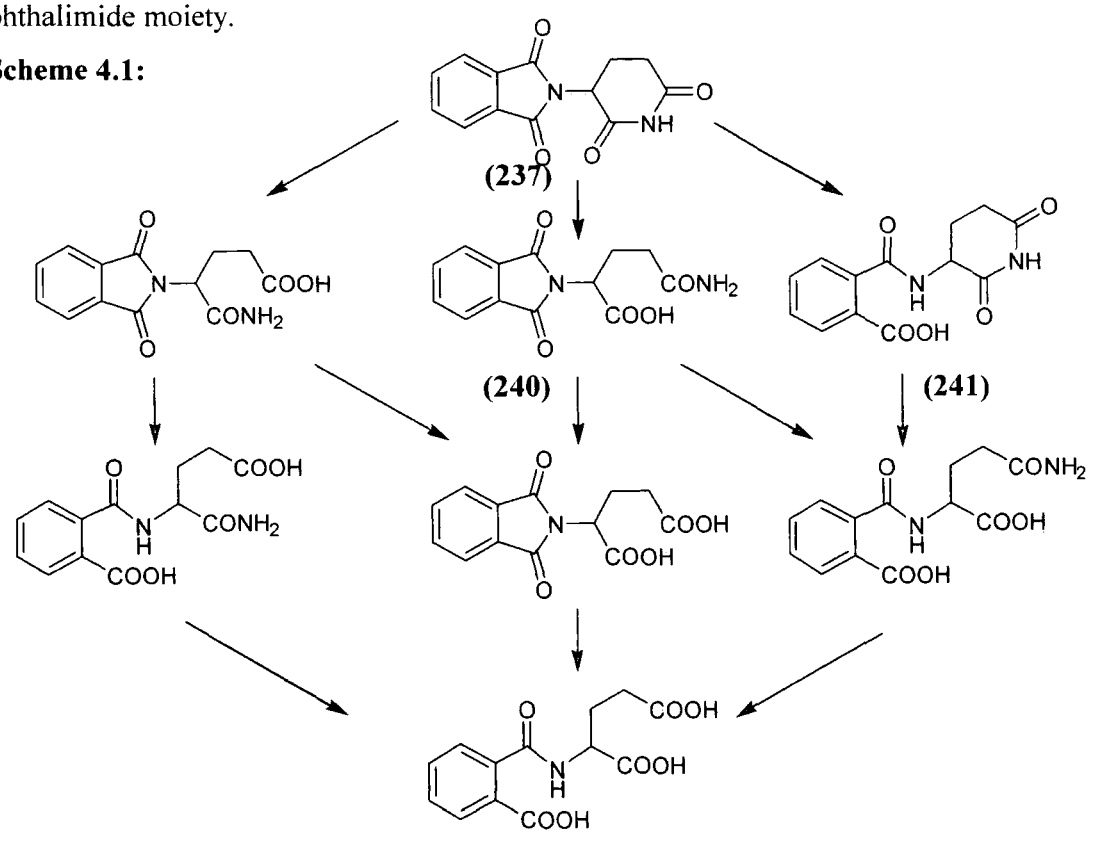

More recently, Meyring *et al*[15] used circular dichroism spectroscopy for the stereochemical characterization of hydroxylated metabolites, formed during *in vitro* biotransformation of thalidomide. It was determined that the chiral centre of thalidomide is unaffected by this stereoselective biotransformation process. Metabolism of the *R*-enantiomer produced mainly one metabolite, (3'*R*, 5'*R*)-*trans*-hydroxythalidomide, **(242)**, (see Scheme 4.2). This then spontaneously epimerizes to the more stable (3'*S*, 5'*R*)-*cis*-isomer, **(243)**. Conversely, the (*S*)-enantiomer is preferentially metabolized by hydroxylation of the phthalimide moiety, resulting in (*S*)-5-hydroxythalidomide, **(244)**. However numerous studies have reported that the levels of these and other metabolites found in human blood are very low.[9]

Scheme 4.2:

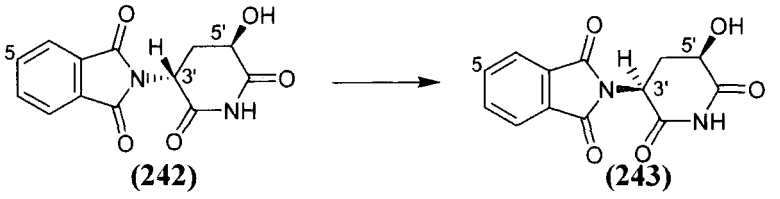

(242)

(3'*R*, 5'*R*)-*trans*-hydroxythalidomide

(243)

(3'*S*, 5'*R*)-*cis*-hydroxythalidomide,

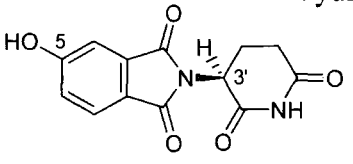

(244)

(*S*)-5-hydroxythalidomide

An interesting result of studies by Meyring *et al*[15] provided evidence that thalidomide itself was not toxic whereas the occurrence of toxicity was coupled with the presence of hepatic enzymes and an NADPH-generating system. This supports speculation that these metabolites may be important for the activation of thalidomide and may cause its teratogenicity, such as through bioactivation of thalidomide by embryonic prostaglandin-H synthase, causing oxidative damage to DNA,[16] or possible metabolic formation of a reactive arene-oxide intermediate which would be later converted to a less reactive phenol.[17]

4.1.3 Analogues of thalidomide

The many areas in which thalidomide has proven to be an effective treatment override the serious side effects produced by the drug. Analogues of thalidomide would seek to optimise the immunological and anticancer activity, while minimizing the sedative and other harmful side effects.

Tumour necrosis factor (TNF)-α is a cytokine involved in systemic inflammation. It is a member of the cytokine family, which stimulate the acute phase reaction. The primary role of (TNF)-α is in the regulation of immune cells. (TNF)-α causes apoptotic cell death, cellular proliferation, differentiation, inflammation, and viral replication. The disregulation, and particularly the overproduction of (TNF)-α has been implicated in a variety of human diseases, including cancer.[18] The ability of thalidomide to suppress or regulate the release of (TNF)-α has prompted the development of numerous analogues such as complex **(245)**[19] (see Figure 4.2) with the aim of improving thalidomide's anti (TNF)-α properties.

Figure 4.2:

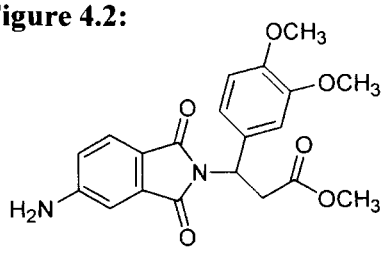

(245)

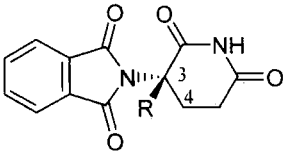

(246)

R = Me,Et,*n*-Pr
CHF_2,CF_3,F

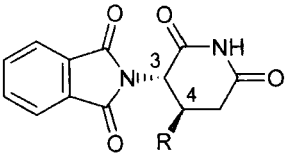

(247)

R = Alkyl, Aryl

As the teratogenic, sedative, or anti-inflammatory properties of thalidomide, are generally associated with only one enantiomer, the design and synthesis of configurationally stable analogues is of great importance. Optically stable analogues of thalidomide have been synthesized by quaternizing the stereogenic centre such as in complex **(246)**. C3 substituents such as alkyl groups,[20] fluoroalkyl groups[21] or a fluorine atom[20] have been successfully employed to this end. Yamada *et al*[22] reported high stereointegrity induced by the introduction of alkyl or aryl substituents in the β-position, such as in complex

(247). Epimerization in this case would lead to formation of an unfavourable *cis*-conformation. Under neutral or slightly acidic conditions (D_2O, 40° C, 8 hr) no deuterium incorporation was observed at the C3 position of derivative **(247)** by ^1H NMR spectroscopy, suggesting that β-substitution sufficiently disfavoured deprotonation leading to enolization at C3. Under basic conditions, (CD_3OD, catalytic amounts of Et_3N, 24 hr), the C3 proton was completely exchanged for deuterium. However there was still no evidence for the formation of the 3,4-*cis* isomer so stereointegrity was maintained.

4.1.4 Chemokine inhibitors.

Chemokines are small protein signalling molecules involved in the regulation of the immune system both during physiological host defence and in pathological inflammation conditions such as guest versus host disease and autoimmune disorders. As chemokines often act in a synergistic fashion, with different chemokines acting in parallel to promote inflammation, it is necessary to have a chemokine inhibitor which acts to inhibit a wide range of chemokines. To date the majority of chemokine inhibitors are limited to acting on one or a small subset of related chemokine receptors. In situations such as an inflammatory response, where several chemokines are active, selective inhibitors may be largely ineffective. A broad-spectrum chemokine inhibitor has so far remained elusive.

Reckless *et al* described a short peptide sequence known as *peptide-3*, derived from chemoattractant protein-1 (MCP-1), a human chemokine monocyte, which simultaneously inhibited activity of wide range of chemokines *in vivo*.[23] More recently, with a view to overcoming the physiological limitations of peptides, Fox *et al*[24] reported the design and synthesis of a series of non-peptide broad-spectrum chemokine inhibitors in the form of *N*-acyl-3-aminoglutarimides, of which compound **(248)** proved the most potent (see Figure 4.5).

Figure 4.5:

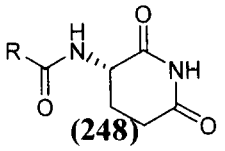

(248)

R = $(CH_2)_{\varnothing}CH{=}CH_2$

Compound **(248)** showed similar properties and potency to those of the short chain *peptide-3* described by Reckless *et al.*[23] It was discovered in this study that neither *peptide-3* nor compound **(248)** could bind to many chemokine receptors which would have been the expected method of inhibition. It is likely, then, that both *peptide-3* and the *N*-acyl-3-aminoglutarimides mediate chemokine inhibition by a mechanism which is yet unidentified and is distinct from that of simple receptor antagonists.

The 3-aminoglutarimide moiety is not commonly found in nature with the exception of in thalidomide. The broad chemokine inhibiting ability of this moiety may give insight into the mechanism by which thalidomide regulates the production of (TNF)-α, since other chemokine inhibitors are known to reduce (TNF)-α biosynthesis.[25]

One unresolved issue of this work is the stereointegrity of the *N*-acyl-3-aminoglutarimide compounds synthesised. As with thalidomide, the proton at the chiral centre is likely to be sufficiently acidic to exchange at an appreciable rate in a protic solvent, leading to racemization. This issue is addressed in this chapter. The generous gift of two such *N*-acyl-3-aminoglutarimides **(249)** and **(250)**, from Dr. David Fox (University of Warwick) enabled us to determine the rates of exchange of the acidic C3-H, and the rates of base catalyzed hydrolysis of these two acylaminolactams.

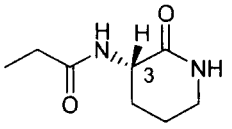

(249)
N-(2-Oxo-piperidine -3-yl)-propionamide

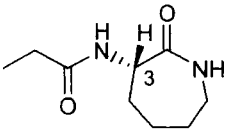

(250)
N-(2-Oxo-azepan-3-yl)-propionamide

The results of this work are reported in this chapter.

4.2.1 Deuterium exchange reactions followed by ^{1}H NMR spectroscopy

The H/D-exchange reactions of thalidomide **(237)**, and the propionamides **(249)** and **(250)** were analyzed using 300 MHz ^{1}H NMR spectroscopy. For propionamides **(249)** and **(250)** disappearance of the peak due to the C3-H in the ^{1}H NMR spectrum was monitored at 25 °C and at ionic strength I = 1.0 (KCl). From these ^{1}H NMR data the first and second order-rate constants for the deprotonation of substrate by deuteroxide ion to give the corresponding carbanion and hydrolysis of the substrate could be estimated. For thalidomide the disappearance of the peak due to the C3-H in the ^{1}H NMR spectra was monitored at 25 °C and ionic strength I = 0.5 (KCl) due to its low solubility in aqueous solution at ionic strength , I = 1.0 (KC).

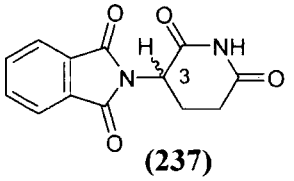

(237)

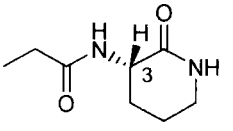

(249)

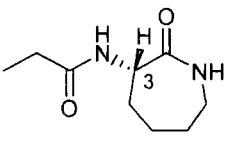

(250)

Scheme 4.3 shows a detailed mechanism for the deuteroxide ion-catalyzed exchange reaction of the propionamides **(249)** and **(250)**. The substrates **(251)** can be deprotonated by a base at the C3 position in D_2O solution to form the corresponding carbanion **(252)**. Resonance delocalization of the charge to oxygen yields the corresponding enolate **(253)**. As with azolium ions, low carbanion concentrations ensure the concentration of DOH formed during this process is negligible in solvent D_2O which means that reprotonation by DOH will also be negligible. Thus deprotonation at C3 and hence enolate formation can be followed by effectively irreversible formation of the deuterium exchange product **(254)**. A similar mechanism is followed in the case of thalidomide **(237)**, leading, in all three cases to a racemic mixture of deuterated products.

Scheme 4.3:

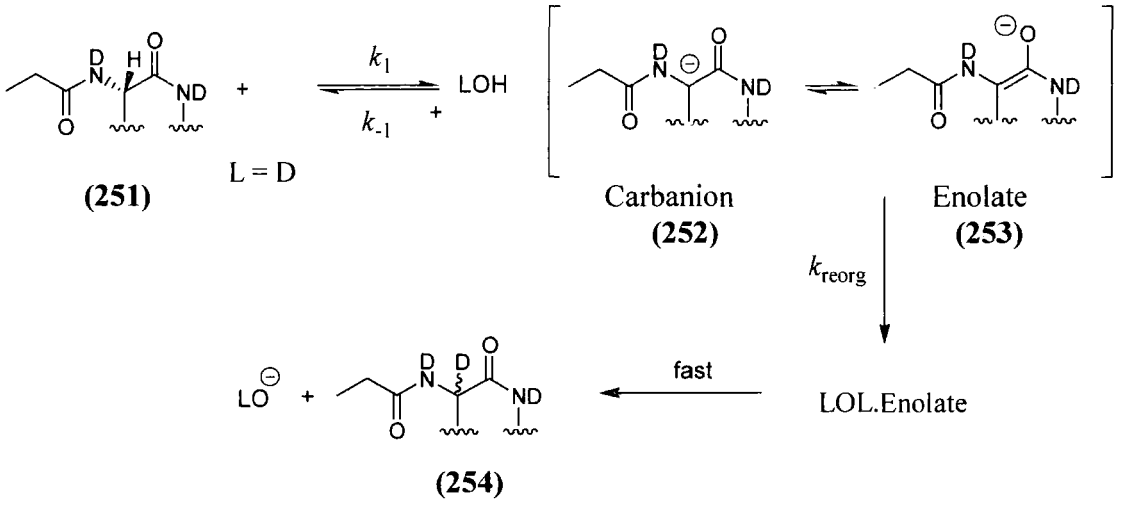

As expected, a competing hydrolysis reaction was observed for thalidomide **(237)** producing potentially a number of hydrolysis products detailed in Section 4.1 (Scheme 4.1). A competing hydrolysis reaction was also observed in the case of propionamides **(249)** and **(250)**.

A likely mechanism for this hydrolysis reaction for the propionamides is shown in Scheme 4.4 for propionamide **(249)** and it is expected to be similar for the seven membered ring analogue **(250)**. Nucleophilic attack of deuteroxide ion at the carbonyl carbon of propionamide **(249)**, would initially give a tetrahedral intermediate **(255)**. Subsequent ring opening of this intermediate by D_2O would most likely occur at N1 resulting in formation of the amino acid **(256)** as a carboxylate anion. This is the most likely product of the hydrolysis reaction according to the ^1H NMR spectra obtained as large chemical shift changes were observed in peaks due to the ring hydrogens. In support of this observation, the ring amide carbonyl, (C2), is likely to be more electrophilic than the propionyl amide carbonyl group. The former has a σ-electron withdrawing nitrogen β to the carbonyl carbon on the opposite side to N1, while the latter carbonyl does not. Further hydrolysis of anion **(256)** is not expected as it is significantly less electrophilic than the parent propionate due to the negative charge of the carboxylate group.

Scheme 4.4:

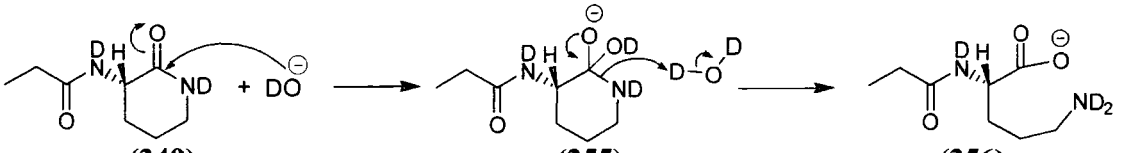

(249) **(255)** **(256)**

A typical exchange experiment for propionamides **(249)** and **(250)** was run in deuteroxide solution in D_2O at 25 °C and ionic strength I = 1.0 (KCl) and was quenched at different time points during the reaction. The signal due to the C3-H of the substrates appears as a triplet in the range 4.2 – 4.6 ppm signal and decays during the reaction due to both deuteroxide ion-catalyzed exchange and hydrolysis of the substrates. The C5-H of unexchanged hydrolysis product **(256)** is far less acidic than C3-H of **(249)** or **(250)** as it is α to a carboxylate anion.[26,‡] The signal due to this proton appears upfield in the range 3.9 – 4.2 ppm. The upfield shift in the ^{1}H NMR spectrum supports a reduction in acidity of this proton as it is more shielded in **(256)** than in the parent acids **(249)** and **(250)**. Further transformations were apparent in the ^{1}H NMR spectra due to hydrolysis of the substrates. A full description of the ^{1}H NMR spectra for propionamides **(249)** and **(250)** is detailed in Section 4.2.2 – 3.

Due to the lower solubility of thalidomide compared to the analogues **(249)** and **(250)** a typical exchange experiment for thalidomide **(237)** was run in D_2O at 25 °C and ionic strength I = 0.5 (KCl). The pD was maintained in the range 6.59 – 9.24 by the use of various buffers. Aliquots were quenched at different time points during the reaction. As discussed in Section 4.1, all the substituted amide bonds of thalidomide are susceptible to hydrolysis at pH 7.4 *via* a similar mechanism to that shown in Scheme 4.2. From pH 6-7

‡ The second order rate constant for deuteroxide ion-catalyzed exchange of an α-hydrogen of acetate anion for deuterium (k_{DO} =8.4 × 10^{-9} $M^{-1}s^{-1}$) is 2260-fold smaller than acetamide (k_{DO} = 1.9 × 10^{-5} $M^{-1}s^{-1}$).[26] A similar difference in reactivity towards deuteroxide ion-catalyzed exchange is expected between the C5 and C5 α-hydrogens of hydrolysis product **(256)** and propionamides **(249)** or **(250)** respectively. [26]

the phthalimide ring cleaves, while above pH 7 the glutarimide moiety is believed to hydrolyse.[12] The possible hydrolysis products are detailed in Scheme 4.1. We have not confirmed the identity of the hydrolysis product(s) under our conditions by using other methods, however given the large change in the chemical shifts of peaks due to aryl hydrogens, it is most likely that hydrolysis of the phthalimide moiety is occurring. If hydrolysis was occurring more remotely from the aryl ring the glutarimide moiety, a smaller change in chemical shift would have been expected.

As with the reactions involving azolium ions, the internal standard used in propionamide experiments was tetramethylammonium deuterio-sulphate (TMADS). The internal standard used in thalidomide experiments was *t*-butanol. The signal due to the twelve methyl hydrogens of the internal standard tetramethylammonium deuteriosulfate, appears as a broad singlet at 3.2 – 3.0 ppm. The signal due to the nine methyl hydrogens of *t*-butanol appears as a broad singlet at 1.13 ppm. The hydrogens of neither internal standard undergo exchange in the reaction conditions investigated.[27]

The progress of reactions for parent acids **(249)** and **(250)** was monitored by determining the integrated area of a substrate peak due to the relevant acidic hydrogen over time relative to the integrated area of peaks due to internal standard which is at a constant concentration throughout the experiment. The fraction of substrate remaining $f(s)$, was determined from Equation 4.1.

$$f(s) = \frac{(A_p/A_{IS})_t}{(A_p/A_{IS})_{t=0}} \qquad \textbf{(Equation 4.1)}$$

The observed pseudo-first-order rate constants for total disappearance of substrate due to both hydrolysis and exchange, k_{obs}, was determined as the slope of semi-logarithmic plots of H/D exchange progress against time (Equation 4.2). Isolated peaks for hydrolysis product permitted the determination of pseudo first order rate constants for hydrolysis only, hence allowing the extraction of a rate constant for exchange only from k_{obs}.

$$\ln f(s) = -k_{obs}t \qquad \textbf{(Equation 4.2)}$$

The pseudo-first-order rate constant for deuterium exchange only is formally the sum of the first order rate constants for exchange catalyzed by solvent, deuteroxide ion and buffer base (Equation 4.3).

$$k_{obs} = k_{D2O} + k_{DO}[DO^-] + k_B[B^-] \qquad \textbf{(Equation 4.3)}$$

In contrast to azolium ions, the contribution of the buffer term ($k_B[B^-]$, s^{-1}) is likely to be significant in these reactions as a stable enolate intermediate potentially forms on deprotonation of the parent acid. The contribution of buffer catalysis has not been fully investigated for these substrates.

4.2.2 N-(2-Oxo-piperidine-3yl)propionamide (249)

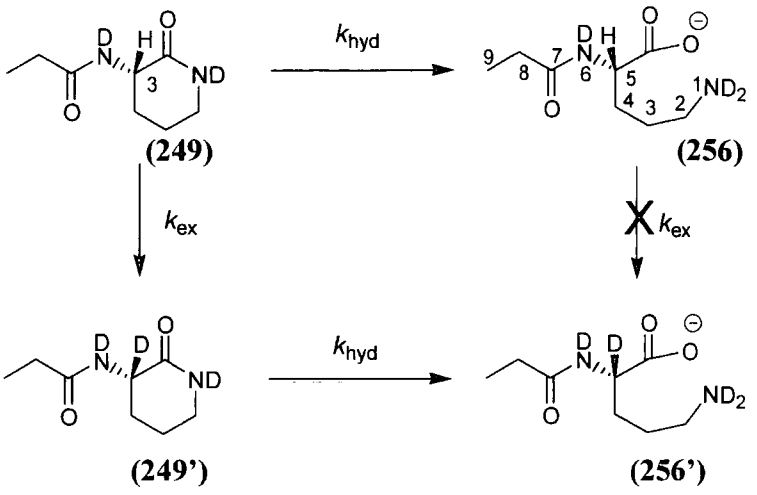

Rates of deuteroxide ion-catalyzed exchange of propionamide **(249)** to form the corresponding deuterated product **(249')** and hydrolysis to form the corresponding amino acids **(256)** were determined by 300 MHz ^{1}H NMR spectroscopy. H/D-exchange is unlikely to occur at C5 in hydrolysis product **(256)** as the acidic proton is α to a carboxylate and so is less acidic than C3-H of **(249)**, therefore any exchange of the C3-H would have occurred prior to hydrolysis.

Figure 4.4 shows representative ^{1}H NMR spectra of propionamide **(249)** (10 mM, 15mM KOD) obtained during the exchange for deuterium of the C3-H in D_2O at 25 °C and ionic strength I = 1.0 (KCl). The signal due to the C3-H appears as an asymmetric triplet at 4.30 – 4.40 ppm (A) due to coupling to the two C4 protons. The signal due to the C6-H_2 appears as a broad quartet at 3.30 – 3.45 ppm (B) due to coupling to C5-H_2, and perhaps long range coupling to the C4-hydrogens or some slight non-equivalence in the C6 or C5-hydrogens. The signal due to the internal standard (TMAHS) appears as a broad singlet at 3.33 ppm. The signal due to the CH_2 group of the ethyl protons of the propionyl side chain appears as a quartet at 2.35 ppm (C) due to coupling to the methyl protons of the propionyl group. The signal due to the C4-H_2 appears as a multiplet at 2.05 – 2.20 ppm (D). The signal due to C5-H_2 appears as a multiplet at 1.75 – 2.05 ppm (E). In the

reactant propionamide **(249)**, the C4 hydrogens are close to both an electron withdrawing nitrogen as well as a carbonyl and are expected to produce a peak with a more downfield chemical shift. However upon hydrolysis this order of chemical shift should reverse as the C4 hydrogens of hydrolysis products are closer to the 'more shielding' negatively charged carboxylate group than the C3 hydrogens. Accurate coupling constant values could not be extracted from the two multiplets (D) and (E) and thus confirmation of chemical shift assignments could not be obtained.

Deuterium exchange at C3 and hydrolysis of the substrate results in the disappearance of the triplet due to C3-H. This is coupled to the appearance of a double doublet at 4.10 – 4.20 ppm (A') due to the C5-H of amino acid **(256)**, which is coupled to the two adjacent non-equivalent C4 protons. It is expected that the change of hydrogen for deuterium at C3 of **(249)** and C5 of **(256)** to give **(249')** and **(256')** will not change the chemical shifts of peaks due to all other hydrogens of reactant and hydrolysis product. Thus any new peaks appearing over time are due to hydrolysis product only. The decay of the asymmetric quartet due to C6-H_2 (B) is matched by the growth of a triplet at 2.75 ppm (B') due to the C2 hydrogens of **(256)** and **(256')**, which are coupled to the adjacent C3 protons. The quartet due to the CH_2 hydrogens of the propionyl group (C) splits into two quartets at 2.35 ppm over the course of the reaction.[26,‡] The decay of the signal due to the C4-H_2 of **(249)** (D) is matched by the growth of a quintet at 1.55 ppm (D') due to the C4 hydrogens of **(256)** and **(256')**, due to coupling to the adjacent C3 and C5 hydrogens. Finally the multiplet due to the C5-H_2 of **(249)** at 1.75 – 2.05 ppm evolves into a larger multiplet at 1.65 – 2.05 ppm, which includes peaks due to the C3 hydrogens of **(256)** and **(256')**.

‡ There is a difference of 0.8 ppm upfield movement in chemical shift between the α-methyl protons of dimethylacetate (δ 2.06 ppm) and acetate anion (δ 1.98 ppm).[1] In the present case, the much smaller < .0.1 ppm dowield shift of the quartet due to the CH_2 as the reaction occurs is evidence that parallel hydrolysis is not occurring at the propionyl carbonyl in addition to at the ring, as an upfield chemical shift would be expected upon the formation of propanoate from the propionamide.

Figure 4.4: Representative ^{1}H NMR spectra at 300 MHz of propionamide (249) (10mM, 15mM KOD), obtained during exchange of the C3-H for deuterium and hydrolysis at C2 in D_2O at 25 °C and ionic strength I = 1.0 (KCl). The extent of deuterium exchange is indicated above each spectrum.

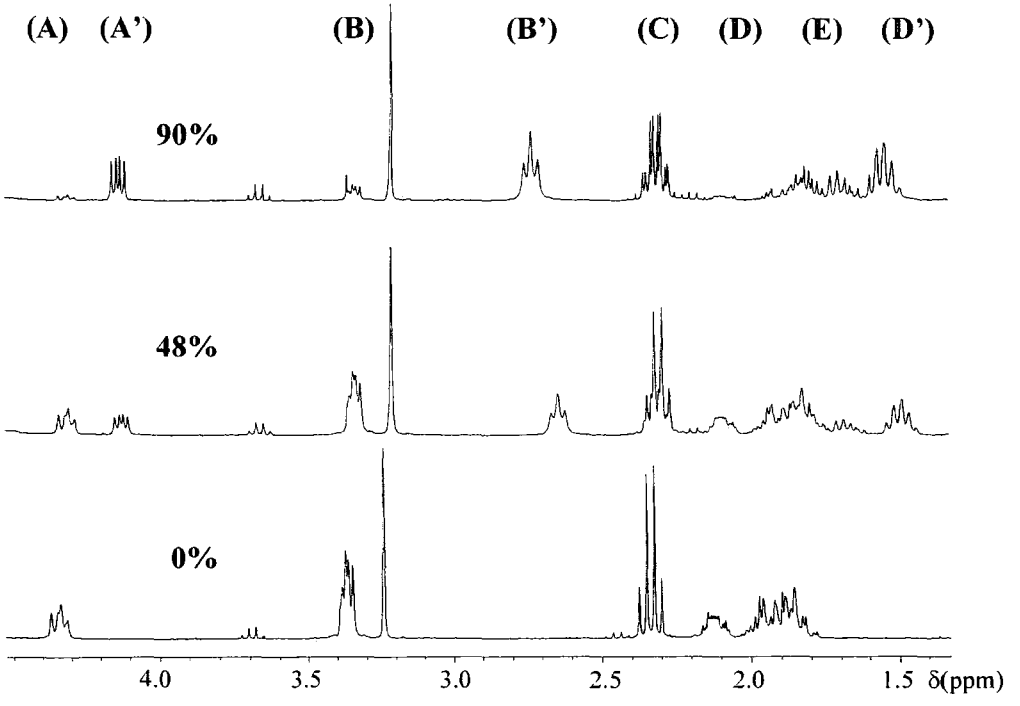

Reaction data and the experimental first-order rate constants for deuterium exchange and hydrolysis (k_{obs}, s^{-1}) at different concentrations of deuteroxide solution are shown in Tables 4.1 and 4.2 respectively. The values for k_{obs} (s^{-1}) shown in Tables 4.2 are obtained from the slopes of semilogarithmic plots (Figure 4.5) of the fraction of unreacted substrate f(s) against time. The observed rate constant of decay of the peak due to C3-H of **(249)**, (k_{obs}, s^{-1}) is the total loss of substrate due to both deuteroxide ion-catalyzed hydrolysis and deuterium exchange at C3. The observed rate constant for hydrolysis ($k_{hydrolysis}$, s^{-1}) of **(249)** to form hydrolysis product **(256)** with a hydrogen at the C3

position was calculated from the slopes of semilogarithmic plots (Figure 4.6) of $f(s')$ (Equation 4.4) against time.

$$f(s') = \left(\frac{\frac{A_{C3\text{-}H(t=0)}}{A_{IS(t=0)}} - \frac{A_{C5\text{-}H(t)}}{A_{IS(t)}}}{\frac{A_{C3\text{-}H(t=0)}}{A_{IS(t=0)}}} \right) \qquad \textbf{(Equation 4.4)}$$

In Equation 4.1 $A_{C3\text{-}H(t=0)}$ is the total area of the peak due to the C3-H at 0% reaction, and $A_{C5\text{-}H(t)}$ is the area of the peak due to the C5-H of **(256)** at different time points as the reaction progressed and A_{IS} is the area of the peak due to the internal standard.

Table 4.1: Analysis of reaction data for the deuterium exchange at C3-H and hydrolysis of propionamide (249) in deuteroxide solution in D_2O at 25 °C and ionic strength I = 1.0 (KCl).

$[DO^-]^a$ (M)	Time (secs)	$f(s)^b$	$f(s')^c$	ln $f(s)$	ln $f(s')$
0.015	0	1	1.000	0.000	0.000
	5.20×10^3	0.872	0.914	-0.137	-0.090
	1.31×10^4	0.753	0.816	-0.284	-0.204
	1.44×10^4	0.759	0.819	-0.276	-0.200
	1.72×10^4	0.712	0.783	-0.340	-0.245
	1.96×10^4	0.674	0.746	-0.395	-0.293
0.025	0	1.000	1.000	0.000	0.000
	5.22×10^3	0.712	0.716	-0.340	-0.334
	1.31×10^4	0.538	0.594	-0.620	-0.520
	1.48×10^4	0.459	0.426	-0.779	-0.854
	1.72×10^4	0.444	0.322	-0.812	-1.132
	1.96×10^4				
0.030	0	1.000	1.000	0.000	0.000
	4.50×10^3	0.684	0.801	-0.380	-0.222
	9.00×10^3	0.536	0.599	-0.625	-0.513
	1.39×10^4	0.357	0.556	-1.031	-0.587
	1.84×10^4	0.257	0.504	-1.360	-0.685

(a) Measurements were made in KOD solution in the 0.015 – 0.030 M range. (b) The fraction of unexchanged substrate remaining $f(s)$, after reaction due to both hydrolysis and exchange was calculated according to Equation 4.1 Measurements were made at an initial substrate concentration of 10 mM. (c) The fraction of substrate remaining after reaction due to hydrolysis only $f(s')$, was calculated according to Equation 4.4.

The first order-rate constant for the deuteroxide ion-catalyzed exchange of the C3-H for deuterium, ($k_{exchange}$, s^{-1}) was calculated using Equation 4.5.

$$k_{exchange} = k_{obs} - k_{hydrolysis} \qquad \textbf{(Equation 4.5)}$$

Table 4.2: First order rate constants for the deuterium exchange at C3-H and hydrolysis of propionamide (249) in deuteroxide solution in D_2O at 25 °C and ionic strength I = 1.0 (KCl).

$[DO^-]$ (M)	k_{obs} $(s^{-1})^a$	$k_{hydrolysis}$ $(s^{-})^b$	$k_{exchange}$ $(s^{-1})^c$
0.015	1.92×10^{-5}	1.43×10^{-5}	4.91×10^{-6}
0.025	4.66×10^{-5}	3.76×10^{-5}	9.00×10^{-6}
0.030	7.30×10^{-5}	6.08×10^{-5}	1.27×10^{-5}

(a) The value of the first-order rate constant (k_{obs}) for the total disappearance of substrate was obtained from the slope of the plot of $\ln f(s)$ against time shown in Figure 4.5. (b) The value of the first order rate constant for the formation of hydrolysis product **(256)** ($k_{hydrolysis}$) was obtained from the slope of the plot of $\ln f(s')$ against time shown in Figure 4.8. (c) The value of the first order rate constant for deuterium exchange of the C3-H ($k_{exchange}$) was obtained using Equation 4.5.

Figure 4.5: Semi-logarithmic plot of the fraction of remaining C3-H against time of propionamide (249) in deuteroxide solution at 0.015 M (♦), 0.025 M (■), and 0.03 M (▲) at 25 °C and ionic strength I = 1.0 (KCl).

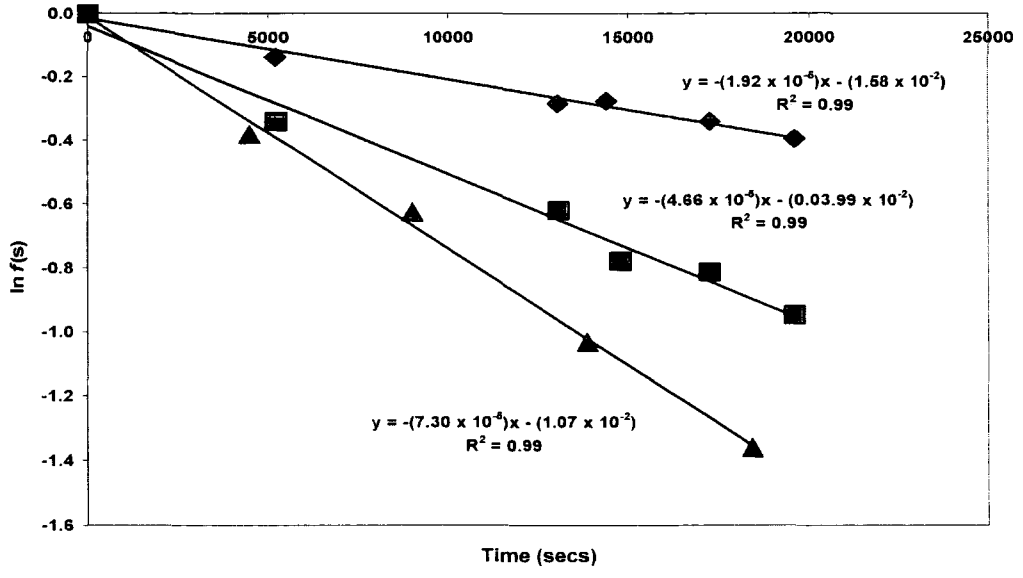

Figure 4.6: Semi-logarithmic plot of the decay of C3-H of propionamide (249) due to the formation of hydrolysis product (256) against time in deuteroxide solution at 0.015 M (♦), 0.025 M (■), and 0.03 M (▲) at 25 °C and ionic strength I = 1.0 (KCl).

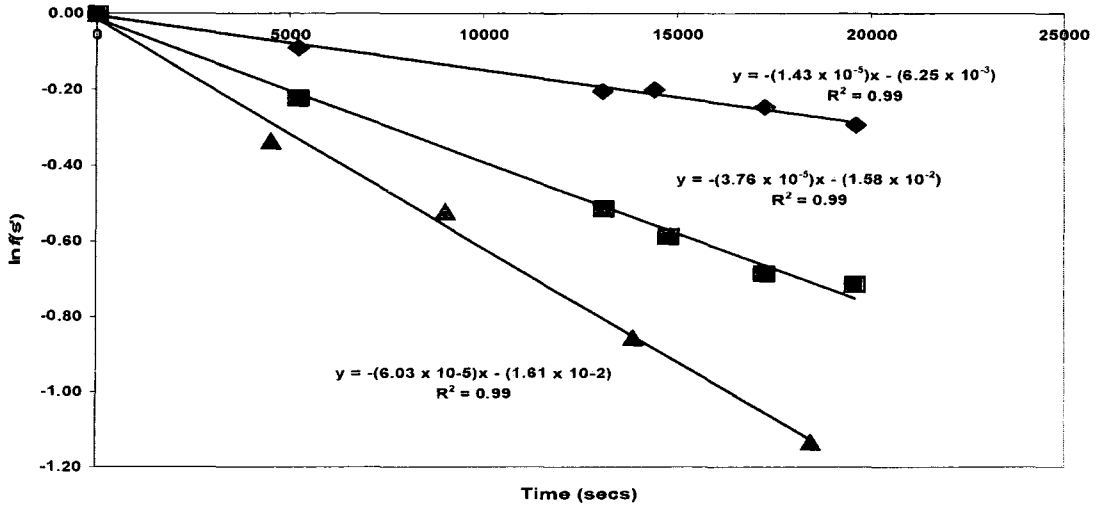

The second-order rate constant for total loss of propionamide **(249)** was calculated from the slope of the plot of k_{obs} against the concentration of deuteroxide ion (Figure 4.7, (♦)) The second-order rate constant for hydrolysis of propionamide **(249)** to form amino acid **(256)** was calculated from the slope of $k_{hydrolysis}$ against the concentration of deuteroxide ion (Figure 4.8, (■)). The second-order rate constant for the deuteroxide ion-catalyzed deuterium exchange of C3-H was calculated from the slope of the plot of the calculated values k_{ex} against the concentration of deuteroxide ion (Figure 4.7,(▲)).

Figure 4.7: Plot of k_{obs}, (♦), $k_{hydrolysis}$, (■) and $k_{exchange}$, (▲) against [DO⁻] for the reaction of propionamide (249) in D_2O at 25 °C and I = 1.0 (KCl).

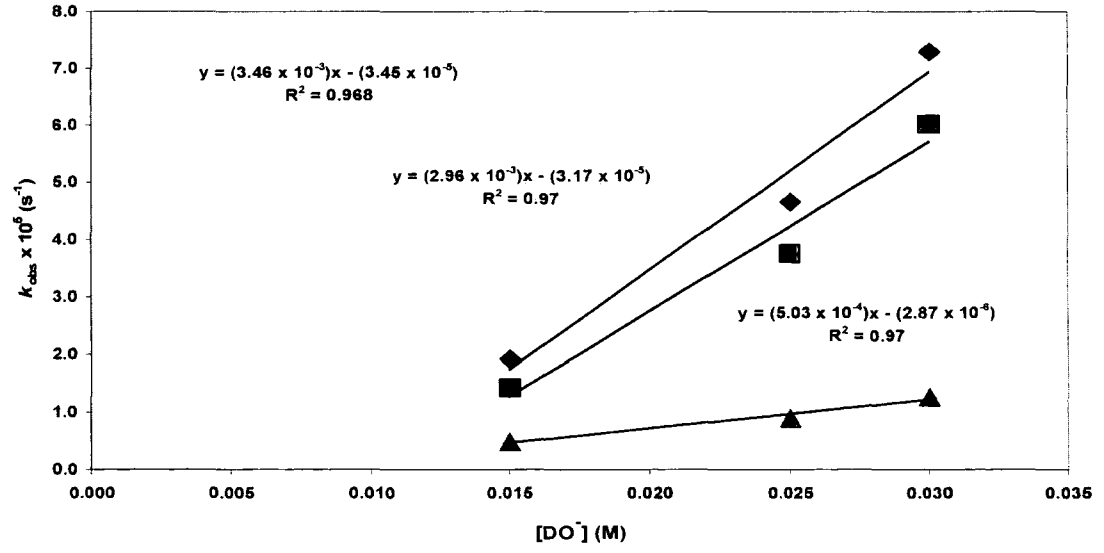

The second-order rate constant for total loss of propionamide **(249)** was calculated as k_{total} = 3.46 × 10^{-3} $M^{-1}s^{-1}$. The second-order rate constant for the hydrolysis of **(249)** to give amino acid **(256)** was calculated as k_{hyd} = 2.96 × 10^{-3} $M^{-1}s^{-1}$, which is six times greater than the calculated rate for deuteroxide ion-catalyzed H/D-exchange at C3 which was estimated to be k_{DO} = 5.30 × 10^{-4} $M^{-1}s^{-1}$.

However, the second order plots in Figure 4.7 have substantial negative y-axis intercepts. This could be due to either error in the NMR analysis or to a higher dependence of k values (s^{-1}) on the concentration of deuteroxide ion as in Equation 4.6 A plot of k (s^{-1})/[DO^-] against [DO^-] should be linear for the second order dependence on deuteroxide ion concentration (Equation 4.7), and would yield as intercept k_{total}, k_{hyd} or k_{DO} respectively.

$$k = k_2[DO^-] + k_3[DO^-]^2 \qquad \textbf{(Equation 4.6)}$$

$$k/[DO^-] = k_2 + k_3[DO^-] \qquad \textbf{(Equation 4.7)}$$

These plots are show in Figure 4.8 and yield the following values: k_{total} = 1.31 × 10^{-4} $M^{-1}s^{-1}$; k_{Hyd} = 1.0 × 10^{-4} $M^{-1}s^{-1}$; k_{DO} = 2.31 × 10^{-4} $M^{-1}s^{-1}$. The plots in Figure 4.8 give poorer linear correlations than those in Figure 4.7, and also yield a k_{DO} value that is higher than both k_{total} and $k_{hydrolysis}$. However the data has been obtained at only three concentrations of deuteroxide ion. Data at a wider range of concentrations would be required to conclusively confirm whether a higher order dependence on [DO^-] exists.

Figure 4.8: **Plot of $k_{obs}/[DO^-]$, (♦), $k_{hydrolysis}/[DO^-]$, (■) and $k_{exchange}/[DO^-]$, (▲) against $[DO^-]$ for the reaction of propionamide (249) in D_2O at 25 °C and I = 1.0 (KCl).**

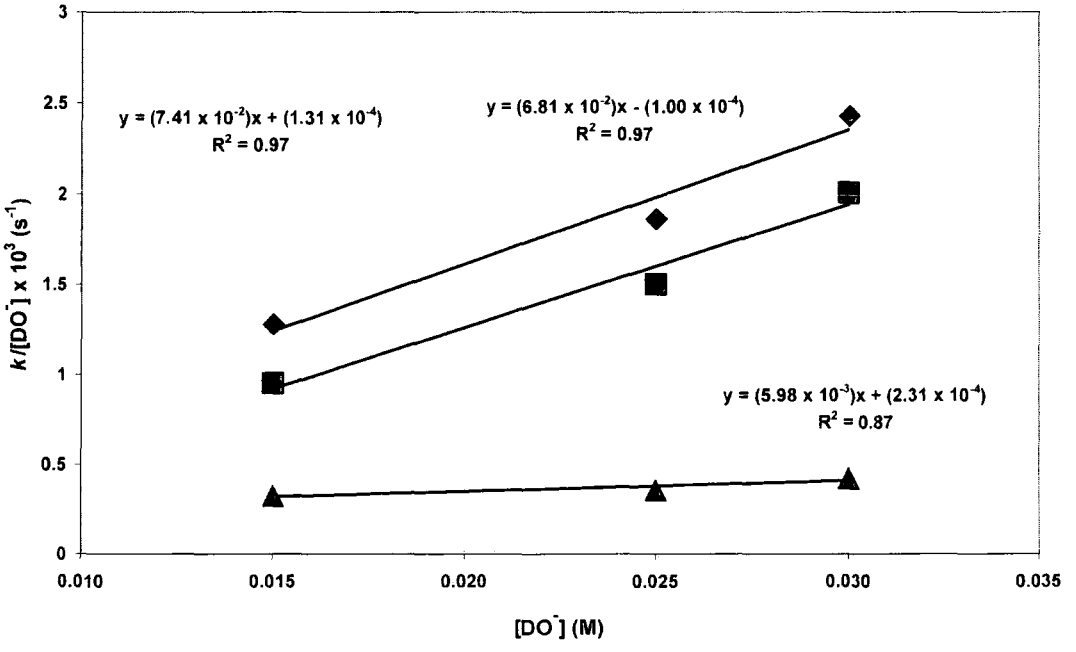

Another possible source of error is that the extents of reaction followed differ at each $[DO^-]$. In particular, only 25% reaction was followed in 0.015 M KOD. Despite this, the individual first order plots in Figures 4.5 – 4.6 give good linear correlations.

Finally deuteroxide ion is consumed in the formation of the carboxylate anion product of the hydrolysis reaction. After the reaction of 25% of 10 mM substrate in 0.015 KOD, approximately 2 mM deuteroxide ion would be consumed due to the formation of hydrolysis product, thus decreasing the KOD concentration by 10% this could result in a smaller than expected rate constant for reaction in 0.015 M KOD, and could account for the negative intercept of the second order plot. Consumption of deuteroxide ion in this fashion would have less of an impact at the higher overall concentration of deuteroxide ion.

4.2.3 N-(2-Oxo-azapan-3-yl)propionamide (250)

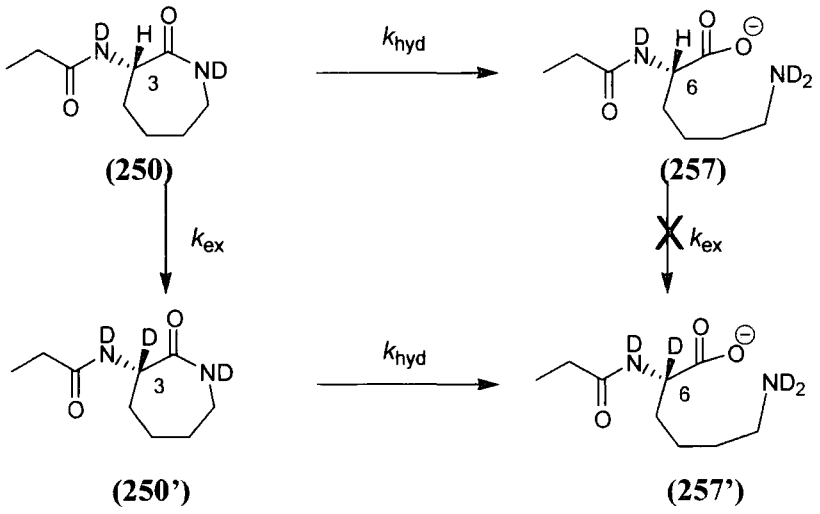

(250) **(257)** **(250')** **(257')**

Rates of deuteroxide ion-catalyzed exchange of propionamide **(250)** to form the corresponding deuterated product **(250')** and hydrolysis to form the corresponding amino acid **(257)** were determined by 300 MHz ^{1}H NMR spectroscopy. H/D-exchange is unlikely to occur at C6 in hydrolysis product **(257)** as the acidic proton is α to a carboxylate and so is less acidic than C(3)-H of **(250)**, therefore any exchange of the C(3)-H would have occurred prior to hydrolysis.

Figure 4.9 shows representative ^{1}H NMR spectra of propionamide **(250)** (10 mM, 0.5 M KOD) obtained during the exchange for deuterium of the C3-H in D_2O at 25 °C and ionic strength I = 1.0 (KCl). At 0% reaction, the signal due to the C3-H appears as a doublet at 4.55 ppm (A). The C3-H should be coupled to the C4-H_2, and thus a triplet would be expected, however the appearance of the peak could be influenced by the proximity of the large DOH peak at 4.67 ppm. The signal due to the C7-H_2 appears as a highly asymmetric broad quartet at 3.30 – 3.45 ppm (B) due to coupling to the likely non-equivalent C6-H_2. The signal due to the CH_2 group of the ethyl protons of the propionyl side chain appears as a quartet at 2.35 ppm (C) due to coupling to the adjacent methyl protons of the propionyl group. The signal due to the C4-H_2 appears as a broad multiplet at 1.90 – 2.05 ppm (D) The signals due to the C5 and C6 hydrogens appear as multiplets at 1.55 – 1.89 ppm (E) and at 1.3 – 1.45 ppm (F). As with propionamide **(249)**, the most

downfield multiplet is assigned to the C4 hydrogens, rather than the C5 or C6 hydrogens, as the former are closer to both an electron withdrawing nitrogen as well as to a carbonyl, and are thus expected to produce a peak with a more downfield chemical shift.

Deuterium exchange at C3 and hydrolysis of the substrate results in the disappearance of the doublet due to C3-H. This is coupled with the appearance of a quartet at 4.05 ppm (A') due to the C6-H of amino acid **(257)**, which is coupled to the two adjacent non-equivalent C5 protons. The decay of the quartet due to C7-H_2 was matched by the growth of a triplet at 2.60 ppm (B') due to the C2-H_2 of **(257)** and **(257')** which are coupled to the adjacent C3-H_2 protons of **(257)** and **(257')**. The multiplets due to the protons on C4 – C6 of hydrolysis product are not clearly distinguishable from each other as decay of the relevant signals due to propionamide **(250)** and growth of signals due to amino acid **(257)** and **(257')** all occur in the range 1.30 - 1.89 ppm. The peak due to C4-H_2 of **(250)** decays over the course of the reaction while peaks (E) and (F) increase in the spectra over time.

Figure 4.9: Representative ^{1}H NMR spectra at 300 MHz of propionamide (250) (10mM, 0.5 M KOD), obtained during hydrolysis and H/D-exchange at C3 in D_2O at 25 °C and ionic strength I = 1.0 (KCl). The extent of reaction is indicated above each spectrum.

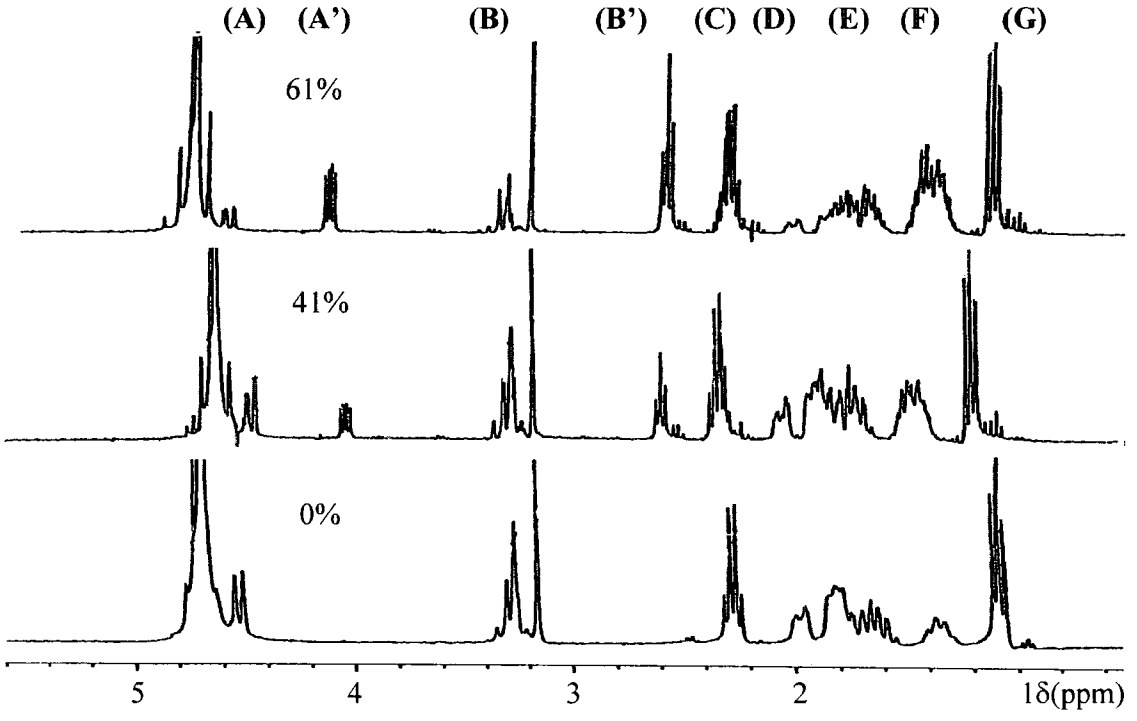

Reaction data and the experimental first-order rate constants for deuterium exchange and hydrolysis (k_{obs}, s^{-1}) at different concentrations of deuteroxide solution are shown in Table 4.3 and 4.4 respectively. The values for k_{obs} (s^{-1}) shown in Table 4.4 are obtained from the slopes of the semilogarithmic plots (Figure 4.10) of the fraction of unreacted substrate against time. The observed rate constant of decay of the peak due to C3-H of **(250)**, (k_{obs}, s^{-1}) is the total loss of substrate due to both deuteroxide ion-catalyzed hydrolysis and deuterium exchange at C3. The observed rate constants for hydrolysis ($k_{hydrolysis}$, s^{-1}) of **(250)** to form hydrolysis product **(257)** with a hydrogen at the C3 position was calculated from the slopes of semilogarithmic plots of $f(s')$ (Equation 4.8) against time (Figure 4.11) as described for the reaction of propionamide **(249)**.

$$f(s') = \left(\frac{\frac{A_{C3\text{-}H(t=0)}}{A_{IS(t=0)}} - \frac{A_{C6\text{-}H(t)}}{A_{IS(t)}}}{\frac{A_{C3\text{-}H(t=0)}}{A_{IS(t=0)}}} \right) \quad \textbf{(Equation 4.8)}$$

Table 4.3: Analysis of reaction for the deuterium exchange at C3-H and hydrolysis of propionamide (250) in deuteroxide solution in D_2O at 25 °C and ionic strength I = 1.0 (KCl).

$[DO^-]^a$ (M)	Time (secs)	$f(s)^b$	$f(s')^c$	ln $f(s)$	ln $f(s')$
0.25	0	1.000	–	0.000	–
	2.08×10^3	0.996		-0.004	
	2.30×10^4	0.925		-0.078	
	5.75×10^4	0.819		-0.199	
	6.59×10^4	0.796		-0.228	
0.50	0	1.000	1.000	0.000	0.000
	3.79×10^3	0.905	0.949	-0.100	-0.052
	1.38×10^4	0.833	0.914	-0.182	-0.090
	3.88×10^4	0.713	0.829	-0.339	-0.188
	6.72×10^4	0.526	0.679	-0.643	-0.387
	1.04×10^5	0.472	0.605	-0.750	-0.503
0.75	0	1.000	1.000	0.000	0.000
	2.92×10^3	0.780	1.000	-0.248	0.000
	1.17×10^4	0.752	0.765	-0.285	-0.268
	2.21×10^4	0.571	0.710	-0.560	-0.343
	7.64×10^4	0.213	0.388	-1.546	-0.947

(a) Measurements were made in KOD solution in the 0.25 – 0.75 M range. (b) The fraction of unexchanged substrate remaining $f(s)$, after reaction due to both hydrolysis and exchange was calculated according to Equation 4.1 Measurements were made at an initial substrate concentration of 10 mM. (c) The fraction of substrate remaining after reaction due to hydrolysis only, $f(s')$, was calculated according to Equation 4.8.

The first order-rate constant for the deuteroxide ion-catalyzed exchange of the C3-H for deuterium, ($k_{exchange}$, s^{-1}) was calculated using Equation 4.5.

Table 4.4: **First order rate constants for the deuterium exchange at C3-H and hydrolysis of propionamide (250) in deuteroxide solution in D_2O at 25 °C and ionic strength I = 1.0 (KCl).**

$[DO^-]$ (M)	k_{obs} $(s^{-1})^a$	$k_{hydrolysis}$ $(s^-)^b$	$k_{exchange}$ $(s^{-1})^c$
0.25	3.51×10^{-6}	2.06×10^{-6}	1.45×10^{-6}
0.50	7.22×10^{-6}	4.84×10^{-6}	2.38×10^{-6}
0.75	1.91×10^{-5}	1.22×10^{-5}	6.88×10^{-6}

(a) The value of the first-order rate constant (k_{obs}) was obtained from the slope of the plot of ln f(s) against time shown in Figure 4.10. (b) The value of the first order rate constant for the formation of hydrolysis product **(257)** ($k_{hydrolysis}$) was obtained from the slope of the plot of ln f(s') against time shown in Figure 4.11. (c) The value of the first order rate constant ($k_{exchange}$) was obtained using Equation 4.5.

The values for the first-order rate constants for the hydrolysis and deprotonation of propionamide **(250)** in 0.25 M KOD were estimated by comparison with the relative rate constants for hydrolysis and overall disappearance of propionamide **(250)** in 0.50 – 0.75 M deuteroxide solution. Only 21% reaction was followed in 0.025 M KOD and peaks due to the C6-H of hydrolysis product could not be accurately measured in this case. According to the latter experimental data, hydrolysis accounted for an average of 66% of the total disappearance of substrate in 0.50 – 0.75 M deuteroxide solution. Hence, a theoretical rate constant for hydrolysis of substrate **(250)** in 0.25 M KOD solution was calculated as 66% of the total rate of disappearance of substrate $k_{hydrolysis} \approx 2.06 \times 10^{-6}\ s^{-1}$. Extending this extrapolation, the first order rate constant for deuteroxide ion-catalyzed H/D-exchange of the C3-H in 0.25 M KOD solution was calculated to be $k_{exchange} \approx 1.45 \times 10^{-6}\ s^{-1}$.

Figure 4.10: Semi-logarithmic plot of the fraction of remaining C3-H against time for the total loss of propionamide (250) in deuteroxide solution at 0.25 M (♦), 0.50 M (■), and 0.75 M (▲) at 25 °C and ionic strength I = 1.0 (KCl).

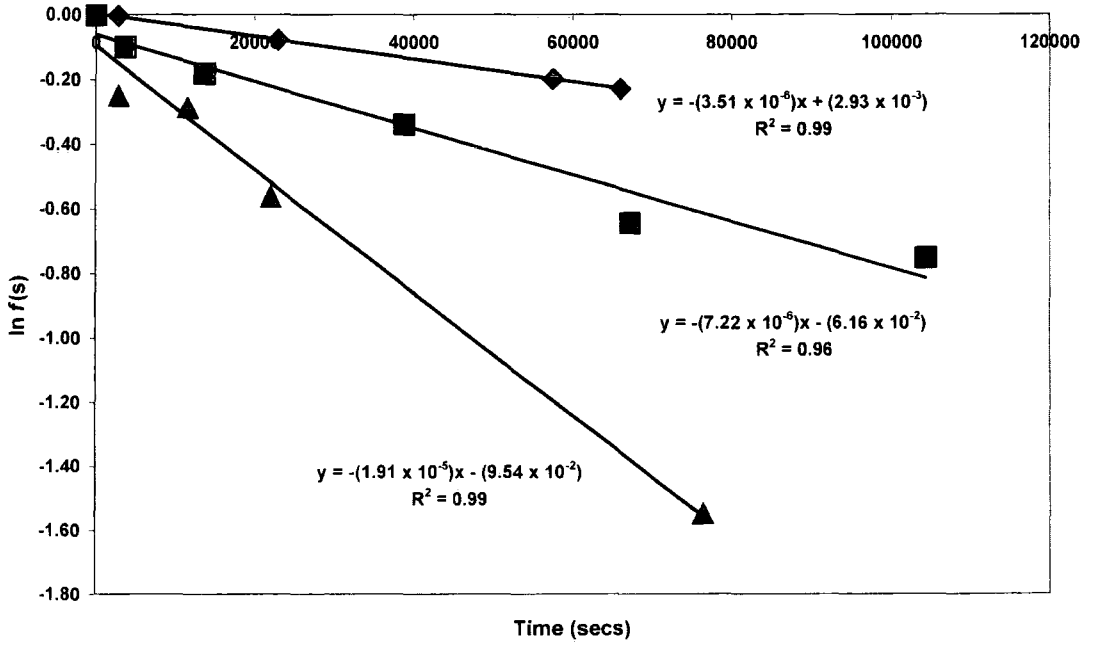

Figure 4.11: Semi-logarithmic plot of the decay of C3-H of propionamide (250) due to hydrolysis against time in deuteroxide solution at 0.50 M (♦) and 0.75 M (■) at 25 °C and ionic strength I = 1.0 (KCl).

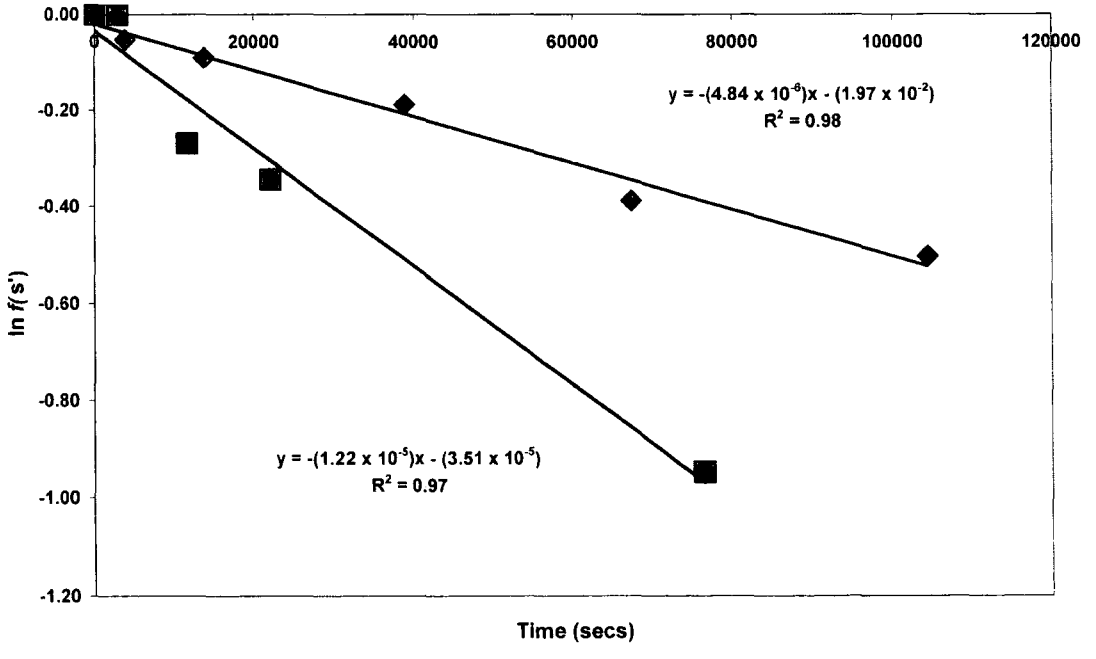

The second-order rate constant for total loss of propionamide **(250)** was calculated from the slope of the plot of k_{obs} (s^{-1}) against the concentration of deuteroxide ion (Figure 4.13, (♦)). The second-order rate constant for hydrolysis of propionamide **(250)** to form amino acid **(257)** was calculated from the slope of $k_{hydrolysis}$ (s^{-1}) against the concentration of deuteroxide ion (Figure 4.12, (■)). The second-order rate constant for the deuteroxide ion-catalyzed deuterium exchange of C3-H was calculated from the slope of the plot of the calculated values $k_{exchange}$, (s^{-1}) against the concentration of deuteroxide ion (Figure 4.12, (▲)).

Figure 4.13: Plot of k_{obs}, (♦), $k_{hydrolysis}$, (■) and $k_{exchange}$, (▲) against [DO^-] for the reaction of propionamide (250) in D_2O at 25 °C and I = 1.0 (KCl).

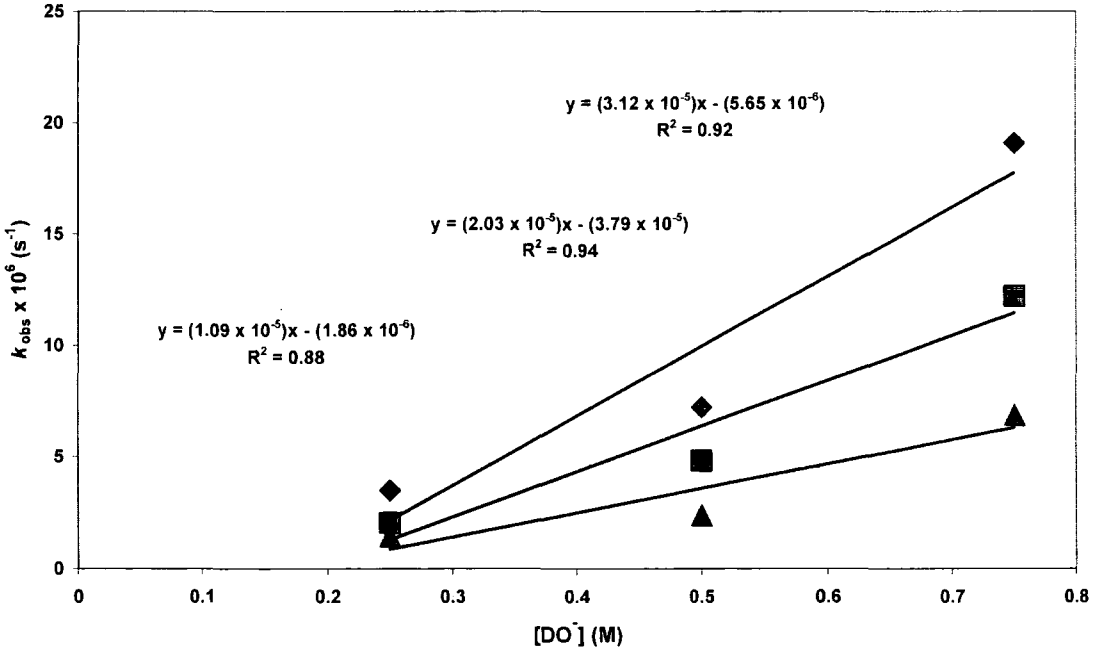

The second-order rate constant for total loss of propionamide **(250)** was calculated as $k_{total} = 3.12 \times 10^{-5}\ M^{-1}s^{-1}$. The second-order rate for the hydrolysis of **(250)** was calculated to be $k_{hyd} = 2.03 \times 10^{-5}\ M^{-1}s^{-1}$, The rate for deuteroxide ion-catalyzed H/D-exchange at C3 which was calculated to be $k_{DO} = 1.09 \times 10^{-5}\ M^{-1}s^{-1}$.

As for propionamide **(249)**, substantial negative intercepts were obtained for each of the second order plots in Figure 4.12 indicating either error in the NMR analysis or a higher than first order dependence on the concentration of deuteroxide ion. However as there are only two deuteroxide concentrations in which exchange and hydrolysis could be independently analysed, further analysis was not performed of the reaction data to account for a higher order dependence on deuteroxide ion concentration.

4.2.4 Thalidomide (237)

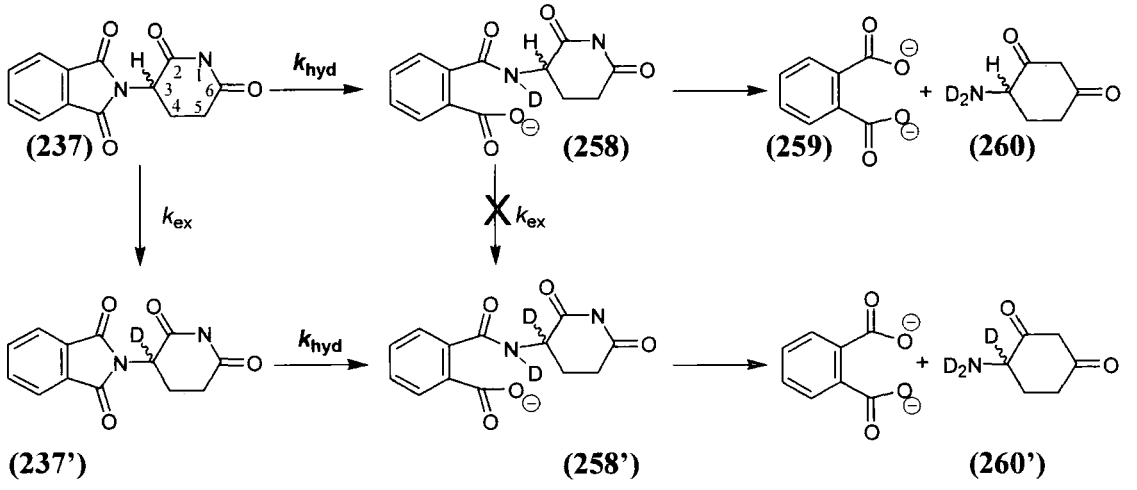

Rates of deuteroxide ion-catalyzed exchange of propionamide **(237)** to form the corresponding deuterated product **(237')** and hydrolysis poduct(s) were determined by 500 MHz ^{1}H NMR spectroscopy. We have not confirmed the identity of the hydrolysis product by using other analytical methods, however given the large change in the chemical shift of peaks due to aryl hydrogens, it is most likely that hydrolysis of the phthalimide moiety is occurring. If hydrolysis was occurring more remotely from the aryl ring at the glutarimide moiety, a smaller change in chemical shift would have been expected.

Figure 4.13a shows a ^{1}H NMR spectrum of thalidomide **(237)** (1 mM) obtained in $CDCl_3$ The signal due to the two *o*-CHs of the aryl ring is expected to appear as a doublet due to coupling to the *m*-CH proton, however the slight non-equivalence of the these protons means that the signal appears as a quartet at 7.83 ppm (A). The latter *meta* hydrogens

give rise to a quartet at 7.78 ppm (B). The signal due to the C3-H appears as a quartet at 5.18 ppm (C) and is coupled to the adjacent C4-H_2. A broad multiplet at 2.65 - 2.90 ppm (D) is the signal due to the C5-H_2 and C4-H(*H*). The signal due to the second C4-*H*(H) appears as a triplet at 2.20 ppm (E). This was confirmed using COSY spectroscopy. Peaks due to thalidomide **(237)** in D_2O solution appeared in a similar location to that described in $CDCl_3$ however the lower solubility in aqueous solution led to significantly lower signal to noise ratio than obtained in chloroform.

Figure 4.13b shows representative ^{1}H NMR spectra of thalidomide **(237)** (0.1 mM, pD 8.67) obtained during the exchange for deuterium of the C3-H in D_2O at 25 °C and ionic strength I = 0.5 (KCl) Deuterium exchange at C3 and hydrolysis of the substrate results in the disappearance of the quartet due to C3-H at 5.18 ppm. The decay of the signals due to the four *o*-CHs and *m*-CHs is matched by the growth of two new quartets at 7.71 ppm and 7.56 ppm respectively. The symmetrical nature of the peaks due to the aryl hydrogens of hydrolysis product suggests that the actual hydrolysis product is benzene dicarboxylic acid **(259)**. Intramolecular nucleophilic catalysis by ortho carboxylate anions of amide hydrolysis in such systems is relatively fast at the pD values of the current experiments[28, 29] and significantly faster than the observed rate constants for hydrolysis given below in Table 4.6. Thus it is likely that the slower initial formation of hydrolysis product **(258)** is followed by fast further hydrolysis to give **(259)**. However as all possible hydrolysis products have four aryl hydrogens on the aryl moiety, the analysis is not impacted. All other peaks due to the substrate were obscured by peaks due to quinuclidinone buffer present in the reaction mixture (not shown). In this case the internal standard used was *t*-butanol which yielded a singlet at 1.13 ppm due to the nine methyl hydrogens. The pD remained constant throughout the reaction and was unchanged prior to quenching.

Figure 4.13a: ^{1}H NMR spectrum at 500 MHz of thalidomide (10 mM) in $CDCl_3$

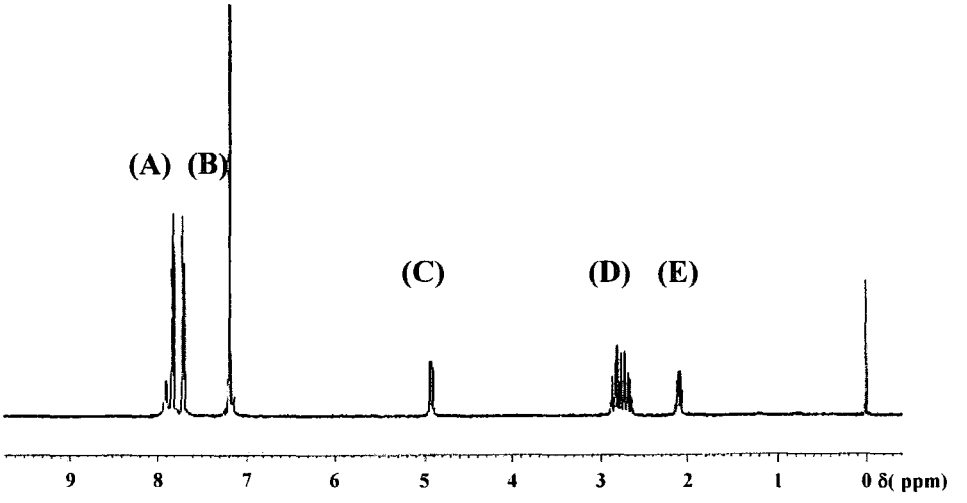

Figure 4.13b: Representative ^{1}H NMR spectra at 300 MHz of thalidomide (237) (0.1 mM, pD 8.67), obtained during exchange of the C3-H for deuterium and hydrolysis at C2 in D_2O at 25 °C and ionic strength I = 0.5 (KCl). The extent of reaction is indicated above each spectrum.

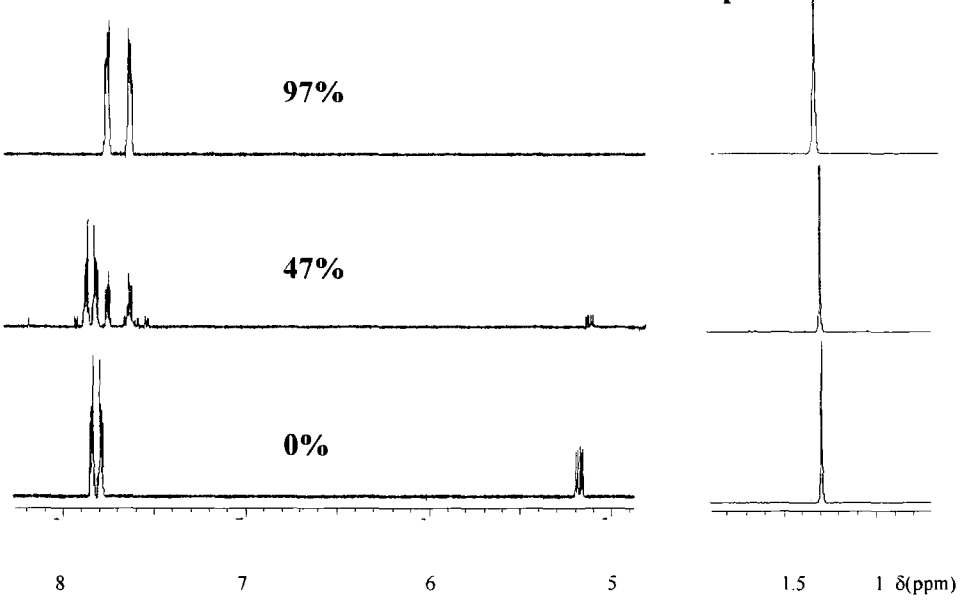

Reaction data and the experimental first-order rate constants for total disappearance of substrate due to both exchange and hydrolysis(k_{obs}, s^{-1}) at different pD values in buffered D_2O solution are shown in Tables 4.5 – 4.6. The values for k_{obs} (s^{-1}) shown in Table 4.6

were obtained from the slopes of the semilogarithmic plots (Figure 4.14) of the fraction of unreacted substrate $f(s)$ against time, where $f(s)$ was calculated using Equation 4.1. The observed rate constants for hydrolysis ($k_{hydrolysis}$, s^{-1}) of thalidomide **(237)** shown in Table 4.6 were calculated from the slope of semilogarithmic plots (Figure 4.15) of the fraction of unhydrolyzed substrate over time. The fraction of substrate remaining after reaction by hydrolysis only, $f(s)$, was calculated using Equation 4.9.

$$f(s') = \left(\frac{(A_{Ar\text{-}thal(t=0)}/A_{IS(t=0)}) - (A_{Ar\text{-}hyd(t)}/A_{IS(t)})}{(A_{Ar\text{-}thal(t=0)}/A_{IS(t=0)})} \right) \qquad \textbf{(Equation 4.9)}$$

In Equation 4.9, $A_{Ar\text{-}thal(t=0)}$, refers to the area of all peaks due to the aryl hydrogens of thalidomide before any reaction has occurred whereas $A_{Ar\text{-}hyd(t)}$, refers to the area of all new peaks at 7.56 – 7.1 ppm due to aryl hydrogens of hydrolysis product at various timepoints during the reaction.

Table 4.5: First order rate data for exchange of the C3-H (237) for deuterium and hydrolysis of thalidomide (237) in quinuclidinone and phosphate buffers (50 mM) in D_2O at 25 °C and ionic strength I = 0.5 (KCl).

Buffer	[DO-][a] (M)	Time (secs)	$f(s)$[b]	$f(s')$[c]	Ln $f(s)$	Ln $f(s')$
phosphate	707×10^{-9} (pD 6.59)	0	1.000	1.000	0.000	0.000
		8.40×10^{4}	0.811	0.963	-0.209	-0.038
		1.81×10^{5}	0.573	0.870	-0.557	-0.139
		2.62×10^{5}	0.469	0.821	-0.757	-0.197
		6.10×10^{5}	0.224	0.659		-0417
phosphate	1.69×10^{-8} (pD 6.97)	0	1.000	1.000	0.000	0.000
		1.63×10^{5}	0.673	0.945	-0.396	-0.057
		4.33×10^{5}	0.282	0.814	-1.266	-0.206
		5.35×10^{5}	0.191	0.693	-1.655	-0.367
		8.45×10^{5}	0.000	0.588		-0.531
quinuclidinone	8.47×10^{-7} (pD 8.67)	0	1.000	1.000	0.000	0.000
		7.72×10^{3}	0.358	0.817	-1.027	-0.202
		1.40×10^{4}	0.258	0.805	-1.355	-0.217
		1.94×10^{4}	0.146	0.699	-1.924	-0.358
		2.62×10^{4}	0.093	0.620	-2.375	-0.478
		8.81×10^{4}	0.000	0.166		-1.796

quinuclidinone	3.13×10^{-6} (pD 9.24)	0	1.000	1.000	0.000	0.000
		1.20×10^{3}	0.831	1.077	-0.185	0.074
		2.41×10^{3}	0.640	1.007	-0.446	0.007
		4.77×10^{3}	0.397	0.923	-0.924	-0.080
		5.98×10^{3}	0.412	0.943	-0.887	-0.059
		8.81×10^{3}	0.265	0.819	-1.328	-0.200

(a) Measurements were made in 50 mM phosphate buffers in the pD 6.59 – 6.97 range and in 50mM quinuclidinone buffers in the pD 8.67 – 9.24 range. $[DO^-]$ was calculated using $[DO^-] = (10^{pD-pK_w})/\gamma_{OL}$ with $pK_w = 14.87$, where $\gamma_{OL} = 0.75$ is the activity correction of lyoxide ion under our experimental conditions. (b) The fraction of unreacted substrate remaining $f(s)$, was calculated according to Equation 4.1 where A_p is the area of the peak due to the C3-H of **(237)** and A_{IS} is that area of the peak due to the internal standard. Measurements were made at an initial substrate concentration of 0.1 mM. (c) The fraction of substrate remaining after reaction by hydrolysis only, $f(s')$, was calculated using Equation 4.9.

Figure 4.14: Semi-logarithmic plot of the fraction of remaining C3-H against time of thalidomide (237) in phosphate and quinuclidine buffers at pD 6.59 (♦), 6.97 (■), 8.67 (▲) and 9.24 (●), at 25 °C and ionic strength I = 0.5 (KCl).

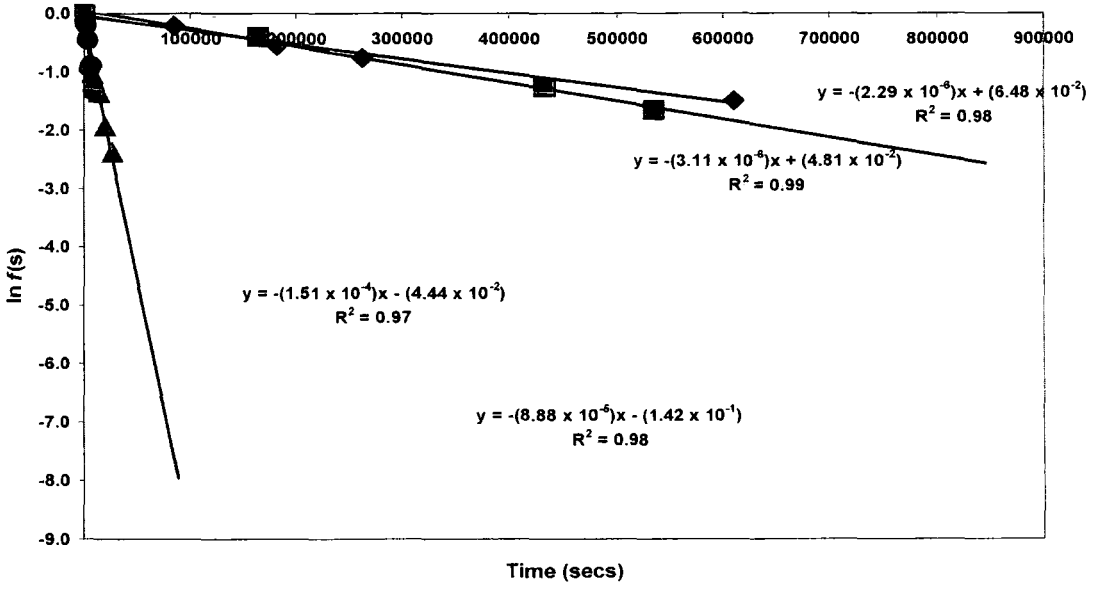

Figure 4.15: Semi-logarithmic plot of the fraction of substrate remaining after hydrolysis of thalidomide (237) against time in phosphate and quinuclidine buffers at pD 6.59 (♦), 6.97 (■), 8.67 (▲) and 9.24 (●), at 25 °C and ionic strength I = 0.5 (KCl).

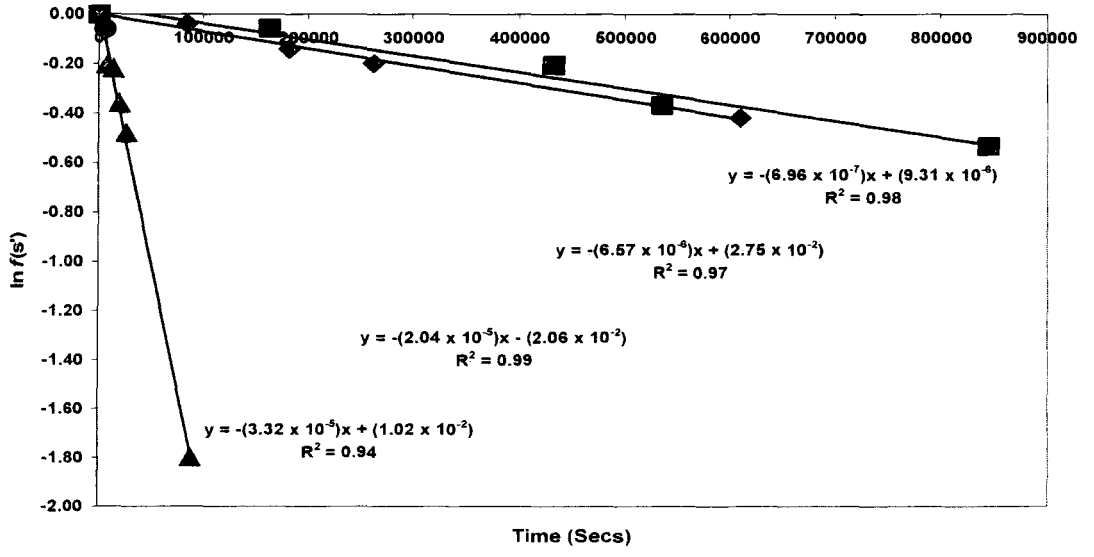

The first order-rate constant for the deuteroxide ion-catalyzed exchange of the C3-H for deuterium, ($k_{exchange}$, s^{-1}) was calculated using Equation 4.1.

Table 4.6: First order rate constants for the deuterium exchange at C3-H and hydrolysis of thalidomide (237) in phosphate and quinuclidinone buffers in D_2O at 25 °C and ionic strength I = 0.5 (KCl).

Buffer	[DO-] (M)	k_{obs} (s^{-1})	$k_{hydrolysis}$ (s^{-1})	$k_{exchange}$ (s^{-1})
phosphate	7.07×10^{-9} (pD 6.59)	2.29×10^{-6}	6.96×10^{-7}	1.43×10^{-6}
phosphate	1.69×10^{-8} (pD 6.97)	3.11×10^{-6}	6.57×10^{-6}	2.99×10^{-6}
quinuclidinone	8.47×10^{-7} (pD 8.67)	8.88×10^{-5}	2.04×10^{-5}	4.76×10^{-5}
quinuclidinone	3.13×1^{-6} (pD 9.24)	1.51×10^{-4}	3.32×10^{-5}	8.05×10^{-5}

(a) The value of the first-order rate constants (k_{obs}, s^{-1} and $k_{hydrolysis}$, s^{-1}) were obtained from the slopes of the plots of ln *f*(s) and ln *f*(s') against time shown in Figure 4.15 and 4.16 respectively.

The second-order rate constant for total loss of thalidomide **(237)**, k_{total} ($M^{-1}s^{-1}$), was calculated from the slope of the plot of k_{obs} (s^{-1}) against the concentration of deuteroxide ion (Figure 4.16, (♦)). The second-order rate constant for hydrolysis of thalidomide **(237)** k_{Hyd} ($M^{-1}s^{-1}$) was calculated from the slope of $k_{hydrolysis}$ (s^{-1}) against the concentration of deuteroxide ion (Figure 4.16, (■)). The second-order rate constant for the deuteroxide ion-catalyzed deuterium exchange of C3-H, k_{DO} ($M^{-1}s^{-1}$), was calculated from the slope of the plot of the calculated values $k_{exchange}$ against the concentration of deuteroxide ion (Figure 4.16, (▲)). It is assumed that contribution of buffer catalysis is the same in the case of phosphate buffers and quinuclidinone buffers as no further analysis on the extent of buffer catalysis has been carried out in this work.

Figure 4.16: Plot of k_{obs}, (♦) $k_{exchange}$, (■), and $k_{hydrolysis}$, (▲) against [DO^-] for the H/D exchange and hydrolysis reaction of thalidomide (237) in buffered solution in D_2O at 25 °C and I = 0.5 (KCl).

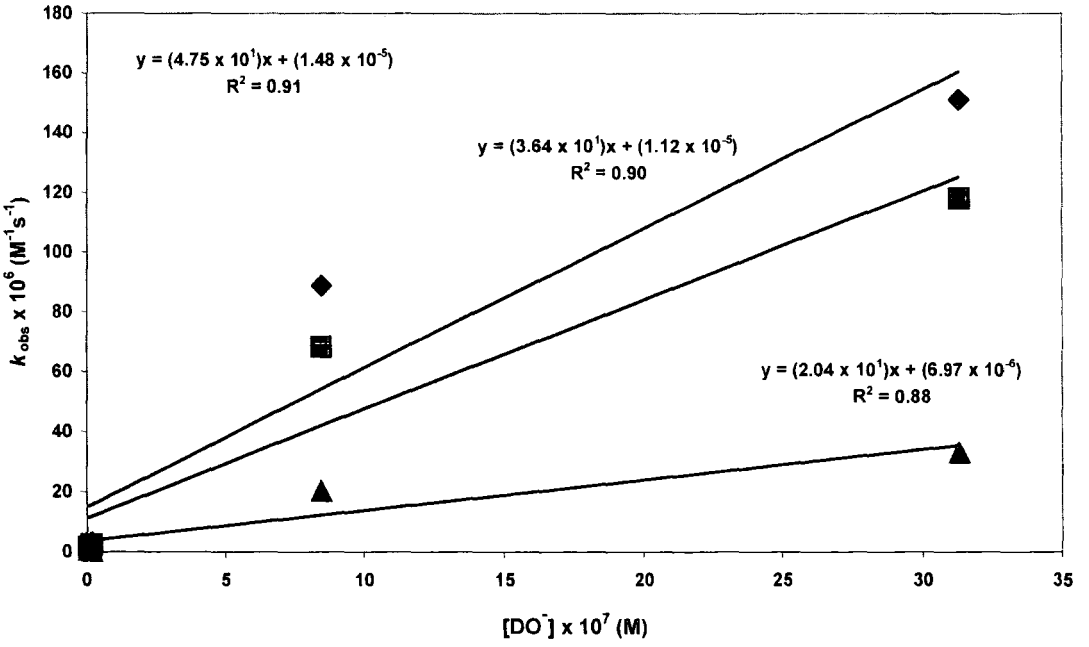

The second-order rate constant for total loss of thalidomide **(237)** was determined as k_{total} = 47.5 $M^{-1}s^{-1}$. The second-order rate constant for the hydrolysis of **(237)** was determined as k_{Hyd} = 20.4 $M^{-1}s^{-1}$, The second-order rate constant for deuteroxide ion-catalyzed H/D-exchange at C3 which was calculated to be k_{DO} = 36.4 $M^{-1}s^{-1}$.

4.2.5 Estimation of k_{H2O} and pK_a determination.

The second order rate constants for deuteroxide ion catalyzed exchange (k_{DO} values) for propionamides **(249)** and **(250)** and for thalidomide **(237)** were obtained as 5.30×10^{-4} $M^{-1}s^{-1}$, 1.09×10^{-5} $M^{-1}s^{-1}$and 36.4 $M^{-1}s^{-1}$ respectively.

The second-order rate constant for hydroxide-ion catalyzed deprotonation (k_{HO}, $M^{-1}s^{-1}$) can be obtained from the experimental k_{DO} value ($M^{-1}s^{-1}$) by using the secondary isotope effect relationship: k_{DO}/k_{HO} = 2.0. Similarly to the DKPs discussed in Chapter 3, the secondary solvent deuterium isotope effect for deprotonation of these carbon acids by lyoxide ion is expected to be larger than k_{DO}/k_{HO} = 1.46 for deprotonation of acetone.[30] However there is no evidence that it is close to the maximum value of k_{DO}/k_{HO} = 2.4 for deprotonation to form very unstable carbanions for which isotope exchange is limited by solvent reorganization. Therefore, an intermediate value of k_{DO}/k_{HO} = 2.0 is used as the secondary solvent isotope effect for deprotonation of the carbon acids discussed in this chapter.

As discussed in Section 3.3 for DKPs **(221)** and **(222)** the reverse rate of protonation of propionamides **(249)**, **(250)** and thalidomide **(237)** is expected to be far below the limiting rate constants determined for the 'clocks' described by Richard *et al*[31] detailed in Chapter 1. Thus a value for k_{HOH} in this case can only be accessed by direct measurement. However a Brønsted plot of log k_{HO} values against pK_a of other simple aldehydes, ketones and esters[32-34] provides a means to estimate the pK_a values of propionamides **(249)** and **(250)** and thalidomide **(237)**. where both literature parameters have been statistically corrected to represent a single acidic proton in the molecule (see Table 4.7 and Figure 4.17). An estimate of the pK_a values for propionamides **(249)** and **(250)** and thalidomide **(237)** can be calculated from the equation of the line in Figure 4.17 together with the experimental k_{HO} values for these substrates. The negative of the slope of the Brønsted correlation in Figure 3.14 is the Brønsted coefficient, β = 0.40.

Table 4.7: Kinetic acidity of C3-H and C6-H of propionamides (249), (250), thalidomide (237) and other simple carbon acids of similar acidity.

Carbon Acid	p[a]	k_{HO} $(M^{-1}s^{-1})$[b]	k_{HO}/p $(M^{-1}s^{-1})$[d]	pK_a[e]	pK_a + Log p[g]
Ph_2CHCHO	1	254	254	10.4	10.4
t-$PhCH_2CHO$	2			12.3	12.6
c-$PhCH_2CHO$	2	20	10	13.1	13.4
CH_3CHO	3	1.17	0.39	16.7	17.2
CH_3COPh	3	0.25	0.083	18.3	18.8
CH_3COCH_3	6	0.22	0.037	19.3	20.1
CH_3COSEt	3	2.0×10^{-2}	6.7×10^{-3}	21.0	21.5
CH_3COOEt	3	1.2×10^{-3}	4.0×10^{-4}	25.6	26.1
CH_3CONH_2	3	9.5×10^{-6}	3.2×10^{-6}	28.4	28.9
N-(2-Oxo-piperidine-3-yl)propionamide	1	2.65×10^{-4}[c]	2.65×10^{-4}	24.9[f]	24.9
N-(2-Oxo-azapan-3-yl)propionamide	1	5.45×10^{-6}[c]	5.45×10^{-6}	29.1[f]	29.1
thalidomide	1	23.8[c]	23.8	12.5[f]	12.5

(a) p is the number of identical acidic protons in the carbon acid. (b) k_{HO} is the second order rate constant for the hydroxide-catalyzed deprotonation of the carbon acid. (c) Experimentally determined in this work. (d) The second order-rate constant for the hydroxide-catalyzed deprotonation of a *single acidic proton* of the carbon acid. (e) Literature pK_a values.[34] (f) Interpolated using the equation that fits the linear plot in Figure 4.17 together with experimental k_{HO} values. (g) Carbon acid pK_a values corrected to represent the ionisation of one acidic proton. (h) Interpolated using the equation to the linear plot in Figure 4.17 together with experimental k_{HO} values.

Figure 4.17: Brønsted plot of statistically corrected second order rate constants k_{HO} for hydroxide ion catalysed deprotonation of carbon acids (♦) against corresponding pK_a values using the literature data in Table 3.5. The interpolated data points for propionamides (249) and (250) and thalidomide (237) are also indicated (●).

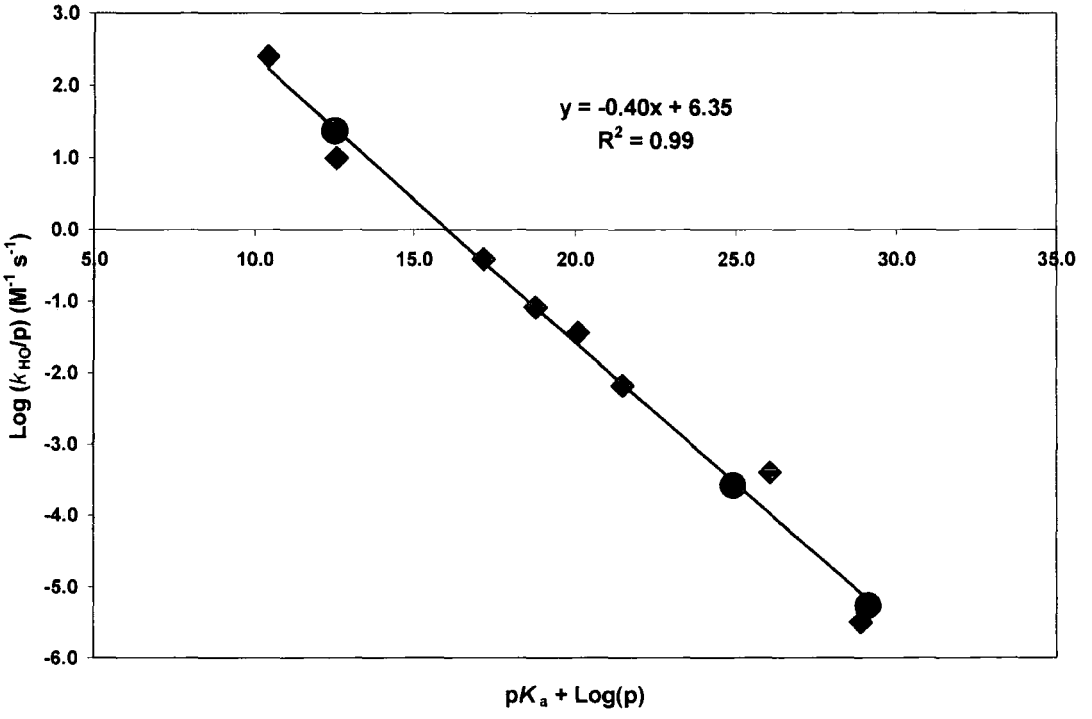

4.3.1 Mechanism of Deuterium Exchange

A detailed mechanism for deuteroxide-ion catalyzed exchange of the acidic proton of thalidomide **(237)** and the chemokine inhibitors **(249)** and **(250)** is shown in Scheme 4.3. In D_2O solution with deuteroxide ion as base, the encounter of the neutral substrate **(251)** and deuteroxide ion results in proton abstraction to give an intimate ion pair. The carbanion formed on loss of a proton can reorganise to form the corresponding enolate **(253)**.

Reprotonation of the enolate/LOD complex by DOH^+ (k_p) would regenerate the protonated substrate, while irreversible protonation by D_2O, initially involving placement of a molecule of DOD in a position to deliver a deuteron to the C3 of the enolate gives exchange product. The solvent reorganization step is irreversible and results in an exchange reaction as the concentration of protonated DOH^+ is negligible. Reprotonation of the enolate intermediate is fast relative to deprotonation of the parent acid. Hence determination of the rate constant for deuterium exchange enables estimation of the rate constant for enolate formation.

The H/D-exchange reactions of propionamide **(249)** and **(250)** and thalidomide **(237)** were monitored by ^1H NMR spectroscopy in D_2O solution, and reaction data was analyzed, as described in Section 4.2. The results are summarized in Table 4.8.

The pK_a values for propionamides **(249)** and **(250)** were estimated to be 24.9 and 29.1 respectively. The pK_a value for thalidomide was estimated to be 12.5.

Table 4.8:

Acid	k_{DO}[a] $(M^{-1}s^{-1})$[a]	k_{HO}[b] $(M^{-1}s^{-1})$[b]	k_{Hyd}[c] $(M^{-1}s^{-1})$[c]	pK_a[d]
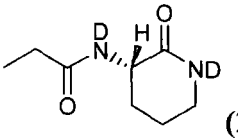 **(249)**	5.30×10^{-4}	2.65×10^{-4}	2.96×10^{-3}	24.9
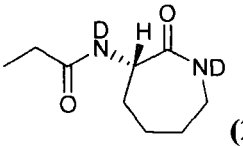 **(250)**	1.09×10^{-5}	5.45×10^{-6}	2.03×10^{-5}	29.1
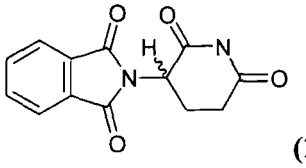 **(237)**	47.5	23.8	20.4	12.5

(a)Second order-rate constant for the deuteroxide ion-catalyzed deuterium exchange reaction at C3, calculated from slope of the plots of the first order-rate constant for exchange ($k_{exchange}$, s^{-1}) against [DO^-] (M) shown in Figures 4.9, 4.13 and 4.17 respectively. (b) Second order rate constant for the hydroxide ion-catalyzed exchange reaction at C3 calculated using the secondary solvent kinetic isotope effect k_{DO}/k_{HO} = 2.0 (c) Second order rate-constant for hydrolysis of substrate in deuteroxide solution. (d) Carbon acid pK_a value interpolated as described in Section 4.2.5.

4.3.2 Rate constants for exchange and hydrolysis of thalidomide (237)

The rate of deuteroxide ion-catalyzed deuterium exchange of the C3-H of thalidomide was found to be 2.3-fold faster than hydrolysis of the substrate in deuteroxide solution at 25 °C and ionic strength I = 0.5 (KCl) (see Table 4.8). There are however few reported rate constants in the literature which can be compared with the data obtained in this work.

According to one study carried out by Eriksson *et al*[35] on the human pharmacokinetics of thalidomide, the rate of chiral inversion of the R- and S-enantiomers of thalidomide in blood were reported to be 8.33×10^{-5} s^{-1} and 8.61×10^{-5} s^{-1} respectively at 37 °C and physiological pH (taken to be pH 7.4 as the standard pH of blood[36]). The rates of

racemization of *in vivo* were reported to be 4.72×10^{-5} s^{-1} (R to S) and 5.00×10^{-5} s^{-1} (S to R).This may be compared to the observed rate constant for exchange at pD 6.9 $k_{exchange}$ = 1.43×10^{-6} s^{-1}. Using Equation 4.7 and the second order rate constant for hydroxide ion-catalyzed exchange for thalidomide, k_{HO} = 23.8 ($M^{-1}s^{-1}$) determined in this work, a value for k_{ex} = 5.12×10^{-6} s^{-1} may be estimated at pH 7.4 in D_2O solution at 25 °C and ionic strength I = 0.5 (KCl).

$$k_{ex} = k_{HO}[HO^-] \qquad \textbf{(Equation 4.7)}$$

The value estimated from this work is 10-fold smaller than that previously reported in blood, A decrease in temperature from 37 °C to 25 °C should decrease the rate by only 2-3-fold, thus the larger value in blood plasma indicates the existence of catalysis by other species present in the blood.

Eriksson *et al*[35] also reported rate constants for elimination - presumed to be primarily due to hydrolysis - of R- and S-thalidomide at 37 °C and physiological pH. The S-enantiomer (k_{elim} = 6.67×10^{-5} s^{-1} S to R) was found to undergo elimination 3-fold faster than the R-enantiomer, (k_{elim} = 2.19×10^{-5} s^{-1} R to S). This may be compared to the value for k_{hyd} = 6.96×10^{-7} s^{-1} for the hydrolysis of thalidomide racemate at 25 °C and pD 6.9. Assuming the rate of hydrolysis in deuteroxide solution is similar to that in hydroxide solution at pH 7.4 the rate of hydrolysis may be estimated using Equation 4.8 and the observed second order-rate constant for the deuteroxide ion-catalyzed hydrolysis of thalidomide to be 2.33×10^{-6} s^{-1}.

$$k_{hydrolysis} = k_{Hyd}[HO^-] \qquad \textbf{(Equation 4.8)}$$

The rate constant for hydrolysis of thalidomide racemate at 25 °C and pH 7.4 estimated in this work is also 10-fold less than the average value reported by Eriksson.[35] Correction for temperature should account for some of this difference in rate. It is also possible that hydrolysis of thalidomide is increased in blood and body tissues relative to aqueous solution as the substrate may be subject to catalysis from another source, although so far this has not been reported to be the case.

4.3.3 k_{DO} ($M^{-1}s^{-1}$) and k_{Hyd}($M^{-1}s^{-1}$) values of thalidomide (237) and propionamides (249) and (250)

Both propionamides **(249)** and **(250)** demonstrate significantly higher stereochemical integrity and hydrolytic stability than thalidomide **(237)** in D_2O solution at 25 °C (see Table 4.8). The second order-rate constant for deuterium exchange at C3 of thalidomide is 9.0×10^4 and 4.4×10^6 fold larger than for propionamides **(249)** and **(250)** respectively. The electron-withdrawing inductive effect of the extra carbonyl groups in thalidomide compared to in the two propionamides is likely the main factor responsible for increasing the rate of exchange in the former case At physiological pH (~ pH 7.0) the rates of racemization of propionamides **(249)** and **(250)** are expected to be in the range $1 \times 10^{-12} - 10^{-13}$ s^{-1} (calculated using Equation 4.7) while the rate of racemization of thalidomide at pH 6.6 was found to be 1.23×10^{-6} s^{-1}. Similarly, the second order-rate constant for hydrolysis of thalidomide **(237)** is $6.8 \times 10^3 - 1.0 \times 10^6$–fold greater than for **(249)** and **(250)** respectively although hydrolysis is occurring at different sites for the former compared to the latter substrates. At pH 7.0 the rates of hydrolysis of propionamides **(249)** and **(250)** are expected to be in the range $10^{-11} - 10^{-13}$ s^{-1} while at pH 6.6 the rate of hydrolysis of thalidomide was estimated to be 658×10^{-7} s^{-1}. It may be assumed that under physiological conditions propionamides **(249)** and **(250)** would be more resistant to both racemization and hydrolysis than thalidomide.

4.3.4 Effects of ring size on k_{DO} ($M^{-1}s^{-1}$) and k_{Hyd} ($M^{-1}s^{-1}$)

It can be seen from Table 4.8 that an increase in ring size from a six-membered ring in **(249)** to a seven-membered ring in **(250)** results in a significant decrease in reactivity. On going from propionamide **(249)** to **(250)** there are 48-fold and 146-fold decreases second order rate constants for exchange and hydrolysis. There is an increase of 4.2 pK units the increase in ring size. This could be due to increased steric hindrance around the acidic C3-H with increased ring size. A similar decrease in reactivity with increasing ring size was seen with the six-membered pyrimidinium ions **(121)** – **(123)** (Chapter 2) which were significantly less acidic than imidazolinium and imidazolium ions also studied.

4.3.5 Relative stability of thalidomide (237) and thalidomide analogues (249) and (250).

As discussed in Section 4.0, propionamides **(249)** and **(250)** are the subjects of a study to identify the essential structural motifs present in peptide 3 which produce the broad-spectrum chemokine inhibition. It was found that *N*-acyl-3-aminoglutarimides were the most active broad-spectrum chemokine inhibitors in this series. *N*-acyl-3-amino-glutarimides retained the characteristic property of peptide 3, which is the ability to inhibit all chemokines tested with very similar potency. This observation strongly suggested that neither peptide 3 nor the *N*-acyl-3-aminoglutarimides were functioning as simple receptor antagonists but as mediators for chemokine inhibition by an as yet unknown mechanism. The unresolved issue of stereointegrity of the active *N*-acyl-3-aminoglutarimides has been addressed in this work. It can be seen from Table 4.8 that the propionamides **(249)** and **(250)** with pK_a values of 24.9 and 29.1 respectively and significantly lower rates of hydrolysis, show significantly higher stereochemical integrity than thalidomide (pK_a 12.5). Although it is unlikely that these analogues of thalidomide will share the teratogenic side effects induced by thalidomide, a full pharmacological assessment of these species remains to be carried out before consideration of their use as anti-inflammatory agents in humans.

Reference:

(1) Eriksson, T., Bjorkman, S., Roth, B., Fyge, A. Hoglund, P., *Chirality* **1996**, *7*, 44.
(2) Teo, S. K., Resztak, K. E., Scheffler, M. A., Kook, K. A., Zeldis, J. B., Stirling, D. I., Thomas, S. D., *Microbes Infect.* **2002**, *4*, 1193.
(3) Sheskin, J. *Clin. Pharmacol. Ther.* **1965**, *6*, 303.
(4) Arora, M., Wagner, J. E., Davies, S. M., Blazar, B. R., Defor, T., Enright, H., Miller, W. J., Weisdorf, D. F., *Biol. Blood Marrow Transplant.* **2001**, *7*, 265.
(5) Gaziev, D., Lucarelli, G., *Expert Opin. Investig. Drugs*, **2001**, *10*, 909.
(6) Grosshans, E., Illy, G., *Int. J. Dermatol.* **1984**, *23*, 598.
(7) Kruse, F. E., Joussen, A. M., Rohrschneider, K., Becker, M. D., Volcker, H. E., *Graefe's Arch. Clin. Exp. Ophthalmol.* **1998**, *236*, 461.
(8) D'Amato, R. J., Loughnan, M. S., Flynn, E., Folkman., *J. Proc. Natl. Acad. Sci. U.S.A.* **1994**, *91*, 4082.
(9) Eriksson T., B., S., Höglund, P., *Eur. J. Clin. Pharmacol.* **2001**, *57*, 365.
(10) Eriksson. T., B., S., Roth, B., Höglund, P., *Chirality* **2000**, *52*, 807.
(11) Chen, T. L., Vogelsang, G. B., Petty, B. G., Brundrett, R. B., Noe, D. A., Santos, G. W., Colvin, O. M., *Drug Metab. Dispos.* **1989**, *17*, 402.
(12) Eriksson T., B., S., Roth, B., *Chirality* **1998**, *10*, 223.
(13) Schumacher, H., Smith, R. L., Williams, R. T., *J. Pharmacol.* **1965**, *25*, 324.
(14) Reist, M., Carrupt, P. A., Francote, E., Testa, B., *Chem. Res. Toxicol.* **1998**, *11*, 1521.
(15) Meyring, M., Mühlbacher, J., Messer, K., Kastner-Pustet, N., Gerhard, B., Mannschreck, A., Blaschke, G. *Anal. Chem.* **2002**, *74*, 3726.
(16) Eriksson T., B., S., Roth, B., Höglund, P., *J. Pharm. Phermacol.* **2000**, *52*, 807.
(17) Koch, H. *Sci. Pharm.* **1981**, *49*, 67.
(18) Lochsley, R. M., Killeen, N., Lenardo, M. J., *Cell* **2001**, *104*, 487.
(19) Muller, G. W., Corral, L. G., Shire, M. G., Wang, H., Moreira, A., Kaplin, G., Stirling, D., *J. Med. Chem.* **1996**, *39*, 3238.
(20) Chung, F., Palmer, B. D., Muller, G. W., Man, H. W., Kestell, P., Baguley, B. C., Ching, L. M., *Oncol. Res.* **2003**, *14*, 75.
(21) Osipiv, S. N., Tsouker, P., Hennig, L., Burger, K., *Tetrahedron* **2004**, *60*, 271.
(22) Yamada, T., Okada, T. Sakiguchi, K., Ohfune, Y., Ueki, H., Soloshonok, V. A., *Org. Lett.* **2006**, *8*, 5625.
(23) Reckless, J., Grainger, D. J., *Biochem. J.* **1999**, *340*, 2049.
(24) Fox, D. J., Reckless, J., Warren, S. G., Grainger, D. J., *J. Med. Chem.* **2002**, *45*, 360.
(25) Reckless, J., Tatalick, L. M., Grainger, D. J., *Immunology* **2001**, *103*, 244.
(26) Richard, J. P., Williams, G., O'Donoghue, A. C., Amyes, T. L. *J. Am. Chem. Soc.* **2002**, *124*, 2957.
(27) Rios, A., O'Donoghue, A. C., Amyes, T. L., Richard, J. P., *Can. J. Chem.* **2005**, *83*, 1536.
(28) Aldersley, M. F., Kirby, A. J., Lancaster, P. W., Mc Donald, R. S., Smith, C. R., *J. Chem. Soc. Perkin II* **1974**, 1487.
(29) Kirby, A. J., Mc Donald, R. S., Smith, C. R., *J. Chem. Soc. Perkin II*

1974, 1495.
(30) Pocker, Y. *Chem. Ind.* **1959**, 1383.
(31) Richard, J. P., Amyes, T. L., Toteva, M. M. *Acc. Chem. Res* **2001**, *34*, 981
(32) Keefe, J. R., Kresge, A. J., *The Chemistry of Enols*; John Wiley and Sons: Chichester, 1990.
(33) Amyes, T. L., Richard, J. P. *J. Am. Chem. Soc* **1992**, *114*, 10297.
(34) Amyes, T. L., Richard, J. P. *J. Am. Chem. Soc* **1996**, *118*, 3129.
(35) Eriksson, T., Bjorkman, S., Roth, B., Fyge, A. Hoglund, P., *Chirality* **1996**, 7, 44.
(36) Campbel, N. A., Reece, J. A., *Biology*, 7 ed.; Benjamin Cummings: San Francisco, 2005.

Chapter 5

Experimental

5.1 Synthesis of substrates for kinetic measurements

5.1.1 Glyoxal-bis(2,4,6-trimethylphenyl)imine (262)[1]

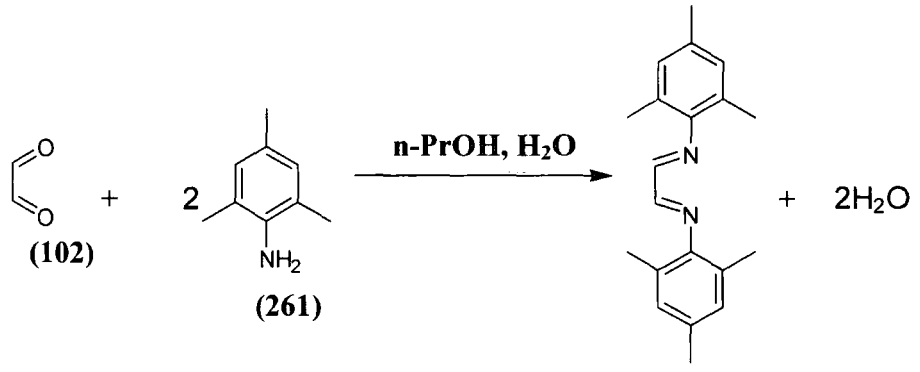

(262)

2,4,6-Trimethylaniline **(261)** (1.35 g, 10.0 mmol) in *n*-propanol (6 mL) was added to glyoxal **(102)** (40 wt % aqueous solution), (0.750 g, 5.16 mmol) in H_2O (1 mL). The dark yellow solution was stirred at room temperature for 24 hours and then refluxed under nitrogen at 60 °C for 6 hours. The solution was then stirred at room temperature for another 24 hours. On cooling a yellow precipitate formed. The mixture was filtered and the precipitate washed with water, and recrystallized from diethyl ether yielding large needle crystals (1.12 g, 74%) Rf 0.8 (ethyl acetate/dichloromethane 1:5), m.p. 158 – 163 °C (lit.[1] 157 - 158°C).

δ^1H / ppm (300 MHz, $CDCl_3$): 2.16 [s, 12H, *o*-CH_3], 2.29 [s, 6H, *p*-CH_3], 6.90 [s, 4H, *m*-CH], 8.10 [s, 2H, C*H*C*H*].

Lit. δ^1H / ppm (300 MHz, $CDCl_3$)[1]: 2.19 [s, 12H,*o*-CH_3], 2.32 [s, 6H *p*-CH_3], 6.93 [s, 4H, *m*-CH], 8.13 [s, 2H, CH].

ν_{max} / cm^{-1}: 1456 (CH), 1617 (N=C), 2958 and 2862 (CH).

ES+ *m/z*: 293.3 (M^+, 100%).

5.1.2. 1,3-Bis(2,4.6-trimethylphenylamino)ethane dihydrochloride (263)[1]

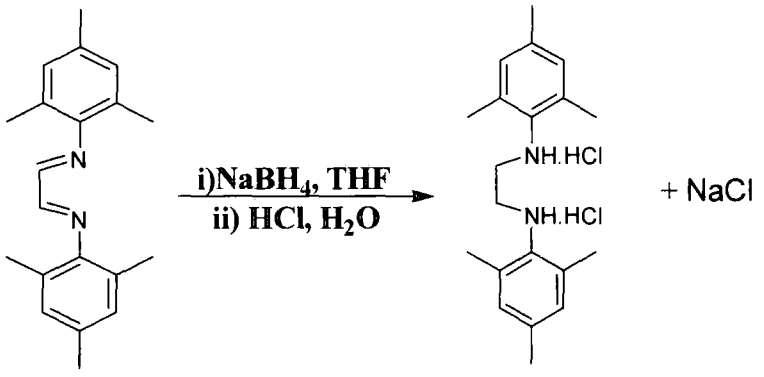

(262) **(263)**

Glyoxal–bis(2,4,6-trimethylphenyl)imine **(262)** (2.95 g, 10.1 mmol), in THF (40 mL) was treated at 0 °C with $NaBH_4$ (3.00 g, 79.3 mmol) and was stirred for 16 hours at 23 °C, and subsequently heated to reflux for 3 hours under nitrogen. The reaction mixture was cooled on ice, and a HCl solution (3 M) was slowly added drop-wise to the mixture until effervescence had ceased. H_2O was added (10 mL), the solution turned cloudy and a white precipitate formed. The amine **(263)** was collected by suction filtration, recrystallized from ethanol to yield a white powder (2.72 g, 74 %), Rf 0.76 (ethyl acetate/dichloromethane 1:4), m.p. > 250 °C (lit.[1] > 250 °C).

δ^1H / ppm (300 MHz, $CDCl_3$): 2.24 [s, 6H, *p*-CH_3], 2.40 [s, 12H, *o*-CH_3], 3.52 [s, 4H, CH_2], 6.83 [s, 4H, *m*-CH].

Lit.[1] δ^1H / ppm (300 MHz, $CDCl_3$): 2.22 [s, 6H, *p*-CH_3], 2.44 [s, 12H, *o*-CH_3], 3.67 [s, 4H, CH_2CH_2], 6.96 [s, 4H, *m*-CH].

ν_{max} / cm^{-1}: 1446 (CH), 1604 (NH) 2850 and 2912 (CH).

5.1.3. 1,3-Bis(2,4,6-trimethylphenyl)-4,5-dihydroimidazolium tetrafluoroborate (264)

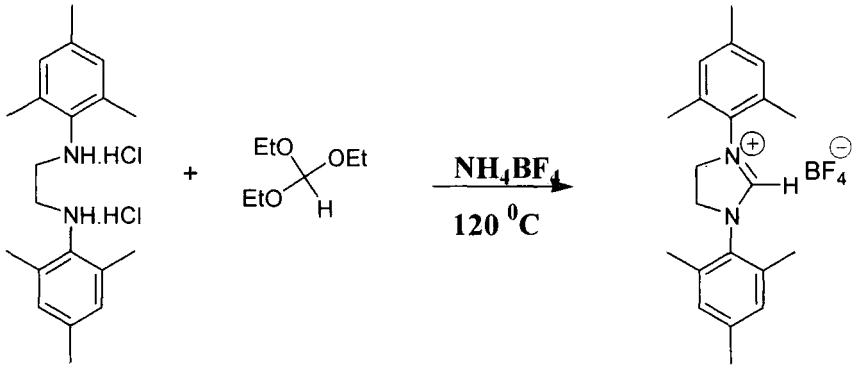

(263) **(264)**

1,3-Bis(2,4,6-trimethylphenylamino)ethane dihydrochloride **(263)** (1.00 g, 2.71 mmol), was added to ammonium tetrafluoroborate (0.280 g, 2.67 mmol) and triethyl orthoformate (3.00 mL, 0.003 mol). The beige liquid obtained yielded a precipitate of similar colour, which was then isolated by suction filtration. Hot ethanol was added to the mother liquor and it was placed in the freezer for three days. The white crystals formed were filtered, washed with hexane, dried *in vacuo* and recrystallized from ethanol to yield tetrafluoroborate product **(264)** was recrystallized from ethanol to yield (1.02 g, 96 %). m.p. > 250 °C (lit.[1] >250°C).

δ^1H / ppm (300 MHz, $CDCl_3$): 2.32 [s, 6H, *p*-CH_3], 2.37 [s, 12H, *o*-CH_3], 4.55 [s, 4H, CH_2CH_2], 7.00 [s, 4H, *m*-CH], 7.91 [s, 1H, NC*H*N].

Lit.[1] δ^1H / ppm (300 MHz, $CDCl_3$): 2.32 [s, 6H, *p*-CH_3], 2.37 [s, 12H, *o*-CH_3], 4.43 [s, 4H, CH_2CH_2], 7.08 [s, 4H, *m*-CH].8.14 [s, 1H, NC*H*N]

^{13}C / ppm (300 MHz, DMSO-d_6): 17.9 [s, *o*-CH_3], 21.3 [s, *p*-CH_3], 51.6 [s, CH_2CH_2], 130.2 [s, *m*-C], 131.6 [s, ipso-C], 136.1 [s, *o*-C], 140.4 [s, *p*-C], 160.5 [s, NCN].

Lit.[1] ^{13}C / ppm (300 MHz, DMSO-d_6)[1]: 17.9 [s, *o*-CH_3], 21.2 [s, *p*-CH_3], 52.2 [s, CH_2CH_2], 130.6 [s, *m*-C], 131.4 [s, ipso-C], 136.5 [s, *o*-C], 140.5 [s, *p*-C], 160.4 [s, NCN].

MS+ *m/z*: 307.3 (M^+, 100%).

5.1.4. 1,3-Bis(2,4,6-trimethylphenyl)-4,5-dihydroimidazolium chloride (117)[1]

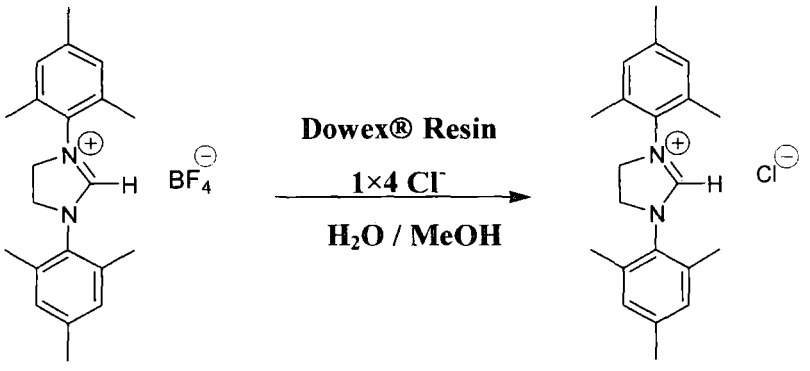

(264) **(117)**

Dowex® anion exchange resin in the chloride form (5.00 g) was fully hydrated into a resin - water slurry, then packed in a column (10 cm). 1,3-Bis(2,4,6-trimethylphenyl)-4,5-dihydroimidazolium tetrafluoroborate **(264)** (0.150 g, 0.381 mmol), was dissolved in a minimum volume of methanol and water (20 mL) and run through the column. The column was washed several times with water and methanol. The resulting analyte solution was concentrated and dried *in vacuo* to give the chloride product as an off-white solid **(117)** (0.131g, 92 %),. m.p. >250 °C (Lit.[1] >250 °C).

δ^1H / ppm (300 MHz, $CDCl_3$): 2.31[s, 6H, *p*-CH_3], 2.42 [s, 12H, *o*-CH_3], 4.68 [s, 4H, CH_2CH_2], 6.99 [s, 4H, *m*-CH], 8.32 [s, NCHN].

Lit.[1] δ^1H / ppm (300 MHz, $CDCl_3$): 2.28 [s, 6H, *p*-CH_3], 2.36 [s, 12H, *o*-CH_3], 4.48 [s, 4H, CH_2CH_2], 7.08 [s, 4H, *m*-CH].9.22 [s, 1H, NC*H*N].

^{13}C / ppm (300 MHz, DMSO-d_6): 16.7[s, *o*-CH_3], 20.1[s, *p*-CH_3], 51.1[s, CH_2CH_2], 129.5[s, *m*-C], 131.4[s, ipso-C], 135.6[s, *o*-C], 140.9[s, *p*-C], 159.9[s, NCN].

Lit.[1] ^{13}C / ppm (300 MHz, DMSO-d_6)[1]: 17.2 [s, *o*-CH_3], 20.5 [s, *p*-CH_3], 50.9 [s, CH_2CH_2], 129.3 [s, *m*-C], 130.8 [s, ipso-C], 135.3 [s, *o*-C], 139.5 [s, *p*-C], 160.2[s, NCN].

ν_{max} / cm^{-1}: 1487 (CH), 1618 (N=C) and 2843 (CH).

$C_{21}H_{27}N_2Cl$

Requires:	%C 73.56	%H 7.94	%N 8.17
Found:	%C 73.44	%H 7.42	%N 8.26

5.1.5. 1,3-Bis(2,4,6-trimethylphenyl)imidazolium chloride (109)[1].

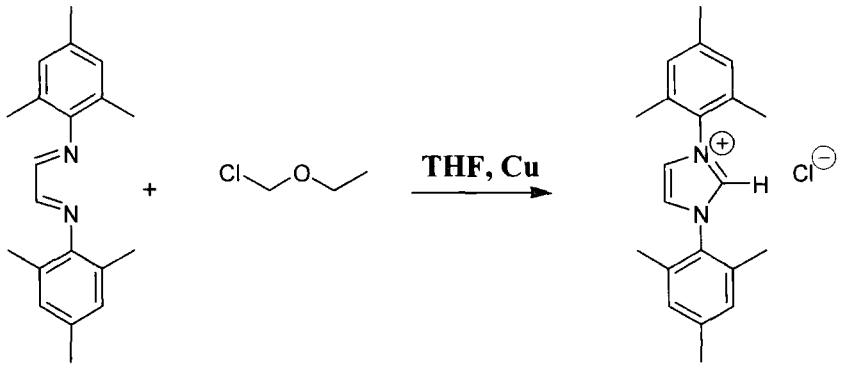

(262) **(109)**

Chloromethylethyl ether (0.300 g, 3.17 mmol) in THF (1 mL) was added to a solution of glyoxal-bis(2,4,6-trimethylphenyl)imine **(260)** (0.900 g, 3.08 mmol) in THF (10 mL). An extraction thimble (15 × 50 mm) charged with 4 Å molecular sieves was suspended in the

reaction flask using copper wire. After 30 min stirring under nitrogen at room temperature, a white solid precipitated. The resulting product was collected by suction filtration and recrystallized from *n*-hexane to yield a white powder **(109)** (0.49 g, 48 %), Rf 0.76 (hexane/dichloromethane 3:2), m.p. > 250 °C, (lit.[1] > 250 °C).

δ^1H / ppm (300 MHz, $CDCl_3$): 2.20 [s, 12H, *o*-CH_3], 2.35 [s, 6H, *p*-CH_3], 7.04 [s, 4H, *m*-CH], 7.57 [s, 2H, C*H*C*H*], 11.04 [s, 1H, NC*H*N].

Lit. δ^1H / ppm (300 MHz, $CDCl_3$): 2.17[s,12H, *o*-CH_3], 2.37 [s, 6H, *p*-CH_3], 7.08 [s, 4H, *m*-CH], 7.61 [s, 2H, C*H*C*H*], 11.05 [s, 1H, NC*H*N].

^{13}C / ppm (300 MHz, DMSO-d_6): 17.7 [s, *o*-CH_3], 21.1 [s, *p*-CH_3], 124.2 [s,*C*H*C*H], 129.9 [s, *o*-C], 130.6 [s, ipso-C], 134.1 [s, *o*-C], 140.0 [s, *p*-C], 141.4 [s,N*C*N].

ν_{max} / cm^{-1}: 1480 (CH), 1537 (CC) and 2892 (CH).

$C_{21}H_{27}N_2BF_4$

Requires:	%C 73.99	%H 7.39	%N 8.22
Found:	%C 73.42	%H 7.26	%N 8.01

5.1.6. Glyoxal-bis(*p*-methoxyphenyl)imine (265)

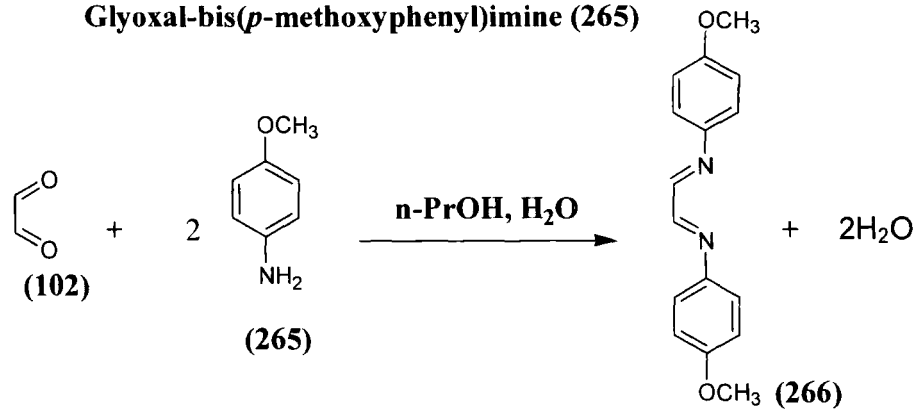

(102) **(265)** **(266)**

p-Anisidine (*p*-methoxyaniline), **(265)** (4.59 g, 37.3 mmol) in *n*-propanol (40 mL) was added to glyoxal **(102)** (40 wt % aqueous solution, 2.16 g, 18.6 mmol) in H_2O (5 mL). The green-yellow solution was stirred at room temperature for 4 hours after which time the reaction was complete. The mixture was filtered and the precipitate washed with water, and recrystallised from ethyl acetate (30 mL). The product **(266)** formed as large yellow needle like crystals (4.99 g, 67 %), Rf 0.83 (petroleum ether /ethyl acetate 3:2), m.p. 166-168 °C.

δ^1H / ppm (300 MHz, $CDCl_3$): 3.82 [s, 6H, *p*-OCH_3], 6.95 [d, $^3J_{H,H}$ = 8.25 Hz, 4H, *m*-CH], 7.32 [d, $^3J_{H,H}$ = 8.25 Hz, 4H, *o*-CH], 8.41 [s, 2H, C*H*C*H*].

^{13}C / ppm (500 MHz, $CDCl_3$): 55.7 [s, OCH_3], 14.8 [s, *m*-CH], 123.2 [s, *o*-CH], 143.2 [s, *p*-C], 157.8 [s, NCH], 159.9 [s, ipso-C].

ν_{max} / cm^{-1}: 824 (CH), 1249 (C-O), 1498 (CH), 1606 (C=N) and 2835 (CH).

$C_{16}H_{16}N_2O_2$

Requires:	%C 71.62	%H 6.01	%N 10.44
Found:	%C 71.51	%H 6.06	%N 10.43

5.1.7. 1,3-Bis(*p*-methoxyphenyl)ethane (267).

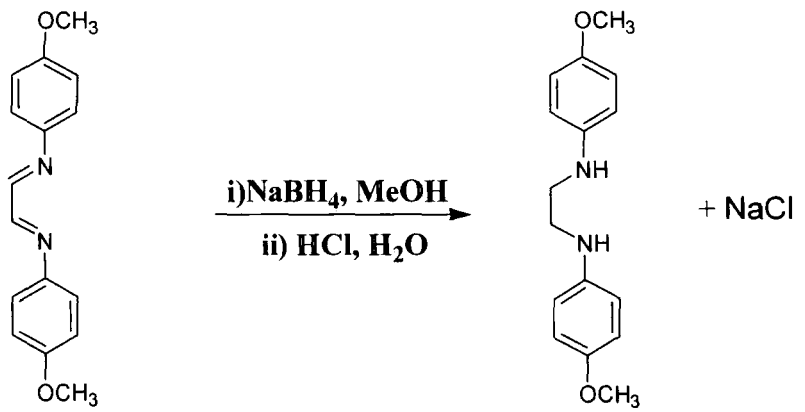

(266) **(267)**

Glyoxal–bis(*p*-methoxyphenyl)imine **(266)** (0.500 g, 1.80 mmol) in methanol (50 mL) and THF (10 mL) was treated at 0 °C with $NaBH_4$ (0.145 g, 3.70 mmol) dissolved in sodium hydroxide (1.50 mL 1.0 N) and water (10 mL). The solution was refluxed for 1 hour at 80 °C, under nitrogen until it turned colourless. A further 10 mL of water was added and the solution was concentrated *in vacuo*. Yellow crystals were observed to precipitate out of solution, which were collected by suction filtration and dried to yield bis amine **(267)** (4.70 g, 78 %). Rf. 0.72 (petroleum ether /ethyl acetate 3:2) m.p. 117-120 °C.

δ^1H / ppm (300 MHz, $CDCl_3$): 3.33 [s, 4H, CH_2CH_2], 3.75 [s, 6H, *p*-OCH_3], 6.50 [d, $^4J_{H,H}$ = 2.4 Hz, 4H, *m*-CH], 6.90 [d, $^3J_{H,H}$ = 2.4 Hz, 4H, *o*-CH].

^{13}C / ppm (500 MHz, $CDCl_3$): 44.6 [s, CH_2CH_2], 56.0 [s, OCH_3], 114.6 [s, *m*-CH], 115.1 [s, *o*-CH], 142.5 [s, *p*-C], 152.6 [s, ipso-C].

ν_{max} / cm^{-1}: 813 (CH) 1226 (CO), 1501 (CC), 3112 (NH).

MS+ *m/z*: 273.2 (M^+, 100%).

5.1.8. 1,3-Bis(*p*-methoxyphenyl)-4,5-dihydroimidazolium tetrafluoroborate (268).

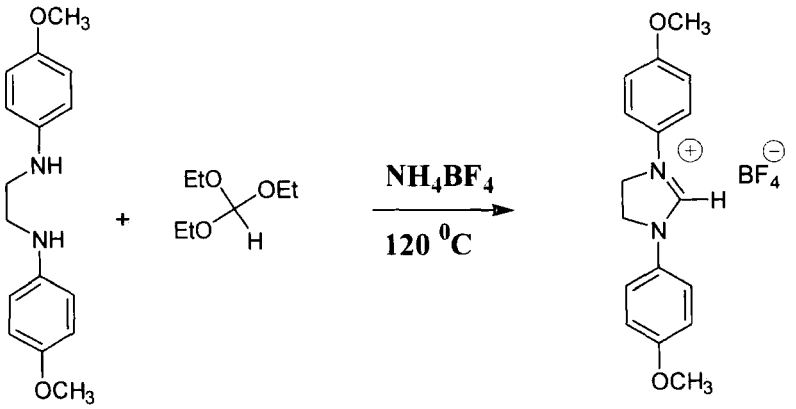

(267) **(268)**

1,3-Bis(*p*-methoxyphenylamino)ethane **(267)** (1.00 g, 0.0036 mol), was added to ammonium tetrafluoroborate (0.380 g, 0.0036 mol) and triethyl orthoformate (10 mL). The mixture was refluxed at 120 °C for 3 hours. The resulting yellow liquid contained a beige precipitate, which was isolated by suction filtration and dried *in vacuo*. Recrystallization from ethanol yielded dihydroimidazolium salt **(268)** (0.35 g, 30 %), Rf 0.18 (Diethyl ether/ethyl acetate 4:3) m.p. > 250 °C.

δ^1H / ppm (300 MHz, $CDCl_3$): 3.80 [s, 6H, *p*-OCH_3], 4.51 [s, 4H, im-CH_2CH_2], 7.10 [d, $^3J_{H,H}$ =3.3, 4H, *m*-CH], 7.55 [d, $^3JH_{,H}$ = 3.3 Hz, 4H, *o*-CH], 9.71 [s, 1H, NC*H*N].

^{13}C / ppm (500 MHz, DMSO-d_6): 49.2 [s, CH_2CH_2], 56.2 [s, OCH_3], 115.4 [s, *m*-CH], 120.6.1 [s, *o*-CH], 130.0 [s, *p*-C], 151.4 [s, NCHN], 158.6 [s, ipso-C].

5.1.9. 1,3-Bis(*p*-methoxyphenyl)-4,5-dihydroimidazolium chloride (118).

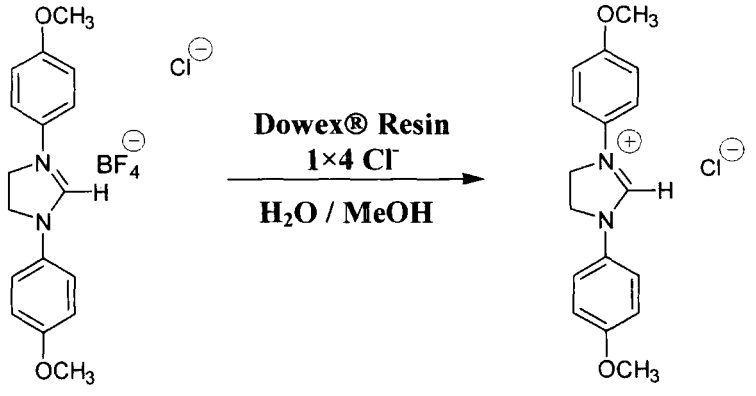

(268) **(118)**

Dowex® anion exchange resin in the chloride form (5.00 g), was fully hydrated into a resin – water slurry then packed in a column (5 mL). 1,3-Bis(*p*-methoxyphenyl)-4,5-dihydroimidazolium tetrafluoroborate **(266)** (1.00 g 3.10 mmol), was dissolved in methanol (30mL) and then water was added (10 mL). The solution was run through the

column and the column was washed with water and methanol. The resulting analyte solution was concentrated and dried *in vacuo* to give the chloride product **(118)** (0.35 g, 100 %), Rf 0.18 (Diethyl ether/ethyl acetate 4:3), m.p. >250 °C.

δ^1H / ppm (300 MHz, $CDCl_3$): 3.80 [s, 6H, *p*-OCH_3], 4.51 [s, 4H, CH_2CH_2], 7.10 [d, $^3J_{H,H}$ =3.3, 4H, *m*-CH], 7.55 [d, $^3J_{H,H}$ = 3.3 Hz, 4H, *o*-CH] , 9.73 [s, 1H, NC*H*N].

^{13}C / ppm (500 MHz, DMSO-d_6): 49.2 [s, CH_2CH_2], 56.2 [s, OCH_3], 115.4 [s, *m*-CH], 120.6.1 [s, *o*-CH], 130.0 [s, *p*-C], 151.4 [s, NCHN], 158.6 [s, ipso-C].

ν_{max} / cm^{-1}: 831(CH), 1287 (C-O), 1515 (CC), 1615 and 3440 (C=N).

MS+ *m/z*: 283.2 (M^+, 100%).

$C_{17}H_{19}N_2O_2Cl$ + 1½(H_2O)

Requires:	%C 59.04	%H 6.41	%N 8.10
Found:	%C 59.12	%H 6.30	%N 7.99

5.1.10. 1,3-Bis(*p*-methoxyphenyl)imidazolium chloride (110).

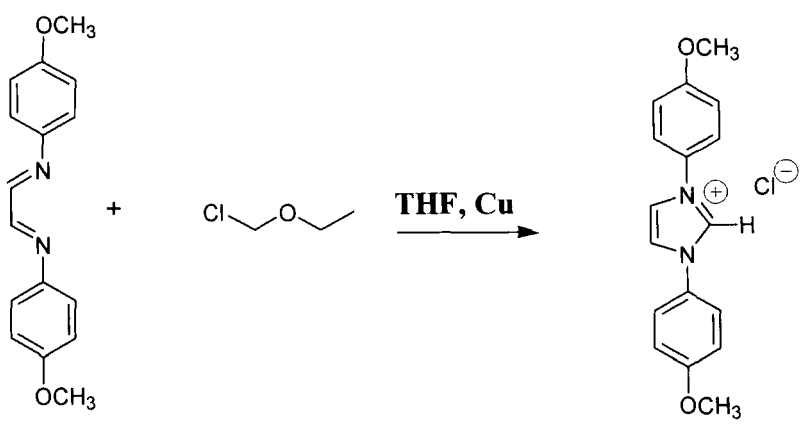

(266) **(110)**

Chloromethylethyl ether (0.330 g, 3.40 mmol) in THF (15 mL) was added to glyoxal-bis(*p*-methoxyphenyl)imine **(266)** (10 g, 3.4 mmol) in a large reaction vessel. An extraction thimble (15 × 50 cm) charged with 4 Å molecular sieves was suspended in the reaction flask using copper wire. After 24 hours stirring under nitrogen at room temperature, a black solid precipitated. The solid was collected by suction filtration and purified by column chromatography on a silica column (methanol/dichloromethane 1:9) to yield product **(110)** as a beige powder (0.980 g, 91 %), Rf 0.32 (methanol/dichloromethane 1:9). m.p. > 250 °C.

δ^1H / ppm (400 MHz, $CDCl_3$): 3.60 [s, 6H, *p*-OCH_3], 6.99 [d, $^3J_{H,H}$ = 9.0 Hz 4H, *m*-CH], 7.60 [d, $^3J_{H,H}$ = 9.0 Hz, 4H, *o*-CH], 8.21 [s, 2H, C*HCH*], 9.98 [s, 1H, NC*H*N].

^{13}C / ppm (500 MHz, $CDCl_3$): 58.4 [s, OCH_3], 118.0 [s, *m*-CH], 125.0 [s, *p*-C], 126.6 [s, *o*-CH], 130.7 [s, *C*HCH], 162.9 [s, NCN].

ν_{max} / cm^{-1}: 820 (CH), 1281(C=O), 1501(CC), 1556 and 3332 (C=N).

MS+ *m/z*: 281.1 (M^+, 100%).

$C_{17}H_{17}N_2O_2Cl$ +1½(H_2O)

Requires:	%C 59.39	%H 5.86	%N 8.15
Found:	%C 59.20	%H 5.60	%N 8.04

The X-ray crystal structure of 1,3-bis(*p*-methoxyphenyl)imidazolium chloride **(110)** determined in this work is described in Section 5.1.16

5.1.11 Glyoxal-bis(2,6-di-*iso*propylphenyl)imine (270).

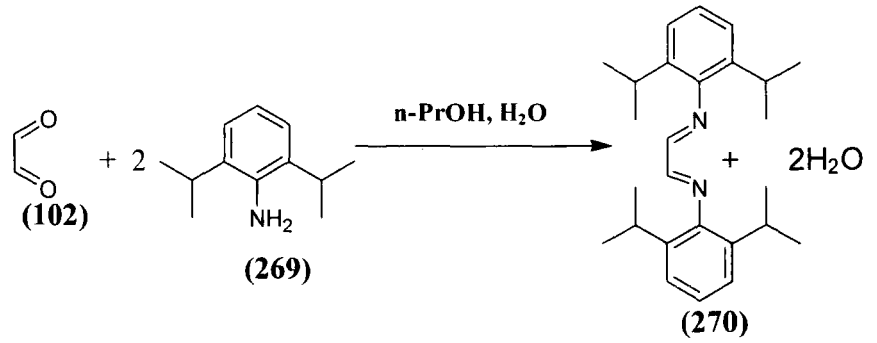

(102) (269) (270)

2,6-Di-*iso*propylaniline **(269)** (3.80 g, 0.010 mol) in *n*-propanol (25mL) was added to glyoxal **(102)** (40 wt % aqueous solution, (0.730 g, 0.005 mol) in H_2O (2 mL). The solution rapidly turned yellow and was stirred at 25 °C overnight. A further addition of water (10 mL) was added the mixture which yielded a bright yellow precipitate. The mixture was filtered and the precipitate washed with water, and recrystallised from ethyl acetate (15 mL) to yield product **(270)** as large cubic crystals (2.98 g, 78%), Rf 0.83 (chloroform) m.p. 130-131 °C.

δ^1H / ppm (400 MHz, $CDCl_3$): 1.20 [d, $^3J_{H,H}$ = 8.5 Hz 24H, $CH(CH_3)_2$], 2.94 [septet, $^3J_{H,H}$ = 8.5 Hz 4H, $CH(CH_3)_2$], 7.15 [m, 6H, Ar-CH], 8.10 [s, 2H, CHCH].

^{13}C / ppm (500 MHz, $CDCl_3$): 23.6 [s, $CH(CH_3)_2$], 28.2 [s, $CH(CH_3)_2$], 123.4 [s, *m*-CH], 125.3 [s, *p*-CH], 136.9 [s, *o*-CH], 148.2 [s, ipso-C], 163.3 [s, NCH].

ν_{max} / cm^{-1}: 1458 (CH), 1624 (CN) and 2958 (CH).

$C_{26}H_{36}N_2$

Requires:	%C 82.93	%H 9.64	%N 7.44
Found:	%C 82.93	%H 9.76	%N 7.21

5.1.12. 1,3-Bis(2,6-di-*iso*propylphenylamino)ethane (271).

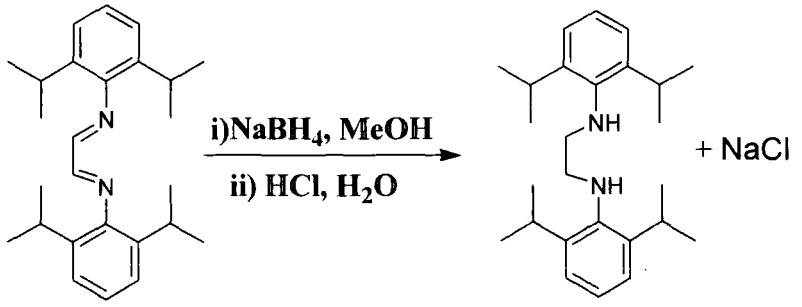

(270) **(271)**

Glyoxal–bis(2,6-di-*iso*propylphenyl)imine **(270)** (1.00 g, 2.70 mmol) in methanol (50mL) and THF (30 mL) was treated at 0 °C with $NaBH_4$ (0.01 g, 2.70 mmol) dissolved in sodium hydroxide (2 mL 1.0 N) and water (5 mL). The solution was refluxed for 16 hours at 80 °C under nitrogen, then quenched with HCl (0.5 M) and a further 30 mL of water was added. The solution was concentrated and a white shiny solid precipitated. The amine **(271)** was collected by suction filtration, and dried *in vacuo* (1.02 g 100%), Rf 0.45 (chloroform) m.p. 218-220 °C.

δ^1H / ppm (400 MHz, $CDCl_3$): 1.25 [d, $^3J_{H,H}$ = 6.8 Hz, 24H, $CH(CH_3)_2$], 3.31 [s, 4H, CH_2CH_2], 3.36 [septet, $^3J_{H,H}$ = 6.8 Hz 4H, $CH(CH_3)_2$], 7.22 [m, 6H, Ar-CH].

ν_{max} / cm^{-1}: 1439 and 2864 (CH), 2960 (NH).

MS+ *m/z*: 381.4 (M^+, 100%).

$C_{26}H_{40}N_2$

Requires:	%C 82.05	%H 10.59	%N 7.36
Found:	%C 81.66	%H 10.52	%N 7.59

5.1.13. 1,3-Bis(2,6-di-*iso*propylphenyl)-4,5-dihydroimidazolium tetrafluoroborate (272)

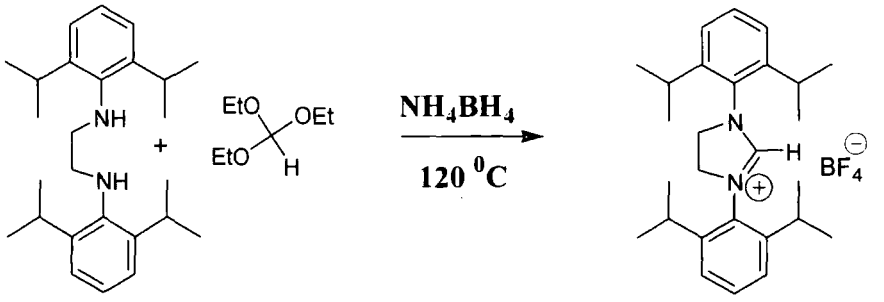

(271) **(272)**

1,3-Bis(2,6-di-*iso*propylphenyl)ethane **(271)** (0.067 g, 0.18 mmol), was added to ammonium tetrafluoroborate (0.018 g, 0.18 mmol) and triethyl orthoformate (10 mL). The mixture was refluxed at 120 °C for 24 hours. The resulting yellow liquid contained a crystalline beige precipitate. The solid was isolated and recrystalized from ethanol to yield product **(272)** as a crystalline solid (0.62 g, 54%), Rf 0.64 (diethyl ether/ethyl acetate 4:3) m.p. > 250 °C.

δ^1H / ppm (300 MHz, DMSO): 1.19 [d, $^3J_{H,H}$ = 7.0 Hz, 12H, CH(C*H*$_3$)$_2$], 1.34 [d, $^3J_{H,H}$ = 7.0 Hz, 12H, CH(C*H*$_3$)$_2$], 3.07 [septet, $^3J_{H,H}$ = 7 Hz, 4H, C*H*(CH$_3$)$_2$], 4.53 [s, 4H, C*H*$_2$C*H*$_2$], 7.42 [d, $^3J_{H,H}$ = 7.5 Hz, 4H, *m*-CH], 7.54 [t, $^3J_{H,H}$ = 7.5 Hz 2H, *p*-CH], 9.43 [s, 1H, NC*H*N].

^{13}C / ppm (500 MHz, DMSO-d_6): 24.0 [s, C(*C*H$_3$)$_3$], 28.9 [s, *C*H$_2$*C*H$_2$], 54.3 [s, *C*(CH$_3$)$_3$], 125.5 [s, *m*-C], 130.5 [s, ipso-C], 131.7 [s, *o*-C], 146.8 [s, *p*-C], 160.7[s, N*C*N].

ν_{max} / cm^{-1}: 1460 (CH), 1625 (C=N).

MS+ *m/z*: 391.4 (M$^+$, 100%).

The X-ray crystal structure of 1,3-bis(2,6-di-*iso*propylphenyl)imidazolium tetrafluouroborate (272) determined in this work is described in Section 5.1.17.

$C_{27}H_{39}N_2\ BF_4\ ½(H_2O)$

Requires:	%C 66.53	%H 8.27	%N 5.75
Found:	%C 66.19	%H 8.10	%N 5.72

5.1.14. 1,3-Bis(2,6-di-*iso*propylphenyl)-4,5-dihydroimidazolium chloride (118).

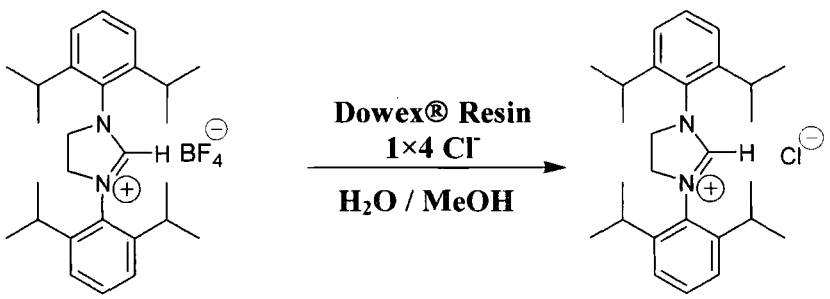

(272) **(118)**

Dowex® anion exchange resin in the chloride form (5 g), was fully hydrated into a resin-water slurry then packed in a column (10 cm). 1,3-Bis(2,6-diisopropylphenyl)-4,5-dihydroimidazolium tetrafluoroborate **(272)** (0.08 g, 0.16mmol), was dissolved in methanol, (15 mL) and water (10 m) and run through the column. The column was then washed with methanol and water. The resulting analyte solution and washings were concentrated and dried *in vacuo* to yield a white solid **(118)** (0.070 g, 100 %), Rf 0.72 (diethyl ether/ethyl acetate 4:3), m.p. >250 °C .

δ^1H / ppm (300 MHz, DMSO): 1.19 [d, $^3J_{H,H}$ = 7.0 Hz, 12H, $CH(CH_3)_2$], 1.34 [d, $^3J_{H,H}$ = 7.0 Hz, 12H, $CH(CH_3)_2$], 3.07 [septet, $^3J_{H,H}$ = 7 Hz, 4H, $CH(CH_3)_2$], 4.53 [s, 4H, CH_2CH_2], 7.42 [d, $^3J_{H,H}$ = 7.5 Hz, 4H, *m*-CH], 7.54 [t, $^3J_{H,H}$ = 7.5 Hz 2H, *p*-CH], 9.43 [s, 1H, NCHN].

^{13}C / ppm (500 MHz, DMSO-d_6): 24.0 [s, $C(CH_3)_3$], 28.9 [s, CH_2CH_2], 54.3 [s, $C(CH_3)_3$], 125.5 [s, *m*-C], 130.5 [s, ipso-C], 131.7 [s, *o*-C], 146.8 [s, *p*-C], 160.7[s, NCN].

$C_{27}H_{39}N_2Cl$

Requires: %C 75.93 %H 9.20 %N 6.56

Found: %C 75.77 %H 9.03 %N 6.50

5.1.15. 1,3-Bis(2,6-di-*iso*propylphenyl)imidazolium chloride (112).

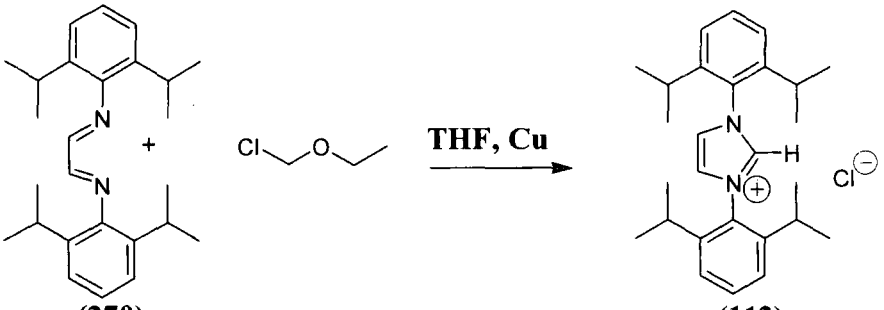

(270) **(112)**

Chloromethylethyl ether (0.250 g, 20.7 mmol) in THF (7 mL) was added to glyoxal-bis(2,6-di-*iso*propylphenyl)imine **(270)** (1.00 g, 2.70 mmol) in a large reaction vessel. An extraction thimble (15 × 50 mm) charged with 4 Å molecular sieves was suspended in the reaction flask using copper wire. After 24 hours stirring under nitrogen at room temperature, a pale precipitate appeared out of the dark red solution. The resulting precipitate was collected by suction filtration and dried to yield the product **(112)** as a powder (1.07 g, 94 %). Rf 0.28 (methanol/dichloromethane 1:9) m.p. > 250 °C.

δ^1H / ppm (400 MHz, $CDCl_3$): 1.22 [d, $^3J_{H,H}$ = 6.6 Hz 12H, $CH(CH_3)_2$], 1.28 [d, $^3J_{H,H}$ = 6.6 Hz 12H, $CH(CH_3)_2$], 2.44 [septet, $^3J_{H,H}$ = 6.6 Hz 4H, $CH(CH_3)_2$], 7.36 [d, $^3J_{H,H}$ = 7.7 Hz 4H, *m*-CH], 7.57 [t, $^3J_{H,H}$ = 7.7 Hz 2H, *p*-CH], 8.09 [s, 2H, CHCH], 9.60 [s, 1H, NCHN].

^{13}C / ppm (300 MHz, DMSO-d_6): 23.7 [s, $C(CH_3)_3$], 29.1 [s, CHCH], 55.2 [s, $C(CH_3)_3$], 124.8 [s, *m*-C], 126.8 [s, *o*-C], 132.2 [s, *p*-C], 139.0 [s, CHCH], 151.0 [s, NCN].

ν_{max} / cm^{-1}: 802, 1461 (CH), 1521 (CC) and 2878 (CH).

MS+ *m/z*: 389.4 (M^+, 100%).

$C_{27}H_{37}N_2Cl_2+0.5(H_2O)$

Requires: %C 71.60 %H 8.73 %N 6.30

Found: %C 72.48 %H 8.45 %N 6.26

5.1.16 X-Ray crystallographic data for 1,3-bis(*p*-methoxyphenyl)-imidazolium chloride (110).

Table 5.1: Crystal data and structure refinement for 1,3-bis(*p*-methoxyphenyl)-imidazolium chloride (110).

Empirical formula	$C_{17}H_{19}N_2O_3Cl$
Molecular formula	$[C_{17}H_{17}N_2O_2]^+Cl^- \times H_2O$
Formula weight	334.79
Temperature	293(2) K
Wavelength	0.71073 Å
Crystal system	Monoclinic
Space group	C2 (#5)
Unit cell dimensions	a = 15.672(2) Å α= 90°.
	b = 9.4073(14) Å β= 90.038(2)°.
	c = 5.3976(8) Å γ = 90°.
Volume	795.8(2) $Å^3$
Z	2
Density (calculated)	1.397 Mg/m^3
Absorption coefficient	0.257 mm^{-1}
F(000)	352
Crystal size	0.40 x 0.20 x 0.20 mm^3
Theta range for data collection	2.53 to 25.99°.
Index ranges	–19<=h<=19, –11<=k<=11, –6<=l<=6
Reflections collected	6158
Independent reflections	1571 [R(int) = 0.0187]
Completeness to theta = 26.00°	100.0 %
Absorption correction	Semi–empirical from equivalents

Max. and min. transmission	0.9504 and 0.8792
Refinement method	Full–matrix least–squares on F^2
Data / restraints / parameters	1571 / 1 / 145
Goodness–of–fit on F^2	1.096
Final R indices [I>2sigma(I)]	R1 = 0.0288, wR2 = 0.0732
R indices (all data)	R1 = 0.0294, wR2 = 0.0738
Absolute structure parameter	0.37(6) [a]
Largest diff. peak and hole	0.150 and –0.234 e.Å^{-3}

[a] hence refined as inversion twin

Table 5.2: Atomic coordinates (x 10^4) and equivalent isotropic displacement parameters (Å^{2}x 10^3) for 1,3-bis(*p*-methoxyphenyl)imidazolium chloride (110). U(eq) is defined as one third of the trace of the orthogonalized U^{ij} tensor.

Atom	x	y	z	U(eq)
C(1)	0	2132(2)	15000	35(1)
N	421(1)	1306(1)	13409(2)	34(1)
C(2)	258(1)	–93(2)	14012(3)	45(1)
C(3)	968(1)	1796(1)	11432(2)	34(1)
C(4)	1044(1)	3242(2)	10968(3)	41(1)
C(5)	1573(1)	3704(2)	9096(3)	45(1)
C(6)	2038(1)	2733(2)	7685(3)	39(1)
O(1)	2558(1)	3306(1)	5925(2)	52(1)
C(9)	3064(1)	2351(2)	4497(3)	55(1)
C(7)	1944(1)	1297(2)	8145(3)	44(1)
C(8)	1408(1)	825(2)	10017(3)	43(1)
Cl	10000	7059(1)	10000	79(1)
O(2)	10000	5373(2)	5000	57(1)

Table 5.3: Bond lengths (Å) and angles (°) for 1,3-bis(*p*-methoxyphenyl)-imidazolium chloride (110).

Bond	Bond Lengths (Å)
C(1)–N	1.3329(16)
C(1)–N#1	1.3329(16)
C(1)–H(1)	0.95(3)
N–C(2)	1.3799(18)
N–C(3)	1.4448(16)
C(2)–C(2)#1	1.339(3)
C(2)–H(2)	0.94(2)
C(3)–C(8)	1.3761(19)
C(3)–C(4)	1.388(2)
C(4)–C(5)	1.378(2)
C(4)–H(4)	0.91(2)
C(5)–C(6)	1.395(2)
C(5)–H(5)	0.84(3)
C(6)–O(1)	1.3629(18)
C(6)–C(7)	1.381(2)
O(1)–C(9)	1.426(2)
C(9)–H(9A)	1.06(2)
C(9)–H(9B)	0.96(2)
C(9)–H(9C)	1.02(3)
C(7)–C(8)	1.388(2)
C(7)–H(7)	0.84(2)
C(8)–H(8)	0.93(2)
O(2)–H(1O2)	0.78(2)

Bond	Bond Angles (°)
N–C(1)–N#1	108.68(17)
N–C(1)–H(1)	125.66(8)
N#1–C(1)–H(1)	125.66(9)
C(1)–N–C(2)	108.22(12)
C(1)–N–C(3)	125.74(12)
C(2)–N–C(3)	126.02(11)
C(2)#1–C(2)–N	107.44(8)
C(2)#1–C(2)–H(2)	130.5(14)
N–C(2)–H(2)	121.9(14)
C(8)–C(3)–C(4)	120.48(12)
C(8)–C(3)–N	119.76(12)
C(4)–C(3)–N	119.76(11)
C(5)–C(4)–C(3)	119.53(13)
C(5)–C(4)–H(4)	119.3(13)
C(3)–C(4)–H(4)	121.1(13)
C(4)–C(5)–C(6)	120.59(14)
C(4)–C(5)–H(5)	119.9(13)
C(6)–C(5)–H(5)	119.5(14)
O(1)–C(6)–C(7)	125.15(13)
O(1)–C(6)–C(5)	115.76(13)
C(7)–C(6)–C(5)	119.08(14)
C(6)–O(1)–C(9)	117.44(14)
O(1)–C(9)–H(9A)	111.6(12)
O(1)–C(9)–H(9B)	105.1(14)
H(9A)–C(9)–H(9B)	116(2)
O(1)–C(9)–H(9C)	107.2(14)
H(9A)–C(9)–H(9C)	107.9(17)
H(9B)–C(9)–H(9C)	108.5(19)
C(6)–C(7)–C(8)	120.56(14)
C(6)–C(7)–H(7)	120.9(15)
C(8)–C(7)–H(7)	118.5(15)
C(3)–C(8)–C(7)	119.72(13)

C(3)–C(8)–H(8)	117.4(12)
C(7)–C(8)–H(8)	122.9(12)

Symmetry transformations used to generate equivalent atoms: #1 –x,y,–z+3

Table 5.4: Anisotropic displacement parameters ($Å^2$x 10^3) for 1,3-bis(*p*-methoxyphenyl)imidazolium chloride (110). The anisotropic displacement factor exponent takes the form: $-2\pi^2[h^2 a^{*2} U^{11} + ... + 2 h k a^* b^* U^{12}]$

Atom	U^{11}	U^{22}	U^{33}	U^{23}	U^{13}	U^{12}
C(1)	39(1)	30(1)	35(1)	0	1(1)	0
N	38(1)	28(1)	35(1)	–2(1)	–1(1)	0(1)
C(2)	61(1)	27(1)	46(1)	–1(1)	5(1)	2(1)
C(3)	34(1)	36(1)	32(1)	–2(1)	–2(1)	0(1)
C(4)	47(1)	32(1)	45(1)	–6(1)	10(1)	2(1)
C(5)	51(1)	32(1)	50(1)	–2(1)	9(1)	–1(1)
C(6)	37(1)	44(1)	35(1)	–3(1)	2(1)	2(1)
O(1)	55(1)	50(1)	50(1)	–4(1)	18(1)	–2(1)
C(9)	47(1)	66(1)	53(1)	–10(1)	14(1)	4(1)
C(7)	48(1)	40(1)	43(1)	–7(1)	7(1)	9(1)
C(8)	52(1)	30(1)	48(1)	–2(1)	5(1)	4(1)
Cl	160(1)	40(1)	38(1)	0	8(1)	0
O(2)	94(1)	31(1)	44(1)	0	11(1)	0

Table 5.5: Hydrogen coordinates (x 10^4) and isotropic displacement parameters ($Å^2$x 10^3) for 1,3-bis(*p*-methoxyphenyl)imidazolium chloride (110).

Atom	x	y	z	U(eq)
H(1)	0	3150(40)	15000	61(8)
H(2)	514(13)	–850(30)	13160(40)	72(6)
H(4)	728(11)	3890(30)	11830(30)	54(5)
H(5)	1622(12)	4580(30)	8810(40)	60(6)
H(9A)	2681(13)	1680(30)	3380(40)	73(6)
H(9B)	3427(13)	1880(30)	5680(40)	71(6)
H(9C)	3436(16)	2950(30)	3350(50)	87(7)
H(7)	2204(13)	690(30)	7290(40)	58(5)
H(8)	1342(11)	–130(20)	10410(30)	52(5)
H(1O2)	9989(14)	5820(30)	6200(40)	65(6)

Table 5.6: Torsion angles (°) for 1,3-bis(*p*-methoxyphenyl)imidazolium chloride (110).

Bond	Torsion Angle (°)
N#1–C(1)–N–C(2)	0.18(8)
N#1–C(1)–N–C(3)	–178.53(12)
C(1)–N–C(2)–C(2)#1	–0.5(2)
C(3)–N–C(2)–C(2)#1	178.22(14)
C(1)–N–C(3)–C(8)	175.92(10)
C(2)–N–C(3)–C(8)	–2.56(18)
C(1)–N–C(3)–C(4)	–4.31(16)
C(2)–N–C(3)–C(4)	177.20(14)
C(8)–C(3)–C(4)–C(5)	–0.9(2)
N–C(3)–C(4)–C(5)	179.38(13)
C(3)–C(4)–C(5)–C(6)	–0.7(2)
C(4)–C(5)–C(6)–O(1)	–178.36(13)
C(4)–C(5)–C(6)–C(7)	1.8(2)

C(7)–C(6)–O(1)–C(9)	–2.0(2)
C(5)–C(6)–O(1)–C(9)	178.12(14)
O(1)–C(6)–C(7)–C(8)	178.83(13)
C(5)–C(6)–C(7)–C(8)	–1.3(2)
C(4)–C(3)–C(8)–C(7)	1.3(2)
N–C(3)–C(8)–C(7)	–178.93(12)
C(6)–C(7)–C(8)–C(3)	–0.2(2)

Symmetry transformations used to generate equivalent atoms: #1 –x,y,–z+3

Table 5.7: Hydrogen bonds for 1,3-bis(*p*-methoxyphenyl)imidazolium chloride (110), (Å and °).

D–H...A	d(D–H)	d(H...A)	d(D...A)	<(DHA)
O(2)–H(1O2)...Cl	0.78(2)	2.36(2)	3.1301(9)	176(3)

Symmetry transformations used to generate equivalent atoms: #1 –x,y,–z+3

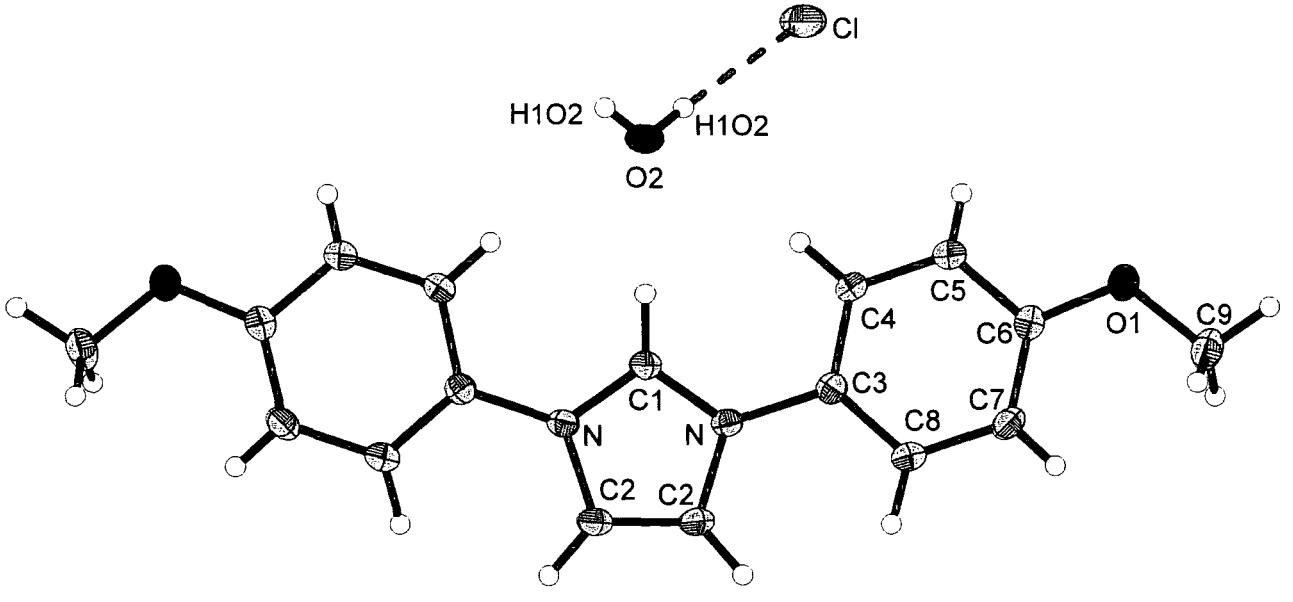

1,3-bis(*p*-methoxyphenyl)imidazolium chloride **(110)**, molecular cation with closest counter ion and water linked to it by hydrogen bonding; thermal ellipsoids are drawn on the 25% probability level.

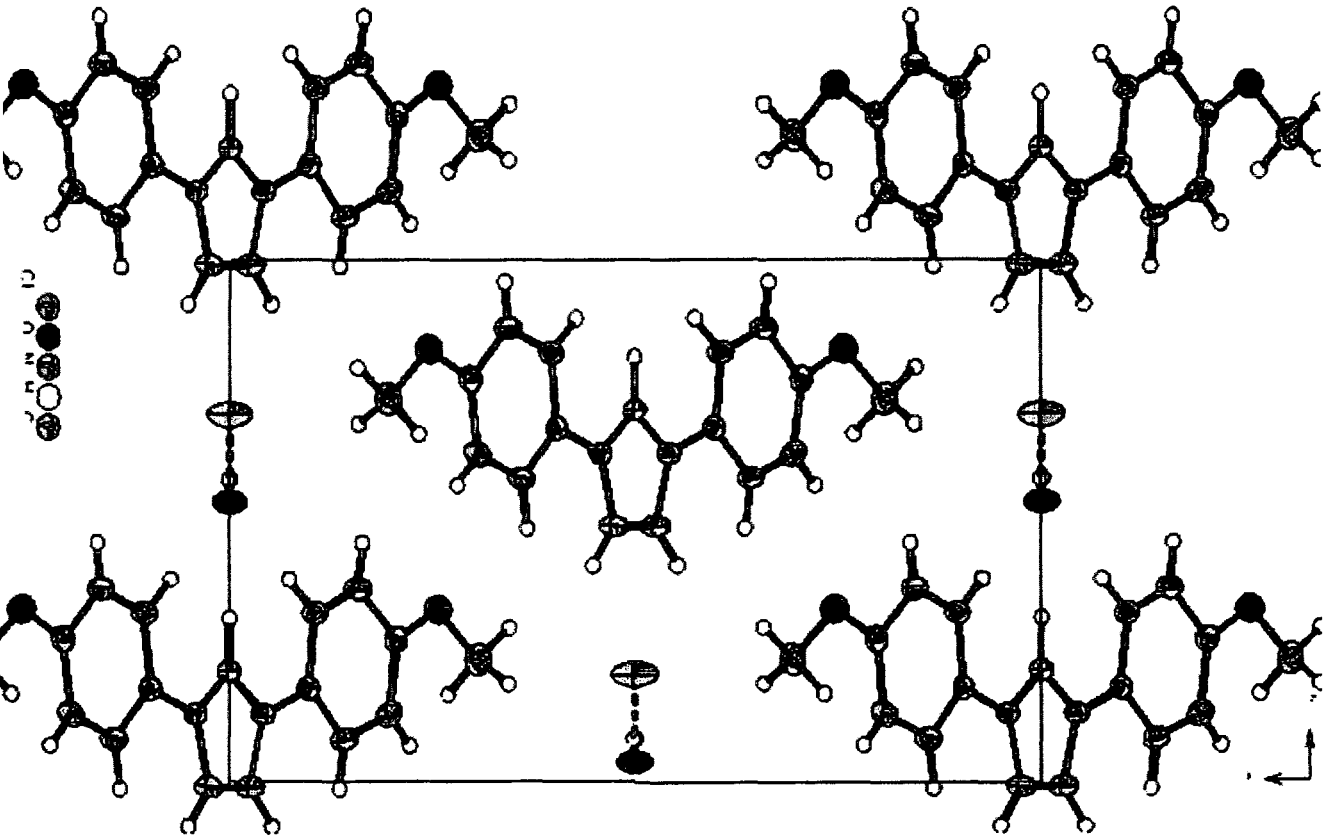

1,3-bis(*p*-methoxyphenyl)imidazolium chloride **(110)**, view along [0 0 1]; thermal ellipsoids are drawn on the 25% probability level

5.1.17 X-Ray crystallographic data for 1,3-bis(di-*iso*propylphenyl)4,5-imidazolium tetrafluoroborate (272).

Table 5.8: Crystal data and structure refinement for 1,3-bis(di-*iso*propylphenyl)-4,5-dihydroimidazolium tetrafluoroborate (272).

Identification code	s256	
Empirical formula	$C_{27}H_{39}N_2 \times B F_4$	
Formula weight	478.41	
Temperature	120(2) K	
Wavelength	0.71073 Å	
Crystal system	Orthorhombic	
Space group	P c c n	
Unit cell dimensions	a = 11.1217(7) Å	α= 90°.
	b = 12.5647(7) Å	β= 90°.
	c = 19.201(1) Å	γ = 90°.
Volume	2683.2(3) $Å^3$	
Z	4	
Density (calculated)	1.184 Mg/m^3	
Absorption coefficient	0.087 mm^{-1}	
F(000)	1024	
Crystal size	0.20 x 0.08 x 0.06 mm^3	
Theta range for data collection	2.12 to 26.00°.	
Index ranges	-13<=h<=13, -15<=k<=15, -23<=l<=23	
Reflections collected	21468	
Independent reflections	2646 [R(int) = 0.1016]	
Completeness to theta = 26.00°	100.0 %	
Absorption correction	None	
Refinement method	Full-matrix least-squares on F^2	
Data / restraints / parameters	2646 / 6 / 232	
Goodness-of-fit on F^2	1.079	
Final R indices [I>2sigma(I)]	R_1 = 0.0757, wR_2 = 0.2014	

R indices (all data)	$R_1 = 0.1220$, $wR_2 = 0.2274$
Extinction coefficient	0.0029(16)
Largest diff. peak and hole	0.838 and -0.810 e.Å^{-3}

Table 5.9: Atomic coordinates (x 10^4) and equivalent isotropic displacement parameters (Å^{2}x 10^3) for 1,3-bis(di-*iso*propylphenyl)-4,5 dihydroimidazolium tetrafluoroborate (272). U(eq) is defined as one third of the trace of the orthogonalized U^{ij} tensor.

Atom	x	y	z	U(eq)
N(1)	2842(2)	1681(2)	4234(1)	22(1)
C(1)	2500	2500	3851(2)	20(1)
C(2)	2773(3)	1934(3)	4987(2)	24(1)
C(3)	3274(3)	684(2)	3956(2)	22(1)
C(4)	2434(3)	-113(3)	3812(2)	26(1)
C(5)	2881(3)	-1050(3)	3519(2)	32(1)
C(6)	4094(4)	-1186(3)	3400(2)	34(1)
C(7)	4903(4)	-384(3)	3562(2)	32(1)
C(8)	4507(3)	572(3)	3842(2)	26(1)
C(9)	5395(3)	1459(3)	3998(2)	31(1)
C(10)	5890(4)	1933(4)	3325(3)	46(1)
C(11)	6407(4)	1087(4)	4472(3)	48(1)
C(12)	1103(3)	4(3)	3959(2)	31(1)
C(13)	621(4)	-918(3)	4393(2)	39(1)
C(14)	387(4)	115(5)	3284(3)	49(1)
B(1)	2500	2500	1895(2)	38(2)
F(1)	1456(4)	2466(4)	2302(2)	33(1)
F(2)	2685(6)	1498(5)	1521(3)	51(2)
F(1A)	1612(4)	2092(5)	2319(3)	42(2)

F(2A)	2803(8)	1818(6)	1404(4)	87(3)

Table 5.10. Anisotropic displacement parameters ($Å^2 x\ 10^3$) for 1,3-bis(di-*iso*propylphenyl)-4,5-dihydroimidazolium tetrafluoroborate (272). The anisotropic displacement factor exponent takes the form: $-2\pi^2[h^2 a^{*2} U^{11} + ... + 2 h k a^* b^* U^{12}]$

Atom	U^{11}	U^{22}	U^{33}	U^{23}	U^{13}	U^{12}
N(1)	29(2)	20(1)	17(1)	0(1)	1(1)	3(1)
C(1)	22(2)	21(2)	18(2)	0	0	-1(2)
C(2)	32(2)	25(2)	16(2)	0(1)	1(1)	1(2)
C(3)	28(2)	19(2)	20(2)	1(1)	2(1)	3(1)
C(4)	29(2)	24(2)	25(2)	0(1)	2(1)	2(1)
C(5)	37(2)	24(2)	34(2)	-7(2)	5(2)	-1(2)
C(6)	41(2)	24(2)	38(2)	-4(2)	11(2)	4(2)
C(7)	29(2)	27(2)	38(2)	3(2)	11(2)	4(2)
C(8)	28(2)	25(2)	23(2)	4(1)	1(1)	1(1)
C(9)	27(2)	28(2)	37(2)	4(2)	3(2)	-3(2)
C(10)	36(2)	50(3)	52(3)	21(2)	-4(2)	-15(2)
C(11)	51(3)	45(3)	49(3)	11(2)	-17(2)	-11(2)
C(12)	30(2)	28(2)	33(2)	-7(2)	1(2)	-1(2)
C(13)	35(2)	39(2)	43(2)	-2(2)	11(2)	-5(2)
C(14)	37(3)	64(3)	47(3)	4(3)	-8(2)	1(2)
B(1)	32(3)	69(5)	12(2)	0	0	-12(3)

Table 5.11: Hydrogen coordinates (x 10^4) and isotropic displacement parameters ($Å^2$x 10 ^{3}) for 1,3-bis(di-*iso*propylphenyl)-4,5-dihydroimidazolium tetrafluoroborate (272).

Atom	x	y	z	U(eq)
H(1)	2500	2500	3380(30)	22(12)
H(21)	3590(40)	1920(30)	5190(20)	39(11)
H(22)	2240(40)	1420(30)	5230(20)	34(10)
H(5)	2270(30)	-1650(30)	3440(20)	35(10)
H(6)	4410(40)	-1900(40)	3190(20)	55(13)
H(7)	5690(40)	-450(30)	3489(19)	31(10)
H(9)	5000(40)	2080(30)	4280(20)	50(12)
H(101)	6370(40)	2560(40)	3440(20)	41(11)
H(102)	5250(40)	2100(40)	3020(20)	52(13)
H(103)	6390(60)	1460(60)	3090(40)	110(20)
H(111)	6980(40)	1720(30)	4610(20)	41(11)
H(112)	6920(40)	540(40)	4210(30)	63(15)
H(113)	6040(40)	790(40)	4950(30)	52(13)
H(12)	960(40)	660(30)	4220(20)	43(12)
H(131)	-290(40)	-780(40)	4480(20)	53(13)
H(132)	1040(40)	-1000(30)	4860(30)	47(12)
H(133)	680(40)	-1610(40)	4120(30)	61(14)
H(141)	-430(50)	190(40)	3420(20)	56(13)
H(142)	700(40)	770(40)	2980(30)	60(14)
H(143)	460(40)	-550(40)	3030(30)	65(16)

Table 512: Selected bond lengths (Å) and angles (°) for 1,3-bis(di-*iso*propylphenyl)-4,5-dihydroimidazolium tetrafluoroborate (272).

Bond	Bond Length (Å)
N(1)-C(1)	1.320(4)
N(1)-C(3)	1.445(4)
N(1)-C(2)	1.483(4)
C(1)-N(1)#1	1.320(4)
C(2)-C(2)#1	1.546(7)
C(3)-C(8)	1.395(5)
C(3)-C(4)	1.397(5)
C(4)-C(5)	1.396(5)
C(4)-C(12)	1.514(5)
C(5)-C(6)	1.380(5)
C(6)-C(7)	1.386(5)
C(7)-C(8)	1.388(5)
C(8)-C(9)	1.519(5)
C(9)-C(11)	1.520(6)
C(9)-C(10)	1.525(6)
C(12)-C(13)	1.524(6)
C(12)-C(14)	1.527(6)

Bond	Bond Angle (°)
C(1)-N(1)-C(3)	124.5(3)
C(1)-N(1)-C(2)	111.1(3)
C(3)-N(1)-C(2)	124.3(3)
N(1)-C(1)-N(1)#1	112.4(4)
N(1)-C(2)-C(2)#1	102.56(17)
C(8)-C(3)-C(4)	123.7(3)
C(8)-C(3)-N(1)	118.2(3)
C(4)-C(3)-N(1)	118.2(3)
C(5)-C(4)-C(3)	116.5(3)
C(5)-C(4)-C(12)	120.3(3)
C(3)-C(4)-C(12)	123.2(3)
C(6)-C(5)-C(4)	121.3(3)
C(5)-C(6)-C(7)	120.5(3)
C(6)-C(7)-C(8)	120.7(4)
C(7)-C(8)-C(3)	117.3(3)
C(7)-C(8)-C(9)	120.3(3)
C(3)-C(8)-C(9)	122.3(3)
C(8)-C(9)-C(11)	112.0(3)
C(8)-C(9)-C(10)	110.7(3)
C(11)-C(9)-C(10)	111.1(4)
C(4)-C(12)-C(13)	111.8(3)
C(4)-C(12)-C(14)	111.2(3)
C(13)-C(12)-C(14)	110.5(4)

Symmetry transformations used to generate equivalent atoms: #1 -x+1/2,-y+1/2,z

Table 5.13: Selected torsion angles (°) for 1,3-bis(di-*iso*propylphenyl)-4,5-dihydroimidazolium tetrafluoroborate (272).

Bond	Torsion Angle (°)
C(3)-N(1)-C(1)-N(1)	-179.2(3)
C(2)-N(1)-C(1)-N(1)#1	-1.59(18)
C(1)-N(1)-C(2)-C(2)#1	3.8(4)
C(3)-N(1)-C(2)-C(2)#1	-178.6(3)
C(1)-N(1)-C(3)-C(8)	90.5(4)
C(2)-N(1)-C(3)-C(8)	-86.8(4)
C(1)-N(1)-C(3)-C(4)	-89.0(4)
C(2)-N(1)-C(3)-C(4)	93.7(4)
C(8)-C(3)-C(4)-C(5)	-1.8(5)
N(1)-C(3)-C(4)-C(5)	177.6(3)
C(8)-C(3)-C(4)-C(12)	178.0(3)
N(1)-C(3)-C(4)-C(12)	-2.5(5)
C(3)-C(4)-C(5)-C(6)	1.8(5)
C(12)-C(4)-C(5)-C(6)	-178.1(3)
C(4)-C(5)-C(6)-C(7)	-0.7(6)
C(5)-C(6)-C(7)-C(8)	-0.5(6)
C(6)-C(7)-C(8)-C(9)	-178.2(3)
C(4)-C(3)-C(8)-C(9)	179.4(3)
N(1)-C(3)-C(8)-C(9)	-0.1(5)
C(7)-C(8)-C(9)-C(11)	-55.1(5)
C(3)-C(8)-C(9)-C(11)	126.3(4)
C(7)-C(8)-C(9)-C(10)	69.4(5)
C(3)-C(8)-C(9)-C(10)	-109.1(4)
C(5)-C(4)-C(12)-C(13)	52.9(5)
C(3)-C(4)-C(12)-C(13)	-127.0(4)
C(5)-C(4)-C(12)-C(14)	-71.1(5)
C(3)-C(4)-C(12)-C(14)	109.0(4)

Symmetry transformations used to generate equivalent atoms: #1 -x+1/2,-y+1/2,z

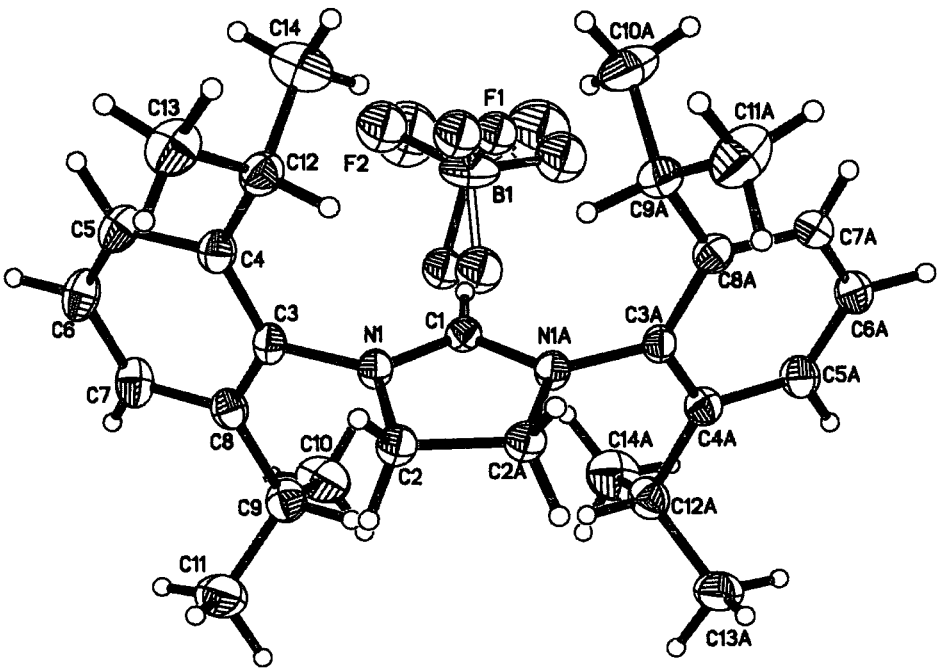

1,3-bis(di-*iso*propylphenyl)-4,5-dihydroimidazolium tetrafluoroborate **(272)**, molecular cation with closest counter ion.

5.2.1 Bis D-Proline diketopiperazine (218).

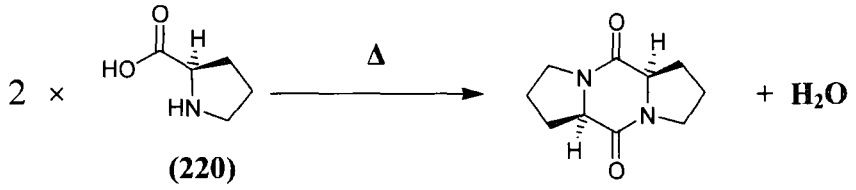

(220) **(218)**

D-Proline **(220)** (1.00 g, 0.009 mol) was placed in a dry flask. Heat was applied using a heat gun until the contents of the flask were completely melted. Heating continued for another 30 seconds and the flask was left to cool. The resulting off-white solid was purified using column chromatography on an aluminium oxide column (methanol 100%) to yield product **(218)** as a white solid (0.75 g, 86%), Rf. 0.5 (MeOH) m.p. 142-145 °C.

δ^1H / ppm (400 MHz, D_2O): 1.77 – 1.86 [m, 4H, NCH_2CH_2], 1.88 – 1.94 [m, 2H, NCH(*H*)], 2.09 – 2.19 [m, 2H, NC*H*(H)] 3.25 – 3.32 [m, 2H COCHCH(*H*)], 3.37 – 3.42 [m, 2H COCHC*H*(H)] 4.27 [t, $^3J_{H,H}$ = 7.8 Hz 2H, COC*H*CH_2].

δ^{13}C / ppm (400 MHz, D_2O): 22.7 [s, NCH_2CH_2], 27.3 [s, $COCHCH_2$], 45.3 [s, NCH], 60.8 [s, COCH], 168.4 [s, CO].

$C_{10}H_{14}N_2O_2$

Requires:	%C 61.84	%H 7.27	%N 14.42
Found:	%C 61.77	%H 7.17	%N 14.40

5.2.2 Bis L-Proline Diketopiperazine (219).

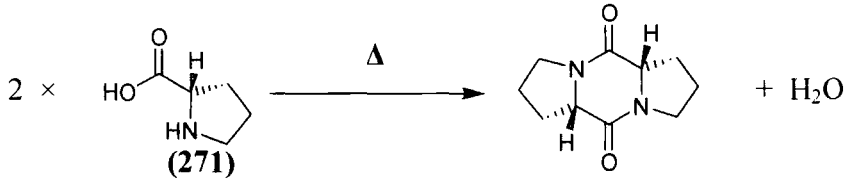

(271) **(219)**

L-Proline **(271)** (1 g, 0.009 mol) was placed in a dry flask. Heat was applied using a heat gun until the contents of the flask were completely melted. Heating continued for another 30 seconds and then the flask was left to cool. The resulting off white solid was purified using column chromatography on a aluminium oxide column (methanol 100%) (0.44 g, 50%), Rf. 0.5 (MeOH) m.p. 151-154 °C

δ^1H / ppm (400 MHz, D_2O): 1.77 – 1.86 [m, 4H, NCH_2CH_2], 1.88 – 1.94 [m, 2H, NCH(*H*)], 2.09 – 2.19 [m, 2H, NC*H*(H)] 3.25 – 3.32 [m, 2H COCHCH(*H*)], 3.37 – 3.42 [m, 2H COCHC*H*(H)], 4.27 [t, $^3J_{H,H}$ = 7.8 Hz 2H, COC*H*CH_2].

δ^{13}C / ppm (400 MHz, D_2O): 22.7 [s, NCH_2CH_2], 27.3 [s, $COCHCH_2$], 45.3 [s, NCH], 60.8 [s, COCH], 168.4 [s, CO].

5.3 General instrumentation

NMR samples were prepared in deuterated chloroform, deuterium oxide and d^6- dimethyl sulfoxide (DMSO). Tetramethylsilane (TMS) was used as an internal reference in deuterated chloroform. ^1H NMR and ^{13}C NMR spectra at 300 and 500 MHz were recorded on Oxford Varian Unity Inova 300 and 500 MHz NMR spectrometers in University College Dublin. In the University of Durham NMR spectra were recorded on a Varian Unity 300, a Bruker Ultrashield 400, and an Oxford Varian Inova 500 spectrometer. ^1H and ^{13}C NMR chemical shifts in $CDCl_3$ are reported relative to $CHCl_3$ at 7.27 ppm and 77.0 ppm respectively. In D_2O ^1H NMR chemical shifts are reported relative to HOD at 4.67 ppm. In d^6-DMSO ^1H NMR and ^{13}C NMR chemical shifts are reported relative to d^5-DMSO at 2.50 ppm and 39.52 ± 0.06 ppm respectively. Elemental analyses were obtained from the Microanalytical Unit, Chemistry Department, UCD, and from the Microanalytical Unit, Chemistry Department, Durham University. Melting points were measured using a Gallenkamp Melting Point Apparatus. Thin Layer Chromatography was carried out using silica-backed Merck Kieselgel 60 F254 plates.

5.4 Materials and preparation of solutions

Deuterium oxide (99.9 % D) was purchased from Apollo Scientific Ltd. Deuterium chloride (35 %, 99.5 % D), potassium deuteroxide (40 wt % 98+ %D) and deuterated chloroform (99.8 % D) were purchased from Aldrich Chemical company. 1,3-Di-*t*-butylimidazolium chloride, (99%) was purchased from Strem Chemicals Ltd. N,N'-Bis(*p*-chlorophenyl)imidazolium chloride (99%) was purchased from Aldrich Chemical company. 1-Ethyl, 3-methyl imidazolium iodide and 1-butyl, 3-methyl imidazolium bromide were a gift from Ms. Daniella Pieraccini, University of Piza. Our thanks to Dr. David Fox, University of Warwick U.K. for an initial sample of Bis-D-proline, although later samples were prepared in our laboratory. Our thanks also to Prof. Roger Alder, University of Bristol U.K. for providing samples of 1,3-di-*iso*propylpyrimidinium hexafluorophosphate, **(120)**, 1,3-di-*iso*propylpyrimidinium bis(trifluoromethylsulfonyl)amide, **(121)** 1,3-diethylpyrimidinium hexafluorophosphate

(122) and N,N'bis(di-*iso*propylamino) formadinium hexafluoro phosphate **(123)**. The internal standard, tetramethylammonium deuteriosulfate was a generous gift from Prof. Tina Amyes, University of Buffalo, New York. All other chemicals were reagent grade and were used without further purification unless otherwise stated.

Stock solutions of potassium deuteroxide and potassium chloride were prepared by dilution and titration of the commercial concentrated solutions. Stock solutions of buffers, K_2DPO_4 and KD_2PO_4, were obtained from potassium phosphate monobasic and dibasic by exchanging the hydrogen atoms for deuterium. This was achieved by dissolving the salts in D_2O, followed by removal of solvent under reduced pressure. The process was repeated five times and the salts were freeze dried. Phosphate buffers were prepared by mixing stock solutions of K_2DPO_4 and KD_2PO_4 in D_2O with addition of KCl to give solutions of buffer at various acid/ base ratios and I=1.0 (KCl).

Stock solutions of quinuclidine-DCl, and quinuclidinone-DCl salts in D_2O were obtained from quinuclidine-HCl and quinucidinone-HCl salts respectively by exchanging the hydrogen atoms for deuterium in a similar method to the phosphate buffer exchange. Quinuclidine and quinuclidinone buffers were prepared by mixing stock solutions of exchanged salt and stock solutions of potassium deuteroxide with the addition of KCl when needed to give solutions of buffer at various acid/base ratios and I=1 (KCl).

Stock solutions of acetate buffers were prepared by mixing stock solutions of potassium acetate and DCl with addition of KCl when needed to give buffer solutions at various acid/base ratios and I=1.0 (KCl).

5.5 Kinetic methods

H/D exchange reactions were carried out in 12.5 mL vials which were incubated at 25 ± 0.1°C in a thermostated water bath. All reactions were carried out in D_2O with the ionic strength maintained at I = 1.0 for with potassium chloride, with the exception of substrates N,N'-bis(*p*-chlorophenyl)imidazolium chloride **(111)** (I = 0.5), N,N'-bis(*p*-methoxyphenyl) imidazolium chloride **(110)** (I = 0.5), N,N'-bis(*p*-methoxyphenyl)-4,5-

dihydroimidazolium chloride **(117)** (I = 0.25) and thalidomide **(237)** (I = 0.5). In these cases poor solubility of the substrate in water necessitated a lower ionic strength. Typically reactions were run on a 5 or 6 mL scale, and were initiated by injection of 500, or 1000 μL of substrate stock solution (50 mM) to the KOD or buffer solution, containing internal standard tetramethylammonium deuteriosulphate. In general, the final substrate and internal standard concentrations in the reaction solutions were 5 - 10 mM and 0.5 - 1 mM, respectively. This ensured an approximately 1:1 ^{1}H NMR integration ratio of the singlet due to relevant acidic hydrogen of substrate and the triplet due to the 12 methyl hydrogens of internal standard. In cases where the phosphate and acetate buffers were used, where the reaction solution had a final pD of around 7 or less, the substrate was added neat to the reaction solution and dissolved with the aid of sonication.

The reaction progress was monitored over time by withdrawing aliquots (~800 μL) at timed intervals. These aliquots were quenched to pD 2-4 by addition of >1 M DCl solution. The samples were either analysed immediately or placed in a sealed plastic bag containing calcium chloride and stored in the freezer for analysis at a later time.

The pD of buffered solutions was determined at 25 °C using a MeterLab^{TM} PHM 290 pH-Stat Controller equipped with a radiometer (pH 4 - 7 - 10 @ 25 °C) combination electrode, that could be standardised between pH 4 - 7 or pH 7 - 10 to encompass the pD of the buffer solution. The hydronium ion concentration at any pH was calculated from $[H_3O^+] = 10^{-pH}/\gamma_H$, where $\gamma_H = 0.9$ is the apparent activity coefficient of hydronium ion under our experimental conditions. To determine a value for γ_H, a series of dilutions of standardised 1M HCl were made to give a titrimetrically known series of HCl solutions in the concentration range 0.001 – 0.1 M. The pD was calculated by adding 0.4 to the observed reading of the pH meter. The deuteroxide concentration was calculated from the equation $[DO^-] = (10^{pD - pKw})/\gamma_{DO}$, where $K_w = 10^{-14.87}$ M^2 is the ion product of D_2O at 25 °C and $\gamma_{DO} = 0.747$ is the apparent activity coefficient of deuteroxide ion under our experimental conditions. The estimated error on the observed pseudo-first-order rate constant (k_{obs}, s^{-1}) is ± 5 % based on the error of the ^{1}H NMR measurement. Although the measurements of k_{obs} and the calculation of pK_a are single determinations, the calculated

error in similar measurements and calculations performed by Richard *et al*[2] is ± 5 % for k_{obs} and ± 0.5 units for the pK_a.

^{1}H NMR spectra of 1,3-bis(2,4,6-trimethylphenyl)imidazolium chloride **(109)**, 1,3-bis(2,4,6-trimethylphenyl)4,5–dihydroimidazolium chloride **(116)**, 1,3-di-*iso*propylpyrimidinium hexafluorophosphate **(120)**, 1,3-diethylpyrimidinium hexafluorophosphate **(122)**, 1,3-di-*iso*propylpyrimidinium bis(trifluoromethylsulfonyl)amide **(121)**, N,N'-bis(di-*iso*propylamino)formadinium hexafluorophosphate **(123)**, bis-D-proline diketopiperazine **(218)**, bis-L-proline diketopiperazine **(219)**, N-(2-oxo-piperidine-3yl)propionamide **(249)** and N-(2-oxo-azapan-3-yl)propionamide **(250)** were recorded on an Oxford Varian Unity Inova 300 spectrometer. A relaxation delay of 1 second was used between pulses for all compounds. Spectra (64 – 128 transients) were recorded with a 45.0 ° pulse angle, sweep width of 2999 Hz, and an acquisition time of 3.744 s (total acquisition time 5-10 min). Baselines were subject to first – order drift correction before integration of the peak areas. Substrate and product peak areas were compared with the peak of the internal standard that was set to an arbitrary figure of 1000.

^{1}H NMR spectra of 1-methyl-3-mesityl-5-*iso*propyl-4-hydroimidazolium iodide **(119)**, 1,3-bis(2,4,6-trimethylphenyl)imidazolium chloride **(109)**, 1-ethyl-3-methylimidazolium iodide **(114)**, 1-butyl-3-methylimidazolium iodide **(115)**, and 1,3-bis(2,6-di-*iso*propylphenyl)imidazolium chloride **(112)** were recorded on a Bruker 400 Ultrashield spectrometer. The relaxation delay between pulses was set to 1 s on this spectrometer. Spectra were recorded at a pulse angle of 90°, a sweep width of 8278.1 Hz, an acquisition time of 7.899 s, and 16 transients (total acquisition time 5-10 min). Baselines were subject to first–order drift correction before integration of the peak areas. The integrated peak area for the singlet due to the C2-H, and in cases where hydrolysis or further reaction occurred the area of other relevant peaks of was compared with the peak of the internal standard that was set to an arbitrary figure of 1000.

^{1}H NMR spectra of 1-ethyl-3-methylimidazolium chloride **(142)**, 1,3-di-*t*-butylimidazolium chloride **(114)**, 1,3-bis(*p*-methoxyphenyl)4,5-dihydroimidazolium chloride **(117)**, 1,3-bis(*p*-methoxyphenyl)imidazolium chloride **(110)**, N,N'-bis(Di-*iso*propylamino)formadinium hexafluorophosphate **(123)**, 1,3-bis(*p*-chlorophenyl)imidazolium chloride **(111)**, were recorded on a Oxford Varian Inova 500 spectrometer with a relaxation delay of 20 s, sweep width of 7996.8 Hz, and acquisition time of between 4 - 6 s, and a 90° pulse angle. Spectra were run with 128 – 1056 transients with a total acquisition time of between 1 - 7 hours. This spectrometer was used in situations where a greater signal/noise ratio was required due to the low solubility of the substrate.

References

(1) Arduengo, A. J., III,Krafczyrk, R., Schmutzler, R. *Tetrahedron* **1999**, *55*, 14523.
(2) Richard, J. P., Williams, G., Gao, J. *J. Am. Chem. Soc.* **1999**, *121*, 715-726.

Acknowledgments

I would like to sincerely thank my supervisor Dr. Ann Marie C. O'Donoghue for the abundant help and guidance she has provided for me over the past few years. I can't imagine more friendly, supportive and inspiring boss.

I would also like to thank the remainder of the academic staff in the Chemistry Department in UCD for all their support and help, and all the academic staff in the University of Durham for the welcome and support I received on transferring to Durham.

Many thanks to all the technical staff in the departments of both UCD and Durham for their willingness and good humour, especially Geraldine Fitzpatrick (for help with the NMR in Dublin), and Alan Kenwright and Catherine Heffernan (for all their patience and help with my endless NMR experiments in Durham).

Thanks to all my lab-mates, Jenny, Barry, Shelly, Terry and Anita and to my extended lab family in 237 in UCD, especially Lisa, (saviour of my sanity on more than one occasion) and Wan Mohamed *Khairul* Bin Wan Mohamed Zin (I'll be visiting you in Malaysia!).

Thanks to my sisters, Joanna, Laila and Zoë for being great in general and to Dan for taking their place when I was alone in England.

Special thanks to Mark for being so supportive and understanding of everything I do, and to my parents Tony and Patricia, for their constant and unconditional support throughout this and every part of my life.

Special thanks also to my Grandmother who inspires me to keep going, stay focused, and be positive, and always remember to enjoy life.